

# Earth-Science Reviews

## Prediction of shoreline–shelf depositional process regime guided by palaeotidal modelling --Manuscript Draft--

<b>Manuscript Number:</b>	EARTH-D-20-00288R1
<b>Article Type:</b>	Review Article
<b>Keywords:</b>	Shoreline-Shelf; Wave; Tide; Fluvial; Process regime; Numerical Modelling; Palaeotidal
<b>Corresponding Author:</b>	Daniel Collins Shell International Ltd London, London UNITED KINGDOM
<b>First Author:</b>	Daniel Collins
<b>Order of Authors:</b>	Daniel Collins Alexandros Avdis Martin H. Wells Christopher D. Dean Andrew J. Mitchell Peter A. Allison Howard D. Johnson Gary J. Hampson Jon Hill Matthew D. Piggott
<b>Abstract:</b>	<p>Ancient shoreline–shelf depositional systems are influenced by an unusually wide array of geological, biological and hydrodynamic processes, with sediment transport and deposition primarily determined by the interaction of river, wave (including storm) and tidal processes, and changes in relative sea level. Understanding the impact of these processes on shoreline–shelf morphodynamics and stratigraphic preservation remains challenging. Numerical modelling integrated with traditional facies analysis provides an increasingly viable approach, with the potential to quantify, and thereby improve understanding of, the impact of these complex coastal sedimentary processes. An integrated approach is presented here that focuses on palaeotidal modelling to investigate the controls on ancient tides and their influence on sedimentary deposition and preservation – one of the three cornerstones of the ternary process classification scheme of shoreline-shelf systems. Numerical tidal modelling methodology is reviewed and illustrated in three palaeotidal model case studies of different scales and focus. The results are synthesised in the context of shoreline–shelf processes, including a critique and modification of the process-based classification scheme.</p> <p>The emphasis on tidal processes reflects their global importance throughout Earth's history. Ancient palaeotidal models are able to highlight and quantify the following four controls on tidal processes: (1) the physiography (shape and depth) of oceans (1000s km scale) determines the degree of tidal resonance; (2) the physiography of ocean connections to partly enclosed water bodies (100–1000s km scale) determines the regional-scale flux of tidal energy (inflow versus outflow); (3) the physiography of continental shelves influences shelf tidal resonance potential; and (4) tides in relatively local-scale embayments (typically 1–10s km scale) are influenced by the balance of tidal amplification due to funnelling, shoaling and resonance effects versus frictional damping. In deep time, palaeogeographic and palaeobathymetric uncertainty can be accounted for in palaeotidal models by performing sensitivity analyses to different scenarios, across this range of spatial scales.</p> <p>These tidal process controls are incorporated into an updated predictive decision tree</p>

	<p>for determining shoreline–shelf process regime in terms of the relative interaction of wave, fluvial and tidal processes. The predictive decision tree considers the effects of basin physiography, shelf width and shoreline morphology on wave, fluvial and tidal processes separately. Uncertainty and ambiguity in applying the widely used three-tier process classification scheme are reduced by using the decision tree in conjunction with a proposed two-tier classification of process regime that is limited to primary and secondary processes. This two-tier classification scheme is illustrated in the three case studies, showing how integration of numerical modelling with facies analysis of the preserved stratigraphic record improves confidence in prediction of tide-influenced shoreline-shelf process regimes. Wider application of this approach will further improve process-based classifications and predictions of modern and ancient shoreline–shelf systems.</p>
<b>Suggested Reviewers:</b>	<p>Valentina Marzia Rossi valentina.rossi@igg.cnr.it Mixed-process shoreline-shelf systems</p> <p>Shahin Dashtgard Simon Fraser University - Surrey sdashtga@sfu.ca Mixed-process shoreline-shelf systems</p> <p>Bruce Ainsworth Chevron Corp bruce.ainsworth@chevron.com Mixed-process shoreline-shelf systems</p> <p>Robert Dalrymple dalrympl@queensu.ca Mixed-process shoreline systems with focus on tidal systems</p> <p>Chris Paola cpaola@umn.edu Numerical modelling of sedimentary systems</p> <p>Zheng Zhou zeng.zhou@hhu.edu.cn</p>
<b>Opposed Reviewers:</b>	
<b>Response to Reviewers:</b>	

Dear Jingping Xu (Editor: ESR),

Many thanks for your editorial comments and the careful reviewer assessments. Please find attached the completed major revisions of manuscript EARTH-D-20-00288. The co-authors and I have systematically addressed the key concerns of the two reviewers. Details of the responses and key revisions in response to major concerns are given in the reviewer's comments. As a consequence of these major revisions and re-structuring, many of the more minor revisions/comments made by reviewer #1 as comments on the manuscript itself have also been addressed.

In response to the reviewer comments concerning the length and focus of the review, we have slightly modified the title *from 'Predicting shoreline depositional process regimes using insights from palaeotidal modelling' to 'Prediction of shoreline–shelf depositional process regime guided by palaeotidal modelling'*. The updated title is succinct and clearly articulates the purpose of the manuscript: to review how predictions and classification of shoreline-shelf depositional process regime can be guided by insights from numerical palaeotidal modelling.

Please contact me directly should you require any further information. We look forward to your reply.

Kind regards,

Daniel Collins, on behalf of all co-authors

**Reviewer #1 comments:**

Comment: *“manuscript far too long! ... review of tidal theory to be too long and repetitive of recently published work. Also, the background provided for each of the three, central paleo-tidal modeling studies (i.e., model design) is excessive. There is also unnecessary repetition, especially relating to various points of the controls on tidal dynamics.”*

Response:

- The revised manuscript has been significantly shortened; from 27,283 words in the original submission to 21,700 words in the revised manuscript – a 23% reduction. Furthermore, the number of figures has reduced from 31 to 25. The reduction was focused on the background and methodology sections, and on the background information of the case studies.
- The review of tidal theory has been shortened significantly to 1089 (new section 2.2.1) from 2543 words (old section 2.1). Details on the methodology of numerical tidal modelling has also been shortened.
- The summary of each case studies, especially the background, are much shorter, with an average word count reduction of 46%.
- In streamlining background and case study summaries, necessary edits have been made to reduce repetition relating to the controls on tides.

Comment: *“Your central message is lost ... I note that the title of the manuscript signals that this paper will be about predicting the nature of coastal zones, and yet this topic is almost completely absent from the Introduction, appearing only as an apparent after-thought as the third objective of the paper. Nowhere in the early part of the manuscript is the rationale for this interest in coastal prediction stated, or the reason why it needs to be re-examined.”*

Response:

- These linked comments have been addressed in focus by a complete re-write of the abstract, conclusions and introduction around the central message – that palaeotidal modelling provides unique insights into understanding, classifying and predicting ancient shoreline-shelf processes.
- The introduction now has the following structure, which clearly articulates the central message
  - Paragraph 1: Overview of the complex controls on sedimentary processes and morphodynamics of shoreline-shelf systems
  - Paragraph 2: The importance of better understanding shoreline-shelf systems
  - Paragraphs 3 and 4: Brief overview of the range of shoreline-shelf classifications and summary of range of related controls that have been investigated using numerical modelling.
  - Paragraph 5: Making the case for integrating numerical tidal modelling with sedimentary and stratigraphic analyses for improving classification, prediction and interpretation of shoreline–shelf depositional process regimes.

Comment: *“The aspect of tidal dynamics that you appear to believe is the most important neglected consideration (large-scale basin morphology) is perhaps under-sold, given that you do not consider*



1 *the fact that entire ocean basins can be "tuned" to particular tidal periods (i.e., the North Atlantic is*  
2 *nearly at resonance with the M2 tide, whereas the modern Pacific accentuates the diurnal tide)."*

3 Response:

- 4
- 5 • This aspect of tidal dynamics – relating to the ‘whole ocean’ (reviewer #1 in-text comment),  
6 is now mentioned, explicitly, in the following:  
7
    - 8 ○ Abstract: ‘(1) the physiography (shape and depth) of oceans (1000s km scale)  
9 determines the degree of tidal resonance;’
    - 10 ○ Background – Tidal theory (section 2.2.1): ‘For example, the modern North Atlantic  
11 Ocean is close to resonance for the semidiurnal M2 tide, whereas the modern Pacific  
12 Ocean accentuates the diurnal (O1 and K1) constituents (Fig. 4).’
    - 13 ○ Discussion – Controls on tidal processes and sedimentation (section 4.2.1): ‘A key  
14 consideration for understanding tidal processes and sedimentation along shorelines  
15 directly facing ocean basins (i.e. open-ocean shoreline systems) is therefore to  
16 estimate the influence of ocean-basin width and depth in controlling tidal  
17 resonance’
    - 18 ○ Conclusions: ‘Tides are controlled by the following physiographic controls on tidal  
19 processes: (1) the impact of physiography – size, shape and bathymetry – on tidal  
20 resonance in the Earth’s global ocean and constituent ocean basins (1000s km-  
21 scale)’
- 22

23 Comment: *"The immediate focus in section 2 on a very detailed review of tidal dynamics makes it*  
24 *appear that this manuscript is exclusively about this subject, when it really isn't. Because of this lack*  
25 *of appropriate "set-up" of the purpose of the manuscript, the apparently sudden digression into*  
26 *coastal classification in section 2.3 is unexpected."*

27 Response:

- 28
- 29 • The background section now starts with, and principally comprises of, a review of  
30 ‘Classification, identification and prediction of clastic depositional shoreline–shelf systems  
31 and process regime (section 2.1)’. This is now reinforced as the central purpose of the  
32 manuscript.
  - 33 • The link between palaeotidal modelling and identification of ancient tidal processes – the  
34 basis of the integrated modelling-facies analysis approach advocated is this review – are  
35 both summarised in section 2.2.
- 36

37 Comment: *"Indeed, there are several instances where material is presented without comment, so*  
38 *that the significance is not obvious. A particular example of this is flagged at Lines 195-199."*

39 Response:

40  
41  
42  
43  
44  
45  
46  
47  
48  
49  
50 In streamlining the structure of the revised manuscript, and significantly reducing its length, we have  
51 consciously tried to avoid presenting material without comment and repetition. This includes the  
52 particular example highlight in the original submission on Lines 195-199, concerning shoaling and  
53 funnelling effects. These equations are no longer included in the revised manuscript and instead:  
54  
55  
56  
57  
58  
59  
60  
61  
62  
63  
64  
65

1 'The most relevant points for understanding controls on tides and predicting shoreline–shelf process  
2 classification are discussed' on Lines 482-510.  
3  
4

5 Comment: *"The very lengthy review of three of your own paleo-tidal Modeling studies is interesting,*  
6 *but is excessive relative to their use in this manuscript ... Rather, it would make the presentation*  
7 *much more streamlined to discuss the results in general terms only, highlighting only those particular*  
8 *points that relate to the topic of predicting the nature of coastal zones. This should be done while*  
9 *presenting the results".*  
10  
11

12 Response:  
13

- 14 • We agree with the reviewer #1's recommendation and we now summarise each case study  
15 in just two parts: 'Background' and 'Model results and rock-record integration'. In the latter,  
16 the key results that give insights on the controls on tidal dynamics, and the evidence  
17 preserved in the time-equivalent rock record, are interwoven. Furthermore, the titles of  
18 each case study illustrate the spatial scale of the tidal controls discussed therein to aid clarity  
19 for the reader.  
20  
21  
22  
23

24 Comment: *"With regard to coastal classification and the discussion of mixed-energy settings and*  
25 *deposits, you and others before you have taken a somewhat negative tone when talking about the*  
26 *first-generation of classifications. As someone who was directly involved in that, I might be slightly*  
27 *sensitive, but I would point out that all of the original classifications recognized clearly and explicitly*  
28 *that mixed-energy systems were common, if not even dominant. This was explicit, for example, in*  
29 *how modern systems were plotted in diagrams such as Figure 3 of Dalrymple et al. (1992). However,*  
30 *at that time there were too few documented examples to allow the creation of multiple models, so*  
31 *the focus on "end members" was a necessary first step."*  
32  
33  
34  
35

36 Response:  
37

- 38 • We apologise that our original phrasing suggesting any negativity towards early  
39 classifications: our opinion is anything but negative. Rightly, we have revised our background  
40 text on these seminal models, including an explanation as to why they necessarily focused  
41 on relative process end-members (section 2.1.1):
  - 42 ○ 'Seminal models for clastic shoreline systems initially focused on modern deltas,  
43 particularly the relationship between delta front morphology and the relative  
44 influence of wave, tidal and fluvial process (Coleman and Wright, 1975; Galloway,  
45 1975). This ternary classification scheme was widely adopted and modified to  
46 include a wider range of depositional settings by Boyd et al. (1992), notably the  
47 bivariate wave versus tide classification of clastic coasts (Hayes, 1975; Hayes, 1979)  
48 and variability in grain size (Orton and Reading, 1993). Boyd et al. (1992) and  
49 Dalrymple et al., (1992) developed predictive evolutionary relationships between  
50 long-term equilibrium depositional environments for a wide range of shoreline–shelf  
51 depositional systems and recognised the overarching control of rate of sediment  
52 supply versus rate of relative sea level change (shoreline transgression vs.  
53 regression). These seminal models and classifications of shoreline–shelf systems  
54 necessarily focused on relative process end-members to establish the full range of  
55  
56  
57  
58  
59  
60  
61  
62  
63  
64  
65

depositional system types in the continuous spectrum of potential mixed-energy systems.’.

Comment: “Similarly, you appear to consider the recent documentation of mixed-energy settings and sedimentary structures to be a cause of “growing uncertainty” (Line 341; i.e., something “negative”) rather than being the positive addition of tools to recognize mixed-energy deposits. I personally prefer the adoption of a more positive tone, emphasizing how knowledge has advanced”

Response:

- Again, any negativity was unintentional and the specific phrasing referred to has been deleted. We also clearly recognise, in section 2.1.3, the positive ‘recent advances over the last 10–15 years in process-based sedimentological analysis of end-member and mixed-energy shoreline–shelf systems has increased confidence in palaeoenvironmental and ancient process interpretations. This is illustrated with a few specific examples, while a more comprehensive analysis of tidal facies is presented later (Section 2.2.3.1).’.

Comment: “the section on the influence of grain size has the potential to be interesting, but I do not see great value with respect to the topic of the manuscript, in its present form. The level of the discussion seems unnecessarily low; as I have noted in a comment, some of the points that you make are topics that I covered in a 2nd-year undergraduate class. Perhaps I taught at an unusually high level, but I suggest either deleting this material, or revising it to make it much more substantive. Given the great length of the manuscript, deletion would seem to be the better option.”

Response:

- This section has been deleted.

Comment: “the focus on the main topic (better prediction of coastal character in ancient successions) needs to be much more obvious, running as a consistent, identifiable thread throughout the entire presentation.”

Response:

- The refocusing of the abstract, introduction, background, case studies – including the titles of each case study – and conclusions, plus shortening discussion section 4.1 and 4.2 relative to section 4.3 – where the revised predictive classification scheme is presented – provides a more focused central message.

**Reviewer ‘#2:**

Comment (1): “The authors’ discussion on process classifications (section 2.3.1) started with the classic ternary classification scheme initially developed for deltas (Galloway, 1975). However, it is increasingly noted that, besides hydrodynamic regime, landscape setting and sedimentology are also equally important determining the shoreline morphology and depositional processes. In fact,

hydrodynamic regime, sedimentology and landscape setting are closely interlinked. This is nicely illustrated in, e.g. Fig.7 of Townend (2012) and Zhou et al. (2017). I recommend the authors to consider and discuss some recent insights related to the original ternary hydrodynamics-based classification.”

Response:

- The reviewer is thanked for providing a lengthy list of very relevant publications. The first paragraph of the revised introduction outlines the full range of controls on shoreline morphology with reference to the above comment and references:
  - ‘The type, morphology, depositional architecture and spatio-temporal evolution of these systems reflect dynamic interactions between three main groups of forcing conditions (e.g. Townend, 2012; Zhou et al., 2017). First, hydrodynamic processes operate on a range of spatio-temporal scales and principally include tides, river flow and wave climate (e.g. Galloway, 1975; Boyd et al., 1992; Ainsworth et al., 2011), but also larger magnitude-lower frequency extreme events such as storms. Second, the ‘sedimentology’ of the system includes both the rate of sediment supply and the range of grain sizes and characteristics of the sediment sources (e.g. Orton & Reading, 1993; Jaffe et al., 2007). Third, landscape setting describes the physiographic characteristics of the land-sea interface and receiving sedimentary basin (e.g. Zhou et al., 2014), which depends on various factors, most notably antecedent geology, sea level change, accommodation space (often related to tectonics) and, increasingly, anthropogenic influence (sediment supply, dredging, vegetation change, etc.).’

Comments (2) and (3):

- *“Although the focus is put on the palaeotidal modelling, I still recommend the authors to include some paragraphs discussing recent progress on ‘process-based’ morphodynamic modelling of shoreline evolution (e.g. de Vriend et al., 1993; van der Wegen and Roelvink, 2008; Nahon et al. 2012; Zhou et al. 2014). In fact, these modelling techniques are gradually capable of dealing with large-scale (100s km) and long-term (100s years) problems”*
- *“Closely linked to the previous comment, I think some recent insights/progress from the long-term process-based morphodynamic modelling approach, to understand shoreline depositional processes need to be discussed (other than common hydrodynamics, i.e. river, tide and wave), such as salinity difference (Olabarrieta et al. 2018; Zhou et al. 2020), sediment sorting processes (Zhou et al. 2015), sediment bedding in deltas (Leonardi et al. 2014) and so on.”*

Response:

- The wider progress in numerical modelling of shoreline morphodynamics is directly acknowledged in the revised introduction paragraph 3, and includes the aforementioned, and related, references:
  - ‘Whilst the variety and variability of controls on shoreline–shelf systems make it impossible to quantitatively understand and fully model ‘real world’ systems, numerical modelling has become an increasingly important tool for simplifying and understanding the diverse and complex set of controls on ‘real world’ shoreline–shelf systems. Numerical models simulate ‘virtual world’ systems subject to selected

1 processes operating under controlled boundary conditions (see Zhou et al., 2017 for  
2 a recent review). Models of virtual systems represent a conceptual idealisation of  
3 the real world for the processes modelled and must therefore be shown to produce  
4 robust, reliable and realistic simulation results comparable to relevant  
5 measurements from the real world. Testing the sensitivity of models to changes in  
6 boundary conditions and comparing to relevant measurement from real world  
7 examples is critical for validating the efficacy of the numerical modelling approach  
8 (Zhou et al., 2017). In the case of shoreline–shelf systems, there is now a wide body  
9 of research that investigate long-term morphodynamics and shoreline depositional  
10 processes using a process-based modelling approach. Most of these studies have so  
11 far investigated the influence of varying tide, river and wave hydrodynamics (e.g. de  
12 Vriend et al., 1993; van der Wegen & Roelvink, 2008; Nahon et al., 2013; Zhou et al.,  
13 2014; Rossi et al., 2016; Zhou et al., 2017), but other factors such as salinity  
14 differences (Olabarrieta et al. 2018; Zhou et al. 2020), sediment sorting processes  
15 (Zhou et al. 2015) and sediment bedding in deltas (Leonardi et al. 2014) have also  
16 been shown to significantly impact shoreline circulation and morphology.’

21  
22  
23 Comment (4): “Throughout the manuscript, the authors used words such as ‘long-term equilibrium’  
24 and ‘disequilibrium’ in a few places. I think it would be useful (for a reader) to define their concepts,  
25 as statistic equilibrium is seldom in natural systems (see, Zhou et al. 2017).”

26  
27  
28 Response:

- 29  
30  
31  
32  
33  
34  
35  
36  
37  
38  
39  
40  
41  
42  
43
- The few mentions ‘long-term equilibrium’ and ‘disequilibrium’ have largely been removed, as they were used somewhat imprecisely and not explicitly relating to the definition outlines in Zhou et al. (2017). However, the term ‘long-term equilibrium’ is still used once, and the simple, intuitive meaning is briefly provided: ‘Boyd et al. (1992) and Dalrymple et al., (1992) developed predictive evolutionary relationships between long-term equilibrium depositional environments – where sediment accumulation and erosion are essentially balanced (e.g. Zhou et al., 2017) – for a wide range of shoreline–shelf depositional systems and recognised the overarching control of rate of sediment supply versus rate of relative sea level change (shoreline transgression vs. regression).’

44  
45  
46  
47  
48  
49

Comment (5): “As a thorough review, I think it would be useful to add some discussion on the role of human influence. In the Anthropocene, the effects of humans modifying shoreline is sometimes overwhelming”

50  
51  
52  
53  
54  
55  
56  
57  
58  
59  
60  
61  
62  
63  
64  
65

Response:

- Anthropogenic influences on shoreline-shelf systems – both direct and indirect - are mentioned in the introduction:
  - ‘Third, landscape setting describes the physiographic characteristics of the land-sea interface and receiving sedimentary basin (e.g. Zhou et al., 2014), which depends on various factors, most notably antecedent geology, sea level change, accommodation space (often related to tectonics) and, increasingly, anthropogenic influence (sediment supply, dredging, vegetation change, etc.).’

- 1  
2  
3  
4  
5  
6  
7  
8  
9  
10  
11  
12  
13  
14  
15  
16  
17  
18  
19  
20  
21  
22  
23  
24  
25  
26  
27  
28  
29  
30  
31  
32  
33  
34  
35  
36  
37  
38  
39  
40  
41  
42  
43  
44  
45  
46  
47  
48  
49  
50  
51  
52  
53  
54  
55  
56  
57  
58  
59  
60  
61  
62  
63  
64  
65
- ‘Anthropogenic climate change has the potential to significantly impact shorelines through changes in sea level and rates of sediment weathering, erosion and supply. Anthropogenic influence on shorelines also extends to direct displacement of large volumes of sediment in engineering works and indirectly through, for example, changes in sediment erosion versus deposition related to vegetation clearing (e.g. Tomasovych and Kidwell, 2017) and modified balances between morphology, hydrodynamics and sediment transport. As such, present-day configurations of shoreline systems are often the result of ongoing and intrinsically coupled natural, social and economic feedbacks, the impacts of which on future long-term shoreline configurations are only just being explored (Zhou et al., 2017).’

Comment (6): *“The current manuscript is a bit lengthy and I think the authors may remove/shorten some very basic knowledge in Section 2 Background, such as sections 2.1.1-2.1.”*

Response:

- As mentioned above, the manuscript has been significantly shortened – main body + caption word count reduced by 23%, or 5583 words.
- Sections 2.1.1-2.1 in the original submission have been shortened or removed – revised sections 2.2.1-2.2.2.

Comment: *Editorial comments listed*

Response:

- Reference errors, also indicated by reviewer #1, have been addressed
- Table 3 (now Table 2) appears fine in the .doc version.

## ABSTRACT

Ancient shoreline–shelf depositional systems are influenced by an unusually wide array of geological, biological and hydrodynamic processes, with sediment transport and deposition primarily determined by the interaction of river, wave (including storm) and tidal processes, and changes in relative sea level. Understanding the impact of these processes on shoreline–shelf morphodynamics and stratigraphic preservation remains challenging. Numerical modelling integrated with traditional facies analysis provides an increasingly viable approach, with the potential to quantify, and thereby improve understanding of, the impact of these complex coastal sedimentary processes. An integrated approach is presented here that focuses on palaeotidal modelling to investigate the controls on ancient tides and their influence on sedimentary deposition and preservation – one of the three cornerstones of the ternary process classification scheme of shoreline-shelf systems. Numerical tidal modelling methodology is reviewed and illustrated in three palaeotidal model case studies of different scales and focus. The results are synthesised in the context of shoreline–shelf processes, including a critique and modification of the process-based classification scheme.

The emphasis on tidal processes reflects their global importance throughout Earth's history. Ancient palaeotidal models are able to highlight and quantify the following four controls on tidal processes: (1) the physiography (shape and depth) of oceans (1000s km scale) determines the degree of tidal resonance; (2) the physiography of ocean connections to partly enclosed water bodies (100–1000s km scale) determines the regional-scale flux of tidal energy (inflow versus outflow); (3) the physiography of continental shelves influences shelf tidal resonance potential; and (4) tides in relatively local-scale embayments (typically 1–10s km scale) are influenced by the balance of tidal amplification due to funnelling, shoaling and resonance effects versus frictional damping. In deep time, palaeogeographic and palaeobathymetric uncertainty can be accounted for in palaeotidal models by performing sensitivity analyses to different scenarios, across this range of spatial scales.

These tidal process controls are incorporated into an updated predictive decision tree for determining shoreline–shelf process regime in terms of the relative interaction of wave, fluvial and tidal processes. The predictive decision tree considers the effects of basin physiography, shelf width and shoreline morphology on wave, fluvial and tidal processes separately. Uncertainty and ambiguity in applying the widely used three-tier process classification scheme are reduced by using the decision tree in conjunction with a proposed two-tier classification of process regime that is limited to primary and secondary processes. This two-tier classification scheme is illustrated in the three case studies, showing how integration of numerical modelling with facies analysis of the preserved stratigraphic record improves confidence in prediction of tide-influenced shoreline-shelf process regimes. Wider

application of this approach will further improve process-based classifications and predictions of modern and ancient shoreline–shelf systems.



**Declaration of interests**

☒ The authors declare that they have no known competing financial interests or personal relationships that could have appeared to influence the work reported in this paper.

☐The authors declare the following financial interests/personal relationships which may be considered as potential competing interests:

# Prediction of shoreline–shelf depositional process regime guided by palaeotidal modelling

Daniel S. Collins<sup>1,2</sup>, Alexandros Avdis<sup>2</sup>, Martin R. Wells<sup>3</sup>, Christopher D. Dean<sup>4</sup>, Andrew J. Mitchell<sup>2</sup>, Peter A. Allison<sup>2</sup>, Howard D. Johnson<sup>2</sup>, Gary J. Hampson<sup>2</sup>, Jon Hill<sup>5</sup>, and Matthew D. Piggott<sup>2</sup>

<sup>1</sup> *Shell International Ltd, London, SE1 7NA, UK*

<sup>2</sup> *Department of Earth Science and Engineering, Imperial College London, South Kensington Campus, London, SW7 2AZ, UK*

<sup>3</sup> *BP plc, Chertsey Road, Sunbury-on-Thames, Middlesex TW16 7LN, UK*

<sup>4</sup> *Department of Earth Science, Natural History Museum, London, SW7 5BD, UK*

<sup>5</sup> *Environment Department, University of York, Heslington, York, YO10 5DD, UK*

## ABSTRACT

Ancient shoreline–shelf depositional systems are influenced by an unusually wide array of geological, biological and hydrodynamic processes, with sediment transport and deposition primarily determined by the interaction of river, wave (including storm) and tidal processes, and changes in relative sea level. Understanding the impact of these processes on shoreline–shelf morphodynamics and stratigraphic preservation remains challenging. Numerical modelling integrated with traditional facies analysis provides an increasingly viable approach, with the potential to quantify, and thereby improve understanding of, the impact of these complex coastal sedimentary processes. An integrated approach is presented here that focuses on palaeotidal modelling to investigate the controls on ancient tides and their influence on sedimentary deposition and preservation – one of the three cornerstones of the ternary process classification scheme of shoreline-shelf systems. Numerical tidal modelling methodology is reviewed and illustrated in three palaeotidal model case studies of different scales and focus. The results are synthesised in the context of shoreline–shelf processes, including a critique and modification of the process-based classification scheme.

The emphasis on tidal processes reflects their global importance throughout Earth’s history. Ancient palaeotidal models are able to highlight and quantify the following four controls on tidal processes: (1) the physiography (shape and depth) of oceans (1000s km scale) determines the degree of tidal resonance;

(2) the physiography of ocean connections to partly enclosed water bodies (100–1000s km scale) determines the regional-scale flux of tidal energy (inflow versus outflow); (3) the physiography of continental shelves influences shelf tidal resonance potential; and (4) tides in relatively local-scale embayments (typically 1–10s km scale) are influenced by the balance of tidal amplification due to funnelling, shoaling and resonance effects versus frictional damping. In deep time, palaeogeographic and palaeobathymetric uncertainty can be accounted for in palaeotidal models by performing sensitivity analyses to different scenarios, across this range of spatial scales.

These tidal process controls are incorporated into an updated predictive decision tree for determining shoreline–shelf process regime in terms of the relative interaction of wave, fluvial and tidal processes. The predictive decision tree considers the effects of basin physiography, shelf width and shoreline morphology on wave, fluvial and tidal processes separately. Uncertainty and ambiguity in applying the widely used three-tier process classification scheme are reduced by using the decision tree in conjunction with a proposed two-tier classification of process regime that is limited to primary and secondary processes. This two-tier classification scheme is illustrated in the three case studies, showing how integration of numerical modelling with facies analysis of the preserved stratigraphic record improves confidence in prediction of tide-influenced shoreline-shelf process regimes. Wider application of this approach will further improve process-based classifications and predictions of modern and ancient shoreline–shelf systems.

**Keywords:** Shoreline–Shelf; Wave; Tide; Fluvial; Process regime; Numerical Modelling; Palaeotidal.

## 1 INTRODUCTION

Shoreline–shelf landscapes at the land-sea interface are some of the most dynamic settings on earth, containing a complex array of sedimentary systems that include deltaic, estuarine, paralic, shallow marine and shelfal environments. The type, morphology, depositional architecture and spatio-temporal evolution of these systems reflect dynamic interactions between three main groups of forcing conditions ([Townend, 2012](#); [Zhou et al., 2017](#)). First, hydrodynamic processes operate on a range of spatio-temporal scales and principally include tides, river flow and wave climate (e.g. [Galloway, 1975](#); [Boyd et al., 1992](#); [Ainsworth et al., 2011](#)), but also larger magnitude-lower frequency extreme events such as storms. Second, the ‘sedimentology’ of the system includes both the rate of sediment supply and the range of grain sizes and characteristics of the sediment sources ([Orton and Reading, 1993](#)). Third, landscape setting describes the physiographic characteristics of the land-sea interface and receiving sedimentary basin ([Zhou et al.,](#)

2014), which depends on various factors, most notably antecedent geology, sea level change, accommodation space (often related to tectonics) and, increasingly, anthropogenic influence (sediment supply, dredging, vegetation change, etc.). Additional processes that mediate interactions between these factors include biological activity (e.g. fauna-sediment reworking) and vegetation cover. Furthermore, feedbacks exist between these controls such that changes, for example, in sea level can influence shoreline morphology (landscape setting) and cause potentially dramatic changes in tide and/or wave influence (e.g. [Yoshida et al., 2007](#); [Collins et al., 2018c](#)). In the case of natural shoreline–shelf systems, morphological change is generally related to the intrinsic feedback between hydrodynamics, sediment transport and morphology, but this feedback is invariably conditioned and constrained by the various factors governing landscape setting and sediment character of the system ([Zhou et al., 2017](#)).

Obtaining a better understanding of shoreline–shelf systems is of increasing importance in the 21<sup>st</sup> Century. Anthropogenic climate change has the potential to significantly impact shorelines through changes in sea level and rates of sediment weathering, erosion and supply. Anthropogenic influence on shorelines also extends to direct displacement of large volumes of sediment in engineering works and indirectly through, for example, changes in sediment erosion versus deposition related to vegetation clearing ([Tomašových and Kidwell, 2017](#)) and modified balances between morphology, hydrodynamics and sediment transport. As such, present-day configurations of shoreline systems are often the result of ongoing and intrinsically coupled natural, social and economic feedbacks, the impacts of which on future long-term shoreline configurations are only just being explored ([Zhou et al., 2017](#)). However, ancient stratigraphic records containing an archive of past changes in shoreline–shelf environments can form a useful reference for interpreting the potential future response of shorelines to changes in climatically-driven processes, provided these can be disentangled from other allogenic and autogenic controls (e.g. [Reading and Collinson, 1996](#); [Hampson, 2016](#)). Some of these ancient stratigraphic units deposited at or near shorelines have contributed significantly to global conventional and unconventional hydrocarbon production. Characterising, classifying and understanding the difference in facies, architecture and morphology between reservoirs formed in different shoreline–shelf systems has underpinned efforts to interpret and predict reservoir distribution and performance, to ultimately improve hydrocarbon recovery. Similar reservoirs also form vital freshwater aquifers, geothermal reservoirs and current and future reservoirs for CO<sub>2</sub> storage in carbon, capture and storage (CCS) projects.

Due to the complexity and evident importance of these settings, a variety of classification systems have evolved for categorising shoreline–shelf depositional systems (see reviews by [Elliott, 1986](#); [Boyd et al., 1992](#); [Johnson and Baldwin, 1996](#); [Reading and Collinson, 1996](#); [James and Dalrymple, 2010](#); [Ainsworth](#)

et al., 2011). However, the most widely applied classifications relate shoreline–shelf morphology and idealised sections of preserved stratigraphy to the relative strength of river, wave and tide processes (Coleman and Wright, 1975; Galloway, 1975; Hayes, 1975; Hayes, 1979; Boyd et al., 1992; Ainsworth et al., 2011), conditioned by the overarching controls of relative sea level change versus sediment supply (Curry, 1964; Boyd et al., 1992; Dalrymple, 1992), sediment grain size (Orton and Reading, 1993) and tectono-physiographic setting (Reading and Collinson, 1996).

Whilst the variety and variability of controls on shoreline–shelf systems make it impossible to quantitatively understand and fully model ‘real world’ systems, numerical modelling has become an increasingly important tool for simplifying and understanding the diverse and complex set of controls on such systems. Numerical models simulate ‘virtual world’ systems subject to selected processes operating under controlled boundary conditions (Zhou et al., 2017). Models of virtual systems represent a conceptual idealisation of the real world for the processes modelled, producing robust, reliable and realistic simulation results calibrated with real world measurements (Zhou et al., 2017). In the case of shoreline–shelf systems, there is now a wide body of research that investigate long-term morphodynamics and shoreline depositional processes using a process-based modelling approach. Most of these studies have so far investigated the influence of varying tide, river and wave hydrodynamics (de Vriend et al., 1993; Van der Wegen and Roelvink, 2008; Nahon et al., 2012; Leonardi et al., 2014; Zhou et al., 2014; Rossi et al., 2016; Zhou et al., 2017), but other factors such as salinity differences (Olabarrieta et al., 2018; Zhou et al., 2020), sediment sorting processes (Zhou et al., 2015) have also been shown to significantly impact shoreline circulation and morphology.

Improved understanding and recognition of process interactions along modern and ancient shorelines has led to refined process-based classifications and predictive models of shoreline systems (Ainsworth et al., 2008; Ainsworth et al., 2011; Vakarelov and Ainsworth, 2013; Nyberg and Howell, 2016). In the case of ancient systems, an important improvement has been wider application of theoretical relationships between the strength of wave or tide processes and shoreline–shelf physiography, derived from palaeogeographic reconstructions, in order to support facies and stratigraphic interpretations of ancient depositional processes, most notably the impact of shoreline geometry and on tidal resonance or amplification (Godin, 1993; Yoshida et al., 2007; van Cappelle et al., 2018; Zuchuat et al., 2019). Simple theoretical relationships provide a quick method of estimating shoreline–shelf wave and tidal potential but lack the ability to assess or understand spatio-temporal variability and the sensitivity to, and interaction of, potential physiographic controls. Instead, hydrodynamic numerical modelling enables deeper discussion of these factors, ranging from multi-process morphodynamic simulations (Geleynse et al.,

2011; [Rossi et al., 2016](#)) to simulations of specific shoreline processes. Of the trivariate controls of tide, river and wave processes, tidal forcing has proven both slightly easier to predict using numerical modelling (given that it relates to well understood planetary motions) and perhaps more relevant to understanding ancient shoreline-shelf processes, given that tides operate globally through the whole Earth system ([Stammer et al., 2014](#)), influence sediment transport to some capacity along all shorelines globally and have operated throughout the vast majority of Earth's history ([Green et al., 2017](#)). In comparison, river processes only operate directly along a small portion of global shorelines, waves depend on wind patterns, fetch and basin physiography, and both river and wave processes depend on complicated atmospheric and climatic processes. As such, numerical tidal simulations (e.g. [Slingerland, 1986](#); [Ericksen and Slingerland, 1990](#); [Martel et al., 1994](#); [Wells et al., 2005a](#); [Mitchell et al., 2010](#); [Collins et al., 2018a](#); [Collins et al., 2018b](#); [Dean et al., 2019](#)) have been extensively validated against modern sedimentary environments and, through integration with sedimentological and stratigraphic datasets, have provided unique information on the physiographic controls on tidal processes and sedimentary preservation along ancient tide-influenced shorelines. However, the implications of ancient tidal model simulations on the classification, prediction and interpretation of shoreline–shelf depositional process regimes have not yet been fully explored.

This review article aims to assess the implications of palaeotidal model simulations for classification and prediction of shoreline depositional process regime by discussing three main questions: (1) How do we classify and predict shoreline-shelf depositional systems, especially regarding hydrodynamic processes? (2) What do existing present-day and ancient numerical tidal models indicate about the controls on tides? (3) How can we use this understanding to improve predictions of shoreline–shelf process regime?

## 2 BACKGROUND

### 2.1 Classification, identification and prediction of clastic depositional shoreline–shelf systems and process regime

#### 2.1.1 Shoreline–shelf classifications

There is no single unifying classification of clastic shorelines and shelves. As with all natural systems, clastic shorelines form in response to multiple controls, and different parameters can be used for the purpose of classification (e.g. [Reading and Collinson, 1996](#)). Seminal models for clastic shoreline systems initially focused on modern deltas, particularly the relationship between delta front morphology and the relative influence of wave, tidal and fluvial process ([Coleman and Wright, 1975](#); [Galloway, 1975](#)). This

ternary classification scheme was widely adopted and modified to include a wider range of depositional settings by [Boyd et al. \(1992\)](#), notably the bivariate wave versus tide classification of clastic coasts ([Hayes, 1975](#); [Hayes, 1979](#)) and variability in grain size ([Orton and Reading, 1993](#)). [Boyd et al. \(1992\)](#) and [Dalrymple \(1992\)](#) developed predictive evolutionary relationships between long-term equilibrium depositional environments, where sediment accumulation and erosion are essentially balanced ([Zhou et al., 2017](#)). These relationships addressed a wide range of shoreline–shelf depositional systems and recognised the overarching control of rate of sediment supply versus rate of relative sea level change (shoreline transgression versus regression). These seminal models and classifications of shoreline–shelf systems necessarily focused on relative process end-members to establish the full range of depositional system types in the continuous spectrum of potential mixed-energy systems.

The extensive range of models provide a means to classify shoreline–shelf systems at a particular time and in a particular location. However, these models were not intended to predict more detailed process variations either spatially at a given time, temporally at a given location, or both spatially and temporally ([Boyd et al., 1992](#)). Such dynamic changes in depositional processes on various spatial and temporal scales may be caused by variations in any of the multitude of controls impacting shoreline–shelf systems. For example, changes in shoreline physiography (morphology and bathymetry), fluctuations in accommodation space creation versus sediment supply rates, and variations in regional basin physiography may all form dominant controls on shoreline-shelf systems.

Within individual shoreline systems, complex arrangements of discrete depositional elements attributed to different combinations of wave, tide and fluvial processes have been recognized in analyses of: (1) modern delta geomorphology and sedimentological data, including the Danube ([e.g. Bhattacharya and Giosan, 2003](#)), Ganges-Brahmaputra ([e.g. Willis, 2005](#)), Mahakam ([e.g. Allen and Chambers, 1998](#)), Mekong ([e.g. Nguyen et al., 2000](#); [Ta et al., 2002b](#)), Mitchell ([e.g. Nanson et al., 2013](#)) and Changjiang (Yangtze) ([e.g. Hori et al., 2002](#)) deltas; and (2) approximately contemporaneous ancient stratigraphic units, including the Permian Kookfontein and Waterford formations in the Karoo Basin ([Gomis-Cartesio et al., 2016](#)), Cretaceous Ferron Sandstone, Western Interior Seaway ([e.g. Gardner et al., 2004](#); [Bhattacharya and MacEachern, 2009](#); [Li et al., 2011](#); [Li et al., 2015](#)), Cretaceous Sego Sandstone, Western Interior Seaway ([Willis and Gabel, 2001](#); [Legler et al., 2014](#); [van Cappelle et al., 2016](#)), Cretaceous Horseshoe Canyon Formation, Western Interior Seaway ([Willis and Gabel, 2001](#); [Legler et](#)



al., 2014; Ainsworth et al., 2015; Ainsworth et al., 2016; van Cappelle et al., 2016) and Miocene Belait Formation, NW Borneo (Lambiase et al., 2003; Collins et al., 2017b; Collins et al., 2018c). Consequently, these and many other depositional systems frequently indicate mixed-process regimes, with variable wave, tide and fluvial interactions in both space (e.g. along and/or perpendicular to depositional strike) and time (on various timescales e.g. daily, seasonal, annual or longer). These mixed-energy systems cannot be fully resolved in the early process classification models (Coleman and Wright, 1975; Galloway, 1975; Boyd et al., 1992). Therefore, Ainsworth et al. (2011) developed a new semi-quantitative, process-based classification scheme based on the relative importance of primary, secondary and tertiary processes: represented by ‘dominated’, ‘influenced’ or ‘affected’ descriptors, respectively. This higher-resolution process-based approach enhances comparison of modern and ancient shoreline deposits (Fig. 1A). However, a quantitative process analysis of modern shorelines by Nyberg and Howell (2016) suggests the thresholds separating primary, secondary and tertiary processes are ambiguous, resulting in these authors favouring a two-tier classification (Fig. 1B). Furthermore, the additional ambiguity in the process interpretation of several common sedimentary structures means that most studies of ancient, mixed-process shoreline deposits have adopted a two-tier process classification (e.g. Bhattacharya and Giosan, 2003; Lambiase et al., 2003; Coates and MacEachern, 2007; Gani and Bhattacharya, 2007; Hansen et al., 2007; Buatois et al., 2012; Vakarelov et al., 2012; Amir Hassan et al., 2013; Legler et al., 2013; Chen et al., 2014; Legler et al., 2014; Ainsworth et al., 2015; Gugliotta et al., 2015; Li et al., 2015; Ainsworth et al., 2016; Amir Hassan et al., 2016; Gomis-Cartesio et al., 2016; Gugliotta et al., 2016a; Rossi and Steel, 2016; Vaucher et al., 2016; Collins et al., 2017b; Collins et al., 2018c).



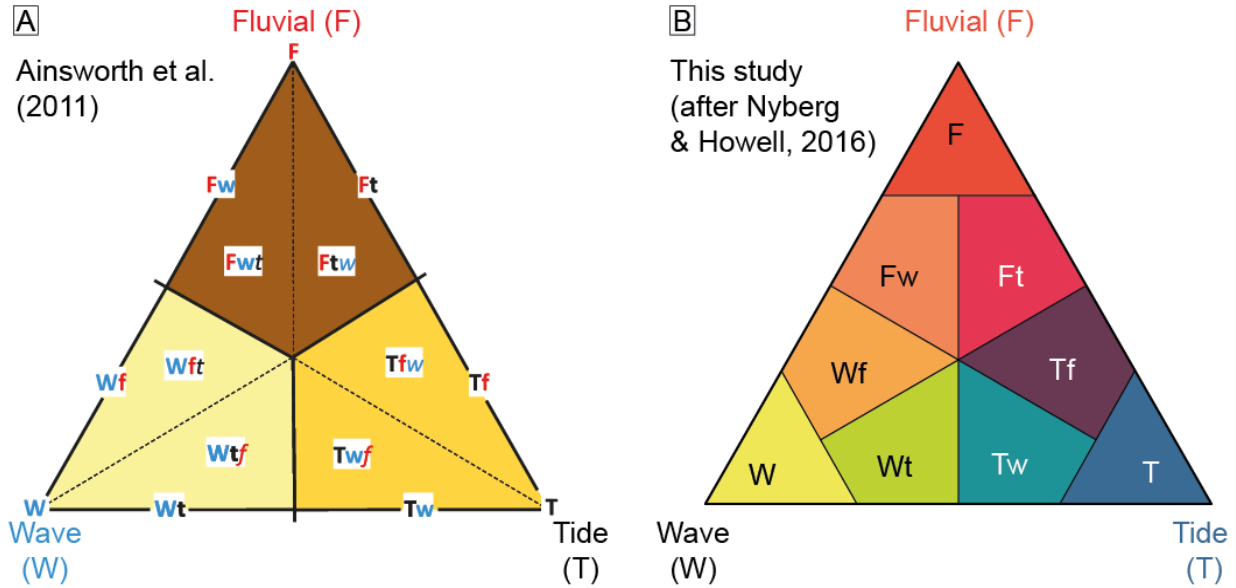


**Fig. 1.** Two contrasting ternary process classifications for shoreline depositional systems. (A) The three-tier classification of Ainsworth et al. (2011) utilizes primary, secondary, and tertiary processes, which are referenced as ‘dominated’ (capitalized and bold), ‘influenced’ (lower case and bold) and ‘affected’ (lower case italics and not bold), respectively. For example, wave dominated, tide influenced and fluvial affected is written **Wtf**. (B) The two-tier classification of Nyberg and Howell (2016) recognizes the primary and secondary processes, and is favored in this study (see text for discussion).

### 2.1.2 Process classification of present-day global shorelines

Nyberg and Howell (2016) developed the first, systematic, semi-automated classification of global shoreline process regime (Fig. 2) by combining several datasets and methodologies: (1) proxies for wave, tide and fluvial processes, including wave height, tidal amplitude and river discharge; (2) depositional versus erosional shorelines, determined by combining global lithology maps and digital elevation models; and (3) algorithms for determining the ‘tidal coefficient’ for modifying tidal amplitude using shoreline rugosity or ‘roughness index’. This integrated approach predicts shoreline classification with an 85% success rate compared to manual interpretation based principally on shoreline morphology (e.g. Ainsworth et al., 2011), and is consistent with earlier comparisons of shoreline morphology with quantitative metrics of wave, tide and river power along large, but non-global, stretches of siliciclastic coastlines (e.g. Harris et al., 2002). By subdividing the global shoreline into 5 km segments, this methodology classifies 28% of global shorelines as depositional, of which 62% are wave-dominated, 35% tide-dominated and 3% fluvial-dominated (Fig. 2A) (Nyberg and Howell, 2016). On a global scale, over 90% of shorelines on narrow shelves ( $\leq 25$  km) are wave-dominated and  $< 5\%$  tide-dominated, whereas

over 30% of shorelines on wide shelves (>75 km) are tide-dominated (Fig. 2B). Along depositional shorelines, tide dominance increases from <20% on narrow shelves to >50% on wide shelves (Fig. 2C). Fluvial-dominated systems are prone to more wave modification on narrow shelves and to more tide modification on wide shelves (Fig. 2B and C).

Tide-dominated deltas are widely distributed (Figs 2A and 4A), including: (1) at low and high latitudes; (2) along open-ocean shorelines and in partly enclosed oceans and seas; and (3) along straight and highly embayed shorelines. Their locations encompass a range of tectonic settings, including strike-slip transtensional rift (e.g. Colorado delta), forearc (e.g. Cooper delta), foreland (e.g. Mahakam and Fly deltas) and passive margin settings (Ganges Brahmaputra delta) (Nyberg and Howell, 2016). Tide-dominated deltas preferentially occur along macrotidal shorelines (Fig. 4A), but they also occur along mesotidal shorelines (e.g. Mekong and Mahakam deltas). However, tide-dominated deltas exclusively occur along shorelines with elevated tidal bed shear stresses, where tidal currents at their maximum strength are capable of transporting at least coarse sand (Fig. 4D).

Although the Nyberg and Howell (2015) classification provides a consistent, reproducible approach for identifying process distribution along global shorelines, it has some limitations. As is observed in modern systems, more rugose and funnel-shaped shorelines are strongly correlated with tide dominance, but not all present-day embayments are tide dominated. Likewise, smoother shorelines are correlated with wave dominance. None of the tidal coefficients consider theoretical and quantifiable relationships between shoreline physiography and the tidal prism (D'Alpaos et al., 2010). Lastly, wave height and tidal range are inadequate proxies for differentiating wave- and tide-dominance in mixed-energy systems (e.g. Anthony and Orford, 2002; Dalrymple, 2010b; Mulhern et al., 2017) because these parameters are not directly related to sediment entrainment (unlike bed shear stress).

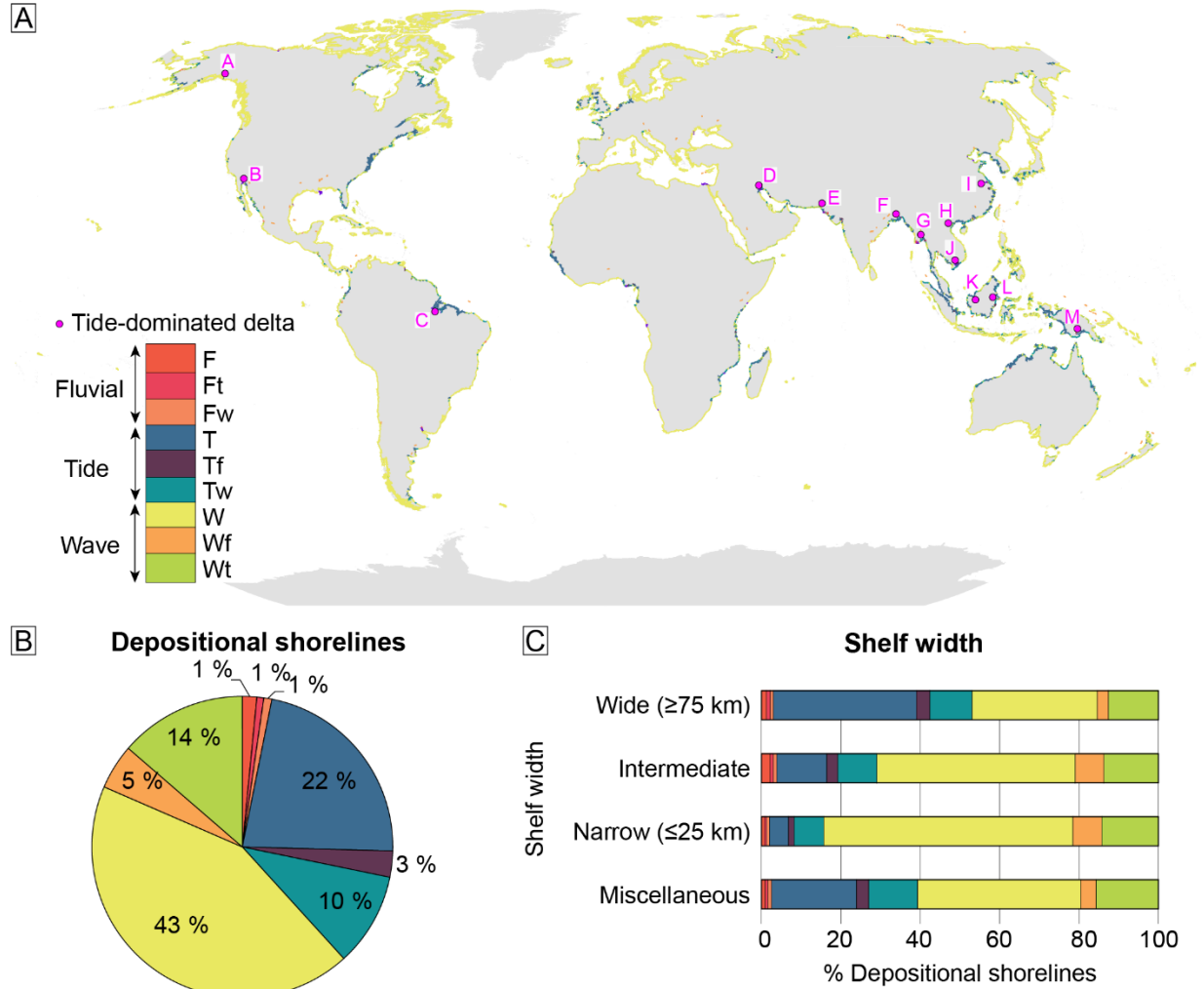


**Fig. 2.** Quantification of modern global shoreline process regimes (from Nyberg and Howell, 2016). (A) Two-tier ternary process classification of modern shorelines (see Fig. 1B) showing the locations (pink dots) of tide-dominated deltas (Goodbred and Saito, 2012): A) Copper; B) Colorado; C) Amazon; D) Shatt-al-Arab; E) Indus; F) Ganges-Brahmaputra; G) Irrawaddy; H) Red River; I) Yangtze; J) Mekong; K) Rajang; L) Mahakam; and M) Fly. Figures 4A and D show the same delta locations on a global map of tidal range and tidal bed shear stress, respectively. (B) Proportion of the two-tier process classifications along depositional shorelines. (C) Relationship between binned shelf width and proportion of the two-tier process classification along depositional shorelines. The miscellaneous class is for shallow seas and seaways (e.g. Baltic Sea).

### 2.1.3 Identification of ancient shoreline–shelf processes

The study and interpretation of ancient physical processes from sedimentary rocks has required a rigorous, multi-scale approach that has developed over the last 60–70 years (see reviews by [Walker and Plint, 1992](#); [Reading, 1996](#)). This methodology is underpinned by rigorous facies analysis, which relies on detailed, qualitative descriptions of distinctive combinations of sedimentary and biological structures (e.g. [Reading, 1978](#); [Reading, 1996](#)). However, small-scale (c. 1–100s cm) facies are typically based on subtle differences that are non-unique in terms of depositional processes and environment ([Walker and James, 1992](#)). Hence, sedimentological and stratigraphic descriptions and interpretations are required across the range of scales and dimensions spanning facies, facies associations, facies successions and architectural elements to characterise and interpret ancient processes and environments ([Elliott, 1986](#); [Walker and James, 1992](#); [Dalrymple, 2010a](#); [Colombera and Mountney, 2020b](#)). Understanding the relationship between process, sedimentation, sedimentary structures and stratigraphic architecture also requires comparison to the modern, where these aspects may be observed and measured directly in different environments ([Middleton, 1965](#); [Allen, 1968](#); [Allen, 1982b](#); [Yang et al., 2008](#); [Collinson and Mountney, 2019](#); [Dalrymple, 2021](#)).

In shoreline–shelf systems, the process-based sedimentological approach centres upon unravelling the relative influence of river, wave and tide processes based on different groups of physical processes, principally unidirectional and bidirectional traction currents and gravitational, oscillatory and suspension flow processes. The confidence level of ancient ternary process interpretations depends on several factors, most notably: (1) the availability and quality of the rock data; (2) the formation and preservation potential of sedimentary facies that can be assigned to specific flow processes; (3) the uncertainty in the process interpretation of sedimentological, stratigraphic and biological features; and (4) the level of existing knowledge of the depositional system under investigation. Recently, a statistical method for classifying shoreline–shelf deposits has been proposed that involves assigning a percentage likelihood that a bed or stratal unit was formed by wave, tide or fluvial processes (‘process percentage’) and quantifying the relative proportion of each bed or stratal unit ([Rossi et al., 2017b](#); [Peng et al., 2018](#)). The ‘process percentage’ is determined based on the proportion of preserved sedimentary structures, and also the proportion of wave-, tide- or fluvial-dominated interpretations of each sedimentary structure in an extensive literature database ([Rossi et al., 2017b](#); [Peng et al., 2018](#)). However, this approach has limitations. First, the volumetric proportion of deposits formed by different processes may not reflect process dominance in the environment of deposition, as highlighted by [Dalrymple et al. \(2015\)](#). Second,

end-member process interpretations of various sedimentary structures are commonly ambiguous. Third, it is difficult to assign percentage values to sedimentary structures formed by combined processes.

Nonetheless, recent advances over the last 10–15 years in process-based sedimentological analysis of end-member and mixed-energy shoreline–shelf systems has increased confidence in palaeoenvironmental and related process interpretations. This is illustrated with a few specific examples, while a more comprehensive analysis of tidal facies is presented later (Section 2.2.3.1). It is now recognized that muddy and sandy heterolithics with a predominance of unidirectional ripple cross-lamination are not limited to tidal settings as was originally emphasized (e.g. [Reineck and Wunderlich, 1968](#)) and occasionally uncritically adopted by some sedimentologists. Instead these facies can form in a wide range of environments and under a spectrum of processes, especially those with mixed fluvial and tidal influence (e.g. [Dalrymple et al., 2015](#); [Gugliotta et al., 2016b](#); [Korcinka et al., 2018](#); [Collins et al., 2020](#); [Van Yperen et al., 2020](#)) ([Thomas et al., 1987](#); [Martinius et al., 2015](#); [Jablonski and Dalrymple, 2016](#)). Likewise, subtle difference in the interpretation of tidal influence (secondary process) versus tidal modulation (tertiary processes) in cross-stratification have been proposed ([Martinius and Gowland, 2011](#); [Gugliotta et al., 2016a](#)) ([Martinius et al., 2015](#)). Hummocky and swaley cross-stratification with mudstone drapes have recently been interpreted to record mixed storm and tidal processes ([Vakarelov et al., 2012](#); [Wei et al., 2016](#)) or inherent flow variability during storm flows (e.g. [Collins et al., 2017b](#)). Lastly, the range of oscillatory to unidirectional flow and the influence of hyperpycnal flow in the origin of hummocky and swaley cross-stratification and related structures (e.g. combined-flow ripples and planar lamination) is now more widely appreciated ([Dott and Bourgeois, 1982](#); [Arnott and Southard, 1990](#); [Myrow and Southard, 1996](#); [Myrow et al., 2002](#); [Dumas and Arnott, 2006](#); [Lamb et al., 2008](#); [Tinterri, 2011](#); [Basilici et al., 2012](#); [Perillo et al., 2014](#)).

#### ***2.1.4 Prediction of ancient shoreline–shelf depositional process regime***

Understanding the physiographic and hydrodynamic controls on the process regime of present-day shorelines (section 2.1.2), and consideration of such controls in ancient case studies, has enabled development of predictive models for ancient shoreline–shelf depositional process regime. [Ainsworth et al. \(2011\)](#) extended previous process-based models of shoreline–shelf systems by including the following aspects: (1) basin physiography (100–1000 km scale), (2) shelf width (10–100 km scale), (3) fluvial versus wave effectiveness, (4) accommodation versus sediment supply (A/S ratio), and (5) shoreline

morphology (1–10 km scale). These were incorporated into a decision tree (Fig. 7A) and two predictive matrices (Fig. 7B and C) for low and high tidal resonance, respectively.

First, basin physiography and shelf width are combined to determine the ‘tidal resonance potential of the basin’ (Fig. 7A). Tidal resonance occurs when the natural period of oscillation within an ocean, water body, on the shelf or within a shoreline embayment, is coincident with the tidal period ([Slingerland, 1986](#); [Allen, 1997](#); [Collins et al., 2018c](#)). The interpretation of tidal resonance potential is calibrated empirically to shelf width ([cf. Howarth, 1982](#)). Present-day shorelines suggest that tide-dominated systems are more likely adjacent to shelves greater than 75 km in width ([Heap et al., 2004](#); [Ainsworth et al., 2011](#)). Hence, shelf width is used as an approximate empirical cut-off to distinguish modern and ancient shorelines with lower (<75 km shelf width) and higher tidal potential (>75 km shelf width), respectively.

The second decision in the tree (Fig. 3) focuses on fluvial versus wave effectiveness, which is also partly related to ancient shoreline palaeogeography. Shorelines facing large open water bodies are likely to be strongly influenced by wind-driven waves, with a large fetch resulting in a relatively high wave effectiveness. In contrast, shorelines that are more sheltered from direct oceanic waves and/or face smaller water bodies experience lower wave effectiveness. Fluvial effectiveness is controlled by a range of continental processes, including climate, weathering, river hydrology, drainage basin area, slope of the alluvial plain, and hinterland relief and gradient. Predictions of higher fluvial effectiveness must be supported by palaeogeographic, palaeodrainage and palaeohydrological reconstructions, especially where these indicate proximity to the outlets of large fluvial drainages. Consequently, wave and fluvial effectiveness are determined by very different factors, requiring independent facies analysis of preserved stratigraphy.

The third decision, the rate of accommodation space creation versus sediment supply (A/S ratio), is a useful theoretical concept ([Muto and Steel, 1997](#)) but difficult to apply practically, even for extensive datasets ([Ainsworth et al., 2008](#); [Ainsworth et al., 2011](#)) and for predictions based on parasequence characteristics ([Colombera and Mountney, 2020a](#)). The A/S ratio does not directly affect shoreline depositional processes but may modify their relative interaction through changes in physiography. For embayed shorelines, which favour tidal amplification, the degree of wave protection will be: (1) reduced

under low A/S conditions because higher progradation rates cause shorelines to straighten more quickly; and (2) increased under high A/S conditions, when accommodation exceeds sediment supply, because the embayed shoreline geometry will more likely persist (Fig. 3) ([Ainsworth et al., 2011](#)). Furthermore, the A/S ratio impacts preservation potential, with more complete preservation of all sub-environments in high A/S settings ([van Vliet and Schwander, 1987](#); [Collins et al., 2018c](#)).

Shoreline morphology (c. 1–10 km scale) is the final decision on the tree (Fig. 3), and can have a significant impact on the relative balance of tide, wave and fluvial processes (Fig. 1) ([Boyd et al., 1992](#); [Dalrymple et al., 1992](#); [Ainsworth et al., 2008](#); [Ainsworth et al., 2011](#)). Highly-embayed, more rugose shoreline morphologies may promote: (1) amplification of the tidal wave by funnelling and/or resonance effects ([Slingerland, 1986](#); [Allen, 1997](#)); and (2) protection from direct wave approach from the open ocean or sea. Therefore, [Ainsworth et al. \(2011\)](#) use shoreline rugosity as a direct proxy for tidal influence, with increasing rugosity corresponding to increased potential for tidal influence (Fig. 3). Their model predicts that all interpreted highly embayed shorelines, and half of interpreted moderately embayed shorelines, are tide-dominated, whereas only a quarter of interpreted straight to lobate shorelines are tide-dominated (Fig. 3A). However, this simplified differentiation is inconsistent with observations of Holocene to present-day embayed shorelines, most notably estuaries (e.g. [Dalrymple, 1992](#); [Roy et al., 2001](#); [Boyd et al., 2006](#); [Dalrymple, 2006](#); [Dalrymple, 2010b](#)), which may be wave-dominated (e.g. [Roy et al., 1980](#); [Honig and Boyd, 1992](#); [Cooper, 2001](#); [Anthony et al., 2002](#)), tide-dominated (e.g. [Hori et al., 2001](#); [Dalrymple et al., 2012](#)), river-dominated (e.g. [Cooper, 1993](#); [Sondi et al., 1995](#)), and mixed process ([d'Anglejan and Brisebois, 1978](#); [Jouanneau and Latouche, 1981](#); [Clifton, 1983](#); [Allen and Posamentier, 1993](#); [Roy et al., 2001](#)). Furthermore, amplifying of tides due to funnelling and resonance effects in embayments may be counteracted by frictional effects (e.g. [Dalrymple et al., 1992](#); [Allen, 1997](#); [Mitchell et al., 2010](#); [Collins et al., 2018a](#); [Collins et al., 2018b](#)). Consequently, the variability in predicted processes for ancient embayed shorelines may be higher than that proposed by [Ainsworth et al. \(2011\)](#) (Fig. 3).

Prediction of shoreline processes in ancient successions is enhanced by access to the following: (1) reliable chronostratigraphic information with an appropriate resolution; and (2) overlapping age ranges ('temporal resolution'). The temporal resolution of data and interpretations relating to the inferred controls varies significantly. For example, the temporal resolution of interpreted system tracts relating to



3<sup>rd</sup>-order (c. 0.5–3.0 Myr) or 4<sup>th</sup>-order (few 10s ka to c. 0.5 Myr) sea-level cycles ([Haq, 2014](#); [Sames et al., 2016](#)) will likely fall within the temporal resolution of regional-scale palaeogeographic maps, which are typically driven by plate tectonics and used for interpreting basin physiography and fluvial versus wave effectiveness ([Markwick and Valdes, 2004](#)). In contrast, the physiography of shoreline embayments and the continental shelf may be driven by relative sea level changes or local tectonics, which vary on much smaller timescales ([Partington et al., 1993a](#); [Partington et al., 1993b](#); [Egbert et al., 2004](#); [Stammer et al., 2014](#); [Collins et al., 2018a](#); [van Cappelle et al., 2018](#)).

Whilst the predictive framework of Ainsworth et al. (2011) provides an improved methodology for interrogating the process classifications of ancient shoreline-shelf systems, the current decision tree does not sufficiently capture the complex impact of basin physiography on tide and wave processes. For tidal processes, basin physiography complicates: (1) the flux of tidal energy into and out of partly enclosed water bodies (referred to herein as tidal inflow and outflow), and (2) the funnelling, shoaling and resonance effects on continental shelves and within shoreline embayments, which occur on a range of scales (c. 1–1000s km width and 1–100s m depth) ([Mitchell et al., 2010](#); [Wells et al., 2010b](#); [Collins et al., 2018c](#)). However, basin physiography does not constitute a separate query in the predictive model (Fig. 3) and is treated as a modifying factor to shelf tidal resonance potential ([Ainsworth et al., 2011](#)). Open oceans are sufficiently large to allow generation of relatively high *in-situ* tides ([Dalrymple, 1992](#)). Therefore, basins that have restricted access to the open oceans generally have a lower potential for producing amplified tidal currents by resonance effects, whereas basins with less restricted access to open oceans have a higher tidal resonance potential. For example, the small tides (typically <1 m tidal range) in the modern Arctic Ocean are primarily due to the restricted access to the Atlantic Ocean preventing northward propagation of the open ocean tidal wave, as well as the basin being too small to have its own tides ([Dalrymple and Padman, 2019](#)). However, an exception is that certain restrictive basin physiographies, typically on a smaller-scale (1–10s km), may cause significant amplification of tides by funnelling, shoaling and/or resonance effects ([Piper et al., 1990](#); [Martel et al., 1994](#)) ([Mitchell et al., 2010](#); [Ainsworth et al., 2011](#); [Mitchell et al., 2011](#)) ([Androsov et al., 2002](#); [Leckie and Rumpel, 2003](#)). On the other hand, smaller basins and large areas of wide, shallow shelves may increase frictional dissipation of tides but also waves and may still be tide dominated even at lower tidal ranges. This is illustrated in the White Sea region of the modern Arctic Ocean, where macrotidal ranges occur due to favourable geomorphology for funnelling and shoaling effects, in combination with rotating tides due to the high Coriolis parameter, whilst mean wave height is low to due restricted ocean access ([Dalrymple and Padman, 2019](#)). Overall, the generalized treatment of basin physiography in the existing predictive model ([Ainsworth et al., 2011](#)) combines two very different effects on tides relating to: (1) basin size (100–1000



km width scale) and bathymetry (100–1000 m depth scale), which has a first order control on the balance of tidal inflow versus outflow; and (2) second-order funnelling and resonance effects relating to basin physiography (10–100s km width scale and 1–100s m depth scale) ([Wells et al., 2005a](#); [Wells et al., 2007](#); [Mitchell et al., 2010](#); [Wells et al., 2010b](#); [Collins et al., 2018a](#); [Collins et al., 2018b](#)). Numerical tidal modelling is particularly well-suited to distinguishing between these two basin physiographic controls ([Slingerland, 1986](#); [Martel et al., 1994](#); [Wells et al., 2007](#); [Collins et al., 2018a](#); [Collins et al., 2018b](#)) and therefore provides information for shoreline–shelf process prediction.

### 1. Tidal resonance potential of basin



Wave (W) Tide (T)

A - Accommodation  
S - Sediment supply  
SL - Straight/lobate  
ME - Moderately embayed  
HE - Highly embayed

		Fluvial effectiveness > Wave effectiveness		Wave effectiveness > Fluvial effectiveness	
		Low A/S	High A/S	Low A/S	High A/S
Shoreline morphology - increased rugosity ↑	Highly embayed	Tf	Tf	Twf ← Tw → T	T
	Moderately embayed	Tf	Tf	Twf ← Tw → T	T ↔ Tw
	Straight to lobate	Tf ↔ Twf	F Ft Fw Ftw Fwf	Twf ← Tw → T	Wf Wt W Wff Wtf

**Increasing wave effectiveness vs. fluvial discharge**

17

1  
2  
3  
4 435 (C) Predictive matrix for settings with a high tidal potential. Abbreviations and color coding are shown in the inset  
5  
6 436 (opposite B).  
7 437  
8  
9 438  
10  
11  
12  
13  
14  
15  
16  
17  
18  
19  
20  
21  
22  
23  
24  
25  
26  
27  
28  
29  
30  
31  
32  
33  
34  
35  
36  
37  
38  
39  
40  
41  
42  
43  
44  
45  
46  
47  
48  
49  
50  
51  
52  
53  
54  
55  
56  
57  
58  
59  
60  
61  
62  
63  
64  
65

## 2.2 Tidal theory, palaeotidal modelling and identification of ancient tidal processes

### 2.2.1 Tidal theory

Since the mathematical and non-mathematical theory of Earth tides has been reviewed extensively and in detail elsewhere ([Defant, 1961](#); [MacMillan, 1966](#); [Pugh, 1987](#); [Dalrymple, 1992](#); [Allen, 1997](#); [Open University Course Team, 1999](#); [Willis, 2005](#); [Kvale, 2006](#); [Kvale, 2012](#); [Longhitano et al., 2012](#); [Reynaud and Dalrymple, 2012](#); [Pugh and Woodworth, 2014](#); [Dalrymple and Padman, 2019](#)), here it will be only briefly discussed in terms of the fundamental concepts and dominant controls impact shallow-water tides (Table 1). Astronomical tides are defined as ‘any periodic fluctuation in the water level that is generated by the gravitational attraction of the Moon and Sun’ ([Dalrymple, 1992](#)) and can be understood by a combination of equilibrium and dynamic theories of tides. In equilibrium tidal theory, the gravitational dynamics of the Earth-Moon-Sun system, combined with the Earth’s rotation, results in two oceanic bulges beneath the moon and on the opposite side of the Earth that move clockwise around the Earth to produce twice daily (semidiurnal) high (flood) and low (ebb) tides. Changes in the magnitude of tide-generating forces by the Moon and Sun on varying timescales, in combination with the Earth’s tilt, produces various tidal variations and cycles (e.g. diurnal inequality, spring and neap cycles etc.). However, the applicability of equilibrium tidal theory to understanding real-world tides is complicated by several factors, most notably that the Earth’s ocean basins are interrupted by significant bathymetric changes and emergent landmasses. Instead, the dynamic tidal theory model tides as the combined effects of many tidal constituents. The 11 most important tidal constituents cause semi-diurnal ( $M_2$ ,  $S_2$ ,  $N_2$ ,  $K_2$ ), diurnal ( $K_1$ ,  $O_1$ ,  $P_1$ ,  $Q_1$ ) and long-period ( $M_f$ ,  $M_m$ ,  $S_{sa}$ ) tides and harmonic convergence and divergence of these constituents result in tidal cycles. The relative importance of diurnal ( $K_1$  and  $O_1$ ) to semidiurnal ( $M_2$  and  $S_2$ ) tides is quantified using the ratio  $F$ , where:

$$F = \left( \frac{K_1 + O_1}{M_2 + S_2} \right)$$

If  $F < 0.25$ , the tide is semi-diurnal, for  $0.25 < F < 1.5$  the tide is mixed semidiurnal dominated, for  $1.5 < F < 3$  the tide is mixed diurnal dominated, and  $F > 3$  the tide is diurnal ([Open University Course Team, 1999](#)).

Name	Description
Astronomical tide	Tide formed by the gravitational and rotational effects of the Moon and Sun on the water in an open ocean or seaway
Bed shear stress	Force per unit area exerted by flow on the sediment surface
Co-oscillating or boundary tide	Tide formed by the propagation of an open-ocean astronomical tide into a connected water body
Coriolis effect and amphidromic cells	The Coriolis effect deflects the tidal wave to the right in the northern hemisphere and left in the southern hemisphere. In the northern hemisphere, this causes the tidal wave to rotate anticlockwise about an amphidromic point of zero tidal range; rotation is clockwise in the southern hemisphere. In enclosed water bodies, the deflected tidal wave (termed a Kelvin wave) pushes against the shoreline, leading to an exponential increase in tidal range from the amphidromic node towards the shoreline. The Coriolis effect also causes asymmetry in the tidal range on either side of elongate water bodies, such as the Yellow Sea, because the incoming tidal wave is larger than the reflected wave.
Diurnal	Once-daily tide where the $K_1$ and $O_1$ constituents are more dominant than the $M_2$ and $S_2$ constituents
Resonance	Resonance occurs when the tidal period matches a natural mode of oscillation within a water body. Maximum resonance typically occurs when shelf width is approximately a quarter the dominant tidal wavelength, and matches a half-wave oscillator or standing wave in an enclosed basin and quarter-wave oscillator in an open-ended embayment (gulf).
Funnelling	Increase in tidal amplitude caused by progressive narrowing and shallowing of a water body
Semidiurnal	Twice-daily tide where the $M_2$ and $S_2$ constituents are more dominant than the $K_1$ and $O_1$ constituents
Shoaling	Increase in tidal amplitude caused by progressive shallowing of a water body
Tidal amplitude	Elevation of tidal high water above mean sea level, equal to half the tidal range
Tidal range	Vertical height between consecutive high and low waters over a tidal cycle (twice the tidal amplitude), classified as microtidal (<2 m), mesotidal (2–4 m) and macrotidal (>4 m)

**Table 1.** Explanations of several tide-related terms used in this paper.

Significant tides, though typically <1 m in tidal range (the difference in sea level between high and low tide), only develop in the open oceans. Open-ocean tides are fundamentally controlled by ocean basin physiography and tides across entire oceans can be ‘tuned’ to particular tidal constituents. For example, the modern North Atlantic Ocean is close to resonance for the semidiurnal  $M_2$  tide, whereas the modern Pacific Ocean accentuates the diurnal ( $O_1$  and  $K_1$ ) constituents (Fig. 4). An ocean basin can house resonant tides when the width of the basin,  $L$  is equal to a multiple of half wavelengths,  $\lambda = \sqrt{gHT}$  ( $T$  is the tidal period,  $g$  is gravity, and  $H$  is water depth) of the tidal wave. Oceanic tides rotate as waves around fixed (amphidromic) points with negligible tidal amplitude (half the tidal range) (Fig. 4). Water on continental shelves and smaller water bodies partly (seas) or fully (lakes) enclosed by land do not develop appreciable *in situ* tides (Dalrymple, 1992). Instead, tides on shelves and in seas rely on the amount of tidal inflow from connected ocean basins which depends on the size, shape and bathymetry of the connection(s) and orientation of connection(s) relative to the oceanic tide (Fig. 4). When oceanic tides

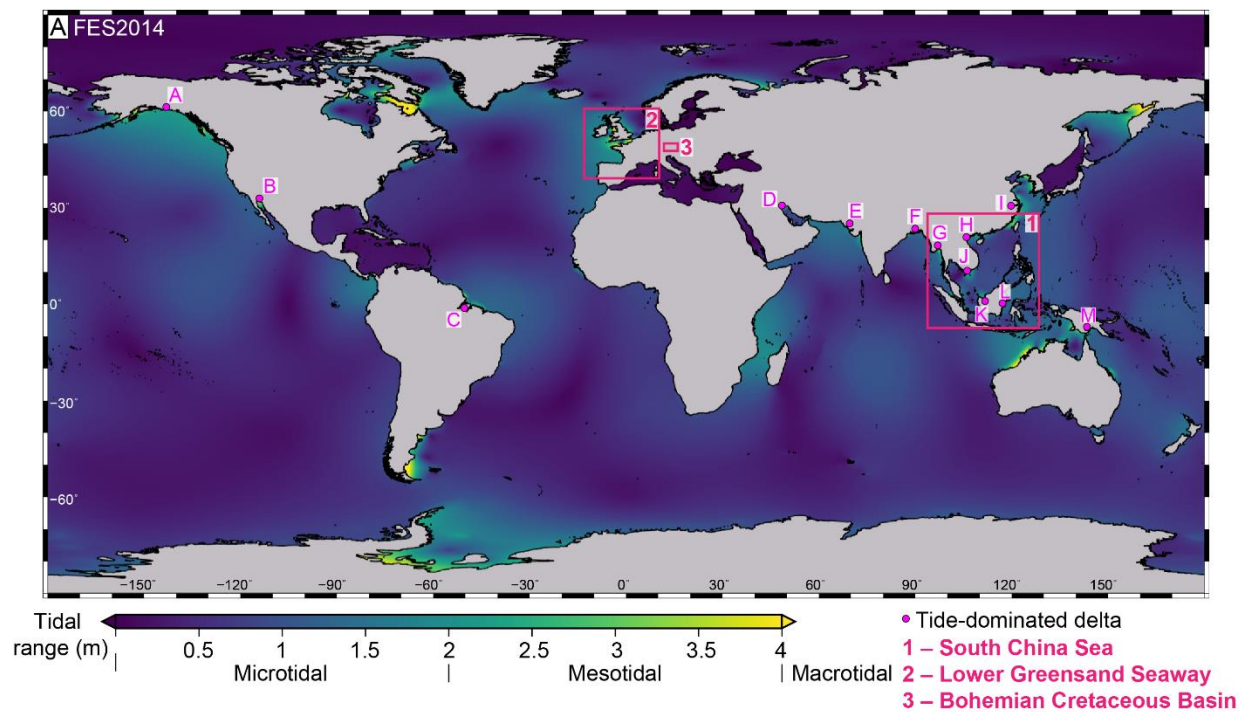
encounter areas of shallower water and constricted physiography, they may undergo amplification due to shoaling, funnelling and resonance (Table 2). Simplified mathematical reviews of these effects are discussed elsewhere ([Proudman, 1953](#); [Howarth, 1982](#); [Slingerland, 1986](#); [Allen, 1997](#); [Wells et al., 2007](#); [Kowalik and Luick, 2013](#)). The most relevant points for understanding controls on tides and predicting shoreline–shelf process classification are discussed below.

First, shoaling effects describe the increase in tidal amplitude and current velocity that occurs when water depth decreases, for example, from the deeper ocean onto the continental shelf, and from deeper shelf to shoreline areas. Second, funnelling effects describe the increase in tidal range as a result of physical constriction of the tidal wave, for example, in straits and shoreline embayments. The combination of shoaling and funnelling effects is referred to as convergence effects and these are an important contributing cause of tidal amplification in shoreline – shelf areas. Third, tidal resonance occurs when the natural period of oscillation on the shelf or within a shoreline bathymetric constriction is coincident with the tidal period ([Slingerland, 1986](#); [Allen, 1997](#)). On the continental shelf, tidal resonance reaches a maximum when shelf width is one-quarter the tidal wavelength (and for widths 3/4, 5/4, etc.) (e.g. [Proudman, 1953](#); [Howarth, 1982](#)). However, this relationship assumes the incident tide is perpendicular to the shelf, friction is inversely proportional to depth and no Coriolis effect, none of which have been widely evaluated. At typical shelf depths (c. 100 m), the quarter wavelength of the dominant semi-diurnal M<sub>2</sub> and diurnal K<sub>1</sub> tides are c. 350 km and 675 km. As the majority (c. 70%) of modern shelves are <75 km wide ([Nyberg and Howell, 2016](#)), tides are closer to resonance as shelf width increases, hence tidal amplitude increases with shelf width ([Redfield, 1958](#); [Off, 1963](#); [de Vries Klein, 1977](#); [Cram, 1979](#); [Ainsworth et al., 2011](#); [Reynaud and Dalrymple, 2012](#)). Within an embayment or gulf, tidal resonance occurs when the amount of time taken for the tidal wave to travel for the embayment mouth, to the apex and back to the mouth is the same, or nearly the same, as the time between high and low tides, effectively forming a high amplitude standing wave. The combination of tidal resonance and convergence effects explains the location of the highest tidal ranges globally ([O'Reilly et al., 2005](#)). In the Bay of Fundy, eastern Canada, tidal ranges up to 17 m are caused principally by the dominant M<sub>2</sub> tide being very close to resonance, with secondary convergence effects in the landward shallowing and narrowing estuary (e.g. [Garrett, 1972](#); [Dalrymple, 2021](#)). In comparison, tides of up to 14m tidal range in the Severn Estuary in the upper reaches of the Bristol Channel, UK, are caused by partial resonance of the dominant M<sub>2</sub> tide plus convergence effects in the funnel-shaped and shallowing Severn Estuary (e.g. [Gao and Adcock, 2017](#)). Simplified numerical relationships for convergence effects and tidal resonance (e.g. [Slingerland, 1986](#); [Allen, 1997](#); [Wells, 2008](#)) can enable first-order interpretations of whether the potentially dominant

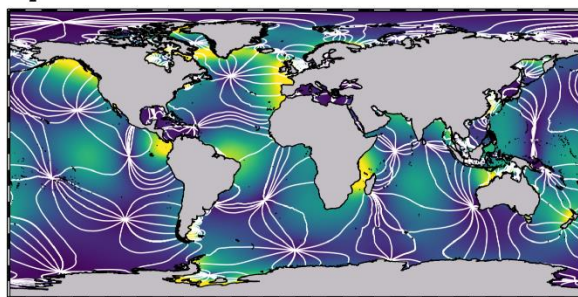
1  
2  
3  
4  
5  
6  
7  
8  
9  
10  
11  
12  
13  
14  
15  
16  
17  
18  
19  
20  
21  
22  
23  
24  
25  
26  
27  
28  
29  
30  
31  
32  
33  
34  
35  
36  
37  
38  
39  
40  
41  
42  
43  
44  
45  
46  
47  
48  
49  
50  
51  
52  
53  
54  
55  
56  
57  
58  
59  
60  
61  
62  
63  
64  
65

511 semi-diurnal or diurnal tidal constituents may be close to resonance and the potential magnitude of  
512 shoaling and funnelling effects in both the modern and ancient.





**B**  $M_2$  tide FES2014



**C**  $K_1$  tide FES2014

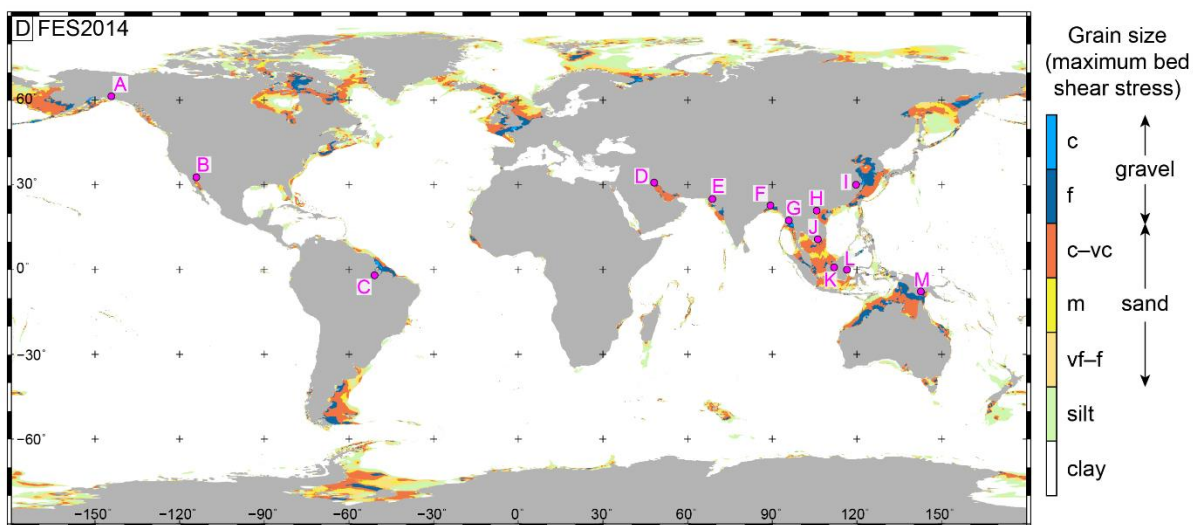
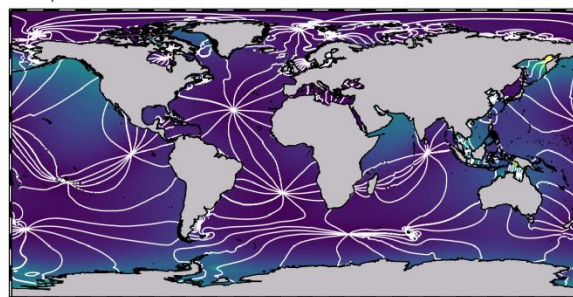




**Fig. 4.** (A) Present day global tidal range based on the FES 2014 tidal model ([Carrère et al., 2015](#)), showing the locations (pink dots) of tide-dominated deltas ([Goodbred and Saito, 2012](#)): A) Copper; B) Colorado; C) Amazon; D) Shatt-al-Arab; E) Indus; F) Ganges-Brahmaputra; G) Irrawaddy; H) Red River; I) Yangtze; J) Mekong; K) Rajang; L) Mahakam; and M) Fly. Pink boxes show approximate locations of the palaeotidal modelling case studies. (B, C) Global map of  $M_2$  (B) and  $K_1$  tidal amplitude (C) from FES 2014. Contours join lines of equal phase in  $30^\circ$  intervals and white arrows give the sense of rotation of the major ocean amphidromic systems. (D) Maximum tidal bed shear stress, plotted as the equivalent grain size that could be entrained if available, for FES2014, including the difference in sediment grain size class. Grain size abbreviations: vf = very fine; f = fine; m = medium; c = coarse; vc = very coarse.

## 2.2.2 Palaeotidal modelling

Palaeotidal numerical modelling can provide quantitative information on ancient shoreline tidal processes and can test their sensitivity to palaeogeographic and palaeobathymetric change and uncertainty (e.g. [Martel et al., 1994](#); [Egbert et al., 2004](#); [Wells et al., 2005a](#); [Uehara et al., 2006](#); [Collins et al., 2018a](#); [Collins et al., 2018b](#)). Computational methods for palaeotidal modelling, including tidal forcing boundary conditions and mesh generation, have advanced since early approaches that used structured meshes and open boundary tidal forcing by the  $M_2$  (principal lunar semi-diurnal) tide only, and output tidal amplitude or range ([Slater, 1985](#); [Slingerland, 1986](#); [Ericksen and Slingerland, 1990](#); [Martel et al., 1994](#)). More recent simulations have investigated tidal amplitude ([Slingerland, 1986](#); [Wells et al., 2005a](#); [Wells et al., 2005b](#); [Wells et al., 2007](#); [Wells et al., 2010a](#); [Wells et al., 2010b](#)) and bed shear stress ([Mitchell et al., 2010](#); [Mitchell et al., 2011](#)) in ancient epicontinental seaways, and tidal range and bed shear stress in ancient seas ([Collins et al., 2017a](#); [Collins et al., 2018a](#); [Collins et al., 2018b](#)), using models with astronomical tidal forcing and unstructured meshes (Table 2). These diverse case studies illustrate how the sensitivity of shoreline tides to various palaeogeographic and palaeobathymetric changes can improve predictive models of depositional process regimes of ancient shoreline systems.

A multitude of globally applicable numerical tidal models exist ([Shum et al., 1997](#); [Stammer et al., 2014](#)), a comprehensive review of which is beyond the aim of this paper. The range of modern ocean tide models can be classified as (1) data-constrained models, those with empirical adjustment to an adopted prior models, (2) barotropic hydrodynamic models that may be constrained by tide information through assimilation, or (3) purely hydrodynamic models with no data constraints ([Stammer et al., 2014](#)). Palaeotidal models, where no empirical tidal data are available, must by definition be purely hydrodynamic. The tidal model used in the ancient case studies discussed herein is Fluidity (<http://fluidityproject.github.io/>), formerly the Imperial College Ocean Model (ICOM), which can be used to simulate both astronomical and co-oscillating boundary tides. Details of the tetrahedral, unstructured meshing and hydrodynamic modelling approach used with Fluidity have been widely documented and will not be repeated herein ([Pain et al., 2005](#); [Wells et al., 2005a](#); [Gorman et al., 2007](#); [Gorman et al., 2008](#); [Piggott et al., 2008](#); [Geuzaine and Remacle, 2009](#); [Avdis et al., 2018](#)) (e.g. [Wells et al., 2010a](#); [Wells et al., 2007a](#); [Mitchell et al., 2010](#)). Likewise, tidal modelling using Fluidity has been extensively validated against real-world modern tidal amplitude ([Wells et al., 2005a](#); [Wells et al., 2005b](#); [Wells et al., 2007](#); [Wells, 2008](#); [Wells et al., 2010a](#); [Wells et al., 2010b](#); [Collins et al., 2017a](#); [Collins et al., 2018a](#); [Collins et al., 2018b](#)) and tidal bed shear stress ([Mitchell et al., 2010](#); [Mitchell et al., 2011](#); [Collins et al., 2017a](#); [Collins et al., 2018a](#); [Collins et al., 2018b](#)), which includes global ([Wells et al., 2010a](#); [Collins et](#)

1  
2  
3  
4 556 [al., 2018a](#); [Collins et al., 2018b](#)) and regional comparisons in the Mediterranean Sea ([Wells et al., 2005a](#)),  
5  
6 557 North Sea ([Wells et al., 2007](#); [Mitchell et al., 2010](#)), Baltic Sea ([Wells, 2008](#)) and South China Sea  
7  
8 558 ([Collins et al., 2017a](#); [Collins et al., 2018a](#); [Collins et al., 2018b](#)) (see Supplementary Material). As well  
9  
10 559 as Fluidity, other modern hydrodynamic tidal models have been used for palaeotidal modelling, notably  
11  
12 560 the Oregon State University Tidal Inversion Software (OTIS) ([Egbert et al., 2004](#); [Green and Huber,](#)  
13  
14 561 [2013](#); [Wilmes and Green, 2014](#); [Green et al., 2017](#)).  
15  
16  
17  
18  
19  
20  
21  
22  
23  
24  
25  
26  
27  
28  
29  
30  
31  
32  
33  
34  
35  
36  
37  
38  
39  
40  
41  
42  
43  
44  
45  
46  
47  
48  
49  
50  
51  
52  
53  
54  
55  
56  
57  
58  
59  
60  
61  
62  
63  
64  
65

Geologic age & reference	Study area	Computational method	Boundary conditions	Key findings
<b>Late Devonian c. 370 Ma (Slingerland, 1986)</b>	Catskill epicontinental sea of North America	Structured grid, finite difference scheme; Navier–Stokes equations; Coriolis parameter (f -plane).	Open boundary tidal forcing, no astronomical tidal forcing; M2 tide only; Variable bathymetry; Chezy approximation for bottom friction.	Microtidal–low mesotidal, locally mesotidal–macrotidal areas due to resonance, funnelling and shoaling effects. Tidal ranges increased by 1) increasing the boundary tidal range; 2) increasing the open boundary width; and 3) increasing the depth of the seaway.
<b>Mid Cretaceous c. 100 Ma (Slater, 1985)</b>	Western Interior Seaway of North America	Structured grid, finite difference scheme; Laplace Tidal Equations; No Coriolis parameter.	Open boundary and astronomical tidal forcing; M2 tide only; Uniform depths; Linear bottom friction with respect to velocity.	Microtidal; Astronomical tidal forcing dominates; Open boundary tide negligible from the Arctic Ocean and possibly significant from the Gulf of Mexico; Tidal range sensitive to water depth (resonance at 200 m water depth).
<b>Mid Cretaceous c. 100 Ma (Erickson and Slingerland, 1990)</b>	Western Interior Seaway of North America	Structured grid, finite difference scheme; Navier Stokes equations; Coriolis parameter (f -plane).	Open boundary tidal forcing, no astronomical tidal forcing; M2 tide only; Variable bathymetry; Chezy approximation for bottom friction.	Microtidal, locally mesotidal–macrotidal near Gulf of Mexico open boundary; Tidal range increases as seaway depth and Gulf of Mexico connection increases; Open boundary tides argued to be dominant

				contributor to tides, not astronomically forced tides (cf. Slater, 1985).
<b>Miocene c. 22 Ma (Martel et al., 1994)</b>	Alpine foreland basin of France and Switzerland	Structured grid, finite difference scheme; Navier Stokes equations; Coriolis Parameter (f -plane).	Open boundary tidal forcing, no astronomical tidal forcing; M2 tide only; Variable bathymetry; Chezy approximation for bottom friction.	Higher tidal current speeds predicted with wider and deeper open-ocean connections and 2m open boundary tide applied.
<b>Late Carboniferous c. 300 Ma (Wells et al., 2005a,b)</b>	Late Carboniferous sea of NW Europe	Unstructured, tetrahedral mesh, finite element scheme; Navier Stokes equations; No Coriolis parameter; Fluidity tidal model.	Astronomical tidal forcing only; M2 tide only; Variable bathymetry; No treatment of bottom friction.	Extremely microtidal seaway (typically <10 cm tidal range) across NW region across various sensitivity tests; Putative tidal deposits interpreted to be confined to localised estuaries.
<b>Late Carboniferous c. 300 Ma (Wells et al., 2008)</b>	Late Carboniferous sea of NW Europe	Unstructured, tetrahedral mesh, finite element scheme; Navier Stokes equations; Coriolis parameter included; Fluidity tidal model.	Astronomical tidal forcing only; M2, S2, N2, K2, Q1, O1, P1, K1, M <sub>f</sub> , M <sub>m</sub> and S <sub>sa</sub> tidal constituents; Variable bathymetry; Bottom drag applied as surface-integral based on quadratic friction law.	Microtidal ranges predicted across the northwest European region (similar to Wells et al., 2005a, b); Extra tidal constituents increase the predicted tidal range to 20–80 cm.

<b>Early Cretaceous, late Aptian, c. 116 Ma (Wells et al., 2010a)</b>	Global	Unstructured, tetrahedral mesh, finite element scheme; Navier Stokes equations; Coriolis parameter included; Fluidity tidal model.	Astronomical tidal forcing only; M2, S2, O1 and K1 tidal constituents modelled independently; Variable bathymetry; Bottom drag applied as surface-integral based on quadratic friction law.	Model results compared to published geologic records; High mesotidal to macrotidal on the Arabian Platform, around India, along the Pacific coast between North and South America, northeast of Australia, and around Southeast Asia; Low microtidal ranges in the proto-South Atlantic Ocean and Weddell Sea.
<b>Early Cretaceous, late Aptian – early Albian, c. 112–107 Ma (Wells et al., 2010b)</b>	Lower Greensand Seaway of NW Europe	Unstructured, tetrahedral mesh, finite element scheme; Navier Stokes equations; Coriolis parameter included; Fluidity tidal model.	Open boundary conditions (from Wells et al., 2010a) and astronomical tidal forcing; M2, S2, O1 and K1 tidal constituents modelled independently; Variable bathymetry; Bottom drag applied as surface-integral based on quadratic friction law.	Overall microtidal increasing to microtidal–macrotidal with increased width and depth of open-ocean connections and more localised funnelling, shoaling and Coriolis effects.
<b>Middle Cretaceous, Early–Middle Turonian, c. 93 Ma (Mitchell et al., 2010)</b>	Bohemian Cretaceous Basin of Central Europe	Unstructured, tetrahedral mesh, finite element scheme; Navier Stokes equations; Coriolis parameter	Open boundary conditions and astronomical tidal forcing; varying combinations of M2, S2, O1 and K1 tidal constituents; Variable bathymetry; Bottom drag	Microtidal–mesotidal across the Bohemian Cretaceous Basin and range of sensitivity tests; Elevated tidal ranges and velocity in local embayments and straits due to funnelling and shoaling effects.

		included; Fluidity tidal model.	applied as surface-integral based on quadratic friction law.	
<b>Early Jurassic, c. 200 Ma (Mitchell et al., 2011)</b>	Laurasian Seaway of NW Europe	Unstructured, tetrahedral mesh, finite element scheme; Navier Stokes equations; Coriolis parameter included; Fluidity tidal model.	Astronomical tidal forcing; M2, S2, O1 and K1 tidal constituents; Variable bathymetry; Bottom drag applied as surface-integral based on quadratic friction law.	Seaway largely microtidal; Flow constriction associated with shallow platforms and straits produced elevated bed shear stresses that were decoupled from tidal range.
<b>Eocene, c. 55 Ma (Green &amp; Huber, 2013)</b>	Global	Finite element grid, 1/4° resolution, Numerical solutions to linearized shallow water equations, including Coriolis parameter; OTIS tidal model.	Includes up to 8 constituents (M2, S2, N2, K2, K1, O1, P1, Q1) and linear bottom drag parameterization (see Egbert et al., 2004); Variable ocean bathymetry and stratification.	Weak M2 tide predicted in Eocene ocean except in the Pacific.
<b>Mesozoic–Cenozoic, 5 timeslices from c. 252 Ma to 3 Ma (Green et al., 2017)</b>	Global	Finite element grid, 1/4° resolution, Numerical solutions to linearized shallow water equations, including Coriolis	M2, S2, K1 and O1 tidal constituents and linear bottom drag parameterization (see Egbert et al., 2004); Variable ocean bathymetry and stratification.	Tidal dissipation during the Cenozoic and Late Cretaceous were weaker than at present, apart from the glacial states over the last 2 Ma.

		parameter; OTIS		
		tidal model.		
<b>Oligocene–</b>	South China	Unstructured,	Astronomical tidal forcing;	Spring tides along South China Sea
<b>Miocene, c. 26–</b>	Sea, SE Asia	tetrahedral mesh,	M2, S2, N2, K2, Q1, O1, P1,	coastline were largely mesotidal–
<b>5 Ma (Collins et</b>		finite element	K1, M <sub>f</sub> , M <sub>m</sub> and S <sub>sa</sub> tidal	macrotidal and capable of
<b>al., 2017a,</b>		scheme; Navier	constituents; Variable	transporting sand throughout the Late
<b>2018a)</b>		Stokes equations;	bathymetry; Bottom drag	Oligocene to Middle Miocene.
		Coriolis parameter	applied as surface-integral	
		included.	based on quadratic friction law.	
<b>Late</b>	Western Interior	Unstructured,	Astronomical tidal forcing;	Regionally microtidal and
<b>Cretaceous</b>	Seaway of North	tetrahedral mesh,	M2, S2, N2, K2, Q1, O1, P1,	mesotidal (2–4 m) along most of the
<b>middle</b>	America	finite element	K1, M <sub>f</sub> , M <sub>m</sub> and S <sub>sa</sub> tidal	eastern margin of the seaway;
<b>Campanian, c.</b>		scheme; Navier	constituents; Variable	increased tidal bed shear stress when
<b>75-77.5 Ma</b>		Stokes equations;	bathymetry; Bottom drag	seaway center and entrance to Gulf
<b>(Dean et al.,</b>		Coriolis parameter	applied as surface-integral	of Mexico are deeper.
<b>2019)</b>		included.	based on quadratic friction law.	

**Table 2.** Summary of previously published palaeotidal models from deep geologic time (excluding the Quaternary).



## 2.2.3 Identification of ancient tidal processes

### 2.2.3.1 Tidal facies analysis

Observations across the range of facies- to facies succession scales interpreted as indicating tidal processes have been widely documented from several different shallow-water depositional environments, most notably deltas, estuaries, barrier inlets, embayments, straits and open shelves ([Johnson and Baldwin, 1996](#); [Reading and Collinson, 1996](#); [Bhattacharya, 2010](#); [Dalrymple, 2010b](#); [Martinius and van den Berg, 2011](#); [Davis and Dalrymple, 2012](#); [Longhitano et al., 2012](#)). The most significant features are those related to tidal flow reversals, flood–ebb tide versus slack water dynamics and tide-related periodicity, particularly the following: (1) bidirectional cross-bedding and cross-lamination (cm–dm-scale), including the relatively rare variant of ‘herringbone’ patterns (e.g. [Van Straaten, 1953](#); [Reineck, 1963](#); [Boersma, 1969](#); [Klein, 1970a](#); [Klein, 1970b](#); [Klein, 1971](#); [Hayes, 1980](#); [Boersma and Terwindt, 1981](#); [Yoshida et al., 2004](#)); (2) larger-scale (10s m-scale) bidirectionality, such as between separate but closely spaced sand bodies with oppositely-dipping cross-bedding, which have been interpreted to reflect mutually evasive ebb- and flood-tidal channels and bars ([Robinson, 1966](#); [Johnson, 1975](#); [Johnson and Levell, 1995](#); [Harris et al., 2004](#); [Sixsmith et al., 2008](#); [Legler et al., 2013](#); [Levell et al., 2020](#)); (3) sigmoidal ‘shovel-shaped’ cross-bed sets, with extended mud-rich toesets, sometimes with oppositely-dipping current ripples (e.g. [Boersma and Terwindt, 1981](#); [Mutti et al., 1984](#); [Mutti et al., 1985](#); [Kreisa and Moila, 1986](#); [Dalrymple and Rhodes, 1995](#); [van den Berg et al., 2007](#); [Tinterri, 2011](#)); (4) multiple reactivation surfaces with an apparent cyclicity or predictable and repeated pattern (e.g. [Boersma, 1969](#); [McCabe and Jones, 1977](#); [Reineck and Singh, 1980](#); [Boersma and Terwindt, 1981](#); [Allen, 1982a](#); [Allen and Homewood, 1984](#)); (5) ‘paired drapes’ or ‘double drapes’ comprising sandy foresets and associated mudstone and/or carbonaceous (typically finely comminuted ‘coffee ground’ type) drapes (mm–cm-scale), which are interpreted to form by semi-diurnal to diurnal tidal inequality (e.g. [Reineck and Singh, 1980](#); [Visser, 1980](#); [Smith, 1988](#); [De Boer et al., 1989](#); [Nio and Yang, 1991](#)); (6) ‘tidal bundles’ in the form of lateral and vertical thickness variations of sandy foresets and associated mudstone/carbonaceous drapes (dm–m-scale) , which have been related to spring–neap semi-lunar cycles (e.g. [Visser, 1980](#); [Allen, 1981b](#); [Boersma and Terwindt, 1981](#); [Allen and Homewood, 1984](#); [Kreisa and Moila, 1986](#); [Nio and Yang, 1991](#)) (cf. [Martinius and Gowland, 2011](#)); (7) heterolithic bedding (cm–m-scale) with apparent, or preferably measured and statistically analysed, cyclicity in the thickness of sandstone–mudstone layers, which are referred to as ‘couplets’ if other evidence of tidal deposition (e.g. bidirectional current ripples etc.) are observed ([Reineck and Wunderlich, 1968](#); [Terwindt, 1971](#); [Terwindt and Breusers, 1972](#); [Reineck and Singh, 1980](#); [Kvale et al., 1989](#); [Archer et al., 1991](#); [Archer, 1995](#); [Greb and Archer, 1995](#); [Kvale, 2006](#); [Kvale, 2012](#)); (8) inclined heterolithic strata (dm–10s m-scale) ([Thomas et al., 1987](#); [Smith,](#)

1988; [Dalrymple et al., 2003](#); [Choi et al., 2004](#); [Dalrymple and Choi, 2007](#)); (cf. [Sisulak and Dashtgard, 2012](#); [Jablonski and Dalrymple, 2016](#)); and (9) ichnofabrics which, in general, show reduced but variable and sporadic bioturbation intensities and predominance of facies-crossing ichnofauna ([MacEachern et al., 2005](#); [McIlroy, 2006](#); [McIlroy, 2007](#); [MacEachern and Bann, 2008](#); [Longhitano et al., 2010](#); [Gingras and MacEachern, 2012](#); [Gingras et al., 2012](#)). In terms of micropalaeontological information, the most important potential indicator of tidal processes are palynomorph acmes of coastal biomes whose distribution, abundance and productivity within a depositional system is strongly related to tidal processes, most notably those associated with deposition in mangrove, seagrass and salt marsh settings (e.g. [Grindrod, 1988](#); [Wolanski et al., 1992](#); [Woodroffe et al., 2016](#)).

Definitive recognition of tide-influenced sedimentation relies on observing combinations of the features described above because, in isolation, some of these features can form by other processes (e.g. wave, storm and/or fluvial) operating by themselves or, especially, in combination with tides (e.g. [Thomas et al., 1987](#); [Hovikoski et al., 2008](#); [Dalrymple, 2010b](#); [Martinius and van den Berg, 2011](#); [Reynaud and Dalrymple, 2012](#); [Dalrymple et al., 2015](#); [Gugliotta et al., 2016a](#); [Gugliotta et al., 2016b](#); [Collins et al., 2020](#)). Mixed-process settings, especially those where fluvial and tidal currents coexist, can exacerbate differences in the strength and sediment transport capacity of ebb- and flood-tidal currents. Strongly skewed palaeocurrent patterns, with one dominant offshore-directed mode, and a weaker oppositely-directed secondary mode, may occur when fluvial, wave and/or storm processes combine with tides, such as in deltaic and estuarine settings ([Legler et al., 2013](#); [van Cappelle et al., 2016](#); [Collins et al., 2020](#); [Levell et al., 2020](#)). For example, in the modern microtidal Po Delta, preserved tidal signals in open-water prodelta facies are correlatable to cyclical variations in water-surface steepness and consequent changes in river discharge velocity and sediment transport capacity in distributary channels ([Maselli et al., 2020](#)). In modern open-marine shelf settings, storm-induced currents can also contribute to tidal current sediment transport asymmetry ([Stride, 1973](#); [Belderson et al., 1982](#); [Stride, 1982](#)). Similarly, storm-enhanced tidal transport systems have been inferred to explain unidirectional palaeocurrent patterns in ancient shallow-marine deposits ([Banks, 1973](#); [Johnson, 1975](#); [Anderton, 1976](#); [Levell, 1980](#)) and, in the modern Fly River delta, sediment transport to and across the delta front may be controlled by wave-induced resuspension together with tides, storm surge and barotropic flow ([Harris et al., 2004](#)). Autogenic tidal processes responsible for mutually evasive ebb and flood tidal channels can also create skewed palaeocurrent patterns in the stratigraphic record, particularly where: (1) channel preservation is unequal, (2) ebb and flood tidal channels are so effectively shielded from each other that evidence of the secondary

reversing tide is absent, and/or (3) incomplete outcrop or subsurface dataset ([Sixsmith et al., 2008](#); [Legler et al., 2014](#)).

Confident identification of tidal influence and its relative importance with respect to other processes (e.g. wave, storm and/or fluvial) requires reconstruction of shoreline palaeo-geomorphology at the scale of the depositional system (c. 1–100s km), based on detailed facies analysis in the context of high-resolution stratigraphic and regional palaeogeographic relationships. Such confidence in interpretation requires data of high quality and density, such as provided by extensive outcrop data (e.g. [Willis and Gabel, 2001](#); [Legler et al., 2013](#); [Legler et al., 2014](#); [Ainsworth et al., 2016](#); [Rossi et al., 2016](#); [van Cappelle et al., 2016](#); [Kurcinka et al., 2018](#); [Van Yperen et al., 2020](#)) or subsurface datasets containing 3D seismic data, densely spaced wells and/or extensive cores (e.g. [Hubbard et al., 2011](#); [Willis and Fitris, 2012](#); [Holgate et al., 2013](#)). In practice, such datasets and confident interpretations are rare. It is therefore appropriate to focus comparison of ‘rock-record’ data with tidal model predictions at bedform scale (c. mm–10s m), at which interpretations of bed shear stress as a proxy for tidal current velocity (section 3.2.3) can be readily made. Other tidal model outputs, including tidal range (section 3.2.2) and tidal phase, are typically less straightforward to interpret from available ‘rock-record’ data ([Wells et al., 2005a](#); [Mitchell et al., 2010](#)).

#### 2.2.3.2 *Palaeotidal range analysis*

Analysis of palaeotidal range from the rock record requires observations and interpretation at a range of scales: depositional system morphology (c. 1–100s km), depositional environments (c. 0.1–1 km) and depositional elements and facies (<1 to 10s m) may all preserve an imprint of tidal sedimentary processes but do not permit accurate constraints on tidal range, often not even the ability to differentiate microtidal, mesotidal and macrotidal regimes (Table 3) ([Wells et al., 2005a](#)). Alternative methods used to estimate palaeotidal range are: (1) interpretations of water depth from stratigraphic position within interpreted fining-upward channel-fill units ([Nio et al., 1983](#)) ([Yang and Nio, 1985](#)); (2) stratigraphic thickness estimates of interpreted intertidal deposits in tidal flat units ([Klein, 1970a](#); [Klein, 1971](#)), although these units are very similar to interpreted channel-fill units within the fluvial-to-marine transition zone (e.g. [Olson, 1972](#); [Dalrymple and Choi, 2007](#); [Amir Hassan et al., 2013](#); [Gugliotta et al., 2016a](#); [Collins et al., 2018c](#); [Collins et al., 2020](#)); and (3) average calculations of characteristic mudstone drape spacings based on groups of sandstone–mudstone couplets from interpreted spring and neap conditions, and various assumptions regarding dune height and speed, dry bulk sediment density, and current velocity for

1  
2  
3  
4 662 sediment entrainment ([Allen, 1981b](#)). Depositional systems subject to higher tidal ranges are more likely  
5  
6 663 to be tide-dominated, but this relationship is inconsistent (e.g. [Hayes, 1979](#); [Mulhern et al., 2017](#)),  
7  
8 664 especially for mixed-process systems ([e.g. Davis and Hayes, 1984](#)). Furthermore, higher tidal ranges may  
9  
10 665 not always correspond to stronger tidal currents ([Dalrymple, 2010b](#)), as shown in both modern macrotidal  
11  
12 666 environments ([e.g. Yang et al., 2008](#)) and palaeotidal models ([Mitchell et al., 2011](#)). Consequently,  
13  
14 667 numerous studies have highlighted that tidal range is, at best, an imperfect indicator of sedimentary  
15  
16 668 response.  
17  
18  
19  
20  
21  
22  
23  
24  
25  
26  
27  
28  
29  
30  
31  
32  
33  
34  
35  
36  
37  
38  
39  
40  
41  
42  
43  
44  
45  
46  
47  
48  
49  
50  
51  
52  
53  
54  
55  
56  
57  
58  
59  
60  
61  
62  
63  
64  
65

Indicator	Size	Description	Tidal range
Delta morphology	10s - 100s km	Tide-dominated deltas display wide, landward-tapering river mouths, elongate shore-normal mouth bars, sinuous tidal creeks, tidal flats, saltmarsh and/or mangroves, and smaller-scale tidal indicators (e.g. Ganges-Brahmaputra, Mahakam, Irrawaddy, Fly deltas)	Mesotidal to macrotidal
		Fluvial-dominated deltas display digitate ('birds-foot') to lobate morphologies and rapid progradation due to higher relative stream power compared to wave/tide reworking (e.g. Mississippi delta).	Microtidal to mesotidal
		Wave-dominated deltas display cusped geometries with intermediate progradation rates due to wave action ('littoral energy fence') (e.g. Baram)	Microtidal to mesotidal
Open shelf tidal sand-sheets (including tidal sand ridges and ribbons)	10s - 100s km	Sheets are tabular sandbodies with planar tops and bases formed by open-shelf tidal currents. Super-imposed sedimentary bodies include tidal sand ridges, linear bedforms with long axes orientated up to 20° obliquely to tidal currents and distinguished from aeolian dunes by the presence of 2 main current directions at 180°, shelly debris, reactivation surfaces, low angle (3–6°) cross-stratification and marine trace fossils (e.g. Norfolk Ridges, southern North Sea). Smaller superimposed bedforms include sand ribbons, scour hollows, longitudinal furrows,	Mesotidal to macrotidal

		obstacle marks, sand waves, rippled sand sheets and longitudinal sand patches.	
Furrows and gravel waves	L < 150 km; W < 50 km	Mostly erosional features with small (ca 1 m high, 10 m wavelength) gravel-rich subaqueous dunes, formed due to low sediment supply and strong tidal currents (e.g. Bristol Channel)	Macrotidal
Estuarine/incised valley-fill tidal sandbodies	W < 30 km; T ca 1 m	Outer estuary characterized by elongate sand ridges and tidal channels with super-imposed, smaller-scale tidal indicators. Middle and inner estuary characterized by heterolithic strata with isolated sandbodies (e.g. Thames estuary, southern North Sea)	Microtidal to macrotidal
Saltmarsh	L 10 km; W < 5 km; T < 10 m	Gently sloping coastal wetland which extends landwards to the high-tide mark. Evaporating pools of saline water form localized 'salt-pans' and fauna and flora adapted to highly fluctuating salinities dominate.	Mesotidal to macrotidal
Mangroves	L < 200 km; W < 60 km; T < 10 m	Densely vegetated forests occupying the lower intertidal zone (ca mean sea level to low-tide mark) of tide-dominated, typically mud-rich deltaic shorelines. Flora sub-zonations related to topography and often diverse fauna adapted to salinity variations (e.g. Mekong, Ganges-Brahmaputra deltas).	Mesotidal to macrotidal

Tidal creeks	W < 100 m; T 10 m	Shore-normal creeks which do not pass into a fluvial system landwards, often mud-rich.	Microtidal to macrotidal
--------------	----------------------	---	--------------------------

**Table 3.** Larger-scale tidal indicators, ranging from depositional environments to systems, and their generalized implication for tidal-range prediction in the geological rock record ([modified after Wells et al., 2005a](#)).

### 2.2.3.3 Ancient bed shear stress analysis

Bed shear is a better indicator than tidal range of sedimentary response as it is a key variable for understanding the initiation and maintenance of grain motion, formation of bedforms (Fig. 5), and both competence-driven and capacity-drive deposition ([Harms et al., 1982](#); [Komar, 1987](#); [Hiscott, 1994](#); [Dalrymple, 2010a](#)). Tidal currents that exceed the critical bed shear stress threshold for sediment entrainment will impact sedimentary processes and preserved sedimentary structures and grain size provide some information on ancient bed shear stress (Fig. 5). However, the type of sedimentary structures formed by currents of varying flow velocity is also strongly dependent on the available grain size and water depth during deposition (Fig. 5), which can only be estimated in the context of facies successions, permitted by the availability of appropriate rock record data. Less reliable predictions of available grain size range may be possible based on catchment area geology, interpreted palaeo-drainages and other indirect data sources (e.g. seismic geometries of clinoforms, seismic amplitudes, well logs and other borehole data). For a given water depth, if tidal bed shear stress was insufficient to rework the minimum grain size available, tides will not have influenced sediment transport. In contrast, the size, type and texture of sedimentary structures may vary depending on tidal current strength and the frequency with which the critical bed shear stress for entrainment of the available grain size range was exceeded.

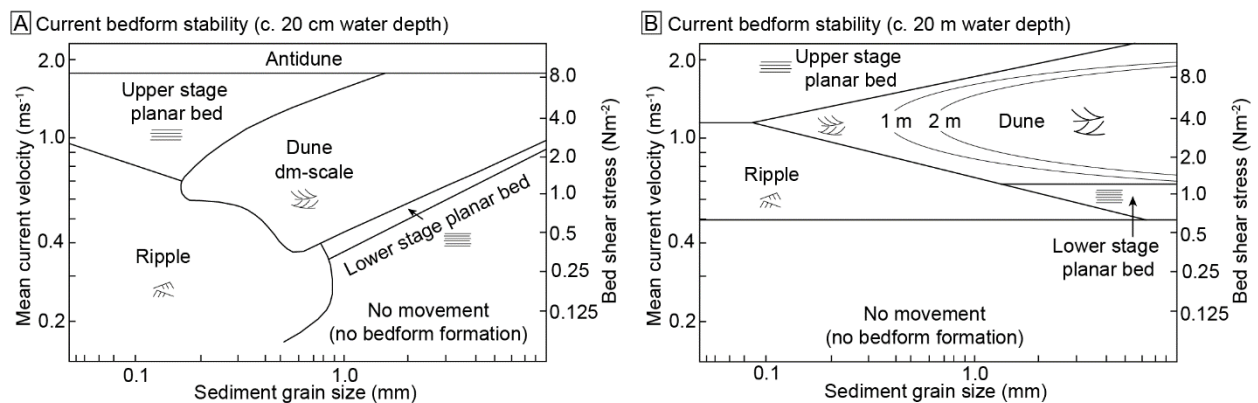


**Fig. 5.** (A) Bedform stability diagram, including bed shear stress, for unidirectional flow at approximately 20 cm water depth (flume tank) ([Harms et al., 1982](#); [Mitchell et al., 2010](#)). (B) Bedform stability diagram, including bed shear stress, for unidirectional flow at approximately 2 m water depth ([Rubin and McCulloch, 1980](#)).



### 3 PALAEOTIDAL MODELLING CASE STUDIES

Several published palaeotidal modelling case studies each provide unique insights into the controls on tidal processes across a range of time periods and geological settings. Herein, we review three case studies that illustrate the range of physiographic controls on tides relevant for improving predictions of shoreline–shelf progress regime. Together these three case studies document changes in tidal processes: (1) across a wide range of spatial scales, from regional scale in open oceans (1000s km) through seaways and enclosed basins (100s – 1000s km), to local scale on continental shelves (10 – 100s km) and in shoreline features (1–10s km); (2) in different basin and tectonic settings; (3) across different time encompassing various changes in basin-to-shoreline physiography; and (4) at various times in Earth history. Below, each case study is summarized in turn, with a brief review of the geological setting followed by a synthesis and discussion of the palaeotidal model results in terms of the influence on tides by larger-scale basin physiography (100–1000 km), shelf width (c. 10–100 km) and shoreline geometry (c. 1–10 km).

#### 3.1 Regional-scale controls on tidal deposition: Oligocene–Miocene South China Sea (SCS), Southeast Asia

##### 3.1.1 Background

During the Oligo–Miocene, the SCS and wider Southeast Asia region experienced geologically rapid and extensive tectonic reorganization, impacting large-scale oceanic flow patterns, in response to major movements of the Indo-Australian, Eurasian, Pacific and Philippine Sea plates (Fig. 6) ([Lee and Lawver, 1995](#); [Hall, 1996](#); [Hall, 2002](#)). In summary, Oligocene–Early Miocene tectonism within the SCS was dominated by active seafloor spreading and broadly occur between c. 32–31 Ma and 20.5 Ma or 15 Ma ([Briaes et al., 1993](#); [Barckhausen et al., 2014](#)) ([Barckhausen and Roeser, 2004](#)). Post-collision uplift formed a foredeep along the NW Borneo margin by the Late Miocene ([Hinz et al., 1989](#); [Hall, 2002](#); [Ingram et al., 2004](#); [Franke et al., 2008](#); [Hutchison, 2010](#)), whilst the Sunda Shelf remained emergent throughout the Oligo–Miocene, in contrast to its present-day drowned state (Fig. 6) ([van Hattum et al., 2006](#); [Hall, 2013](#); [Shoup et al., 2013](#)) (e.g. [Gordon et al., 2012](#); [Hu et al., 2015](#)). At the eastern SCS margin, clockwise rotation and northward movement of the Philippine Sea Plate and the Izu-Bonin-Mariana (IBM) arc formed the present-day Philippines by the Middle–Late Miocene and narrowed oceanic connections into the SCS from the Pacific Ocean north of the IBM arc, which is modelled as emergent in some palaeogeographies due to physiographic uncertainty (Fig. 6) ([Collins et al., 2017a](#); [Collins et al., 2018a](#); [Collins et al., 2018b](#)). At the western SCS margin, variable extension, compression, eustatic sea level and sediment supply impacted formation,

development and infill of several shelf basins ([Doust and Sumner, 2007](#); [Miller et al., 2011](#); [Shoup et al., 2013](#); [Morley, 2016](#); [Collins et al., 2018a](#); [Collins et al., 2018b](#)).

Numerical palaeotidal modelling was undertaken to understand the spatial and temporal impact that regional-scale, tectonic- driven physiographic changes had on shoreline–shelf tides and the corresponding stratigraphic record during the Late Oligocene–Miocene interval. Palaeotidal modelling with Fluidity used full astronomical tidal forcing and global multi-scale meshes with a maximum *ca* 10 km resolution ([Collins et al., 2017a](#); [Collins et al., 2018a](#); [Collins et al., 2018b](#)).

Model outputs included herein ([Collins et al., 2018a](#)) are maximum spring tidal range and maximum tidal bed shear stress, plotted as the equivalent grain size capable of being transported if present (see Section 2.2.3.3). ‘Base case’ models used the preferred palaeogeographic interpretations at sea level highstand for three time intervals in the Early, Middle and Late Miocene (Fig. 7). Sensitivity tests included tidal models for 50 m sea level lowstand palaeogeographies for Late Oligocene–Late Miocene time intervals, and a Late Miocene (6 Ma) tidal model for a palaeogeography with a submerged (10 m) IBM arc.

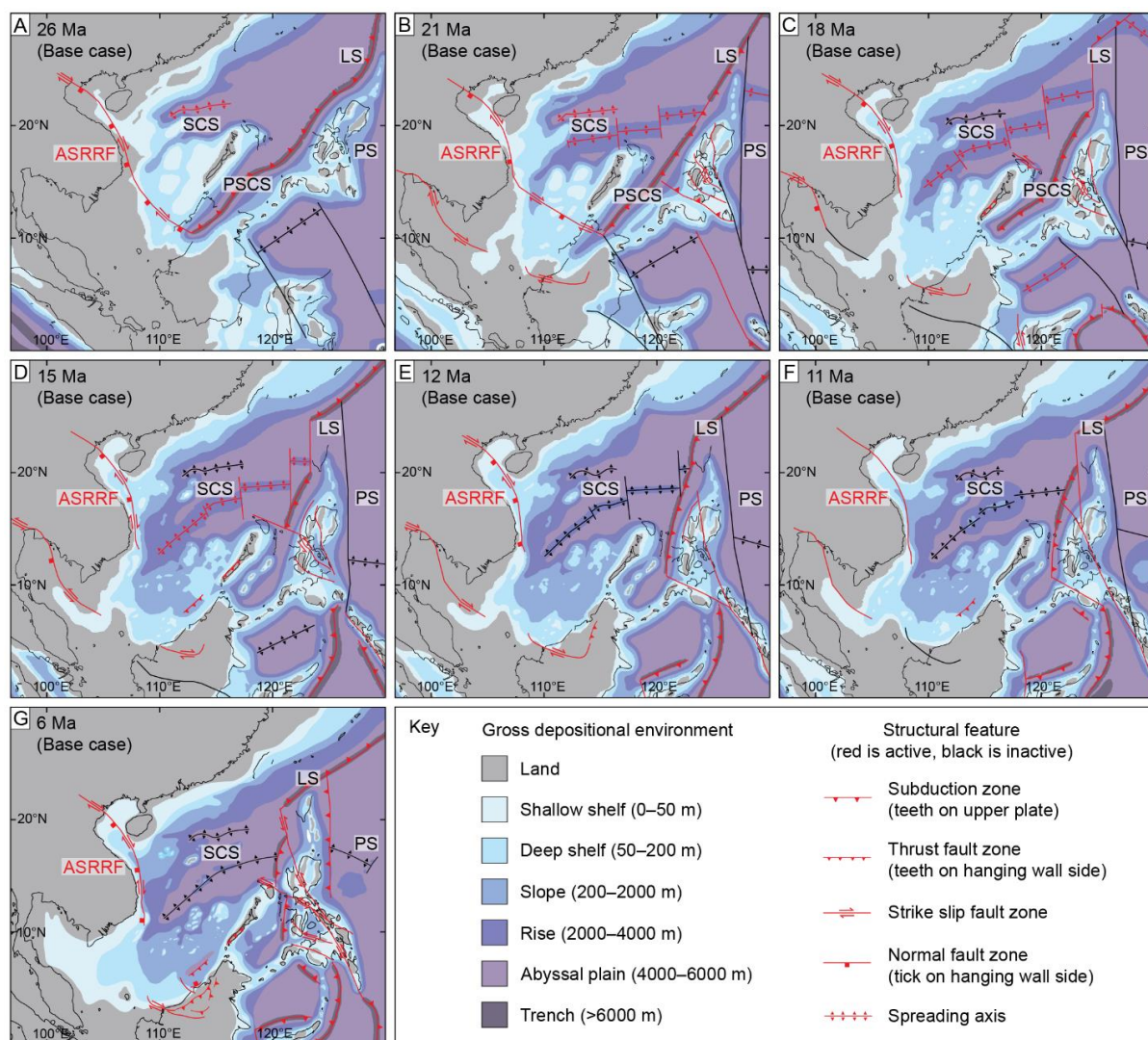


**Fig. 6.** Gross depositional environmental reconstructions for the Late Oligocene–Late Miocene in Southeast Asia based on sea-level highstand for eight time-slices: (A) 26 Ma (Chattian); (B) 21 Ma (Aquitainian); (C) 18 Ma (Burdigalian); (D) 15 Ma (Langhian); (E) 12 Ma (Serravallian); (F) 11 Ma (Tortonian); (G) 6 Ma (Messinian). Alternative gross depositional environmental reconstructions include a submerged Palawan: (H) 26 Ma (Chattian); (I) 21 Ma (Aquitainian); (J) 18 Ma (Burdigalian). After [Collins et al. \(2018a\)](#).

### 3.1.2 Model results and rock-record integration

In the Oligocene–Miocene SCS, regional (100–1000s km) and tectonic-driven palaeogeographic changes caused a significant decrease in the overall extent and magnitude of tidal processes. Most notably during the Miocene, reduced oceanic inflow and boundary tide related to narrowing of the Pacific Ocean connection via the Luzon Strait (from c. 1500 km to 350 km) and north of the IBM arc (from c. 1600 km to 370 km) coincided with no ocean outflow from the SW SCS due to the emergent Sunda Shelf. Consequently, tides in the central SCS decreased from macrotidal (>4 m), and capable of coarse sand to gravel transport in the Early Miocene, to mesotidal (>2 to 4 m), and capable of fine

1 sand to silt transport in the Middle–Late Miocene (Fig. 7). The importance of regional-scale ocean  
2 inflow on tides is further indicated by sensitivity analyses. Shutdown of oceanic throughflow into the  
3 Sea of Japan during lowstands increased tidal inflow and boundary tides to the SCS, resulting in  
4 larger and stronger tides than during equivalent highstands (Fig. 8A–B). Likewise, submerging the  
5 IBM arc (to only 10 m water depth) in the Late Miocene causes substantially larger and stronger tides  
6 across the SCS (Fig. 8C–D). Overall, tides were diurnal to mixed diurnal dominated (F-ratio >1.5),  
7 reflecting amplification and dominance of diurnal tides in the Pacific Ocean, similar to the present  
8 day.  
9

10  
11  
12  
13  
14  
15  
16 On a local-scale, tidal range and bed shear stress maxima in the Oligo–Miocene SCS invariably  
17 occurred within embayed shoreline areas, particularly those with (1) relatively wide and deep  
18 entrances open to the incoming tide, and (2) high resonance and theoretical funnelling potential  
19 ([Collins et al., 2018a](#)). For example, widening and deepening the entrance to the Gulf of Thailand  
20 (western SCS) permitted greater tidal inflow and a larger tidal prism, potentially enhanced by  
21 resonance effects, resulting in an increase from microtidal to low mesotidal conditions during the  
22 Miocene ([Collins et al., 2018a](#)).  
23  
24  
25  
26  
27  
28  
29  
30

31 Model results are supported by sedimentological and micropalaeontological data (Fig. 9) and are  
32 consistent with previous Miocene palaeoenvironmental stratigraphic interpretations ([e.g. Doust and](#)  
33 [Sumner, 2007](#)), including the distribution of interpreted mangrove-related facies in the western SCS  
34 ([Morley et al., 2011](#); [Shoup et al., 2013](#)). Preserved Oligocene–Middle Miocene strata in several  
35 basins within areas of high modelled tidal range and bed shear stress include interpretable evidence  
36 for tidal processes on different scales (e.g. facies to facies successions), and mangrove palynomorph  
37 data, notably acmes in mangrove pollen (Fig. 8) ([Morley et al., 2011](#); [Shoup et al., 2013](#)). Tidal  
38 processes are commonly interpreted to have operated together with river processes, and to a lesser  
39 extent wave processes. Mixed fluvial and tidal preservatons is often expressed within heterolithic  
40 facies and facies associations, where variations in sandstone-bed thickness, the ratio of sandstone-to-  
41 mudstone, and bioturbation on a cm-to-metre scale can be attributed to variations in river discharge  
42 and tides ([Amir Hassan et al., 2013](#); [Amir Hassan et al., 2016](#); [Collins et al., 2018c](#); [Collins et al.,](#)  
43 [2020](#)). Tidal processes are also interpreted for sandstone-dominated facies associations and  
44 successions predominantly characterised by trough-cross stratification, often but not exclusively with  
45 long rippled toesets and/or bi-modal palaeocurrent directions. Significantly, this occurs in association  
46 with paralic coals and mudstones deposited within or in close relation to mangroves, including *in situ*  
47 occurrences ([Morley et al., 2011](#); [Amir Hassan et al., 2013](#); [Togunwa et al., 2015](#); [Amir Hassan et al.,](#)  
48  
49  
50  
51  
52  
53  
54  
55  
56  
57  
58  
59



2016; [Murtaza et al., 2018](#)). Tidal signals are less widespread in Middle–Late Miocene strata (Fig. 9), preferentially occurring in embayed shoreline settings coincident with relative highs in modelled tidal range and bed shear stress, such as in the Gulf of Thailand ([Morley et al., 2011](#); [Ridd et al., 2011](#); [Shoup et al., 2013](#)) and in areas of NW Borneo ([Hadley et al., 2006](#); [Collins et al., 2018c](#)). Preserved sections in open-coastline systems are mostly interpreted to have been dominated by wave processes, even in areas of modelled high tidal bed shear stress such as along SE Vietnam ([Morley et al., 2011](#); [Chung et al., 2015](#)), suggesting wave processes may have overprinted evidence of tides.

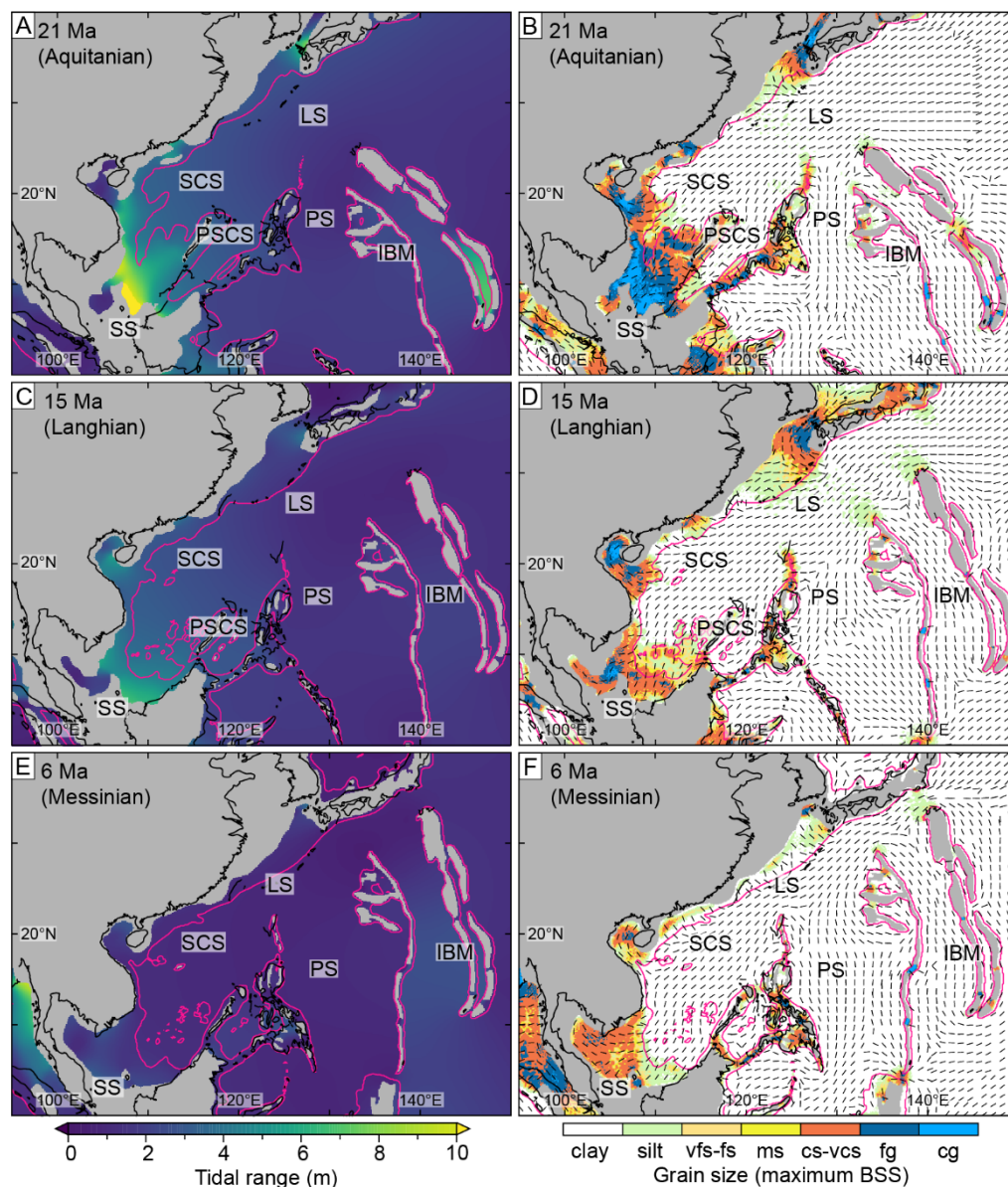


**Fig. 7.** Palaeotidal model results in the Oligo–Miocene South China Sea for tidal range (A, C, E) and maximum tidal bed shear stress plotted as the maximum sediment caliber entrained (B, D, F), for three ‘base case’ palaeogeographic reconstructions: (A, B) Early Miocene at 21 Ma; (C, D) Middle Miocene at 15 Ma; and (E, F) Late Miocene at 6 Ma (see Fig. 6). The thicker black line (A–F) is the reconstructed present-day coastline. The thinner black lines in the bed shear stress plots indicate the orientation of maximum tidal bed shear stress. The pink lines (A–F) indicate the interpreted 200 m palaeobathymetric contour and approximate palaeo-shelf edge. See [Collins et al. \(2018a\)](#) for all model results and sensitivity analyses. Map abbreviations: IBM – Izu-Bonin-Mariana Arc; LS – Luzon strait; PS – Philippine Sea; SCS – South China Sea; SS – Sunda Shelf. Grain size abbreviations: vfs = very fine sand; fs = fine sand; ms = medium sand; cs = coarse sand; vcs = very coarse sand; fg = fine gravel; cg = coarse gravel.

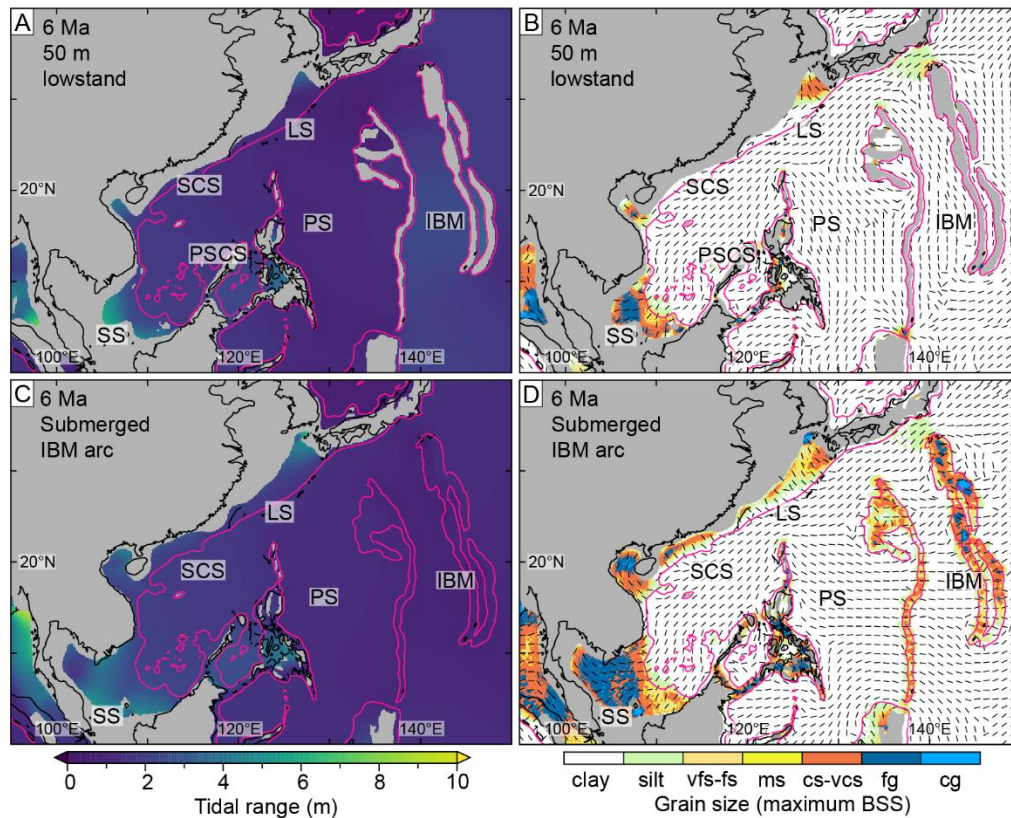


**Fig. 8.** Sensitivity analyses of the base-case for the Late Miocene (6 Ma) base case palaeogeographic reconstruction (cf. Fig. 7E, F) showing modeled tidal range (A, C) and maximum tidal bed shear stress, plotted as the maximum sediment caliber entrained (B, D), for a 50 m sea-level lowstand reconstruction (A, B) and submerged Izu-Bonin-Mariana (IBM) arc (C, D). Refer to Fig. 7 for abbreviations.

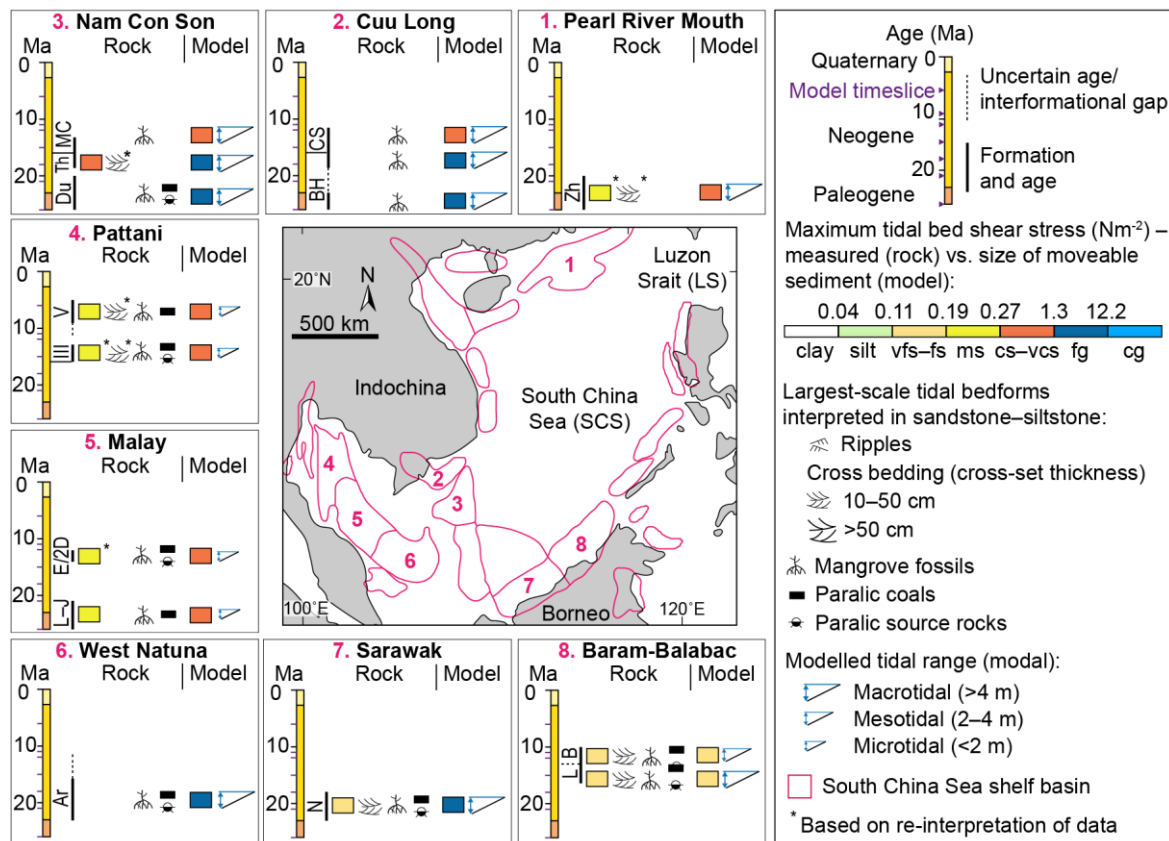


**Fig. 9.** Evidence of tide-influenced deposition based on sedimentological and micropalaeontological data, mainly from petroleum exploration wells, and comparison to base case tidal model results (Fig. 7) in South China Sea shelf basins. Rock-record data include grain size, cross lamination (ripples) and/or cross bedding interpreted to preserve evidence of tidal process (e.g. bidirectional palaeocurrents, scoop-shaped foresets, mudstone drapes), mangrove pollen acmes and the occurrence of paralic, mangrove-bearing coals and source rocks. Studied formations and key references for each basin are: (1) Upper Zhuhai (Zh) Formation, Pearl River Mouth Basin ([Zheng and Deng, 2012](#)); (2) Bach Ho (BH) and Con Son (CS) formations, Cuu Long Basin ([Morley et al., 2011](#)); (3) Dua (Du), Thong (Th) and Mang Cau (MC) formations, Nam Con Son Basin ([Tin and Ty, 1995](#); [Morley et al., 2011](#)); (4) Sequences II–IV, Pattani Basin ([Jardine, 1997](#); [Lockhart et al., 1997](#)); (5) Groups L–J and E, Malay Basin ([Morley et al., 2011](#)); (6) Arang (Ar) Formation, West Natuna Basin ([Morley et al., 2011](#)); (7) Nyalau (Ny) Formation, Balingian Province, Sarawak Basin ([Amir Hassan et al., 2013](#); [Amir Hassan et al., 2016](#)); (8) Lambir (L) and Belait (B) formations, Baram Delta Province, Baram-Balabac Basin ([Lambiase et al., 2003](#); [Collins et al.](#)).

## 3.2 Regional- to local-scale controls on tidal deposition: Early Cretaceous (Aptian–Albian) Lower Greensand Seaway, north-west Europe

### 3.2.1 Background

The Early Cretaceous (Aptian–Albian) ‘Lower Greensand Seaway’ (LGS), used here to refer to the interconnected network of three main seaways connecting with larger marine bodies (i.e. Boreal, proto-Atlantic and Neothys; Fig. 10A–B), contrasts markedly to the SCS example: it covers a much smaller area, it was part of a larger epicontinental sea and it was entirely shallow water, far removed from coeval oceanic basins. The larger-scale (10–100s km) basin physiography was determined by a series of precursor, west-east-trending, rift basins (c. 50–100 km long and 10–30 km wide; e.g. Weald, Wessex and Channel basins; Fig. 10 C–D) that were initiated during the Early Cretaceous (e.g. [Ziegler, 1990](#); [Hawkes et al., 1998](#)). Aptian-Albian deposits in the LGS comprise shallow-marine sandstones (Lower Greensand Group; Fig. 10E), divided informally herein into two stratigraphic intervals: (1) the upper part of the *fissicostatus–martinioides* Zone (labelled ‘FH’, Fig. 10E) comprising deposits with negligible evidence of tidal currents, suggesting low tidal range (microtidal–low mesotidal) ([Ruffell and Wach, 1991](#); [Wells et al., 2010b](#)); (2) the mid-to-upper part of the *upper martinioides–lower tardefurcata* Zone (labelled ‘FSW’ in Fig. 10E), represented by several units, with exemplary evidence of deposition by strong tidal currents within an inferred macrotidal, ebb-dominated diurnal, or mixed, predominantly diurnal tidal regime (e.g. [De Raaf and Boersma, 1977](#)) ([Allen, 1982a](#); [Bridges, 1982](#); [Johnson and Levell, 1995](#); [Wonham and Elliott, 1996](#); [Yoshida et al., 2004](#)). These ‘greensands’ deposits are overlain by offshore marine mudstones (Gault Clay Formation). Hence, the Aptian-Albian succession reflects overall marine transgression, which was accompanied by an overall increase in basin width, length, bathymetry and connectivity. Consequently, predicting tidal circulation in this setting is complicated by several uncertainties, most notably: (1) variability in palaeobathymetry caused by the drowning of previously separate rift basins (potentially forming various ‘straits’) with differing initial water depths (Fig. 10C–D); and (2) complex marine flooding of these basins, with competing marine incursions entering the LGS through connections to the Boreal Sea (to the north), proto-Atlantic Ocean (to the south-west), and Neotethys Ocean (to the south-east) (Fig. 10A–B).

Palaeotidal modelling and comparison to the Lower Greensand Group in the two stratigraphic intervals outlined above (‘FH’ and ‘FSW’ in Fig. 10E) allows uncertainty analyses across a range of different age, palaeobathymetric and palaeogeographic scenarios ([Wells et al., 2010b](#)). Regional-scale tidal simulations for tidal amplitude and phase represent both astronomical ( $M_2$ ,  $S_2$ ,  $K_1$ , and  $O_1$ ) and boundary tidal forcing, the latter generated using a global Aptian model ([Wells et al., 2010a](#)). Two base-case palaeogeographies (‘Scenario 1’), based on modified published interpretations (see [Wells, 2008](#); [Wells et al., 2010b](#)), were generated for the ‘FH’ and ‘FSW’ stratigraphic intervals (Fig. 10E),



referred to as FH1 (Fig. 11A–B) and FSW1 (Fig. 11C–D), respectively. A key difference between the ‘base case’ scenarios for these two timeslices is widening of the oceanic connections, especially through the Paris Basin, in the upper *martinioides*–lower *tardefurcata* Zone due to transgression in the *nutfieldensis* Zone (Casey, 1961; Wells et al., 2010b). Four out of seven sensitivity analyses for each base-case palaeogeography are discussed herein, corresponding to scenarios 2, 4, 6 and 8 in Wells et al. (2010b): Scenario 2 has closure of the Paris Basin connection to the Neotethys Ocean (FH2 and FSW2); Scenario 4 has a connection through the Pewsey Basin to the proto-Atlantic Ocean (FH4 and FSW4); Scenario 6 has opening of all oceanic connections (FH6 and FSW6); and Scenario 8 has a doubled water depth between 0 and 200 m (FH8 and FSW8).

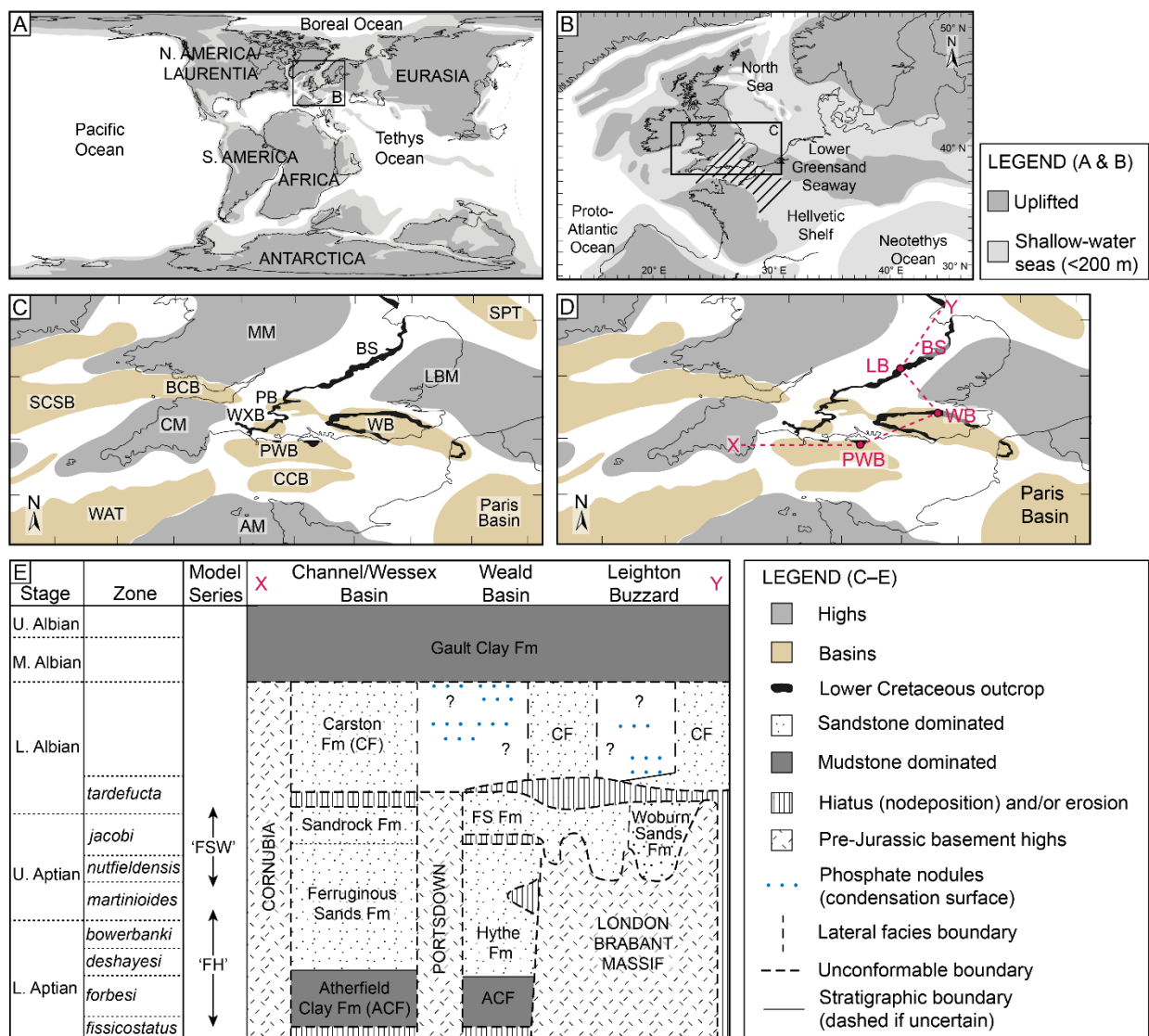


**Fig. 10.** Geological and stratigraphic framework of the Early Cretaceous ‘Lower Greensand Seaway’, NW Europe. (A) Global Aptian palaeogeographic framework. (B) Aptian palaeogeographic framework of northwest

Eurasia. In A and B, darker grey are significant uplifted highs and lighter grey shallow-water seas (< 200 m depth). (C) Aptian palaeogeographic map of southern UK and northern France with significant uplifted highs in dark grey and basins in light brown. Basin abbreviations: BCB – Bristol Channel Basin; BS – Bedfordshire Strait; CCB – Central Channel Basin; PB – Pewsey Basin; PWB – Purbeck-Wright Basin; SCSB – South Celtic Sea Basin; WAT – Western Approaches Trough; WB – Weald Basin. High abbreviations: AM – Armorican Massif; CM – Cornubian Massif; LBM – London-Brabant Massif; MM – Midlands Massif. (D) Aptian palaeogeographic map illustrating key locations for the chronostratigraphic and lithostratigraphic framework of the Lower Greensand Group (section X–Y in E). Location abbreviations in addition to those labelled in C: LB – Leighton Buzzard. (E) Illustrative chronostratigraphic and lithostratigraphic section of the Lower Greensand Group in southern England. Two ‘base case’ palaeogeographies are considered (Fig. 11): ‘FH’ represents the upper part of the *fissicostatus*–*martinioides* Zone depositional sequence, corresponding to the Ferruginous Sands Formation on the Isle of Wight and the Hythe Formation in the Weald; ‘FSW’ represents the mid to upper part of the upper *martinioides*–lower *tardefurcata* Zone depositional sequence, corresponding to the Folkestone Sands Formation in the Weald, the Sandrock Formation on the Isle of Wight, and the Woburn Sands Formation around Leighton Buzzard. After [Wells et al. \(2010b\)](#), [Yoshida et al. \(2004\)](#) and references therein.

### 3.2.2 Model results and rock-record integration

The range of tidal model scenarios illustrates the regional-scale (100s km) interplay between tidal inflow and outflow. This has a first-order control on tides in smaller-scale (10s km) areas and can supersede funnelling effects within some smaller physiographic constrictions, such as in straits and embayments. In the LGS, predicted tidal ranges in simulations of the upper *martinioides*–lower *tardefurcata* Zone (‘FSW’) (Figs. 11B, D, 12B, D, F, H) are consistently higher than in equivalent base-case and sensitivity simulations of the *fissicostatus*–*martinioides* Zone (‘FH’; Figs. 11 A, C, 12A, C, E, G), and are interpreted to relate to increased inflow of tidal energy due to the greater width of the seaway and its ocean connections in ‘FSW’ simulations. This is especially pronounced for the Paris Basin, because the maximum depth is similar in equivalent FSW and FH simulations and the same open tidal boundary conditions are used in both cases. In addition, for all scenarios and both timeslices, tidal range is higher along the eastern margins of the seaway and the Paris Basin, due to Coriolis deflection of the northward propagating tidal wave from the Neotethys Ocean.

Modelled high mesotidal to low macrotidal conditions for the FSW interval are supported by widespread interpreted tidal deposits throughout the seaway at this time. Evidence of tidal processes ranges in scale from facies (e.g. sedimentary structures, palaeocurrents and ichnology), through facies associations to facies successions (see Section 2.2.3), and include various combinations of tidal indicators such as the following: (1) mudstone draped cross-set, including some double-drapes and possible spring-neap bundles; (2) compound cross-stratification; (3) bidirectional palaeocurrent

1 directions on a range of scales, including ebb- and flood-dominated patterns in 10s m-thick intervals;  
2 (4) reactivation surfaces; (5) wavy-, flaser- and lenticular-bedded heterolithic cross-bed toesets; (6)  
3 shallow-marine, variable intensity, low diversity ichnofauna; and (7) vertical and lateral facies and  
4 facies association relationships, including grain size trends and the geometry of bounding surfaces e.g.  
5 ([Bridges, 1982](#); [Johnson and Levell, 1995](#); [Wonham and Elliott, 1996](#); [Yoshida et al., 2004](#); [Wells et](#)  
6 [al., 2010b](#)), ([Allen, 1982a](#); [Bridges, 1982](#)). Overall, these deposits are interpreted to record deposition  
7 under strong tidal currents, with probable mesotidal to macrotidal ranges ([Allen, 1981b](#)), in tidal  
8 estuarine to embayment environments ([Yoshida et al., 2004](#)). This is consistent with palaeotidal  
9 model results that include local-scale amplification through shoaling and funnelling effects (Fig. 12B  
10 and 13). Furthermore, the predicted diurnal-dominated tidal regime in the LGS in all modelled  
11 scenarios (Fig. 13) matches the interpretation of diurnal-dominated spring–neap tidal bundles in the  
12 Folkestone Sands Formation ([Allen, 1981a](#); [Allen, 1982a](#)).

13 Modelled microtidal to low mesotidal conditions for the FH interval is broadly consistent with little  
14 evidence of tidal influence in the time-equivalent stratigraphic record (see review in [Wells et al.](#)  
15 [\(2010b\)](#)). The only putative tidal deposits of this age, occurring in the western Weald Basin, are  
16 limited in areal extent and contain no published evidence of bidirectional currents or mud drapes,  
17 decreasing the confidence in interpretation ([Casey, 1961](#); [Narayan, 1971](#); [Bridges, 1982](#); [Ruffell and](#)  
18 [Wach, 1991](#); [Rawson, 2006](#)).

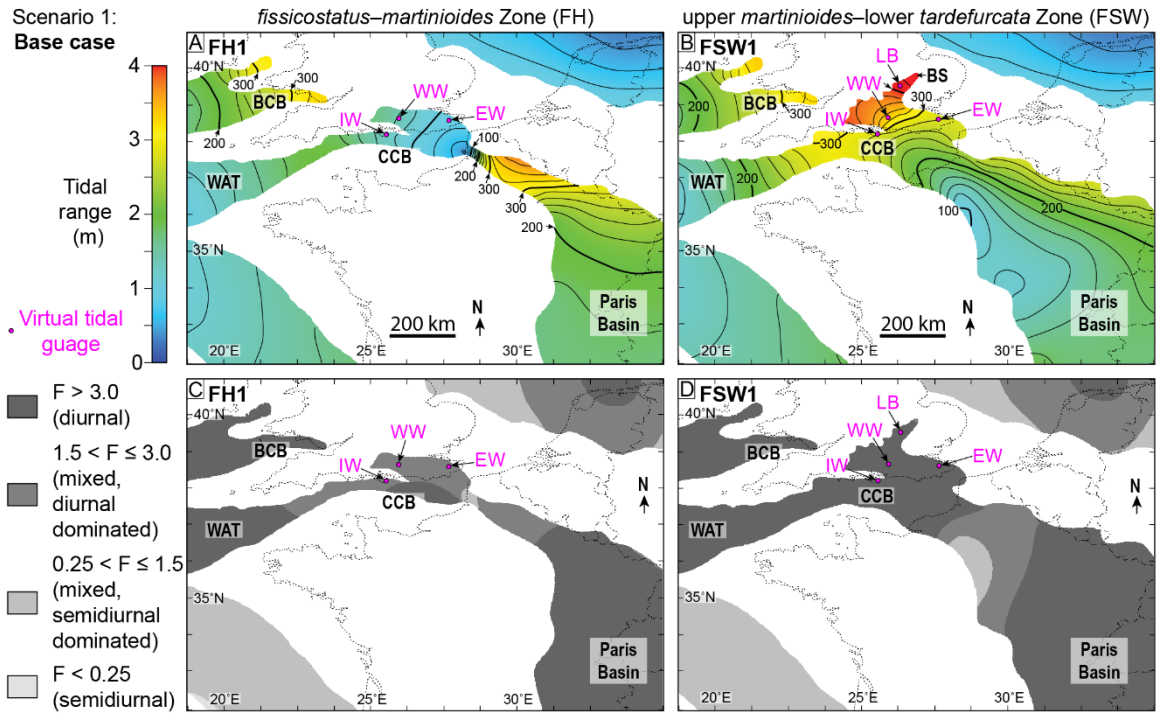


**Fig. 11.** Base case palaeotidal model results in the Early Cretaceous Lower Greensand Seaway for the *fissicostatus–martinioides* Zone (A, C) and upper *martinioides–lower tardefurcata* Zone (B, D) timeslices (respectively ‘FH’ and ‘FSW’ in Fig. 10D) showing modelled tidal range (0–4 m) for the four principal tidal constituents ( $M_2 + S_2 + K_1 + O_1$ ), with 20 cm contours and bold, annotated contours every 100 cm (A–B), and the ‘F-ratio’ between the amplitudes of diurnal and semidiurnal tidal constituents (C–D). After [Wells et al. \(2010b\)](#). Pink labelled dots show positions of ‘virtual tidal gauges’ in the East Weald Basin (EW), Isle of Wight (IW), Leighton Buzzard (LB) and West Weald Basin (WW). Basin abbreviations: CCB – Central Channel Basin; BCB – Bristol Channel Basin; BS – Bedfordshire Strait; CCB – Central Channel Basin; PB – Pewsey Basin; WAT – Western Approaches Trough. Modified from [Wells et al. \(2010b\)](#).



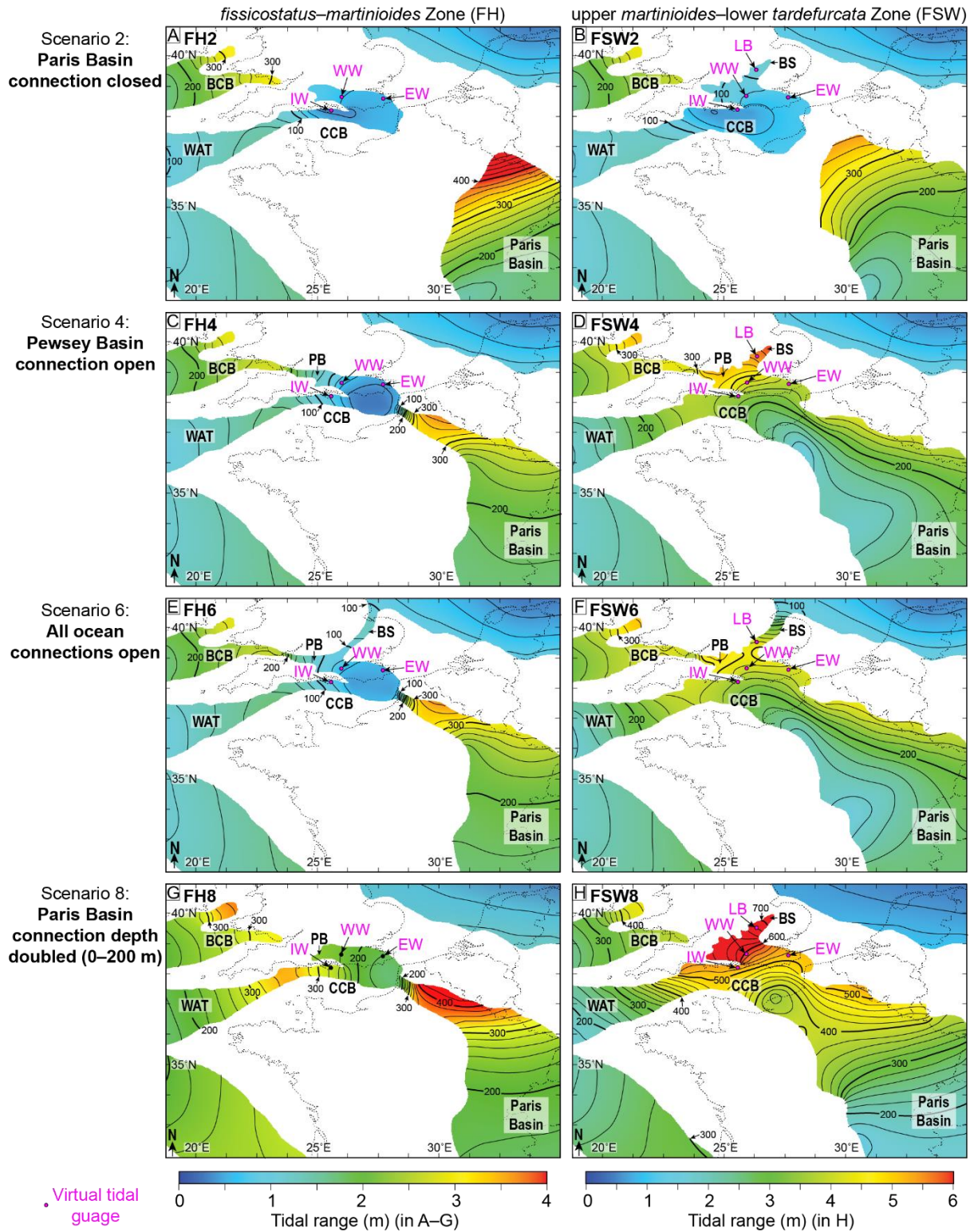


**Fig. 12.** Modelled tidal range for the four principal tidal constituents ( $M_2 + S_2 + K_1 + O_1$ ) in sensitivity analyses of base-case reconstructions for the *fissicostatus*–*martinioides* Zone (A, C, E, G) and upper *martinioides*–lower *tardefurcata* Zone (B, D, F, H) timeslices in the Early Cretaceous Lower Greensand Seaway (respectively ‘FH’ and ‘FSW’ in Fig. 10D); tidal range contours are drawn for 20 cm intervals and bold, annotated contours every

100 cm. Pink labelled dots show positions of ‘virtual tidal gauges’ in the East Weald Basin (EW), Isle of Wight (IW), Leighton Buzzard (LB) and West Weald Basin (WW). Basin abbreviations: CCB – Central Channel Basin; BCB – Bristol Channel Basin; BS – Bedfordshire Strait; CCB – Central Channel Basin; PB – Pewsey Basin; WAT – Western Approaches Trough. Modified from [Wells et al. \(2010b\)](#).

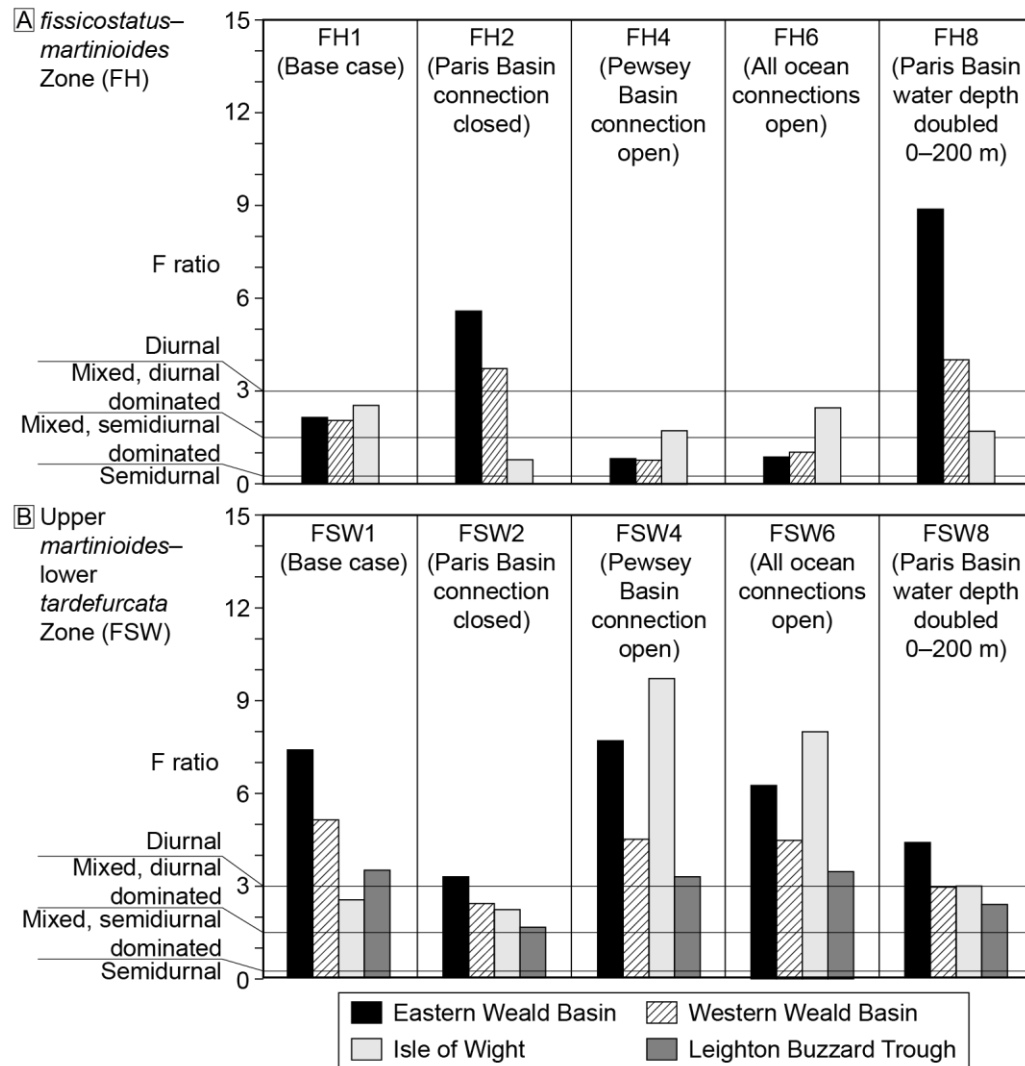


**Fig. 13.** Bar graphs of modelled tidal range at ‘virtual tide gauge’ locations (see Fig. 11 & 12) for base-case (Fig. 11) and sensitivity simulations (Fig. 12) for the *fissicostatus-martinioides* Zone (A) and upper *martinioides-lower tardefurcata* Zone (B) timeslices (respectively ‘FH’ and ‘FSW’ in Fig. 10D). Modified from [Wells et al. \(2010b\)](#).

### 3.3 Local-scale controls on tidal deposition: Late Cretaceous (Turonian-Cenomanian), Bohemian Cretaceous Basin, Central Europe

#### 3.3.1 Background

The Bohemian Cretaceous Basin (BCB) was a slowly subsiding, transtensional basin that linked with other basins to form the large and shallow Mid-Cretaceous European Epicontinental Sea (MCEES) (e.g. [Ziegler, 1990](#); [Mitchell et al., 2010](#)). As with the LGS example presented above, the BCB was far removed from coeval oceanic basins; over a thousand kilometres from the Neotethys Ocean to the southeast and the Proto-Atlantic Ocean to the west (Fig. 14) (e.g. [Ziegler, 1990](#); [Mitchell et al., 2010](#)). Several emergent landmasses lay in between these oceans and the BCB (Fig. 14), such that boundary tides are likely to have been significantly blocked and damped by seabed friction ([Mitchell et al., 2010](#)). However, funnelling and shoaling effects in local-scale straits (c. 10s km wide) may have been important within the basin (Fig. 15). In this context, two depositional models have been proposed for Turonian-to-early-Coniacian shallow-marine sandstones in the BCB. An early model of large offshore bedforms sculpted by storms and tides (cf. tidal sand banks or ridges) (e.g. [Jerzykiewicz and Wojewoda, 1986](#)) has been superseded by one of top-truncated, coarse-grained deltaic shorelines that were reworked by tidal currents ([Uličný, 2001](#); [Uličný et al., 2009](#)); both models are discussed here.

Palaeotidal modelling in the MCEES and BCB has focused on the early Middle Turonian interval ('TUR 2' genetic sequence of [Uličný et al. \(2009\)](#)) with two main aims: (1) to understand how boundary tides from the Neotethys and Proto-Atlantic oceans were expressed as tidal circulation in the BCB, by considering regional-scale (10–100s km) basin physiography (Fig. 14); and (2) to assess whether modelled tidal bed shear stress was capable of generating the grain-size distributions, bedform types and palaeocurrent orientations observed at local-scale (1s–10s km) in the Turonian-to-early-Coniacian shallow-marine sandstones (Fig. 15) ([Mitchell et al., 2010](#)). A dataset combining outcrops and densely spaced boreholes provides good constraint on the basin-fill thickness and syn-depositional physiography of the BCB ([Uličný et al., 2009](#)), which contained islands with intervening, 10s km-wide straits (e.g. 'Elbe Strait'; Fig. 15). However, the physiography of many areas in the wider epicontinental sea is uncertain, with differences of up to 100 m water depth in basin centres outside the BCB (Fig. 14B–C) ([Ziegler, 1990](#)). Palaeotidal model simulations for the MCEES and BCB were forced with both astronomical ( $M_2$ ,  $S_2$ ,  $K_1$  and  $O_1$ ), and co-oscillating boundary tides adjacent to the deep, and expansive Proto-Atlantic and Neotethys oceans (Fig. 14) ([Wells et al., 2007](#); [Mitchell et al., 2010](#)). The co-oscillating boundary tide was set in phase with the natural resonance at each respective boundary to give the maximum tidal potential in the seaway. Two sensitivity cases of tides in the MCEES were considered: (1) palaeobathymetric uncertainty was tested using 'minimum' and maximum' depth scenarios (Fig. 14D, E); and (2) resonance of different tidal constituents was



tested by imposing different boundary tides weighted towards semi-diurnal ( $M_2$ ,  $S_2$ ) and diurnal components ( $K_1$ ,  $O_1$ ). These regional-scale tidal simulations were subsequently investigated on a more local scale in the BCB.

**Fig. 14.** (A) Stratigraphic chart showing the chronostratigraphy (modified after [Ogg et al. \(2004\)](#)), main lithofacies in the Lužice-Jizera Sub-basin (see Fig. 15A), genetic sequences recognized in this paper, and phases of basin evolution (after [Uličný et al., 2009](#)). (B) Regional palaeogeography for the Mid-Cretaceous European



Epicontinental Sea (Ziegler, 1990; Dercourt et al., 2000; Golonka, 2004; Gil et al., 2006; Golonka et al., 2006; Golonka, 2007; Mitchell et al., 2010). The approximate outline of the Bohemian Cretaceous Basin (BCB) is shown in red. (c) Gross depositional environmental map of central-western mainland Europe for the Cenomanian–Turonian (from Ziegler, 1990). (D–E Regional palaeobathymetries for palaeotidal modelling of the Mid-Cretaceous European Epicontinental Sea (MCEES), showing major contours for (D) minimum and (E) maximum depth scenarios (after Mitchell et al., 2010). Red box shows the position of the BCB. Abbreviations: AM = American Massif; BCB = Bohemian Cretaceous Basin; BM = Bohemian Massif; C = Cracow Swell; CM = Cornubian Massif; CCM = Central Carpathian Massif; CSH = Corso-Sardinian High; EH = Ebro High; FH = Faeroe High; GH = Grampian High; HB = Hatton Bank; HP = Hebrides Platform; IbM = Iberian Massif; IM = Irish Massif; M = Moesia; MC = Massif Central; SP = Shetland Platform; R = Rodopes; RB = Rockall Bank; RM = Rhenish Massif.

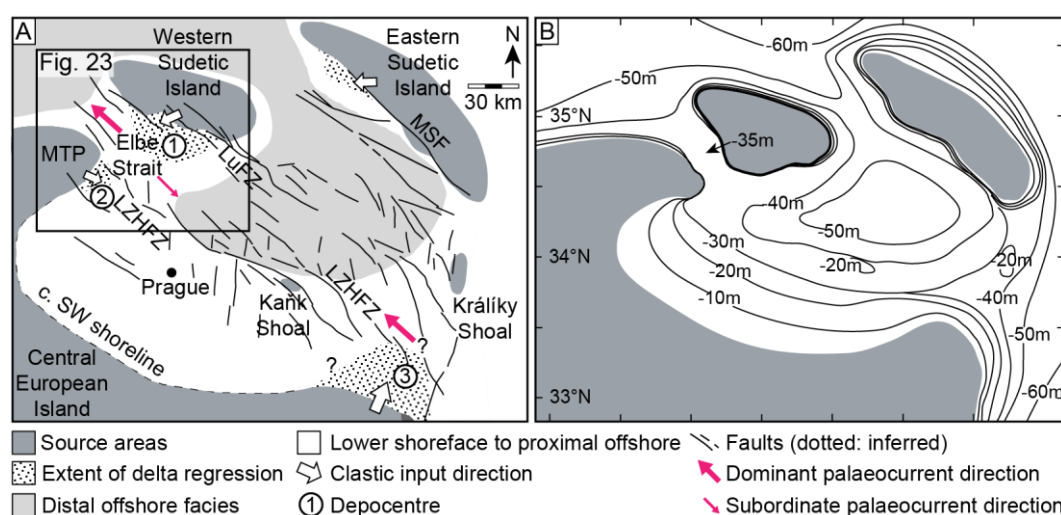


**Fig. 15.** Local scale palaeogeography (A) and palaeobathymetric (B) for the early Middle Turonian Bohemian Cretaceous Basin (onset of *Collignoniceras woollgarii* Zone). The extent of deltaic depocenters correspond to intermediate regression of the ‘TUR 2’ siliciclastic wedge (see Fig. 19A). Circled numbers (1) to (3) indicate the three main depocenters: (1) the Lužice-Jizera Sub-basin; (2) the Ohře Ramp; and (3) the Orlice-Žďár Sub-basin. MTP – Most-Teplice Palaeohigh; LuFZ – Lužice (Lausitz) Fault Zone; LZHFZ – Labe-Železné Hory Fault Zone. Modified after (Uličný et al., 2009). (B) Palaeobathymetric interpretation based on facies analysis of preserved outcrop and subsurface data (Uličný, 2001; Uličný et al., 2009). The heights of delta-front clinoforms suggests minimum depths of c. 35 m in the Elbe Strait, whereas a maximum depth of c. 50 m is estimated for the basin interior as inferred from trace fossil assemblages. After Mitchell et al. (2010).

### 3.3.2 *Model results and rock-record integration*

On a regional scale, modelled tidal range in the MCEES interior is consistently microtidal to mesotidal (Fig. 16), which supports attenuation of the tidal wave by seabed friction and emergent landmasses during propagation across the continental shelf ([Shaw, 1964](#); [Hallam, 1981](#); [Wells et al., 2005a](#); [Mitchell et al., 2010](#)). These results could be consistent with early interpretations of Turonian-to-early-Coniacian sandstones as large tidal bedforms, which do not necessarily require macrotidal conditions cf. ([Stride, 1973](#); [Stride, 1982](#); [Jerzykiewicz and Wojewoda, 1986](#)). Tidal amplification forming macrotidal conditions is limited to embayments and straits, however, this only occurs with specific boundary and bathymetric conditions, consistent with the influence of tidal resonance ([Wells et al., 2007](#)). Overall, these results more closely support a tide-influenced deltaic depositional model ([Uličný, 2001](#); [Uličný et al., 2009](#); [Mitchell et al., 2010](#)), in which fluvio-deltaic sediment supplied laterally from the basin margins was reworked along the basin axis by strong, locally constricted tidal currents. This model is similar to mixed fluvial and tidal deposition in other tidal straits (e.g. [Longhitano and Steel, 2017](#); [Rossi et al., 2017a](#)).

At a local-scale, modelled tidal range in the BCB varies from microtidal to mesotidal (Fig. 16) and modelled maximum tidal bed shear stress is consistently elevated within palaeogeographic constrictions between islands, including the Elbe Strait (Fig. 17). All modelled scenarios with forced boundary conditions generated maximum bed shear stresses in excess of c.  $2.0 \text{ Nm}^{-2}$  in the Elbe Strait (Fig. 17), which is capable of forming 3D dunes in coarse sand in up to c. 20 m water depths. These predicted tidal processes are more than sufficient to form the dm-scale cross bedding with common reactivation surfaces, finer-grained foreset drapes (some in doublets) and WNW-dominated to bidirectional palaeocurrents observed in age-equivalent sandstones within the Elbe Strait and north-western Lužice-Jizera Sub-basin (Figs 20 & 22) (e.g. [Harms et al., 1982](#); [Jerzykiewicz and Wojewoda, 1986](#); [Southard and Boguchwal, 1990](#); [Uličný, 2001](#); [Uličný et al., 2009](#); [Mitchell et al., 2010](#)). Sensitivity analysis suggests that modelled maximum bed shear stress values significantly increase for a higher boundary tide magnitude (Fig. 17A–B). Furthermore, water depth in the regional seaway influences the modelled maximum bed shear stresses locally in the BCB: modelled values are higher in the minimum depth scenario for the semi-diurnal regime, but higher in the maximum depth scenario for the diurnal tidal regime (Fig. 17C, D). This result suggests variations in resonance potential between boundary tide and palaeobathymetry scenarios, likely a result of relatively complex, constructive interaction between different co-oscillating boundary tides ([Mitchell et al., 2010](#)). Nonetheless, instantaneous bed shear stress vectors in all models show clear northwest- and southeast-directed transport patterns in the Elbe Strait, consistent with measured palaeocurrent directions (Fig. 18) ([Voigt and Tröger, 1996](#); [Uličný et al., 2009](#); [Mitchell et al., 2010](#)).

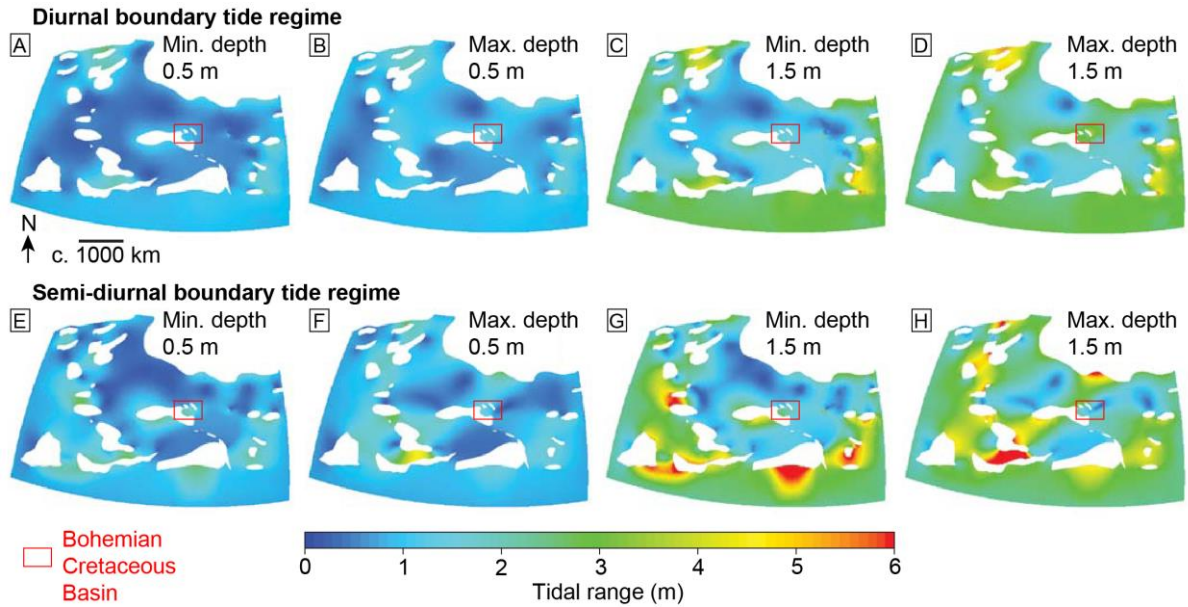


**Fig. 16.** Modelled tidal range in the Mid-Cretaceous European Epicontinental Sea (MCEES) for eight sensitivity tests for co-oscillating diurnal (A–D) versus semi-diurnal (E–H) boundary tide regimes, 0.5 m (A, B, E, F) versus 1.5 m (C, D, G, H) boundary tidal range, and minimum (min.) (A, C, E, G) and maximum (max.) (B, D, F, H) regional palaeobathymetry in the MCEES. Fluidity consistently predicts a microtidal to mesotidal range in the interior of the seaway, suggesting attenuation of the boundary tidal waves across the continental shelf by bed friction and blocking by emergent landmasses. After [Mitchell et al. \(2010\)](#).

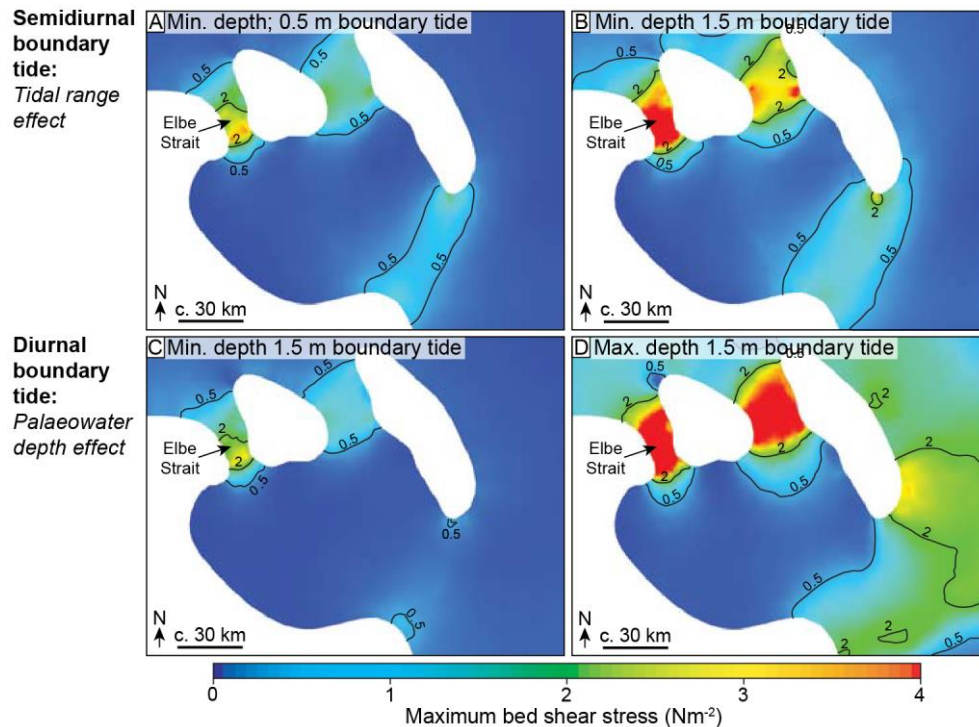


**Fig. 17.** Modeled maximum bed shear stress in the Bohemian Cretaceous Basin. The  $0.5 \text{ Nm}^{-2}$  contours show the approximate minimum bed shear stress required for the formation of dunes in coarse sand (Fig. 5) (Harms et al., 1982), whereas  $1.0 \text{ Nm}^{-2}$  is the approximate minimum bed shear stress required to form the observed scale of 3D dunes in coarse-grained sand in the Elbe Strait. Results for a 0.5 m (A) and 1.5 m (B) semi-diurnal boundary tide regime in the minimum (min.) depth regional palaeobathymetric domain (Fig. 14D) indicate that the modeled maximum bed shear stress is strongly dependent on the amplitude of the co-oscillating boundary tide. Results for the 1.5 m diurnal boundary tide regime in (C) minimum and (D) maximum (max.) regional palaeobathymetries indicate that the modeled maximum bed shear stress is strongly dependent on regional palaeobathymetry (Fig. 14D, E). After Mitchell et al. (2010).

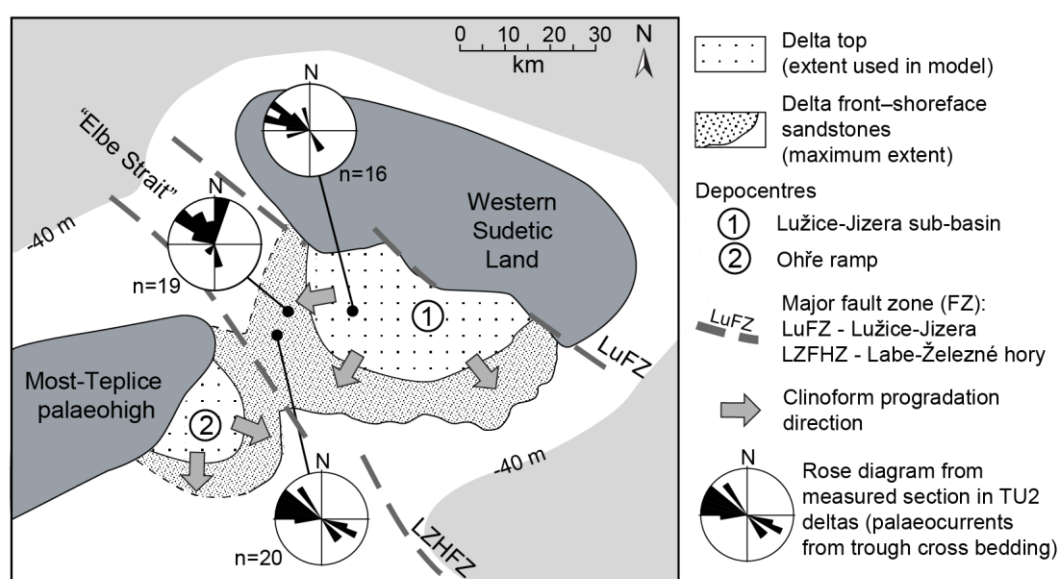


**Fig. 18.** Close-up view of the Elbe Strait area within the BCB (Fig. 15), showing the progradation extent and direction of sandy clinoforms (Voigt and Tröger, 1996; Uličný et al., 2009), and typical palaeocurrent rose diagrams for small-scale cross-sets in clinoforms recording intermediate regression of TUR 2 deltas. Circled numbers indicate (1) the Lužice-Jizera Sub-basin; (2) the Ohře Ramp.

## 4 DISCUSSION

### 4.1 Comparing tidal model and rock record data

The comparison of palaeotidal model to rock-record data involves the evaluation of different data types with contrasting dimensions and spatial-temporal scales (Fig. 19). This review has highlighted favourable comparisons between palaeotidal model predictions of tidal range and tidal bed shear stress with the occurrence of tidally-influenced strata in the spatial and temporal domains of the respective models. However, the comparison of palaeotidal model results and the time-equivalent rock record is limited by three key challenges: (1) confidently recognising tidal influence in the rock record, (2) inferring ancient bed shear stress and, especially, tidal range, and (3) the spatial and temporal resolutions of palaeogeographic data and subsequent interpretations underpinning palaeotidal simulations (e.g. basin morphology, palaeobathymetry, gross depositional environments).

Palaeogeographic reconstructions underpinning palaeotidal simulations involve combining, simplifying and averaging multiple geological data types (e.g. sedimentological, biostratigraphic, seismic). Each data type contains uncertainties, especially the quality and resolution of age dating and geological interpretations ([Markwick and Valdes, 2004](#)). With increasing spatial extent, the minimum temporal resolution of the geologic data underpinning palaeogeographic maps generally coarsens, becomes more variable and forms a composite ‘time-slice’ rather than a single ‘time plane’ (Fig. 19A).

Palaeotidal modelling provides areal (2D) and temporal data on three main parameters: (1) tidal amplitude, (2) tidal range and (3) tidal bed shear stress (magnitude and direction of instantaneous, mean and maximum values). In existing palaeotidal simulations, the maximum spatial resolution of computational meshes is on the order of 10 km and the temporal duration represented by a composite ‘timeslice’ (i.e. time interval) is typically c. 2–5 Ma (Fig. 19B and C), but both vary on a case-by-case basis (Table 3). Rock record data is typically one-dimensional (e.g. stratigraphic logs, core and well data), occasionally two-dimensional (e.g. outcrop panels, well-log correlation panels, seismic cross-sections and maps) and rarely three-dimensional (e.g. curvilinear and/or multiple outcrop panels, multiple and closely-spaced cores and wells, 3D seismic volumes) (Fig. 19B). Such data may lie at spatial resolutions much smaller than those of palaeotidal model meshes and model timeslices. It is possible to address the discrepancy in spatial scales between rock record data and palaeotidal models by combining rock record data from multiple locations, although such amalgamation of data should be carried out carefully so as not to obscure important local patterns. For example, in palaeotidal models of the BCB (Section 3.3), instantaneous bed shear stress provides a more reliable model output for



comparison with rock-record palaeocurrent data than values of mean and maximum bed shear stress collated over multiple tidal cycles ([Mitchell et al., 2010](#)).

Facies modelling aimed at deciphering the relative influence of tide, wave and fluvial processes involves analysis at a wide range of scales, from facies (mm–m) to systems tracts (10–100s km) ([Van Wagoner et al., 1990](#); [Walker and James, 1992](#); [Posamentier and Walker, 2006](#); [Hampson et al., 2008](#)). [Vakarelov and Ainsworth \(2013\)](#) have formalized this approach for shoreline depositional systems into five stratigraphic hierarchical levels, each with different spatial resolutions and dimensions (Fig. 20): (1) facies (element), a component of a depositional element; (2) facies association (element set), a depositional environment; (3) a facies model for part of a depositional system (element complex assemblage); (4) a facies model for a whole depositional system (element complex assemblage set); and (5) a transgressive-regressive tongue or parasequence, which captures the temporal evolution of the facies model for a whole depositional system during one episode of shoreline advance and subsequent retreat. Comparing tidal model and rock-record data most often occurs at the facies, facies-association and parasequence levels, and possibly at larger scales (e.g. parasequence set). This is due in part to data availability, but also because the variability in process dominance and preservation typically increases up the stratigraphic levels. For example, mixed-energy depositional systems (level 4 and above) often comprise several depositional sub-environments (level 3) with varying degrees of tide, wave and/or fluvial influence (e.g. [Ainsworth et al., 2011](#); [Vakarelov and Ainsworth, 2013](#)).

Deciphering the degree and extent of tidal influence is further complicated by incomplete stratigraphic preservation, including preservational bias. Tidal deposits may be preferentially preserved in a wide range of depositional environments but with variable extent and significance. For example, such deposits are often particularly significant in coastal embayments and at the mouths of fluvially incised valleys, but geographically restricted elsewhere, such as in tidal inlets within larger barrier-lagoon systems. However, the maximum resolution of computational meshes used in palaeotidal modelling, especially for regional-scale studies, is significantly larger than the typical spatial dimensions of facies (mm–m) and facies associations (1–100s m) (Fig. 19B). Furthermore, across all spatial scales, the topographically lower components of these depositional systems have higher preservation potential and, generally, their deposits tend to be coarser grained ([Dalrymple, 2010a](#)). Hence there is an almost inevitable bias in the preserved sedimentary and stratigraphic features indicative of certain depositional processes and sub-environments. For example, in a mixed fluvial-tidal setting with channel-bar topography, fluvial currents are likely to preferentially influence coarser-grained

deposition in deeper channel axes, with variable superimposed influence of tides, especially ebb tidal currents. These coarser-grained deposits are likely to have a higher preservation potential compared to finer-grained, typically more heterolithic and more strongly tide-influenced deposits of topographically higher parts of tidal bars (e.g. [Levell et al., 2020](#)). Consequently, despite a depositional environment reflecting mixed river and tidal processes, fluvially influenced deposits may be preferentially preserved and the record of tidal deposition diminished. This is further supported by the frequent paucity of intertidal deposits and dominance of subtidal deposits in many ancient tide-dominated successions ([Legler et al., 2013](#); [van Cappelle et al., 2016](#); [Archer et al., 2019](#); [Collins et al., 2020](#); [Levell et al., 2020](#)). Consequently, the comparison of model to rock-record data may be biased by the varying preservation of tide-influenced deposits in relation to spatial and temporal changes in depositional processes across a range of scales. These primary depositional biases are further exacerbated where limited rock-record data is available in the present-day and where data are selectively compared to model results.

For one- and two-dimensional stratigraphic data, interpretation of areal depositional morphology and its relationship to the depositional system scale are typically guided by comparison to process-based interpretations of modern shoreline environments (Fig. 20B). Process-based classifications of modern shoreline systems are principally based on 2D areal morphology, ideally supported by data on hydrodynamics and sediment type (e.g. [Coleman and Wright, 1975](#); [Galloway, 1975](#); [Hayes, 1979](#); [Boyd et al., 1992](#); [Hori and Saito, 2007](#); [Ainsworth et al., 2011](#); [Nyberg and Howell, 2016](#)) and sedimentary facies characteristics (e.g. [Ta et al., 2002a](#); [Lambiase et al., 2003](#); [Salahuddin and Lambiase, 2013](#); [Fanget et al., 2014](#); [Gugliotta et al., 2018](#)). Hence, the 2D morphologies of end-member tide-, wave- and fluvial-dominated shorelines are embedded in ternary-process models of shoreline depositional systems ([Ainsworth et al., 2011](#); [Vakarelov and Ainsworth, 2013](#); [Nyberg and Howell, 2016](#)).

Tide-dominated shorelines typically display the following morphological characteristics: (1) complex and intricately branching networks of funnel-shaped (seaward-flaring) tidal channels, (2) elongate tidal bars (mainly subtidal but often with subaerial tops), which partly infill tidal channels and often extend seaward from channel mouths, and (3) more extensive ('land-fringing') intertidal and supratidal areas with, depending principally on latitude, salt marsh or mangrove colonization (e.g. [Ainsworth et al., 2011](#); [Nyberg and Howell, 2016](#)). Tide-dominated shorelines are more likely to be rugose to funnel shaped, and *vice versa*, whereas straighter shorelines are more likely to be wave-dominated, and *vice versa* (e.g. Fig. 2) (e.g. [Ainsworth et al., 2011](#); [Nyberg and Howell, 2016](#)). These

generalized relationships are useful but oversimplified, especially when they are an intrinsic component of algorithms for classifying modern shoreline process regime ([Nyberg and Howell, 2016](#)). For example, this relationship does not include quantifiable variations in tidal range, tidal prism and/or tidal bed shear with shoreline rugosity, or complex related feedbacks (e.g. [D'Alpaos et al., 2010](#)). A more rigorous, albeit ambitious, approach for determining the process regime along shorelines would be to compare measured values of tidal strength (bed shear stress), tidal range, wave strength, wave height and fluvial discharge ([Harris et al., 2002](#)) with those from numerical models, preferably including data assimilation.

The temporal resolution of rock-record data is highly dependent on the methodology of absolute dating and the degree of interpolation between control ages (Fig. 19C). For example, in the Cretaceous of the Western Interior Basin of North America, an estimated temporal resolution of c. 200 ka has been achieved because high-resolution ammonite biozones have been calibrated to radiometric age dates ([Obradovich, 1993](#)) ([Krystinik and DeJarnett, 1995](#)). In contrast, a paucity of absolute age dates in the Miocene–Pliocene Baram Delta Province, and the vast majority of similar Tertiary delta provinces around the world, means biostratigraphic zones have a temporal resolution of >1 Ma ([Sandal, 1996](#)).



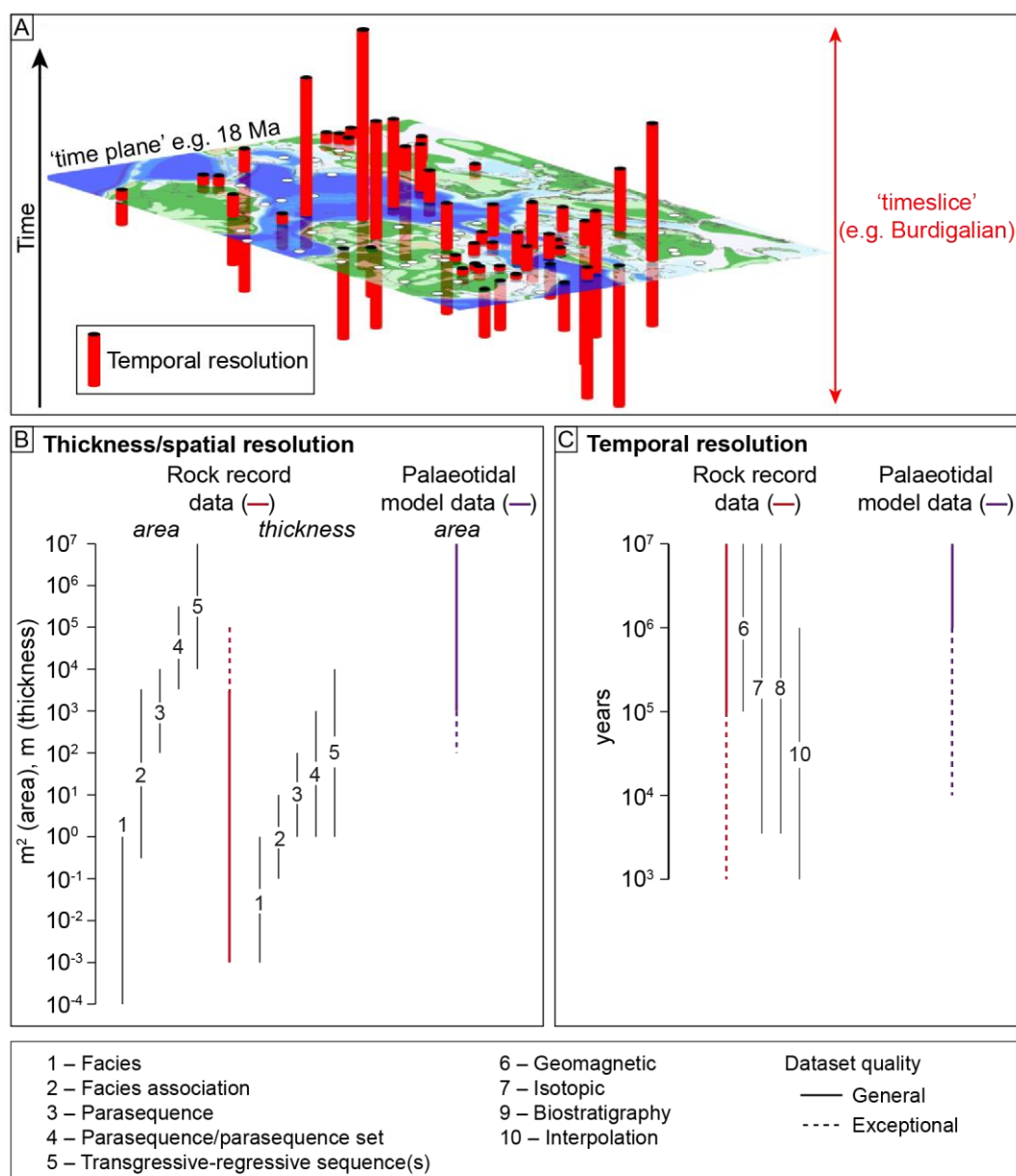


**Fig. 19.** Variable resolution of palaeogeographic, tidal modelling and rock record data. (A) Illustration of the minimum temporal resolution of geologic data underpinning a palaeogeographic 'timeslice' (after [Markwick and Valdes, 2004](#)). Each data point is assumed to represent a single observation of equivalent area, but the temporal resolution of each point is generally variable (red cylinders), due in part to imprecise or uncertain dating and correlation. Defining a timeslice instead of a time-plane maximizes data density. (B) Thickness and spatial resolution of rock and model data. Rock data are differentiated by general versus exceptional dataset quality: in this context, exceptional means extensive and continuous outcrops or several tens of correlated cores and well logs. Numbers 1-5 represent five hierarchical levels of rock data (e.g. the "levels" of [or levels; e.g. Vakarelov and Ainsworth, 2013](#)), showing varying areal and thickness scales (see full text and legend in the bottom panel). Tidal model data is area based. (C) Temporal resolution of rock and model data, showing (i) five hierarchical levels of rock data ([Vakarelov and Ainsworth, 2013](#)); (ii) the most common



## 4.2 Controls on tidal processes and sedimentation

### 4.2.1 Basin physiography

The overall physiography – size, shape and bathymetry – of the Earth’s global ocean, and constituent ocean basins (at present, the Pacific, Atlantic, Southern and Arctic oceans) is the first-order, largest-scale (1000s km) control on astronomical tides. A key consideration for understanding tidal processes and sedimentation along shorelines directly facing ocean basins (i.e. open-ocean shoreline systems) is therefore to estimate the influence of ocean-basin width and depth in controlling tidal resonance (Section 2.2.1). On geological timescales, of the order of 10s–100s Myr plate movements, ocean basins can move in and out of tidal resonant states in response to changing physiography ([Green et al., 2017](#)). For present-day open-ocean systems, there is no obvious systematic, qualitative relationship between tidal amplitude and latitude (e.g. Fig. 4) ([Dalrymple and Padman, 2019](#)). This is due to strong modification of tidal circulation by rotational, funnelling, shoaling and resonance effects, especially in shallower bathymetric areas and shoreline constrictions ([Allen, 1997](#); [Wells, 2008](#); [Dalrymple and Padman, 2015](#); [Dalrymple and Padman, 2019](#)). These effects are complicated and difficult to predict. However, numerical tidal modelling provides a proven, robust method to understand the cumulative influence of these effects. This results in more rigorous and quantitative predictions of tidal potential in modern and ancient, open-ocean systems.

Shoreline systems facing water bodies that are partly enclosed by land, referred to herein as ‘partly enclosed’ systems, have variable degrees of connectivity to adjacent open ocean basin(s), and display a large variation in size (100s to 1000s km) (e.g. present-day North Sea). The case studies presented earlier (Section 3) are all partly enclosed systems. For partly enclosed systems, the foremost control on shoreline tides is the balance between the amount of tidal energy entering and exiting the basin – the tidal inflow and outflow (Fig. 21). Tidal potential is highest when tidal inflow exceeds outflow. Tidal inflow is mainly controlled by the physiography of the basin entrance(s) and the angle between the basin entrance(s) and tidal flow in the adjacent open ocean (Fig. 21A), which principally depends on latitude and Coriolis rotation ([Leeder, 2011](#)). Tidal inflow will be relatively high where open-ocean tides flow directly towards the basin entrance, minimizing loss of tidal energy to frictional damping, and/or the entrance is relatively wide, deep and unobstructed (Fig. 21A). Tidal outflow depends on the number, size, configuration and physiography of outflow connections (Fig. 21B). Tidal outflow is highest if there are multiple, wide, deep and unobstructed outflow connections (Fig. 27B). The tidal energy distribution within partly enclosed systems depends on the relative locations of inflow positions versus outflow positions and embayments, and the tidal flow dynamics within the

basin. This point is clearly illustrated in palaeotidal modelling sensitivity tests of the Lower Greensand Seaway (section 4.2), in which the number and location of tidal inflow and outflow positions is varied (Fig. 12).

Partly enclosed systems may also include relatively shallow (up to a few hundreds of metres) but wide (up to several 100s km) basins, for example, the present-day Baltic Sea and ancient epicontinental seaways. The physiography of these systems may also result in tidal resonance of the incoming boundary tide due to the tidal periodicity matching a natural oscillation frequency of water within the basin. Tidal resonance potential has been approximated for simple, rectangular-shaped, open-ended water bodies (Wells, 2008). However, more complex ancient basin physiographies can be modelled to provide quantitative information on integrated resonance potential for all tidal constituents.

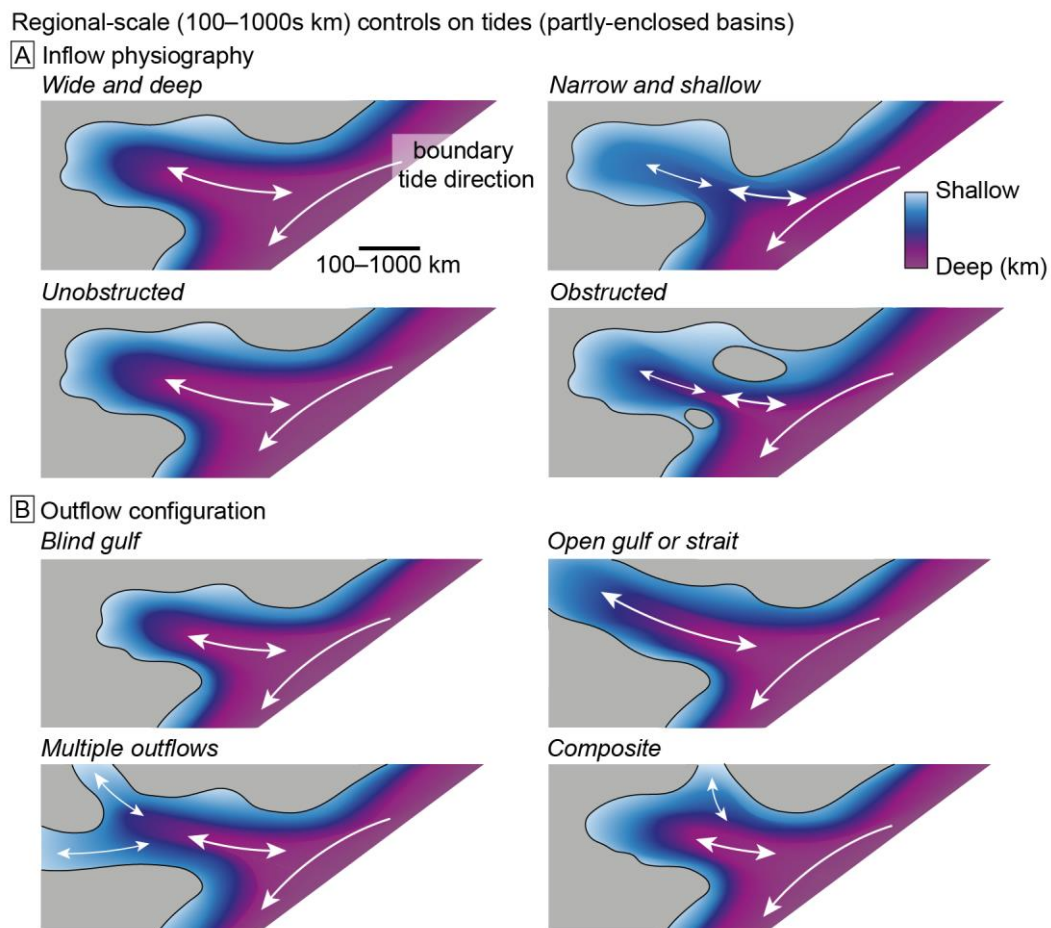


**Fig. 21.** Regional-scale (100–1000s km) basin physiographic controls on tidal energy potential in partly-enclosed basins, related to the balance in tidal energy flux into (inflow) and out (outflow) of the partly enclosed basin. (A) The control of inflow physiography on tidal inflow includes the width, depth and degree of

obstruction of the main tidal inflow position to the basin. Larger, thicker arrows indicate higher tidal energy flux into the partly enclosed basin. (B) The control of outflow physiography on tidal outflow includes the number, width, depth and degree of obstruction of main tidal outflow positions and their configuration with respect to the main tidal inflow positions and boundary tide pathway.

#### 4.2.2 *Tidal resonance on continental shelves*

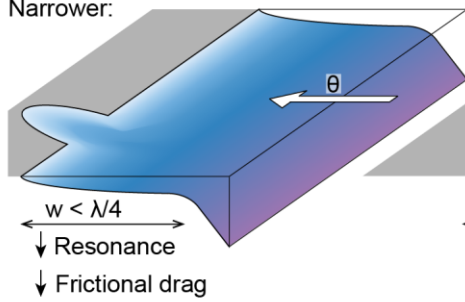
Funnelling, shoaling and resonance effects across continental shelves are widely recognised 10s–100s km-scale controls on tides (sections 2.1.4 and 2.2.1). Analysis of modern tides suggests that the relative importance of tides compared to wave and fluvial processes increases with shelf width perpendicular to the coastline (e.g. [Redfield, 1958](#); [Cram, 1979](#); [Howarth, 1982](#); [Ainsworth et al., 2011](#)). This is principally due to an increase in tidal resonance with shelf width (Section 2.2.1) ([Howarth, 1982](#); [Ainsworth et al., 2011](#)), but some tidal energy will be lost to frictional drag on wider shelves ([Allen, 1997](#)). Furthermore, the relationship between shelf width, tidal range and tidal dominance ([Nyberg and Howell, 2016](#)) varies globally due to changes in the following controls (Fig. 22): (1) the relative amplitude of semi-diurnal to diurnal tidal constituents, which have significantly different wavelengths (e.g. [Kowalik and Luick, 2013](#)); (2) the geometry of continental shelves; (3) the incidence angle of tides and tidal flow patterns, which partly relates to latitude and Coriolis rotation; and (4) frictional effects, which may exceed tidal amplification across wide shelves and seaways. Continental shelf width may change significantly on short geological timescales due to relative sea level changes related to global eustasy, isostatic adjustment, and tectonic subsidence and uplift (e.g. [Miller et al., 2005](#); [Haq, 2014](#); [Sames et al., 2016](#)). Furthermore, within short-term eustatic sea level changes (10–100s ka), shelf width may change due to shoreline progradation, which is likely to be pronounced adjacent to major delta systems (e.g. [Burgess and Hovius, 1998](#); [Hori et al., 2001](#); [Ta et al., 2002a](#); [Chamberlain et al., 2018](#)). In addition, changes to regional-scale tidal flow can supersede the effect of shelf width changes on shelf tidal resonance. For example, despite a decrease in shelf width during 50 m sea-level lowstands, tidal range along northern SCS coastlines was higher during the Late Oligocene–Late Miocene because the boundary tide had a higher tidal range (section 3.1; Figs. 7, 8). Likewise, resonance of the M2 tide in the modern Atlantic Ocean provides a higher boundary tide to the higher latitude Arctic Ocean (Fig. 4A).



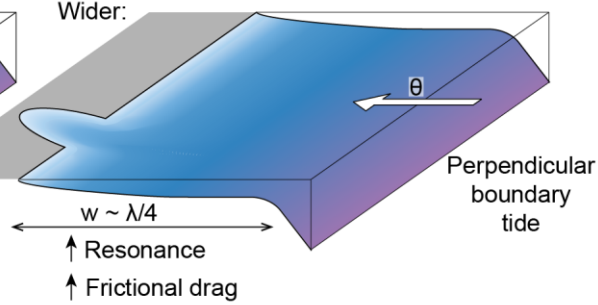
#### Local-scale (10–100s km) controls on continental shelf tidal resonance

##### A Straight shelf (simple resonance scenario)

Narrower:



Wider:



##### B Curvilinear shelf (real-world resonance scenario)

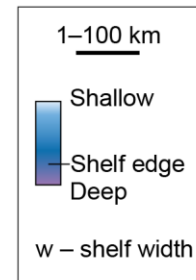
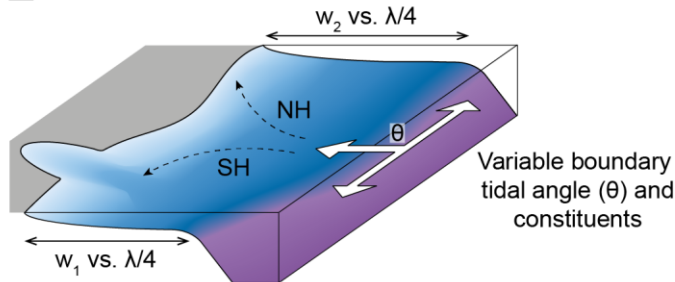


**Fig. 22.** Local-scale (10–100s km) controls on continental shelf tidal resonance. (A–B) Simple resonance scenario for a straight shelf, perpendicular boundary tide and uniform shelf width ( $w$ ), where maximum tidal resonance occurs when shelf width is one-quarter the tidal wavelength ( $\lambda$ ) (after Howarth, 1982). (C) A more realistic resonance scenario for a curvilinear shelf, variable angle ( $\theta$ ) and dominant tidal constituent of the boundary tide, Coriolis rotation and variable shelf width ( $w_1$  versus  $w_2$ ) compared to one-quarter the tidal wavelength. NH = Northern Hemisphere. SH = Southern Hemisphere.

### 4.2.3 Shoreline geometry

Tidal amplification due to funnelling, shoaling and resonance effects in shoreline embayments are potentially very important smaller-scale (1–10s km) controls on tides (e.g. Slingerland, 1986; Dalrymple, 1992; Wells et al., 2007; Ainsworth et al., 2011). However, as outlined below, modern tides and palaeotidal modelling suggest that tidal amplification in coastal embayments is variable and depends on the balance between tidal amplification and frictional damping.

Modern river-linked embayments (e.g. estuaries and interdistributary bays) are typically classified as either hyposynchronous, where tidal range decreases landward because frictional damping exceeds tidal amplification, or hypersynchronous, where tidal range initially increases landward due tidal amplification exceeding frictional damping, before decreasing to the tidal limit (e.g. Godin, 1999; Dalrymple and Choi, 2007). The degree of tidal amplification versus frictional damping can vary between adjacent embayments and show complex patterns within embayments, as seen along eastern

1 North America and western India (Fig. 23). Differentiating between ancient hypersynchronous and  
2 hyposynchronous embayments is difficult and requires interpretation of the process balance and  
3 extent of turbidity maximum zone in the fluvial-to-marine transition zone (e.g. [Gugliotta et al.,](#)  
4 [2016a](#)). However, palaeotidal modelling can reveal spatial and temporal variations in tidal processes  
5 within ancient embayments. For example, as the entrance to the palaeo-Gulf of Thailand became  
6 wider and deeper during the Miocene, greater tidal inflow and reduced frictional damping shifted the  
7 tidal maximum landward (Fig. 7).

11 The relative strength of tidal amplification versus frictional damping depends on several factors:

- 14 (1) The geometry and bathymetry of the embayment, especially its sinuosity (e.g. [Slingerland,](#)  
15 [1986](#); [Allen, 1997](#)). Frictional effects will be higher in more sinuous and rapidly shallowing  
16 embayments compared to straighter, gently shallowing embayments (Fig. 23, 24A).
- 17 (2) The geometry and bathymetry of the embayment entrance impacts inflow and outflow of tidal  
18 energy. A narrower, shallower and obstructed entrance increases dissipation and reflection of  
19 tidal energy (e.g. Mediterranean Ocean; Chesapeake Bay), whereas a wider, deeper and  
20 unobstructed entrance permits greater tidal inflow (e.g. Bay of Fundy) (Figs. 23, 24C).
- 21 (3) The angle between the embayment axis and incoming tide influences tidal inflow. Tidal  
22 inflow increases and frictional effects decrease when the incoming tide is more parallel to the  
23 embayment axis (Fig. 23, 24B).
- 24 (4) Embayment physiography and the dominant tidal constituent control the resonance potential  
25 of embayment tides (Section 2.3).

26 Hyposynchronous embayments are more likely if the tidal inflow and resonance potential are low and  
27 frictional drag potential is high (Fig. 23A). Hypersynchronous embayments are more likely if tidal  
28 inflow and resonance potential are high and frictional drag potential is low (Fig. 23B). However, even  
29 if tidal amplification exceeds frictional effects, embayments may be dominated by fluvial or wave  
30 processes ([Dalrymple, 1992](#)).

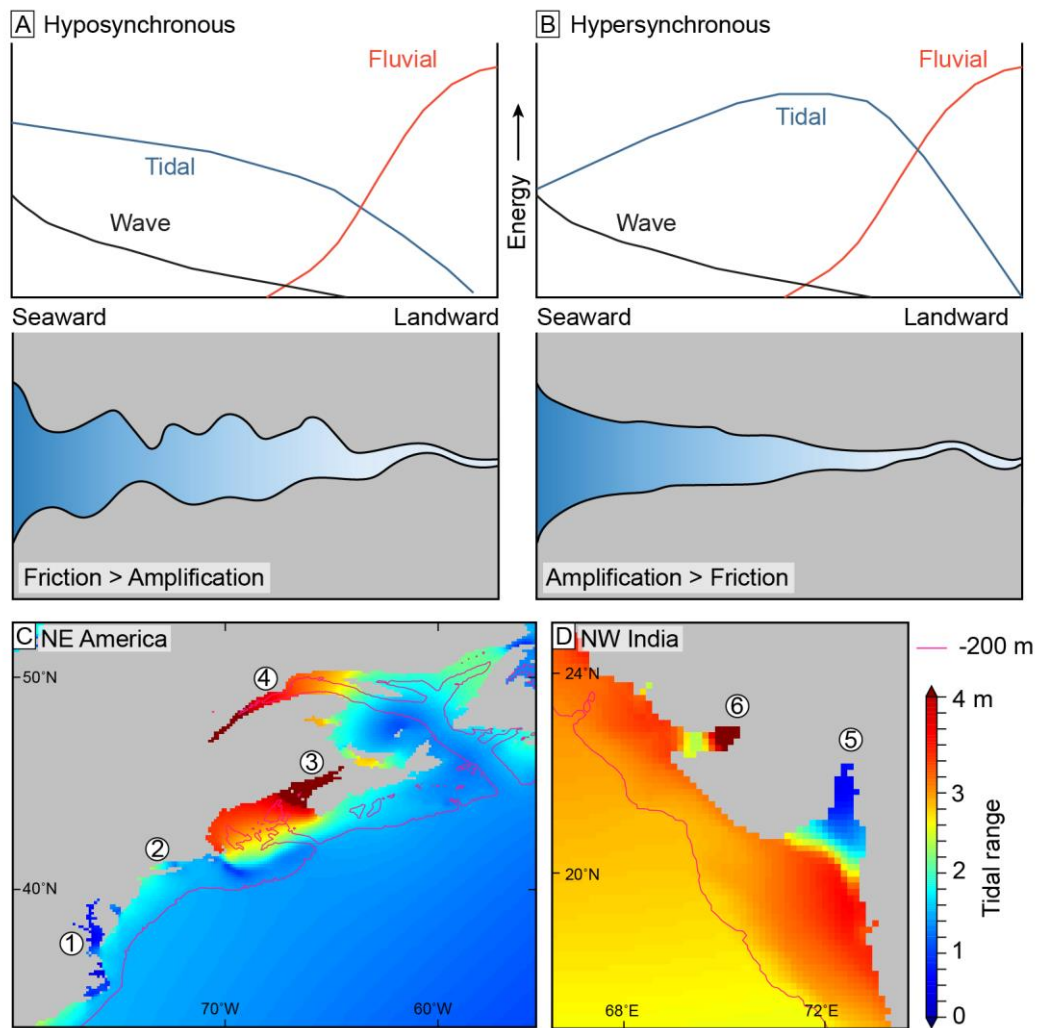


**Fig. 23.** Tides in shoreline embayments. (A) A hyposynchronous system in which frictional damping exceeds amplification of tides due to funneling, shoaling and resonance effect, resulting in a seaward to landward decrease in tidal range and tidal current speed. (B) A hypersynchronous system in which tidal amplification exceeds friction, causing a seaward-to-landward increase in tidal range and current speed, before friction causes tidal range and current speed to decrease to zero at the tidal limit (after Dalrymple and Choi, 2007). (C, D) Modeled tidal range from FES 2012 for north-east America (C) and north-west India (D) illustrating the varying relationship between tidal range and position within adjacent embayments: (1) hyposynchronous Chesapeake Bay; (2) moderately hypersynchronous Long Island Sound; (3) strongly hypersynchronous Bay of Fundy; (4) strongly hypersynchronous St. Lawrence River mouth; (5) strongly hyposynchronous Gulf of Khambhat; and (6) complex hyposynchronous and hypersynchronous Gulf of Kutch.



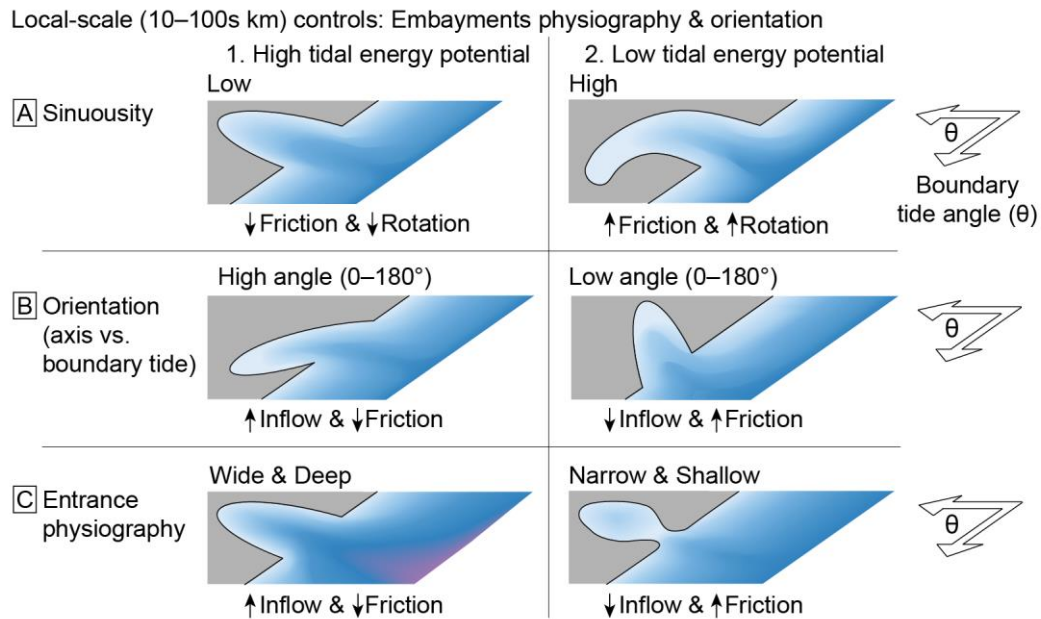


**Fig. 24.** Physiographic controls on tides in shoreline embayments. A schematic matrix includes the influence of (A) shoreline geometry, for example, sinuosity and rugosity, (B) the relative orientation of the embayment axis and incoming tide, and (C) the physiography of the embayment entrance, on (1) high versus (2) low tidal energy potential within the embayment. Note this matrix excludes the influence of wave or fluvial processes.

### 4.3 Modified decision tree for prediction of shoreline–shelf depositional process regime

The original process-based, decision tree hierarchy for predicting shoreline-shelf systems uses the following sequential assessment procedure (Ainsworth et al., 2011) (Fig. 3A): (1) tidal resonance potential, (2) fluvial versus wave effectiveness, (3) low versus high A/S, (4) shoreline geometry (relative degree of rugosity), and (5) coastal process dominance (relative degree of fluvial, wave and tidal processes). We propose replacing this procedure with one that uses two decision trees, reflecting low and high wave energy potential, respectively. The procedure for using each decision tree comprises the following hierarchy (compare Figs. 3A and 26): (1) wave energy potential, (2) tidal energy potential, (3) shelf tidal resonance potential, (4) fluvial potential, and (5) shoreline geometry. The justification for this revision is outlined below, based on the preceding review of tidal theory, the physiographic influence on modern tides and present-day shoreline process regimes (e.g. Nyberg and Howell, 2016), and the physiographic controls on tides highlighted by palaeotidal modelling studies and the time-equivalent stratigraphic record with preserved tidal indicators.

The dominance of wave-dominated process regimes along present-day depositional shorelines (Fig. 2) (Nyberg and Howell, 2016) supports this being the first decision for predicting shoreline process regime (hierarchical query #1 in Fig. 25). In modern systems, the height and strength of wind-generated surface waves are primarily controlled by the speed, duration and fetch of the wind (e.g. Allen, 1997). Wave dominance also depends on the frequency of larger-magnitude storms, overall meteorological conditions and the orientation of the shoreline relative to the wave-generating standing body of water. In ancient domains, determining the speed and duration of wind, and the effect on wave processes, would ideally require sophisticated analyses integrating palaeogeographic reconstructions and numerical climate and wave modelling. More generally, predicting wave energy potential along ancient shorelines relies on larger scale palaeogeographic reconstructions. If a system is open to a large water body or ocean, wave fetch and consequently wave potential would be relatively high. Any protection that restricts access to oceanic waves will lower wave potential (e.g. Ainsworth et al., 2011). Protection from ocean waves may be tectonic (e.g. emergent fault blocks, tectonically controlled seaways) or depositional (e.g. rugose coastal morphology, depositional headland, barrier islands, asymmetrical deltas).

The tidal energy potential of a basin (hierarchical query #2 in Fig. 25) is first dependent on whether the connected open ocean is at resonance with a particular tidal constituent (thus impacting the boundary tide amplitude), and second, whether the study area directly faces the open ocean or instead faces a partly enclosed water body. For systems facing an open ocean, tidal energy potential is assumed to be relatively high because of the relative lack of dissipation effects compared to partly enclosed systems. However, the absolute amount and distribution of tidal energy in an open-ocean basin relates to its size, shape, bathymetry, which together determine resonance, and only partly relates to latitude (Dalrymple and Padman, 2019). As discussed (Section 4.2.1), the tidal energy potential in partly enclosed systems depends on the balance of tidal energy inflow versus outflow (Fig. 21), as well as resonance (Section 2.2.1).

Shelf resonance potential (hierarchical query #3 in Fig. 25) is related to shelf width and the dominant tidal constituent of the incoming tide (Figs. 4, 23). Analysis of modern shoreline processes suggest a cut-off of c. 75 km between mainly tide-dominated (>75 km) and wave-dominated (<75 km) systems (Ainsworth et al., 2011). However, tides only dominate on c. 50% of depositional shorelines associated with shelf widths of >75 km, with 47% being wave dominated (Fig. 2) (Nyberg and Howell, 2016). This suggests that a more representative shelf width threshold may be even higher, which would be closer to the theoretical shelf width for resonance of the typically dominant semi-

diurnal M<sub>2</sub> or diurnal K<sub>1</sub> tidal components (Fig 23). However, without a more accurate and globally applicable cut-off value, the 75 km cut-off is retained in the proposed process prediction decision tree (Fig. 25). Nevertheless, this should be critically assessed on a case-by-case basis, considering other local geological factors.

Assessing fluvial potential (hierarchical query #4 in Fig. 25) relies on (1) measured or inferred drainage area, hinterland relief and rock types ([Milliman and Syvitski, 1992](#); [Syvitski and Milliman, 2007](#); [Sømme et al., 2009](#)); (2) palaeoclimate and its effects on water and sediment discharge ([Hovius, 1998](#); [Syvitski et al., 2003](#); [Milliman and Farnsworth, 2011](#)), and/or (3) observational evidence of fluvial influence in the rock record ([Bhattacharya and Walker, 1992](#); [MacEachern and Bann, 2008](#); [Ainsworth et al., 2016](#)). In general, large drainage basins would have higher fluvial potential than smaller drainage basins. Conversely, large rivers may have a disproportionate likelihood of being strongly tide influenced, or even tide dominated, at their mouth because of the larger tidal prism that is generated by the width of the river channel and its flat gradient, promoting long-distance penetration of the tide ([Dalrymple, 2010b](#)). An exception may be river systems with short, steep drainage basins subject to high rainfall storms, which often preserve river-influenced shoreline deposits (e.g. [Bhattacharya and MacEachern, 2009](#); [Collins et al., 2017b](#)). The overwhelming dominance of wave- and tide-dominated shoreline morphologies along present-day coastlines indicates effective reworking of riverine sediment by marine processes (Fig. 6). However, sedimentary dynamics and deposition may still be dominated by river floods, even in deltas with lobate-to-cusate geometries typical of wave dominance ([Rodriguez et al., 2000](#); [Fielding et al., 2005](#); [Gani and Bhattacharya, 2007](#)). Consequently, for ancient shoreline systems, any information indicating close proximity to a river system may suggest relatively high potential for river influence (Fig. 25).

Shoreline geometry (hierarchical query #5 in Fig. 25) mainly relates to the degree of rugosity, recognizing that tides are commonly amplified in many modern embayments and along embayed shorelines. However, modern embayments and those in palaeotidal simulations are not exclusively tide dominated (e.g. Figs. 2, 4, 26; cf. Fig. 2) due to variations in the balance between frictional damping and tidal amplification, due to funnelling, shoaling and/or resonance (as discussed in Section 4.2.3). Embayed shorelines are also inevitably more protected from direct wave processes. However, wave processes may still be dominant along the back of moderately embayed shorelines, especially where embayment mouths allow direct access to open ocean waves (Fig. 25). In fluvially linked

embayments, river processes may dominate over tides and waves (e.g. Dalrymple and Choi, 2007). Therefore, shoreline geometry can have a variable potential influence on depositional processes.

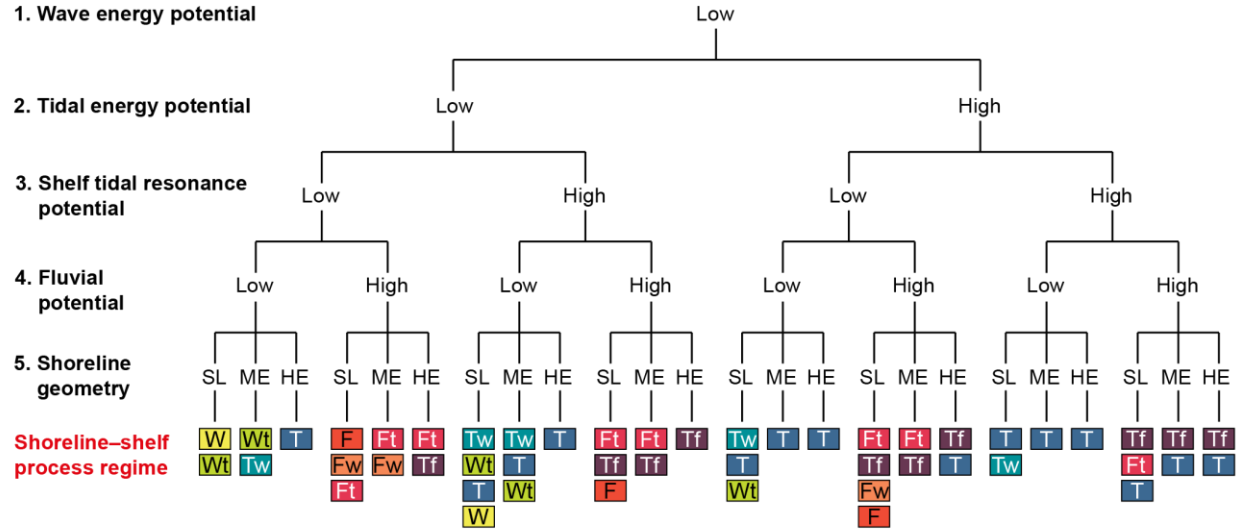
The A/S ratio of a shoreline–shelf system is a widely-used theoretical concept that links tectonics, eustatic sea-level change and sediment supply (Muto and Steel, 1997), and features prominently in the original process-based decision tree of Ainsworth et al. (2011) (hierarchical query #3 in Fig. 3A). However, A/S ratio has been removed from our revised predictive decision tree (Fig. 25) due to limitations with the concept. For example, identifying relatively ‘high’ and ‘low’ A/S ratio relies on generalized relationships between A/S ratio and sequence stratigraphic systems tracts, which in turn relies on extensive datasets for sequence stratigraphic and/or shoreline trajectory analysis (Ainsworth et al., 2008). Quantification of ‘high’ versus ‘low’ A/S ratios also relies upon sufficient well log, core and/or outcrop data to calculate the thickness of a sedimentary unit to approximate accommodation and the sand-to-shale ratio and approximate coarse sediment supply rate (Ainsworth, 2003; Ainsworth, 2005; Ainsworth et al., 2008; Ainsworth et al., 2018). However, even if sufficient data are available, the exact ratios for ‘high’ and ‘low’ A/S regimes are yet to be determined. The reliance on available data and interpretations reduces the applicability of the A/S ratio for predicting shoreline processes in ancient systems, especially where data are limited. Furthermore, the A/S ratio is a subordinate control on tides compared to the tidal energy potential of a basin, shelf tidal resonance potential and shoreline geometry. Process changes relating to A/S ratio only apply for moderately- to highly-embayed shorelines and are captured in changes to shoreline geometry (Section 1.2) (Ainsworth et al., 2011).

We propose to replace the original three-tier process prediction scheme (Figs. 3A) (Ainsworth et al., 2011) with a two-tier scheme that reflects the primary and secondary processes (Figs. 1, 26). Analysis of modern shorelines suggests the thresholds for process classification in a three-tier scheme can be ambiguous (e.g. Fig. 2) (Nyberg and Howell, 2016). While a three-tier scheme has the superficial appearance of greater precision (Figs. 1A, 3) (Ainsworth et al., 2011), it requires definitive process classification and potential quantification of formative processes for sedimentary structures that is rarely, if ever, possible. At present, the range of mixed-process sedimentary structures and variability between different modern and ancient depositional systems is incomplete, including ambiguities in the process interpretations of several sedimentary structures (Section 2.2). A more holistic framework for interpreting mixed-process deposition and preservation would also include the effect of grain size availability on sedimentary facies characteristics and preservation, plus integration with a range of observational and interpretational techniques from both modern and ancient systems (including

numerical modelling). However, such holistic analysis of the ancient record is still limited by several factors, notably preservation bias, dataset quality, and time available for data study. The process prediction scheme proposed herein provides a quick, easily applied and robust interpretation of shoreline–shelf process regime to use, test and refine in subsequent studies. The scheme directly incorporates learnings from several numerical tidal modelling studies and can therefore be applied with a fair degree of confidence in the absence of potentially time-consuming and expensive numerical modelling.

Decision trees for prediction of shoreline–shelf depositional process regime

**A Low wave energy potential:**



**B High wave energy potential:**

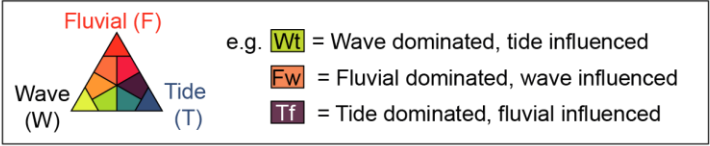
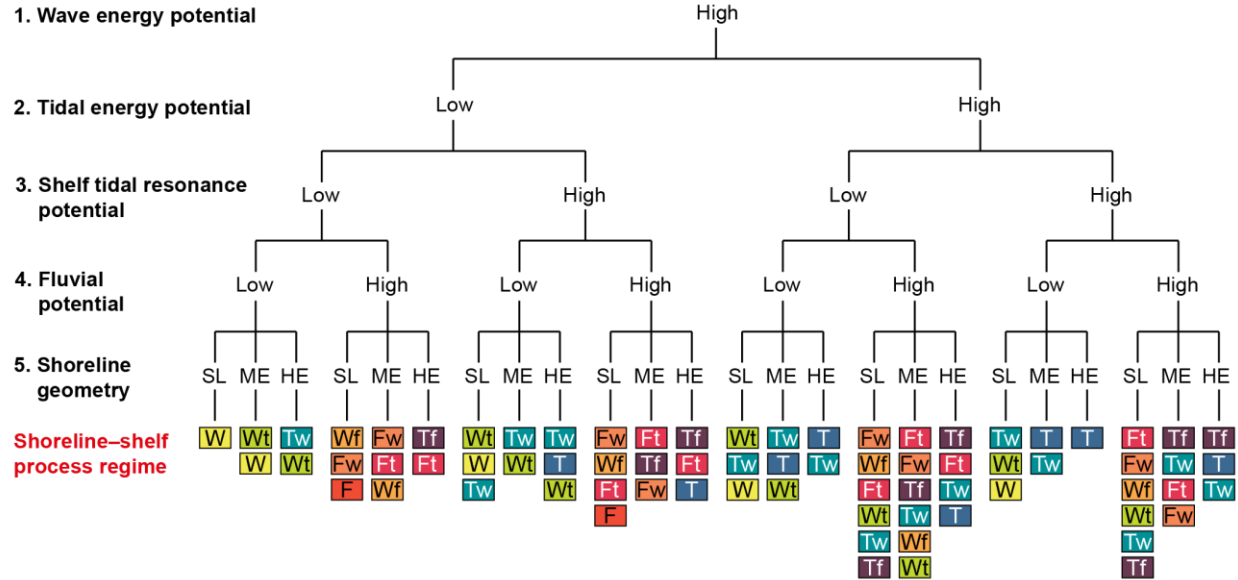


**Fig. 25.** Proposed revision to decision trees for predicting shoreline process dominance (cf. Fig. 3A) (after Ainsworth et al., 2011) for systems with (A) low wave energy potential, and (B) high wave energy. The two decision trees each include five hierarchical queries: (1) wave energy potential of the basin; (2) tidal energy potential of the basin; (3) shelf tidal resonance potential; (4) fluvial potential; and (5) shoreline geometry. Key to colour coding is shown in the inset. Shoreline geometry abbreviations: SL-straight/lobate; ME-moderately embayed; HE-highly embayed.

## 5 CONCLUSIONS

For shoreline–shelf systems, river, wave (including storm) and tide interactions are the primary determinants of sediment transport, morphodynamics and sedimentary preservation and are the cornerstones of process classification schemes. The preserved sedimentary record of these process interactions is widely interpreted, though the range of characteristics and corresponding process interpretation are debated and often ambiguous. Understanding the controls on river, wave and tidal processes benefits from an integrated approach combining numerical modelling and traditional facies analysis, which in turn improves prediction of shoreline–shelf processes classifications. We illustrate this approach in three case studies that combine palaeotidal modelling with process-based facies analysis of time-equivalent stratigraphy. The inferred controls on tides are discussed in the context of modern tidal processes and shoreline–shelf process regimes, resulting in a modification of predictive classification schemes for shoreline–shelf systems.

Tides are controlled by the following physiographic controls: (1) the impact of physiography – size, shape and bathymetry – on tidal resonance in the Earth’s global ocean and constituent ocean basins (1000s km-scale), (2) in partly-enclosed water bodies, the physiography of ocean connections controls the balance between the amount of tidal energy entering and exiting the basin – the tidal inflow and outflow; (3) shelf physiography (10–100 km-scale) and the boundary tide orientation and dominant tidal constituent control shelf tidal resonance; and (4) embayment physiography (1–10 km-scale), especially at the entrance, and the relative orientation of the incoming tide, control tidal amplification (funnelling and shoaling) versus frictional effects in shoreline embayments. Validation of palaeotidal simulations using the rock record requires observations and process interpretations across a range of scales, from facies to depositional sequences, ideally integrating diverse data types. However, the validation is limited by three main uncertainties: (1) ancient tidal range prediction from stratigraphic data; (2) determining the processes of primary sedimentary structures, and (3) preservational bias in the stratigraphic record. In contrast, numerical modelling of tides and other hydrodynamic processes are uniquely powerful tools in providing quantitative insights into the nature and intensity of ancient hydrodynamic processes. We show how this can significantly reduce ambiguities in palaeoenvironmental interpretations in a range of contrasting geological settings.

The overwhelming dominance of waves along modern shorelines indicates existing shoreline–shelf process regime models overstate the role of tides relative to waves. We propose a modified classification scheme for shoreline–shelf process regime that places wave fetch and associated meteorological conditions as the first-order control, with two initial strands for low and high wave energy potential, respectively. These two decision trees each include five hierarchical queries: (1)

1 wave energy potential of the basin; (2) tidal energy potential of the basin; (3) shelf tidal resonance  
2 potential; (4) fluvial potential; and (5) shoreline geometry. The tidal prediction elements of both  
3 decision trees can be significantly enhanced-by calibration with numerical palaeotidal modelling, as  
4 demonstrated by the case studies.  
5  
6  
7

8 Determining process regime from ancient shoreline successions continues to be limited by two critical  
9 aspects: (1) uncertainty and biases in the process classification of common sedimentary structures;  
10 and (2) skewed preservation of certain depositional processes in different environments and on  
11 different timescales. These aspects, combined with the challenges in unravelling modern mixed-  
12 process regimes, lends support to a two-tier, rather than a three-tier, process classification of  
13 shoreline–shelf systems, in which emphasis is placed on only primary and secondary processes. Wider  
14 utilisation of this simpler yet robust predictive classification should enable more consistent and  
15 structured comparisons between ancient shoreline–shelf systems.  
16  
17  
18  
19  
20  
21  
22  
23

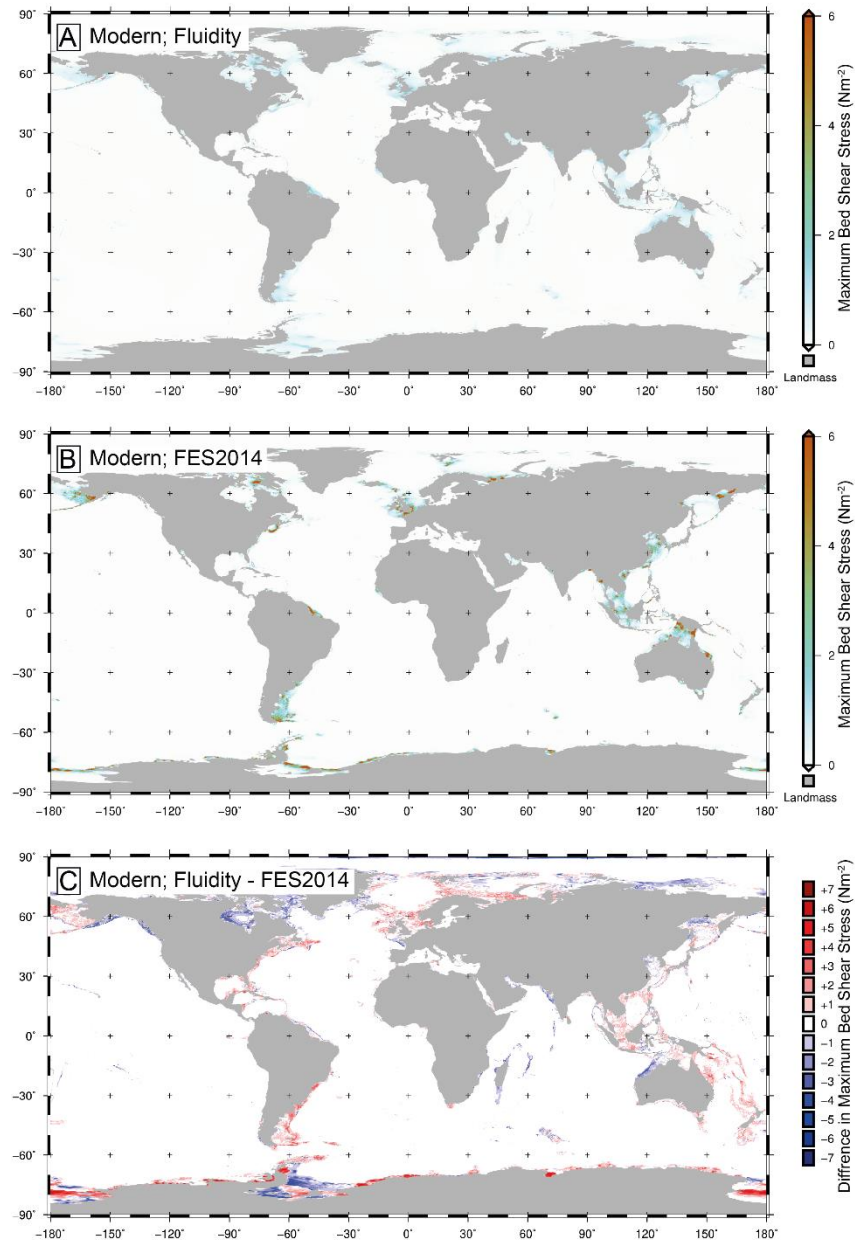
## 24 **ACKNOWLEDGEMENTS**

25 The authors acknowledge financial support from Natural Environment Research Council (NERC),  
26 Leverhulme Trust, Shell International Exploration and Production, and the Academy of Sciences of  
27 the Czech Republic. The authors thank Bob Dalrymple and Zheng Zhou for thorough, constructive  
28 reviewers and Jingping Xu for editorial comments. We also acknowledge support of Getech and  
29 Imperial College’s Grantham Institute and High-Performance Computing Service. D.M. Hodgson,  
30 B.K. Levell, R.B. Ainsworth and B.K. Vakarelov are thanked for valuable comments and discussion.  
31  
32  
33  
34  
35  
36  
37

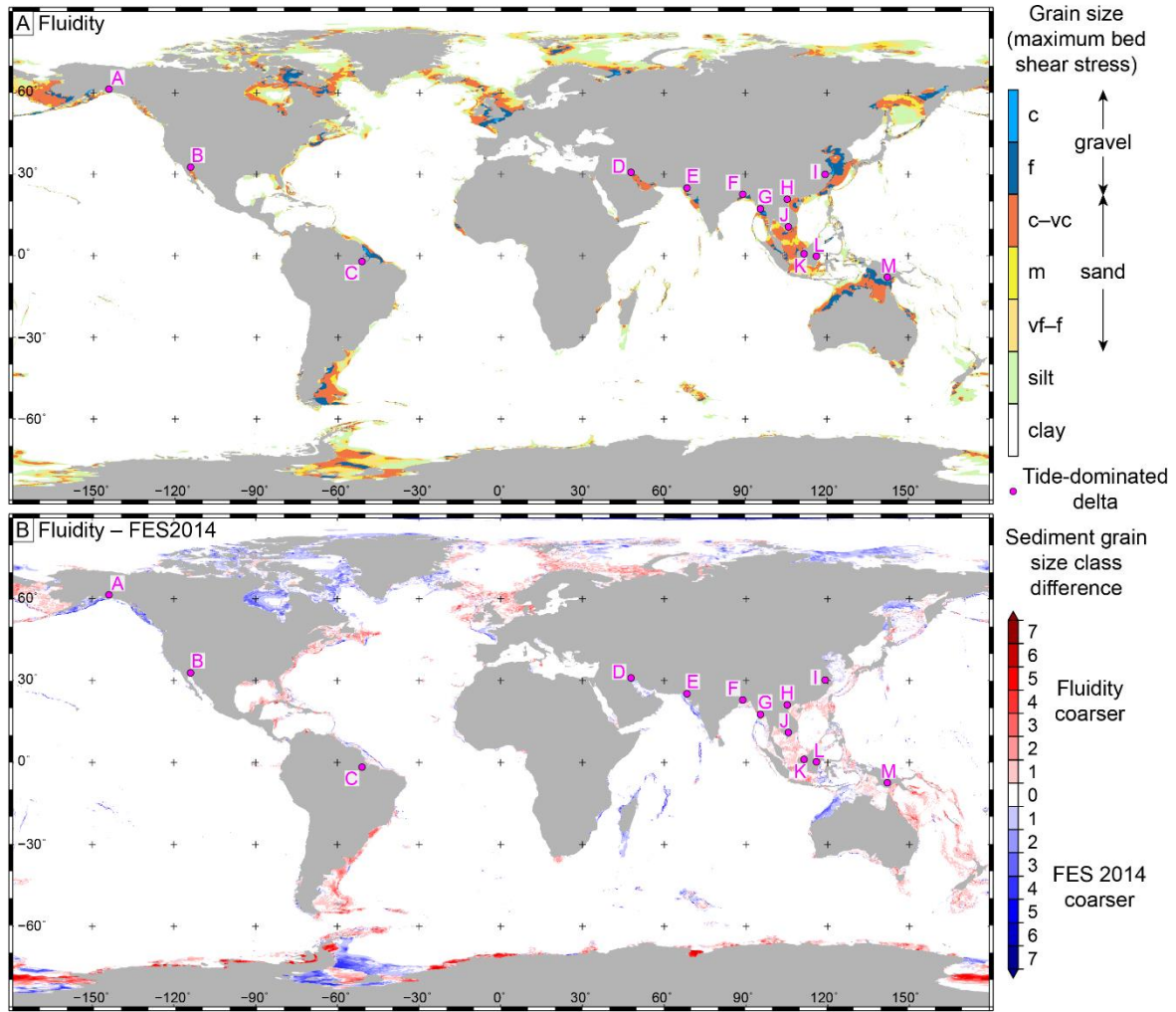
## 38 **SUPPLEMENTARY MATERIAL**

39  
40  
41  
42  
43  
44  
45  
46  
47  
48  
49  
50  
51  
52  
53  
54  
55  
56  
57  
58  
59  
60  
61  
62  
63  
64  
65

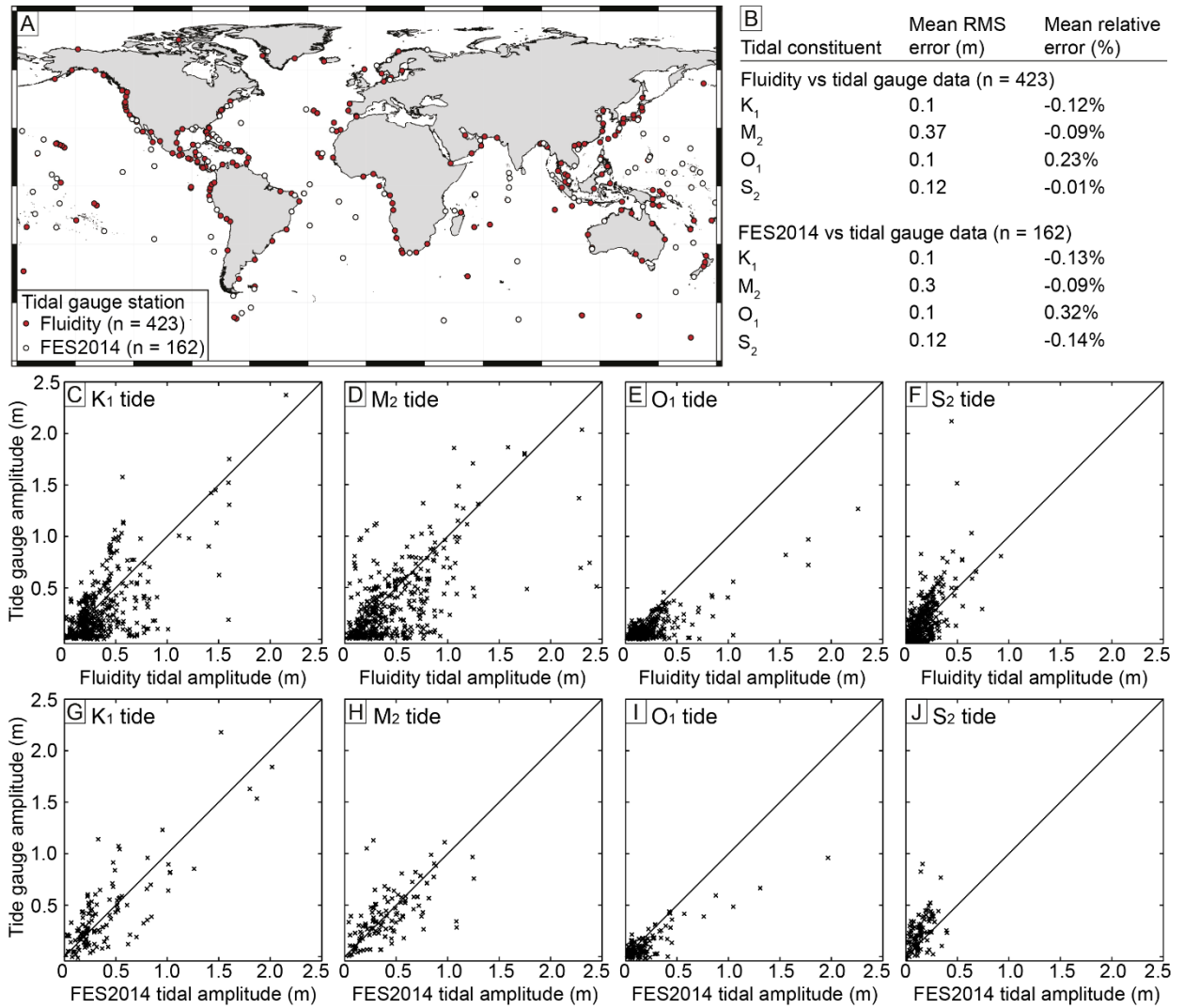




**Supplementary Fig. 1.** Global map of modern tidal bed shear stress calculated from (A) tidal modelling using Fluidity and (B) tidal velocity magnitude from FES2014. C) Difference in maximum tidal bed shear stress between (A) Fluidity and (B) FES2014; Blue indicates FES2014 has a higher maximum tidal bed shear stress.



**Supplementary Fig. 2.** (A) Maximum tidal bed shear stress modeled using Fluidity, plotted as the equivalent grain size that could be entrained if available. (B) Difference in sediment grain size class between maximum tidal bed shear stress for Fluidity (A) and FES2014 (Fig. 2D) (Carrère et al., 2015). Grain size abbreviations: vf = very fine; f = fine; m = medium; c = coarse; vc = very coarse. Pink dots show location of tide-dominated deltas (Goodbred and Saito, 2012): A) Copper; B) Colorado; C) Amazon; D) Shatt-al-Arab; E) Indus; F) Ganges-Brahmaputra; G) Irrawaddy; H) Red River; I) Yangtze; J) Mekong; K) Rajang; L) Mahakam; and M) Fly.



**Supplementary Fig. 3.** Validation of modeled tidal amplitude using Fluidity and FES2014 ([Carrère et al., 2015](#)). (A) Number (n) and position of a global set of tidal stations used for the comparisons to FES2014 (white circles, n = 162) and Fluidity (red circles, n = 423) model data. (B) Summary of root-mean-squared (RMS) and relative percentage errors between the model and tidal gauge data of tidal constituent amplitude. Tidal gauge amplitude data was derived by tidal harmonic analysis of sea surface elevation data. (C–J) Plots of tidal gauge versus modeled tidal amplitude for the  $K_1$  (C, G),  $M_2$  (D, H),  $O_1$  (E, I) and  $S_2$  (F, J) tidal constituents using Fluidity (C–F) and FES2014 (G–J).

## REFERENCES

- Ainsworth, R.B., 2003. Sequence stratigraphic-based analysis of depositional connectivity using 3-D reservoir modelling techniques, University of Liverpool, UK, 310 pp.
- Ainsworth, R.B., 2005. Sequence stratigraphic-based analysis of reservoir connectivity: influence of depositional architecture – a case study from a marginal marine depositional setting. *Petroleum Geoscience*, 11: 257–276.
- Ainsworth, R.B., Flint, S.S. and Howell, J.A., 2008. Predicting coastal depositional style: influence of basin morphology and accommodation to sediment supply ratio within a sequence stratigraphic framework. In: G.J. Hampson, R.J. Steel, P.M. Burgess and R.W. Dalrymple (Editors), *Recent Advances in Models of Siliclastic Shallow-Marine Stratigraphy*. SEPM Special Publication, pp. 237–263.
- Ainsworth, R.B., McArthur, J.B., Lang, S.C. and Vonk, A.J., 2018. Quantitative sequence stratigraphy. *AAPG Bulletin*, 102: 1913-1939.
- Ainsworth, R.B., Vakarelov, B.K., Lee, C., MacEachern, J.A., Montgomery, A.E., Ricci, L.P. and Dashtgard, S.E., 2015. Architecture and evolution of a regressive, tide-influenced marginal marine succession, Drumheller, Alberta, Canada. *Journal of Sedimentary Research*, 85: 596–625.
- Ainsworth, R.B., Vakarelov, B.K., MacEachern, J.A., Nanson, R.A., Lane, T.I., Rarity, F. and Dashtgard, S.E., 2016. Process-Driven Architectural Variability In Mouth-Bar Deposits: A Case Study From A Mixed-Process Mouth-Bar Complex, Drumheller, Alberta, Canada. *Journal of Sedimentary Research*, 86: 512-541.
- Ainsworth, R.B., Vakarelov, B.K. and Nanson, R.A., 2011. Dynamic spatial and temporal prediction of changes in depositional processes on clastic shorelines: Toward improved subsurface uncertainty reduction and management. *AAPG Bulletin*, 95: 267–297.
- Allen, G.P. and Chambers, J.L.C., 1998. Sedimentation in the modern and Miocene Mahakam Delta. Indonesian Petroleum Association, Jakarta, 236 pp.
- Allen, G.P. and Posamentier, H.W., 1993. Sequence stratigraphy and facies model of an incised valley fill; the Gironde Estuary, France. *Journal of Sedimentary Research*, 63: 378-391.
- Allen, J., 1981a. Lower Cretaceous tides revealed by cross-bedding with mud drapes. *Nature*, 289: 579.
- Allen, J.R.L., 1968. Current Ripples: their relation to patterns of water and sediment motion. North Holland, Amsterdam, 433 pp.
- Allen, J.R.L., 1981b. Palaeotidal speeds and ranges estimated from cross-bedding sets with mud drapes. *Nature*, 293: 394-396.
- Allen, J.R.L., 1982a. Mud drapes in sand-wave deposits: a physical model with application to the Folkestone Beds (early Cretaceous, southeast England). *Philosophical Transactions of the Royal Society of London A: Mathematical, Physical and Engineering Sciences*, 306: 291-345.
- Allen, J.R.L., 1982b. Sedimentary structures, their character and physical basis, 1. Elsevier, Amsterdam, 592 pp.
- Allen, P. and Homewood, P., 1984. Evolution and mechanics of a Miocene tidal sandwave. *Sedimentology*, 31: 63-81.
- Allen, P.A., 1997. *Earth Surface Processes*. Blackwell Scientific Publications, Oxford, U.K., 404 pp.
- Amir Hassan, M.H., Johnson, H.D., Allison, P.A. and Abdullah, W.H., 2013. Sedimentology and stratigraphic development of the upper Nyalau Formation (Early Miocene), Sarawak, Malaysia: A mixed wave- and tide-influenced coastal system. *Journal of Asian Earth Sciences*, 76: 301–311.
- Amir Hassan, M.H., Johnson, H.D., Allison, P.A. and Abdullah, W.H., 2016. Sedimentology and stratigraphic architecture of a Miocene retrogradational, tide-dominated delta system: Balingian Province, offshore Sarawak, Malaysia. In: G.J. Hampson, A.D. Reynolds, B. Kostic and M.R. Wells (Editors), *Sedimentology of Paralic Reservoirs: Recent Advances*. Special Publications. Geological Society of London, London, UK, pp. SP444.12, 36 p.

- Anderton, R., 1976. Tidal-shelf sedimentation: an example from the Scottish Dalradian. *Sedimentology*, 23: 429-458.
- Androsof, A., Kagan, B., Romanenkov, D. and Voltzinger, N., 2002. Numerical modelling of barotropic tidal dynamics in the strait of Messina. *Advances in Water Resources*, 25: 401-415.
- Anthony, E.J. and Orford, J.D., 2002. Between wave-and tide-dominated coasts: the middle ground revisited. *Journal of Coastal Research*, 36: 8-15.
- Anthony, E.J., Oyédé, L.M. and Lang, J., 2002. Sedimentation in a fluvially infilling, barrier- bound estuary on a wave- dominated, microtidal coast: the Ouémé River estuary, Benin, west Africa. *Sedimentology*, 49: 1095-1112.
- Archer, A.W., 1995. Modeling of cyclic tidal rhythmites based on a range of diurnal to semidiurnal tidal-station data. *Marine Geology*, 123: 1-10.
- Archer, A.W., Kvale, E.P. and Johnson, H.R., 1991. Analysis of modern equatorial tidal periodicities as a test of information encoded in ancient tidal rhythmites. In: S. DG, R. GE, Z. BA and R. RA (Editors), *Clastic Tidal Sedimentology*. Memoir of the Canadian Society of Petroleum Geologists, pp. 189-196.
- Archer, S.G., Steel, R.J., Mellere, D., Blackwood, S. and Cullen, B., 2019. Response of Middle Jurassic shallow-marine environments to syn-depositional block tilting: Isles of Skye and Raasay, NW Scotland. *Scottish Journal of Geology*, 55: 35-68.
- Arnott, R.W.C. and Southard, J.B., 1990. Exploratory flow-duct experiments on combined-flow bed configurations, and some implications for interpreting storm-event stratification. *Journal of Sedimentary Research*, 60: 211-219.
- Avdis, A., Candy, A.S., Hill, J., Kramer, S.C. and Piggott, M.D., 2018. Efficient unstructured mesh generation for marine renewable energy applications. *Renewable Energy*, 116: 842-856.
- Banks, N., 1973. Tide- dominated offshore sedimentation, Lower Cambrian, north Norway. *Sedimentology*, 20: 213-228.
- Barckhausen, U., Engels, M., Franke, D., Ladage, S. and Pubellier, M., 2014. Evolution of the South China Sea: Revised ages for breakup and seafloor spreading. *Marine and Petroleum Geology*, 58: 599-611.
- Barckhausen, U. and Roeser, H.A., 2004. Seafloor spreading anomalies in the South China Sea revisited. In: P. Clift, W. Kuhnt, P. Wang and D. Hayes (Editors), *Continent-Ocean Interactions Within East Asian Marginal Seas*. Geophysical Monograph Series. AGU, Washington, DC, pp. 121-125.
- Basilici, G., de Luca, P.H.V. and Poiré, D.G., 2012. Hummocky cross-stratification-like structures and combined-flow ripples in the Punta Negra Formation (Lower-Middle Devonian, Argentine Precordillera): A turbiditic deep-water or storm-dominated prodelta inner-shelf system? *Sedimentary Geology*, 267-268: 73-92.
- Belderson, R., Johnson, M., Kenyon, N. and Stride, A., 1982. Bedforms. In: A.H. Stride (Editor), *Offshore tidal sands: processes and deposit*. Chapman and Hall, pp. 27-57.
- Bhattacharya, J.P., 2010. Deltas. In: N.P. James and R.W. Dalrymple (Editors), *Facies Models 4*. Geotext 6. Geological Association of Canada, pp. 233-264.
- Bhattacharya, J.P. and Giosan, L., 2003. Wave-influenced deltas: Geomorphological implications for facies reconstruction. *Sedimentology*, 50: 187-210.
- Bhattacharya, J.P. and MacEachern, J.A., 2009. Hyperpycnal Rivers and Prodeltaic Shelves in the Cretaceous Seaway of North America. *Journal of Sedimentary Research*, 79: 184-209.
- Bhattacharya, J.P. and Walker, R.G., 1992. Deltas. In: R.G. Walker and N.P. James (Editors), *Facies Models: Response to Sea-Level Change*. Geological Association of Canada, St. John's, NL, pp. 157-177.
- Boersma, J. and Terwindt, J., 1981. Neap-spring tide sequences of intertidal shoal deposits in a mesotidal estuary. *Sedimentology*, 28: 151-170.
- Boersma, J.R., 1969. Internal structure of some tidal mega-ripples on a shoal in the Westerschelde estuary, the Netherlands: report of a preliminary investigation. *Geologie en Mijnbouw* (Netherlands Journal of Geosciences), 48: 409-414.

- Boyd, R., Dalrymple, R.W. and Zaitlin, B.A., 1992. Classification of clastic coastal depositional environments. *Sedimentary Geology*, 80: 139-150.
- Boyd, R., Dalrymple, R.W. and Zaitlin, B.A., 2006. Estuarine and incised-valley facies models. In: H.W. Posamentier, Walker, R.G. (Editor), *Facies Models Revisited*. SEPM Special Publication, pp. 171-234.
- Briaies, A., Patriat, P. and Tapponnier, P., 1993. Updated interpretation of magnetic anomalies and seafloor spreading stages in the south China Sea: Implications for the Tertiary tectonics of Southeast Asia. *Journal of Geophysical Research*, 98: 6299-6328.
- Bridges, P.H., 1982. Ancient offshore tidal deposits. In: A.H. Stride (Editor), *Offshore Tidal Sands, Processes and Deposits*. Chapman & Hall, London, UK, pp. 172-192.
- Buatois, L.A., Santiago, N., Herrera, M., Plink-Björklund, P., Steel, R.J., Espin, M. and Parra, K., 2012. Sedimentological and ichnological signatures of changes in wave, river and tidal influence along a Neogene tropical deltaic shoreline. *Sedimentology*, 59: 1568–1612.
- Burgess, P.M. and Hovius, N., 1998. Rates of delta progradation during highstands: consequences for timing of deposition in deep-marine systems. *Journal of the Geological Society*, 155: 217-222.
- Carrère, L., Lyard, F., Cancet, M. and Guillot, A., 2015. FES 2014, a new tidal model on the global ocean with enhanced accuracy in shallow seas and in the Arctic regio, EGU General Assembly 2015, Vienna, Austria.
- Casey, R., 1961. The stratigraphical palaeontology of the Lower Greensand. *Palaeontology*, 3: 487-621.
- Chamberlain, E.L., Törnqvist, T.E., Shen, Z., Mauz, B. and Wallinga, J., 2018. Anatomy of Mississippi Delta growth and its implications for coastal restoration. *Science advances*, 4: eaar4740.
- Chen, S., Steel, R.J., Dixon, J.F. and Osman, A., 2014. Facies and architecture of a tide-dominated segment of the Late Pliocene Orinoco Delta (Morne L'Enfer Formation) SW Trinidad. *Marine and Petroleum Geology*, 57: 208–232.
- Choi, K.S., Dalrymple, R.W., Chun, S.S. and Kim, S.-P., 2004. Sedimentology of modern, inclined heterolithic stratification (IHS) in the macrotidal Han River delta, Korea. *Journal of Sedimentary Research*, 74: 677–689.
- Chung, N.H., Quang, C.D. and Tham, N.T., 2015. A Review of Tertiary Palynomorph Assemblage in Cuu Long Basin: Case Study of Palynomorphs in Miocene–Oligocene Sediments. *International Journal of Sciences: Basic and Applied Research*, 24: 103-111.
- Clifton, H.E., 1983. Discrimination between subtidal and intertidal facies in Pleistocene deposits, Willapa Bay, Washington. *Journal of Sedimentary Research*, 53: 353-369.
- Coates, L. and MacEachern, J.A., 2007. The ichnological signatures of river-and wave-dominated delta complexes: differentiating deltaic and non-deltaic shallow marine successions, Lower Cretaceous Viking Formation and Upper Cretaceous Dunvegan Formation, west-central Alberta. In: J.A. MacEachern, K.L. Bann, M.K. Gingras and S.G. Pemberton (Editors), *Applied Ichnology. Short Course Notes 52*. SEPM, Tulsa, Oklahoma, pp. 227–254.
- Coleman, J.M. and Wright, L.D., 1975. Modern river deltas: variability of processes and sand bodies. In: M.L. Broussard (Editor), *Deltas: Models for Exploration*. Houston Geological Society, Houston, Texas, pp. 99-149.
- Collins, D.S., Avdis, A., Allison, P.A., Johnson, H.D., Hill, J. and Piggott, M.D., 2018a. Controls on tidal sedimentation and preservation: Insights from numerical tidal modelling in the Late Oligocene–Miocene South China Sea, Southeast Asia. *Sedimentology*, 65: 2468-2505.
- Collins, D.S., Avdis, A., Allison, P.A., Johnson, H.D., Hill, J., Piggott, M.D., Amir Hassan, M.H. and Damit, A.R., 2018b. Controls on Tidal Sedimentation and Preservation: Insights from Numerical Tidal Modelling in the Late Oligocene–Miocene South China Sea, Southeast Asia. *Sedimentology*, Accepted; In Press.
- Collins, D.S., Avdis, A., Allison, P.A., Johnson, H.D., Hill, J., Piggott, M.D., Hassan, M.H.A. and Damit, A.R., 2017a. Tidal dynamics and mangrove carbon sequestration during the Oligo–Miocene in the South China Sea. *Nature Communications*, 8: 15698.

- 1 Collins, D.S., Johnson, H.D., Allison, P.A. and Damit, A.R., 2018c. Mixed Process, Humid-Tropical,  
2 Shoreline–Shelf Deposition: Middle Miocene–Modern Baram Delta Province, North-West  
3 Borneo. *Journal of Sedimentary Research*, 88: 399–430.
- 4 Collins, D.S., Johnson, H.D., Allison, P.A., Guilpain, P. and Damit, A.R., 2017b. Coupled ‘storm-  
5 flood’ depositional model: Application to the Miocene–Modern Baram Delta Province, north-  
6 west Borneo. *Sedimentology*, 64: 1203–1235.
- 7 Collins, D.S., Johnson, H.D. and Baldwin, C.T., 2020. Architecture and preservation in the fluvial to  
8 marine transition zone of a mixed- process humid- tropical delta: Middle Miocene Lambir  
9 Formation, Baram Delta Province, north- west Borneo. *Sedimentology*, 67: 1-46.
- 10 Collinson, J. and Mountney, N.P., 2019. *Sedimentary Structures*. Dunedin Academic Press Ltd, 320  
11 pp.
- 12 Colombera, L. and Mountney, N.P., 2020a. Accommodation and sediment- supply controls on clastic  
13 parasequences: A meta- analysis. *Sedimentology*, 67: 1667-1709.
- 14 Colombera, L. and Mountney, N.P., 2020b. On the geological significance of clastic parasequences.  
15 *Earth-Science Reviews*, 201: 103062.
- 16 Cooper, J., 2001. Geomorphological variability among microtidal estuaries from the wave-dominated  
17 South African coast. *Geomorphology*, 40: 99-122.
- 18 Cooper, J.A.G., 1993. Sedimentation in a river dominated estuary. *Sedimentology*, 40: 979-1017.
- 19 Cram, J.M., 1979. The influence of continental shelf width on tidal range: paleoceanographic  
20 implications. *The Journal of Geology*, 87: 441-447.
- 21 Curray, J.R., 1964. Transgressions and regressions. In: R.L. Miller (Editor), *Papers in Marine*  
22 *Geology*. Macmillan, New York, pp. 175-203.
- 23 D'Alpaos, A., Lanzoni, S., Marani, M. and Rinaldo, A., 2010. On the tidal prism–channel area  
24 relations. *Journal of Geophysical Research: Earth Surface*, 115: F01003.
- 25 d'Anglejan, B. and Brisebois, M., 1978. Recent sediments of the St. Lawrence middle estuary. *Journal*  
26 *of Sedimentary Research*, 48: 951-964.
- 27 Dalrymple, R.W., 1992. Tidal depositional systems. In: R.G. Walker and N.P. James (Editors), *Facies*  
28 *Models: Response to Sea Level Change*. Geological Association of Canada, St. John's,  
29 Newfoundland, pp. 195-218.
- 30 Dalrymple, R.W., 2006. Incised valleys in time and space: an introduction to the volume and an  
31 examination of the controls on valley formation and filling. In: R.W. Dalrymple, D.A. Leckie  
32 and R.W. Tillman (Editors), *Incised Valleys in Time and Space*. SEPM Special Publication,  
33 pp. 5–12.
- 34 Dalrymple, R.W., 2010a. Interpreting sedimentary successions: facies, facies analysis and facies  
35 models. In: N.P. James and R.W. Dalrymple (Editors), *Facies Models 4*. Geological  
36 Association of Canada, pp. 3-18.
- 37 Dalrymple, R.W., 2010b. Tidal depositional systems. In: R.W. Dalrymple and N.P. James (Editors),  
38 *Facies models 4*. Geological Association of Canada, St. Johns, NL, pp. 201–231.
- 39 Dalrymple, R.W., 2021. Sedimentation on high- energy sand flats in the Bay of Fundy: The record of  
40 tidal- bore activity and deposition from high- concentration suspensions of sand.  
41 *Sedimentology*, Accepted Article.
- 42 Dalrymple, R.W., Baker, E.K., Harris, P.T. and Hughes, M.G., 2003. Sedimentology and stratigraphy  
43 of a tide-dominated, foreland-basin delta (Fly River, Papua New Guinea). In: F.H. Sidi, D.  
44 Nummedal, P. Imbert, H. Darman and H.W. Posamentier (Editors), *Tropical Deltas of*  
45 *Southeast Asia—Sedimentology, Stratigraphy, and Petroleum Geology*. SEPM Spec. Publ.,  
46 pp. 147–173.
- 47 Dalrymple, R.W. and Choi, K., 2007. Morphologic and facies trends through the fluvial–marine  
48 transition in tide-dominated depositional systems: A schematic framework for environmental  
49 and sequence-stratigraphic interpretation. *Earth-Science Reviews*, 81: 135–174.
- 50 Dalrymple, R.W., Kurcinka, C.E., Jablonski, B.V.J., Ichaso, A.A. and Mackay, D.A., 2015.  
51 Deciphering the relative importance of fluvial and tidal processes in the fluvial–marine  
52 transition. In: P.J. Ashworth, J.L. Best and D.R. Parsons (Editors), *Fluvial–Tidal*  
53 *Sedimentology*. *Developments in Sedimentology*. Elsevier, pp. 3–45.



- Dalrymple, R.W., Mackay, D.A., Ichaso, A.A. and Choi, K.S., 2012. Processes, morphodynamics, and facies of tide-dominated estuaries. In: R.A.J. Davis and R.W. Dalrymple (Editors), *Principles of Tidal Sedimentology*. Springer, New York, pp. 79-108.
- Dalrymple, R.W. and Padman, L., 2015. Tides at high latitudes, AAPG Hedberg Research Conference, Latitudinal Controls on Stratigraphic Models and Sedimentary Concept. AAPG Search and Discovery Article #120178, Banff.
- Dalrymple, R.W. and Padman, L., 2019. Are tides controlled by latitude? . In: C. Fraticelli, A.W. Martinius, J.R. Suter and P.J. Markwick (Editors), *Latitudinal controls on stratigraphic models and sedimentary concepts*. SEPM Special Publication 108, pp. 29-45.
- Dalrymple, R.W. and Rhodes, R.N., 1995. Estuarine dunes and bars. In: P. G.M.E. (Editor), *Geomorphology and Sedimentology of Estuaries*. Developments in Sedimentology. Elsevier, Amsterdam, pp. 359–422.
- Dalrymple, R.W., Zaitlin, B.A. and Boyd, R., 1992. Estuarine facies models: conceptual basis and stratigraphic implications: perspective. *Journal of Sedimentary Petrology*, 62: 1130–1146.
- Davis, R.A. and Dalrymple, R.W., 2012. *Principles of Tidal Sedimentology*. Springer, New York, 621 pp.
- Davis, R.A. and Hayes, M.O., 1984. What is a wave-dominated coast? *Marine Geology*, 60: 313-329.
- De Boer, P.L., Oost, A. and Visser, M., 1989. The diurnal inequality of the tide as a parameter for recognizing tidal influences. *Journal of Sedimentary Research*, 59: 912-921.
- De Raaf, J.F.M. and Boersma, J.R., 1977. Tidal deposits and their sedimentary structures (seven examples from Western Europe). *Geologie en Mijnbouw*, 50: 479-504.
- de Vriend, H.J., Capobianco, M., Cheshier, T., De Swart, H.d., Latteux, B. and Stive, M., 1993. Approaches to long-term modelling of coastal morphology: a review. *Coastal engineering*, 21: 225-269.
- de Vries Klein, G., 1977. Tidal circulation model for deposition of clastic sediment in epeiric and mioclinical shelf seas. *Sedimentary Geology*, 18: 1-12.
- Dean, C.D., Collins, D.S., van Cappelle, M., Avdis, A. and Hampson, G.J., 2019. Regional-scale paleobathymetry controlled location, but not magnitude, of tidal dynamics in the Late Cretaceous Western Interior Seaway, USA. *Geology*, 47: 1083-1087.
- Defant, A., 1961. *Physical Oceanography*, 11. Pergamon, New York, 598 pp.
- Dercourt, J., Gaetani, M., Vrielynck, B., Barrier, E., Biju-Duval, B., Brunet, M.-F., Cadet, J.P., Crasquin, S. and Sandulescu, M., 2000. *Atlas Peri-Tethys Palaeogeographical Maps, I-XX*. CCGM/CGMW, 269 pp.
- Dott, R.H. and Bourgeois, J., 1982. Hummocky stratification: significance of its variable bedding sequences. *Geological Society of America Bulletin*, 93: 663–680.
- Doust, H. and Sumner, H.S., 2007. Petroleum systems in rift basins—a collective approach in Southeast Asian basins. *Petroleum Geoscience*, 13: 127-144.
- Dumas, S. and Arnott, R.W.C., 2006. Origin of hummocky and swaley cross-stratification— The controlling influence of unidirectional current strength and aggradation rate. *Geology*, 34: 1073–1076.
- Egbert, G.D., Ray, R.D. and Bills, B.G., 2004. Numerical modeling of the global semidiurnal tide in the present day and in the last glacial maximum. *Journal of Geophysical Research: Oceans*, 109.
- Elliott, T., 1986. Deltas. In: H.G. Reading (Editor), *Sedimentary environments and facies*. Blackwell Scientific Publications, Oxford, UK, pp. 113-154.
- Ericksen, M.C. and Slingerland, R., 1990. Numerical simulations of tidal and wind-driven circulation in the Cretaceous Interior Seaway of North America. *Geological Society of America Bulletin*, 102: 1499-1516.
- Fanget, A.-S., Berné, S., Jouet, G., Bassetti, M.-A., Dennielou, B., Maillet, G.M. and Tondut, M., 2014. Impact of relative sea level and rapid climate changes on the architecture and lithofacies of the Holocene Rhone subaqueous delta (Western Mediterranean Sea). *Sedimentary Geology*, 305: 35-53.

- Fielding, C.R., Trueman, J. and Alexander, J., 2005. Sedimentology of the modern and Holocene Burdekin River Delta of north Queensland, Australia—controlled by river output, not by waves and tides. In: L. Giosan and J.P. Bhattacharya (Editors), *River Deltas—Concepts, Models, and Examples* Special Publication 18, pp. 467–496.
- Franke, D., Barckhausen, U., Heyde, I., Tingay, M. and Ramli, N., 2008. Seismic images of a collision zone offshore NW Sabah/Borneo. *Marine and Petroleum Geology*, 25: 606–624.
- Galloway, W.E., 1975. Process framework for describing the morphologic and stratigraphic evolution of deltaic depositional systems. In: M.L. Broussard (Editor), *Deltas: Models for Exploration*. Houston Geological Society, Houston, USA, pp. 87–98.
- Gani, M.R. and Bhattacharya, J.P., 2007. Basic building blocks and process variability of a Cretaceous delta: Internal facies architecture reveals a more dynamic interaction of river, wave, and tidal processes than is indicated by external shape. *Journal of Sedimentary Research*, 77: 284–302.
- Gao, C. and Adcock, T.A., 2017. On the tidal resonance of the Bristol Channel. *International Journal of Offshore and Polar Engineering*, 27: 177–183.
- Gardner, M.H., Cross, T.A., Levorsen, M., Chidsey, T., Adams, R. and Morris, T., 2004. Stacking patterns, sediment volume partitioning, and facies differentiation in shallow-marine and coastal-plain strata of the Cretaceous Ferron Sandstone, Utah. In: T.C. Chidsey, R.D. Adams and T.H. Morris (Editors), *Regional to Wellbore Analog for Fluvial–Deltaic Reservoir Modeling: The Ferron Sandstone of Utah*. American Association of Petroleum Geologists, Studies in Geology pp. 95–124.
- Garrett, C., 1972. Tidal resonance in the Bay of Fundy and Gulf of Maine. *Nature*, 238: 441–443.
- Geleynse, N., Storms, J.E.A., Walstra, D.-J.R., Jagers, H.R.A., Wang, Z.B. and Stive, M.J.F., 2011. Controls on river delta formation: insights from numerical modelling. *Earth and Planetary Science Letters*, 302: 217–226.
- Geuzaine, C. and Remacle, J.F., 2009. Gmsh: A 3-D finite element mesh generator with built-in pre- and post-processing facilities. *International Journal for Numerical Methods in Engineering*, 79: 1309–1331.
- Gil, J., García-Hidalgo, J., Segura, M., García, A. and Carenas, B., 2006. Stratigraphic architecture, palaeogeography and sea-level changes of a third order depositional sequence: the late Turonian–early Coniacian in the northern Iberian Ranges and Central System (Spain). *Sedimentary Geology*, 191: 191–225.
- Gingras, M.K. and MacEachern, J.A., 2012. Tidal ichnology of shallow-water clastic settings. In: R.A. Davis and R.W. Dalrymple (Editors), *Principles of Tidal Sedimentology*. Springer, New York, pp. 57–77.
- Gingras, M.K., MacEachern, J.A. and Dashtgard, S.E., 2012. The potential of trace fossils as tidal indicators in bays and estuaries. *Sedimentary Geology*, 279: 97–106.
- Godin, G., 1993. On tidal resonance. *Continental Shelf Research*, 13: 89–107.
- Godin, G., 1999. The propagation of tides up rivers with special considerations on the upper Saint Lawrence River. *Estuarine, Coastal and Shelf Science*, 48: 307–324.
- Golonka, J., 2004. Plate tectonic evolution of the southern margin of Eurasia in the Mesozoic and Cenozoic. *Tectonophysics*, 381: 235–273.
- Golonka, J., 2007. Late Triassic and Early Jurassic palaeogeography of the world. *Palaeogeography, Palaeoclimatology, Palaeoecology*, 244: 297–307.
- Golonka, J., Gahagan, L., Krobicki, M., Marko, F. and Oszczyk, N., 2006. Plate-tectonic evolution and paleogeography of the circum-Carpathian region. In: J. Golonka and F.J. Picha (Editors), *The Carpathians and their Foreland: Geology and Hydrocarbon Resources*. AAPG Memoir, pp. 11–46.
- Gomis-Cartesio, L.E., Poyatos-Moré, M., Flint, S.S., Hodgson, D.M., Brunt, R.L. and Wickens, H.D., 2016. Anatomy of a mixed-influence shelf edge delta, Karoo Basin, South Africa. In: G.J. Hampson, A.D. Reynolds, B. Kostic and M.R. Wells (Editors), *Sedimentology of Paralic*

- Reservoirs: Recent Advances. Special Publication 444. Geological Society of London, pp. SP444.5.
- Goodbred, S.L. and Saito, Y., 2012. Tide-dominated deltas. In: R.A. Davis and R.W. Dalrymple (Editors), *Principles of Tidal Sedimentology*. Springer, New York, pp. 129-149.
- Gordon, A.L., Huber, B.A., Metzger, E.J., Susanto, R.D., Hurlburt, H.E. and Adi, T.R., 2012. South China Sea throughflow impact on the Indonesian throughflow. *Geophysical Research Letters*, 39: 1-7.
- Gorman, G.J., Piggott, M. and Pain, C.C., 2007. Shoreline approximation for unstructured mesh generation. *Computers & geosciences*, 33: 666-677.
- Gorman, G.J., Piggott, M., Wells, M., Pain, C.C. and Allison, P., 2008. A systematic approach to unstructured mesh generation for ocean modelling using GMT and Terreno. *Computers & Geosciences*, 34: 1721-1731.
- Greb, S.F. and Archer, A.W., 1995. Rhythmic sedimentation in a mixed tide and wave deposit, Hazel Patch sandstone (Pennsylvanian), eastern Kentucky coal field. *Journal of Sedimentary Research*, 65: 96-106.
- Green, J. and Huber, M., 2013. Tidal dissipation in the early Eocene and implications for ocean mixing. *Geophysical Research Letters*, 40: 2707-2713.
- Green, J.A.M., Huber, M., Waltham, D., Buzan, J. and Wells, M., 2017. Explicitly modelled deep-time tidal dissipation and its implication for Lunar history. *Earth and Planetary Science Letters*, 461: 46-53.
- Grindrod, J., 1988. The palynology of Holocene mangrove and saltmarsh sediments, particularly in northern Australia. *Review of Palaeobotany and Palynology*, 55: 229-245.
- Gugliotta, M., Flint, S.S., Hodgson, D.M. and Veiga, G.D., 2015. Stratigraphic record of river-dominated crevasse subdeltas with tidal influence (Lajas Formation, Argentina). *Journal of Sedimentary Research*, 85: 265-284.
- Gugliotta, M., Flint, S.S., Hodgson, D.M. and Veiga, G.D., 2016a. Recognition criteria, characteristics and implications of the fluvial to marine transition zone in ancient deltaic deposits (Lajas Formation, Argentina). *Sedimentology*, 63: 1971-2001.
- Gugliotta, M., Kurcinka, C.E., Dalrymple, R.W., Flint, S.S. and Hodgson, D.M., 2016b. Decoupling seasonal fluctuations in fluvial discharge from the tidal signature in ancient deltaic deposits: an example from the Neuquén Basin, Argentina. *Journal of the Geological Society of London*, 173: 94-107.
- Gugliotta, M., Saito, Y., Nguyen, V.L., Oanh Ta, T.K. and Tamura, T., 2018. Sediment distribution and depositional processes along the fluvial to marine transition zone of the Mekong River delta, Vietnam. *Sedimentology*, Accepted; In Press.
- Hadley, D.F., Arochukwu, E.C., Nishi, K., Sarginson, M.J., Salleh, H. and Omar, M., 2006. *Depositional Modelling of Champion Field, Brunei*, Society of Petroleum Engineers Asia Pacific Oil and Gas Conference and Exhibition. Society of Petroleum Engineers, Adelaide, Australia.
- Hall, R., 1996. Reconstructing Cenozoic SE Asia. In: R. Hall and D. Blundell (Editors), *Tectonic Evolution of Southeast Asia*. Geological Society, London, Special Publications, London, UK, pp. 153-184.
- Hall, R., 2002. Cenozoic geological and plate tectonic evolution of SE Asia and the SW Pacific: computer-based reconstructions, model and animations. *Journal of Asian Earth Sciences*, 20: 353-431.
- Hall, R., 2013. The palaeogeography of Sundaland and Wallacea since the Late Jurassic. *Journal of Limnology*, 72: 1-17.
- Hallam, A., 1981. *Facies Interpretation and the Stratigraphic Record*. W.H. Freeman, Oxford, 291 pp.
- Hampson, G.J., 2016. Towards a sequence stratigraphic solution set for autogenic processes and allogenic controls: Upper Cretaceous strata, Book Cliffs, Utah, USA. *Journal of the Geological Society*, 173: 817-836.

- Hampson, G.J., Rodriguez, A.B., Storms, J.E.A., Johnson, H.D. and Meyer, C.T., 2008. Geomorphology and High-Resolution Stratigraphy of Progradational Wave-Dominated Shoreline Deposits: Impact on Reservoir-Scale Facies Architecture. 117-142.
- Hansen, C.D., MacEachern, J.A., Bann, K., Gingras, M. and Pemberton, S., 2007. Application of the asymmetric delta model to along-strike facies variations in a mixed wave-and river-influenced delta lobe, Upper Cretaceous Basal Belly River Formation, central Alberta. In: J.A. MacEachern, K.L. Bann, M.K. Gingras and S.G. Pemberton (Editors), *Applied Ichnology*. SEPM Short Course Notes 52. SEPM, Tulsa, Oklahoma, pp. 255–271.
- Haq, B.U., 2014. Cretaceous eustasy revisited. *Global and Planetary Change*, 113: 44-58.
- Harms, J.C., Southard, J.B. and Walker, R.G., 1982. Structures and Sequences in Clastic Rocks. Short Course 9. SEPM, Tulsa, Oklahoma, 249 pp.
- Harris, P.T., Heap, A.D., Bryce, S.M., Porter-Smith, R., Ryan, D.A. and Heggie, D.T., 2002. Classification of Australian Clastic Coastal Depositional Environments Based Upon a Quantitative Analysis of Wave, Tidal, and River Power. *Journal of Sedimentary Research*, 72: 858-870.
- Harris, P.T., Hughes, M.G., Baker, E.K., Dalrymple, R.W. and Keene, J.B., 2004. Sediment transport in distributary channels and its export to the pro-deltaic environment in a tidally dominated delta: Fly River, Papua New Guinea. *Continental Shelf Research*, 24: 2431-2454.
- Hawkes, P., Fraser, A. and Einchcomb, C., 1998. The tectono-stratigraphic development and exploration history of the Weald and Wessex basins, Southern England, UK, Development, Evolution and Petroleum Geology of the Wessex Basin. Special Publications 133. Geological Society, London, pp. 39-65.
- Hayes, M.O., 1975. Morphology of sand accumulations in estuaries: an introduction to the symposium. In: L.E. Cronin (Editor), *Estuarine Research*. Academic Press, New York, N.Y., pp. 3–22.
- Hayes, M.O., 1979. Barrier island morphology as a function of tidal and wave regime. In: S.P. Leatherman (Editor), *Barrier Islands*. Academic Press, New York, pp. 1-27.
- Hayes, M.O., 1980. General morphology and sediment patterns in tidal inlets. *Sedimentary geology*, 26: 139-156.
- Heap, A.D., Bryce, S. and Ryan, D.A., 2004. Facies evolution of Holocene estuaries and deltas: a large-sample statistical study from Australia. *Sedimentary Geology*, 168: 1-17.
- Hinz, K., Fritsch, J., Kempter, E., Mohammad, M.A.M., Meyer, J., Mohamed, M.D., Vosberg, D.G.H., Weber, D.I.J. and Benavidez, M.J., 1989. Thrust tectonics along the north-western continental margin of Sabah/Borneo. *Geologische Rundschau*, 78: 705-730.
- Hiscott, R.N., 1994. Loss of capacity, not competence, as the fundamental process governing deposition from turbidity currents. *Journal of Sedimentary Research*, 64: 209-214.
- Holgate, N.E., Jackson, C.A.L., Hampson, G.J. and Dreyer, T., 2013. Sedimentology and sequence stratigraphy of the Middle-Upper Jurassic Krossfjord and Fensfjord formations, Troll Field, northern North Sea. *Petroleum Geoscience*, 19: 237-258.
- Honig, C. and Boyd, R., 1992. Estuarine sedimentation on the eastern shore of Nova Scotia. *Journal of Sedimentary Research*, 62: 569-583.
- Hori, K. and Saito, Y., 2007. Classification, architecture, and evolution of large-river deltas. In: A. Gupta (Editor), *Large rivers: geomorphology and management*. John Wiley & Sons, Chichester, UK, pp. 75-96.
- Hori, K., Saito, Y., Zhao, Q., Cheng, X., Wang, P., Sato, Y. and Li, C., 2001. Sedimentary facies of the tide-dominated paleo-Changjiang (Yangtze) estuary during the last transgression. *Marine Geology*, 177: 331-351.
- Hori, K., Saito, Y., Zhao, Q. and Wang, P., 2002. Architecture and evolution of the tide-dominated Changjiang (Yangtze) River delta, China. *Sedimentary Geology*, 146: 249-264.
- Hovikoski, J., Räsänen, M., Gingras, M., Ranzi, A. and Melo, J., 2008. Tidal and seasonal controls in the formation of Late Miocene inclined heterolithic stratification deposits, western Amazonian foreland basin. *Sedimentology*, 55: 499–530.

- Hovius, N., 1998. Controls on sediment supply by large rivers. In: K.W. Shanley and P.J. McCabe (Editors), *Relative Role of Eustasy, Climate and Tectonics in Continental Rocks* SEPM Special Publication 59, pp. 3-16.
- Howarth, M.J., 1982. Tidal currents of the continental shelf. In: A.H. Stride (Editor), *Offshore Tidal Sands: Processes and Deposits*. Chapman & Hall, London, pp. 10-26.
- Hu, D., Wu, L., Cai, W., Gupta, A.S., Ganachaud, A., Qiu, B., Gordon, A.L., Lin, X., Chen, Z. and Hu, S., 2015. Pacific western boundary currents and their roles in climate. *Nature*, 522: 299–308.
- Hubbard, S.M., Smith, D.G., Nielsen, H., Leckie, D.A., Fustic, M., Spencer, R.J. and Bloom, L., 2011. Seismic geomorphology and sedimentology of a tidally influenced river deposit, Lower Cretaceous Athabasca oil sands, Alberta, Canada. *AAPG bulletin*, 95: 1123-1145.
- Hutchison, C.S., 2010. The North-West Borneo Trough. *Marine Geology*, 271: 32-43.
- Ingram, G.M., Chisholm, T.J., Grant, C.J., Hedlund, C.A., Stuart-Smith, P. and Teasdale, J., 2004. Deepwater North West Borneo: hydrocarbon accumulation in an active fold and thrust belt. *Marine and Petroleum Geology*, 21: 879-887.
- Jablonski, B.V.J. and Dalrymple, R.W., 2016. Recognition of strong seasonality and climatic cyclicity in an ancient, fluvially dominated, tidally influenced point bar: Middle McMurray Formation, Lower Steepbank River, north-eastern Alberta, Canada. *Sedimentology*, 63: 552–585.
- James, N.P. and Dalrymple, R.W., 2010. *Facies Models 4*. Geological Association of Canada, 586 pp.
- Jardine, E., 1997. Dual petroleum systems governing the prolific Pattani Basin, offshore Thailand. In: J.V.C. Howes and R.A. Noble (Editors), *International Conference on Petroleum Systems of SE Asia and Australasia*, Indonesian Petroleum Association, Jakarta, Indonesia, pp. 351-363.
- Jerzykiewicz, T. and Wojewoda, J., 1986. The Radków and Szczeliniec sandstones: an example of giant foresets on a tectonically controlled shelf of the Bohemian Cretaceous Basin (Central Europe). In: J.R. Knight and J.R. McLean (Editors), *Shelf Sands and Sandstones*. Canadian Society of Petroleum Geologists, Memoir 11, pp. 1-15.
- Johnson, H.D., 1975. Tide- and wave- dominated inshore and shoreline sequences from the late Precambrian, Finnmark, North Norway. *Sedimentology*, 22: 45-74.
- Johnson, H.D. and Baldwin, C.T., 1996. *Shallow Clastic Seas*. In: H. Reading (Editor), *Sedimentary Environments: processes, facies and stratigraphy*. Blackwell Scientific Publications, Oxford, pp. 236-286.
- Johnson, H.D. and Levell, B.K., 1995. Sedimentology of a transgressive, estuarine sand complex: the Lower Cretaceous Woburn Sands (Lower Greensand), southern England. In: A.G. Plint (Editor), *Sedimentary Facies Analysis: a Tribute to the Research and Teaching of Harold G. Reading*. IAS Special Publication 22. Blackwell Publishing Ltd., Oxford, UK, pp. 17-46.
- Jouanneau, J.-M. and Latouche, C., 1981. *The Gironde Estuary*. Contributions to Sedimentology, 10. E. Schweizerbart'sche Verlagsbuchhandlung, Stuttgart.
- Klein, G.d., 1970a. Depositional and dispersal dynamics of intertidal sand bars. *Journal of Sedimentary Research*, 40: 1095-1127.
- Klein, G.D., 1970b. Tidal origin of a Precambrian quartzite; the Lower Fine-grained quartzite (middle Dalradian) of Islay, Scotland. *Journal of Sedimentary Research*, 40: 973-985.
- Klein, G.D., 1971. A sedimentary model for determining paleotidal range. *Geological Society of America Bulletin*, 82: 2585-2592.
- Komar, P.D., 1987. Selective gravel entrainment and the empirical evaluation of flow competence. *Sedimentology*, 34: 1165-1176.
- Kowalik, Z. and Luick, J., 2013. *The Oceanography of Tides*. University of Alaska Fairbanks, Fairbanks, Alaska, 157 pp.
- Kreisa, R. and Moila, R., 1986. Sigmoidal tidal bundles and other tide-generated sedimentary structures of the Curtis Formation, Utah. *Geological Society of America Bulletin*, 97: 381-387.
- Krystinik, L.F. and DeJarnett, B.B., 1995. Lateral variability of sequence stratigraphic framework in the Campanian and Lower Maastrichtian of the Western Interior Seaway. In: J.C. Van Wagoner and G.T. Bertram (Editors), *Sequence Stratigraphy of Foreland Basin Deposits*:

- Outcrop and Subsurface Examples from the Cretaceous of North America. Memoir 64. AAPG, Tulsa, Oklahoma, pp. 11–26.
- Kurcinka, C., Dalrymple, R.W. and Gugliotta, M., 2018. Facies and architecture of river-dominated to tide-influenced mouth bars in the lower Lajas Formation (Jurassic), Argentina. *AAPG Bulletin*, 102: 885-912.
- Kvale, E.P., 2006. The origin of neap–spring tidal cycles. *Marine Geology*, 235: 5-18.
- Kvale, E.P., 2012. Tidal constituents of modern and ancient tidal rhythmites: criteria for recognition and analyses. In: R.A. Davis and R.W. Dalrymple (Editors), *Principles of Tidal Sedimentology*. Springer, New York, pp. 1-17.
- Kvale, E.P., Archer, A.W. and Johnson, H.R., 1989. Daily, monthly, and yearly tidal cycles within laminated siltstones of the Mansfield Formation (Pennsylvanian) of Indiana. *Geology*, 17: 365-368.
- Lamb, M.P., Myrow, P.M., Lukens, C., Houck, K. and Strauss, J., 2008. Deposits from Wave-Influenced Turbidity Currents: Pennsylvanian Minturn Formation, Colorado, U.S.A. *Journal of Sedimentary Research*, 78: 480-498.
- Lambiase, J.J., Damit, A.R., Simmons, M.D., Abdoerrias, R. and Hussin, A., 2003. A depositional model and the stratigraphic development of modern and ancient tide-dominated deltas in NW Borneo. In: F.H. Sidi, D. Nummedal, P. Imbert, H. Darman and H.W. Posamentier (Editors), *Tropical Deltas of Southeast Asia—Sedimentology, Stratigraphy, and Petroleum Geology* SEPM Spec. Publ., pp. 109–123.
- Leckie, D.A. and Rumpel, T., 2003. Tide-influenced sedimentation in a rift basin—Cretaceous Qishn Formation, Masila Block, Yemen: A billion barrel oil field. *AAPG Bulletin*, 87: 987-1013.
- Lee, T.-Y. and Lawver, L.A., 1995. Cenozoic plate reconstruction of Southeast Asia. *Tectonophysics*, 251: 85-138.
- Leeder, M.R., 2011. *Sedimentology and sedimentary basins: from turbulence to tectonics*. Wiley-Blackwell, Oxford, UK, 784 pp.
- Legler, B., Hampson, G.J., Jackson, C.A.L., Johnson, H.D., Massart, B.Y.G., Sarginson, M. and Ravnås, R., 2014. Facies relationships and stratigraphic architecture of distal, mixed tide- and wave-influenced deltaic deposits: Lower Sego Sandstone, Western Colorado, U.S.A. *Journal of Sedimentary Research*, 84: 605–625.
- Legler, B., Johnson, H.D., Hampson, G.J., Massart, B.Y.G., Jackson, C.A.L., Jackson, M.D., El-Barkooky, A. and Ravnås, R., 2013. Facies model of a fine-grained, tide-dominated delta: Lower Dir Abu Lifa Member (Eocene), Western Desert, Egypt. *Sedimentology*, 60: 1313–1356.
- Leonardi, N., Sun, T. and Fagherazzi, S., 2014. Modeling tidal bedding in distributary-mouth bars. *Journal of Sedimentary Research*, 84: 499-512.
- Levell, B.K., 1980. A late Precambrian tidal shelf deposit, the Lower Sandfjord Formation, Finnmark, north Norway. *Sedimentology*, 27: 539-557.
- Levell, B.K., Johnson, H.D., Collins, D.S. and Van Cappelle, M., 2020. Deposition and preservation of fluvio- tidal shallow- marine sandstones: A re- evaluation of the Neoproterozoic Jura Quartzite (western Scotland). *Sedimentology*, 67: 173-206.
- Li, W., Bhattacharya, J.P., Zhu, Y., Garza, D. and Blankenship, E., 2011. Evaluating delta asymmetry using three- dimensional facies architecture and ichnological analysis, Ferron ‘Notom Delta’, Capital Reef, Utah, USA. *Sedimentology*, 58: 478-507.
- Li, Z., Bhattacharya, J.P. and Schieber, J., 2015. Evaluating along-strike variation using thin-bedded facies analysis, Upper Cretaceous Ferron Notom Delta, Utah. *Sedimentology*, 62: 2060–2089.
- Lockhart, B.E., Chinoroje, O., Enomoto, C.B. and Hollomon, G.A., 1997. Early Tertiary deposition in the southern Pattani Trough, Gulf of Thailand. In: P. Dheeradilok, C. Hinthong, P. Chaodumrong, P. Putthaphiban, W. Tansathien, C. Utha-aroon, N. Sattarak, T. Nuchanong and S. Techawan (Editors), *The International Conference on Stratigraphy and Tectonic Evolution of Southeast Asia and the South Pacific*, Bangkok, Thailand, pp. 476-489.
- Longhitano, S.G., Mellere, D., Steel, R.J. and Ainsworth, R.B., 2012. Tidal depositional systems in the rock record: A review and new insights. *Sedimentary Geology*, 279: 2-22.

- Longhitano, S.G., Sabato, L., Tropeano, M. and Gallicchio, S., 2010. A mixed bioclastic–siliciclastic flood-tidal delta in a micro tidal setting: depositional architectures and hierarchical internal organization (Pliocene, Southern Apennine, Italy). *Journal of Sedimentary Research*, 80: 36–53.
- Longhitano, S.G. and Steel, R.J., 2017. Deflection of the progradational axis and asymmetry in tidal seaway and strait deltas: insights from two outcrop case studies. In: G.J. Hampson, A.D. Reynolds, B. Kostic and M.R. Wells (Editors), *Sedimentology of Paralic Reservoirs: Recent Advances* Special Publication 444, Geological Society of London pp. 141–172.
- MacEachern, J.A. and Bann, K.L., 2008. The role of ichnology in refining shallow marine facies models. In: G.J. Hampson, R.J. Steel, P.M. Burgess and R.W. Dalrymple (Editors), *Recent Advances in Models of Siliciclastic Shallow-Marine Stratigraphy*. SEPM Spec. Publ., pp. 73–116.
- MacEachern, J.A., Bann, K.L., Bhattacharya, J.P. and Howell, C.D., 2005. Ichnology of deltas: organism responses to the dynamic interplay of rivers, waves, storms, and tides. In: L. Giosan and J.P. Bhattacharya (Editors), *River Deltas—Concepts, Models, and Examples*. SEPM Special Publication. SEPM, pp. 45–85.
- MacMillan, D.H., 1966. *Tides*. American Elsevier Publishing Company, New York, 240 pp.
- Markwick, P.J. and Valdes, P.J., 2004. Palaeo-digital elevation models for use as boundary conditions in coupled ocean–atmosphere GCM experiments: a Maastrichtian (late Cretaceous) example. *Palaeogeography Palaeoclimatology Palaeoecology*, 213: 37–63.
- Martel, A.T., Allen, P.A. and Slingerland, R., 1994. Use of tidal-circulation modeling in paleogeographical studies: an example from the Tertiary of the Alpine perimeter. *Geology*, 22: 925–928.
- Martinius, A.W. and Gowland, S., 2011. Tide-influenced fluvial bedforms and tidal bore deposits (late Jurassic Lourinhã Formation, Lusitanian Basin, Western Portugal). *Sedimentology*, 58: 285–324.
- Martinius, A.W., Jablonski, B.V.J., Fustic, M., Strobl, R. and van den Berg, J.H., 2015. Fluvial to tidal transition zone facies in the McMurray Formation (Christina River, Alberta, Canada), with emphasis on the reflection of flow intensity in bottomset architecture. In: P.J. Ashworth, J.L. Best and D.R. Parsons (Editors), *Fluvial–Tidal Sedimentology*. Developments in Sedimentology. Elsevier, pp. 445–480.
- Martinius, A.W. and van den Berg, J.H., 2011. *Atlas of sedimentary structures in estuarine and tidally-influenced river deposits of the Rhine-Meuse-Scheldt system*. EAGE Publications BV, Houten, 298 pp.
- Maselli, V., Normandeau, A., Nones, M., Tesi, T., Langone, L., Trincardi, F. and Bohacs, K.M., 2020. Tidal modulation of river-flood deposits: How low can you go? *Geology*, 48: 663–667.
- McCabe, P.J. and Jones, C.M., 1977. Formation of reactivation surfaces within superimposed deltas and bedforms. *Journal of Sedimentary Research*, 47: 707–715.
- McIlroy, D., 2006. Ichnology of a macrotidal tide-dominated deltaic depositional system: Lajas Formation, Neuquén Province, Argentina. In: R. Bromley, L.A. Buatois, J. Genise, M.G. Mángano and R. Melchor (Editors), *Sediment–Organism Interactions: A Multifaceted Ichnology*. Special Publication 88. SEPM, Tulsa, Oklahoma, pp. 195–211.
- McIlroy, D., 2007. Lateral variability in shallow marine ichnofabrics: implications for the ichnofabric analysis method. *Journal of the Geological Society*, 164: 359–369.
- Middleton, G.V., 1965. Primary sedimentary structures and their hydrodynamic interpretation, 12. SEPM Special Publication 265 pp.
- Miller, K.G., Kominz, M.A., Browning, J.V., Wright, J.D., Mountain, G.S., Katz, M.E., Sugarman, P.J., Cramer, B.S., Christie-Blick, N. and Pekar, S.F., 2005. The Phanerozoic record of global sea-level change. *Science*, 310: 1293–1298.



- 1 Miller, K.G., Mountain, G.S., Wright, J.D. and Browning, J.V., 2011. A 180-Million-Year Record of  
2 Sea Level and Ice Volume Variations from Continental Margin and Deep-Sea Isotopic  
3 Records. *Oceanography*, 24: 40-53.
- 4 Milliman, J.D. and Farnsworth, K.L., 2011. River discharge to the coastal ocean: a global synthesis.  
5 Cambridge University Press, Cambridge, UK, 381 pp.
- 6 Milliman, J.D. and Syvitski, J.P., 1992. Geomorphic/tectonic control of sediment discharge to the  
7 ocean: the importance of small mountainous rivers. *The Journal of Geology*, 100: 525-544.
- 8 Mitchell, A.J., Allison, P.A., Gorman, G.J., Piggott, M.D. and Pain, C.C., 2011. Tidal circulation in an  
9 ancient epicontinental sea: The Early Jurassic Laurusian Seaway. *Geology*, 39: 207-210.
- 10 Mitchell, A.J., Uličný, D., Hampson, G.J., Allison, P.A., Gorman, G.J., Piggott, M.D., Wells, M.R.  
11 and Pain, C.C., 2010. Modelling tidal current-induced bed shear stress and palaeocirculation  
12 in an epicontinental seaway: the Bohemian Cretaceous Basin, Central Europe.  
13 *Sedimentology*, 57: 359-388.
- 14 Morley, C.K., 2016. Major unconformities/termination of extension events and associated surfaces in  
15 the South China Seas: Review and implications for tectonic development. *Journal of Asian  
16 Earth Sciences*, 120: 62-86.
- 17 Morley, R.J., Swiecicki, T. and Pham, D.T.T., 2011. A sequence stratigraphic framework for the  
18 Sunda region, based on integration of biostratigraphic, lithological and seismic data from  
19 Nam Con Son basin, Vietnam, Indonesian Petroleum Association 35th Annual Convention,  
20 Jakarta, Indonesia, pp. IPA11-G-002.
- 21 Mulhern, J.S., Johnson, C.L. and Martin, J.M., 2017. Is barrier island morphology a function of tidal  
22 and wave regime? *Marine Geology*, 387: 74-84.
- 23 Murtaza, M., Rahman, A.H.A., Sum, C.W. and Konjing, Z., 2018. Facies associations, depositional  
24 environments and stratigraphic framework of the Early Miocene–Pleistocene successions of  
25 the Mukah–Balingian Area, Sarawak, Malaysia. *Journal of Asian Earth Sciences*, 152: 23-38.
- 26 Muto, T. and Steel, R.J., 1997. Principles of regression and transgression: the nature of the interplay  
27 between accommodation and sediment supply. *Journal of Sedimentary Research*, 67: 994-  
28 1000.
- 29 Mutti, E., Allen, G. and Rosell, J., 1984. Sigmoidal cross stratification and sigmoidal bars:  
30 depositional features diagnostic of tidal sandstones, 5th IAS European Regional Meeting,  
31 Marsiglia, pp. 312-313.
- 32 Mutti, E., Rosell, J., Allen, G., Fonnesu, F. and Sgavetti, M., 1985. The Eocene Baronia tide  
33 dominated delta-shelf system in the Ager Basin. In: M.D. Mila and J. Rosell (Editors),  
34 Excursion guidebook: 6th International Association of Sedimentologists European Regional  
35 Meeting. International Association of Sedimentologists, Lleida, Spain, pp. 579-600.
- 36 Myrow, P.M., Fischer, W. and Goodge, J.W., 2002. Wave-modified turbidites: combined-flow  
37 shoreline and shelf deposits, Cambrian, Antarctica. *Journal of Sedimentary Research*, 72:  
38 641-656.
- 39 Myrow, P.M. and Southard, J.B., 1996. Tempestite deposition. *Journal of Sedimentary Research*, 66:  
40 992-1007.
- 41 Nahon, A., Bertin, X., Fortunato, A.B. and Oliveira, A., 2012. Process-based 2DH morphodynamic  
42 modeling of tidal inlets: A comparison with empirical classifications and theories. *Marine  
43 Geology*, 291: 1-11.
- 44 Nanson, R.A., Vakarelov, B.K., Ainsworth, R.B., Williams, F.M. and Price, D.M., 2013. Evolution of  
45 a Holocene, mixed-process, forced regressive shoreline: the Mitchell River delta, Queensland,  
46 Australia. *Marine Geology*, 339: 22-43.
- 47 Narayan, J., 1971. Sedimentary structures in the lower Greensand of the Weald, England, and Bas-  
48 Boulonnais, France. *Sedimentary Geology*, 6: 73-109.
- 49 Nguyen, V.L., Ta, T.K.O. and Tateishi, M., 2000. Late Holocene depositional environments and  
50 coastal evolution of the Mekong River Delta, Southern Vietnam. *Journal of Asian Earth  
51 Sciences*, 18: 427-439.

- Nio, S.-D. and Yang, C.-S., 1991. Diagnostic attributes of clastic tidal deposits: a review. In: D. Smith, G.G.E. Reinson, B.A. Zaitlin and R.A. Rahmani (Editors), *Clastic Tidal Sedimentology*. Canadian Society of Petroleum Geologists, Memoir 16, pp. 3-27.
- Nio, S., Siegenthaler, C. and Yang, C., 1983. Megaripple cross-bedding as a tool for the reconstruction of the paleo-hydraulics in a Holocene subtidal environment, SW Netherlands. *Geologie en Mijnbouw*, 62: 499-510.
- Nyberg, B. and Howell, J.A., 2015. Is the present the key to the past? A global characterization of modern sedimentary basins. *Geology*, 43: 643-646.
- Nyberg, B. and Howell, J.A., 2016. Global distribution of modern shallow marine shorelines. Implications for exploration and reservoir analogue studies. *Marine and Petroleum Geology*, 71: 83-104.
- O'Reilly, C.T., Solvason, R. and Solomon, C., 2005. Where are the world's largest tides? In: J. Ryan (Editor), *BIO Annual Report "2004 in Review"*, Washington, D. C., pp. 44-46.
- Obradovich, J.D., 1993. A Cretaceous time scale. In: W.G.E. Caldwell and E.G. Kauffman (Editors), *Evolution of the Western Interior Basin*. Geological Association of Canada, Special Paper 39, St. John's, Newfoundland, pp. 379-396.
- Off, T., 1963. Rhythmic linear sand bodies caused by tidal currents. *AAPG Bulletin*, 47: 324-341.
- Ogg, J.G., Agterberg, F.P. and Gradstein, F.M., 2004. The Cretaceous period. In: G. F.M., O. J.G. and S. A.G (Editors), *A Geologic Time Scale 2004*. Cambridge University Press, Cambridge, pp. 344-383.
- Olabarrieta, M., Geyer, W.R., Coco, G., Friedrichs, C.T. and Cao, Z., 2018. Effects of density- driven flows on the long- term morphodynamic evolution of funnel- shaped estuaries. *Journal of Geophysical Research: Earth Surface*, 123: 2901-2924.
- Olson, W.S., 1972. Sedimentary Model for Determining Paleotidal Range: Discussion. *Geological Society of America Bulletin*, 83: 537-538.
- Open University Course Team, 1999. *Waves, Tides and Shallow-water Processes: Second Edition*. Butterworth-Heinemann, Oxford, UK, 227 pp.
- Orton, G.J. and Reading, H.G., 1993. Variability of deltaic processes in terms of sediment supply, with particular emphasis on grain size. *Sedimentology*, 40: 475-512.
- Pain, C.C., Piggott, M.D., Goddard, A.J.H., Fang, F., Gorman, G.J., Marshall, D.P., Eaton, M.D., Power, P.W. and De Oliveira, C.R.E., 2005. Three-dimensional unstructured mesh ocean modelling. *Ocean Modelling*, 10: 5-33.
- Partington, M., Copestake, P., Mitchener, B.a. and Underhill, J.R., 1993a. Biostratigraphic calibration of genetic stratigraphic sequences in the Jurassic–lowermost Cretaceous (Hettangian to Ryazanian) of the North Sea and adjacent areas, Geological Society, London, Petroleum Geology Conference Series. Geological Society of London, pp. 371-386.
- Partington, M., Mitchener, B., Milton, N. and Fraser, A., 1993b. Genetic sequence stratigraphy for the North Sea Late Jurassic and Early Cretaceous: distribution and prediction of Kimmeridgian–Late Ryazanian reservoirs in the North Sea and adjacent areas, Geological Society, London, Petroleum Geology Conference series. Geological Society of London, pp. 347-370.
- Peng, Y., Steel, R.J., Rossi, V.M. and Olariu, C., 2018. Mixed-energy process interactions read from a compound-clinoform delta (paleo–Orinoco Delta, Trinidad): preservation of river and tide signals by mud-induced wave damping. *Journal of Sedimentary Research*, 88: 75-90.
- Perillo, M.M., Best, J.L. and Garcia, M.H., 2014. A new phase diagram for combined-flow bedforms. *Journal of Sedimentary Research*, 84: 301-313.
- Piggott, M.D., Gorman, G.J., Pain, C.C., Allison, P.A., Candy, A.S., Martin, B.T. and Wells, M.R., 2008. A new computational framework for multi-scale ocean modelling based on adapting unstructured meshes. *International Journal for Numerical Methods in Fluids*, 56: 1003-1015.
- Piper, D.J., Kontopoulos, N., Anagnostou, C., Chronis, G. and Panagos, A., 1990. Modern fan deltas in the western Gulf of Corinth, Greece. *Geo-Marine Letters*, 10: 5-12.
- Posamentier, H.W. and Walker, R.G. (Editors), 2006. *Facies models revisited*. SEPM Special Publication 84.
- Proudman, J., 1953. *Dynamical Oceanography*. Methuen-John Wiley, London, 409 pp.

- Pugh, D. and Woodworth, P., 2014. Sea-level science: understanding tides, surges, tsunamis and mean sea-level changes. Cambridge University Press, Cambridge, UK, 407 pp.
- Pugh, D.T., 1987. Tides, surges and mean sea-level: a handbook for engineers and scientists. John Wiley & Sons, Chichester, UK, 472 pp.
- Rawson, P.F., 2006. Cretaceous: sea levels peak as the North Atlantic opens, *The Geology of England and Wales*, 2nd Edition. Geological Society, London, London, UK, pp. 365-393.
- Reading, H.G., 1978. *Sedimentary Environments and Facies*, 60. Blackwell Scientific Publications, Oxford, 557 pp.
- Reading, H.G., 1996. *Sedimentary environments: processes, facies and stratigraphy*. Blackwell Publishing Ltd, Oxford, U.K., 615 pp.
- Reading, H.G. and Collinson, J.D., 1996. Clastic coasts. In: H.G. Reading (Editor), *Sedimentary Environments; Processes, Facies and Stratigraphy*. Blackwell Science Ltd, Oxford, UK, pp. 154–231.
- Redfield, A.C., 1958. The influence of the continental shelf on the tides of the Atlantic coast of the United States. *Journal of Marine Research*, 17: 432-448.
- Reineck, H.-E., 1963. Sedimentgefüge im Bereich der südlichen Nordsee. *Senckenbergische Naturforschende Gesellschaft, Abhandlungen*, 505: 1–138.
- Reineck, H.-E. and Singh, I.B., 1980. *Depositional Sedimentary Environments: With Reference to Terrigenous Clastics*. Springer, Berlin, 549 pp.
- Reineck, H.-E. and Wunderlich, F., 1968. Classification and Origin of Flaser and Lenticular Bedding. *Sedimentology*, 11: 99-104.
- Reynaud, J.-Y. and Dalrymple, R.W., 2012. Shallow-marine tidal deposits. In: R.A. Davies Jr. and R.W. Dalrymple (Editors), *Principles of Tidal Sedimentology*. Springer, New York, pp. 335-369.
- Ridd, M.F., Barber, A.J. and Crow, M.J., 2011. *The Geology of Thailand*. Geological Society of London, London, UK, 626 pp.
- Robinson, A., 1966. Residual currents in relation to shoreline evolution of the East Anglian coast. *Marine Geology*, 4: 57-84.
- Rodriguez, A.B., Hamilton, M.D. and Anderson, J.B., 2000. Facies and evolution of the modern Brazos Delta, Texas: wave versus flood influence. *Journal of Sedimentary Research*, 70: 283-295.
- Rossi, V.M., Kim, W., Leva López, J., Edmonds, D., Geleynse, N., Olariu, C., Steel, R.J., Hiatt, M. and Passalacqua, P., 2016. Impact of tidal currents on delta-channel deepening, stratigraphic architecture, and sediment bypass beyond the shoreline. *Geology*, 44: 927-930.
- Rossi, V.M., Longhitano, S.G., Mellere, D., Dalrymple, R.W., Steel, R.J., Chiarella, D. and Olariu, C., 2017a. Interplay of tidal and fluvial processes in an early Pleistocene, delta-fed, strait margin (Calabria, Southern Italy). *Marine and Petroleum Geology*, In Press, Accepted Article.
- Rossi, V.M., Perillo, M.M., Steel, R.J. and Olariu, C., 2017b. Quantifying mixed-process variability in shallow-marine depositional systems: What are sedimentary structures really telling us? *Journal of Sedimentary Research*, 87: 1060-1074.
- Rossi, V.M. and Steel, R.J., 2016. The role of tidal, wave and river currents in the evolution of mixed-energy deltas: Example from the Lajas Formation (Argentina). *Sedimentology*, 63: 824–864.
- Roy, P., Thom, B. and Wright, L., 1980. Holocene sequences on an embayed high-energy coast: an evolutionary model. *Sedimentary Geology*, 26: 1-19.
- Roy, P., Williams, R., Jones, A., Yassini, I., Gibbs, P., Coates, B., West, R., Scanes, P., Hudson, J. and Nichol, S., 2001. Structure and function of south-east Australian estuaries. *Estuarine, Coastal and Shelf Science*, 53: 351-384.
- Rubin, D.M. and McCulloch, D.S., 1980. Single and superimposed bedforms: a synthesis of San Francisco Bay and flume observations. *Sedimentary Geology*, 26: 207-231.
- Ruffell, A.H. and Wach, G.D., 1991. Sequence stratigraphic analysis of the Aptian-Albian Lower Greensand in southern England. *Marine and Petroleum Geology*, 8: 341-353.

- Salahuddin and Lambiase, J.J., 2013. Sediment Dynamics and Depositional Systems of the Mahakam Delta, Indonesia: Ongoing Delta Abandonment On A Tide-Dominated Coast. *Journal of Sedimentary Research*, 83: 503–521.
- Sames, B., Wagreich, M., Wendler, J., Haq, B., Conrad, C., Melinte-Dobrinescu, M., Hu, X., Wendler, I., Wolfgring, E. and Yilmaz, I., 2016. Short-term sea-level changes in a greenhouse world—A view from the Cretaceous. *Palaeogeography, Palaeoclimatology, Palaeoecology*, 441: 393-411.
- Sandal, S.T., 1996. The Geology and Hydrocarbon Resources of Negara Brunei Darussalam. Brunei Shell Petroleum Company, Brunei Museum, Bandar Seri Begawan, Brunei Darussalam, 243 pp.
- Shaw, D.P., 1964. *Time in Stratigraphy*. McGraw Hill, New York, 365 pp.
- Shoup, R.C., Morley, R.J., Swiecicki, T. and Clark, S., 2013. Tectono-stratigraphic Framework and Tertiary Paleogeogeography of Southeast Asia; Gulf of Thailand to South Vietnam Shelf. *Houston Geological Society Bulletin*, 55: 27-39.
- Shum, C., Woodworth, P., Andersen, O., Egbert, G.D., Francis, O., King, C., Klosko, S., Le Provost, C., Li, X. and Molines, J.M., 1997. Accuracy assessment of recent ocean tide models. *Journal of geophysical research: oceans*, 102: 25173-25194.
- Sisulak, C.F. and Dashtgard, S.E., 2012. Seasonal Controls On the Development And Character of Inclined Heterolithic Stratification In A Tide-Influenced, Fluvially Dominated Channel: Fraser River, Canada. *Journal of Sedimentary Research*, 82: 244–257.
- Sixsmith, P.J., Hampson, G.J., Gupta, S., Johnson, H.D. and Fofana, J.F., 2008. Facies architecture of a net transgressive sandstone reservoir analog: The Cretaceous Hosta Tongue, New Mexico. *AAPG Bulletin*, 92: 513-547.
- Slater, R.D., 1985. A numerical model of tides in the Cretaceous Seaway of North America. *The Journal of Geology*, 93: 333-345.
- Slingerland, R., 1986. Numerical computation of co-oscillating palaeotides in the Catskill epeiric Sea of eastern North America. *Sedimentology*, 33: 487-497.
- Smith, D.G., 1988. Tidal bundles and mud couplets in the McMurray Formation, northeastern Alberta, Canada. *Bulletin of Canadian Petroleum Geology*, 36: 216-219.
- Sømme, T.O., Helland-Hansen, W., Martinsen, O.J. and Thurmond, J.B., 2009. Relationships between morphological and sedimentological parameters in source-to-sink systems: a basis for predicting semi-quantitative characteristics in subsurface systems. *Basin Research*, 21: 361-387.
- Sondi, I., Juračić, M. and Pravdić, V., 1995. Sedimentation in a disequilibrium river- dominated estuary: the Raša River Estuary (Adriatic Sea, Croatia). *Sedimentology*, 42: 769-782.
- Southard, J.B. and Boguchwal, L.A., 1990. Bed configurations in steady unidirectional water flows. Part 2. Synthesis of flume data. *Journal of Sedimentary Research*, 60.
- Stammer, D., Ray, R.D., Andersen, O.B., Arbic, B.K., Bosch, W., Carrère, L., Cheng, Y., Chinn, D.S., Dushaw, B.D., Egbert, G.D., Erofeeva, S.Y., Fok, H.S., Green, J.A.M., Griffiths, S., King, M.A., Lapin, V., Lemoine, F.G., Luthcke, S.B., Lyard, F., Morison, J., Müller, M., Padman, L., Richman, J.G., Shriver, J.F., Shum, C.K., Taguchi, E. and Yi, Y., 2014. Accuracy assessment of global barotropic ocean tide models. *Reviews of Geophysics*, 52: 243-282.
- Stride, A.H., 1973. Sediment transport by the North Sea. In: E.D. Goldberg (Editor), *North Sea Science*. MIT Press, Cambridge, MA, pp. 101-130.
- Stride, A.H., 1982. *Offshore tidal sands: processes and deposits*. Chapman & Hall, London, 222 pp.
- Syvitski, J.P. and Milliman, J.D., 2007. Geology, geography, and humans battle for dominance over the delivery of fluvial sediment to the coastal ocean. *The Journal of Geology*, 115: 1-19.
- Syvitski, J.P., Peckham, S.D., Hilberman, R. and Mulder, T., 2003. Predicting the terrestrial flux of sediment to the global ocean: a planetary perspective. *Sedimentary Geology*, 162: 5-24.
- Ta, T.K.O., Nguyen, V.L., Tateishi, M., Kobayashi, I., Saito, Y. and Nakamura, T., 2002a. Sediment facies and Late Holocene progradation of the Mekong River Delta in Bentre Province,

- southern Vietnam: an example of evolution from a tide-dominated to a tide- and wave-dominated delta. *Sedimentary Geology*, 152: 313-325.
- Ta, T.K.O., Nguyen, V.L., Tateishi, M., Kobayashi, I., Tanabe, S. and Saito, Y., 2002b. Holocene delta evolution and sediment discharge of the Mekong River, southern Vietnam. *Quaternary Science Reviews*, 21: 1807-1819.
- Terwindt, J. and Breusers, H., 1972. Experiments on the origin of flaser, lenticular and sand- clay alternating bedding. *Sedimentology*, 19: 85-98.
- Terwindt, J.H., 1971. Litho-facies of inshore estuarine and tidal-inlet deposits. *Geologie en Mijnbouw*, 50: 515-526.
- Thomas, R.G., Smith, D.G., Wood, J.M., Visser, J., Calverley-Range, E.A. and Koster, E.H., 1987. Inclined heterolithic stratification—terminology, description, interpretation and significance. *Sedimentary Geology*, 53: 123–179.
- Tin, N.T. and Ty, N.D., 1995. Petroleum geology of the Nam Con Son Basin. *Bulletin of the Geological Society of Malaysia*, 37: 1-11.
- Tinterri, R., 2011. Combined flow sedimentary structures and the genetic link between sigmoidal-and hummocky-cross stratification. *GeoActa*, 10: 1–43.
- Togunwa, O.S., Abdullah, W.H., Hakimi, M.H. and Barbeito, P.J., 2015. Organic geochemical and petrographic characteristics of Neogene organic-rich sediments from the onshore West Baram Delta Province, Sarawak Basin: Implications for source rocks and hydrocarbon generation potential. *Marine and Petroleum Geology*, 63: 115-126.
- Tomašových, A. and Kidwell, S.M., 2017. Nineteenth-century collapse of a benthic marine ecosystem on the open continental shelf. *Proceedings of the Royal Society B: Biological Sciences*, 284: 20170328.
- Townend, I., 2012. The estimation of estuary dimensions using a simplified form model and the exogenous controls. *Earth Surface Processes and Landforms*, 37: 1573-1583.
- Uehara, K., Scourse, J.D., Horsburgh, K.J., Lambeck, K. and Purcell, A.P., 2006. Tidal evolution of the northwest European shelf seas from the Last Glacial Maximum to the present. *Journal of Geophysical Research: Oceans*, 111: C09025.
- Uličný, D., 2001. Depositional systems and sequence stratigraphy of coarse- grained deltas in a shallow- marine, strike- slip setting: the Bohemian Cretaceous Basin, Czech Republic. *Sedimentology*, 48: 599-628.
- Uličný, D., Laurin, J. and Čech, S., 2009. Controls on clastic sequence geometries in a shallow-marine, transtensional basin: the Bohemian Cretaceous Basin, Czech Republic. *Sedimentology*, 56: 1077-1114.
- Vakarelov, B.K. and Ainsworth, R.B., 2013. A hierarchical approach to architectural classification in marginal-marine systems: Bridging the gap between sedimentology and sequence stratigraphy. *AAPG Bulletin*, 97: 1121–1161.
- Vakarelov, B.K., Ainsworth, R.B. and MacEachern, J.A., 2012. Recognition of wave-dominated, tide-influenced shoreline systems in the rock record: Variations from a microtidal shoreline model. *Sedimentary Geology*, 279: 23-41.
- van Cappelle, M., Hampson, G.J. and Johnson, H.D., 2018. Spatial and Temporal Evolution of Coastal Depositional Systems and Regional Depositional Process Regimes: Campanian Western Interior Seaway, USA. *Journal of Sedimentary Research*, 88: 873-897.
- van Cappelle, M., Stukins, S., Hampson, G.J. and Johnson, H.D., 2016. Fluvial to tidal transition in proximal, mixed tide-influenced and wave-influenced deltaic deposits: Cretaceous lower Sego Sandstone, Utah, USA. *Sedimentology*, 63: 1333–1361.
- van den Berg, J.H., Boersma, J.R. and Gelder, A.v., 2007. Diagnostic sedimentary structures of the fluvial-tidal transition zone—Evidence from deposits of the Rhine and Meuse. *Netherlands Journal of Geosciences/Geologie en Mijnbouw*, 86: 287–306.
- Van der Wegen, M. and Roelvink, J., 2008. Long- term morphodynamic evolution of a tidal embayment using a two- dimensional, process- based model. *Journal of Geophysical Research: Oceans*, 113.

- van Hattum, M.W.A., Hall, R., Pickard, A.L. and Nichols, G.J., 2006. Southeast Asian sediments not from Asia: Provenance and geochronology of north Borneo sandstones. *Geology*, 34: 589.
- Van Straaten, L., 1953. Megaripples in the Dutch Wadden Sea and in the basin of Arcachon (France). *Geol. Mijnbouw*, 15: 1-11.
- van Vliet, A. and Schwander, M.M., 1987. Stratigraphic interpretation of a regional seismic section across the Labuan syncline and its flank structures, Sabah, North Borneo. In: A.W. Bailey (Editor), *Atlas of Seismic Stratigraphy*. AAPG Studies in Geology 27, pp. 163-167.
- Van Wagoner, J.C., Mitchum, R.M., Campion, K.M. and Rahmanian, V.D., 1990. Siliciclastic Sequence Stratigraphy in Well Logs, Cores, and Outcrops: Concepts for High-Resolution Correlation of Time and Facies. *Methods in Exploration*, 7. AAPG, 55 pp.
- Van Yperen, A.E., Poyatos- Moré, M., Holbrook, J.M. and Midtkandal, I., 2020. Internal mouth- bar variability and preservation of subordinate coastal processes in low- accommodation proximal deltaic settings (Cretaceous Dakota Group, New Mexico, USA). *The Depositional Record*.
- Vaucher, R., Pittet, B., Hormière, H., Martin, E.L. and Lefebvre, B., 2016. A wave-dominated, tide-modulated model for the Lower Ordovician of the Anti-Atlas, Morocco. *Sedimentology*, 64: 777-807.
- Visser, M.J., 1980. Neap-spring cycles reflected in Holocene subtidal large-scale bedform deposits: a preliminary note. *Geology*, 8: 543-546.
- Voigt, T. and Tröger, K., 1996. Sea-level changes during Late Cenomanian and early Turonian in the Saxonian Cretaceous Basin. *Mitteilungen aus dem Geologisch-Paläontologischen Institut der Universität Hamburg*, 77: 275-290.
- Walker, R.G. and James, N.P., 1992. *Facies Models: Response to Sea Level Change*. Geotext, 1. Geological Association of Canada, 409 pp.
- Walker, R.G. and Plint, A.G., 1992. Wave-and storm-dominated shallow marine systems. In: R.G. Walker and N.P. James (Editors), *Facies Models: Response to Sea-Level Change*. Geological Association of Canada, St. John's, Newfoundland, pp. 219-238.
- Wei, X., Steel, R.J., Ravnås, R., Jiang, Z., Olariu, C. and Li, Z., 2016. Variability of tidal signals in the Brent Delta Front: New observations on the Rannoch Formation, northern North Sea. *Sedimentary Geology*, 335: 166-179.
- Wells, M.R., 2008. *Tidal modelling of modern and ancient seas and oceans*, Imperial College London, 527 pp.
- Wells, M.R., Allison, P.A., Hampson, G.J., Piggott, M.D. and Pain, C.C., 2005a. Modelling ancient tides: the Upper Carboniferous epi-continental seaway of Northwest Europe. *Sedimentology*, 52: 715-735.
- Wells, M.R., Allison, P.A., Piggott, M.D., Gorman, G.J., Hampson, G.J., Pain, C.C. and Fang, F., 2007. Numerical Modeling of Tides in the Late Pennsylvanian Midcontinent Seaway of North America with Implications for Hydrography and Sedimentation. *Journal of Sedimentary Research*, 77: 843-865.
- Wells, M.R., Allison, P.A., Piggott, M.D., Hampson, G.J., Pain, C.C. and Gorman, G.J., 2010a. Tidal Modeling of an Ancient Tide-Dominated Seaway, Part 1: Model Validation and Application to Global Early Cretaceous (Aptian) Tides. *Journal of Sedimentary Research*, 80: 393-410.
- Wells, M.R., Allison, P.A., Piggott, M.D., Hampson, G.J., Pain, C.C. and Gorman, G.J., 2010b. Tidal Modeling of an Ancient Tide-Dominated Seaway, Part 2: The Aptian Lower Greensand Seaway of Northwest Europe. *Journal of Sedimentary Research*, 80: 411-439.
- Wells, M.R., Allison, P.A., Piggott, M.D., Pain, C.C., Hampson, G.J. and De Oliveira, C.R., 2005b. Large sea, small tides: the Late Carboniferous seaway of NW Europe. *Journal of the Geological Society*, 162: 417-420.
- Willis, B.J., 2005. Deposits of tide-influenced river deltas. In: L. Giosan and J.P. Bhattacharya (Editors), *River Deltas—Concepts, Models, and Examples*. SEPM Special Publication, pp. 87-129.
- Willis, B.J. and Fitris, F., 2012. Sequence Stratigraphy of Miocene Tide-Influenced Sandstones In the Minas Field, Sumatra, Indonesia. *Journal of Sedimentary Research*, 82: 400-421.

- Willis, B.J. and Gabel, S., 2001. Sharp-based, tide-dominated deltas of the Sego Sandstone, Book Cliffs, Utah, USA. *Sedimentology*, 48: 479–506.
- Wilmes, S.-B. and Green, J.A.M., 2014. The evolution of tides and tidal dissipation over the past 21,000 years. *Journal of Geophysical Research: Oceans*, 119: 4083–4100.
- Wolanski, E.E.J., Mazda, Y.Y. and Ridd, P.P.V., 1992. Mangrove hydrodynamics. In: A.I. Robertson and D.M. Alongi (Editors), *Tropical Mangrove Ecosystems. Coastal and Estuarine Studies*. American Geophysical Union, Washington, DC, pp. 43–62.
- Wonham, J.P. and Elliott, T., 1996. High-resolution sequence stratigraphy of a mid-Cretaceous estuarine complex: the Woburn Sands of the Leighton Buzzard area, southern England. In: S.P. Hesselbo and D.N. Parkinson (Editors), *Sequence Stratigraphy in the British Isles. Special Publications 103*. Geological Society, London, pp. 41–62.
- Woodroffe, C.D., Rogers, K., McKee, K.L., Lovelock, C.E., Mendelsohn, I.A. and Saintilan, N., 2016. Mangrove sedimentation and response to relative sea-level rise. *Annual Review of Marine Science*, 8: 243–66.
- Yang, B., Gingras, M.K., Pemberton, S.G. and Dalrymple, R.W., 2008. Wave-generated tidal bundles as an indicator of wave-dominated tidal flats. *Geology*, 36: 39.
- Yang, C.S. and Nio, S.D., 1985. The estimation of palaeohydrodynamic processes from subtidal deposits using time series analysis methods. *Sedimentology*, 32: 41–57.
- Yoshida, S., Johnson, H.D., Pye, K. and Dixon, R.J., 2004. Transgressive changes from tidal estuarine to marine embayment depositional systems: The Lower Cretaceous Woburn Sands of southern England and comparison with Holocene analogs. *AAPG Bulletin*, 88: 1433–1460.
- Yoshida, S., Steel, R.J. and Dalrymple, R.W., 2007. Changes in depositional processes—an ingredient in a new generation of sequence-stratigraphic models. *Journal of Sedimentary Research*, 77: 447–460.
- Zheng, W. and Deng, H., 2012. The Tidal Sandstone Characteristic of the Zhuhai Formation, Huizhou Oil Field, Pearl River Mouth Basin, South China Sea. *Petroleum Science and Technology*, 30: 567–574.
- Zhou, Z., Chen, L., Tao, J., Gong, Z., Guo, L., van der Wegen, M., Townend, I. and Zhang, C., 2020. The role of salinity in fluvio- deltaic morphodynamics: A long- term modelling study. *Earth Surface Processes and Landforms*, 45: 590–604.
- Zhou, Z., Coco, G., Jiménez, M., Olabarrieta, M., Van der Wegen, M. and Townend, I., 2014. Morphodynamics of river- influenced back- barrier tidal basins: The role of landscape and hydrodynamic settings. *Water Resources Research*, 50: 9514–9535.
- Zhou, Z., Coco, G., Townend, I., Olabarrieta, M., Van Der Wegen, M., Gong, Z., D'alpaos, A., Gao, S., Jaffe, B.E. and Gelfenbaum, G., 2017. Is “morphodynamic equilibrium” an oxymoron? *Earth-Science Reviews*, 165: 257–67.
- Zhou, Z., Coco, G., van der Wegen, M., Gong, Z., Zhang, C. and Townend, I., 2015. Modeling sorting dynamics of cohesive and non-cohesive sediments on intertidal flats under the effect of tides and wind waves. *Continental Shelf Research*, 104: 76–91.
- Ziegler, P.A., 1990. *Geological Atlas of Western and Central Europe*. Maatschappij B.V., Shell Internationale Petroleum, The Hague, 239 pp.
- Zuchuat, V., Sleveland, A.R., Pettigrew, R.P., Dodd, T.J., Clarke, S.M., Rabbal, O., Braathen, A. and Midtkandal, I., 2019. Overprinted allocyclic processes by tidal resonance in an epicontinental basin: The Upper Jurassic Curtis Formation, east- central Utah, USA. *The Depositional Record*, 5: 272–305.



1  
2  
3  
4  
5  
6  
7  
8  
9  
10  
11  
12  
13  
14  
15  
16  
17  
18  
19  
20  
21  
22  
23  
24  
25  
26  
27  
28  
29  
30  
31  
32  
33  
34  
35  
36  
37  
38  
39  
40  
41  
42  
43  
44  
45  
46  
47  
48  
49  
50  
51  
52  
53  
54  
55  
56  
57  
58  
59  
60  
61  
62  
63  
64  
65

~~Predicting~~Prediction of shoreline–shelf depositional process  
~~regimes using insights from~~regime guided by palaeotidal  
modelling

Daniel S. Collins<sup>1,2</sup>, Alexandros Avdis<sup>2</sup>, Martin R. ~~Wells~~<sup>3</sup>Wells<sup>3</sup>, ~~Christopher D. Dean~~<sup>4</sup>A,  
~~Andrew J. Mitchell~~<sup>2</sup>, Peter A. Allison<sup>2</sup>, Howard D. Johnson<sup>2</sup>, Gary J. Hampson<sup>2</sup>, Jon ~~Hill~~<sup>4</sup>,  
~~Christopher D. Dean~~<sup>5</sup>Hill<sup>5</sup>, and Matthew D. Piggott<sup>2</sup>

<sup>1</sup> Shell International Ltd, London, SE1 7NA, UK  
<sup>2</sup> ~~Department of Earth Science and Engineering, Imperial College London, South Kensington~~  
Campus, London, SW7 2AZ, UK  
<sup>3,3</sup> BP plc, Chertsey Road, Sunbury-on-Thames, Middlesex TW16 7LN, UK  
<sup>4</sup> ~~Department of Earth Science, Natural History Museum, London, SW7 5BD, UK~~  
<sup>4</sup>~~Environment~~<sup>5</sup>Environment Department, University of York, Heslington, York, YO10 5DD, UK  
<sup>5</sup>~~School of Geography, Earth & Environmental Sciences, University of Birmingham,~~  
~~Birmingham, B15 2TT, UK~~

ABSTRACT

~~Tides are a fundamental element of predictive~~Ancient shoreline–shelf depositional ~~models~~–systems  
~~are influenced by an unusually wide array of geological, biological and hydrodynamic processes, with~~  
~~sediment transport and deposition primarily determined by the interaction of ancient shoreline process~~  
~~regimes. These models principally relate ancient river, wave (including storm) and tidal processes,~~  
~~and changes in relative sea level. Understanding the impact of these processes on shoreline–shelf~~  
~~morphodynamics and stratigraphic preservation remains challenging. Numerical modelling integrated~~

Style Definition: Normal: Font: (Default) Times New Roman, 12 pt, Space After: 0 pt, Line spacing: Double
Style Definition: Heading 4: Font: Bold
Style Definition: Heading 5
Style Definition: Heading 6
Style Definition: Heading 7
Style Definition: Heading 8
Style Definition: Heading 9
Style Definition: Header
Style Definition: Footer
Style Definition: Base_Heading
Style Definition: Base_Text
Style Definition: Balloon Text: Font: (Default) Tahoma, 8 pt, Line spacing: Double
Style Definition: Body Text Indent
Style Definition: Body Text Indent 2
Style Definition: Body Text Indent 3
Style Definition: Caption
Style Definition: EndNote Bibliography Title: Font: 12 pt
Style Definition: EndNote Bibliography: Font: 12 pt
Style Definition: Comment Text: Font: (Default) Times New Roman, Space After: 0 pt, Line spacing: Double
Style Definition: Normal (Web)
Style Definition: No Spacing: Font: 12 pt
Style Definition: Revision
Style Definition: Title
Style Definition: paragraph
Formatted: Art title, Line spacing: Double
Commented [CDSS1]: Modified to to 'Prediction of shoreline–shelf depositional process regime guided by palaeotidal modelling'. The updated title is succinct and clearly articulates the purpose of the manuscript: to review how predictions and classification of shoreline-shelf depositional process regime can be guided by insights from numerical palaeotidal modelling.
Formatted: English (United Kingdom)
Formatted: Not Superscript/ Subscript
Formatted: Line spacing: single
Formatted: Indent: Left: 0", Hanging: 0.3", Line spacing: Double
Formatted: Default Paragraph Font, Font: 12 pt
Formatted: Default Paragraph Font, Font: 12 pt
Formatted: Default Paragraph Font, Font: 12 pt

with traditional facies analysis provides an increasingly viable approach, with the potential to shelf width (e.g. quantify, and thereby improve understanding of, the impact of these complex coastal sedimentary processes. An integrated approach is presented here that focuses on palaeotidal modelling to investigate the controls on ancient tides and their influence on sedimentary deposition and preservation – one of the three cornerstones of the ternary process classification scheme of shoreline-shelf systems. Numerical tidal modelling methodology is reviewed and illustrated in three palaeotidal model case studies of different scales and focus. The results are synthesised in the context of shoreline-shelf processes, including a critique and modification of the process-based classification scheme.

The emphasis on tidal processes reflects their global importance throughout Earth's history. Ancient palaeotidal models are able to highlight and quantify the following four controls on tidal processes: (1) ~~100 km) and shoreline geometry (e.g. 1–10 km)~~ but rarely consider larger-scale basin) the physiography (100–1000 km) or variability related to changing shoreline geometry. A refined shape and depth of oceans (1000s km scale) determines the degree of tidal resonance; (2) the physiography of ocean connections to partly enclosed water bodies (100–1000s km scale) determines the regional-scale flux of tidal energy (inflow versus outflow); (3) the physiography of continental shelves influences shelf tidal resonance potential; and (4) tides in relatively local-scale embayments (typically 1–10s km scale) are influenced by the balance of tidal amplification due to funnelling, shoaling and resonance effects versus frictional damping. In deep time, palaeogeographic and palaeobathymetric uncertainty can be accounted for in palaeotidal models by performing sensitivity analyses to different scenarios, across this range of spatial scales.

These tidal process controls are incorporated into an updated predictive decision tree for ancient shoreline process regimes is developed based on a review of modern determining shoreline processes, supported by new insight from numerical palaeotidal modelling studies. Modern depositional shorelines are overwhelmingly wave dominated, suggesting a first-order control – shelf process regime in terms of the relative interaction of wave-fetch and wave-generating wind conditions on shoreline processes. Several numerical palaeotidal modelling studies highlight the following controls on tidal processes: (1) 100–1000 km-scale basin-physiography on tidal inflow

versus outflow; (2) 10–100 km scale shelf physiography on shelf tidal resonance potential; (3) tidal amplification (funnelling and shoaling) versus frictional effects in shoreline embayments (1–10 km scale); and (4) palaeogeographic uncertainty, which affects prediction of these latter three controls, fluvial and tidal processes. The predictive decision tree considers the effects of basin physiography, shelf width and shoreline morphology on wave, tide and fluvial and tidal processes separately. The uncertainty and ambiguity in applying the widely used three-tier process classification scheme are reduced by using the decision tree in conjunction with a proposed two-tier classification of process regime in the decision tree (that is limited to primary and secondary processes) reflects uncertainty and ambiguity in applying three. This two-tier process classification schemes to modern shorelines and, especially, to ancient shoreline deposits. This review demonstrates scheme is illustrated in the benefit three case studies, showing how integration of numerical tidal modelling, calibrated by integrated comparison to with facies analysis of the preserved stratigraphic record, and offers a refined classification and improves confidence in prediction of tide-influenced shoreline-shelf process regimes. Wider and consistent utilisation of these concepts, and numerical simulations of other depositional processes; application of this approach will further improve process-based classifications and predictions of modern and ancient shoreline-shelf systems.

Keywords: Numerical Modelling; Shoreline-Shelf; Wave; Tide; Fluvial; Process regime; Numerical Modelling; Palaeotidal; Mixed process; Shoreline; Deltaic; Shelf; Sedimentary Preservation.

## 1 INTRODUCTION

**Commented [CDSS2]:** Rewritten with the intention of clarifying:

- Broader understanding on the complexity of shoreline – shelf systems
- Impact of improving understanding of these systems
- Including the ocean-scale controls on tides
- More emphasis on the revised predictive classification of shoreline-shelf process regime guided by insights from numerical tidal modelling

**Formatted:** Default Paragraph Font, Font: 12 pt

**Formatted:** Default Paragraph Font, Font: 12 pt

**Formatted:** Line spacing: Double

Shorelines are amongst the most geologically variable, environmentally diverse and climatically sensitive sedimentary environments, with important social and economic implications (Giosan and Bhattacharya, 2005; Syvitski and Saito, 2007). Physical, biological and chemical exchange between the continents and oceans across this interface is fundamentally impacted by the interaction of hydrodynamic processes relating to fluvial, wave and tidal influence. Shoreline-shelf landscapes at the land-sea interface are some of the most dynamic settings on earth, containing a complex array of sedimentary systems that include deltaic, estuarine, paralic, shallow marine and shelfal environments. The type, morphology, depositional architecture and spatio-temporal evolution of these systems reflect dynamic interactions between three main groups of forcing conditions (Townend, 2012; Zhou et al., 2017). First, hydrodynamic processes operate on a range of spatio-temporal scales and principally include tides, river flow and wave climate (e.g. Galloway, 1975; Boyd et al., 1992; Ainsworth et al., 2011), but also larger magnitude-lower frequency extreme events such as storms. Second, the ‘sedimentology’ of the system includes both the rate of sediment supply and the range of grain sizes and characteristics of the sediment sources (Orton and Reading, 1993). Third, landscape setting describes the physiographic characteristics of the land-sea interface and receiving sedimentary basin (Zhou et al., 2014), which depends on various factors, most notably antecedent geology, sea level change, accommodation space (often related to tectonics) and, increasingly, anthropogenic influence (sediment supply, dredging, vegetation change, etc.). Additional processes that mediate interactions between these factors include biological activity (e.g. fauna-sediment reworking) and vegetation cover. Furthermore, feedbacks exist between these controls such that changes, for example, in sea level can influence shoreline morphology (landscape setting) and cause potentially dramatic changes in tide and/or wave influence (e.g. Yoshida et al., 2007; Collins et al., 2018c). In the case of natural shoreline-shelf systems, morphological change is generally related to the intrinsic feedback between hydrodynamics, sediment transport and morphology, but this feedback is invariably conditioned and constrained by the various factors governing landscape setting and sediment character of the system (Zhou et al., 2017). Obtaining a better understanding of shoreline-shelf systems is of increasing importance in the 21<sup>st</sup> Century. Anthropogenic climate change has the potential to significantly impact shorelines through changes in sea level and rates of sediment weathering, erosion and supply.

Anthropogenic influence on shorelines also extends to direct displacement of large volumes of sediment in engineering works and indirectly through, for example, changes in sediment erosion versus deposition related to vegetation clearing (Tomašových and Kidwell, 2017) and modified balances between morphology, hydrodynamics and sediment transport. As such, present-day configurations of shoreline systems are often the result of ongoing and intrinsically coupled natural, social and economic feedbacks, the impacts of which on future long-term shoreline configurations are only just being explored (Zhou et al., 2017). However, ancient stratigraphic records containing an archive of past changes in shoreline–shelf environments can form a useful reference for interpreting the potential future response of shorelines to changes in climatically-driven processes, provided these can be disentangled from other allogenic and autogenic controls (e.g. Reading and Collinson, 1996; Hampson, 2016). Some of these ancient stratigraphic units deposited at or near shorelines have contributed significantly to global conventional and unconventional hydrocarbon production. Characterising, classifying and understanding the difference in facies, architecture and morphology between reservoirs formed in different shoreline–shelf systems has underpinned efforts to interpret and predict reservoir distribution and performance, to ultimately improve hydrocarbon recovery. Similar reservoirs also form vital freshwater aquifers, geothermal reservoirs and current and future reservoirs for CO<sub>2</sub> storage in carbon, capture and storage (CCS) projects.

Due to the complexity and evident importance of these settings, a variety of classification systems have evolved for categorising shoreline–shelf depositional systems (see reviews by Elliott, 1986; Boyd et al., 1992; Johnson and Baldwin, 1996; Reading and Collinson, 1996; James and Dalrymple, 2010; Ainsworth et al., 2011). However, the most widely applied classifications relate shoreline–shelf morphology and idealised sections of preserved stratigraphy to the relative strength of river, wave and tide processes (Coleman and Wright, 1975; Galloway, 1975; Hayes, 1975; Hayes, 1979; Boyd et al., 1992; Ainsworth et al., 2011), conditioned by the overarching controls of relative sea level change versus sediment supply (Curray, 1964; Boyd et al., 1992; Dalrymple, 1992), sediment grain size (Orton and Reading, 1993) and tectono-physiographic setting (Reading and Collinson, 1996).

Whilst the variety and variability of controls on shoreline–shelf systems make it impossible to quantitatively understand and fully model ‘real world’ systems, numerical modelling has become

an increasingly important tool for simplifying and understanding the diverse and complex set of controls on such systems. Numerical models simulate ‘virtual world’ systems subject to selected processes operating under controlled boundary conditions (Zhou et al., 2017). Models of virtual systems represent a conceptual idealisation of the real world for the processes modelled, producing robust, reliable and realistic simulation results calibrated with real world measurements (Zhou et al., 2017). In the case of shoreline–shelf systems, there is now a wide body of research that investigate long-term morphodynamics and shoreline depositional processes using a process-based modelling approach. Most of these studies have so far investigated the influence of varying tide, river and wave hydrodynamics (de Vriend et al., 1993; Van der Wegen and Roelvink, 2008; Nahon et al., 2012; Leonardi et al., 2014; Zhou et al., 2014; Rossi et al., 2016; Zhou et al., 2017), but other factors such as salinity differences (Olabarrieta et al., 2018; Zhou et al., 2020), sediment sorting processes (Zhou et al., 2015) have also been shown to significantly impact shoreline circulation and morphology.

Improved understanding and recognition of process interactions along modern and ancient shorelines has led to refined process-based classifications and predictive models of shoreline systems (Ainsworth et al., 2008; Ainsworth et al., 2011; Vakarelov and Ainsworth, 2013; Nyberg and Howell, 2016)(Ainsworth et al., 2008; Ainsworth et al., 2011; Vakarelov and Ainsworth, 2013; Nyberg and Howell, 2016)). An important component improvement has been wider application of theoretical relationships between the strength of wave or tide processes and shoreline–shelf -physiography, derived from palaeogeographic reconstructions, in order to support facies and stratigraphic interpretations of ancient depositional processes, most notably the impact of shoreline geometry and on tidal resonance or amplification (Godin, 1993; Yoshida et al., 2007; van Cappelle et al., 2018; Zuchuat et al., 2019)(Godin, 1993; Yoshida et al., 2007; van Cappelle et al., 2018; Zuchuat et al., 2019)). Simple theoretical relationships ~~are~~ provide a quick method of estimating shoreline–shelf wave and tidal potential; but ~~without~~ lack the ability to assess or understand spatio-temporal

Formatted: Line spacing: single

variability and the sensitivity to, and interaction of, potential physiographic controls. Instead, hydrodynamic numerical modelling enables deeper discussion of these factors, ranging from multi-process morphodynamic simulations (Geleynse et al., 2011; Rossi et al., 2016) to simulations of specific shoreline processes. In particular, numerical tidal simulations (e.g. Slingerland, 1986; Ericksen and Slingerland, 1990; Martel et al., 1994; Wells et al., 2005a; Mitchell et al., 2010; Collins et al., 2018a; Dean et al., 2019) to simulations of specific shoreline processes. Of the trivariate controls of tide, river and wave processes, tidal forcing has proven both slightly easier to predict using numerical modelling (given that it relates to well understood planetary motions) and perhaps more relevant to understanding ancient shoreline-shelf processes, given that tides operate globally through the whole Earth system (Stammer et al., 2014), influence sediment transport to some capacity along all shorelines globally and have operated throughout the vast majority of Earth's history (Green et al., 2017). In comparison, river processes only operate directly along a small portion of global shorelines, waves depend on wind patterns, fetch and basin physiography, and both river and wave processes depend on complicated atmospheric and climatic processes. As such, numerical tidal simulations (e.g. Slingerland, 1986; Ericksen and Slingerland, 1990; Martel et al., 1994; Wells et al., 2005a; Mitchell et al., 2010; Collins et al., 2018a; Collins et al., 2018b; Dean et al., 2019) have been extensively validated against modern sedimentary environments and, through integration with sedimentological and stratigraphic datasets, have provided unique information on the physiographic controls on tidal processes and sedimentary preservation along ancient tide-influenced shorelines. However, the implications of ancient tidal model simulations on the classification, prediction and interpretation of shoreline-shelf depositional process regimes have not yet been fully explored.



The aims of this review article are threefold. First, the results of three palaeotidal modelling studies are integrated aims to identify the dominant physiographic controls on shoreline tidal processes. The three case studies investigated ancient tides in strongly contrasting geological settings and on various spatial and temporal scales: (1) the Oligocene–Miocene South China Sea (SCS); (2) the Early Cretaceous Lower Greensand Seaway, NW Europe; and (3) the Late Cretaceous Bohemian Cretaceous Basin, Central Europe. Second, the comparison between model results and sedimentological and stratigraphic data in the rock record establishes the strengths, limitations and potential biases of the palaeotidal modelling approach. Third, assess the implications of palaeotidal model simulations for classification and prediction of shoreline depositional process regime are assessed.

## 2 BACKGROUND

### 2.1 Tidal theory and numerical modelling

#### 2.1.1 Equilibrium tidal theory

The non-mathematical theory of Earth tides has been extensively reviewed (Defant, 1961; MacMillan, 1966; Dalrymple, 1992; Allen, 1997; Open University Course Team, 1999; Willis, 2005; Kvale, 2006; Kvale, 2012; Longhitano et al., 2012). Astronomical tides are defined as ‘any periodic fluctuation in the water level that is generated by the gravitational attraction of the Moon and Sun’ (Dalrymple, 1992). The Moon, although smaller than the Sun, accounts for c. 70% of the tide-raising force due to its closer proximity. However, the tide-generating forces are small. Significant tides, though typically <1 m in tidal range (the difference in sea level between

**Commented [CDSS3]:** Introduction has been extensively rewritten and lengthened in order to improve the ‘setup’ of the article’s main focus – as indicated more explicitly in the revised title and abstract, address additional review comments and broaden impact of the review article, especially with wider research community applying numerical modelling to understanding shoreline-shelf systems.

**Formatted:** Line spacing: single

**Commented [CDSS4]:** Section 2 BACKGROUND and 3 METHODS have been combined in the revised manuscript.

We have also reordered subsections, in line with reviewer #1’s comment that to improve the ‘setup’ of the article. Therefore, the sections on classification and prediction of shoreline-shelf process regime (section 2.3 in the original submission) occurs before a much-shortened section 2.1. Furthermore, the original section 2.2 is combined with the original section 2.3; likewise the original section 3.1 is combined with section 2.1.

As a consequence of shortening the background on tidal modelling, and changing the order, the number and order of figures has been significantly revised – including less of the tidal theory to focus on classification and prediction of shoreline-shelf process regime

**Commented [CDSS5]:** This section has been significantly shortened, with a detailed list of reviews on these topics included

~~high and low tide), only develop in the open oceans. Smaller enclosed water bodies (seas, lakes) and water on continental shelves do not develop appreciable *in situ* tides (Dalrymple, 1992).~~

Tides are most commonly understood in the context of equilibrium tidal theory, in which the Earth is covered by water of uniform depth that responds instantaneously to changes in tractive forces and the Moon rotates around the equator at a constant distance (e.g. MacMillan, 1966; Dalrymple, 1992). The lunar tidal force, in combination with centrifugal forces associated with the rotation of the earth-moon system about its common centre of mass, leads to the development of two oceanic tidal bulges: one beneath the moon, one on the opposite side of the Earth. The rotation of Earth every 24 hours, and the Moon around the Earth every 29 days (in the same direction as the Earth rotates), means these bulges appear to move clockwise around the Earth. This produces two high and two low (semi-diurnal) tides each day at a period of 12.42 hours, with rising and falling tides termed ‘flood tide’ and ‘ebb tide’, respectively (Dalrymple, 1992).

Equilibrium model tides vary on many timescales due to changes in the magnitude of the tide-generating forces produced by the Sun and Moon (Defant, 1961; MacMillan, 1966; Dalrymple, 1992; Kvale, 2006). For example, spring-neap tidal cycles (14.77 days) are caused by the relative positioning of the Earth, Sun and Moon. Spring tides occur when the Earth, Moon and Sun are aligned in a straight line at new or full Moon, resulting in greater than average tidal ranges. In contrast, neap tides occur when the Sun and Moon are at right angles to the Earth at first- and third-quarter phases of the Moon, resulting in smaller tidal ranges (Fig. 1A and B). The time between successive new moons is called the ‘synodic month’, which has a modern period of 29.53 days and encompasses two spring-neap cycles. For semi-diurnal tides, each spring-neap cycle (every 14.77 days) contains up to 28 tidal cycles (Dalrymple, 1992; Kvale, 2006).

Furthermore, due to the tilt of the Earth's axis, the declination of the Moon varies by  $28.5^\circ$  north and south of the equator monthly (Fig. 1C). Daily, the declination of the Moon can lead to one semi-diurnal tide being higher (dominant) than the other (subordinate), which is termed 'diurnal inequality' (Fig. 1D). Monthly, there is a 'tropical' spring-neap cyclicity with increased diurnal inequality when the Moon is at its maximum declination (Fig. 1D) (e.g. Kvale, 2012).

While equilibrium tidal theory explains the astronomical forcing causing tides, real-world tides are complicated by several factors. First, a mean ocean depth of c. 22 km is needed to account for rotation of a tidal bulge around the circumference of the Earth in 24 hours, whereas the mean measured ocean depth is c. 4 km (Wells et al., 2005a). Second, ocean basins are interrupted by landmasses and the ocean water depth varies globally, which means two bulges either side of the Earth cannot exist. Instead, oceanic tides rotate as waves around fixed (amphidromic) points with negligible tidal amplitude (half the tidal range) (Fig. 2). Third, inertia and friction mean that the ocean does not respond instantaneously to the tidal forcing. Last, equilibrium tidal theory does not explain the occurrence of the following: (1) diurnal (one high tide and one low tide in a tidal day) tides in low latitude positions, which are only predicted at high latitudes; (2) mid-latitude semi-diurnal tides with minimal diurnal inequality; and (3) spring-neap cycles synchronized with the 27.32 day (tropical month) lunar orbital cycle of the Moon (tropical month), rather than the more common 29.53 day cycle of lunar phases (synodic month or 'lunar month').

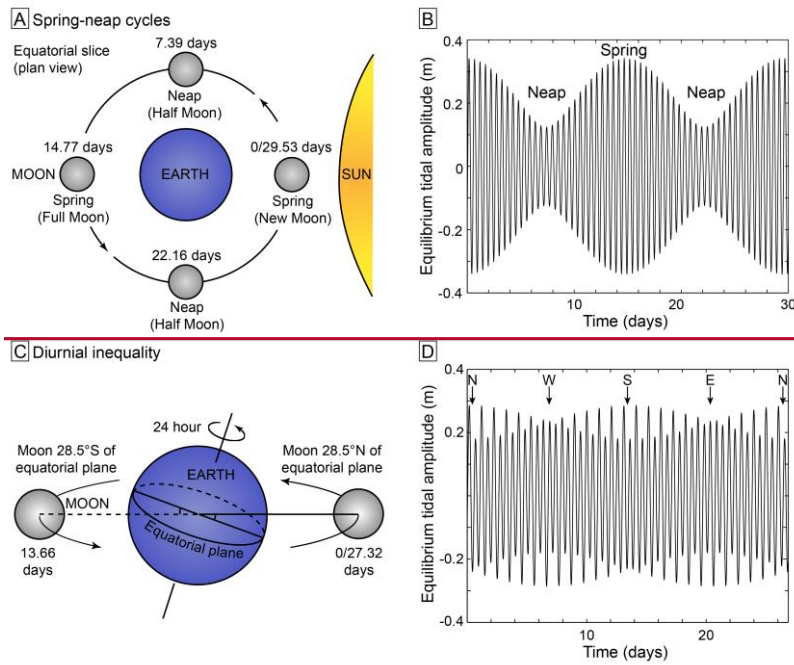


**Fig. 1.** (A) Astronomical explanation of synodic spring-neap tidal cycles. Synodic spring tides occur when the Sun and Moon are above the same line of Earth's longitude (conjunction) or are  $180^\circ$  of longitude apart (opposition). Synodic neap tides occur when the Sun and Moon are separated by  $90^\circ$  of Earth's longitude. (B) Graph of equilibrium tidal amplitude over a 30-day period displaying synodic spring-neap tidal cycles caused by the interaction of  $M_2$  and  $S_2$  tidal constituents. (C) Monthly variation in the Moon's declination between  $28.5^\circ$  north and south of the Earth's equatorial plane caused by the tilt of the Earth's axis, which is accounted for by the  $K_1$  and  $O_1$  tidal constituents (Table 1). (D) Graph of equilibrium tidal amplitude over a 27-day period caused by the interaction of the  $M_2$  and  $K_1$  tidal constituents. Daily, one tide is larger than the other (diurnal inequality). Monthly, there is a 'tropical' spring-neap cyclicity of more pronounced diurnal inequality when the Moon is at its maximum declination north or south of the equator. N—Moon north of the Equator; W—Moon west of the equator; S—Moon south of the equator; E—Moon east of the equator. After Wells (2008).

Commented [CDSS6]: Removed

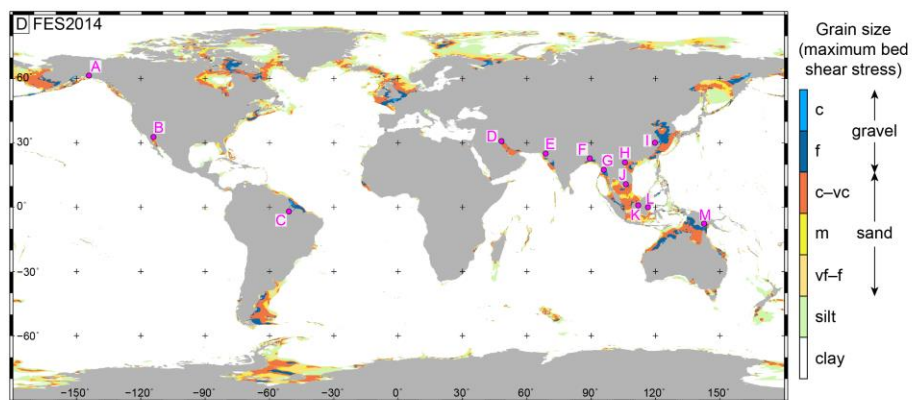
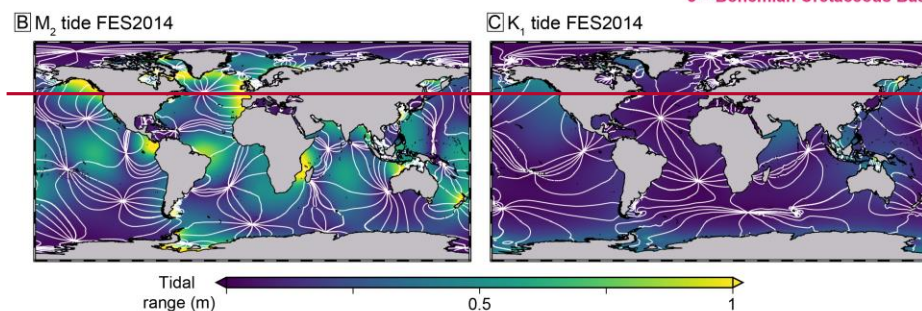
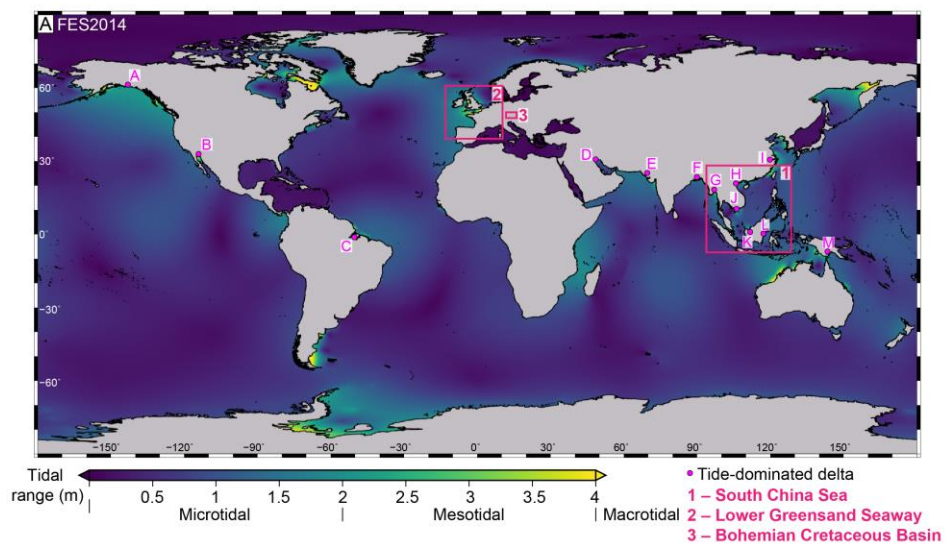


**Fig. 2.** (A) Present day global tidal range based on the FES 2014 tidal model (Carrère et al., 2015), showing the locations (pink dots) of tide-dominated deltas (Goodbred and Saito, 2012): A) Copper; B) Colorado; C) Amazon; D) Shatt-al-Arab; E) Indus; F) Ganges-Brahmaputra; G) Irrawaddy; H) Red River; I) Yangtze; J) Mekong; K) Rajang; L) Mahakam; and M) Fly. Pink boxes show approximate locations of the palaeotidal modelling case studies. (B, C) Global map of  $M_2$  (B) and  $K_1$  tidal amplitude (C) from FES 2014. Contours join lines of equal phase in  $30^\circ$  intervals and white arrows give the sense of rotation of the major ocean amphidromic systems. (D) Maximum tidal bed shear stress, plotted as the equivalent grain size that could be entrained if available, for FES2014, including the difference in sediment grain size class. Grain size abbreviations: vf = very fine; f = fine; m = medium; c = coarse; vc = very coarse.

### 2.1.2 Dynamic tidal theory

Given the limitations of equilibrium tidal theory, real-world tides are more accurately explained by dynamic tidal theory. In this model, the tidal forcing due to the movement and angular speed of the Moon and Sun are modelled as the combined effects of a series of imaginary satellites (Foreman and Henry, 1979; Pugh, 1987; Kvale, 2006; Kvale, 2012). Each modelled satellite generates its own tidal wave of a given tidal amplitude, period and phase angle (response time) moving around an amphidromic point (Pugh, 1987; Kvale, 2006; Kvale, 2012). Each tide is referred to as a tidal constituent, each of which are represented by alphanumeric terms and can be derived from the harmonic decomposition of tidal station water level measurements. From over 100 possible tidal constituents, 11 account for c. 82% of the variability observed in measured tides (Table 1) (e.g. Defant, 1961; Kantha and Clayson, 2000). The by discussing three main tidal cycles (i.e. synodic, tropical and anomalistic) are related to harmonic convergence and divergence of major tidal constituents, most notably: (1) diurnal inequality exists because the  $O_1$  and  $M_2$  tidal constituents are in phase only once a day; (2) synodic neap-spring cycles are

generated when the  $M_2$  and  $S_2$  constituents are in phase (every 14.77 days); and (3) tropical neap-spring cycles reflect the convergence of the  $K_1$  and  $O_1$  constituents (every 13.66 days) (Kvale, 2006; Kvale, 2012). Amphidromic systems are primarily the result of the combined interaction of tidal constituents, basin geometry and the Coriolis force. Table 2 provides a summary of key tide related terms.

Name	Description	Period (hr or day)	Equilibrium amplitude (m)
<b>Semidiurnal</b>			
$M_2^{*†§}$ Principal Lunar	Rotation of Earth with respect to the Moon	12.42 hr	0.242334
$S_2^{*†§}$ Principal Solar	Rotation of Earth with respect to the Sun	12.00 hr	0.112841
$N_2^*$ Lunar elliptic	Eccentricity of Lunar orbit	12.66 hr	0.046398
$K_2^*$ Luni-solar declinational	Modulation of $M_2$ and $S_2$ due to Lunar and Solar declination changes	11.97 hr	0.030704
<b>Diurnal</b>			
$K_1^{*†§}$ Luni-Solar declinational	Change in Lunar and Solar declination	23.94 hr	0.141565
$O_1^{*†§}$ Principal Lunar	Change in Lunar declination	25.82 hr	0.100514
$P_1^*$ Principal Solar	Change in Solar declination	24.07 hr	0.046843
$Q_1^*$ Lunar elliptic	Modulation of $O_1$ due to the elliptical orbit of the Moon	26.87 hr	0.019256
<b>Long-period</b>			
$M_f^*$ Lunar fortnightly	Non-sinusoidal Lunar declination changes	13.66 d	0.041742
$M_m^*$ Lunar monthly	Irregularities in the rate of change of distance and speed of the Moon in orbit	27.55 d	0.022026
$S_{sa}^*$ Solar semi-annual	Non-uniform changes in the Sun's declination and distance	182.6 d	0.019446

\* tidal constituent used in Collins et al. (2017) and Collins et al. (2018) (Oligocene–Miocene South China Sea)

† tidal constituent used in Wells et al. (2010b) (Early Cretaceous Lower Greensand Seaway)

§ tidal constituent used in Mitchell et al. (2010) (Late Cretaceous Bohemian Cretaceous Basin)

**Table 1. Origin, period (in solar hours, hr or days, d) and equilibrium amplitude of 11 important tidal constituents (after Defant, 1961; Kantha and Clayson, 2000; Wells, 2008).**

Commented [CDSS7]: Removed



Name	Description
Astronomical tide	Tide formed by the gravitational and rotational effects of the Moon and Sun on the water in an open ocean or seaway
Bed shear stress	Force per unit area exerted by flow on the sediment surface
Co-oscillating or boundary tide	Tide formed by the propagation of an open-ocean astronomical tide into a connected water body
Coriolis effect and amphidromic cells	The Coriolis effect deflects the tidal wave to the right in the northern hemisphere and left in the southern hemisphere. In the northern hemisphere, this causes the tidal wave to rotate anticlockwise about an amphidromic point of zero tidal range. In enclosed water bodies, the deflected tidal wave (termed a Kelvin wave) pushes against the shoreline, leading to an exponential increase in tidal range from the amphidromic node towards the shoreline.
<del>Diurnal</del>	<del>Once-daily tide where the <math>K_1</math> and <math>O_1</math> constituents are more dominant than the <math>M_2</math> and <math>S_2</math> constituents</del>
Resonance	Resonance occurs when the tidal period matches a natural mode of oscillation within a water body. Maximum resonance typically occurs when shelf width is approximately a quarter the dominant tidal wavelength, and matches a half-wave oscillator or standing wave in an enclosed basin and quarter-wave oscillator in an open-ended embayment (gulf).
Funnelling	Increase in tidal amplitude caused by progressive narrowing of a water body
Semidiurnal	Twice-daily tide where the $M_2$ and $S_2$ constituents are more dominant than the $K_1$ and $O_1$ constituents
Shoaling	Increase in tidal amplitude caused by progressive shallowing of a water body
Tidal amplitude	Elevation of tidal high water above mean sea level
Tidal range	Vertical height between consecutive high and low waters over a tidal cycle (twice the tidal amplitude), classified as microtidal (<2 m), mesotidal (2–4 m) and macrotidal (>4 m)

**Table 2. Explanations of several tide-related terms used in this paper (modified from Wells et al., 2010b).**

### ***2.1.3 Shoaling, funnelling and resonance effects on tides***

~~When oceanic tides encounter areas of shallower water and constricted physiography, they may undergo amplification due to shoaling, funnelling and resonance (Table 2).~~

~~Shoaling effects involve a transformation of the tidal wave in order to conserve the energy flux.~~

~~This occurs by a reduction in the wave speed and wavelength and an associated increase in the wave amplitude and the current velocity (Allen, 1997). Assuming a flat bed and ignoring~~

reflected energy and bottom drag, the relative change in amplitude is proportional to the quadratic root of the relative change in water depth:

$$\frac{h_1}{h_2} = \left( \frac{A_2}{A_1} \right)^4$$

where,  $h_1$  and  $h_2$  are the deep and shallow water depths and  $A_1$  and  $A_2$  are the corresponding amplitudes, respectively (Allen, 1997). The relative current velocity  $U$  ( $\text{ms}^{-1}$ ) increases by

$$\frac{h_1}{h_2} = \left( \frac{U_1}{U_2} \right)^{\frac{3}{4}}$$

where subscripts 1 and 2 denote the initial deep shallow water depths, respectively (Allen, 1997).

Funnelling of a tidal wave occurs when the flow is physically constricted by a physiographic feature like a strait or embayment. For a landward tapering and landward shallowing embayment, assuming that energy is conserved and ignoring bottom friction, the combined effect of funnelling and shoaling (convergence effects) are estimated by

$$\frac{A_e}{A_o} = \left( \frac{w_o}{w_e} \right)^{1/2} \left( \frac{h_o}{h_e} \right)^{1/4}$$

where  $A$  = tidal range (m),  $w$  = water body width (m),  $h$  = water body depth (m), subscript 'o' denotes the open deeper water body and subscript 'e' the constricted shallower water body (Slingerland, 1986; Allen, 1997). The comparison between theoretical convergence effects ( $A_e/A_o$ ) on tides in ancient physiographic embayments calculated using this equation, and tidal amplitude and convergence effects predicted by palaeotidal modelling, can illustrate the possible effects of bottom friction and attenuation by physiographic features (e.g. shoals, islands, headlands) (Wells et al., 2007a; Collins et al., 2018a).

Resonance occurs when the natural period of oscillation on the shelf, or within a shoreline bathymetric constriction, is coincident with the tidal period (Slingerland, 1986; Allen, 1997). For an idealized straight and laterally extensive continental shelf, tidal resonance reaches a maximum when shelf width is one quarter the tidal wavelength (and for widths 3/4, 5/4, etc.), assuming the incident tide is perpendicular to the shelf, friction is inversely proportional to depth and no Coriolis effect (Fig. 3A) (e.g. Proudman, 1953; Howarth, 1982). The resonance pattern is likely to be similar if bathymetry and rotational effects are included (Howarth, 1982). However, the wavelength of tides strongly depends on the dominant phase and water depth (Fig. 3B). At typical continental shelf water depths (100 m), the wavelengths of the semi-diurnal  $M_2$  and diurnal  $K_1$  tides are 1,400 km and 2,700 km, respectively (Fig. 3B) (Kowalik and Luick, 2013). Therefore, resonance of  $M_2$  and  $K_1$  tides requires very different shelf widths of 350 km and 675 km, respectively. As the majority (c. 70%) of modern shelves are <75 km wide (Nyberg and Howell, 2016), tides are closer to resonance as shelf width increases, hence tidal amplitude increases with shelf width (Redfield, 1958; Off, 1963; de Vries Klein, 1977; Cram, 1979; Ainsworth et al., 2011). High tidal ranges along embayed coasts occur partly as a consequence of the effective widening of the shelf, with the tidal system closer to resonance (e.g. Willis, 2005). For a closed or 'blind' embayment (gulf), the simplest period of resonance ( $T$ ) is a quarter wavelength

$$T = \frac{4l}{\sqrt{gh}}$$

Formatted: Font: Not Bold

where  $l$  = embayment length (m),  $g$  = gravitational acceleration ( $\text{ms}^{-2}$ ), and  $h$  = embayment depth (m) (e.g. Allen, 1997). In an ‘enclosed’ water body, the simplest period of resonance ( $T$ ) is a half wavelength

$$T = \frac{2l}{\sqrt{gh}}$$

where  $l$  = basin width (m),  $g$  = gravitational acceleration ( $\text{ms}^{-2}$ ) and  $h$  = water depth (m) (e.g. Allen, 1997). In these situations, resonance occurs when the tidal wave reflected off one boundary of the embayment entrance reaches the opposite boundary (for a partly enclosed water body) at the same time as another tidal wave begins to propagate, such that the waves constructively interfere.

Tidal resonance in embayments is illustrated by using the tidal model Fluidity (Section 3.1) and simple physiographic box models that were centred on the equator, ranged between 0 to 3000 km wide and 0 to 300 m deep (192 experiments in total), and had a constant bottom drag coefficient of 0.0025 and mesh resolution of c. 15 km (Fig. 4) (Wells, 2008). The model was forced with the  $M_2$ ,  $S_2$ ,  $K_1$ , and  $O_1$  tidal constituents such that the total boundary tide amplitude was 1 m, the total amplitudes of semidiurnal (i.e.  $M_2 + S_2$ ) and diurnal (i.e.  $K_1 + O_1$ ) constituents were equal, and the ratios of the  $M_2$  to  $S_2$  constituents and  $K_1$  to  $O_1$  constituents were equal to the ratio of their equilibrium amplitudes (Table 1). The modelled tidal range at the head of the embayment was plotted on a graph of basin width versus depth, which illustrates that even the shallowest basins must be several hundred kilometres wide to attain resonance (Fig. 4). The relative importance of diurnal ( $K_1$  and  $O_1$ ) to semidiurnal ( $M_2$  and  $S_2$ ) tides is quantified using the ratio  $F$ , where

$$F = \left( \frac{K_1 + O_1}{M_2 + S_2} \right)$$

If  $F < 0.25$ , the tide is semi diurnal,  $0.25 < F < 3$ , the tide is mixed, and  $F > 3$ , the tide is diurnal

(Open University Course Team, 1999).

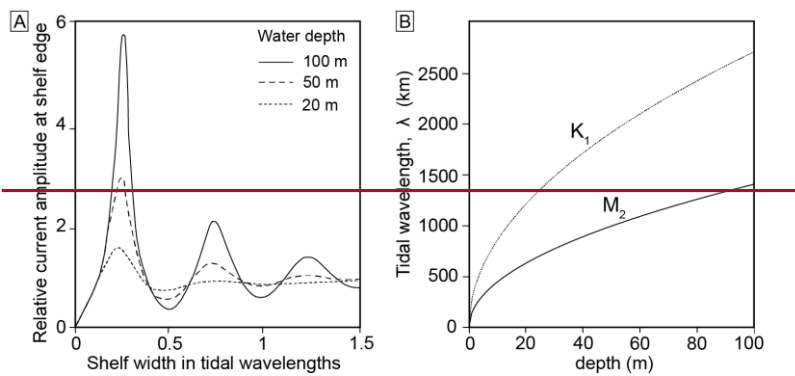


**Fig. 3.** Influence of shelf width on tidal resonance. (A) Plot of tidal resonance widths of straight shelves in terms of tidal wavelengths for water depths of 100, 50 and 25 m. Relative current amplitude is the amplitude divided by the current amplitude of a progressive wave (after Howarth, 1982). (B) Relationship between tidal wavelengths and water depth for the  $M_2$  and  $K_1$  tidal constituents (after Kowalik and Luick, 2013).

Commented [CDSS8]: Removed

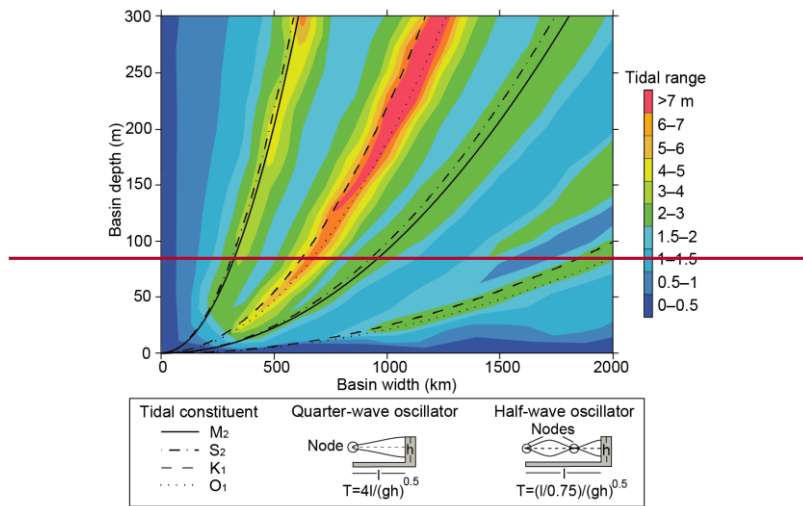


**Fig. 4.** Tidal resonance effect in embayments. Graph shows increase in modeled tidal range for the semidiurnal ( $M_2$ ,  $S_2$ ) and diurnal ( $K_1$ ,  $O_1$ ) tidal constituents at the head of embayments of various dimensions for simple box models using the Fluidity tidal model (from Wells, 2008; Collins et al., 2018a).

Commented [CDSS9]: Removed

#### 2.1.4 Numerical palaeotidal modelling

Palaeotidal numerical modelling can provide quantitative information on ancient shoreline tidal processes and can test their sensitivity to palaeogeographic and palaeobathymetric uncertainty (e.g. Martel et al., 1994; Wells et al., 2005a; Collins et al., 2018a). Computational methods for ancient tidal modelling, including tidal forcing boundary conditions and mesh generation, have advanced since early approaches that used structured meshes and open boundary tidal forcing by the  $M_2$  (principal lunar semi-diurnal) tide only, and output tidal amplitude or range (Slater, 1985; Slingerland, 1986; Ericksen and Slingerland, 1990; Martel et al., 1994). More recent simulations have investigated tidal amplitude (Slingerland, 1986; Wells et al., 2005a; Wells et al., 2005b;

Wells et al., 2007a; Wells et al., 2010a; Wells et al., 2010b) and bed shear stress (Mitchell et al., 2010; Mitchell et al., 2011) in ancient epicontinental seaways, and tidal range and bed shear stress in ancient seas (Collins et al., 2017a; Collins et al., 2018a), using models with astronomical tidal forcing and unstructured meshes (Table 3). ~~These diverse case studies illustrate how the sensitivity of shoreline tides to various palaeogeographic and palaeobathymetric changes can improve predictive models of depositional process regimes of ancient shoreline systems.~~



Geologic age & reference	Study area	Computational method	Boundary conditions	Key findings	Formatted: Font: 11 pt
Late Devonian c. 370 Ma (Slingerland, 1986)	Catskill epicontinental sea of North America	Structured grid; finite difference scheme; Navier Stokes equations; Coriolis parameter ( $f$ -plane).	Open boundary tidal forcing; no astronomical tidal forcing; M2 tide only; Variable bathymetry; Chezy approximation for bottom friction.	Microtidal–low mesotidal, locally mesotidal–macrotidal areas due to resonance, funnelling and shoaling effects. Tidal ranges increased by: 1) increasing the boundary tidal range; 2) increasing the open boundary width; and 3) increasing the depth of the seaway.	Formatted: Font: 11 pt
Mid Cretaceous c. 100 Ma (Slater, 1985)	Western Interior Seaway of North America	Structured grid; finite difference scheme; Laplace Tidal Equations; No Coriolis parameter.	Open boundary and astronomical tidal forcing; M2 tide only; Uniform depths; Linear bottom friction with respect to velocity.	Microtidal; Astronomical forcing dominates; Open boundary tide negligible; Arctic Ocean and possibly significant from the Gulf of Mexico; Tidal range sensitive to water depth (resonance at 200 m water depth).	Formatted: Font: 11 pt Formatted: Font: 11 pt Formatted: Line spacing: single Formatted: Font: 11 pt, Not Bold
Mid Cretaceous c. 100 Ma (Erickson and Slingerland, 1990)	Western Interior Seaway of North America	Structured grid; finite difference scheme; Navier Stokes equations; Coriolis parameter ( $f$ -plane).	Open boundary tidal forcing; no astronomical tidal forcing; M2 tide only; Variable bathymetry; Chezy approximation for bottom friction.	Microtidal, locally mesotidal near Gulf of Mexico; open boundary; Tidal increases as seaway depth and Gulf of Mexico connection increases; Open boundary argued to be dominant contributor to tides, not astronomically forced tides (cf. Slater, 1985).	Formatted: Font: 11 pt Formatted: Font: 11 pt Formatted: Line spacing: single Formatted: Font: 11 pt, Not Bold
Miocene c. 22 Ma (Martel et al., 1994)	Alpine foreland basin of France and Switzerland	Structured grid; finite difference scheme; Navier Stokes equations; Coriolis Parameter ( $f$ -plane).	Open boundary tidal forcing; no astronomical tidal forcing; M2 tide only; Variable bathymetry; Chezy approximation for bottom friction.	Higher tidal current speed predicted with wider open ocean connection; open boundary tide applied.	Formatted: Font: 11 pt Formatted: Line spacing: single Formatted: Font: 11 pt Formatted: Font: 11 pt, Not Bold
Late Carboniferous c. 300 Ma (Wells et al., 2005a,b)	Late Carboniferous sea of NW Europe	Unstructured; tetrahedral mesh; finite element scheme; Navier Stokes equations; No Coriolis parameter.	Astronomical tidal forcing only; M2 tide only; Variable bathymetry; No treatment of bottom friction.	Extremely microtidal seaway (typically <10 cm tidal range) across NW region across various sensitivity tests; Putative tidal deposits interpreted to be confined to localised estuaries.	
Late Carboniferous c. 300 Ma (Wells et al., 2008)	Late Carboniferous sea of NW Europe	Unstructured; tetrahedral mesh; finite element scheme; Navier Stokes equations;	Astronomical tidal forcing only; M2, S2, N2, K2, Q1, O1, P1, K1, M <sub>2</sub> , M <sub>2</sub> <sub>in</sub> and S <sub>2</sub> <sub>in</sub> tidal constituents; Variable bathymetry; Bottom drag applied as surface integral	Microtidal ranges predicted across the northwest European region (similar to Wells et al., 2005a, b); Extra tidal constituents increase the predicted tidal range to 20–80 cm.	

		Coriolis parameter included.	based on quadratic friction law.	
Early Cretaceous, late Aptian, c. 116 Ma (Wells et al., 2010a)	Global	Unstructured, tetrahedral mesh; finite element scheme; Navier Stokes equations; Coriolis parameter included.	Astronomical tidal forcing only; M2, S2, O1 and K1 tidal constituents modelled independently; Variable bathymetry; Bottom drag applied as surface integral based on quadratic friction law.	Model results compared to published geologic records; High mesotidal to macrotidal on the Arabian Platform, around India, along the Pacific coast between North and South America, northeast of Australia, and around Southeast Asia; Low microtidal ranges in the proto-South Atlantic Ocean and Weddell Sea.
Early Cretaceous, late Aptian—early Albian, c. 112–107 Ma (Wells et al., 2010b)	Lower Greensand Seaway of NW Europe	Unstructured, tetrahedral mesh; finite element scheme; Navier Stokes equations; Coriolis parameter included.	Open boundary conditions (from Wells et al., 2010a) and astronomical tidal forcing; M2, S2, O1 and K1 tidal constituents modelled independently; Variable bathymetry; Bottom drag applied as surface integral based on quadratic friction law.	Overall microtidal increasing to microtidal–macrotidal with increased width and depth of open ocean connections and more localised funnelling, shoaling and Coriolis effects.
Middle Cretaceous, Early–Middle Turonian, c. 93 Ma (Mitchell et al., 2010)	Bohemian Cretaceous Basin of Central Europe	Unstructured, tetrahedral mesh; finite element scheme; Navier Stokes equations; Coriolis parameter included.	Open boundary conditions and astronomical tidal forcing; varying combinations of M2, S2, O1 and K1 tidal constituents; Variable bathymetry; Bottom drag applied as surface integral based on quadratic friction law.	Microtidal–mesotidal across the Bohemian Cretaceous Basin and range of sensitivity tests; Elevated tidal ranges and velocity in local embayments and straits due to funnelling and shoaling effects.
Early Jurassic, c. 200 Ma (Mitchell et al., 2011)	Laurasian Seaway of NW Europe	Unstructured, tetrahedral mesh; finite element scheme; Navier Stokes equations; Coriolis parameter included.	Astronomical tidal forcing; M2, S2, O1 and K1 tidal constituents; Variable bathymetry; Bottom drag applied as surface integral based on quadratic friction law.	Seaway largely microtidal; Flow constriction associated with shallow platforms and straits produced elevated bed shear stresses that were decoupled from tidal range.
Oligocene–Miocene, c. 26–5 Ma (Collins et al., 2017, 2018)	South China Sea, SE Asia	Unstructured, tetrahedral mesh; finite element scheme; Navier Stokes equations; Coriolis parameter included.	Astronomical tidal forcing; M2, S2, N2, K2, Q1, O1, P1, K1, M <sub>2</sub> , M <sub>4</sub> and S <sub>2m</sub> tidal constituents; Variable bathymetry; Bottom drag applied as surface integral based on quadratic friction law.	Spring tides along South China Sea coastline were largely mesotidal–macrotidal and capable of transporting sand throughout the Late Oligocene to Middle Miocene.
Late Cretaceous	Western Interior	Unstructured, tetrahedral mesh,	Astronomical tidal forcing; M2, S2, N2, K2, Q1, O1,	Regionally microtidal.

Formatted: Font: 11 pt

Formatted: Line spacing: single

Formatted: Font: 11 pt

Formatted: Font: 11 pt, English (United States)

middle Campanian, c. 75–77.5 Ma (Dean et al., 2019)	Seaway of North America	finite element scheme; Navier Stokes equations; Coriolis parameter included;	P1, K1, M <sub>2</sub> , M <sub>4</sub> and S <sub>2</sub> tidal constituents; Variable bathymetry; Bottom drag applied as surface integral based on quadratic friction law;	mesotidal (2–4 m) along most of the eastern margin of the seaway; increased tidal bed shear stress when seaway center and entrance to Gulf of Mexico are deeper;
---	-------------------------	--	--	--

**Table 3.** Summary of previously published palaeotidal models from deep geologic time (excluding the Quaternary).

**Commented [CDSS10]:** We've added additional studies by Green & Huber 2013, Green et al. 2017 and Dean et al., 2019

## 2.2 Process-based sedimentological analysis

**Commented [CDSS11]:** Changes in this section (revised section 2.1.3):  
 -Clarification on interpreting depositional processes at a range of scales, and using a range of data across these scales  
 -Remove reference to 'tiering'  
 -Additional, recommendation referencing

The study and interpretation of ancient physical processes from sedimentary rocks requires a rigorous, multi-scale approach that has developed over the last 60–70 years (see reviews by Walker and Plint, 1992; Reading, 1996). The approach is underpinned by rigorous facies analysis, which relies on detailed, qualitative descriptions of distinctive combinations of sedimentary and biological structures (e.g. Reading, 1978; Reading, 1996) (De Raaf et al., 1965; Walker, 1979; Anderton, 1985). However, small-scale (c. 1–100s cm) facies are typically based on subtle differences that are non-unique in terms of depositional processes and environment (Walker and James, 1992). Process and environment interpretation more readily occurs at the facies association (typically several metres to 10s metre) and facies succession (10s–100s m) levels but even at these scales process and environment interpretation may remain ambiguous (Walker and James, 1992; Dalrymple, 2010; Colombero and Mountney, 2020b). Understanding the relationship between process, sedimentation and resultant sedimentary structures and stratigraphy ideally requires close comparison to the modern, where these aspects may be observed and measured directly in different environments (Middleton, 1965; Allen, 1968; Allen,

**Formatted:** Font: 12 pt

1982b; Collinson and Mountney, 2019) questions: (1) How do we classify and predict shoreline-shelf depositional systems?

In shoreline systems, the process-based sedimentological approach centres upon determining the relative influence of river, wave and tide processes, with the inherent understanding that these are characterised by different groups of physical process types, principally unidirectional and bidirectional traction currents and gravitational, oscillatory and suspension flow processes. The application of a three-tier process classification depends on: (1) the availability and quality of the rock data; and (2) the process implications of sedimentological and biological features. However, both these considerations are subject to potential biases. For example, higher quality exposure may be sandstone-dominated due to preferential weathering of finer grained or thinner bedded facies, the identification and interpretation of which often requires exceptional outcrop or core data quality. Furthermore, sediment texture, particularly grain size distribution, has a significant control on the type of sedimentary structures and facies formed, and can vary significantly between different sedimentary systems (Jopling and Walker, 1968; Allen, 1982b; Harms et al., 1982; Kvale et al., 1989; Orton and Reading, 1993; Yoshida et al., 2007).

A statistical method for classifying shoreline deposits involves assigning a percentage likelihood that a bed or stratal unit was formed by wave, tide or fluvial processes ('process percentage') and quantifying the relative proportion of each bed or stratal unit (Rossi et al., 2017; Peng et al., 2018). The 'process percentage' is determined based on the proportion of preserved sedimentary structures, and also the proportion of wave, tide or fluvial dominated interpretations of each sedimentary structure in an extensive literature database (Rossi et al., 2017; Peng et al., 2018).

Formatted: Font: 11 pt

Formatted: Font: 12 pt

However, end-member process interpretations of various sedimentary structures are commonly ambiguous, and it is difficult to assign percentage values to those formed by combined processes. Whilst this statistical method provides a theoretical framework for more accurate estimation of process variability, in reality interpretations may be subjective and biased, partly reflecting uncertainties in original literature studies and revisions in process interpretations of different sedimentary structures. Indeed, original literature interpretations may have skewed, and even self-reinforced, the process interpretation of some key sedimentary structures and facies (Colombera et al., 2012; Rossi et al., 2017). For example, it is now recognized that heterolithic facies are not limited to tidal settings, as was originally emphasized (e.g. Reineck and Wunderlich, 1968), but can form in a wider range of depositional environments (e.g. Ainsworth et al., 2012). This effect is captured in the growing uncertainty regarding the process classification of heterolithic deposits in terms of the balance of fluvial versus tidal processes, especially: (1) those displaying unidirectional-dominated, current ripple cross-lamination (e.g. Dalrymple et al., 2015; Gugliotta et al., 2016b; Kureinka et al., 2018; Collins et al., 2020; Van Yperen et al., 2020), including within inclined heterolithic strata (Thomas et al., 1987; Martinus et al., 2015; Jablonski and Dalrymple, 2016); and (2) discriminating between tidal influence (secondary process) versus tidal modulation (tertiary processes) in cross-stratification (Martinus and Gowland, 2011; Gugliotta et al., 2016a) (Martinus et al., 2015). Similarly, hummocky and swaley cross-stratification with mudstone drapes have been interpreted to record mixed storm and tidal processes (Vakarelov et al., 2012; Wei et al., 2016), but the variability in flow and sedimentation required for mud draping may occur inherently occur during storm flows (e.g. Collins et al., 2017b). A further example is the process origin of hummocky and swaley cross-stratification and related structures (e.g. combined flow ripples and planar lamination), including

the balance of oscillatory to unidirectional flow and the influence of hyperpycnal flow (Dott and Bourgeois, 1982; Arnott and Southard, 1990; Myrow and Southard, 1996; Myrow et al., 2002; Dumas and Arnott, 2006; Lamb et al., 2008; Tinterri, 2011; Basilei et al., 2012; Perillo et al., 2014). Consequently, assigning the relative contribution of wave, tidal or fluvial processes to a given sedimentary structure remains uncertain.

**1.1 Classification and prediction of shoreline depositional regarding hydrodynamic processes? (2) What do existing present-day and ancient numerical tidal models indicate about the controls on tides? (3) How can we use this understanding to improve predictions of shoreline-shelf process regime? process regime**

## **2 BACKGROUND**

### **2.1 Classification, identification and prediction of clastic depositional shoreline-shelf systems and process regime**

#### **2.2.1.1 Shoreline-shelf Process classifications**

Shoreline systems encompass a wide range of depositional settings, including deltas, strandplains, estuaries, barrier islands and a host of sub-environments (e.g. lagoons, tidal flats, distributary channels, mouth bars, etc.). Seminal models for clastic shoreline systems initially focused on modern deltas, particularly the relationship between delta front morphology and the relative influence of wave, tidal and fluvial process (Coleman and Wright, 1975; Galloway, 1975). This ternary classification scheme was widely adopted and modified to include a wider range of depositional settings by Boyd et al. (1992), notably the bivariate wave versus tide classification of elastic coasts (Hayes, 1975; Hayes, 1979) and variability in grain size (Orton and Reading, 1993). Furthermore, Boyd et al. (1992) and Dalrymple et al. (1990) interpreted the

Formatted: Heading 2, Line spacing: single

Formatted: Line spacing: 1.5 lines

Formatted: Line spacing: Double

1  
2  
3  
4  
5  
6  
7  
8  
9  
10  
11 495 predictive evolutionary relationships between long-term equilibrium depositional environments  
12  
13 496 and the rates of sediment supply versus relative sea-level change (shoreline transgression vs.  
14  
15 497 regression). The most recent manifestation of the ternary classification scheme has been a more  
16  
17 498 detailed descriptive process model of the spectrum of shoreline systems, including aspects of  
18  
19 499 their spatial and temporal variability (Ainsworth et al., 2011).

20 500  
21  
22 501 However, Ainsworth et al. (2011) also noted that these relatively long-term equilibrium models  
23  
24 502 are unable to predict more precise process variations in space at a given time ('environmental  
25  
26 503 disequilibrium'; There is no single unifying classification of clastic shorelines and shelves. As  
27  
28 504 with all natural systems, clastic shorelines form in response to multiple controls, and different  
29  
30 505 parameters can be used for the purpose of classification (e.g. Reading and Collinson, 1996).  
31  
32 506 Seminal models for clastic shoreline systems initially focused on modern deltas, particularly the  
33  
34 507 relationship between delta front morphology and the relative influence of wave, tidal and fluvial  
35  
36 508 process (Coleman and Wright, 1975; Galloway, 1975). This ternary classification scheme was  
37  
38 509 widely adopted and modified to include a wider range of depositional settings by Boyd et al.  
39  
40 510 (1992), notably the bivariate wave versus tide classification of clastic coasts (Hayes, 1975;  
41  
42 511 Hayes, 1979) and variability in grain size (Orton and Reading, 1993). Boyd et al. (1992) and  
43  
44 512 Dalrymple (1992) developed predictive evolutionary relationships between long-term  
45  
46 513 equilibrium depositional environments, where sediment accumulation and erosion are essentially  
47  
48 514 balanced (Zhou et al., 2017). These relationships addressed a wide range of shoreline-shelf  
49  
50 515 depositional systems and recognised the overarching control of rate of sediment supply versus  
51  
52 516 rate of relative sea level change (shoreline transgression versus regression). These seminal  
53  
54 517 models and classifications of shoreline-shelf systems necessarily focused on relative process

Formatted: Line spacing: single



end-members to establish the full range of depositional system types in the continuous spectrum of potential mixed-energy systems(Boyd et al., 1992). In addition, they cannot convolve the effects of dynamic temporal changes (at varying timescales) in depositional processes caused by (1) changes in shoreline physiography (morphology and bathymetry), (2) fluctuations in accommodation space creation versus sediment supply rates, and (3) variations in regional basin physiography.

The extensive range of models provide a means to classify shoreline–shelf systems at a particular time and in a particular location. However, these models were not intended to predict more detailed process variations either spatially at a given time, temporally at a given location, or both spatially and temporally (Boyd et al., 1992)(Boyd et al., 1992). In addition, they cannot convolve the effects of Such dynamic temporal changes (at varying timescales) in depositional processes on various spatial and temporal scales may be caused by (1) variations in any of the multitude of controls impacting shoreline–shelf systems. For example, changes in shoreline physiography (morphology and bathymetry), (2) fluctuations in accommodation space creation versus sediment supply rates, and (3) variations in regional basin physiography, may all form dominant controls on shoreline-shelf systems.

Within individual shoreline systems, complex arrangements of discrete depositional elements attributed to different combinations of wave, tide and fluvial processes have been recognized in analyses of: (1) modern delta geomorphology and sedimentological data, including the Danube (e.g. Bhattacharya and Giosan, 2003)(e.g. Bhattacharya and Giosan, 2003), Ganges Brahmaputra (e.g. Willis, 2005)(e.g. Willis, 2005), Mahakam (e.g. Allen and Chambers, 1998)(e.g. Allen and Chambers, 1998), Mekong (e.g. Nguyen et al., 2000; Ta et al., 2002b)(e.g. Nguyen et al., 2000; Ta et al., 2002b), Mitchell (e.g. Nanson et al., 2013)(e.g. Nanson et al., 2013) and Changjiang (Yangtze) (e.g. Hori et al., 2002)(e.g. Hori et al., 2002) deltas; and (2) approximately

contemporaneous ancient stratigraphic units, including the Permian Kookfontein and Waterford formations in the Karoo Basin (Gomis-Cartesio et al., 2016)(Gomis-Cartesio et al., 2016); Cretaceous Ferron Sandstone, Western Interior Seaway

Within individual shoreline systems, complex arrangements of discrete depositional elements attributed to different combinations of wave, tide and fluvial processes have been recognized in analyses of: (1) modern delta geomorphology and sedimentological data, including the Danube (e.g. Bhattacharya and Giosan, 2003), Ganges-Brahmaputra (e.g. Willis, 2005), Mahakam (e.g. Allen and Chambers, 1998), Mekong (e.g. Nguyen et al., 2000; Ta et al., 2002b), Mitchell (e.g. Nanson et al., 2013) and Changjiang (Yangtze) (e.g. Hori et al., 2002) deltas; and (2) approximately contemporaneous ancient stratigraphic units, including the Permian Kookfontein and Waterford formations in the Karoo Basin (Gomis-Cartesio et al., 2016), Cretaceous Ferron Sandstone, Western Interior Seaway (e.g. Gardner et al., 2004; Bhattacharya and MacEachern, 2009; Li et al., 2011; Li et al., 2015), Cretaceous Sego Sandstone, Western Interior Seaway (Willis and Gabel, 2001; Legler et al., 2014; van Cappelle et al., 2016), Cretaceous Sego SandstoneHorseshoe Canyon Formation, Western Interior Seaway (Willis and Gabel, 2001; Legler et al., 2014; van Cappelle et al., 2016)(Willis and Gabel, 2001; Legler et al., 2014; van Cappelle et al., 2016); Ainsworth et al., 2015; Ainsworth et al., 2016; van Cappelle et al., 2016); Cretaceous Horseshoe Canyon and Miocene Belait Formation, Western Interior SeawayNW Borneo (Lambiase et al., 2003; Collins et al., 2017b; Collins et al., 2018b). Consequently, these and many other depositional systems indicate frequent mixed-process regimes, with variable wave, tide and fluvial interactions in both space (e.g. along and/or perpendicular to depositional strike) and time (on various timescales e.g. daily, seasonal, annual or longer). These mixed-energy systems cannot be fully resolved in the early process classification models -and Miocene

Belait Formation, NW Borneo (Coleman and Wright, 1975; Galloway, 1975; Boyd et al., 1992).  
Consequently, these and many other depositional systems frequently . Therefore, Ainsworth et  
al. (2011) developed a new semi-quantitative, process-based classification scheme based on the  
relative importance of primary, secondary and tertiary processes (generating ‘dominated’,  
‘influenced’ or ‘affected’ descriptors, respectively). This higher-resolution process-based  
approach enables a more rigorous comparison of modern and ancient shoreline deposits (Fig.  
5A). However, a quantitative process analysis of modern shorelines by Nyberg and Howell  
(2016) suggests the thresholds separating primary, secondary and tertiary processes are  
ambiguous, resulting in these authors favouring a two-tier classification (Fig. 5B). Furthermore,  
the additional ambiguity in the process interpretation of several common sedimentary structures  
means that most studies of ancient, mixed-process shoreline deposits have adopted a two-tier  
process classification (e.g. Bhattacharya and Giosan, 2003; Lambiase et al., 2003; Coates and  
MacEachern, 2007; Gani and Bhattacharya, 2007; Hansen et al., 2007; Buatois et al., 2012;  
Vakarelov et al., 2012; Amir Hassan et al., 2013; Legler et al., 2013; Chen et al., 2014; Legler et  
al., 2014; Ainsworth et al., 2015; Gugliotta et al., 2015; Li et al., 2015; Ainsworth et al., 2016;  
Amir Hassan et al., 2016; Gomis-Cartesio et al., 2016; Gugliotta et al., 2016a; Rossi and Steel,  
2016; Vaucher et al., 2016; Collins et al., 2017b; Collins et al., 2018b).  
indicate frequent mixed-process regimes, with variable wave, tide and fluvial interactions in both  
space (e.g. along and/or perpendicular to depositional strike) and time (on various timescales e.g.  
daily, seasonal, annual or longer). These mixed-energy systems cannot be fully resolved in the  
early process classification models (Coleman and Wright, 1975; Galloway, 1975; Boyd et al.,  
1992)(Coleman and Wright, 1975; Galloway, 1975; Boyd et al., 1992). Therefore, Ainsworth et  
al. (2011) Ainsworth et al. (2011) developed a new semi-quantitative, process-based  
classification scheme based on the relative importance of primary, secondary and tertiary  
processes (generating: represented by ‘dominated’, ‘influenced’ or ‘affected’ descriptors,

Formatted: Line spacing: 1.5 lines

respectively)). This higher-resolution process-based approach enables a more rigorous enhances  
comparison of modern and ancient shoreline deposits (Fig. 5A1A). However, a quantitative  
process analysis of modern shorelines by Nyberg and Howell (2016) Nyberg and Howell (2016)  
suggests the thresholds separating primary, secondary and tertiary processes are ambiguous,  
resulting in these authors favouring a two-tier classification (Fig. 5B1B). Furthermore, the  
additional ambiguity in the process interpretation of several common sedimentary structures  
means that most studies of ancient, mixed-process shoreline deposits have adopted a two-tier  
process classification (e.g. Bhattacharya and Giosan, 2003; Lambiase et al., 2003; Coates and  
MacEachern, 2007; Gani and Bhattacharya, 2007; Hansen et al., 2007; Buatois et al., 2012;  
Vakarelov et al., 2012; Amir Hassan et al., 2013; Legler et al., 2013; Chen et al., 2014; Legler et  
al., 2014; Ainsworth et al., 2015; Gugliotta et al., 2015; Li et al., 2015; Ainsworth et al., 2016;  
Amir Hassan et al., 2016; Gomis Cartesio et al., 2016; Gugliotta et al., 2016a; Rossi and Steel,  
2016; Vaucher et al., 2016; Collins et al., 2017b; Collins et al., 2018b)(e.g. Bhattacharya and  
Giosan, 2003; Lambiase et al., 2003; Coates and MacEachern, 2007; Gani and Bhattacharya,  
2007; Hansen et al., 2007; Buatois et al., 2012; Vakarelov et al., 2012; Amir Hassan et al., 2013;  
Legler et al., 2013; Chen et al., 2014; Legler et al., 2014; Ainsworth et al., 2015; Gugliotta et al.,  
2015; Li et al., 2015; Ainsworth et al., 2016; Amir Hassan et al., 2016; Gomis Cartesio et al.,  
2016; Gugliotta et al., 2016a; Rossi and Steel, 2016; Vaucher et al., 2016; Collins et al., 2017b;  
Collins et al., 2018c).

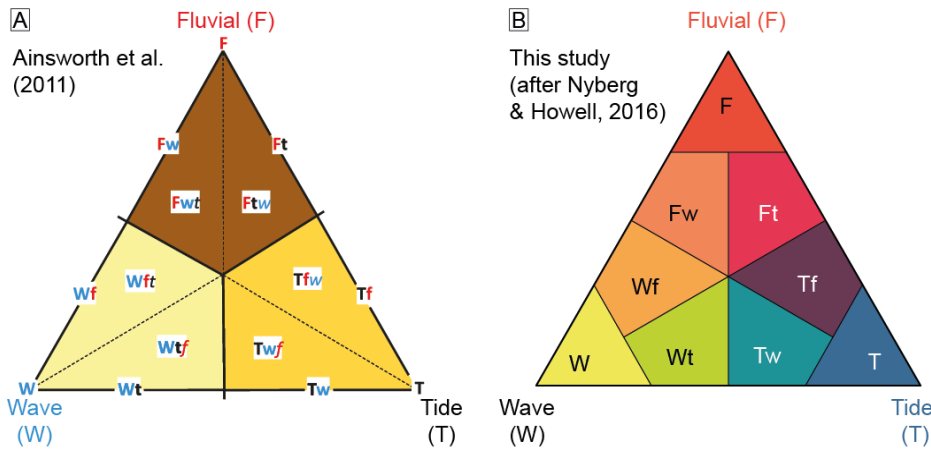


**Fig. 51.** Two contrasting ternary process classifications for shoreline depositional systems. (A) The three-tier classification of Ainsworth et al. (2011) utilizes primary, secondary, and tertiary processes, which are referenced as ‘dominated’ (capitalized and bold), ‘influenced’ (lower case and bold) and ‘affected’ (lower case italics and not bold), respectively. For example, wave dominated, tide influenced and fluvial affected is written **Wt<sub>f</sub>**. (B) The two-tier classification of Nyberg and Howell (2016) recognizes the primary and secondary processes, and is favored in this study (see text for discussion).

## 2.2.22.1.2 Process classification of present-day global shorelines

Nyberg and Howell (2016) developed the first, systematic, semi-automated classification of global shoreline process regime (Fig. 62) by combining several datasets and methodologies: (1) proxies for wave, tide and fluvial processes, including wave height, tidal amplitude and river discharge; (2) depositional versus erosional shorelines, determined by combining global lithology maps and digital elevation models; and (3) algorithms for determining the ‘tidal coefficient’ for modifying tidal amplitude using shoreline rugosity or

Formatted: Line spacing: Double

Formatted: Line spacing: single

‘roughness index’. This integrated approach predicts shoreline classification with an 85% success rate compared to manual interpretation based principally on shoreline morphology (~~e.g. Ainsworth et al., 2011~~)(e.g. Ainsworth et al., 2011)), and is consistent with earlier comparisons of shoreline morphology with quantitative metrics of wave, tide and river power along large, but non-global, stretches of siliciclastic coastlines (~~e.g. Harris et al., 2002~~)(e.g. Harris et al., 2002)). By subdividing the global shoreline into 5 km segments, this methodology classifies 28% of global shorelines as depositional, of which 62% are wave-dominated, 35% tide-dominated and 3% fluvial-dominated (Fig. 6A2A) (~~Nyberg and Howell, 2016~~)(Nyberg and Howell, 2016)). On a global scale, over 90% of shorelines on narrow shelves ( $\leq 25$  km) are wave-dominated and <5% tide-dominated, whereas over 30% of shorelines on wide shelves ( $> 75$  km) are tide-dominated (Fig. 6B2B). Along depositional shorelines, tide dominance increases from <20% on narrow shelves to >50% on wide shelves (Fig. 6C2C). Fluvial-dominated systems ~~along shorelines are prone to more wave modifiedmodification~~ on narrow shelves and ~~to more tide modifiedmodification~~ on wide shelves (Fig. 6B2B and C).

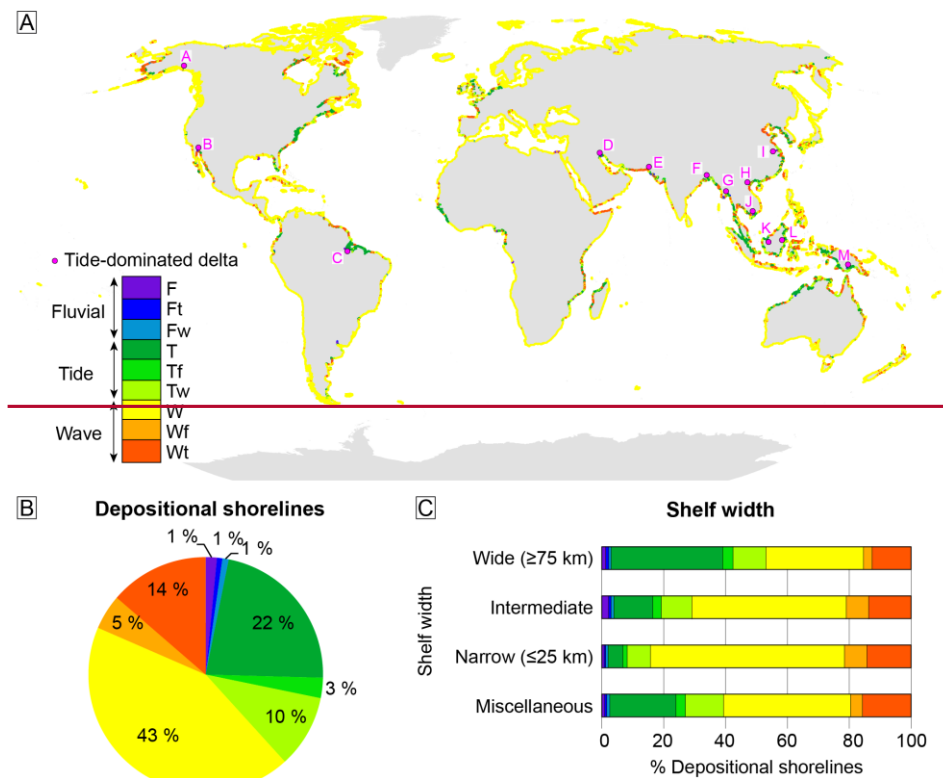
Tide-dominated deltas are widely distributed (Figs 2A and 6A4A), including: (1) at low and high latitudes; (2) along open-ocean shorelines and in partly enclosed oceans and seas; and (3) along straight and highly embayed shorelines. Their locations encompass a range of tectonic settings, including strike-slip transtensional rift (e.g. Colorado delta), forearc (e.g. Cooper delta), foreland (e.g. Mahakam and Fly deltas) and passive margin settings (Ganges Brahmaputra delta) (~~Nyberg and Howell, 2016~~)(Nyberg and Howell, 2016)). ~~Whilst tide~~Tide-dominated deltas preferentially occur along macrotidal shorelines (Fig. 2A), 4A), but they also occur along mesotidal shorelines (e.g. Mekong and Mahakam deltas). However, tide-dominated deltas exclusively occur along

shorelines with elevated tidal bed shear stresses, where tidal currents at their maximum strength are capable of transporting at least coarse sand (Fig. 2D4D).

Although the ~~Nyberg and Howell (2015)~~Nyberg and Howell (2015)-classification provides a consistent, reproducible approach for identifying process distribution along global shorelines, it has significant ~~some~~ limitations. There are inherent biases between shoreline morphology and process dominance: i.e. As is observed in modern systems, more rugose and funnel-shaped shorelines are inherently biased towards strongly correlated with tide dominance and, but not all present-day embayments are tide dominated. Likewise, smoother shorelines towards are correlated with wave dominance. None of the tidal coefficients consider theoretical and quantifiable relationships between shoreline physiography and the tidal prism. (D'Alpaos et al., 2010). Lastly, wave height and tidal range are inadequate proxies for differentiating wave- and tide dominance in mixed-energy systems (e.g. Anthony and Orford, 2002; Mulhern et al., 2017)(e.g. Anthony and Orford, 2002; Dalrymple, 2010b; Mulhern et al., 2017) classification provides a consistent, reproducible approach for identifying process distribution along global shorelines, it has significant limitations. There are inherent biases between shoreline morphology and process dominance: i.e. more rugose and funnel-shaped shorelines are inherently biased towards tide dominance and smoother shorelines towards wave-dominance. None of the tidal coefficients consider theoretical and quantifiable relationships between shoreline physiography and the tidal prism. Lastly, wave height and tidal range are inadequate proxies for differentiating wave- and tide-dominance in mixed-energy systems (e.g. Anthony and Orford, 2002; Mulhern et al., 2017) because these parameters are not directly related to sediment entrainment (unlike bed shear stress).



1  
2  
3  
4  
5  
6  
7  
8  
9  
10  
11  
12  
13  
14  
15  
16  
17  
18  
19  
20  
21  
22  
23  
24  
25  
26  
27  
28  
29  
30  
31  
32  
33  
34  
35  
36  
37  
38  
39  
40  
41  
42  
43  
44  
45  
46  
47  
48  
49  
50  
51  
52  
53  
54  
55  
56  
57  
58  
59  
60  
61  
62  
63  
64  
65



**Commented [CDSS12]:** Colours are now consistent with revised colour scheme used in this paper (Fig. 5B)

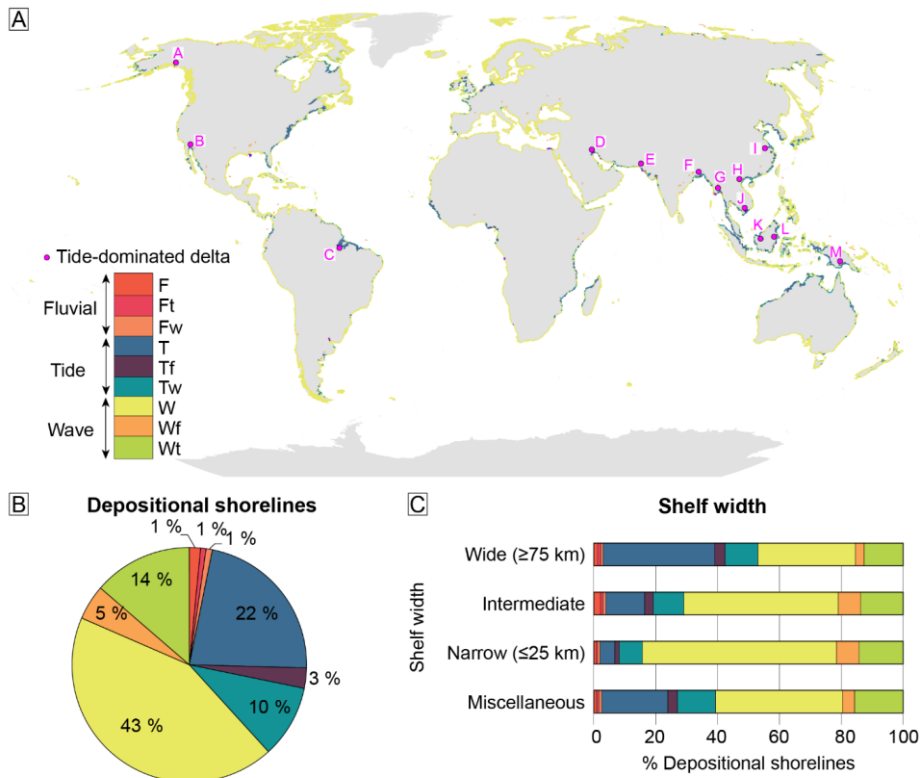


**Fig. 62.** Quantification of modern global shoreline process regimes (from Nyberg and Howell, 2016). (A) Two-tier ternary process classification of modern shorelines (see Fig. 5B1B) showing the locations (pink dots) of tide-dominated deltas (Goodbred and Saito, 2012): A) Copper; B) Colorado; C) Amazon; D) Shatt-al-Arab; E) Indus; F) Ganges-Brahmaputra; G) Irrawaddy; H) Red River; I) Yangtze; J) Mekong; K) Rajang; L) Mahakam; and M) Fly. Figures 2A4A and D show the same delta locations on a global map of tidal range and tidal bed shear stress, respectively. (B) Proportion of the two-tier process classifications along depositional shorelines. (C) Relationship between binned shelf width and proportion of the two-tier process classification along depositional shorelines. The miscellaneous class is for shallow seas and seaways (e.g. Baltic and Red seas Sea).

### 2.1.3 Identification of ancient shoreline–shelf processes

The study and interpretation of ancient physical processes from sedimentary rocks has required a rigorous, multi-scale approach that has developed over the last 60–70 years (see reviews by Walker and Plint, 1992; Reading, 1996). This methodology is underpinned by rigorous facies analysis, which relies on detailed, qualitative descriptions of distinctive combinations of sedimentary and biological structures (e.g. Reading, 1978; Reading, 1996). However, small-scale (c. 1–100s cm) facies are typically based on subtle differences that are non-unique in terms of depositional processes and environment (Walker and James, 1992). Hence, sedimentological and stratigraphic descriptions and interpretations are required across the range of scales and dimensions spanning facies, facies associations, facies successions and architectural elements to characterise and interpret ancient processes and environments (Elliott, 1986; Walker and James, 1992; Dalrymple, 2010a; Colomera and Mountney, 2020b). Understanding the relationship between process, sedimentation, sedimentary structures and stratigraphic architecture also requires comparison to the modern, where these aspects may be observed and measured directly in different environments (Middleton, 1965; Allen, 1968; Allen, 1982b; Yang et al., 2008; Collinson and Mountney, 2019; Dalrymple, 2021).

In shoreline–shelf systems, the process-based sedimentological approach centres upon unravelling the relative influence of river, wave and tide processes based on different groups of physical processes, principally unidirectional and bidirectional traction currents and gravitational, oscillatory and suspension flow processes. The confidence level of ancient ternary process interpretations depends on several factors, most notably: (1) the availability and quality of the rock data; (2) the formation and preservation potential of sedimentary facies that can be assigned to specific flow processes; (3) the uncertainty in the process interpretation of sedimentological, stratigraphic and biological features; and (4) the level of existing knowledge of the depositional system under investigation. Recently, a statistical method for classifying shoreline–shelf deposits has been proposed that involves assigning a percentage likelihood that a bed or stratal unit was formed by wave, tide or fluvial processes (‘process percentage’) and quantifying the relative proportion of each bed or stratal unit (Rossi et al., 2017b; Peng et al., 2018). The ‘process percentage’ is determined based on the proportion of preserved sedimentary structures, and also the proportion of wave-, tide- or fluvial-dominated interpretations of each sedimentary structure in an extensive literature database (Rossi et al., 2017b; Peng et al., 2018). However, this approach has limitations. First, the volumetric proportion of deposits formed by different processes may not reflect process dominance in the environment of deposition, as highlighted by Dalrymple et al. (2015). Second,

Formatted: Font: 11 pt

Formatted: Font: 11 pt

end-member process interpretations of various sedimentary structures are commonly ambiguous. Third, it is difficult to assign percentage values to sedimentary structures formed by combined processes.

Nonetheless, recent advances over the last 10–15 years in process-based sedimentological analysis of end-member and mixed-energy shoreline–shelf systems has increased confidence in palaeoenvironmental and related process interpretations. This is illustrated with a few specific examples, while a more comprehensive analysis of tidal facies is presented later (Section 2.2.3.1). It is now recognized that muddy and sandy heterolithics with a predominance of unidirectional ripple cross-lamination are not limited to tidal settings as was originally emphasized (e.g. Reineck and Wunderlich, 1968) and occasionally uncritically adopted by some sedimentologists. Instead these facies can form in a wide range of environments and under a spectrum of processes, especially those with mixed fluvial and tidal influence (e.g. Dalrymple et al., 2015; Gugliotta et al., 2016b; Kurcinka et al., 2018; Collins et al., 2020; Van Yperen et al., 2020) (Thomas et al., 1987; Martinius et al., 2015; Jablonski and Dalrymple, 2016). Likewise, subtle difference in the interpretation of tidal influence (secondary process) versus tidal modulation (tertiary processes) in cross-stratification have been proposed (Martinius and Gowland, 2011; Gugliotta et al., 2016a) (Martinius et al., 2015). Hummocky and swaley cross-stratification with mudstone drapes have recently been interpreted to record mixed storm and tidal processes (Vakarelov et al., 2012; Wei et al., 2016) or inherent flow variability during storm flows (e.g. Collins et al., 2017b). Lastly, the range of oscillatory to unidirectional flow and the influence of hyperpycnal flow in the origin of hummocky and swaley cross-stratification and related structures (e.g. combined-flow ripples and planar lamination) is now more widely appreciated (Dott and Bourgeois, 1982; Arnott and Southard, 1990; Myrow and Southard, 1996; Myrow et al., 2002; Dumas and Arnott, 2006; Lamb et al., 2008; Tinterri, 2011; Basilici et al., 2012; Perillo et al., 2014).

#### **2.2.3.2.1.4 Prediction of ancient shoreline–shelf depositional process regime**

Ainsworth et al. (2011) Understanding the physiographic and hydrodynamic controls on the process regime of present-day shorelines (section 2.1.2), and consideration of such controls in ancient case studies, has enabled development of predictive models for ancient shoreline–shelf depositional process regime. Ainsworth et al. (2011) extended previous process-based models of shoreline–shelf systems by introducing other critical including the following aspects to the

Formatted: Line spacing: Double

Formatted: Line spacing: single

~~palaeoenvironmental diagnosis, most notably:~~ (1) basin physiography (100–1000 km scale), (2) shelf width (10–100 km scale), (3) fluvial versus wave effectiveness, (4) accommodation versus sediment supply (A/S ratio), and (5) shoreline morphology (1–10 km scale). These were incorporated into a ~~predictive~~ decision tree (Fig. 7A) and two predictive matrices (Fig. 7B and C) for ~~shoreline depositional process regime~~ low and high tidal resonance, respectively.

~~Basin physiography and shelf width are combined to determine the ‘tidal resonance potential of the basin’, which is the first query on the decision tree (Fig. 7A) and distinguishes two predictive matrices (Fig. 7B and C). Tidal resonance occurs when the natural period of oscillation on the shelf, or within a shoreline embayment, is coincident with the tidal period (Slingerland, 1986; Allen, 1997; Collins et al., 2018b). In the predictive model, the interpretation of tidal resonance potential is calibrated empirically to shelf width (cf. Howarth, 1982). Since analysis of present-day shorelines suggests that they are more likely to be tide dominated adjacent to shelves greater than 75 km in width (Heap et al., 2004; Ainsworth et al., 2011), a shelf width of 75 km is an approximate empirical cut-off between modern and ancient shorelines with lower (<75 km shelf width) and higher tidal potential (>75 km shelf width), respectively.~~

~~The effect of basin physiography is complicated by (1) the influence of tidal inflow versus outflow to partly enclosed water bodies, and (2) the funnelling, shoaling and resonance effects on continental shelves and within shoreline embayments, which occur on a range of scales (c. 1–1000s km width and 1–100s m depth) (Mitchell et al., 2010; Wells et al., 2010b; Collins et al., 2018b). However, despite this complexity, basin physiography does not constitute a separate query in the predictive model (Fig. 7) and is treated as a modifying factor to shelf tidal resonance~~

potential ([Ainsworth et al., 2011](#)). Open oceans are sufficiently large to allow generation of relatively high *in situ* tides ([Dalrymple, 1992](#)). Therefore, basins that have restricted access to the open oceans generally have a lower potential for producing amplified tidal currents by resonance effects, whereas basins with less restricted access to open oceans have a higher tidal resonance potential. An exception is that certain restrictive basin physiographies, typically on a smaller scale (1–10s km), may cause significant amplification of tides by funnelling, shoaling and/or resonance effects ([Piper et al., 1990](#); [Martel et al., 1994](#)) ([Mitchell et al., 2010](#); [Ainsworth et al., 2011](#); [Mitchell et al., 2011](#)) ([Androsov et al., 2002](#); [Leekie and Rumpel, 2003](#)). Consequently, the generalized treatment of basin physiography in the existing predictive model ([Ainsworth et al., 2011](#)) combines two very different effects on tides relating to: (1) basin geography (100–1000 km width scale) and bathymetry (100–1000 m depth scale), which has a first order control on the balance of tidal inflow versus outflow; and (2) second order funnelling and resonance effects relating to basin physiography (10–100s km width scale and 1–100s m depth scale) ([Wells et al., 2005a](#); [Wells et al., 2007a](#); [Mitchell et al., 2010](#); [Wells et al., 2010b](#); [Collins et al., 2018a](#)). Distinguishing between these two controls of basin physiography is achieved most rigorously through numerical tidal modelling ([Slingerland, 1986](#); [Martel et al., 1994](#); [Wells et al., 2007a](#); [Collins et al., 2018a](#)).

**Fluvial** First, basin physiography and shelf width are combined to determine the ‘tidal resonance potential of the basin’ (Fig. 7A). Tidal resonance occurs when the natural period of oscillation within an ocean, water body, on the shelf or within a shoreline embayment, is coincident with the tidal period ([Slingerland, 1986](#); [Allen, 1997](#); [Collins et al., 2018c](#)). The interpretation of tidal resonance potential is calibrated empirically to shelf width (cf. [Howarth, 1982](#)). Present-day shorelines suggest that tide-dominated systems are more likely adjacent to shelves greater than

75 km in width (Heap et al., 2004; Ainsworth et al., 2011). Hence, shelf width is used as an approximate empirical cut-off to distinguish modern and ancient shorelines with lower (<75 km shelf width) and higher tidal potential (>75 km shelf width), respectively.

The second decision in the tree (Fig. 3) focuses on fluvial ~~versus wave effectiveness, which is~~ also partly related to ancient shoreline palaeogeography. Hence, shorelines ~~Shorelines~~ Fluvial versus wave effectiveness is related to ancient shoreline palaeogeography. Hence, shorelines facing large open water bodies are likely to be strongly influenced by wind-driven waves, with a large fetch resulting in a relatively high wave effectiveness. In contrast, shorelines that are more sheltered from direct oceanic waves and/or face smaller water bodies experience lower wave effectiveness. Fluvial effectiveness is controlled by a range of continental processes, including climate, weathering, river hydrology, drainage basin area, slope of the alluvial plain, and hinterland relief and gradient. Predictions of higher fluvial effectiveness must be supported by palaeogeographic, palaeodrainage and palaeohydrological reconstructions, especially where these indicate proximity to the outlets of large fluvial drainage areas ~~drainages~~. Consequently, wave and fluvial effectiveness are determined by very different factors. ~~Hence, determining the nature of wave and fluvial interactions, including predictions of their relative effectiveness, must rely on, requiring independent~~ facies analysis of preserved stratigraphy.

The third decision, the rate of accommodation space creation versus sediment supply (A/S ratio) ~~is~~ is a useful theoretical concept ~~(Muto and Steel, 1997)~~ (Muto and Steel, 1997) but difficult to apply practically, even for extensive datasets ~~(Ainsworth et al., 2008; Ainsworth et al., 2011)~~ (Ainsworth et al., 2008; Ainsworth et al., 2011) and for predictions based on parasequence characteristics ~~(Colombera and Mountney, 2020a)~~ (Colombera and Mountney,



2020a)). The A/S ratio does not directly affect shoreline depositional processes but may modify their relative interaction through changes in physiography. For embayed shorelines, which favour tidal amplification, the degree of wave protection will be: (1) reduced under low A/S conditions because higher progradation rates cause shorelines to straighten more quickly; and (2) increased under high A/S conditions, when accommodation exceeds sediment supply, because the embayed shoreline geometry will more likely persist (Fig. 73) (Ainsworth et al., 2011)(Ainsworth et al., 2011Ainsworth et al., 2011). Furthermore, the A/S ratio impacts preservation potential, with more complete preservation of all sub-environments in high A/S settings (van Vliet and Schwander, 1987; Collins et al., 2018c).

Shoreline morphology (c. 1–10 km scale) is the final decision on the tree (Fig. 3), and can have a significant impact on the relative balance of tide, wave and fluvial processes (Fig. 21) (Boyd et al., 1992; Dalrymple et al., 1992; Ainsworth et al., 2008; Ainsworth et al., 2011)(Boyd et al., 1992; Dalrymple et al., 1992; Ainsworth et al., 2008; Ainsworth et al., 2011). Highly-embayed, more rugose shoreline morphologies may promote: (1) amplification of the tidal wave by funnelling and/or resonance effects (Slingerland, 1986; Allen, 1997)(Slingerland, 1986; Allen, 1997); and (2) protection from direct wave approach from the open ocean or sea. Therefore, Ainsworth et al. (2011)Ainsworth et al. (2011) use shoreline rugosity as a direct proxy for tidal influence; with increasing rugosity corresponds corresponding to increased potential for tidal influence (Fig. 73). Their model predicts that all interpreted highly embayed shorelines, and half of interpreted moderately embayed shorelines, are tide-dominated, whereas only a quarter of interpreted straight to lobate shorelines are tide-dominated (Fig. 7A3A). However, this simplified differentiation is inconsistent with observations of Holocene to present-day embayed shorelines,

Formatted: Font: Bold

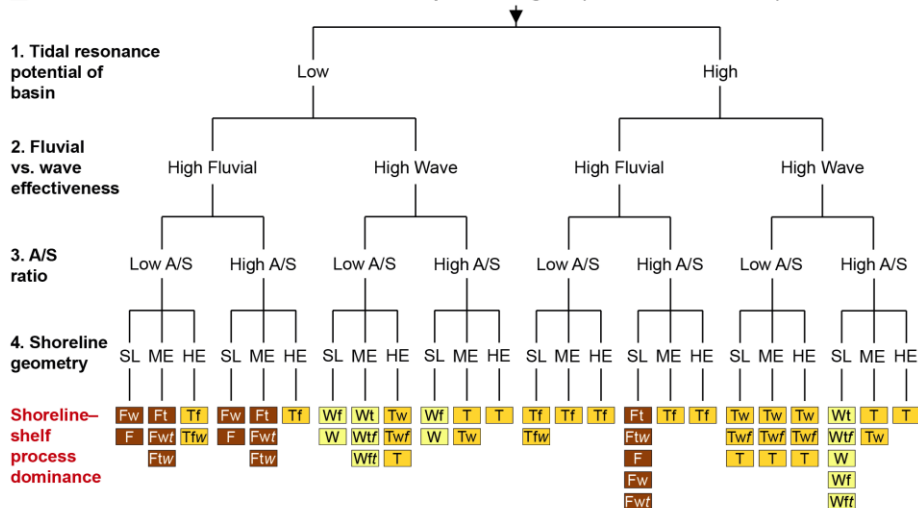
most notably estuaries (e.g. Dalrymple, 1992; Roy et al., 2001; Boyd et al., 2006; Dalrymple, 2006), which may be wave-dominated (e.g. Roy et al., 1980; Honig and Boyd, 1992; Cooper, 2001; Anthony et al., 2002)(e.g. Dalrymple, 1992; Roy et al., 2001; Boyd et al., 2006; Dalrymple, 2006; Dalrymple, 2010b)), tide-dominated (e.g. Hori et al., 2001; Dalrymple et al., 2012), river-dominated (e.g. Cooper, 1993; Sondi et al., 1995), and mixed process (d'Anglejan and Brisebois, 1978; Jouanneau and Latouche, 1981; Clifton, 1983; Allen and Posamentier, 1993; Roy et al., 2001). Furthermore, amplifying of tides due to funnelling and resonance effects in embayments may be counteracted by frictional effects, which may be wave-dominated (e.g. Dalrymple et al., 1992; Allen, 1997; Mitchell et al., 2010; Collins et al., 2018a), tide-dominated (e.g. Hori et al., 2001; Dalrymple et al., 2012), river-dominated (e.g. Cooper, 1993; Sondi et al., 1995), and mixed process (e.g. Dalrymple et al., 1992; Allen, 1997; Mitchell et al., 2010; Collins et al., 2018a)(d'Anglejan and Brisebois, 1978; Jouanneau and Latouche, 1981; Clifton, 1983; Allen and Posamentier, 1993; Roy et al., 2001). Consequently, the variability in predicted processes for ancient embayed shorelines may be higher than that proposed by Ainsworth et al. (2011) (Fig. 7).

For prediction of ancient shorelines, amplifying of tides due to funnelling and resonance effects in embayments may be counteracted by frictional effects (e.g. Dalrymple et al., 1992; Allen, 1997; Mitchell et al., 2010; Collins et al., 2018a; Collins et al., 2018b). Consequently, the variability in predicted processes for ancient embayed shorelines may be higher than that proposed by Ainsworth et al. (2011) (Fig. 3).

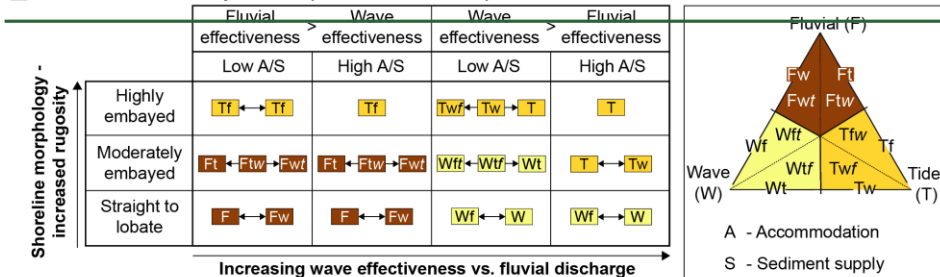
Prediction of shoreline processes, it is important that the data used in ancient successions is enhanced by access to interpret the impact of the different controls on shoreline processes

1  
2  
3  
4  
5  
6  
7  
8  
9  
10  
11 have the following: (1) reliable chronostratigraphic information with an appropriate resolution;  
12  
13 and (2) overlapping age ranges ('temporal resolution'). The temporal resolution of data and  
14  
15 interpretations relating to the inferred controls varies significantly. For example, the temporal  
16  
17 resolution of interpreted system tracts relating to 3rd-order (c. 0.5–3.0 Myr) or 4<sup>th</sup>-order (few 10s  
18  
19 ka to c. 0.5 Myr) sea-level cycles (~~Haq, 2014; Sames et al., 2016~~)(Haq, 2014; Sames et al.,  
20  
21 2016)) will likely fall within the temporal resolution of regional-scale palaeogeographic maps,  
22  
23 which are typically driven by plate tectonics and used for interpreting basin physiography and  
24  
25 fluvial versus wave effectiveness (~~Markwick and Valdes, 2004~~)(Markwick and Valdes, 2004)).  
26  
27 In contrast, the physiography of shoreline embayments and the continental shelf may be driven  
28  
29 by relative sea level changes or local tectonics, which vary on much smaller timescales (~~e.g.~~  
30  
31 ~~Collins et al., 2018a~~)(Partington et al., 1993a; Partington et al., 1993b; Egbert et al., 2004;  
32  
33 ~~Stammer et al., 2014; Collins et al., 2018a; van Cappel et al., 2018~~)(e.g. Collins et al., 2018a).  
34  
35  
36  
37  
38  
39  
40  
41  
42  
43  
44  
45  
46  
47  
48  
49  
50  
51  
52  
53  
54  
55  
56  
57  
58  
59  
60  
61  
62  
63  
64  
65

**A Predictive decision tree for shoreline–shelf process regime (Ainsworth et al. 2011)**



**B Low tidal resonance potential (shelf width <75 km)**



**C High tidal resonance potential (shelf width >75 km)**

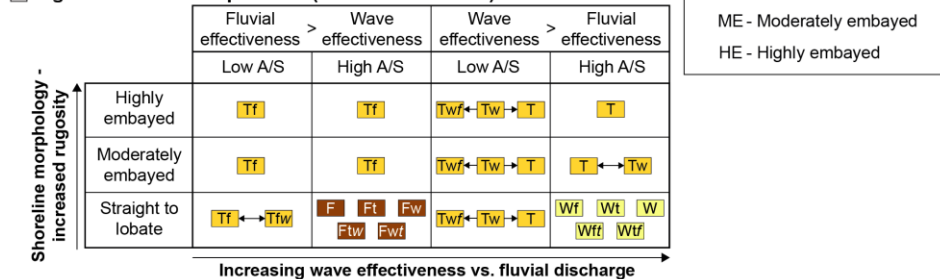


**Fig. 7. Predictive model for shoreline process regime (modified from Ainsworth et al. (2011)).**

(A) Decision tree with four main queries predicting shoreline process regime. (B) Predictive

matrix for settings with a low tidal potential. (C) Predictive matrix for settings with a high tidal potential. Abbreviations and color coding are shown in the inset (opposite B).

## **METHODS**

### **Numerical tidal modelling**

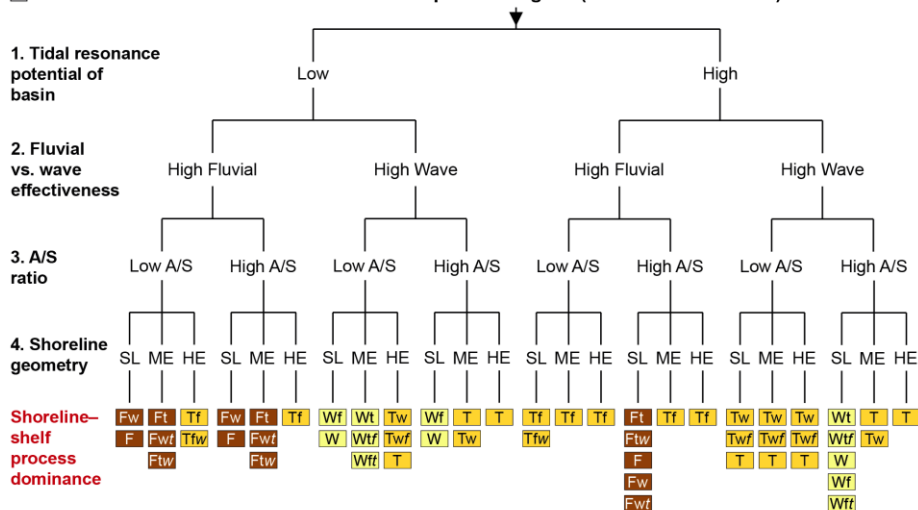
### **Mesh generation**

Whilst the predictive framework of Ainsworth et al. (2011) provides an improved methodology for interrogating the process classifications of ancient shoreline-shelf systems, the current decision tree does not sufficiently capture the complex impact of basin physiography on tide and wave processes. For tidal processes, basin physiography complicates: (1) the flux of tidal energy into and out of partly enclosed water bodies (referred to herein as tidal inflow and outflow), and (2) the funnelling, shoaling and resonance effects on continental shelves and within shoreline embayments, which occur on a range of scales (c. 1–1000s km width and 1–100s m depth) (Mitchell et al., 2010; Wells et al., 2010b; Collins et al., 2018c). However, basin physiography does not constitute a separate query in the predictive model (~~Fig. 3~~) and is treated as a modifying factor to shelf tidal resonance potential (Ainsworth et al., 2011). Open oceans are sufficiently large to allow generation of relatively high *in-situ* tides (Dalrymple, 1992). Therefore, basins that have restricted access to the open oceans generally have a lower potential for producing amplified tidal currents by resonance effects, whereas basins with less restricted access to open oceans have a higher tidal resonance potential. For example, the small tides (typically <1 m tidal range) in the modern Arctic Ocean are primarily due to the restricted access to the Atlantic Ocean preventing northward propagation of the open ocean tidal wave, as well as the basin being too small to have its own tides (Dalrymple and Padman, 2019). However, an exception is that certain restrictive basin physiographies, typically on a smaller-scale (1–10s km), may cause significant amplification of tides by funnelling, shoaling and/or resonance effects (Piper et al., 1990; Martel et al., 1994) (Mitchell et al., 2010; Ainsworth et al., 2011; Mitchell et al., 2011) (Androsoy et al., 2002; Leckie and Rumpel, 2003). On the other hand, smaller basins and large areas of wide, shallow shelves may increase frictional dissipation of tides but also waves and may still be tide dominated even at lower tidal ranges. This is illustrated in the White Sea region

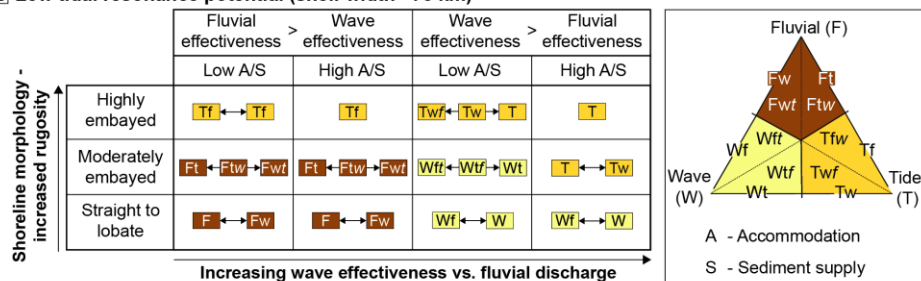
Formatted: Font: Bold

of the modern Arctic Ocean, where macrotidal ranges occur due to favourable geomorphology for funnelling and shoaling effects, in combination with rotating tides due to the high Coriolis parameter, whilst mean wave height is low due restricted ocean access (Dalrymple and Padman, 2019). Overall, the generalized treatment of basin physiography in the existing predictive model (Ainsworth et al., 2011) combines two very different effects on tides relating to: (1) basin size (100–1000 km width scale) and bathymetry (100–1000 m depth scale), which has a first order control on the balance of tidal inflow versus outflow; and (2) second-order funnelling and resonance effects relating to basin physiography (10–100s km width scale and 1–100s m depth scale) (Wells et al., 2005a; Wells et al., 2007; Mitchell et al., 2010; Wells et al., 2010b; Collins et al., 2018a; Collins et al., 2018b). Numerical tidal modelling is particularly well-suited to distinguishing between these two basin physiographic controls (Slingerland, 1986; Martel et al., 1994; Wells et al., 2007; Collins et al., 2018a; Collins et al., 2018b) and therefore provides information for shoreline–shelf process prediction.

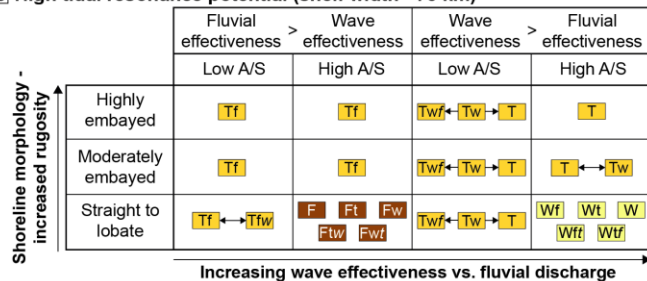
**A Predictive decision tree for shoreline–shelf process regime (Ainsworth et al. 2011)**



**B Low tidal resonance potential (shelf width <75 km)**



**C High tidal resonance potential (shelf width >75 km)**





**A Predictive decision tree for shoreline–shelf process regime (Ainsworth et al. 2011)**



Fluvial (F)

Wave (W) Tide (T)

A - Accommodation  
S - Sediment supply  
SL - Straight/lobate  
ME - Moderately embayed  
HE - Highly embayed

		Fluvial effectiveness > Wave effectiveness		Wave effectiveness > Fluvial effectiveness	
		Low A/S	High A/S	Low A/S	High A/S
Shoreline morphology - increased rugosity ↑	Highly embayed	Tf	Tf	Twf ← Tw → T	T
	Moderately embayed	Tf	Tf	Twf ← Tw → T	T ↔ Tw
	Straight to lobate	Tf ↔ Tw	F   Ft   Fw Ftw   Fwt	Twf ← Tw → T	Wf   Wt   W Wft   Wtf

**Increasing wave effectiveness vs. fluvial discharge**

~~Fig. 7. Predictive model for shoreline process regime (modified from Ainsworth et al. (2011)).~~  
~~Predictive model for shoreline process regime (modified from Ainsworth et al. (2011)). (A)~~  
~~Decision tree with four main queries predicting shoreline process regime. (B) Predictive matrix~~  
~~for settings with a low tidal potential. (C) Predictive matrix for settings with a high tidal~~  
~~potential. Abbreviations and color coding are shown in the inset (opposite D).~~

## ~~3.1. METHODS~~

### ~~3.1.1. Numerical tidal modelling~~

#### ~~3.1.1.1. Mesh generation~~

## 2.2 Tidal theory, palaeotidal modelling and identification of ancient tidal processes

### 2.2.1 Tidal theory

Since the mathematical and non-mathematical theory of Earth tides has been reviewed extensively and in detail elsewhere (Defant, 1961; MacMillan, 1966; Pugh, 1987; Dalrymple, 1992; Allen, 1997; Open University Course Team, 1999; Willis, 2005; Kvale, 2006; Kvale, 2012; Longhitano et al., 2012; Reynaud and Dalrymple, 2012; Pugh and Woodworth, 2014; Dalrymple and Padman, 2019), here it will be only briefly discussed in terms of the fundamental concepts and dominant controls impact shallow-water tides (Table 1). Astronomical tides are defined as ‘any periodic fluctuation in the water level that is generated by the gravitational attraction of the Moon and Sun’ (Dalrymple, 1992) and can be understood by a combination of equilibrium and dynamic theories of tides. In equilibrium tidal theory, the gravitational dynamics of the Earth-Moon-Sun system, combined with the Earth’s rotation, results in two oceanic bulges beneath the moon and on the opposite side of the Earth that move clockwise around the Earth to produce twice daily (semidiurnal) high (flood) and low (ebb) tides. Changes in the magnitude of tide-generating forces by the Moon and Sun on varying timescales, in combination with the Earth’s tilt, produces various tidal variations and cycles (e.g. diurnal inequality, spring and neap cycles etc.). However, the applicability of equilibrium tidal theory to understanding real-world tides is complicated by several factors, most notably that the Earth’s ocean basins are interrupted by significant bathymetric changes and emergent landmasses. Instead, the dynamic tidal theory model tides as the combined effects of many tidal constituents. The 11 most important tidal constituents cause semi-diurnal ( $M_2$ ,  $S_2$ ,  $N_2$ ,  $K_2$ ), diurnal ( $K_1$ ,  $O_1$ ,  $P_1$ ,  $Q_1$ ) and long-period ( $M_f$ ,  $M_m$ ,  $S_{sa}$ ) tides and harmonic convergence and divergence of these constituents result in tidal cycles. The relative importance of diurnal ( $K_1$  and  $O_1$ ) to semidiurnal ( $M_2$  and  $S_2$ ) tides is quantified using the ratio  $F$ , where:

$$F = \left( \frac{K_1 + O_1}{M_2 + S_2} \right)$$

If  $F < 0.25$ , the tide is semi-diurnal, for  $0.25 < F < 1.5$  the tide is mixed semidiurnal dominated, for  $1.5 < F < 3$  the tide is mixed diurnal dominated, and  $F > 3$  the tide is diurnal (Open University Course Team, 1999).

Name	Description
Astronomical tide	Tide formed by the gravitational and rotational effects of the Moon and Sun on the water in an open ocean or seaway
Bed shear stress	Force per unit area exerted by flow on the sediment surface
Co-oscillating or boundary tide	Tide formed by the propagation of an open-ocean astronomical tide into a connected water body
Coriolis effect and amphidromic cells	The Coriolis effect deflects the tidal wave to the right in the northern hemisphere and left in the southern hemisphere. In the northern hemisphere, this causes the tidal wave to rotate anticlockwise about an amphidromic point of zero tidal range; rotation is clockwise in the southern hemisphere. In enclosed water bodies, the deflected tidal wave (termed a Kelvin wave) pushes against the shoreline, leading to an exponential increase in tidal range from the amphidromic node towards the shoreline. The Coriolis effect also causes asymmetry in the tidal range on either side of elongate water bodies, such as the Yellow Sea, because the incoming tidal wave is larger than the reflected wave.
Diurnal	Once-daily tide where the $K_1$ and $O_1$ constituents are more dominant than the $M_2$ and $S_2$ constituents
Resonance	Resonance occurs when the tidal period matches a natural mode of oscillation within a water body. Maximum resonance typically occurs when shelf width is approximately a quarter the dominant tidal wavelength, and matches a half-wave oscillator or standing wave in an enclosed basin and quarter-wave oscillator in an open-ended embayment (gulf).
Funnelling	Increase in tidal amplitude caused by progressive narrowing and shallowing of a water body
Semidiurnal	Twice-daily tide where the $M_2$ and $S_2$ constituents are more dominant than the $K_1$ and $O_1$ constituents
Shoaling	Increase in tidal amplitude caused by progressive shallowing of a water body
Tidal amplitude	Elevation of tidal high water above mean sea level, equal to half the tidal range
Tidal range	Vertical height between consecutive high and low waters over a tidal cycle (twice the tidal amplitude), classified as microtidal (<2 m), mesotidal (2–4 m) and macrotidal (>4 m)

**Table 1. Explanations of several tide-related terms used in this paper.**

Significant tides, though typically <1 m in tidal range (the difference in sea level between high and low tide), only develop in the open oceans. Open-ocean tides are fundamentally controlled by ocean basin physiography and tides across entire oceans can be ‘tuned’ to particular tidal constituents. For example, the modern North Atlantic Ocean is close to resonance for the semidiurnal  $M_2$  tide, whereas the modern Pacific Ocean accentuates the diurnal ( $O_1$  and  $K_1$ ) constituents (Fig. 4). An ocean basin can house resonant tides when the width of the basin,  $L$  is equal to a multiple of half wavelengths,  $\lambda = \sqrt{gHT}$  ( $T$  is the tidal period,  $g$  is gravity, and  $H$  is water depth) of the tidal wave. Oceanic tides rotate as waves around fixed (amphidromic) points with negligible tidal amplitude (half the tidal range) (Fig. 4). Water on continental shelves and smaller water bodies partly (seas) or fully (lakes) enclosed by land do not develop appreciable *in situ* tides (Dalrymple, 1992). Instead, tides on shelves and in seas rely on the amount of tidal

inflow from connected ocean basins which depends on the size, shape and bathymetry of the connection(s) and orientation of connection(s) relative to the oceanic tide (Fig. 4). When oceanic tides encounter areas of shallower water and constricted physiography, they may undergo amplification due to shoaling, funnelling and resonance (Table 2). Simplified mathematical reviews of these effects are discussed elsewhere (Proudman, 1953; Howarth, 1982; Slingerland, 1986; Allen, 1997; Wells et al., 2007; Kowalik and Luick, 2013). The most relevant points for understanding controls on tides and predicting shoreline–shelf process classification are discussed below.

First, shoaling effects describe the increase in tidal amplitude and current velocity that occurs when water depth decreases, for example, from the deeper ocean onto the continental shelf, and from deeper shelf to shoreline areas. Second, funnelling effects describe the increase in tidal range as a result of physical constriction of the tidal wave, for example, in straits and shoreline embayments. The combination of shoaling and funnelling effects is referred to as convergence effects and these are an important contributing cause of tidal amplification in shoreline – shelf areas. Third, tidal resonance occurs when the natural period of oscillation on the shelf or within a shoreline bathymetric constriction is coincident with the tidal period (Slingerland, 1986; Allen, 1997). On the continental shelf, tidal resonance reaches a maximum when shelf width is one-quarter the tidal wavelength (and for widths 3/4, 5/4, etc.) (e.g. Proudman, 1953; Howarth, 1982). However, this relationship assumes the incident tide is perpendicular to the shelf, friction is inversely proportional to depth and no Coriolis effect, none of which have been widely evaluated. At typical shelf depths (c. 100 m), the quarter wavelength of the dominant semi-diurnal M2 and diurnal K1 tides are c. 350 km and 675 km. As the majority (c. 70%) of modern shelves are <75 km wide (Nyberg and Howell, 2016), tides are closer to resonance as shelf width increases, hence tidal amplitude increases with shelf width (Redfield, 1958; Off, 1963; de Vries Klein, 1977; Cram, 1979; Ainsworth et al., 2011; Reynaud and Dalrymple, 2012). Within an embayment or gulf, tidal resonance occurs when the amount of time taken for the tidal wave to travel for the embayment mouth, to the apex and back to the mouth is the same, or nearly the same, as the time between high and low tides, effectively forming a high amplitude standing wave. The combination of tidal resonance and convergence effects explains the location of the highest tidal ranges globally (O'Reilly et al., 2005). In the Bay of Fundy, eastern Canada, tidal

ranges up to 17 m are caused principally by the dominant  $M_2$  tide being very close to resonance, with secondary convergence effects in the landward shallowing and narrowing estuary (e.g. Garrett, 1972; Dalrymple, 2021). In comparison, tides of up to 14m tidal range in the Severn Estuary in the upper reaches of the Bristol Channel, UK, are caused by partial resonance of the dominant  $M_2$  tide plus convergence effects in the funnel-shaped and shallowing Severn Estuary (e.g. Gao and Adcock, 2017). Simplified numerical relationships for convergence effects and tidal resonance (e.g. Slingerland, 1986; Allen, 1997; Wells, 2008) can enable first-order interpretations of whether the potentially dominant semi-diurnal or diurnal tidal constituents may be close to resonance and the potential magnitude of shoaling and funnelling effects in both the modern and ancient.

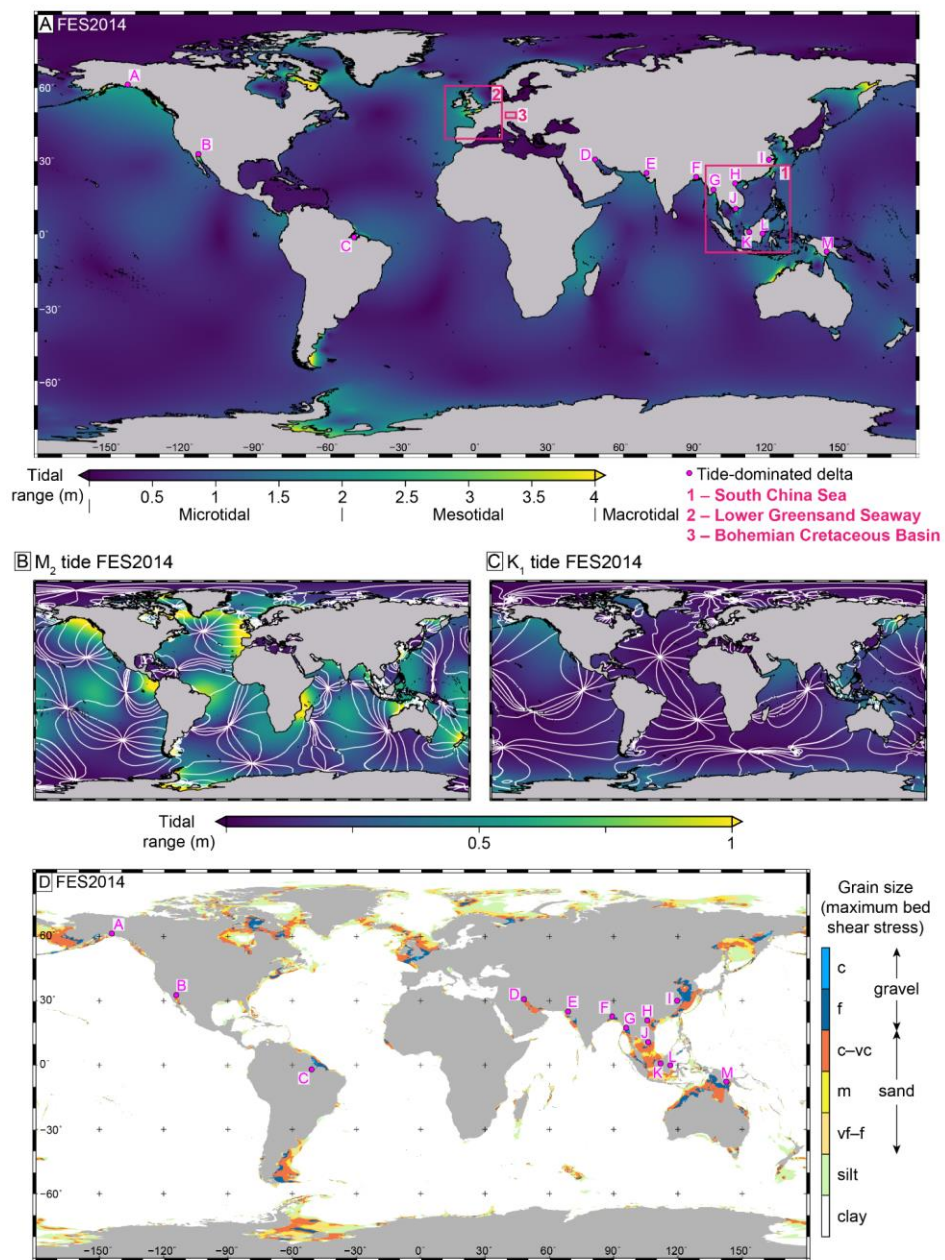




**Fig. 4.** (A) Present day global tidal range based on the FES 2014 tidal model (Carrère et al., 2015), showing the locations (pink dots) of tide-dominated deltas (Goodbred and Saito, 2012): A) Copper; B) Colorado; C) Amazon; D) Shatt-al-Arab; E) Indus; F) Ganges-Brahmaputra; G) Irrawaddy; H) Red River; I) Yangtze; J) Mekong; K) Rajang; L) Mahakam; and M) Fly. Pink boxes show approximate locations of the palaeotidal modelling case studies. (B, C) Global map of  $M_2$  (B) and  $K_1$  tidal amplitude (C) from FES 2014. Contours join lines of equal phase in  $30^\circ$  intervals and white arrows give the sense of rotation of the major ocean amphidromic systems. (D) Maximum tidal bed shear stress, plotted as the equivalent grain size that could be entrained if available, for FES2014, including the difference in sediment grain size class. Grain size abbreviations: vf = very fine; f = fine; m = medium; c = coarse; vc = very coarse.

Formatted: Font: Bold

### 2.2.2 Palaeotidal modelling

Palaeotidal numerical modelling can provide quantitative information on ancient shoreline tidal processes and can test their sensitivity to palaeogeographic and palaeobathymetric change and uncertainty (e.g. Martel et al., 1994; Egbert et al., 2004; Wells et al., 2005a; Uehara et al., 2006; Collins et al., 2018a; Collins et al., 2018b). Computational methods for palaeotidal modelling, including tidal forcing boundary conditions and mesh generation, have advanced since early approaches that used structured meshes and open boundary tidal forcing by the  $M_2$  (principal lunar semi-diurnal) tide only, and output tidal amplitude or range (Slater, 1985; Slingerland, 1986; Ericksen and Slingerland, 1990; Martel et al., 1994). More recent simulations have investigated tidal amplitude (Slingerland, 1986; Wells et al., 2005a; Wells et al., 2005b; Wells et al., 2007; Wells et al., 2010a; Wells et al., 2010b) and bed shear stress (Mitchell et al., 2010; Mitchell et al., 2011) in ancient epicontinental seaways, and tidal range and bed shear stress in ancient seas (Collins et al., 2017a; Collins et al., 2018a; Collins et al., 2018b), using models with astronomical tidal forcing and unstructured meshes (Table 2). These diverse case studies illustrate how the sensitivity of shoreline tides to various palaeogeographic and palaeobathymetric changes can improve predictive models of depositional process regimes of ancient shoreline systems.

Fluidity (<http://fluidityproject.github.io/>), formerly the Imperial College Ocean Model (ICOM), is a hydrodynamic, finite element ocean model that solves the Navier-Stokes equations and uses unstructured, multi-scale, three-dimensional, tetrahedral meshes that (1) smoothly and accurately conform to coastline and bathymetry, (2) have focused resolution in areas of complex bathymetry (e.g. straits and embayments), along coastlines and/or in areas of interest, and (3) maximize computational accuracy and efficiency (Pain et al., 2005; Wells et al., 2005a; Gorman et al., 2007; Gorman et al., 2008; Piggott et al., 2008; Geuzaine and Remacle, 2009; Avdis et al., 2018). Meshes used in Fluidity palaeotidal simulations may be global or regional and have been constructed using Terreno (Gorman et al., 2007; Gorman et al., 2008) or qmsh (Avdis et al., 2018). By working directly on an arbitrary geodetic in Cartesian space, Fluidity eliminates the

‘pole problem’ by which lines of constant longitude converge at the poles producing very small elements (Madee and Imbard, 1996; Comblen et al., 2009; Wells et al., 2010a). A minimum depth of 10 m along the shoreline prevents the free surface from intersecting the bottom surface as it propagates but the increased water depth impacts shallow water current velocities and possibly tidal amplification effects (e.g. Wells et al., 2010a).

### 3.1.2—Hydrodynamic modelling of astronomical and forced boundary tides

Fluidity can simulate both astronomical and co-oscillating boundary tides (Table 2). The astronomical tide results directly from the tide-generating force on the water in an open ocean or seaway due to the gravitational and rotational effects of the Moon and Sun. Astronomical tidal potential is calculated at each mesh node for each time step using the multi-constituent equilibrium theory of tides:

$$\eta_{eq}(\lambda, \theta, t) = \sin^2 \theta \sum_i K_i \cos(\sigma_i t + \chi_i + 2\lambda) + \sin 2\theta \sum_j K_j \cos(\sigma_j t + \chi_j + \lambda) + (3 \sin^2 \theta - 2) \sum_k K_k \cos(\sigma_k t + \chi_k)$$

where  $\eta_{eq}$  = equilibrium tidal potential (m),  $\lambda$  = east longitude (radians),  $\theta$  = colatitude ( $\pi/2$  – latitude, radians),  $\chi$  = astronomical argument (radians),  $\sigma$  = frequency of tidal constituent ( $s^{-1}$ ),  $t$  = universal standard time (s) and  $K$  = equilibrium amplitude of tidal constituent (m). Subscripts  $i$ ,  $j$  and  $k$  represents the semidiurnal, diurnal and long period tidal constituents, respectively, which allows constituents to be modelled individually or in combination (Schwiderski, 1980; Kantha and Clayson, 2000; Wells et al., 2007a; Mitchell et al., 2010). The overall forcing is applied as

the product of the equilibrium tidal potential gradient and the gravitational acceleration ( $g$ )

(Mellor, 1996; Kantha and Clayson, 2000).

The co-oscillating or boundary tide results from propagation of the astronomical tidal wave into a connected water body. This is especially important for simulations of tides in partly enclosed seas and shallow seaways (straits), which typically have limited potential for internally generated astronomical tides because of their smaller water masses (Tsimplis et al., 1995; Wells et al., 2005a). Co-oscillating tides along designated open boundaries are forced as either one fixed cosine wave of constant amplitude and phase applied across the entire boundary length or interpolated as many cosine waves of different amplitudes and phases at a series of points along the boundary. Ideally, the amplitude and phase values for each tidal constituent would be derived from a larger scale model of the adjacent water body.

The bottom drag is applied as a surface integral boundary condition based on a quadratic friction law of the form  $-C_D \bar{u} |\bar{u}|$  where  $C_D$  = drag coefficient and depth averaged current velocity  $|\bar{u}| = \sqrt{u^2 + v^2 + w^2}$ , where  $u$ ,  $v$  and  $w$  represent the velocities in the x, y, and z dimensions, respectively ( $\text{ms}^{-1}$ ) (Wells et al., 2007a; Mitchell et al., 2010). The drag coefficient is set as 0.0025, a generic value used in most ocean models (Pietrzak et al., 2002), but the drag coefficient may vary between  $10^{-2}$ – $10^{-3}$  as a function of bathymetry and sediment grain size, shape and sorting (Safak, 2016).

A spin-up period of at least 120 hours (five days) simulation time is sufficient to remove spin-up effects and reach steady state. A multitude of globally applicable numerical tidal models exist

(Wells et al., 2007a; Wells et al., 2007b), a comprehensive review of which is beyond the aim of this paper. The range of modern ocean tide models can be classified as (1) data-constrained models, those with empirical adjustment to an adopted prior models, (2) barotropic hydrodynamic models that may be constrained by tide information through assimilation, or (3) purely hydrodynamic models with no data constraints (Stammer et al., 2014). Palaeotidal models, where no empirical tidal data are available, must by definition be purely hydrodynamic. The tidal model used in the ancient case studies discussed herein is Fluidity (<http://fluidityproject.github.io/>), formerly the Imperial College Ocean Model (ICOM), which can be used to simulate both astronomical and co-oscillating boundary tides. Details of the tetrahedral, unstructured meshing and hydrodynamic modelling approach used with Fluidity have been widely documented and will not be repeated herein (Pain et al., 2005; Wells et al., 2005a; Gorman et al., 2007; Gorman et al., 2008; Piggott et al., 2008; Geuzaine and Remacle, 2009; Avdis et al., 2018) (e.g. Wells et al., 2010a) Wells et al., 2007a; Mitchell et al., 2010). Likewise, tidal modelling using Fluidity has been extensively validated against real-world modern tidal amplitude (Wells et al., 2005a; Wells et al., 2005b; Wells et al., 2007; Wells, 2008; Wells et al., 2010a; Wells et al., 2010b; Collins et al., 2017a; Collins et al., 2018a; Collins et al., 2018b) and tidal bed shear stress (Mitchell et al., 2010; Mitchell et al., 2011; Collins et al., 2017a; Collins et al., 2018a; Collins et al., 2018b), which includes global (Wells et al., 2010a; Collins et al., 2018a; Collins et al., 2018b) and regional comparisons in the Mediterranean Sea (Wells et al., 2005a), North Sea (Wells et al., 2007; Mitchell et al., 2010), Baltic Sea (Wells, 2008) and South China Sea (Wells et al., 2007a; Wells et al., 2007b)(Collins et al., 2017a; Collins et al., 2018a; Collins et al., 2018b) (see Supplementary Material). As well as Fluidity, other modern hydrodynamic tidal models have been used for palaeotidal modelling, notably the Oregon State University Tidal Inversion Software (OTIS) (Egbert et al., 2004; Green and Huber, 2013; Wilmes and Green, 2014; Green et al., 2017).

Formatted: Line spacing: 1.5 lines

<u>Geologic age &amp; reference</u>	<u>Study area</u>	<u>Computational method</u>	<u>Boundary conditions</u>	<u>Key findings</u>
<u>Late Devonian c. 370 Ma (Slingerland, 1986)</u>	<u>Catskill epicontinental sea of North America</u>	<u>Structured grid, finite difference scheme; Navier– Stokes equations; Coriolis parameter (f - plane).</u>	<u>Open boundary tidal forcing, no astronomical tidal forcing; M2 tide only; Variable bathymetry; Chezy approximation for bottom friction.</u>	<u>Microtidal–low mesotidal, locally mesotidal–macrotidal areas due to resonance, funnelling and shoaling effects. Tidal ranges increased by 1) increasing the boundary tidal range; 2) increasing the open boundary width; and 3) increasing the depth of the seaway.</u>
<u>Mid Cretaceous c. 100 Ma (Slater, 1985)</u>	<u>Western Interior Seaway of North America</u>	<u>Structured grid, finite difference scheme; Laplace Tidal Equations; No Coriolis parameter.</u>	<u>Open boundary and astronomical tidal forcing; M2 tide only; Uniform depths; Linear bottom friction with respect to velocity.</u>	<u>Microtidal; <del>A strong</del> forcing dominates; Open boundary tide negligible from the Arctic Ocean and possibly significant from the Gulf of Mexico; Tidal range sensitive to water depth (resonance at 200 m water depth).</u>
<u>Mid Cretaceous c. 100 Ma (Ericksen and Slingerland, 1990)</u>	<u>Western Interior Seaway of North America</u>	<u>Structured grid, finite difference scheme; Navier Stokes equations; Coriolis parameter (f - plane).</u>	<u>Open boundary tidal forcing, no astronomical tidal forcing; M2 tide only; Variable bathymetry; Chezy approximation for bottom friction.</u>	<u>Microtidal, <del>locally</del> macrotidal near Gulf of Mexico open boundary; Tidal range increases as seaway depth and Gulf of Mexico connection increases; Open boundary tides argued to be dominant contributor to tides.</u>

				<u>not astronomically forced tides (cf. Slater, 1985).</u>
<u>Miocene c. 22 Ma (Martel et al., 1994)</u>	<u>Alpine foreland basin of France and Switzerland</u>	<u>Structured grid, finite difference scheme; Navier Stokes equations; Coriolis Parameter (f - plane).</u>	<u>Open boundary tidal forcing, no astronomical tidal forcing; M2 tide only; Variable bathymetry; Chezy approximation for bottom friction.</u>	<u>Higher tidal current predicted with wider and deeper open-ocean connections and 2m open boundary tide applied.</u>
<u>Late Carboniferous c. 300 Ma (Wells et al., 2005a,b)</u>	<u>Late Carboniferous sea of NW Europe</u>	<u>Unstructured, tetrahedral mesh, finite element scheme; Navier Stokes equations; No Coriolis parameter; Fluidity tidal model.</u>	<u>Astronomical tidal forcing only; M2 tide only; Variable bathymetry; No treatment of bottom friction.</u>	<u>Extremely microtidal seaway (typically &lt;10 cm tidal range) across NW region across various sensitivity tests; Putative tidal deposits interpreted to be confined to localised estuaries.</u>
<u>Late Carboniferous c. 300 Ma (Wells et al., 2008)</u>	<u>Late Carboniferous sea of NW Europe</u>	<u>Unstructured, tetrahedral mesh, finite element scheme; Navier Stokes equations; Coriolis parameter included; Fluidity tidal model.</u>	<u>Astronomical tidal forcing only; M2, S2, N2, K2, Q1, O1, P1, K1, Mf, Mm and Ssa tidal constituents; Variable bathymetry; Bottom drag applied as surface-integral based on quadratic friction law.</u>	<u>Microtidal ranges predicted across the northwest European region (similar to Wells et al., 2005a, b); Extra tidal constituents increase the predicted tidal range to 20–80 cm.</u>
<u>Early Cretaceous,</u>	<u>Global</u>	<u>Unstructured, tetrahedral mesh,</u>	<u>Astronomical tidal forcing only; M2, S2, O1</u>	<u>Model results compared to published geologic records;</u>

Formatted: Line spacing: 1.5 lines



<u>late Aptian, c. 116 Ma (Wells et al., 2010a)</u>		<u>finite element scheme; Navier Stokes equations; Coriolis parameter included; Fluidity tidal model.</u>	<u>and K1 tidal constituents modelled independently; Variable bathymetry; Bottom drag applied as surface-integral based on quadratic friction law.</u>	<u>High mesotidal to macrotidal on the Arabian Platform, around India, along the Pacific coast between North and South America, northeast of Australia, and around Southeast Asia; Low microtidal ranges in the proto-South Atlantic Ocean and Weddell Sea.</u>
<u>Early Cretaceous, late Aptian – early Albian, c. 112–107 Ma (Wells et al., 2010b)</u>	<u>Lower Greensand Seaway of NW Europe</u>	<u>Unstructured, tetrahedral mesh, finite element scheme; Navier Stokes equations; Coriolis parameter included; Fluidity tidal model.</u>	<u>Open boundary conditions (from Wells et al., 2010a) and astronomical tidal forcing; M2, S2, O1 and K1 tidal constituents modelled independently; Variable bathymetry; Bottom drag applied as surface-integral based on quadratic friction law.</u>	<u>Overall microtidal increasing to microtidal–macrotidal with increased width and depth of open-ocean connections and more localised funnelling, shoaling and Coriolis effects.</u>
<u>Middle Cretaceous, Early–Middle Turonian, c. 93 Ma (Mitchell et al., 2010)</u>	<u>Bohemian Cretaceous Basin of Central Europe</u>	<u>Unstructured, tetrahedral mesh, finite element scheme; Navier Stokes equations; Coriolis parameter included; Fluidity tidal model.</u>	<u>Open boundary conditions and astronomical tidal forcing; varying combinations of M2, S2, O1 and K1 tidal constituents; Variable bathymetry; Bottom drag applied as surface-</u>	<u>Microtidal–mesotidal across the Bohemian Cretaceous Basin and range of sensitivity tests; Elevated tidal ranges and velocity in local embayments and straits due to funnelling and shoaling effects.</u>

			<u>integral based on</u> <u>quadratic friction law.</u>	
<u>Early</u> <u>Jurassic, c.</u> <u>200 Ma</u> <u>(Mitchell et</u> <u>al., 2011)</u>	<u>Laurasian</u> <u>Seaway of</u> <u>NW Europe</u>	<u>Unstructured,</u> <u>tetrahedral mesh,</u> <u>finite element</u> <u>scheme; Navier</u> <u>Stokes equations;</u> <u>Coriolis</u> <u>parameter</u> <u>included; Fluidity</u> <u>tidal model.</u>	<u>Astronomical tidal</u> <u>forcing; M2, S2, O1 and</u> <u>K1 tidal constituents;</u> <u>Variable bathymetry;</u> <u>Bottom drag applied as</u> <u>surface-integral based on</u> <u>quadratic friction law.</u>	<u>Seaway largely microtidal;</u> <u>Flow constriction associated</u> <u>with shallow platforms and</u> <u>straits produced elevated bed</u> <u>shear stresses that were</u> <u>decoupled from tidal range.</u>
<u>Eocene, c. 55</u> <u>Ma (Green &amp;</u> <u>Huber, 2013)</u>	<u>Global</u>	<u>Finite element</u> <u>grid, 1/4°</u> <u>resolution,</u> <u>Numerical</u> <u>solutions to</u> <u>linearized</u> <u>shallow water</u> <u>equations,</u> <u>including</u> <u>Coriolis</u> <u>parameter; OTIS</u> <u>tidal model.</u>	<u>Includes up to</u> <u>8 constituents (M2, S2,</u> <u>N2, K2, K1, O1, P1, Q1)</u> <u>and linear bottom drag</u> <u>parameterization (see</u> <u>Egbert et al., 2004);</u> <u>Variable ocean</u> <u>bathymetry and</u> <u>stratification.</u>	<u>Weak M2 tide predicted in</u> <u>Eocene ocean except in the</u> <u>Pacific.</u>
<u>Mesozoic–</u> <u>Cenozoic, 5</u> <u>timeslices</u> <u>from c. 252</u> <u>Ma to 3 Ma</u> <u>(Green et al.,</u> <u>2017)</u>	<u>Global</u>	<u>Finite element</u> <u>grid, 1/4°</u> <u>resolution,</u> <u>Numerical</u> <u>solutions to</u> <u>linearized</u> <u>shallow water</u>	<u>M2, S2, K1 and O1 tidal</u> <u>constituents and linear</u> <u>bottom drag</u> <u>parameterization (see</u> <u>Egbert et al., 2004);</u> <u>Variable ocean</u>	<u>Tidal dissipation during the</u> <u>Cenozoic and Late Cretaceous</u> <u>were weaker than at present,</u> <u>apart from the glacial states</u> <u>over the last 2 Ma.</u>

		<u>equations, including Coriolis parameter; OTIS tidal model.</u>	<u>bathymetry and stratification.</u>	
<u><b>Oligocene–Miocene, c. 26–5 Ma</b></u> <u><b>(Collins et al., 2017a, 2018a)</b></u>	<u>South China Sea, SE Asia</u>	<u>Unstructured, tetrahedral mesh, finite element scheme; Navier Stokes equations; Coriolis parameter included.</u>	<u>Astronomical tidal forcing; M2, S2, N2, K2, Q1, O1, P1, K1, M<sub>f</sub>, M<sub>m</sub> and S<sub>sa</sub> tidal constituents; Variable bathymetry; Bottom drag applied as surface-integral based on quadratic friction law.</u>	<u>Spring tides along South China Sea coastline were largely mesotidal–macrotidal and capable of transporting sand throughout the Late Oligocene to Middle Miocene.</u>
<u><b>Late Cretaceous middle Campanian, c. 75–77.5 Ma</b></u> <u><b>(Dean et al., 2019)</b></u>	<u>Western Interior Seaway of North America</u>	<u>Unstructured, tetrahedral mesh, finite element scheme; Navier Stokes equations; Coriolis parameter included.</u>	<u>Astronomical tidal forcing; M2, S2, N2, K2, Q1, O1, P1, K1, M<sub>f</sub>, M<sub>m</sub> and S<sub>sa</sub> tidal constituents; Variable bathymetry; Bottom drag applied as surface-integral based on quadratic friction law.</u>	<u>Regionally microtidal mesotidal (2–4 m) along most of the eastern margin; seaway; increased tidal bed shear stress when seaway center and entrance to Gulf of Mexico are deeper.</u>

Formatted: English (United Kingdom)

Formatted: Line spacing: 1.5 lines

Formatted: English (United Kingdom)

Formatted: Line spacing: 1.5 lines

Formatted: Font: Bold

**Table 7.2**, after which all fields are set to zero.

The equations of motion describing the movement of the tidal bulge include the Coriolis acceleration ( $f$ ), which is simplified to  $f = 2\Omega \sin \phi$  (Cushman-Roisin, 1994; Cushman-Roisin and Beckers, 2011), where  $\Omega$  is the rotation rate of the Earth ( $7.27 \times 10^{-5} \text{ rad s}^{-1}$ ) and  $\phi$  is the latitude.

Model outputs are the amplitude of tidal components, tidal range, average and maximum tidal current velocity, the magnitude and direction of average and maximum tidal bed shear stress, and the tidal phase. Tidal range is calculated as the difference between the maximum and minimum free surface heights over the post spin-up simulation period, which approximately equals the maximum spring tidal range. The amplitude and phase of the four major tidal constituents ( $M_2$ ,  $S_2$ ,  $K_1$  and  $O_1$ ) are determined using tidal harmonic analysis of the modelled time series of free surface heights (Foreman, 1979). Tidal bed shear stress ( $\tau$ ) is the frictional force exerted by tides on the sediment surface and is calculated using  $\tau = \rho C_D \bar{u} |\bar{u}|$  where  $\rho$  = the density of water ( $1023 \text{ kg m}^{-3}$ ) (Pingree and Griffiths, 1979; Wells et al., 2007a; Mitchell et al., 2010). Bed shear stress magnitudes can be converted to the equivalent grain size that could be entrained by the tidal flow based on the modelled and calculated critical bed shear stress values for sediment transport (Miller et al., 1977; Soulsby et al., 1993; Julien and Raslan, 1998).

### 3.1.3 Validation of tidal model results

Tidal modelling using Fluidity has been extensively validated against real world modern tidal amplitude (Wells et al., 2005a; Wells et al., 2005b; Wells et al., 2007a; Wells, 2008; Wells et al., 2010a; Wells et al., 2010b; Collins et al., 2017a; Collins et al., 2018a) and tidal bed shear stress (Mitchell et al., 2010; Mitchell et al., 2011; Collins et al., 2017a; Collins et al., 2018a). This includes global (Wells et al., 2010a; Collins et al., 2018a) and regional comparisons in the Mediterranean Sea (Wells et al., 2005a), North Sea (Wells et al., 2007a; Mitchell et al., 2010), Baltic Sea (Wells, 2008) and South China Sea (Collins et al., 2017a; Collins et al., 2018a).

On a global scale, comparison of the modeled amplitude of the  $M_2$ ,  $S_2$ ,  $K_1$  and  $O_1$  tidal constituents using Fluidity, which utilises the GEBCO (General Bathymetric Chart of the Oceans) 2014 bathymetric data and an unstructured mesh with maximum resolution of 10 km, to tidal gauge data and the FES 2014 tidal model, clearly illustrates that Fluidity accurately predicts tidal range without the need for data assimilation (Fig. 8). Tidal constituent amplitudes at 423 stations were calculated using tidal harmonic analysis of sea surface elevation data (Caldwell et al., 2015) (Fig. 8A–F) and the calculated mean root-mean-squared (RMS) error includes absolute values of both tidal amplitude and phase (Cummins and Thupaki, 2018). Fluidity very slightly underpredicts tidal amplitude compared to tidal gauge data, with the relative error varying between 0.01% ( $S_2$  tide) to 0.23% ( $O_1$  tide) and the root-mean-squared (RMS) amplitude varying between 0.10 m ( $K_1$  and  $O_1$  tide) to 0.37 m ( $M_2$  tide) (Fig. 8B–F). However, these errors are comparable to those between the FES 2014 tidal model and tidal gauge data for 162 stations (Fig. 8B, G–J), despite the FES2014 model using tidal data from satellite altimetry and gauges, highly accurate global and regional bathymetries, an unstructured mesh with up to c. 7 km ( $1/16^\circ$ ) resolution, and corrections for internal and load tides (Carrère et al., 2015). Local scale differences between the Fluidity model and the FES 2014 model and tidal gauge data are likely caused by (1) mesh resolution limitations that simplify bathymetry (e.g. between islands) and affect modelled tidal flow and frictional effects, (2) the lack of correction for internal drag and load tides, and (3) frictional drag parameterisation (Egbert et al., 2004; Wells et al., 2010a). Overall, tidal modelling using Fluidity accurately predicts present-day global tidal amplitude without the need for data assimilation and to a degree of accuracy that is sedimentologically useful, most notably predicting the following: (1) tidal amplitude and range to a decimetre-scale accuracy; (2) microtidal (<2 m), mesotidal (2–4 m) and macrotidal (>4 m) regimes, which is

Formatted: Font: Not Bold

within the limit of ancient tidal range estimates e.g. (Wells et al., 2005a); (3) the position of amphidromic systems; (4) predominance of semidiurnal versus diurnal tides; and (5) areas of tidal amplification due to shoaling, funnelling and/or resonance effects.

On a global scale, the maximum bed shear stress and potential sediment grain size transport modeled by Fluidity (Fig. 2B) have been compared to those modeled using FES 2014 (Fig. 9), which were calculated based on the modeled tidal current velocity vectors (Equation 1) (Supplementary Fig. 1). Overall, the patterns of potential sediment mobility are similar for the two models, with elevated bed shear stress (and equivalent grain size) in areas of shallower bathymetry and/or physiographic constriction (Fig. 9A and B). However, the potential sediment grain size mobility in shelf areas modeled using Fluidity tends to be one or two grain size classes above or below that modeled by FES 2014 (Fig. 10A and B). Overprediction most likely reflects insufficient frictional damping of modeled tidal energy due to locally coarser mesh and bathymetry resolution and lack of internal drag in the Fluidity model. Underprediction is especially common in relatively large, shallow areas that are partially restricted from the open ocean due to complex physiography. For example, results from the high latitude seas of North America probably reflect reduced penetration of the ocean tidal wave through the constricted physiography due to coarse mesh and bathymetry resolution. Despite these differences, modeled bed shear stress using Fluidity and FES2014 are closely matched in many areas, notably the Gulf of Saint Lawrence, Mediterranean Sea, North Sea and South China Sea. These results illustrate that Fluidity is capable of reproducing the first order variability in modeled tidal bed shear stress related to physiography in modern domains and is capable of modelling the same in ancient

Formatted: Font: Not Bold

domains, provided that palaeobathymetric and palaeogeographic uncertainties are adequately defined.

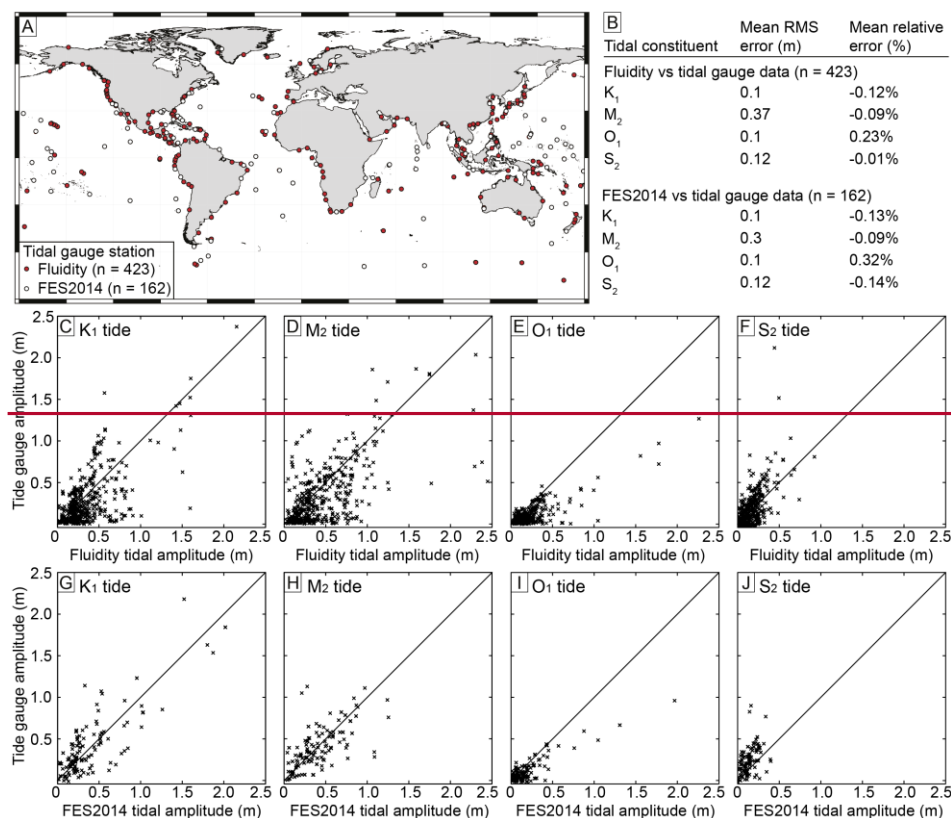


**Fig. 8.** Validation of modeled tidal amplitude using Fluidity and FES2014 (Carrère et al., 2015). (A) Number (n) and position of a global set of tidal stations used for the comparisons to FES2014 (white circles, n = 162) and Fluidity (red circles, n = 423) model data. (B) Summary of root mean squared (RMS) and relative percentage errors between the model and tidal gauge data of tidal constituent amplitude. Tidal gauge amplitude data was derived by tidal harmonic analysis of sea surface elevation data. (C-J) Plots of tidal gauge versus modeled tidal amplitude for the

$K_1$  (C, G),  $M_2$  (D, H),  $O_1$  (E, I) and  $S_2$  (F, J) tidal constituents using Fluidity (C–F) and FES2014 (G–J).

Commented [CDSS13]: Moved to Supplementary Material

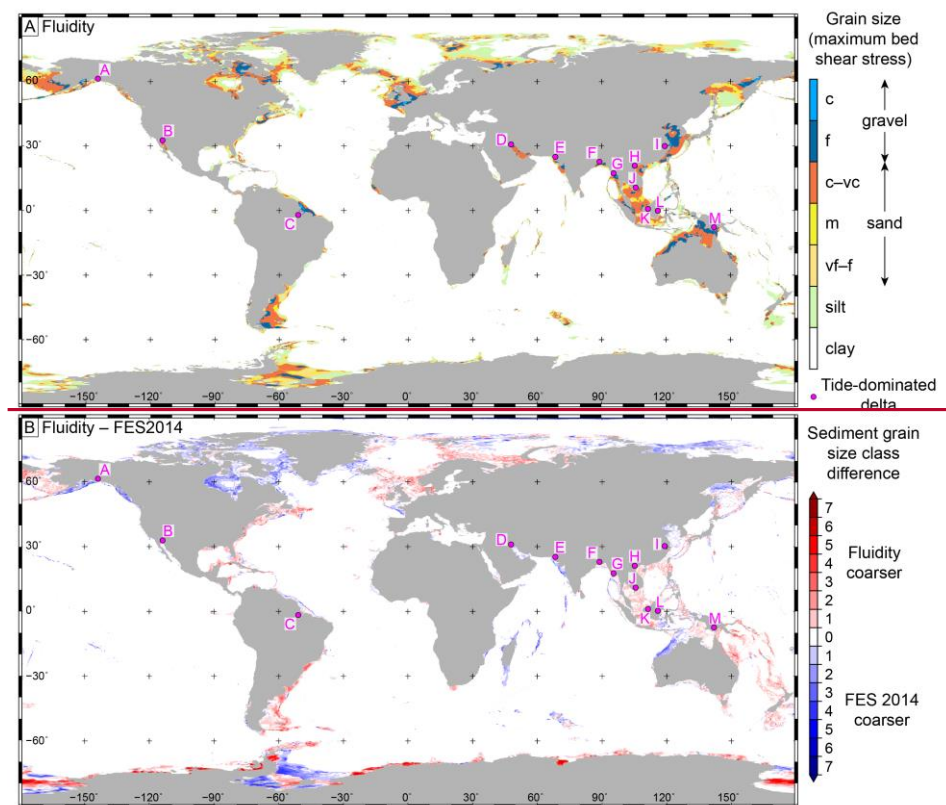


**Fig. 9.** (A) Maximum tidal bed shear stress modeled using Fluidity, plotted as the equivalent grain size that could be entrained if available. (B) Difference in sediment grain size class between maximum tidal bed shear stress for Fluidity (A) and FES2014 (Fig. 2D) (Carrère et al., 2015). Grain size abbreviations: vf = very fine; f = fine; m = medium; e = coarse; ve = very coarse. Pink dots show location of tide-dominated deltas (Goodbred and Saito, 2012): A) Copper; B) Colorado; C) Amazon; D) Shatt al-Arab; E) Indus; F) Ganges-Brahmaputra; G) Irrawaddy; H) Red River; I) Yangtze; J) Mekong; K) Rajang; L) Mahakam; and M) Fly.

Commented [CDSS14]: Moved to Supplementary Material



### 3.2— Comparison of tidal model results with the rock record

For each case study, tidal model results have been compared to available ‘rock record’ data, notably palaeogeographic, stratigraphic, sedimentological and micropaleontological information and interpretations. The majority of referenced datasets invariably include both (1) well-documented sedimentological and/or micropaleontological data, and (2) interpretations of depositional processes and environments that are supported by the available data. Comparison of tidal model results with rock record data from the equivalent stratigraphic interval relies on several steps at different scales but is fundamentally underpinned by detailed facies analysis.

2. Summary of previously published palaeotidal models from deep geologic time (excluding the Quaternary).

#### 2.2.3 Identification of ancient tidal processes

#### 2.2.4 Tidal facies analysis

##### 3.2.1—Observations across the range of facies analysis

Validation of tidal model results using sedimentological data relies on recognising sedimentary characteristics at the bedform scale (c. mm–10s m scale) that are indicative of to facies succession scales interpreted as indicating tidal processes. These have been widely documented from several different shallow-water depositional environments, most notably deltas, estuaries, barrier inlets, embayments, straits and open shelves (e.g. De Raaf and Boersma, 1971; Ginsburg, 1975; De Raaf and Boersma, 1977; Reineck and Singh, 1980; Terwindt, 1981; De Boer et al., 1988; Nio and Yang, 1991; Smith et al., 1991; Shanley et al., 1992; Flemming and Bartholoma, 1995; Willis, 2005; van den Berg et al., 2007; MacEachern and Bann, 2008; Martinius and van den Berg, 2011; Davis, 2012; Shanmugam, 2013)(Johnson and Baldwin, 1996; Reading and Collinson, 1996; Bhattacharya, 2010; Dalrymple, 2010b; Martinius and van den Berg, 2011;

**Commented [CDSS15]:** The number or references has been rationalised in this section

**Commented [CDSS16]:** The number or references has been rationalised in this section

**Formatted:** Heading 3, Line spacing: single

[Davis and Dalrymple, 2012; Longhitano et al., 2012](#)). The most significant features are those related to tidal flow reversals, flood–ebb tide versus slack water dynamics, ~~and~~ tide-related periodicity ~~and/or physico-chemical stress~~, particularly the following: (1) bidirectional cross-bedding and cross-lamination (cm–dm-scale), including the relatively rare variant of ‘herringbone’ patterns (~~e.g. [Van Straaten, 1953; Reineck, 1963; Boersma, 1969; Klein, 1970a; Klein, 1970b; Klein, 1971; Hayes, 1980; Boersma and Terwindt, 1981; Yoshida et al., 2004](#)~~)(~~e.g. [Van Straaten, 1953; Reineck, 1963; Boersma, 1969; Klein, 1970a; Klein, 1970b; Klein, 1971; Hayes, 1980; Boersma and Terwindt, 1981; Yoshida et al., 2004](#)~~); (2) larger-scale (10s m-scale) bidirectionality, such as between separate but closely spaced sand bodies with oppositely-dipping cross-bedding, which have been interpreted to reflect mutually evasive ebb- and flood-tidal channels and bars (~~[Robinson, 1966; Johnson, 1975; Johnson and Levell, 1995; Sixsmith et al., 2008; Legler et al., 2013; Levell et al., 2020](#)~~)(~~Robinson, 1966; Johnson, 1975; Johnson and Levell, 1995; Harris et al., 2004; Sixsmith et al., 2008; Legler et al., 2013; Levell et al., 2020~~); (3) sigmoidal ‘shovel-shaped’ cross-bed sets, with extended mud-rich toesets, sometimes with oppositely-dipping current ripples (~~e.g. [Boersma and Terwindt, 1981; Mutti et al., 1984; Mutti et al., 1985; Kreisa and Moila, 1986; Dalrymple and Rhodes, 1995; van den Berg et al., 2007; Tinterri, 2011](#)~~)(~~e.g. [Boersma and Terwindt, 1981; Mutti et al., 1984; Mutti et al., 1985; Kreisa and Moila, 1986; Dalrymple and Rhodes, 1995; van den Berg et al., 2007; Tinterri, 2011](#)~~); (4) multiple reactivation surfaces with an apparent cyclicity or predictable and repeated pattern (~~e.g. [Boersma, 1969; McCabe and Jones, 1977; Reineck and Singh, 1980; Boersma and Terwindt, 1981; Allen, 1982a; Allen and Homewood, 1984](#)~~)(~~e.g. [Boersma, 1969; McCabe and Jones, 1977; Reineck and Singh, 1980; Boersma and Terwindt, 1981; Allen, 1982a; Allen and Homewood, 1984](#)~~); (5) ‘paired drapes’ or ‘double drapes’ comprising sandy foresets and associated mudstone and/or carbonaceous (typically finely comminuted ‘coffee ground’ type) drapes (mm–cm-scale), which are interpreted to form by semi-diurnal to diurnal tidal inequality (~~e.g. [Reineck and Singh, 1980; Visser, 1980; Smith, 1988; De Boer et al., 1989; Nio and Yang, 1991](#)~~)(~~e.g. [Reineck and Singh, 1980; Visser, 1980; Smith, 1988; De Boer et al., 1989; Nio and Yang, 1991](#)~~); (6) ‘tidal bundles’ in the form of lateral and vertical thickness variations of sandy foresets and associated mudstone/carbonaceous drapes (dm–m-scale) , which have been related to spring–neap semi-lunar cycles (~~e.g. [Visser, 1980; Allen, 1981b; Boersma and Terwindt, 1981](#)~~;

~~Allen and Homewood, 1984; Kreisa and Moila, 1986; Nio and Yang, 1991~~(e.g. Visser, 1980; Allen, 1981b; Boersma and Terwindt, 1981; Allen and Homewood, 1984; Kreisa and Moila, 1986; Nio and Yang, 1991)) ~~(cf. Martinius and Gowland, 2011)~~(cf. Martinius and Gowland, 2011)); (7) heterolithic bedding (cm–m-scale) with apparent, or preferably measured and statistically analysed, cyclicity in the thickness of sandstone–mudstone layers, which are referred to as ‘couplets’ if other evidence of tidal deposition (e.g. bidirectional current ripples etc.) are observed (~~Reineck and Wunderlich, 1968; Terwindt, 1971; Terwindt and Breusers, 1972; Reineck and Singh, 1980; Kvale et al., 1989; Archer et al., 1991; Archer, 1995; Greb and Archer, 1995; Kvale, 2006; Kvale, 2012~~(Reineck and Wunderlich, 1968; Terwindt, 1971; Terwindt and Breusers, 1972; Reineck and Singh, 1980; Kvale et al., 1989; Archer et al., 1991; Archer, 1995; Greb and Archer, 1995; Kvale, 2006; Kvale, 2012)); (8) inclined heterolithic strata (dm–10s m-scale) (~~Thomas et al., 1987; Smith, 1988; Dalrymple et al., 2003; Choi et al., 2004; Dalrymple and Choi, 2007~~)(Thomas et al., 1987; Smith, 1988; Dalrymple et al., 2003; Choi et al., 2004; Dalrymple and Choi, 2007)); (cf. ~~Sisulak and Dashtgard, 2012; Jablonski and Dalrymple, 2016~~)(cf. Sisulak and Dashtgard, 2012; Jablonski and Dalrymple, 2016)); and (9) ichnofabrics which, in general, show reduced but variable and sporadic bioturbation intensities and predominance of facies-crossing ichnofauna (~~MacEachern et al., 2005; McIlroy, 2006; McIlroy, 2007; MacEachern and Bann, 2008; Longhitano et al., 2010; Gingras and MacEachern, 2012; Gingras et al., 2012~~)(MacEachern et al., 2005; McIlroy, 2006; McIlroy, 2007; MacEachern and Bann, 2008; Longhitano et al., 2010; Gingras and MacEachern, 2012; Gingras et al., 2012)). In terms of micropalaeontological information, the most important potential indicator of tidal processes are palynomorph acmes of coastal biomes whose distribution, abundance and productivity within a depositional system is strongly related to tidal processes, most notably those associated with deposition in mangrove, seagrass and salt marsh settings (e.g. Grindrod, 1988; Wolanski et al., 1992; Woodroffe et al., 2016).

Definitive recognition of tide-influenced sedimentation relies on observing combinations of the features described above because, in isolation, some of these features can form by other processes (e.g.

Definitive recognition of tide-influenced sedimentation relies on observing combinations of the features described above because, in isolation, some of these features can form by other processes (e.g., wave, storm and/or fluvial) operating by themselves or, especially, in combination with tides (e.g. Thomas et al., 1987; Hovikoski et al., 2008; Dalrymple, 2010b; Martinius and van den Berg, 2011; Reynaud and Dalrymple, 2012; Dalrymple et al., 2015; Gugliotta et al., 2016a; Gugliotta et al., 2016b; Collins et al., 2020). Mixed-process settings, especially those where fluvial and tidal currents coexist, can exacerbate differences in the strength and sediment transport capacity of ebb- and flood-tidal currents, wave, storm and/or fluvial) operating by themselves or, especially, in combination with tides (Frey and Howard, 1986; Thomas et al., 1987; Shanley et al., 1992; Hovikoski et al., 2008; MacEachern and Bann, 2008; Ichaso and Dalrymple, 2009; Martinius and Gowland, 2011; Tinterri, 2011; Sisulak and Dashtgard, 2012; Vakarelov et al., 2012; Johnson and Dashtgard, 2014; Dalrymple et al., 2015; Gugliotta et al., 2016a; Gugliotta et al., 2016b; Jablonski and Dalrymple, 2016; Kureinka et al., 2018). Mixed-process settings, especially those where fluvial and tidal currents coexist, can exacerbate differences in the strength and sediment transport capacity of ebb- and flood-tidal currents. Strongly skewed palaeocurrent patterns, with one dominant offshore-directed mode, and a weaker oppositely-directed secondary mode, may occur when fluvial, wave and ebb-tidal/or storm processes are combined combine with tides, such as in deltaic and estuarine settings (Legler et al., 2013; van Cappelle et al., 2016; Collins et al., 2020; Levell et al., 2020)(Legler et al., 2013; van Cappelle et al., 2016; Collins et al., 2020; Levell et al., 2020)). For example, in the modern microtidal Po Delta, preserved tidal signals in open-water prodelta facies are correlatable to cyclical variation variations in water-surface steepness and consequent changes in river discharge velocity and sediment transport capacity in distributary channels (Maselli et al.,

~~2020)(Maselli et al., 2020)).~~ In modern open-marine shelf settings, storm-induced currents can  
 also contribute to tidal current sediment transport asymmetry (~~Stride, 1973; Belderson et al.,~~  
~~1982; Stride, 1982)(Stride, 1973; Belderson et al., 1982; Stride, 1982)).~~ Similarly, storm-  
 enhanced tidal transport systems have been inferred to explain unidirectional palaeocurrent  
 patterns in ancient shallow-marine deposits (~~Banks, 1973; Johnson, 1975; Anderton, 1976;~~  
~~Levell, 1980)(Banks, 1973; Johnson, 1975; Anderton, 1976; Levell, 1980))-~~ and, in the modern  
 Fly River delta, sediment transport to and across the delta front may be controlled by wave-  
 induced resuspension together with tides, storm surge and barotropic flow (Harris et al., 2004).  
~~Autogenic tidal processes responsible for. Autogenic tidal processes responsible~~ mutually  
 evasive ebb and flood tidal channels can also create skewed palaeocurrent patterns in the  
 stratigraphic record, particularly where: (1) channel preservation is unequal, (2) ebb and flood  
 tidal channels are so effectively shielded from each other that evidence of the secondary  
 reversing tide is absent, and/or (3) incomplete outcrop or subsurface dataset (~~Sixsmith et al.,~~  
~~2008; Legler et al., 2014)(Sixsmith et al., 2008; Legler et al., 2014)).~~

Confident identification of tidal influence and its relative importance with respect to other  
 processes (e.g. wave, storm and/or fluvial) requires reconstruction of shoreline palaeo-  
 geomorphology at the scale of the depositional system (c. 1–100s km), based on detailed facies  
 analysis in the context of high-resolution stratigraphic and regional palaeogeographic  
 relationships. Such confidence in interpretation requires data of high quality and density, such as  
 provided by extensive outcrop data (~~e.g. Willis and Gabel, 2001; Legler et al., 2013; Legler et~~  
~~al., 2014; Ainsworth et al., 2016; Rossi et al., 2016; van Cappelle et al., 2016; Kurcinka et al.,~~  
~~2018; Van Yperen et al., 2020)(e.g. Willis and Gabel, 2001; Legler et al., 2013; Legler et al.,~~

2014; Ainsworth et al., 2016; Rossi et al., 2016; van Cappelle et al., 2016; Kurcinka et al., 2018; Van Yperen et al., 2020)) or subsurface datasets containing 3D seismic data, densely spaced wells and/or extensive cores (e.g. Hubbard et al., 2011; Willis and Fitris, 2012; Holgate et al., 2013)(e.g. Hubbard et al., 2011; Willis and Fitris, 2012; Holgate et al., 2013)). In practice, such datasets and confident interpretations are rare. It is therefore appropriate to focus comparison of ‘rock-record’ data with tidal model predictions at bedform scale (c. mm–10s m), at which interpretations of bed shear stress as a proxy for tidal current velocity (section 3.2.3) can be readily made. Other tidal model outputs, including tidal range (section 3.2.2) and tidal phase, are typically less straightforward to interpret from available ‘rock-record’ data (e.g. Wells et al., 2005a; (Mitchell et al., 2010))(Wells et al., 2005a; Mitchell et al., 2010).

### 3.2.1.2.5 Palaeotidal range analysis

Analysis of palaeotidal range from the rock record requires observations and interpretation at a range of scales: depositional system morphology (c. 1–100s km), depositional environments (c. 0.1–1 km) and depositional elements and facies (<1 to 10s m) may all preserve an imprint of tidal sedimentary processes, but do not offer more detailed permit accurate constraints on tidal range beyond inferring, often not even the ability to differentiate microtidal, mesotidal and macrotidal regimes (Table 43) (Wells et al., 2005a)(Wells et al., 2005a)). Alternative methods used to estimate palaeotidal range are: (1) interpretations of water depth from stratigraphic position within interpreted fining-upward channel-fill units (Nio et al., 1983)(Nio et al., 1983)) (Yang and Nio, 1985)(Yang and Nio, 1985)); (2) stratigraphic thickness estimates of interpreted intertidal deposits in tidal flat units (Klein, 1970a; Klein, 1971)(Klein, 1970a; Klein, 1971)), although these units are very similar to interpreted channel-fill units within the fluvial-to-marine

**Commented [CDSS17]:** This section includes a comment that ‘Consequently, numerous studies have highlighted that tidal range is, at best, an imperfect indicator of sedimentary response.

**Formatted:** Font: Not Bold, English (United Kingdom)

transition zone (~~e.g. Olson, 1972; Dalrymple and Choi, 2007; Amir Hassan et al., 2013;~~  
~~Gugliotta et al., 2016a; Collins et al., 2018b; Collins et al., 2020)~~(e.g. Olson, 1972; Dalrymple  
and Choi, 2007; Amir Hassan et al., 2013; Gugliotta et al., 2016a; Collins et al., 2018c; Collins et  
al., 2020)); and (3) average calculations of characteristic mudstone drape spacings based on  
groups of sandstone–mudstone couplets from interpreted spring and neap conditions, and various  
assumptions regarding dune height and speed, dry bulk sediment density, and current velocity for  
sediment entrainment (~~Allen, 1981b)(Allen, 1981b)). Depositional systems subject to higher tidal~~  
~~ranges are more likely to be tide dominated, but this relationship is inconsistent, especially for~~  
~~mixed-process systems (e.g. Davis and Hayes, 1984). Furthermore, higher tidal ranges may not~~  
~~always correspond to stronger tidal currents (Mitchell et al., 2011).~~

1  
2  
3  
4  
5  
6  
7  
8  
9  
10  
11  
12  
13  
14  
15  
16  
17  
18  
19  
20  
21  
22  
23  
24  
25  
26  
27  
28  
29  
30  
31  
32  
33  
34  
35  
36  
37  
38  
39  
40  
41  
42  
43  
44  
45  
46  
47  
48  
49  
50  
51  
52  
53  
54  
55  
56  
57  
58  
59  
60  
61  
62  
63  
64  
65

. Depositional systems subject to higher tidal ranges are more likely to be tide-dominated, but this relationship is inconsistent (e.g. Hayes, 1979; Mulhern et al., 2017), especially for mixed-process systems (e.g. Davis and Hayes, 1984). Furthermore, higher tidal ranges may not always correspond to stronger tidal currents (Dalrymple, 2010b), as shown in both modern macrotidal environments (e.g. Yang et al., 2008) and palaeotidal models (Mitchell et al., 2011). Consequently, numerous studies have highlighted that tidal range is, at best, an imperfect indicator of sedimentary response.



Indicator	Size	Description	Tidal range
Delta morphology	10s - 100s km	Tide-dominated deltas display wide, landward-tapering river mouths, elongate shore-normal mouth bars, sinuous tidal creeks, tidal flats, saltmarsh and/or mangroves, and smaller-scale tidal indicators (e.g. Ganges-Brahmaputra, <u>Mahakam</u> , Irrawaddy, Fly deltas).	Mesotidal to macrotidal
		Fluvial-dominated deltas display digitate ('birds-foot') to lobate morphologies and rapid progradation due to higher relative stream power compared to wave/tide reworking (e.g. Mississippi delta).	Microtidal to mesotidal
		Wave-dominated deltas display cusped geometries with intermediate progradation rates due to wave action ('littoral energy fence') (e.g. Baram)	Microtidal to mesotidal
Open shelf tidal sand-sheets (including tidal sand ridges and ribbons)	10s - 100s km	<u>Tabular</u> Sheets are <u>tabular</u> sandbodies with planar tops and bases formed by open-shelf tidal currents. Super-imposed sedimentary structures including bodies include tidal sand ridges, linear bedforms with long axes orientated up to 20° obliquely to tidal currents and distinguished from aeolian dunes by the presence of 2 main current directions at 180°, shelly debris, reactivation surfaces, low angle (3–6°) cross-stratification and marine trace fossils (e.g. Norfolk Ridges, southern North Sea). Smaller superimposed bedforms include sand ribbons, scour hollows, longitudinal furrows, obstacle marks, sand ribbons, sand waves, rippled sand sheets and longitudinal sand patches.	Mesotidal to macrotidal

Furrows and gravel waves	L < 150 km; W < 50 km	Mostly erosional features with small (ca 1 m high, 10 m wavelength) gravel-rich subaqueous dunes, formed due to low sediment supply and strong tidal currents (e.g. Bristol Channel)	Macrotidal
Offshore tidal sand ridges	L ca 50 km; W 1–3 km; T 10–50 m	Linear bedforms with long axes orientated up to 20° obliquely to tidal currents. Distinguished from Aeolian dunes by the presence of 2 main current directions at 180°, shelly debris, mud drapes, reactivation surfaces, low angle (3–6°) cross-stratification and marine trace fossils (e.g. Norfolk Ridges, southern North Sea).	Mesotidal to macrotidal
Estuarine/incised valley-fill tidal sandbodies	W < 30 km; T ca 1 m	Outer estuary characterized by elongate sand ridges and tidal channels with super-imposed, smaller-scale tidal indicators. Middle and inner estuary characterized by heterolithic strata with isolated sandbodies (e.g. Thames estuary, southern North Sea).	Microtidal to macrotidal
Sand ribbons	L < 15 km; W < 200 m; T ca 1 m	Ribbons or strips of sand elongated parallel to tidal currents consisting of sand waves/trains (e.g. western English Channel).	Mesotidal to Macrotidal
Saltmarsh	L 10 km; W < 5 km; T < 10 m	Gently sloping coastal wetland which extends landwards to the high-tide mark. Evaporating pools of saline water form localized 'salt-pans' and fauna and flora adapted to highly fluctuating salinities dominate.	Mesotidal to macrotidal

Formatted: Font: Calibri, 11 pt

Formatted: Line spacing: single

Commented [CDSS18]: Included the subsection on 'Open shelf tidal sand-sheets'

Formatted: Font: 11 pt

Formatted: Font: 11 pt

Formatted: Font: 11 pt

Formatted: Font: Calibri, 11 pt

Formatted: Line spacing: single

Formatted: Font: Calibri

Formatted: Font: (Default) Calibri, 11 pt

Commented [CDSS19]: Included the subsection on 'Open shelf tidal sand-sheets'

Formatted: Font: 11 pt

Formatted: Font: 11 pt

Formatted: Font: Calibri, 11 pt

Formatted: Line spacing: single

Mangroves	L <200 km; W <60 km; T <10 m	Densely vegetated forests occupying the lower intertidal zone (ca mean sea level to low-tide mark) of tide-dominated, typically mud-rich deltaic shorelines. Flora sub-zonations related to topography and often diverse fauna adapted to salinity variations (e.g. Mekong, Ganges-Brahmaputra deltas).	Mesotidal to macrotidal
Tidal creeks	W < 100 m; T 10 m	Shore-normal creeks which do not pass into a fluvial system landwards, often mud-rich.	Microtidal to macrotidal

**Table 43.** Larger-scale tidal indicators, ranging from depositional environments to systems, and their generalized implication for tidal-range prediction in the geological rock record (~~modified after Wells et al., 2005a~~)(modified after Wells et al., 2005a)).

### 3.2.1.22.2.6 Ancient bed shear stress analysis

~~Analysis of ancient bed shear stress is possible based on preserved grain size distribution and sedimentary structures (Fig. 10). Bed shear is a better indicator than tidal range of sedimentary response as it is a key variable for understanding the initiation and maintenance of grain motion, formation of bedforms (Fig. 5), and both competence-driven and capacity-drive deposition (Harms et al., 1982; Komar, 1987; Hiscott, 1994; Dalrymple, 2010a).10).~~ Tidal currents that exceed the critical bed shear stress threshold for sediment entrainment will impact sedimentary processes ~~(Mitchell et al., 2011; Collins et al., 2018a)-and preserved sedimentary structures and grain size provide some information on ancient bed shear stress (Fig. 5).~~ However, the type of sedimentary structures formed by currents of varying flow velocity is also strongly dependent on the available grain size and water depth during deposition (Fig. ~~105~~), which can only be estimated in the context of facies successions, permitted by the availability of appropriate rock record data. Less reliable predictions of available grain size range may be possible based on catchment area geology, interpreted palaeo-~~drainage systems~~drainages and other indirect data sources (e.g. seismic geometries of clinoforms, seismic amplitudes, well logs and other borehole data). For a given water depth, if tidal bed shear stress was insufficient to rework the minimum grain size available, tides will not have influenced sediment transport. In contrast, the size, type and texture of sedimentary structures may vary depending on tidal current strength and the frequency with which the critical bed shear stress for entrainment of the available grain size range was exceeded.

~~Comparison of tidal model results to micropaleontological information strongly depends on the availability of suitable data. The most important potential indicator of tidal processes are~~

**Formatted:** Width: 8.5", Height: 11", Header distance from edge: 0.5", Footer distance from edge: 0.5", Numbering: Continuous

palynomorph assemblages of coastal biomes whose distribution, abundance and productivity within a depositional system is strongly related to tidal processes, most notably those associated with deposition in mangrove, seagrass and salt marsh settings (e.g. Grindrod, 1988; Wolanski et al., 1992; Woodroffe et al., 2016).

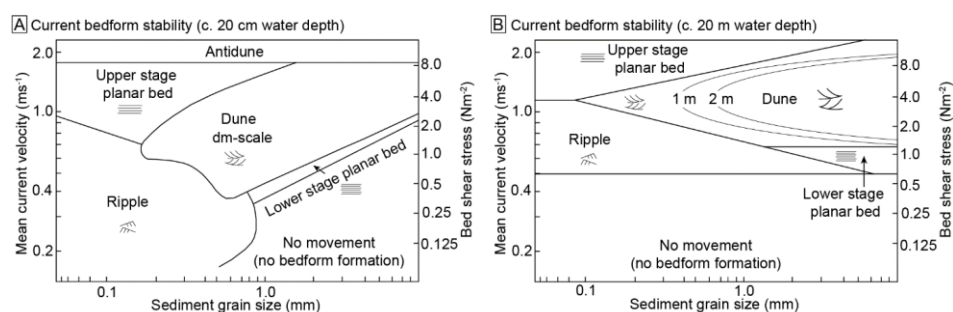


**Fig. 105.** (A) Bedform stability diagram, including bed shear stress, for unidirectional flow at approximately 20 cm water depth (flume tank) (Harms et al., 1982; Mitchell et al., 2010)(Harms et al., 1982; Mitchell et al., 2010)). (B) Bedform stability diagram, including bed shear stress, for unidirectional flow at approximately 2 m water depth (Rubin and McCulloch, 1980).

Field Code Changed

### 3 PALAEOOTIDAL MODELLING CASE STUDIES

Several published palaeotidal modelling case studies each provide unique insights into the controls on tidal processes across a range of time periods and geological settings. Herein, we review three case studies that illustrate the range of physiographic controls on tides relevant for improving predictions of shoreline–shelf progress regime. Together these three case studies document changes in tidal processes: (1) across a wide range of spatial scales, from regional scale in open oceans (1000s km) through seaways and enclosed basins (100s – 1000s km), to local scale on continental shelves (10 – 100s km) and in shoreline features (1–10s km); (2) in different basin and tectonic settings; (3) across different time encompassing various changes in basin-to-shoreline physiography; and (4) at various times in Earth history. Below, each case study is summarized in turn, with a brief review of the geological setting followed by a synthesis and discussion of the palaeotidal model results in terms of the influence on tides by larger-scale basin physiography (100–1000 km), shelf width (c. 10–100 km) and shoreline geometry (c. 1–10 km).

### 4 Regional-scale controls on tidal deposition: RESULTS

#### 4.1 Oligocene–Miocene South China Sea, (SCS), Southeast Asia

##### 4.1.1 Overview

*The Oligocene–Miocene SCS provides a compelling case study for investigating the impact of regional-scale (100–1000s km) physiographic changes on shoreline tidal processes and stratigraphic preservation for several reasons. Firstly, the region underwent significant, geologically rapid, tectonically-driven (plate-related)*

**Commented [CDSS20]:** The results sections has been shortened significantly. Instead of an overview and length reviews of geological setting and model setup/outputs, these three sub-section have been combined into one 'background' section, and shortened dramatically, with the focus being on key aspects of the geological setting relevant to a discussion of tidal model results and controls on associated sedimentation, and the intent of the tidal model studies.

Additionally, the 'Model results' and 'Comparison to the rock record' sections for each case studies are combined and only the key results relating to different spatial scales of tidal controls are including. The evidence (or lack of) for tidal sedimentation in the time-equivalent, preserved rock record is interwove.

**Commented [CDSS21]:** The results sections has been shortened significantly. Instead of an overview and length reviews of geological setting and model setup/outputs, these three sub-section have been combined into one 'background' section, and shortened dramatically, with the focus being on key aspects of the geological setting relevant to a discussion of tidal model results and controls on associated sedimentation, and the intent of the tidal model studies.

Additionally, the 'Model results' and 'Comparison to the rock record' sections for each case studies are combined and only the key results relating to different spatial scales of tidal controls are including. The evidence (or lack of) for tidal sedimentation in the time-equivalent, preserved rock record is interwove.

**Formatted:** Line spacing: Double

*palaeogeographic changes during a c. 25 Myr time period in the Oligo–Miocene,  
which would have impacted large-scale oceanic flow patterns* Background

During the Oligo–Miocene, the SCS and wider Southeast Asia region experienced geologically  
rapid and extensive tectonic reorganization, impacting large-scale oceanic flow patterns, in  
response to major movements of the Indo-Australian, Eurasian, Pacific and Philippine Sea plates  
(Fig. 6) (e.g. Kuhnt et al., 2004; Hall, 2009; Hall, 2011)(Lee and Lawver, 1995; Hall, 1996; Hall,  
2002)). Second, several circum-SCS Oligocene–Miocene basins with high tectonic subsidence  
and sediment supply rates preserve stratigraphic archives of sedimentary environment and  
process changes (e.g. Doust and Sumner, 2007). During this period, there was considerable  
variability in the physiographic configuration of the SCS, which resulted in the formation of  
several shoreline embayments that were influenced by local-scale (10–100s km) tidal processes  
(Collins et al., 2017a; Collins et al., 2018a).

#### **4.1.2—Geological Setting**

During the Oligo–Miocene, the SCS and wider Southeast Asia region experienced extensive  
tectonic reorganization of several microplates and sub-plates in response to major movements of  
the Indo-Australian, Eurasian, Pacific and Philippine Sea plates (Fig. 11). In summary,  
Oligocene–Early Miocene tectonism within the SCS was dominated by active seafloor spreading  
and broadly occur between c. 32–31 Ma and 20.5 Ma or 15 Ma (Briais et al., 1993; Barckhausen  
et al., 2014) (Barckhausen and Roeser, 2004). Post-collision uplift formed a foredeep along the  
NW Borneo margin by the Late Miocene (Lee and Lawver, 1995; Hall, 1996; Hall,  
2002)(Hinz et al., 1989; Hall, 2002; Ingram et al., 2004; Franke et al., 2008; Hutchison, 2010)).  
Extensional rifting preceding oceanic spreading in the SCS occurred from the latest Cretaceous  
(e.g. Hinz and Schlüter, 1985; Ru and Pigott, 1986). Active spreading of the SCS initiated in the  
Early Oligocene at c. 32 Ma (Briais et al., 1993; Barckhausen et al., 2014) or 31 Ma  
(Barckhausen and Roeser, 2004) due to the combination of (1) slab-pull effect due to subduction

of the proto-SCS beneath north-west Borneo, which caused rifting along southern China (Fig. 3), whilst the Sunda Shelf remained emergent throughout the Oligo-Miocene, in contrast to its present-day drowned state (Fig. 6) (van Hattum et al., 2006; Hall, 2013; Shoup et al., 2013) (e.g. Gordon et al., 2012; Hu et al., 2015). At the eastern SCS margin, clockwise rotation and northward movement of the Philippine Sea Plate and the Izu-Bonin-Mariana (IBM) arc formed the present-day Philippines by the Middle-Late Miocene and narrowed oceanic connections into the SCS from the Pacific Ocean north of the IBM arc, which is modelled as emergent in some palaeogeographies due to physiographic uncertainty (Fig. 6) (Collins et al., 2017a; Collins et al., 2018a; Collins et al., 2018b). At the western SCS margin, variable extension, compression, eustatic sea level and sediment supply impacted formation, development and infill of several shelf basins (Holloway, 1982; Taylor and Hayes, 1983; Huchon et al., 1994; Hall, 1996) (Doust and Sumner, 2007; Miller et al., 2011; Shoup et al., 2013; Morley, 2016; Collins et al., 2018a; Collins et al., 2018b), and (2) extrusion of Indochina along the sinistral Ailao Shan Red River Fault Zone, and other faults, during collision of the India-Australia plate with Eurasia. Numerical palaeotidal modelling was undertaken to understand the spatial and temporal impact that regional-scale, tectonic-driven physiographic changes had on shoreline-shelf tides and the corresponding stratigraphic record during the Late Oligocene-Miocene interval. Palaeotidal modelling with Fluidity used full astronomical tidal forcing and global multi-scale meshes with a maximum *ca* 10 km resolution (e.g. Tapponnier et al., 1982; Tapponnier et al., 1986; Peltzer and Tapponnier, 1988; Replumaz and Tapponnier, 2003) (Collins et al., 2017a; Collins et al., 2018a; Collins et al., 2018b). Spreading ceased at around 20.5 Ma (Barekhausen and Roeser, 2004) or 15 Ma (Briais et al., 1993); tectonic flow lines of the c. 32–15 Ma spreading model (Briais et al., 1993) are consistent with the trend of ocean floor fracture zones, unlike the c. 31–20.5 Ma model (Barekhausen and Roeser, 2004), but the c. 32–20.5 Ma spreading model (Barekhausen et al., 2014) has not yet been tested (Mazur et al., 2012). Cessation of spreading was approximately simultaneous with final closure of the proto-SCS and subsequent collision between Borneo and



extended continental crust from the rifted South China margin (Taylor and Hayes, 1983; Hall, 2002; Hutchison, 2010), as evidenced by the 17–15 Ma Deep Regional Unconformity (in Sabah) and its broadly equivalent Base-Middle Miocene Unconformity (in Sarawak) throughout the Neogene basins of NW Borneo (Levell, 1987; Hazebroek and Tan, 1993; Hutchison, 1996; Hutchison et al., 2000). Post-collision uplift resulted in formation of a foredeep trough along NW Borneo by the Late Miocene (Fig. 11) (Hinz et al., 1989; Hall, 2002; Ingram et al., 2004; Franke et al., 2008; Hutchison, 2010).

During the Oligocene–Miocene, clockwise rotation and northward translation of the Philippine Sea Plate, and the Izu–Bonin–Mariana (IBM) arc along its eastern margin, was associated with (1) complex assembly of the present-day Philippine islands by the Middle–Late Miocene, (2) narrowing of the oceanic connections into the SCS (Luzon Strait) and to the Pacific Ocean (north of the IBM arc), and (3) back-arc rifting in the IBM arc (Taylor, 1992; Hall et al., 1995; Hall, 2002; Gaina and Müller, 2007), which is modelled as emergent in some palaeogeographic interpretations due to physiographic uncertainty (Fig. 11) (Collins et al., 2017a; Collins et al., 2018a). Emergence of the Sunda Shelf created a ‘blind gulf’ type basin morphology throughout the Oligocene–Miocene (Fig. 11) (van Hattum et al., 2006; Hall, 2013; Shoup et al., 2013). In contrast, the Sunda Shelf is presently submerged, which facilitates ocean outflow from the SCS, with connections via the Malacca Straits, among others, into the Indian Ocean (e.g. Gordon et al., 2012; Hu et al., 2015). The western SCS margin experienced spatially and temporally variable extension and compression, combined with frequent variations in eustatic sea level and sediment supply. This resulted in the rapid subsidence and infill of several shelf basins, including

the Gulf of Thailand and, further south, the Malay, Penyu and West Natuna basins (Doust and Sumner, 2007; Miller et al., 2011; Shoup et al., 2013; Morley, 2016; Collins et al., 2018a).

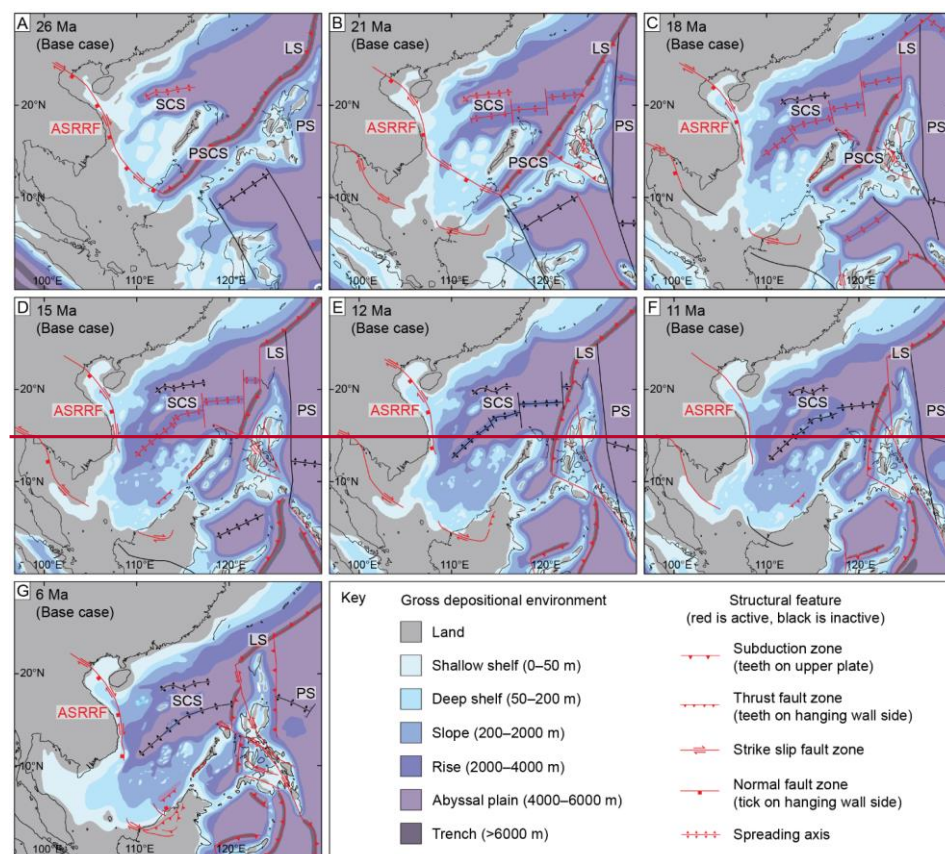


**Fig. 11.** Gross depositional environmental reconstructions for the Late Oligocene–Late Miocene in Southeast Asia based on sea-level highstand for eight time-slices: (A) 26 Ma (Chattian); (B) 21 Ma (Aquitainian); (C) 18 Ma (Burdigalian); (D) 15 Ma (Langhian); (E) 12 Ma (Serravallian); (F) 11 Ma (Tortonian); (G) 6 Ma (Messinian). Alternative gross depositional environmental reconstructions include a submerged Palawan: (H) 26 Ma (Chattian); (I) 21 Ma (Aquitainian); (J)

Formatted: No Spacing, Line spacing: single

Formatted: Font: Bold

18 Ma (Burdigalian). Model outputs included herein (Collins et al., 2018a) are maximum spring tidal range and maximum tidal bed shear stress, plotted as the equivalent grain size capable of being transported if present (see Section 2.2.3.3). 'Base case' models used the preferred palaeogeographic interpretations at sea level highstand for three time intervals in the Early, Middle and Late Miocene (Fig. 7). Sensitivity tests included tidal models for 50 m sea level lowstand palaeogeographies for Late Oligocene–Late Miocene time intervals, and a Late Miocene (6 Ma) tidal model for a palaeogeography with a submerged (10 m) IBM arc. After Collins et al. (2018a).

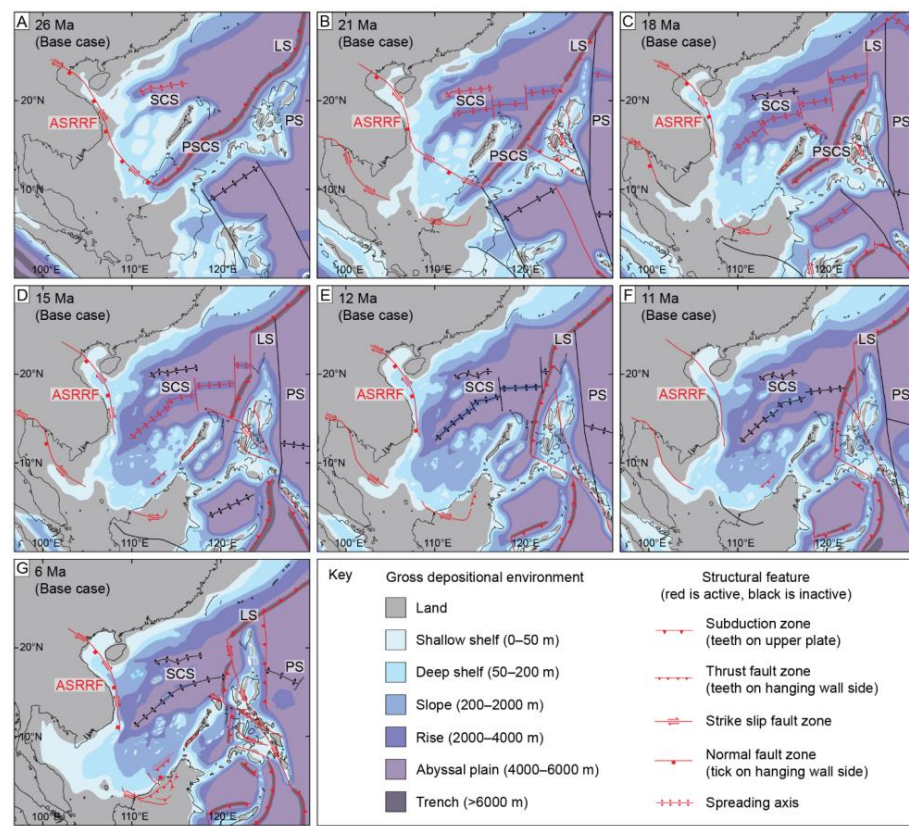


**Fig. 6.** Gross depositional environmental reconstructions for the Late Oligocene–Late Miocene in Southeast Asia based on sea level highstand for eight time slices: (A) 26 Ma (Chattian); (B)

21 Ma (Aquitanian); (C) 18 Ma (Burdigalian); (D) 15 Ma (Langhian); (E) 12 Ma (Serravallian);  
(F) 11 Ma (Tortonian); (G) 6 Ma (Messinian). Alternative gross depositional environmental  
reconstructions include a submerged Palawan; (H) 26 Ma (Chattian); (I) 21 Ma (Aquitanian); (J)  
18 Ma (Burdigalian). After Collins et al. (2018a).

#### 4.1.34.1.2 Model Setup results and Outputs rock-record integration

In the Oligocene–Miocene SCS, regional (100–1000s km) and tectonic-driven palaeogeographic  
changes caused a significant decrease in the overall extent and magnitude of tidal processes.  
Most notably during the Miocene, reduced oceanic inflow and boundary tide related to  
narrowing of the Pacific Ocean connection via the Luzon Strait (from c. 1500 km to 350 km) and  
north of the IBM arc (from c. 1600 km to 370 km) coincided with no ocean outflow from the SW  
SCS due to the emergent Sunda Shelf. Consequently, tides in the central SCS decreased from  
macrotidal (>4 m), and capable of coarse sand to gravel transport in the Early Miocene, to  
mesotidal (>2 to 4 m), and capable of fine sand to silt transport in the Middle–Late Miocene  
(Fig. 7). The importance of regional-scale ocean inflow on tides is further indicated by sensitivity  
analyses. Shutdown of oceanic throughflow into the Sea of Japan during lowstands increased tidal  
inflow and boundary tides to the SCS, resulting in larger and stronger tides than during equivalent  
highstands (Fig. 8A–B). Likewise, submerging the IBM arc (to only 10 m water depth) in the Late  
Miocene causes substantially larger and stronger tides across the SCS (Fig. 8C–D). Overall, tides  
were diurnal to mixed diurnal dominated (F-ratio >1.5), reflecting amplification and dominance of  
diurnal tides in the Pacific Ocean, similar to the present day.

On a local-scale, tidal range and bed shear stress maxima in the Oligo–Miocene SCS invariably  
occurred within embayed shoreline areas, particularly those with (1) relatively wide and deep  
entrances open to the incoming tide, and (2) high resonance and theoretical funnelling potential  
(Collins et al., 2018a). For example, widening and deepening the entrance to the Gulf of  
Thailand (western SCS) permitted greater tidal inflow and a larger tidal prism, potentially  
enhanced by resonance effects, resulting in an increase from microtidal to low mesotidal  
conditions during the Miocene (Collins et al., 2018a).

Formatted: Line spacing: Double

Model results are supported by sedimentological and micropalaeontological data (Fig. 9) and are consistent with previous Miocene palaeoenvironmental stratigraphic interpretations (e.g. Doust and Sumner, 2007), including the distribution of interpreted mangrove-related facies in the western SCS (Morley et al., 2011; Shoup et al., 2013). Preserved Oligocene–Middle Miocene strata in several basins within areas of high modelled tidal range and bed shear stress include interpretable evidence for tidal processes on different scales (e.g. facies to facies successions), and mangrove palynomorph data, notably acmes in mangrove pollen (Fig. 8) (Morley et al., 2011; Shoup et al., 2013). Tidal processes are commonly interpreted to have operated together with river processes, and to a lesser extent wave processes. Mixed fluvial and tidal preservations is often expressed within heterolithic facies and facies associations, where variations in sandstone-bed thickness, the ratio of sandstone-to-mudstone, and bioturbation on a cm-to-metre scale can be attributed to variations in river discharge and tides (Amir Hassan et al., 2013; Amir Hassan et al., 2016; Collins et al., 2018c; Collins et al., 2020). Tidal processes are also interpreted for sandstone-dominated facies associations and successions predominantly characterised by trough-cross stratification, often but not exclusively with long rippled toesets and/or bi-modal palaeocurrent directions. Significantly, this occurs in association with paralic coals and mudstones deposited within or in close relation to mangroves, including *in situ* occurrences (Morley et al., 2011; Amir Hassan et al., 2013; Togunwa et al., 2015; Amir Hassan et al., 2016; Murtaza et al., 2018). Tidal signals are less widespread in Middle–Late Miocene strata (Fig. 9), preferentially occurring in embayed shoreline settings coincident with relative highs in modelled tidal range and bed shear stress, such as in the Gulf of Thailand (Morley et al., 2011; Ridd et al., 2011; Shoup et al., 2013) and in areas of NW Borneo (Hadley et al., 2006; Collins et al., 2018c). Preserved sections in open-coastline systems are mostly interpreted to have been dominated by wave processes, even in areas of modelled high tidal bed shear stress such as along SE Vietnam (Morley et al., 2011; Chung et al., 2015), suggesting wave processes may have overprinted evidence of tides.



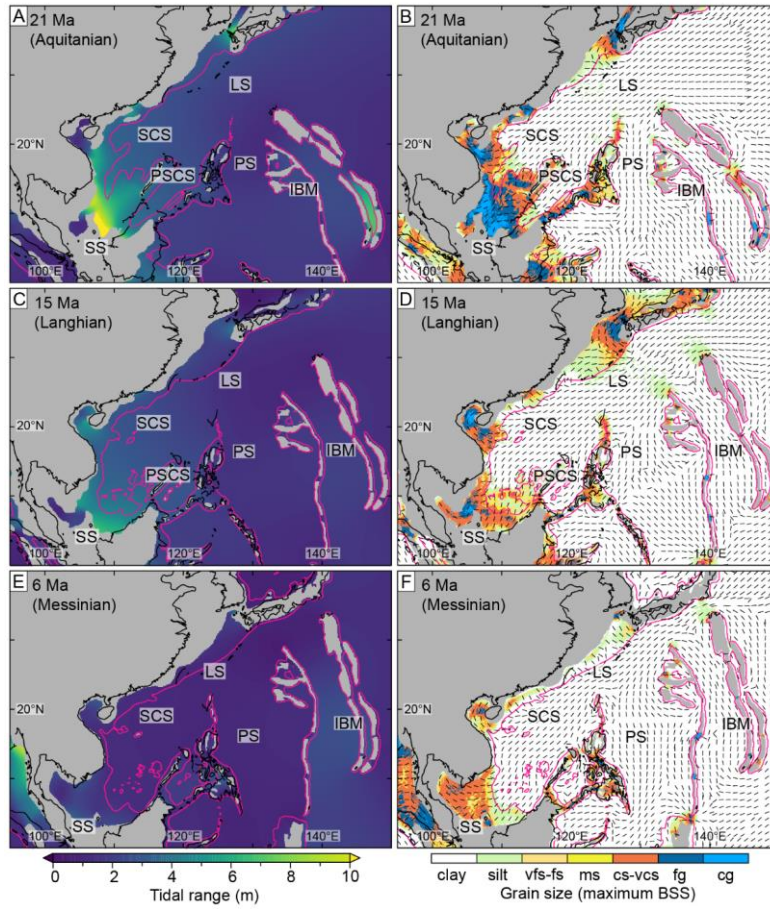


**Fig.** Global simulations using Fluidity represent full astronomical tidal forcing with a spin-up period of period of 120 hours and no open boundary tidal forcing or data assimilation. Global computational meshes produced using qmsh (Avdis et al., 2018) were three-dimensional and multi-scale, with the highest mesh resolution of *ca* 10 km in areas of complex bathymetry. Model outputs included herein are maximum spring tidal range and the magnitude and direction

**Formatted:** Font: Bold

of maximum tidal bed shear stress, plotted as the equivalent grain size capable of being transported (see Section 3.1.3). ‘Base case’ model simulations use the preferred palaeogeographic interpretations at sea level highstand for three timeslices in the Early, Middle and Late Miocene (Fig. 12). Sensitivity tests of the base case models include (1) tidal models for 50 m sea level lowstand palaeogeographic interpretations for Late Oligocene–Late Miocene timeslices, and (2) a Late Miocene (6 Ma; Messinian) tidal model for a palaeogeographic reconstruction with a submerged (10 m) IBM arc. A wider range of model outputs, timeslices and sensitivity analyses have also been evaluated (Collins et al., 2017a; Collins et al., 2018a).

#### **4.1.4 Model Results**

On a regional scale, the base case palaeotidal model suggests an overall decrease in prevailing maximum tidal range and bed shear stress through the Miocene in the SCS (Fig. 12). Tidal range in the central part of the SCS decreased from macrotidal (>4 m) in the Early Miocene (Fig. 12A) to mesotidal (>2 to 4 m) in the Middle–Late Miocene (Figs 12C, E). This was contemporaneous with a decrease in the incoming boundary tide from the Pacific Ocean, from high microtidal–mesotidal in the Early Miocene to microtidal in the Middle–Late Miocene. Along shorelines in the central SCS, maximum strength tidal currents in base case simulations could generally transport up to coarse sand to gravel in the Early Miocene (Fig. 12B), fine to coarse sand in the Middle Miocene (Fig. 12D), and fine sand to silt in the Late Miocene (Fig. 12F). These regional-scale changes in modelled tidal processes were coincident with (1) narrowing of the Luzon Strait from c. 1500 km to 350 km and the Pacific Ocean connection between the IBM arc and Eurasia from c. 1600 km to 370 km through the Miocene (Fig. 11), and (2) obstruction of a major outflow from the SCS at its southwestern end due to the emergent Sunda Shelf.

Sensitivity analyses also emphasize the potential impact of regional-scale physiographic changes on shoreline tides. Tidal models for sea-level lowstand during the Miocene suggest that shutdown of throughflow into the Sea of Japan increased tidal inflow into the SCS. This causes an increase in modelled maximum tidal range and bed shear stress along SCS shorelines (Fig. 13A–B) compared to equivalent highstand models (Fig. 12E–F). A Late Miocene tidal model with a submerged IBM are (to only 10 m water depth) causes a substantial increase in maximum tidal range and bed shear stress in all areas of the SCS (Fig. 13C–D) compared to the base-case model (Fig. 12E–F).

On a local scale, temporal variation in the magnitude of modelled tidal processes generally reflects the fundamental control of regional-scale tectonophysiographic changes. However, whereas on a regional scale tidal range decreased through the Miocene, tidal range in the Gulf of Thailand (western SCS) generally increased from microtidal to low-mesotidal (cf. Figs. 12C, E); widening and deepening of the submerged region permitted greater tidal inflow and larger tidal prism, potentially enhanced by resonance effects (Collins et al., 2018a). Furthermore, the disconnection between calculated and modelled funnelling potential in the Miocene Gulf of Thailand illustrates the strong modifying effect of embayment physiography relative to incoming tidal potential: the narrow and shallow entrance in the Early–Middle Miocene initially prevented tidal inflow into the restricted embayment despite the higher-magnitude regional tides. Nonetheless, tidal range and bed shear stress maxima in the Oligo–Miocene SCS invariably occurred within embayed shoreline areas, particularly those with (1) relatively wide and deep



entrances open to the incoming tide, and (2) high resonance and theoretical funnelling potential  
(Collins et al., 2018a).

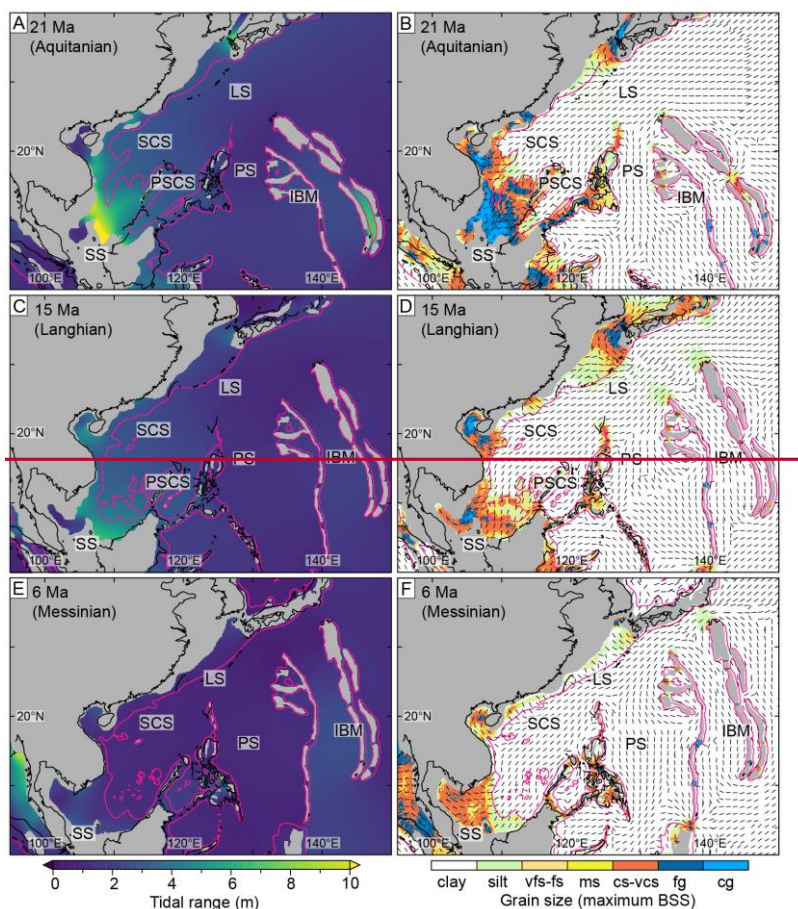
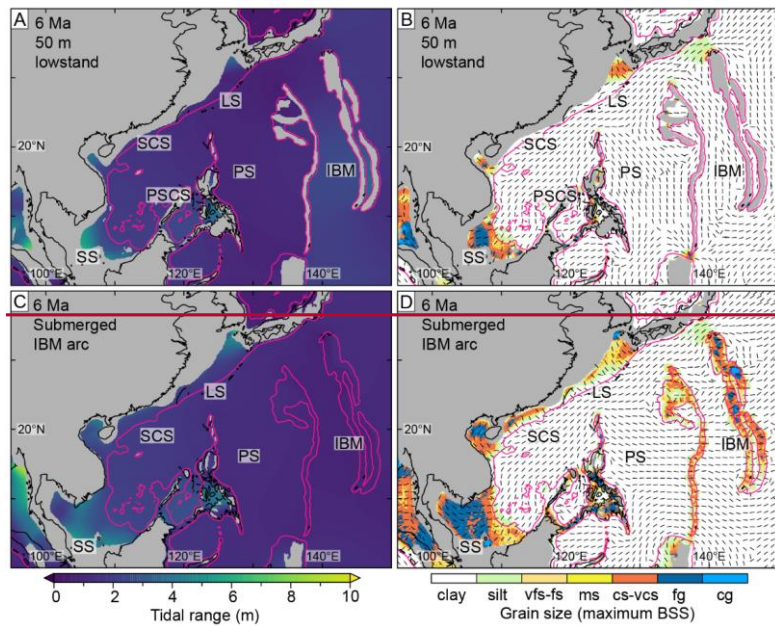


**Fig. 127.** Palaeotidal model results in the Oligo-Miocene South China Sea for tidal range (A, C, E) and maximum tidal bed shear stress plotted as the maximum sediment calibre entrained (B, D, F), for three ‘base case’ palaeogeographic reconstructions: (A, B) Early Miocene at 21 Ma; (C, D) Middle Miocene at 15 Ma; and (E, F) Late Miocene at 6 Ma (see Fig. 116). The

thicker black line (A–F) is the reconstructed present-day coastline. The thinner black lines in the bed shear stress plots indicate the orientation of maximum tidal bed shear stress. The pink lines (A–F) indicate the interpreted 200 m palaeobathymetric contour and approximate palaeo-shelf edge. See Collins et al. (2018a) for all model results and sensitivity analyses. Map abbreviations: IBM – Izu-Bonin-Mariana Arc; LS – Luzon strait; PS – Philippine Sea; SCS – South China Sea; SS – Sunda Shelf. Grain size abbreviations: vfs = very fine sand; fs = fine sand; ms = medium sand; cs = coarse sand; vcs = very coarse sand; fg = fine gravel; cg = coarse gravel.



Formatted: English (United Kingdom)

Formatted: No Spacing, Centered, Line spacing: single

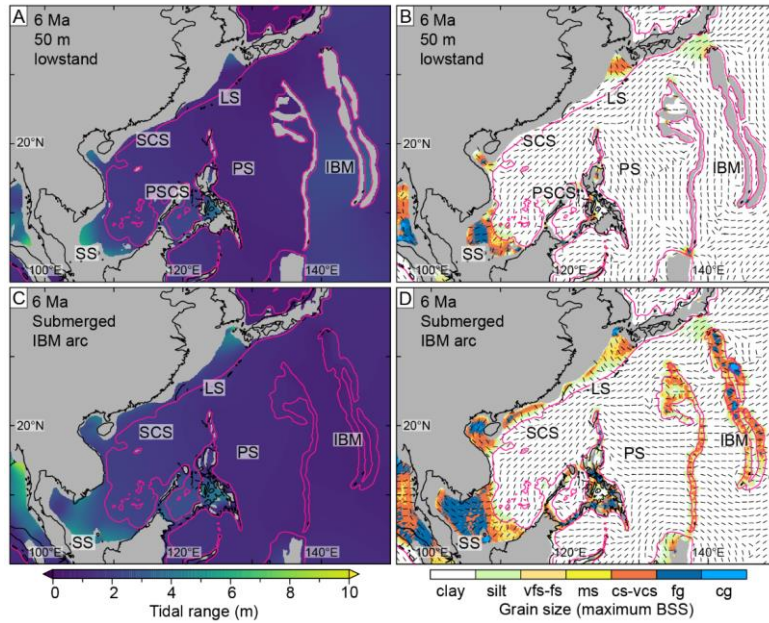
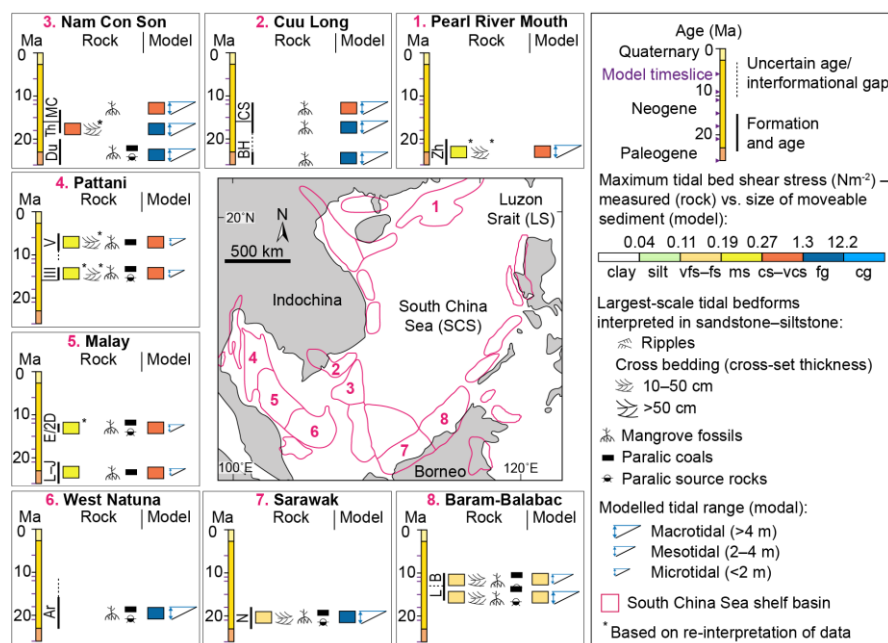


**Fig. 138.** Sensitivity analyses of the base-case for the Late Miocene (6 Ma) base case palaeogeographic reconstruction (cf. Fig. 127E, F) showing modeled tidal range (A, C) and maximum tidal bed shear stress, plotted as the maximum sediment caliber entrained (B, D), for a 50 m sea-level lowstand reconstruction (A, B) and submerged Izu-Bonin-Mariana (IBM) arc (C, D). Refer to Fig. 127 for abbreviations.



**4.1.5—Fig. 9. Evidence of tide-influenced deposition based on sedimentological and micropalaeontological data, mainly from petroleum exploration wells, and comparison to base case tidal model results (Fig. 7) in South China Sea shelf basins. Rock-record data include grain size, cross lamination (ripples) and/or cross bedding interpreted to preserve evidence of tidal process (e.g. bidirectional palaeocurrents, scoop-shaped foresets, mudstone drapes), mangrove pollen acmes and the occurrence of paralic, mangrove-bearing coals and source rocks. Studied formations and key references for each basin are: (1) Upper Zhuhai (Zh) Formation, Pearl River Mouth Basin**  
**Comparison with the rock record**

Maximum tidal range and bed shear stress model results have been compared with Miocene sedimentological and micropaleontological data for several circum SCS basins (Collins et al., 2017a; Collins et al., 2018a).

Model results are broadly corroborated by sedimentological and micropaleontological data (Fig. 14) and are consistent with previous Miocene paleoenvironmental stratigraphic interpretations (e.g. Doust and Sumner, 2007), including the distribution of interpreted mangrove-related facies in the western SCS (Morley et al., 2011; Shoup et al., 2013). Modelled highs in regional-scale tidal range and bed shear stress compare favourably with Late Oligocene to Middle Miocene sedimentological and mangrove palynomorph data in several basins (Fig. 14), including the following open shoreline systems: (1) mangrove palynomorph-acmes in the approximately Late Oligocene, late Early Miocene and Middle Miocene Bach Ho and Con Son Formations in the Cuu Long Basin (basin 2—Fig. 14) (Morley et al., 2011; Chung et al., 2015); (2) the Late Oligocene–Early Miocene Dua Formation in the Nam Con Son Basin, southern Vietnam (basin 3—Fig. 14), which contains paralic coals and mudstones with abundant mangrove pollen (Zheng and Deng, 2012); (2) Bach Ho (BH) and Con Son (CS) formations, Cuu Long Basin (Morley et al., 2011); (3) Dua (Du), Thong (Th) and Mang Cau (MC) formations, Nam Con Son Basin (Tin and Ty, 1995; Morley et al., 2011); (4) Sequences II–IV, Pattani Basin (Jardine, 1997; Lockhart et al., 1997); (5) Groups L–J and E, Malay Basin (Morley et al., 2011)(Morley et al., 2011)14), which contains paralic coals and mudstones with abundant mangrove pollen (Morley et al., 2011) and tide-influenced fine- to medium-grained sandstones (Tin and Ty, 1995); (3) very fine- to fine-grained tidal cross-bedded sandstones and heterolithic facies, and interstratified carbonaceous mudstone and coals, with abundant mangrove material and pollen, in the Early



Miocene Nyalau Formation, Sarawak Basin; (6) Arang (Ar) Formation, West Natuna Basin  
 (Morley et al., 2011); (7) Nyalau (Ny) Formation, Balingian Province, Sarawak Basin (Wan  
 Hasiah, 2003; Amir Hassan et al., 2013; Togunwa et al., 2015; Amir Hassan et al., 2016;  
 Murtaza et al., 2018)(Amir Hassan et al., 2013; Amir Hassan et al., 2016); and (4) mixed fluvial-  
 and tide-influenced, very fine to fine-grained cross-bedded sandstones and heterolithic facies,  
 and mangrove-bearing carbonaceous mudstones in mixed-process deltaic units in the early  
 Middle Miocene Lambir Formation, Baram-Balabac Basin (basin 8—Fig.(Wan Hasiah, 2003;  
 Amir Hassan et al., 2013; Togunwa et al., 2015; Amir Hassan et al., 2016; Murtaza et al., 2018);  
 and (4) mixed fluvial- and tide-influenced, very fine- to fine-grained cross-bedded sandstones  
 and heterolithic facies, and mangrove-bearing carbonaceous mudstones in mixed-process deltaic  
 units in the early Middle Miocene Lambir Formation, Baram-Balabac Basin (basin 8—Fig. 44)  
 (Collins et al., 2020). Evidence of tidal influence is also preserved from the Late Oligocene–  
 Early Miocene embayed Gulf of Thailand, most notably: (1) medium-grained tidal sandstones  
 and abundant mangrove pollen in carbonaceous mudstones and coals in the Early Miocene  
 Pattani Basin (basin 4 Fig. 14) (Jardine, 1997; Lockhart et al., 1997; Charusiri and Pum-Im,  
 2009; Ridd et al., 2011); and (2) paralic mudstones and coals with abundant mangrove and  
 freshwater flora pollen in the Late Oligocene–Early Miocene Malay Basin (basin 5—Fig. 6)  
 (Todd et al., 1997; Morley et al., 2011; Shoup et al., 2013). However, sedimentary evidence for  
 preservation of wave-dominated processes (e.g. swaley and hummock cross-stratification) and  
 environments in regions of modelled tidal range and bed shear stress include: (1) interpreted  
 barred, wave- and storm-dominated, shoreface-shelf system in the Early Miocene, southern  
 Malay Basin (Ramli, 1986); and (2) wave- and storm-dominated environments in locations  
 relatively distal and/or lateral to tidally-influenced coastal-delta environments in the Early

1  
2  
3  
4  
5  
6  
7  
8  
9  
10  
11  
12  
13  
14  
15  
16  
17  
18  
19  
20  
21  
22  
23  
24  
25  
26  
27  
28  
29  
30  
31  
32  
33  
34  
35  
36  
37  
38  
39  
40  
41  
42  
43  
44  
45  
46  
47  
48  
49  
50  
51  
52  
53  
54  
55  
56  
57  
58  
59  
60  
61  
62  
63  
64  
65

Miocene Nyalau Formation (Amir Hassan et al., 2013; Amir Hassan et al., 2016; Murtaza et al., 2018) and early Middle Miocene Miri Formation (Abieda et al., 2005; Siddiqui et al., 2016; Collins et al., 2020) in the Sarawak and Baram-Balabac basins, NW Borneo, respectively.  
; (8) Lambir (L) and Belait (B) formations, Baram Delta Province, Baram-Balabac Basin (Lambiase et al., 2003; Collins et al.).

Regional- to local-scale controls on tidal deposition: ~~Tidal signals are less widespread in Middle-Late Miocene strata (Fig. 14) but preferentially occurred in the embayed shoreline settings, including: (1) medium-grained sandstones with mangrove-bearing mudstones and coals in the Middle-Late Miocene Pattani Basin, Gulf of Thailand (Jardine, 1997; Lockhart et al., 1997; Charusiri and Pum-Im, 2009; Ridd et al., 2011); (2) medium-grained sandstones and mangrove-bearing mudstones and coals deposited under tidally influenced conditions in the Middle Miocene Malay Basin (Todd et al., 1997; Morley et al., 2011; Shoup et al., 2013); and (3) tide-influenced deltaic units (e.g. channels) comprising very fine- to fine-grained sandstone and mangrove-bearing mudstones in embayed areas in the Baram-Balabac Basin, NW Borneo (Hadley et al., 2006; Ainsworth et al., 2011; Collins et al., 2018b). This distribution is consistent with the preferential occurrence of tidal shoreline environments and mangroves within present-day embayed areas, such as the NE shoreline of the Gulf of Thailand and, in NW Borneo. The latter includes the Lupar embayment, which hosts the tide-dominated Rajang delta (Staub and Gastaldo, 2000), and Brunei Bay (e.g. Staub and Esterle, 1994; Nyberg and Howell, 2016; Collins et al., 2018b; Twilley et al., 2018). However, open coastline systems in the Middle-Late Miocene overwhelmingly preserve evidence for reduced tidal influence, most notably: (1) a pronounced decrease in abundance of mangrove pollen and increase in freshwater pollen in shallow-marine strata after the Middle Miocene in the Cuu Long Basin (Chung et al., 2015); (2) a sharp reduction in terrestrial and mangrove-derived pollen and transition from tidally-influenced deltaic to shoreface-shelf deposition through the Middle Miocene in the Nam Con Son Basin, mostly due to increased sea level in the Middle Miocene thermal maximum (Morley et al., 2011); (3) overall decrease in abundance of mangrove pollen and extent of interpreted mangrove-bearing environments in the Middle-Late Miocene Gulf of Thailand (Shoup et al.,~~



1  
2  
3  
4  
5  
6  
7  
8  
9  
10  
11  
12  
13  
14  
15  
16  
17  
18  
19  
20  
21  
22  
23  
24  
25  
26  
27  
28  
29  
30  
31  
32  
33  
34  
35  
36  
37  
38  
39  
40  
41  
42  
43  
44  
45  
46  
47  
48  
49  
50  
51  
52  
53  
54  
55  
56  
57  
58  
59  
60  
61  
62  
63  
64  
65

~~2013); and (4) storm-dominated, fluvial-influenced and tide-affected deposition in open-coastline  
areas of the Middle-Late Miocene Baram-Balabac Basin (Lambiase et al., 2003; Hadley et al.,  
2006; Ainsworth et al., 2011; Collins et al., 2018b) (Collins et al., 2017b). In open-coastline  
settings of the Middle-Late Miocene, as well as lower modelled tidal potential, a large fetch and  
possible increased influence of typhoons (Collins et al., 2017b) would have increased the  
potential for wave and storm overprinting of higher frequency, lower magnitude tidal processes  
(e.g. Dott, 1983; Dott, 1996; Miall, 2015; Collins et al., 2018a; Collins et al., 2018b).  
Nonetheless, mixed wave- and tide-influenced, mangrove-bearing, open-coastline and deltaic  
strata are preserved in the Middle Miocene Cuu Long Basin, which are similar to the present day,  
mixed wave- and tide-influenced, mangrove-bearing Mekong delta, southern Vietnam (e.g. Ta et  
al., 2002a).~~

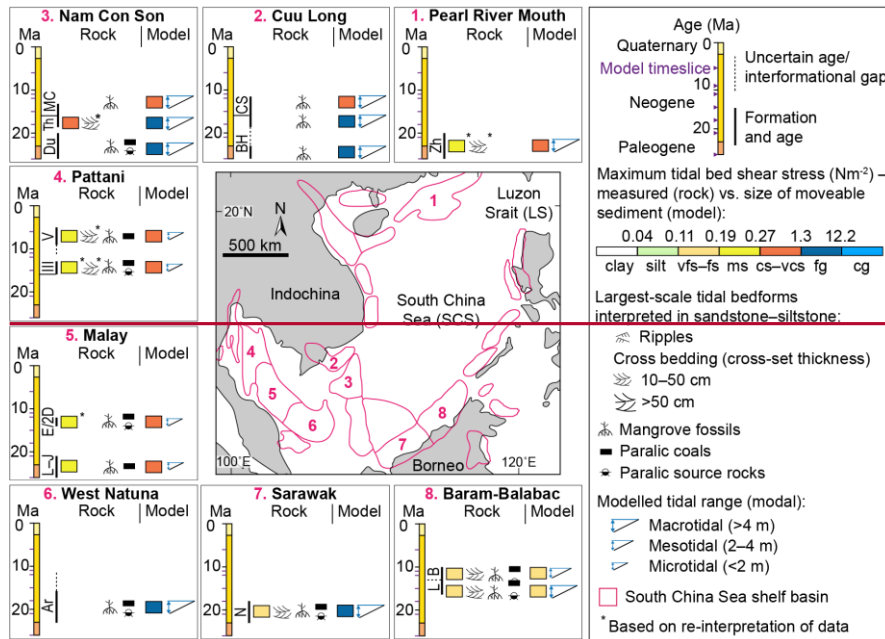


**Fig. 14. Evidence of tide-influenced deposition based on sedimentological and micropaleontological data, mainly from petroleum exploration wells, and comparison to base case tidal model results (Fig. 12) in South China Sea shelf basins. Rock record data include grain size, cross lamination (ripples) and/or cross bedding interpreted to preserve evidence of tidal process (e.g. bidirectional palaeocurrents, scoop-shaped foresets, mudstone drapes), mangrove pollen aemes and the occurrence of paralic, mangrove-bearing coals and source rocks. Studied formations and key references for each basin are: (1) Upper Zhuhai (Zh) Formation, Pearl River Mouth Basin (Zheng and Deng, 2012); (2) Bach Ho (BH) and Con Son (CS) formations, Cuu Long Basin (Morley et al., 2011); (3) Dua (Du), Thong (Th) and Mang Cau (MC) formations, Nam Con Son Basin (Tin and Ty, 1995; Morley et al., 2011); (4) Sequences II–IV, Pattani Basin (Jardine, 1997; Lockhart et al., 1997); (5) Groups L–J and E, Malay Basin (Morley et al., 2011); (6) Arang (Ar) Formation, West Natuna Basin (Morley et al., 2011); (7) Nyalau (Ny) Formation, Balingian Province, Sarawak Basin (Amir Hassan et al., 2013; Amir Hassan et al., 2016); (8)**

Lambir (L) and Belait (B) formations, Baram Delta Province, Baram-Balabac Basin (Lambiase et al., 2003; Collins et al.).

## 4.2 Early Cretaceous (Aptian–Albian) Lower Greensand Seaway, north-west Europe

### 4.2.1 Overview

#### 4.2.1 Background

The Early Cretaceous (Aptian–Albian) ‘Lower Greensand Seaway’ (LGS), used here to refer to the interconnected network of three main seaways connecting with larger marine bodies (i.e. Boreal, proto-Atlantic and Neothys; Fig. The Early Cretaceous Lower Greensand Group in Southeast England is well known for its tidal sandstone deposits (Allen, 1982a; Bridges, 1982; Johnson and Levell, 1995; Wonham and Elliott, 1996; Yoshida et al., 2004). The study area is very different to our previous (SCS)10A–B), contrasts markedly to the SCS example: it covers a much smaller area, it was part of a larger epicontinental sea and it was entirely shallow water, far removed from coeval oceanic basins. The larger-scale (10–100s km) basin physiography was determined by a series of precursor, west-east-trending, rift basins (c. 50–100 km long and 10–30 km wide; e.g. Weald-, Wessex and Channel basins; Fig. 10 C–D) that were initiated during the Early Cretaceous (e.g. Ziegler, 1990; Hawkes et al., 1998) (e.g. Ziegler, 1990; Hawkes et al., 1998)). These basins were initially (Berriasian–Barremian) filled by thick (100s m; up to ca 1 km) alluvial plain successions (Wealden Group). These successions were succeeded by Aptian–Albian deposits that, Aptian–Albian deposits in the LGS comprise shallow marine sandstones (Lower Greensand Group); Fig. 10E), divided informally herein into two stratigraphic intervals: (1) the upper part of the *fissicostatus–martinioides* Zone (labelled ‘FH’, Fig. 10E) comprising deposits with negligible evidence of tidal currents, suggesting low tidal range (microtidal–low mesotidal) (Ruffell and Wach, 1991; Wells et al., 2010b); (2) the mid-to-upper part of the *upper martinioides–lower tardefurcata* Zone (labelled ‘FSW’ in Fig. 10E), represented by several units, with exemplary evidence of tidal sedimentation deposition by strong tidal currents within an inferred macrotidal, ebb-dominated diurnal, or mixed, predominantly diurnal tidal regime comprise shallow-marine sandstones (Lower Greensand Group) with exemplary evidence of tidal sedimentation (e.g. De Raaf and Boersma, 1977) (e.g. De Raaf and Boersma, 1977)) (Allen,

Formatted: Line spacing: Double

1982a; Bridges, 1982; Johnson and Levell, 1995; Wonham and Elliott, 1996; Yoshida et al., 2004). These ‘greensands’ deposits are overlain by offshore marine mudstones (Gault Clay Formation). Hence, the Aptian-Albian succession reflects overall marine transgression, which was accompanied by an overall increase in basin width, length, bathymetry and connectivity. Consequently, predicting tidal circulation in this setting is complicated by several uncertainties, most notably: (1) variability in palaeobathymetry caused by the drowning of previously separate rift basins (potentially forming various ‘straits’) with differing initial water depths, (Fig. 10C–D); and (2) complex marine flooding of these basins, with competing marine incursions entering the Weald Basin LGS through connections to three major marine water bodies during drowning: the Boreal Sea (to the north), proto-Atlantic Ocean (to the south-west), and Neotethys Ocean (to the south-east) (Fig. 10A–B).

Palaeotidal modelling and comparison to the stratigraphic record, with emphasis on the Lower Greensand Group, has been used to understand these uncertainties in the two stratigraphic intervals outlined above (‘FH’ and ‘FSW’ in Fig. 10E) allows uncertainty analyses across a range of different age, palaeobathymetric and palaeogeographic scenarios (Wells et al., 2010b) (Wells et al., 2010b). Regional-scale tidal simulations for tidal amplitude and phase represent both astronomical ( $M_2$ ,  $S_2$ ,  $K_1$ , and  $O_1$ ) and boundary tidal forcing, the latter generated using a global Aptian model (Wells et al., 2010a). Two base-case palaeogeographies (‘Scenario 1’), based on modified published interpretations (see Wells, 2008; Wells et al., 2010b), were generated for the ‘FH’ and ‘FSW’ stratigraphic intervals (Fig. 10E), referred to as FH1 (Fig. 11A–B) and FSW1 (Fig. 11C–D), respectively. A key difference between the ‘base case’ scenarios for these two timeslices is widening of the oceanic connections, especially through the Paris Basin, in the upper *martinioides*–lower *tardefurcata* Zone due to transgression in the *nutfieldensis* Zone (Casey, 1961; Wells et al., 2010b). Four out of seven sensitivity analyses for each base-case palaeogeography are discussed herein, corresponding to scenarios 2, 4, 6 and 8 in Wells et al. (2010b): Scenario 2 has closure of the Paris Basin connection to the Neotethys

Ocean (FH2 and FSW2); Scenario 4 has a connection through the Pewsey Basin to the proto-Atlantic Ocean (FH4 and FSW4); Scenario 6 has opening of all oceanic connections (FH6 and FSW6); and Scenario 8 has a doubled water depth between 0 and 200 m (FH8 and FSW8)..

#### ***4.2.2—Geological Setting***

During the Early Cretaceous, an increase in eustatic sea level, and a waning of rift-related subsidence, resulted in the marine flooding and connection of several previously isolated continental rift basins (Fig. 15A–C). Many of these basins became connected as marine transgression flooded several relatively narrow (c. 10s km wide) seaways, which exploited pre-existing structural lineaments, including basement-linked syn-rift faults (Hawkes et al., 1998). Thus, the Weald and Paris basins were connected via a northwest-southeast-trending seaway along the major Pays de Bray Fault, while the Weald and Southern North Sea basins were connected across the London-Brabant Massif via the northeast-southwest-trending ‘Bedfordshire Strait’ (Ziegler, 1990). Transgression of the Wessex Basin exploited the major basin-bounding Purbeck-Isle of Wight Fault Zone (Gupta and Johnson, 2002).

The various sedimentary basins were infilled with highly diachronous, but broadly Aptian–Albian age, glauconite-rich shallow-marine sandstones, informally referred to ‘greensands’. The first of these shallow-marine sandstone units, the Lower Greensand Group (LGG), is the primary focus of this review. The term ‘Lower Greensand Seaway’ is used here to refer to an interconnected network of three main seaways of latest Aptian–Albian age, each one connecting

with larger marine water bodies (i.e.

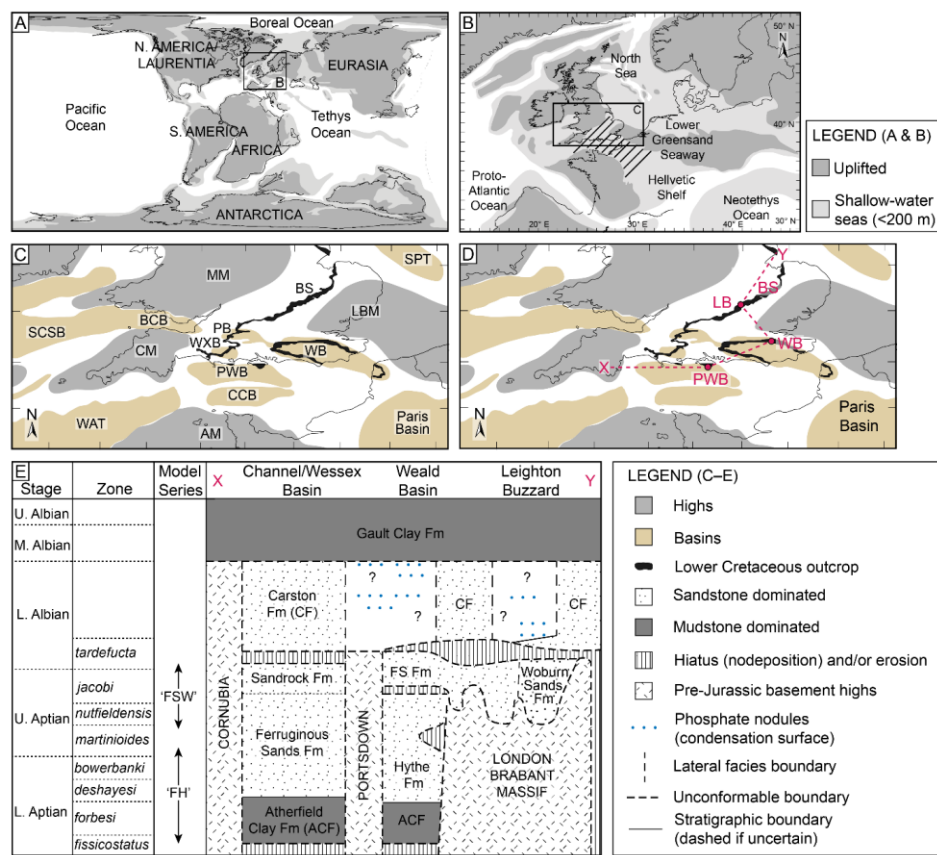


**Fig. 10.** Boreal, proto Atlantic and Neothys; Fig. 15A–B). The LGG stratigraphy and palaeogeography is supported by a robust ammonite biostratigraphic framework and contains unconformities of local to regional extent (Fig. 15D) (Bridges, 1982). Two stratigraphic intervals and associated phases of basin-fill deposition are considered below. The first phase of deposition (labelled ‘FH’ in Fig. 15D) is represented by the upper part of the *fissicostatus*–*martinioides* Zone, which comprises the Ferruginous Sands Formation (Isle of Wight, Wessex

and Channel basins) ([Ruffell, 1992](#)) and the Hythe Formation (Weald Basin) ([Bridges, 1982](#); [Ruffell, 1992](#); [Rawson, 2006](#)). These deposits display negligible evidence of tidal currents, suggesting low tidal range (microtidal–low mesotidal) ([Ruffell and Wach, 1991](#); [Wells et al., 2010b](#)). The second phase of deposition (labelled ‘FSW’ in Fig. 15E) is represented by the mid- to upper part of the *upper martinioides*–*lower tardefurecata* Zone, and comprises several high-energy, shallow marine sandstone units, most notably (1) the Woburn Sands Formation (in Leighton Buzzard) ([Johnson and Levell, 1995](#); [Wonham and Elliott, 1996](#); [Yoshida et al., 2004](#)); (2) the Folkestone Sands Formation (Weald Basin) ([Allen, 1981a](#); [Allen, 1981b](#); [Allen, 1982a](#); [Bridges, 1982](#)); and (3) the Sandrock Formation (Isle of Wight, Wessex and Channel basins) ([Ruffell and Wach, 1991](#); [Insole et al., 1998](#); [Rawson, 2006](#)) (Fig. 15D). These deposits all display compelling evidence of deposition by strong tidal currents within an inferred macro-tidal setting ([Allen, 1982a](#); [Johnson and Levell, 1995](#)). Mud drape spacing in the Folkestone Sands has been interpreted to form spring–neap tidal bundles that were deposited in an ebb-dominated diurnal, or mixed, predominantly diurnal tidal regime ([Allen, 1982a](#)). The LGG succession is capped everywhere by offshore marine mudstones of the Gault Clay Formation, which transgressively onlaps the underlying tidal sandstones ([Johnson and Levell, 1995](#)). Palaeotidal modelling has focused on the two stratigraphic intervals outlined above (‘FH’ and ‘FSW’ in Fig. 15D) ([Wells et al., 2010b](#)), as summarised below:

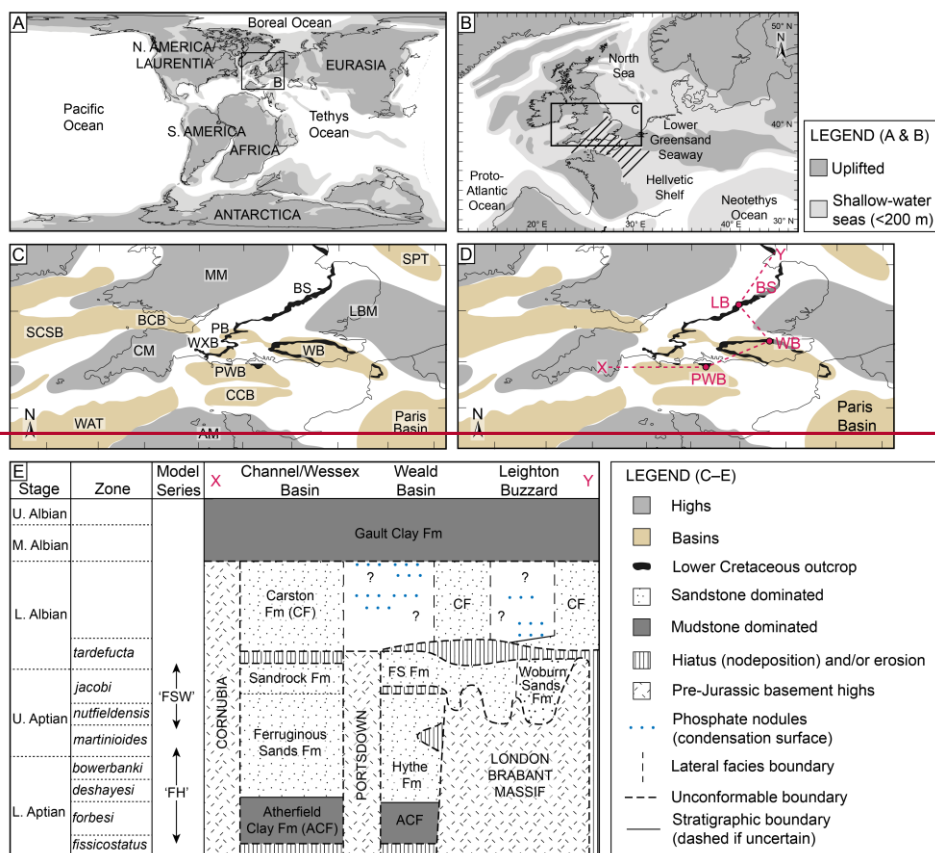


**Fig. 15.** Geological and stratigraphic framework of the Early Cretaceous 'Lower Greensand Seaway', NW Europe. (A) Global Aptian palaeogeographic framework. (B) Aptian palaeogeographic framework of northwest Eurasia. In A and B, darker grey are significant uplifted highs and lighter grey shallow-water seas (< 200 m depth). (C) Aptian palaeogeographic map of southern UK and northern France with significant uplifted highs in dark grey and basins in light brown. Basin abbreviations: BCB – Bristol Channel Basin; BS – Bedfordshire Strait; CCB – Central Channel Basin; PB – Pewsey Basin; PWB – Purbeck-Wright Basin; SCSB –



1  
2  
3  
4  
5  
6  
7  
8  
9  
10  
11  
12  
13  
14  
15  
16  
17  
18  
19  
20  
21  
22  
23  
24  
25  
26  
27  
28  
29  
30  
31  
32  
33  
34  
35  
36  
37  
38  
39  
40  
41  
42  
43  
44  
45  
46  
47  
48  
49  
50  
51  
52  
53  
54  
55  
56  
57  
58  
59  
60  
61  
62  
63  
64  
65

South Celtic Sea Basin; WAT – Western Approaches Trough; WB – Weald Basin. High abbreviations: AM – Armorican Massif; CM – Cornubian Massif; LBM – London-Brabant Massif; MM – Midlands Massif. (D) Aptian palaeogeographic map illustrating key locations for the chronostratigraphic and lithostratigraphic framework of the Lower Greensand Group (section X–Y in E). Location abbreviations in addition to those labelled in C: LB – Leighton Buzzard. (E) Illustrative chronostratigraphic and lithostratigraphic section of the Lower Greensand Group in southern England. Two “base case” palaeogeographies are considered (Fig. 4611): ‘FH’ represents the upper part of the *fissicostatus–martinioides* Zone depositional sequence, corresponding to the Ferruginous Sands Formation on the Isle of Wight and the Hythe Formation in the Weald; ‘FSW’ represents the mid to upper part of the upper *martinioides*–lower *tardefurcata* Zone depositional sequence, corresponding to the Folkestone Sands Formation in the Weald, the Sandrock Formation on the Isle of Wight, and the Woburn Sands Formation around Leighton Buzzard. After Wells et al. (2010b), Yoshida et al. (2004) After Wells et al. (2010b), Yoshida et al. (2004) and references therein.

**4.2.34.2.2 Model Setup results and rock-record integration**

Regional scale tidal simulations were forced with both astronomical and boundary tides for the four most significant tidal constituents ( $M_2$ ,  $S_2$ ,  $K_1$ , and  $O_1$ ) (Kantha and Clayson, 2000); each constituent was run independently for an 8-day period (simulated time), with a time step of 5 minutes, in order to reach a steady state solution. Tidal amplitude and phase were calculated using harmonic analysis on the last 30 hours of the simulated free surface height; tidal range is twice the total tidal amplitude values.

Formatted: Line spacing: Double

Tidal open boundary conditions for regional scale tidal simulations were generated using a global scale Lower Cretaceous (Aptian) palaeotidal model (Wells et al., 2010a) along the southern (Neo-Tethys) and western (proto-Atlantic) margins, and positioned oceanward of the shelf edge, in order to better resolve the propagation of the oceanic tidal wave onto the continental shelf and minimised boundary effects within the Lower Greensand Seaway. The plate tectonic and palaeocoastline reconstructions were based on the Palaeogeographic Atlas Project (Paul Markwick, personal communication 2007), underpinned by ocean floor ages (Müller et al., 1997) and further literature review (Wells et al., 2010a). Palaeobathymetry was estimated by reference to modern analogues (Wells et al., 2010a). The Aptian global palaeotidal model predicts low microtidal ranges in the proto-Atlantic (<1 m) and Boreal (<0.5 m) oceans, and higher diurnal dominated microtidal (c. 1.5–2 m) ranges in the Neotethys (Wells et al., 2010a).

Modified versions of the published Lower Greensand Seaway palaeocoastline (Tyson and Funnell, 1987; Ziegler, 1990; Hancock and Rawson, 1992) were used in regional scale tidal simulations of the Lower Greensand Seaway (Wells, 2008; Wells et al., 2010b). Maximum modelled water depths in the seaway are typically 25 m and do not exceed 75 m by analogy to sand-wave deposits in the present day English Channel and Southern North Sea (Allen, 1982a; Stride, 1982). Numerous sensitivity tests were performed on two ‘base-case’ palaeogeographies for (1) the upper part of the *fissicostatus–martinioides* Zone depositional sequence (the ‘FH’ series, Fig. 15E), referred to as FH1 (Fig. 16A–B), and (2) mid to upper part of the upper *martinioides*–lower *tardefurcata* Zone depositional sequence (the ‘FSW’ series, Fig. 15E), referred to as FSW1 (Fig. 16C–D). A key difference between the ‘base-case’ scenarios for these

two timeslices is widening of the oceanic connections, especially through the Paris Basin, in the upper *martinioides*–lower *tardefurcata* Zone due to transgression in the *nutfieldensis* Zone (Casey, 1961; Wells et al., 2010b).

Eight sensitivity analyses were performed for each ‘base case’ palaeogeography (Wells et al., 2010b), of which four are discussed herein (Scenarios 2, 4, 6 and 8, using the numbering system of Wells et al. (2010b)): (1) closure of the Paris Basin connection to the Neotethys Ocean (Scenario 2: cases FH2 and FSW2; Fig. 17A, B); (2) connection through the Pewsey Basin to the proto-Atlantic Ocean (Scenario 4; FH4 and FSW4; Fig. 17C, D); (3) opening of all oceanic connections (Scenario 6; FH6 and FSW6; Fig. 17E, F); and (4) doubling the water depth between 0 and 200 m, whilst maintain the same palaeoshoreline (Scenario 8; FH8 and FSW8; Fig. 17G, H).

#### 4.2.4 Model Results

Base case simulations for both timeslices suggest propagation of two progressive tidal waves into the Lower Greensand Seaway: (1) a generally dominant tide from the Neotethys Ocean to the south-east, via the Paris Basin, and (2) a generally subordinate tide from the proto-Atlantic Ocean to the west and south-west, via Western Approaches Trough (Fig. 16). A connection to the Boreal Ocean to the north, via the ‘Bedfordshire Strait’ and North Sea (Fig. 15C, D), had not yet been established in either base case simulation (Fig. 16). In the base case simulation of the older timeslice (scenario FH1; Fig. 16A), a microtidal (c. 1–2 m) diurnal-dominated tidal regime in the Lower Greensand Seaway is predicted. The restricted connection between the seaway and Paris Basin is associated with funnelling, shoaling and amplification of tides in the northern Paris

Basin, and decreased tidal inflow into the Weald Basin (e.g. Guillocheau et al., 2000). In the 'base case' simulation of the younger timeslice (scenario FSW1; Fig. 16B), tides in the Lower Greensand Seaway are diurnal-dominated but higher than in scenario FH1: high mesotidal to low macrotidal in the western Weald and Leighton Buzzard–Bedfordshire Strait area, and mesotidal in the rest of the seaway. The simulation shows the northward-propagating tidal wave from the Neotethys Ocean being significantly amplified by funnelling and shoaling effects as the seaway narrows and shallows towards the northwest (Fig. 16B). Furthermore, Coriolis deflection to right steers the tidal wave into the funnel-shaped 'Leighton Buzzard Trough', causing further amplification and formation of macrotidal conditions here (Fig. 16B).

Compared to the base case simulations (Fig. 16), four sensitivity analyses (Scenarios 2, 4, 6 and 8) indicate the following effects on tides in the Lower Greensand Seaway:

- (1) Scenarios FH2 and FSW2 represents closure of the Paris Basin connection to the Neotethys Ocean, and therefore loss of the dominant tidal inflow into the seaway. This substantially decreases modelled tidal range within the seaway in both timeslices, decreasing tidal range by up to c. 75% to microtidal in scenario FSW2 (Fig. 17A–B), and causing local increases in semi-diurnal tides (Fig. 18).
- (2) Scenarios FH4 and FSW4 includes an additional connection to the proto-Atlantic Ocean through the Pewsey Basin, which decreases modelled tidal range within the seaway in both time-slices (Fig. 17C–D). Tidal range is decreased due to destructive interference of out-of-phase tidal waves, which enter from the Weald Basin from the Pewsey Basin and the Paris Basin in scenario FH4, and from the English Channel Basin and the Paris Basin

in scenario FSW4 (Fig. 17C–D). Additionally, some tidal energy may outflow through the Pewsey Basin in both scenarios.

(3) Scenarios FH6 and FSW6 reflects opening of an additional oceanic connection through the Bedfordshire Strait (Fig. 15D) and first communication with the Boreal Sea, to the north. This results in decreased modelled tidal range across much of the LGS because the various tidal waves are not in phase, leading to destructive interference (Fig. 17E–F). Additionally, rather than being trapped, funnelled, and amplified within the seaway, the dominant incoming tide from the southeast may outflow via the additional connections. Tides in the seaway become more semi-diurnal influenced in scenario FH6 but remain diurnal dominated in scenario FSW6 (Fig. 18).

(4) Scenarios FH8 and FSW8 comprises a doubling the water depth between 0 and 200 m, whilst maintaining the same palaeoshoreline. This significantly increases modelled tidal range in both timeslices, to high microtidal-mesotidal (c. 1.8–3 m) in scenario FH8 and macrotidal (c. 5–7 m) in scenario FSW8. This is partially due to enhanced inflow of tidal energy and shoaling caused by the larger change in water depth across the shelf. However, the ratio of diurnal to semi-diurnal tides changes in both time-slices, which suggests that regional physiography also had an important effect on tidal resonance (Fig. 18).

These scenarios illustrate that the regional-scale (100s km) balance between tidal inflow and outflow. The range of tidal model scenarios illustrates the regional-scale (100s km) interplay between tidal inflow and outflow. This has a first-order control on tides in smaller-scale (10s km) areas and can supersede funnelling effects within some smaller physiographic constrictions, such

as in straits and embayments. ~~Predicted~~In the LGS, predicted tidal ranges in simulations of the upper *martinioides*–lower *tardefurcata* Zone (‘FSW’ ~~;~~) (Figs. ~~46B~~11B, D, ~~47B~~12B, D, F, H) are consistently higher ~~in the Lower Greensand Seaway~~ than in equivalent base-case and sensitivity simulations of the *fissicostatus*–*martinioides* Zone (‘FH’; Figs. ~~46A~~11 A, C, ~~47A~~12A, C, E, G) ~~The larger tidal ranges in the FSW simulations result from~~, and are interpreted to relate to increased inflow of tidal energy due to the greater width of the seaway and its ocean connections. ~~in ‘FSW’ simulations.~~ This is especially ~~the case~~pronounced for the Paris Basin, because the maximum depth is similar in equivalent FSW and FH simulations and the same open tidal boundary conditions are used in ~~FSW and FH simulations both cases~~. In addition, ~~infor~~ for all scenarios ~~for each timeslice~~and both timeslices, tidal range is higher along the eastern margins of the seaway and the Paris Basin, due to Coriolis deflection of the northward propagating tidal wave from the Neotethys Ocean.

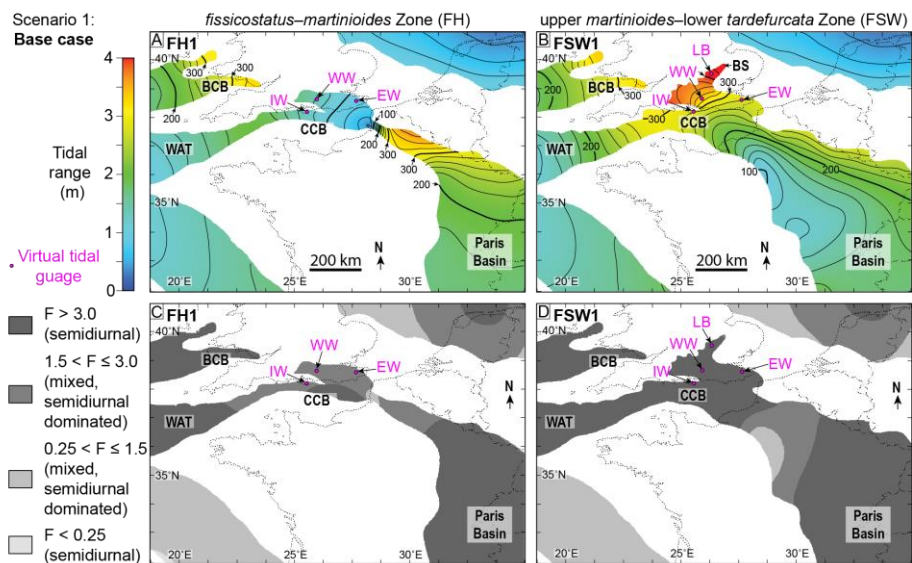


**Fig. 16.** Base case palaeotidal model results in the Early Cretaceous Lower Greensand Seaway for the *fissicostatus–martinioides* Zone (A, C) and upper *martinioides*–lower *tardefurcata* Zone (B, D) timeslices (respectively 'FH' and 'FSW' in Fig. 15D) showing modelled tidal range (0–4 m) for the four principal tidal constituents ( $M_2 + S_2 + K_1 + O_1$ ), with 20 cm contours and bold, annotated contours every 100 cm (A–B), and the 'F-ratio' between the amplitudes of diurnal and semidiurnal tidal constituents (C–D). After Wells et al. (2010b). Pink labelled dots show positions of 'virtual tidal gauges' in the East Weald Basin (EW), Isle of Wight (IW), Leighton Buzzard (LB) and West Weald Basin (WW). Basin abbreviations: CCB – Central Channel Basin; BCB – Bristol Channel Basin; BS – Bedfordshire Strait; CCB – Central Channel Basin; PB – Pewsey Basin; WAT – Western Approaches Trough. Modified from Wells et al. (2010b).

Formatted: Font: Bold



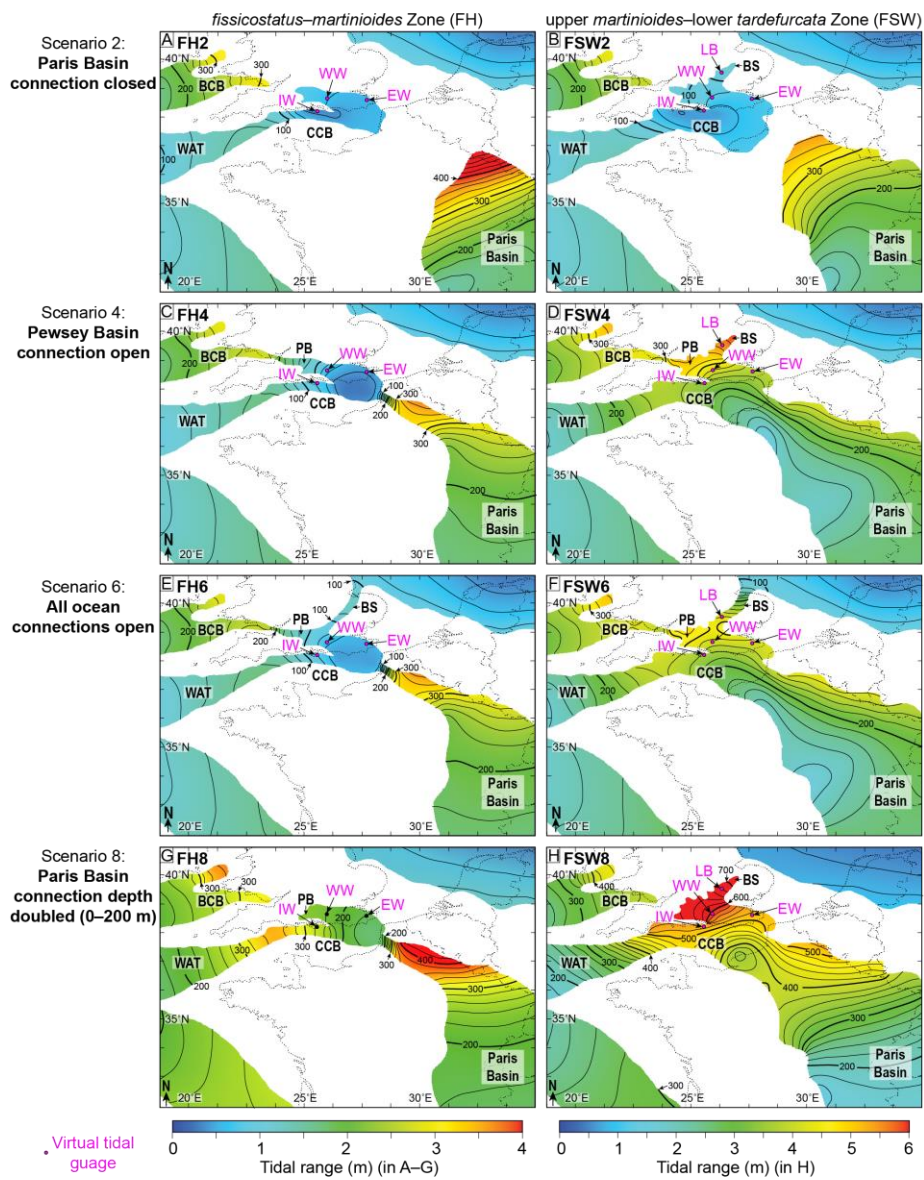
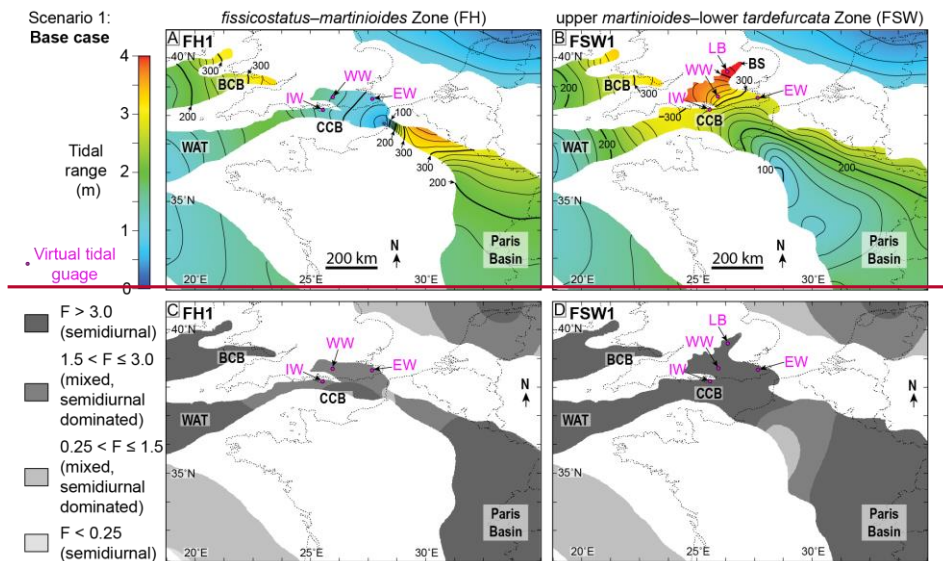


**Fig.**

**Formatted:** Font: Bold

**Formatted:** Line spacing: 1.5 lines

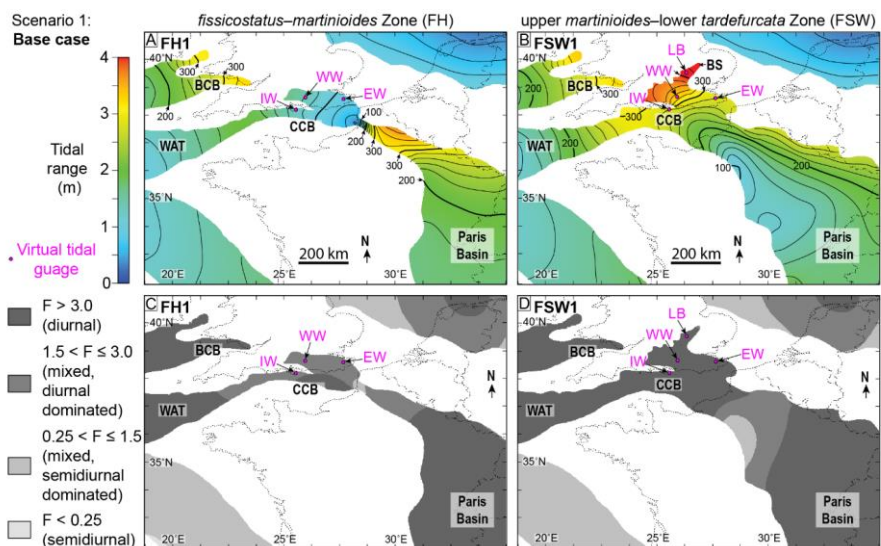




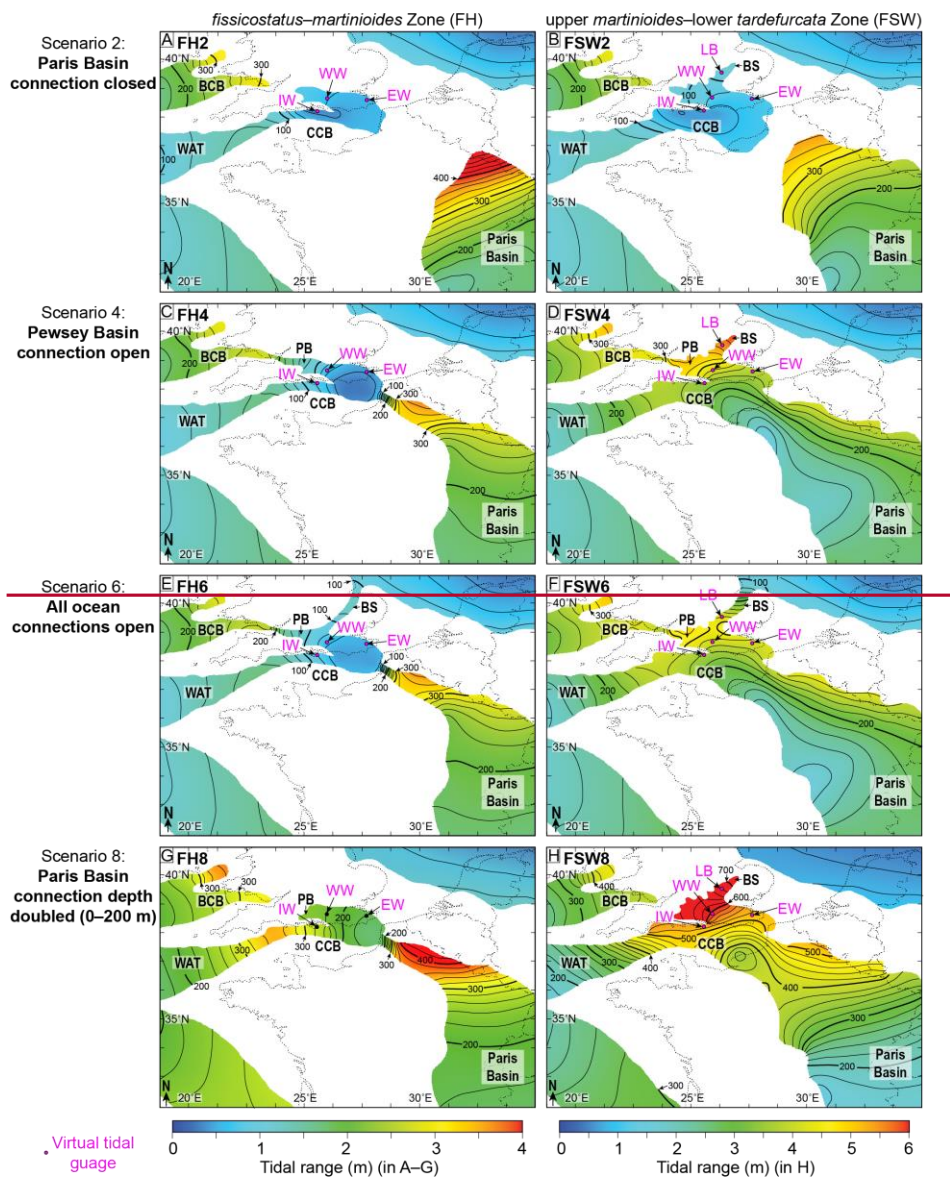
**Fig. 16.** Modelled high mesotidal to low macrotidal conditions for the FSW interval are supported by widespread interpreted tidal deposits throughout the seaway at this time. Evidence of tidal processes ranges in scale from facies (e.g. sedimentary structures, palaeocurrents and ichnology), through facies associations to facies successions (see Section 2.2.3), and include various combinations of tidal indicators such as the following: (1) mudstone draped cross-set, including some double-drapes and possible spring-neap bundles; (2) compound cross-stratification; (3) bidirectional palaeocurrent directions on a range of scales, including ebb- and flood-dominated patterns in 10s m-thick intervals; (4) reactivation surfaces; (5) wavy-, flaser- and lenticular-bedded heterolithic cross-bed toesets; (6) shallow-marine, variable intensity, low diversity ichnofauna; and (7) vertical and lateral facies and facies association relationships, including grain size trends and the geometry of bounding surfaces e.g. (Bridges, 1982; Johnson and Levell, 1995; Wonham and Elliott, 1996; Yoshida et al., 2004; Wells et al., 2010b), (Allen, 1982a; Bridges, 1982). Overall, these deposits are interpreted to record deposition under strong tidal currents, with probable mesotidal to macrotidal ranges (Allen, 1981b), in tidal estuarine to embayment environments (Yoshida et al., 2004). This is consistent with palaeotidal model results that include local-scale amplification through shoaling and funnelling effects (Fig. 12B

1  
2  
3  
4  
5  
6  
7  
8  
9  
10  
11  
12  
13  
14  
15  
16  
17  
18  
19  
20  
21  
22  
23  
24  
25  
26  
27  
28  
29  
30  
31  
32  
33  
34  
35  
36  
37  
38  
39  
40  
41  
42  
43  
44  
45  
46  
47  
48  
49  
50  
51  
52  
53  
54  
55  
56  
57  
58  
59  
60  
61  
62  
63  
64  
65

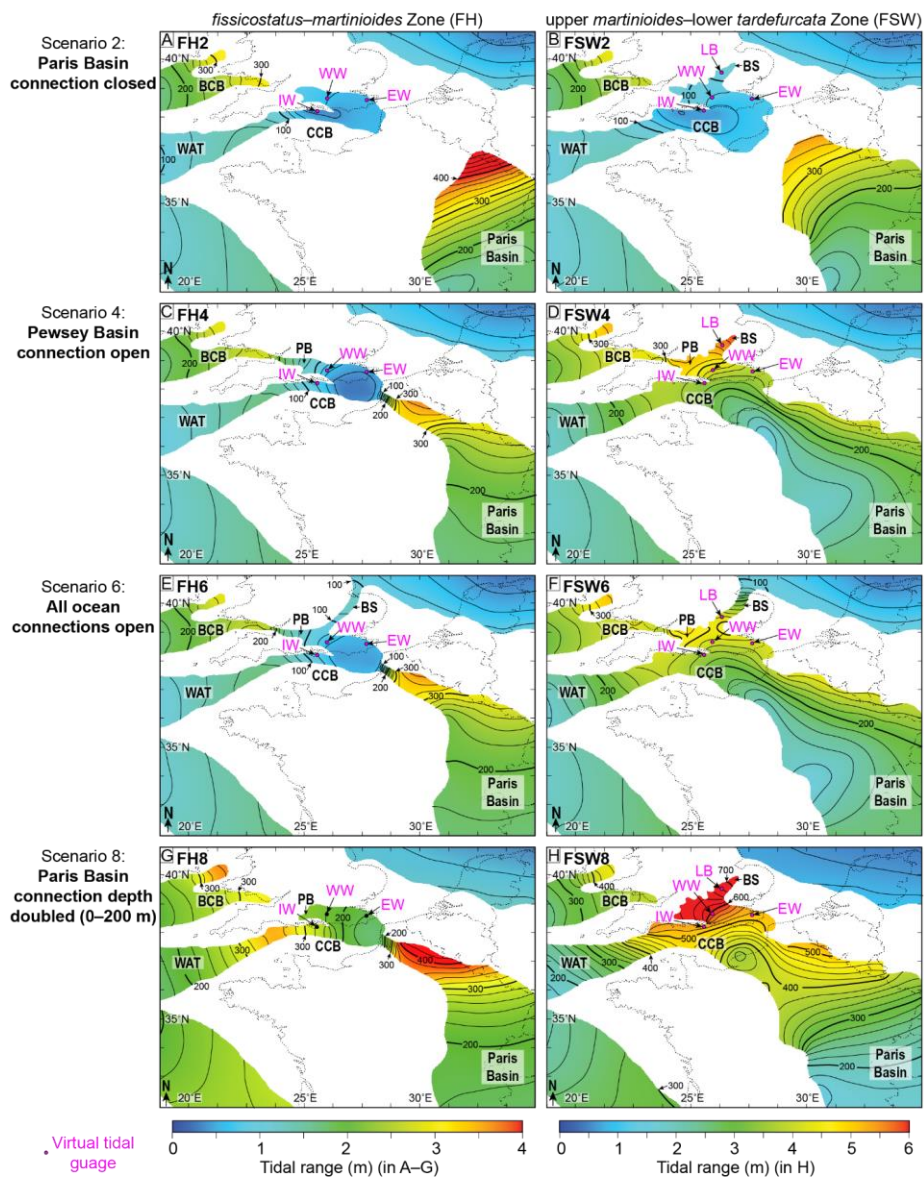
and 13). Furthermore, the predicted diurnal-dominated tidal regime in the LGS in all modelled scenarios (Fig. 13) matches the interpretation of diurnal-dominated spring–neap tidal bundles in the Folkestone Sands Formation (Allen, 1981a; Allen, 1982a). Modelled microtidal to low mesotidal conditions for the FH interval is broadly consistent with little evidence of tidal influence in the time-equivalent stratigraphic record (see review in Wells et al. (2010b). The only putative tidal deposits of this age, occurring in the western Weald Basin, are limited in areal extent and contain no published evidence of bidirectional currents or mud drapes, decreasing the confidence in interpretation (Casey, 1961; Narayan, 1971; Bridges, 1982; Ruffell and Wach, 1991; Rawson, 2006).



**Fig. 11.** Base-case palaeotidal model results in the Early Cretaceous Lower Greensand Seaway for the *fissicostatus–martinioides* Zone (A, C) and *upper martinioides–lower tardefurcata* Zone (B, D) timeslices (respectively ‘FH’ and ‘FSW’ in Fig. 15D10D) showing modelled tidal range (0–4 m) for the four principal tidal constituents ( $M_2 + S_2 + K_1 + O_1$ ), with 20 cm contours and bold, annotated contours every 100 cm (A–B), and the ‘F ratio’ between the amplitudes of diurnal and semidiurnal tidal constituents (C–D). After Wells et al. (2010b)17. Pink labelled dots show positions of ‘virtual tidal gauges’ in the East Weald Basin (EW), Isle of Wight (IW), Leighton Buzzard (LB) and West Weald Basin (WW). Basin abbreviations: CCB – Central Channel Basin; BCB – Bristol Channel Basin; BS – Bedfordshire Strait; CCB – Central Channel Basin; PB – Pewsey Basin; WAT – Western Approaches Trough. Modified from Wells et al. (2010b).

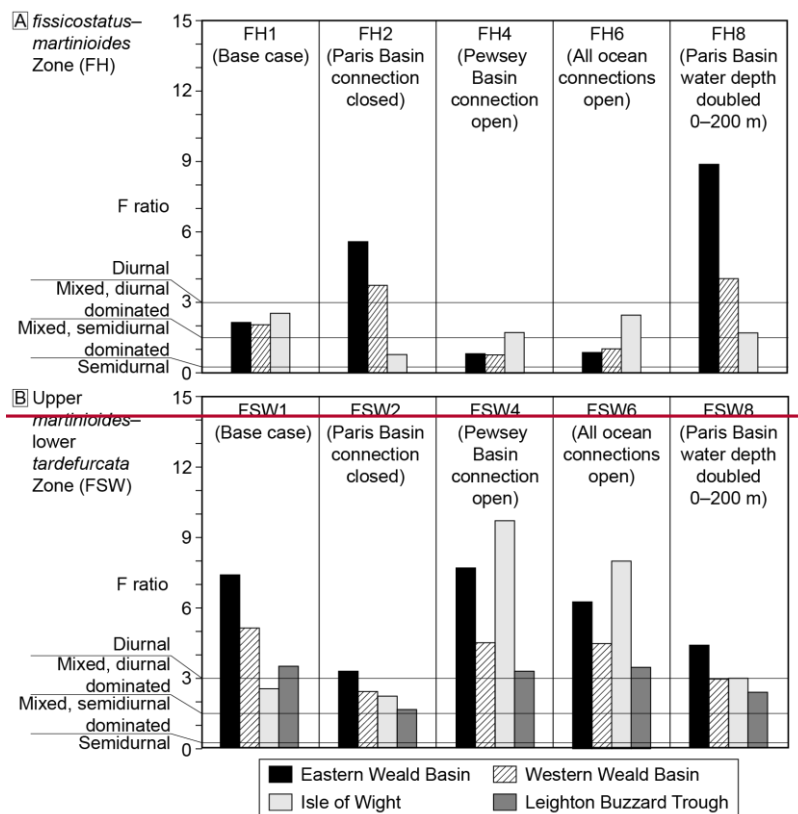






1  
2  
3  
4  
5  
6  
7  
8  
9  
10  
11 **Fig. 17.12.** Modelled tidal range for the four principal tidal constituents ( $M_2 + S_2 + K_1 + O_1$ ) in  
12  
13 sensitivity analyses of base-case reconstructions for the *fissicostatus*–*martinioides* Zone (A, C, E,  
14  
15 G) and upper *martinioides*–lower *tardefurcata* Zone (B, D, F, H) timeslices in the Early  
16  
17 Cretaceous Lower Greensand Seaway (respectively ‘FH’ and ‘FSW’ in Fig. ~~15D~~ 10D); tidal  
18  
19 range contours are drawn for 20 cm intervals and bold, annotated contours every 100 cm. Pink  
20  
21 labelled dots show positions of ‘virtual tidal gauges’ in the East Weald Basin (EW), Isle of  
22  
23 Wight (IW), Leighton Buzzard (LB) and West Weald Basin (WW). Basin abbreviations: CCB –  
24  
25 Central Channel Basin; BCB – Bristol Channel Basin; BS – Bedfordshire Strait; CCB – Central  
26  
27 Channel Basin; PB – Pewsey Basin; WAT – Western Approaches Trough. Modified from [Wells](#)  
28  
29 [et al. \(2010b\)](#).

Field Code Changed



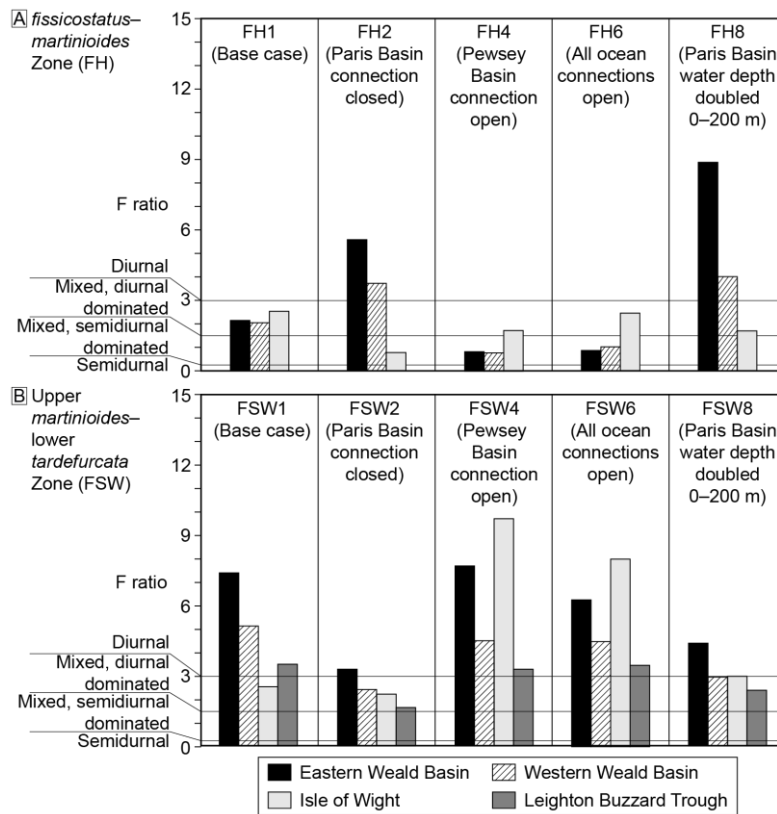


**Fig. 4.13.** Bar graphs of modelled tidal range at ‘virtual tide gauge’ locations (see Fig. 4.6 & 4.711 & 12) for base-case (Fig. 4.611) and sensitivity simulations (Fig. 4.712) for the *fissicostatus*–*martinioides* Zone (A) and upper *martinioides*–lower *tardefurcata* Zone (B) timeslices (respectively ‘FH’ and ‘FSW’ in Fig. 4.5D10D). Modified from Wells et al. (2010b) Wells et al. (2010b).

#### 4.2.5 Comparison with the Rock Record



Modelled tides for the *fissicostatus–martinioides* Zone ('FH' in Fig. 15D) predict microtidal conditions across most models (FH2, FH4 and FH6 scenarios; Fig. 17A, C, E) and low mesotidal in scenario FH8 (Fig. 17G). These results are broadly consistent with the time-equivalent sedimentary record, which contains little evidence of tidal influence on deposition (see review in Wells et al. (2010b)). In the western Weald Basin, putative tidal deposits in the uppermost part of this interval (Hythe Formation) are of limited areal extent and contain no published evidence of bidirectional currents or mud drapes (Casey, 1961; Narayan, 1971; Bridges, 1982; Ruffell and Wach, 1991; Rawson, 2006). This comparison supports modest tidal amplification and high microtidal–low mesotidal tides in the western Weald Basin (Figs. 16A and 17). The comparison also suggests that the connection between the Lower Greensand Seaway and Paris Basin may have been wider, which decreases amplification within the strait and increases tidal inflow into the seaway (see scenario FH7 in Wells et al. (2010b)).

Modelled tides for the upper *martinioides–lower tardefurcata* Zone ('FSW' in Fig. 15D) consistently predict high mesotidal to low macrotidal conditions across all model scenarios (Figs 16B, 17D, F, H, 18B), except when the Paris Basin is not connected (Fig. 17B). Closure of the Paris Basin connection may have occurred for a short time during a global eustatic sea level fall in the *jacobi* Zone, as indicated by a minor non-depositional or erosional hiatus (Fig. 15D) (Casey, 1961). Tidal deposits are widespread throughout the seaway at this time, including the following: (1) mudstone draped cross-bedding and brackish ichnofauna in the Sandrock Formation (Isle of Wight, English Channel Basin) (Ruffell and Wach, 1991; Insole et al., 1998; Rawson, 2006); (2) various combinations of large cross-sets (up to 15 m thick) with mudstone drapes (some double mudstone drapes), reactivation surfaces and bidirectional palaeocurrent

directions, wavy, flaser- and lenticular-bedded heterolithic toesets, and a shallow-marine ichnofauna in the Woburn Sands Formation ('Leigh Buzzard Trough') (Bridges, 1982; Johnson and Levell, 1995; Wonham and Elliott, 1996; Yoshida et al., 2004; Wells et al., 2010b), which are interpreted to preserve large migrating bedforms in tide-dominated estuaries and marine embayments (e.g. Yoshida et al., 2004); and (3) compound cross-bedded sandstones with abundant mud drapes, reactivation surfaces, spring-neap tidal bundles, heterolithics and a shallow-marine ichnofauna in the Folkestone Sands Formation (Weald Basin), which are interpreted to preserve tidal sand waves formed in a shallow sea (Allen, 1982a; Bridges, 1982). These deposits record deposition under strong tidal currents, with probable mesotidal to macrotidal ranges (Allen, 1981b), which is supported by palaeotidal model results (Fig. 17B and 18). Furthermore, the predicted diurnal-dominated tidal regime in the LGS in all modelled scenarios (Fig. 18) matches the interpretation of diurnal-dominated spring-neap tidal bundles in the Folkestone Sands Formation (Allen, 1981a; Allen, 1982a).

### **4.3—Late Cretaceous (Turonian–Cenomanian), Bohemian Cretaceous Basin, Central**

#### **Europe**

##### **4.3.1—Overview**

### 4.3 Local-scale controls on tidal deposition: Late Cretaceous (Turonian-Cenomanian), Bohemian Cretaceous Basin, Central Europe

#### 4.3.1 Background

The Bohemian Cretaceous Basin (BCB) ~~contains prominent tide-influenced shallow marine sandstones of Turonian to early Coniacian age (e.g. Jerzykiewicz and Wojewoda, 1986; Uličný, 2001; Uličný et al., 2009; Mitchell et al., 2010).~~ The BCB was a slowly subsiding, transtensional basin that ~~together linked~~ with other, ~~linked~~ basins ~~formed to form the~~ large and shallow ~~epicontinental sea across much of Europe~~ Mid-Cretaceous European Epicontinental Sea (MCEES) (e.g. Ziegler, 1990; Mitchell et al., 2010) (e.g. Ziegler, 1990; Mitchell et al., 2010)). As with the LGS example presented above, the BCB was far removed from coeval oceanic basins; over a thousand kilometres from the Neotethys Ocean to the southeast and the Proto-Atlantic Ocean to the west (Fig. ~~1914~~) (e.g. Ziegler, 1990; Mitchell et al., 2010) (e.g. Ziegler, 1990; Mitchell et al., 2010)). Several emergent landmasses lay in between these oceans and the BCB (Fig. ~~1914~~), such that boundary tides are likely to have been significantly blocked and damped by seabed friction (~~Mitchell et al., 2010~~) (Mitchell et al., 2010)). However, funnelling and shoaling effects ~~may have been important~~ in local-scale straits (c. 10s km wide) ~~may have been important~~ within the basin (Fig. 2015). In this context, two depositional models have been proposed for Turonian-to-early-Coniacian shallow-marine sandstones in the BCB. ~~Early models interpreted the sandstones as the deposits~~ An early model of large offshore bedforms sculpted by storms and tides (cf. tidal sand banks or ridges) ~~and accumulated in fault-bounded bathymetric depressions (e.g. Jerzykiewicz and Wojewoda, 1986) (e.g. Jerzykiewicz and Wojewoda, 1986)).~~ More recently, the sandstones were re-interpreted as the deposits of localised, ~~has been superseded by one of~~ top-truncated, coarse-grained deltaic shorelines that were reworked by tidal currents ~~in the basin (Uličný, 2001; Uličný et al., 2009) (Uličný, 2001; Uličný et al., 2009))~~; both models are discussed here.

Palaeotidal modelling ~~has been used in the MCEES and BCB~~ has focused on the early Middle Turonian interval ('TUR 2' genetic sequence of Uličný et al. (2009) with two ~~main~~ aims (Mitchell et al., 2010): (1) to understand how boundary tides from the Neotethys and Proto-

Atlantic oceans were expressed as tidal circulation in the BCB, by considering regional-scale (10–100s km) basin physiography (Fig. 14); and (2) to assess whether modelled tidal bed shear stress was capable of generating the grain-size distributions, bedform types and palaeocurrent orientations observed at local-scale (1s–10s km) in the Turonian-to-early-Coniacian shallow-marine sandstones (Fig. 15) (Mitchell et al., 2010). A dataset combining outcrops and densely spaced boreholes provides good constraint on the basin-fill thickness and syn-depositional physiography of the BCB (Uličný et al., 2009), which contained islands with intervening, 10s km-wide straits (e.g. ‘Elbe Strait’; Fig. 15). However, the physiography of many areas in the wider epicontinental sea is uncertain, with differences of up to 100 m water depth in basin centres outside the BCB (Fig. 14B–C) (Ziegler, 1990). Palaeotidal model simulations for the MCEES and BCB were forced with both astronomical ( $M_2$ ,  $S_2$ ,  $K_1$  and  $O_1$ ), and co-oscillating boundary tides adjacent to the deep, and expansive Proto-Atlantic and Neotethys oceans (Fig. 14) (Wells et al., 2007; Mitchell et al., 2010). The co-oscillating boundary tide was set in phase with the natural resonance at each respective boundary to give the maximum tidal potential in the seaway. Two sensitivity cases of tides in the MCEES were considered: (1) palaeobathymetric uncertainty was tested using ‘minimum’ and maximum’ depth scenarios (Fig. 14D, E); and (2) resonance of different tidal constituents was tested by imposing different boundary tides weighted towards semi-diurnal ( $M_2$ ,  $S_2$ ) and diurnal components ( $K_1$ ,  $O_1$ ). These regional-scale tidal simulations were subsequently investigated on a more local scale in the BCB.

#### 4.3.2 Geological Setting

Turonian to early Coniacian strata in the BCB were deposited shortly after peak eustatic flooding at the Cenomanian–Turonian boundary and the maximum extent of the Cretaceous

shallow epicontinental sea in Europe (Fig. 19) ([Hancock and Kauffman, 1979](#); [Ziegler, 1990](#); [Miller et al., 2003](#)). These strata record drowning of Cenomanian fluvio-estuarine deposits around the basin margin ([Uličný and Špičáková, 1996](#)), and the onset of open marine conditions throughout the BCB. Turonian and early Coniacian strata contain eight basinward thinning sandstone wedges ('TUR1-7' and 'CON1' genetic sequences of [Uličný et al. \(2009\)](#)), some of which terminate against or show abrupt thickness changes across syn-depositional faults ([Jerzykiewicz and Wojewoda, 1986](#); [Uličný et al., 2009](#)). Each wedge consists of several tongues, and the basinward-lying part of each tongue contains a single, basinward-dipping set of thick (up to 80 m), steeply dipping (up to 30°) foresets. Each tongue is interpreted to record the progradation of a coarse-grained, Gilbert-type delta from the basin margin, with delta topsets having been removed by later transgressive erosion ([Uličný, 2001](#); [Uličný et al., 2009](#)). Tidal influence was pervasive, as indicated by: (1) cross-bedded, coarse-grained sandstones with bidirectional palaeocurrents oriented parallel to the basin axis, commonly perpendicular to the delta-front foresets that contain the cross-beds; (2) reactivation surfaces in cross-bed sets; and (3) mudstone, siltstone and silty sandstone drapes, which are sometimes paired, along the foresets of cross-beds (e.g. [Jerzykiewicz and Wojewoda, 1986](#); [Uličný, 2001](#); [Uličný et al., 2009](#); [Mitchell et al., 2010](#)). A dataset combining outcrops and densely spaced boreholes provides good constraint on the basin-fill thickness and syn-depositional physiography of the BCB ([Uličný et al., 2009](#)), which contained islands with intervening, fault-bounded, local-scale (c. 10s km) straits (e.g. 'Elbe Strait' of [Mitchell et al. \(2010\)](#); Fig. 20). However, the physiography of many areas in the wider European epicontinental sea is poorly constrained ([Ziegler, 1990](#)). Consequently, modelled palaeobathymetric scenarios are similar for the BCB, but differ by up to 100 m water depth in other basin centres in the epicontinental European seaway (Fig. 19B–C).

Palaeotidal modelling work on the BCB has focussed on Early to Middle Turonian deltaic to shallow marine strata, which form the intermediate part of the 'TUR 2' genetic sequence of Uličný et al. (2009), and occur in three tectonically controlled depocenters: (1) the Lužice Jizera Sub-basin in the eastern Elbe Strait, fed by sediment sourced from the Western Sudetic Island; (2) the Ohře Ramp on the western flank of the Elbe Strait, fed by sediment sourced from the Most-Teplíce Palaeohigh; and (3) Orlice-Žďár Sub-basin, fed by sediment sourced from an unnamed palaeohigh at the south-eastern edge of the Central European Island (Fig. 20A). The Lužice Jizera Sub-basin records a major regressive episode in the TUR 2 genetic sequence, comprising a 20–35 m-thick delta-front clinoform set, which prograded into the up to ca. 40 m-deep Elbe Strait (Fig. 20B) (Uličný, 2001; Uličný et al., 2009; Mitchell et al., 2010). Palaeocurrent data from deposits representing early to intermediate regression of the TUR 2 deltas (i.e. the modelled interval) in the Elbe Strait and north-western Lužice Jizera Sub-basin indicate dominant palaeoflow towards the northwest (Fig. 20A; Uličný et al., 2009; Mitchell et al., 2010), while palaeocurrent data for late TUR 2 deltaic regression in the central Lužice Jizera Sub-basin indicate dominant palaeoflow towards the southeast (Uličný, 2001; Uličný et al., 2009). In the Ohře Ramp depocenter, TUR 2 clinoforms are mud-dominated with a large-scale sigmoidal geometry (Uličný et al., 2009; Mitchell et al., 2010). In the Orlice-Žďár Sub-basin, the correlative unit to the TUR 2 sequence in the Elbe Strait comprises erosively-based, channelised sandstones interpreted as tidal shoals deposited during a relative sea-level lowstand (Čech and Uličný, 1996).

**Formatted:** No Spacing, Left, Line spacing: single

palaeogeography for the Mid-Cretaceous European Epicontinental Sea (Ziegler, 1990; Dercourt et al., 2000; Golonka, 2004; Gil et al., 2006; Golonka et al., 2006; Golonka, 2007; Mitchell et al., 2010). The approximate outline of the Bohemian Cretaceous Basin (BCB) is shown in red. (c) Gross depositional environmental map of central-western mainland Europe for the Cenomanian–Turonian (from Ziegler, 1990). (D–E Regional palaeobathymetries for palaeotidal modelling of the Mid-Cretaceous European Epicontinental Sea (MCEES), showing major contours for (D) minimum and (E) maximum depth scenarios (after Mitchell et al., 2010). Red box shows the position of the BCB. Abbreviations: AM = American Massif; BCB = Bohemian Cretaceous Basin; BM = Bohemian Massif; C = Cracow Swell; CM = Cornubian Massif; CCM = Central Carpathian Massif; CSH = Corso-Sardinian High; EH = Ebro High; FH = Faeroe High; GH = Grampian High; HB = Hatton Bank; HP = Hebrides Platform; IbM = Iberian Massif; IM = Irish Massif; M = Moesia; MC = Massif Central; SP = Shetland Platform; R = Rodopes; RB = Rockall



Bank; RM = Rhenish Massif.

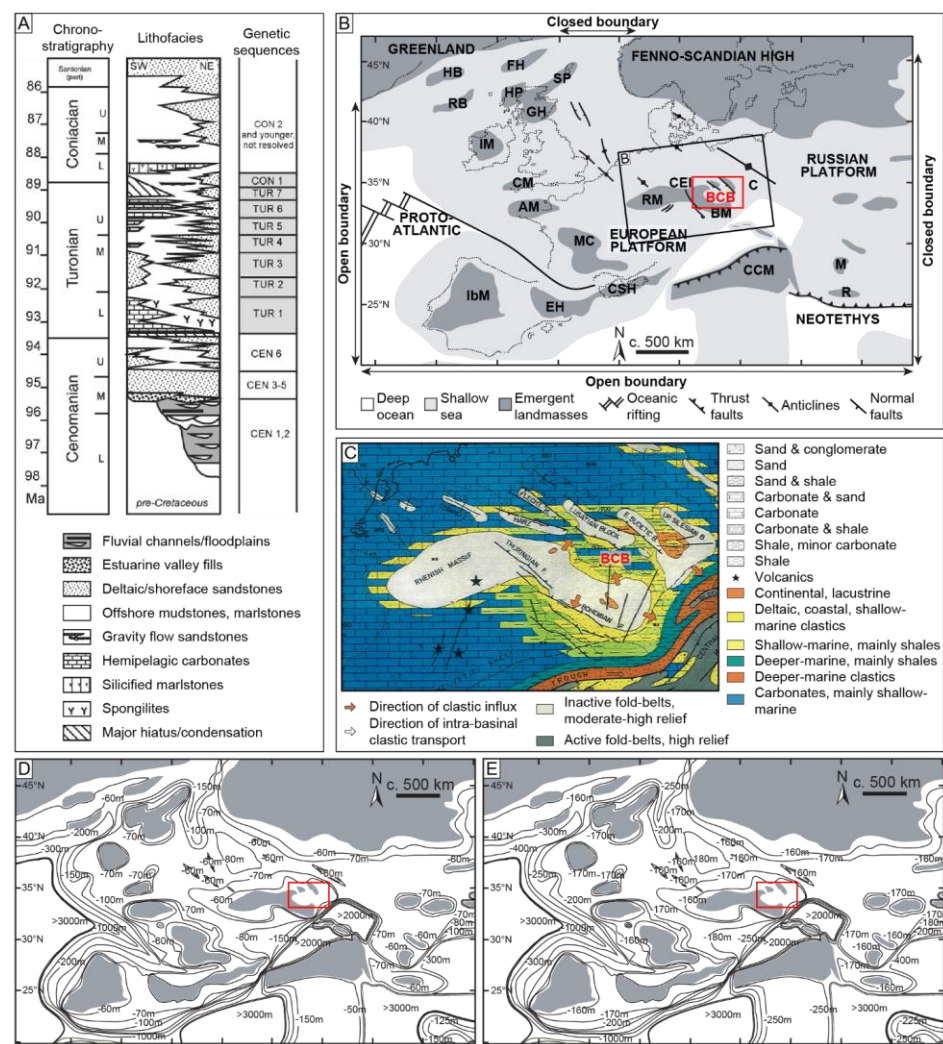


**Fig. 14.** (A) Stratigraphic chart showing the chronostratigraphy (modified after Ogg et al. (2004)Ogg et al. (2004)), main lithofacies in the Lužice Jizera Sub-basin (see Fig. 20A15A), genetic sequences recognized in this paper, and phases of basin evolution (after Uličný et al. (2009)(after Uličný et al., 2009). (B) Regional palaeogeography for the Mid-Cretaceous European

Epicontinental Sea (Ziegler, 1990; Dercourt et al., 2000; Golonka, 2004; Gil et al., 2006; Golonka et al., 2006; Golonka, 2007; Mitchell et al., 2010). The approximate outline of the Bohemian Cretaceous Basin (BCB) is shown in red. (c) Gross depositional environmental map of central-western mainland Europe for the Cenomanian–Turonian (Ziegler, 1990; Dercourt et al., 2000; Golonka, 2004; Gil et al., 2006; Golonka et al., 2006; Golonka, 2007; Mitchell et al., 2010). The approximate outline of the Bohemian Cretaceous Basin (BCB) is shown in red. (e) Gross depositional environmental map of central western mainland Europe for the Cenomanian–Turonian (from Ziegler, 1990) (from Ziegler, 1990). (D–E) Regional palaeobathymetries for palaeotidal modelling of the Mid-Cretaceous European Epicontinental Sea (MCEES), showing major contours for (D) minimum and (E) maximum depth scenarios (after Mitchell et al., 2010) (after Mitchell et al., 2010).

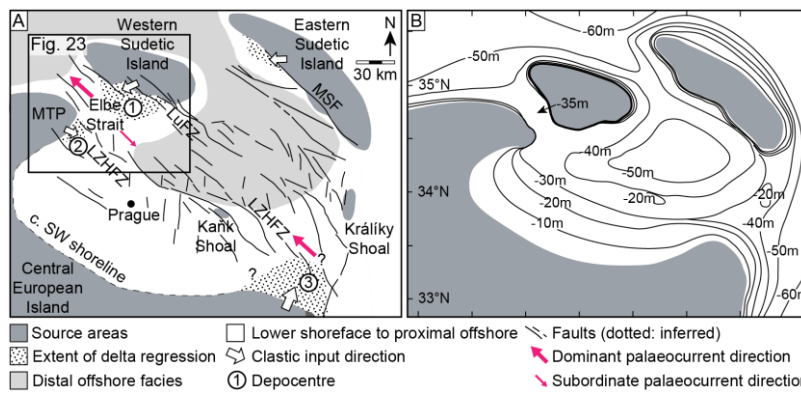


**Fig. 20.** Red box shows the position of the BCB. Abbreviations: AM – American Massif; BCB – Bohemian Cretaceous Basin; BM – Bohemian Massif; C – Cracow Swell; CM – Cornubian Massif; CCM – Central Carpathian Massif; CSH – Corso Sardinian High; EH – Ebro High; FH – Faeroe High; GH – Grampian High; HB – Hatton Bank; HP – Hebrides Platform; IbM – Iberian Massif; IM – Irish Massif; M – Moesia; MC – Massif Central; SP – Shetland Platform; R – Rodope; RB – Rockall Bank; RM – Rhenish Massif.

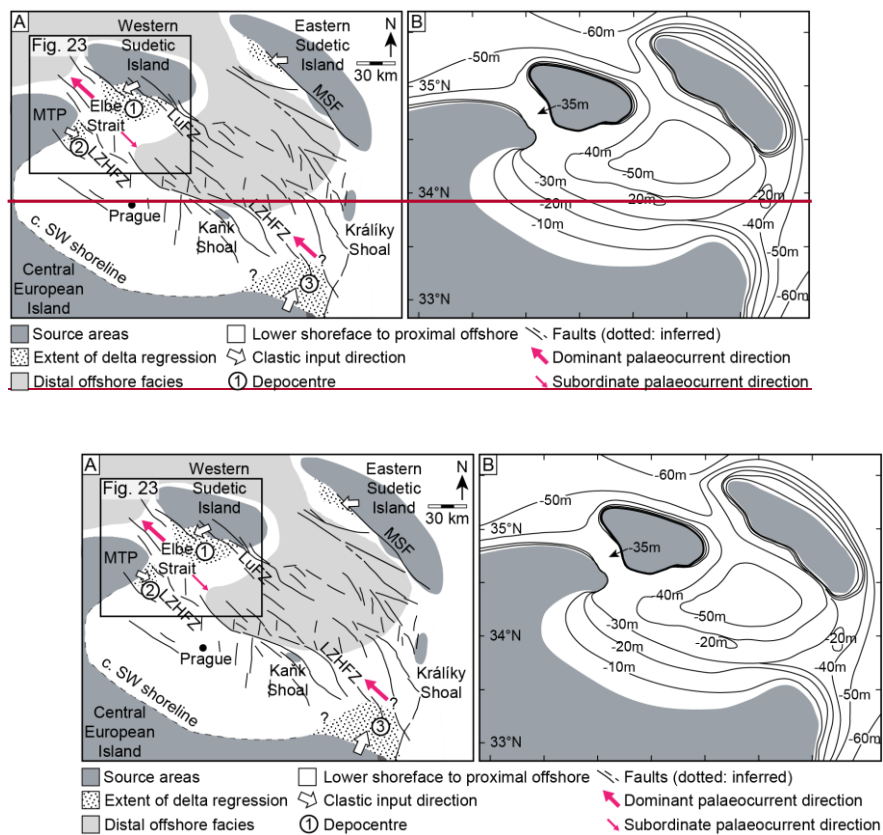


**Fig. 2015.** Local scale palaeogeography (A) and palaeobathymetric (B) for the early Middle Turonian Bohemian Cretaceous Basin (onset of *Collignoniceras woollgarii* Zone). The extent of deltaic depocenters correspond to intermediate regression of the ‘TUR 2’ siliciclastic wedge (see Fig. 19A). Circled numbers (1) to (3) indicate the three main depocenters: (1) the Lužice-Jizera Sub-basin; (2) the Ohře Ramp; and (3) the Orlice-Žďár Sub-basin. MTP – Most-Teplice Palaeohigh; LuFZ – Lužice (Lausitz) Fault Zone; LZHFZ – Labe-Železné Hory Fault Zone. Modified after (Uličný et al., 2009)(Uličný et al., 2009)). (B) Palaeobathymetric interpretation based on facies analysis of preserved outcrop and subsurface data (Uličný, 2001; Uličný et al., 2009)(Uličný, 2001; Uličný et al., 2009)). The heights of delta front clinoforms suggests

1  
2  
3  
4  
5  
6  
7  
8  
9  
10  
11  
12  
13  
14  
15  
16  
17  
18  
19  
20  
21  
22  
23  
24  
25  
26  
27  
28  
29  
30  
31  
32  
33  
34  
35  
36  
37  
38  
39  
40  
41  
42  
43  
44  
45  
46  
47  
48  
49  
50  
51  
52  
53  
54  
55  
56  
57  
58  
59  
60  
61  
62  
63  
64  
65

~~minimum depths of c. 35 m in the Elbe Strait, whereas a maximum depth of c. 50 m is estimated  
for the basin interior as inferred from trace fossil assemblages. After Mitchell et al. (2010).~~  
  
~~. The heights of delta-front clinoforms suggests minimum depths of c. 35 m in the Elbe Strait,  
whereas a maximum depth of c. 50 m is estimated for the basin interior as inferred from trace  
fossil assemblages. After Mitchell et al. (2010).~~

### 4.3.3 Model Setup

#### 4.3.4 Palaeotidal model simulations in the Mid-Cretaceous European Epicontinental Sea

(MCEES) results and BCB were forced with both astronomical and co-oscillating boundary tides with the four main tidal constituents ( $M_2$ ,  $S_2$ ,  $K_1$  and  $O_1$ ). To reduce the impact of uncertain co-oscillating boundary tides in the BCB, the regional-scale modelled domain covers much of the surrounding MCEES (Fig. 19). Open boundaries occur adjacent to the deep, expansive Proto-Atlantic and Neotethys oceans, whereas the boundaries adjacent to the extensive shallow seas of Arctic region and Russian Platform are unforced, because they are deemed unlikely to have had a significant tidal range (Fig. 19) (Wells et al., 2007a; Mitchell et al., 2010). The co-oscillating boundary tide is set in phase with the natural resonance at each respective boundary to give the maximum tidal potential in the seaway. This is determined by running a model with astronomical forcing, undertaking harmonic analysis of tidal amplitude time series collected at various points along the forced boundary, and interpolating the phase values at each point along the boundary so that the spacing between them matches the resolution of the mesh (Section 3.1.2) (Wells et al., 2007a; Mitchell et al., 2010). rock-record integration

Two sensitivity cases of tides in the MCEES were considered: (1) palaeobathymetric uncertainty was tested using two scenarios (Fig. 19D, E), and (2) resonance of different tidal constituents was tested by imposing different boundary tides weighted towards semi-diurnal ( $M_2$ ,  $S_2$ ; F ratio of 0.1) and diurnal components ( $K_1$ ,  $O_1$ ; F ratio of 10). All simulations included a spin-up period of five days and were run for a single spring-neap cycle lasting 14.8 days with a time step of 5

min. These regional-scale tidal simulations were subsequently investigated on a more local scale in the BCB.

#### 4.3.5 Model Results

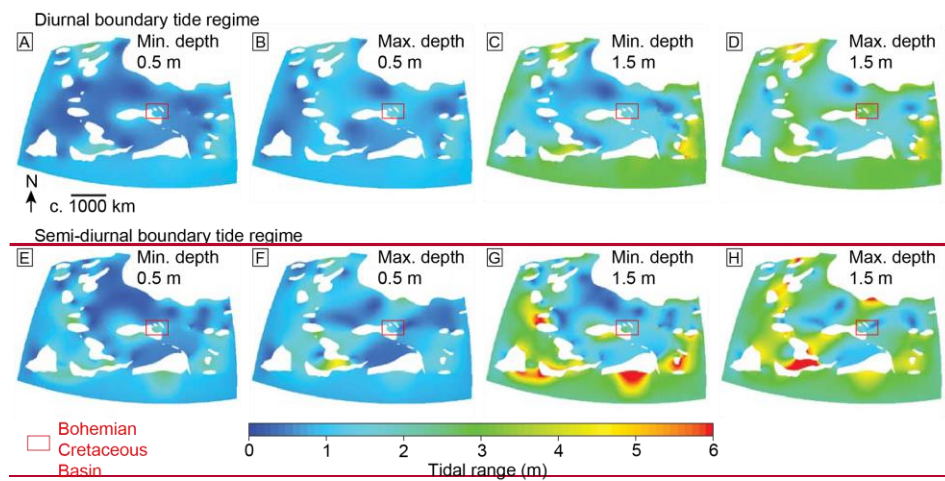
On a regional scale, modelled tidal range in the MCEES interior of the MCEES is consistently microtidal to mesotidal (Fig. 2416), which supports attenuation of the tidal wave by seabed friction and emergent landmasses as it propagated during propagation across the continental shelf (Shaw, 1964; Hallam, 1981; Wells et al., 2005a; Mitchell et al., 2010) (Shaw, 1964; Hallam, 1981; Wells et al., 2005a; Mitchell et al., 2010)). Tidal amplification forming macrotidal conditions is limited to embayments and straits. For example, macrotidal conditions are predicted on the southern margin of the Fenno-Scandian High (Fig. 21), but this only occurs with specific boundary and bathymetric conditions, consistent with the influence of tidal resonance (Fig. 7) (Wells et al., 2007a).

On a local scale, these results could be consistent with early interpretations of Turonian-to-early-Coniacian sandstones as large tidal bedforms, which do not necessarily require macrotidal conditions cf. (Stride, 1973; Stride, 1982; Jerzykiewicz and Wojewoda, 1986). Tidal amplification forming macrotidal conditions is limited to embayments and straits, however, this only occurs with specific boundary and bathymetric conditions, consistent with the influence of tidal resonance (Wells et al., 2007). Overall, these results more closely support a tide-influenced deltaic depositional model (Uličný, 2001; Uličný et al., 2009; Mitchell et al., 2010), in which fluvio-deltaic sediment supplied laterally from the basin margins was reworked along the basin axis by strong, locally constricted tidal currents. This model is similar to mixed fluvial and tidal deposition in other tidal straits (e.g. Longhitano and Steel, 2017; Rossi et al., 2017a).

~~At a local scale within the BCB, modelled tidal range also~~ On a local scale within the  
 BCB, modelled tidal range also varies from microtidal to mesotidal, ~~with elevated tidal ranges~~  
 mainly restricted to the embayed western and southern margins (Fig. 21). Modelled values of  
 (Fig. 16) and modelled maximum tidal bed shear stress ~~are~~ is consistently elevated ~~locally~~  
~~in~~ within palaeogeographic constrictions between islands, including the Elbe Strait (Fig. 17). All  
 modelled scenarios with forced boundary conditions generated maximum bed shear stresses in  
 excess of c.  $2.0 \text{ Nm}^{-2}$  in the Elbe Strait (Fig. 22). ~~Maximum bed shear~~ 17), which is capable  
 of forming 3D dunes in coarse sand in up to c. 20 m water depths. These predicted tidal  
 processes are more than sufficient to form the dm-scale cross bedding with common reactivation  
 surfaces, finer-grained foreset drapes (some in doublets) and WNW-dominated to bidirectional  
 palaeocurrents observed in age-equivalent sandstones within the Elbe Strait and north-western  
 Lužice-Jizera Sub-basin (Figs 20 & 22) (e.g. Harms et al., 1982; Jerzykiewicz and Wojewoda,  
 1986; Southard and Boguchwal, 1990; Uličný, 2001; Uličný et al., 2009; Mitchell et al., 2010).  
 Sensitivity analysis suggests that modelled maximum bed shear stress values ~~are slightly higher~~  
 for the diurnal regime compared to the semidiurnal regime (Fig. 22B, D), and significantly  
 increase ~~with increasing for a higher~~ boundary tide magnitude (Fig. 22A, 17A–B).  
~~Water~~ Furthermore, water depth in the regional seaway ~~also~~ influences the ~~predicted~~ modelled  
 maximum bed shear stresses locally in the BCB: modelled values are higher in the minimum  
 depth scenario for the semi-diurnal regime, but higher in the maximum depth scenario for the  
 diurnal tidal regime (Fig. 22C, 17C, D). This result suggests variations in resonance potential  
 between boundary tide and palaeobathymetry scenarios. ~~However, this inference is not shown in~~  
 the modelled tidal range (Fig. 21) or explained by simple models of tidal resonance (e.g. Fig. 7),  
 which indicate that slower and shorter wave semi-diurnal tides are typically closer to resonance



in deeper domains (Wells, 2008; Mitchell et al., 2010). Instead, these modelled bed shear stress patterns probably, likely a result from of relatively complex, constructive interaction between the different co-oscillating boundary tides and the relative depths of the otherwise unchanged domains (Mitchell et al., 2010)(Mitchell et al., 2010)). Nonetheless, instantaneous bed shear stress vectors in all models show clear northwest- and southeast-directed transport patterns in the Elbe Strait, consistent with measured palaeocurrent directions (Fig. 18) (Voigt and Tröger, 1996; Uličný et al., 2009; Mitchell et al., 2010)-.





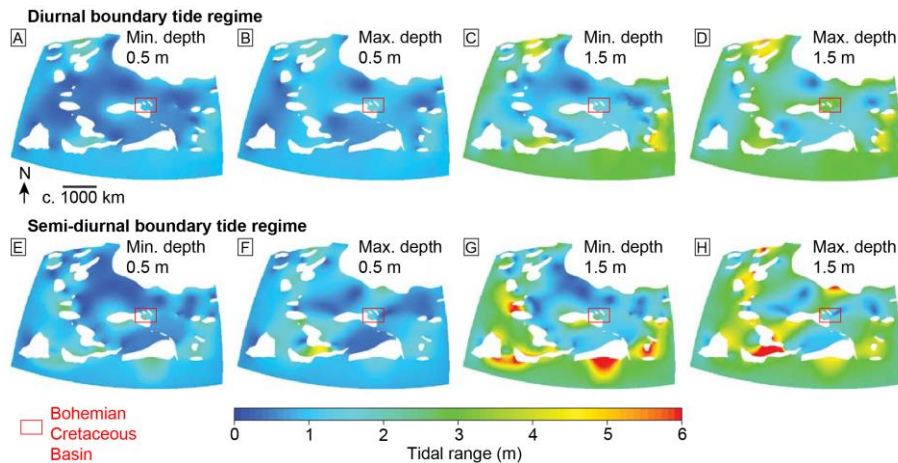


**Fig. 24-16.** Modelled tidal range in the Mid-Cretaceous European Epicontinental Sea (MCEES) for eight sensitivity tests for co-oscillating diurnal (A–D) versus semi-diurnal (E–H) boundary tide regimes, 0.5 m (A, B, E, F) versus 1.5 m (C, D, G, H) boundary tidal range, and minimum (min.) (A, C, E, G) and maximum (max.) (B, D, F, H) regional palaeobathymetry in the MCEES. Fluidity consistently predicts a microtidal to mesotidal range in the interior of the seaway, suggesting attenuation of the boundary tidal waves across the continental shelf by bed friction and blocking by emergent landmasses. After [Mitchell et al. \(2010\)](#).

Field Code Changed

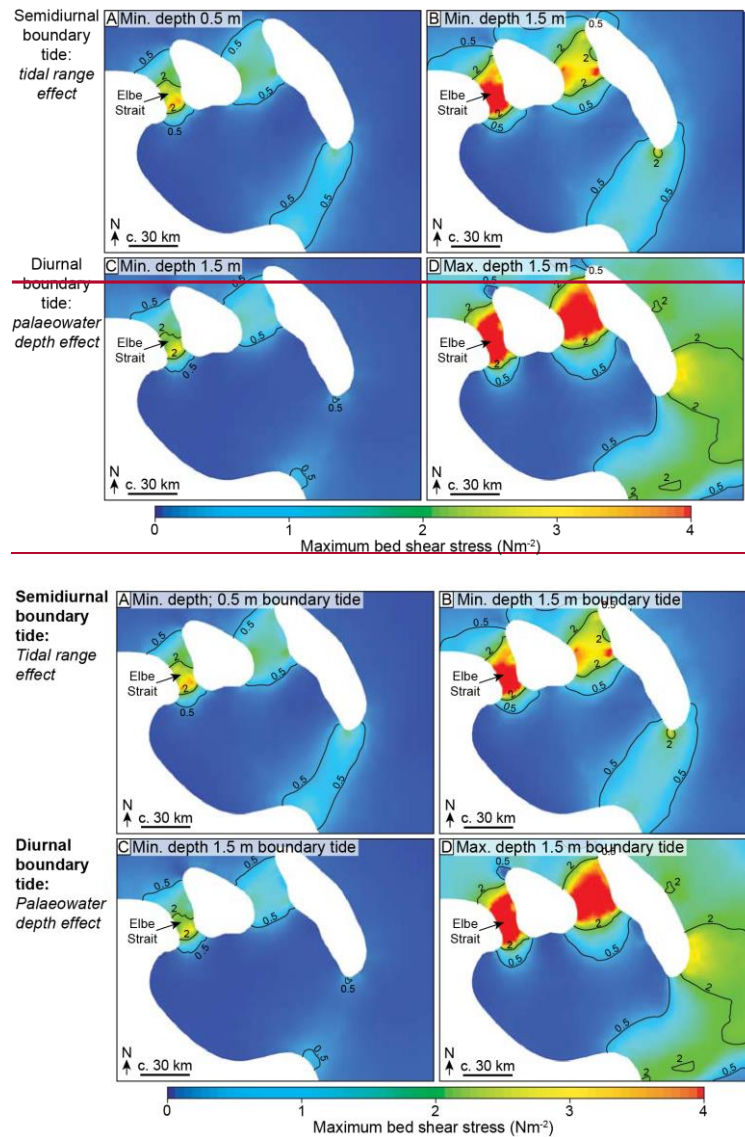


**Fig. 2217.** Modeled maximum bed shear stress in the Bohemian Cretaceous Basin. The 0.5 Nm<sup>-2</sup> contours show the approximate minimum bed shear stress required for the formation of dunes in coarse sand (Fig. 105) (Harms et al., 1982)(Harms et al., 1982)), whereas 1.0 Nm<sup>-2</sup> is the

approximate minimum bed shear stress required to form the observed scale of 3D dunes in coarse-grained sand in the Elbe Strait. Results for a 0.5 m (A) and 1.5 m (B) semi-diurnal boundary tide regime in the minimum (min.) depth regional palaeobathymetric domain (Fig. 19D, 14D) indicate that the modeled maximum bed shear stress is strongly dependent on the amplitude of the co-oscillating boundary tide. Results for the 1.5 m diurnal boundary tide regime in (C) minimum and (D) maximum (max.) regional ~~paleobathymetries~~palaeobathymetries indicate that the modeled maximum bed shear stress is strongly dependent on regional palaeobathymetry (Fig. 19D, 14D, E). After Mitchell et al. (2010) 19D, E). After Mitchell et al. (2010).

#### ***4.3.6—Comparison with the Rock Record***

~~At the regional scale, palaeotidal modelling demonstrates that it is plausible for boundary tides from the Neotethys and Proto-Atlantic oceans to have propagated into the BCB and influenced water circulation here during the late Cretaceous, even allowing for uncertainty in the physiography and boundary tides of the European Mid-Cretaceous European Epicontinental Sea (Fig. 21). Modelled tidal range in the BCB is microtidal to mesotidal, due to attenuation and blocking of the boundary tidal waves as they propagated from the open ocean. These results are inconsistent with early interpretations of Turonian to early Coniacian sandstones as large tidal bedforms (Jerzykiewicz and Wojewoda, 1986), which implies a macro-tidal regime (Stride, 1973; Stride, 1982). Modelled bed shear stress in the BCB is only sufficiently high to transport coarse sand where the shoreline is constricted along straits and embayments. These results support recent interpretations of a tide-influenced deltaic origin for the Turonian to early-Coniacian sandstones (Uličný, 2001; Uličný et al., 2009; Mitchell et al., 2010), in which fluvio-deltaic sediment supplied laterally from the basin margins was reworked along the basin axis by strong, locally constricted tidal currents.~~

Within the Elbe Strait and northwestern Lužice Jizera Sub-basin (Figs 20 & 22), the early to intermediate regressive part of the TUR 2 genetic sequence comprises an upward coarsening, 20-35 m-thick delta-front clinoform set that is dominated by coarse-grained sandstone. The dominant cross-bedding, including in gravelly sandstones to granule conglomerates, displays the following characteristics: (1) cross-sets 10 cm thick in the lower parts of the clinoform set and up to 30–40 cm thick in its upper parts; (2) tabular sets with abundant reactivation surfaces in the middle parts of the clinoform set; (3) silty, fine-grained to very fine-grained sandstone drapes occur locally on foresets; and (4) consistent WNW-directed palaeoflow in the lower to middle part and bi-directional trough cross-sets in the upper part of the clinoform set (Fig. 23) (Mitchell et al., 2010). These features indicate extensive reworking of the seabed by tidal currents with velocities in excess of  $0.6$  to  $0.8 \text{ ms}^{-1}$ , equivalent to bed shear stresses in excess of c.  $1.0 \text{ Nm}^{-2}$  (Fig. 10) (Harms et al., 1982; Southard and Boguchwal, 1990). All modelled scenarios with forced boundary conditions generated maximum bed shear stresses in excess of c.  $2.0 \text{ Nm}^{-2}$  in the Elbe Strait (Fig. 22), which is capable of forming 3D dunes in coarse sand in up to c. 20 m water depths. Instantaneous bed shear stress vectors in all models show clear northwest and southeast-directed bi-polarity in the Elbe Strait, in accordance with the flood and ebb of the tide, and consistent with recorded palaeocurrent directions (Mitchell et al., 2010). In contrast, maximum and mean bed shear stress vectors, which are time-averaged over each model run, lack a consistent pattern across the range of palaeogeographic sensitivity tests, and are instead highly sensitive to subtle changes in local palaeogeography (Mitchell et al., 2010). The range and variability of maximum and mean bed shear stress vectors in palaeogeographic sensitivity tests encompasses the dominant WNW-directed palaeocurrents from early to intermediate regression

of the TUR 2 deltas in the Elbe Strait and northwestern Lužice-Jizera Sub-basin (Fig. 23; Uličný et al., 2009; Mitchell et al., 2010) and also the dominant southeast-directed palaeocurrents from late regression of the TUR 2 deltas in the central Lužice-Jizera Sub-basin (Uličný, 2001; Uličný et al., 2009), but there are insufficient data to constrain detailed local palaeogeography such that a dominant tidal palaeoflow direction can be confidently predicted from model output (Mitchell et al., 2010). This result demonstrates the limitation of paleotidal modelling for prediction at a higher resolution than available geological data can support. In addition, the outcrop-scale detail of the extensive current modification of delta-front clinoforms recorded by the sedimentary structures represents the time-integrated record of local tidal reworking during specific increments of delta progradation at specific locations, at higher spatial resolutions and potentially lower temporal resolutions than palaeotidal model runs.

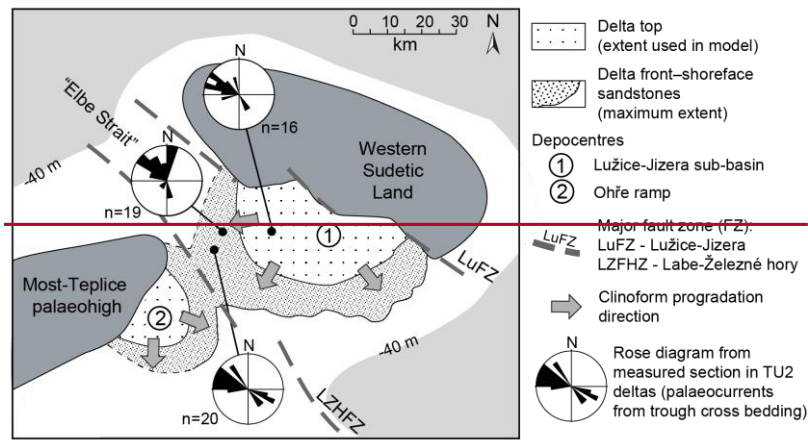


**Fig. 23.** Close-up view of the Elbe Strait area within the BCB (Fig. 20), showing the progradation extent and direction of sandy clinoforms (Voigt and Tröger, 1996; Uličný et al., 2009), and typical palaeocurrent rose diagrams for small-scale cross-sets in clinoforms recording

intermediate regression of TUR 2 deltas. Circled numbers indicate (1) the Lužice-Jizera Sub-basin; (2) the Ohře Ramp.

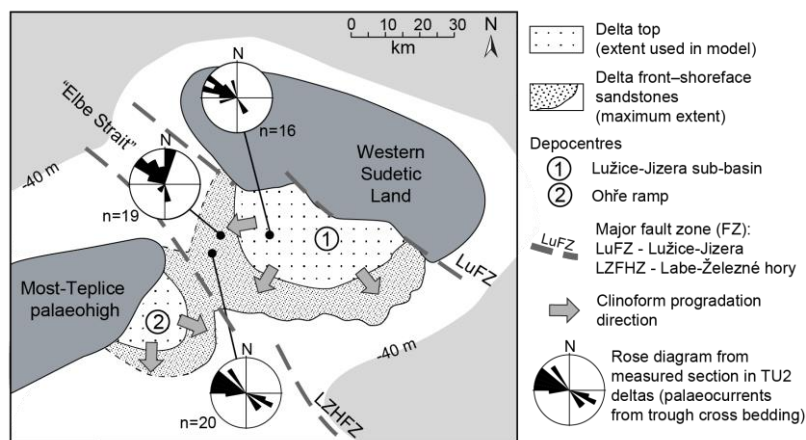


**Fig. 18.** Close-up view of the Elbe Strait area within the BCB (Fig. 15), showing the progradation extent and direction of sandy clinoforms (Voigt and Tröger, 1996; Uličný et al., 2009), and typical palaeocurrent rose diagrams for small-scale cross-sets in clinoforms recording intermediate regression of TUR 2 deltas. Circled numbers indicate (1) the Lužice-Jizera Sub-basin; (2) the Ohře Ramp.

## 5 DISCUSSION

### 5.1 Comparing ~~Tidal Model~~tidal model and ~~Rock Record Data~~rock record data

The comparison of palaeotidal model to rock-record data involves the evaluation of different data types with contrasting dimensions and spatial-temporal scales (Fig. 2419). This review has highlighted favourable comparisons between ~~(1)~~palaeotidal model predictions of tidal range (~~Wells et al., 2005a; Wells et al., 2007a; Wells et al., 2010a; Wells et al., 2010b; Collins et al., 2017a; Collins et al., 2018a; Dean et al., 2019~~) and tidal bed shear stress (~~Mitchell et al., 2010; Collins et al., 2017a; Collins et al., 2018a; Dean et al., 2019~~), with ~~(2)~~with the occurrence of tidally-influenced strata in the spatial and temporal domains of the ~~modelled areas, respective models~~. However, the comparison of palaeotidal model results and the time-equivalent rock record is limited by ~~several factors, three key challenges: (1) confidently recognising tidal influence in particular: (1) the rock record, (2) inferring ancient bed shear stress and, especially, tidal range, and (3) the spatial and temporal resolutions of the palaeogeographic data and related subsequent interpretations underpinning palaeotidal simulations (e.g. basin morphology, palaeobathymetry, gross depositional environments); and (2) the relationship between model outputs (e.g. palaeotidal range and bed shear stress) and interpretations of shoreline depositional processes and geomorphology based on rock record observations. These issues are discussed below.~~

#### 5.1.1 *Spatial and temporal resolution*

Palaeogeographic reconstructions underpinning palaeotidal simulations involve combining, simplifying and averaging multiple geological data types (e.g. sedimentological, biostratigraphic, seismic). Each data type contains uncertainties, especially the quality and resolution of age

Formatted: Line spacing: Double

Formatted: Heading 3, Line spacing: single

1  
2  
3  
4  
5  
6  
7  
8  
9  
10  
11 dating and geological interpretations (~~Markwick and Valdes, 2004~~)(Markwick and Valdes,  
12 ~~2004~~)). ~~The resolution of geologic data used to underpin palaeogeographic maps is user defined~~  
13 ~~and may vary depending on many factors, including available data and project aims.~~ With  
14  
15 increasing spatial extent, the minimum temporal resolution of the geologic data underpinning  
16  
17 palaeogeographic maps generally coarsens, becomes more variable and forms a composite ‘time-  
18  
19 slice’ rather than a single ‘time plane’ (Fig. ~~24A~~19A).  
20  
21  
22  
23  
24 Palaeotidal modelling provides areal (2D) and temporal data on three main parameters: (1) tidal  
25  
26 amplitude, (2) tidal range and (3) tidal bed shear stress (magnitude and direction of  
27  
28 instantaneous, mean and maximum values). In existing palaeotidal simulations, the maximum  
29  
30 spatial resolution of computational meshes is on the order of 10 km and the temporal  
31  
32 ~~resolution~~duration represented by a composite ‘timeslice’ (i.e. time interval) is typically c. 2–5  
33  
34 Ma (Fig. ~~24B~~19B and C). ~~However, the resolutions of model timeslices are often much broader~~  
35  
36 ~~and), but both~~ vary ~~significantly~~ on a case-by-case basis (Table 3). Rock record data is typically  
37  
38 one-dimensional (e.g. stratigraphic logs, core and well data), occasionally two-dimensional (e.g.  
39  
40 outcrop panels, well-log correlation panels, seismic cross-sections and maps) and rarely three-  
41  
42 dimensional (e.g. curvilinear and/or multiple outcrop panels, multiple and closely-spaced cores  
43  
44 and wells, 3D seismic volumes) (Fig. ~~24B~~19B). Such data may lie at spatial resolutions much  
45  
46 smaller than those of palaeotidal model meshes and model timeslices ~~(e.g. individual~~  
47  
48 ~~stratigraphic logs, cores, wells and outcrop panels)~~. It is possible to address the discrepancy in  
49  
50 spatial scales between rock record data and palaeotidal models by combining rock record data  
51  
52 from multiple locations, although such amalgamation of data should be carried out carefully so  
53  
54 as not to obscure important local patterns ~~(e.g. within the context of facies analysis carried out in~~



the hierarchical stratigraphic framework of [Vakarelov and Ainsworth \(2013\)](#), as outlined below).

For example, in paleotidal models of the Bohemian Cretaceous Basin (section 4. For example, in paleotidal models of the BCB (Section 3-3), instantaneous bed shear stress provides a more reliable model output for comparison with rock-record ~~paleocurrent~~ [paleocurrent](#) data than values of mean and maximum bed shear stress collated over multiple tidal cycles ([Mitchell et al., 2010](#)).

Facies modelling aimed at deciphering the relative influence of tide, wave and fluvial processes involves analysis at a wide range of scales, from facies (mm–m) to systems tracts (10–100s km) (~~Van Wagoner et al., 1990; Walker and James, 1992; Posamentier and Walker, 2006; Hampson et al., 2008~~)([Van Wagoner et al., 1990; Walker and James, 1992; Posamentier and Walker, 2006; Hampson et al., 2008](#))). [Vakarelov and Ainsworth \(2013\)](#). [Vakarelov and Ainsworth \(2013\)](#) have formalized this ~~range~~ [approach](#) for shoreline depositional systems into five stratigraphic hierarchical levels, each with different spatial resolutions and dimensions (Fig. ~~2520~~): (1) facies (element), a component of a depositional element; (2) facies association (element set), a depositional environment; (3) ~~parasequence (element complex assemblage)~~, a facies model for part of a depositional system; ~~(element complex assemblage)~~; (4) ~~parasequence or parasequence set~~ [a facies model for a whole depositional system](#) (element complex assemblage set); ~~a depositional system model~~; and (5) a transgressive-regressive ~~sequence or sequences, atongue or parasequence, which captures the temporal depositional system evolution of the facies model for a whole depositional system evolution model~~ [during one episode of shoreline advance and subsequent retreat](#) [model](#). Comparing tidal model and rock-record data most often occurs at the facies, facies-association and parasequence levels, and possibly ~~the~~ [at larger scales \(e.g.](#)

parasequence-~~set-level-1~~. This is due in part to data availability, but also because the variability in process dominance and preservation typically increases up the stratigraphic levels. For example, mixed-energy depositional systems (~~parasequence-set-level 4~~ and above) often comprise several depositional sub-environments (~~parasequence-level 3~~) with varying degrees of tide, wave and/or fluvial influence (~~e.g. Ainsworth et al., 2011; Vakarelov and Ainsworth, 2013~~)(e.g. Ainsworth et al., 2011; Vakarelov and Ainsworth, 2013)).

Deciphering the degree and extent of tidal influence is further complicated by incomplete stratigraphic preservation, including preservational bias. Tidal deposits may be preferentially preserved in a wide range of depositional environments ~~and with variable significance. For example, such deposits are often widespread in coastal embayments, but geographically restricted elsewhere, such as in tidal inlets within larger barrier lagoon systems. However, the maximum resolution of computational meshes used in palaeotidal modelling, especially for regional-scale studies, is significantly larger than the typical spatial dimensions of facies (mm-m) and facies associations (1–100s m) (Fig. 24B). Consequently, the comparison of model to rock record data may be biased by the preservation of tide-influenced deposits related to smaller-scale spatial and temporal changes in tidal processes, especially for depositional systems with limited rock record data and where data are selectively compared to model results. Hence, it is important to consider the potential for any preservational bias in the rock record regarding depositional processes. This could be highlighted by apparently unfavourable comparisons between model outputs and rock record data, but with variable extent and significance. For example, such deposits are often particularly significant in coastal embayments and at the mouths of fluvially incised valleys, but geographically restricted elsewhere, such as in tidal inlets~~

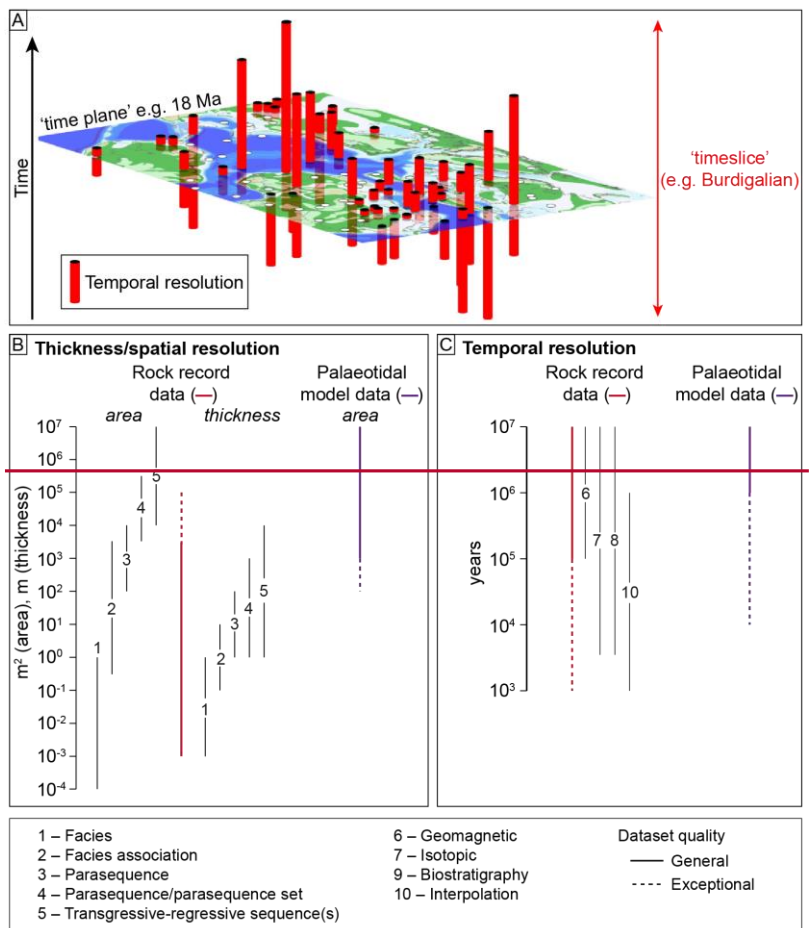
1  
2  
3  
4  
5  
6  
7  
8  
9  
10  
11 within larger barrier-lagoon systems. However, the maximum resolution of computational  
12  
13 meshes used in palaeotidal modelling, especially for regional-scale studies, is significantly larger  
14  
15 than the typical spatial dimensions of facies (mm–m) and facies associations (1–100s m) (Fig.  
16  
17 19B). Furthermore, across all spatial scales, the topographically lower components of these  
18  
19 depositional systems have higher preservation potential and, generally, their deposits tend to be  
20  
21 coarser grained (Dalrymple, 2010a). Hence there is an almost inevitable bias in the preserved  
22  
23 sedimentary and stratigraphic features indicative of certain depositional processes and sub-  
24  
25 environments. For example, in a mixed fluvial-tidal setting with channel-bar topography, fluvial  
26  
27 currents are likely to preferentially influence coarser-grained deposition in deeper channel axes,  
28  
29 with variable superimposed influence of tides, especially ebb tidal currents. These coarser-  
30  
31 grained deposits are likely to have a higher preservation potential compared to finer-grained,  
32  
33 typically more heterolithic and more strongly tide-influenced deposits of topographically higher  
34  
35 parts of tidal bars (e.g. Levell et al., 2020). Consequently, despite a depositional environment  
36  
37 reflecting mixed river and tidal processes, fluvially influenced deposits may be preferentially  
38  
39 preserved and the record of tidal deposition diminished. This is further supported by the frequent  
40  
41 paucity of intertidal deposits and dominance of subtidal deposits in many ancient tide-dominated  
42  
43 successions (Legler et al., 2013; van Cappelle et al., 2016; Archer et al., 2019; Collins et al.,  
44  
45 2020; Levell et al., 2020). Consequently, the comparison of model to rock-record data may be  
46  
47 biased by the varying preservation of tide-influenced deposits in relation to spatial and temporal  
48  
49 changes in depositional processes across a range of scales. These primary depositional biases are  
50  
51 further exacerbated where limited rock-record data is available in the present-day and where data  
52  
53 are selectively compared to model results.

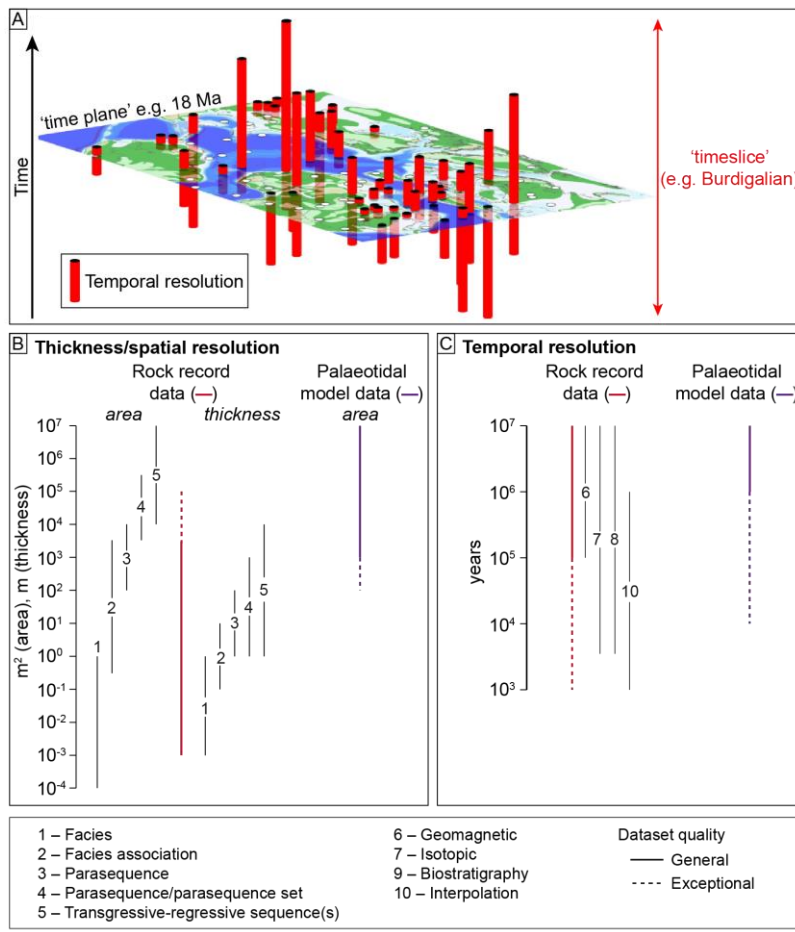
For one- and two-dimensional stratigraphic data, interpretation of areal depositional morphology and ~~up-sealing its relationship~~ to the depositional system scale ~~is~~are typically guided by comparison to process-based interpretations of modern shoreline environments (Fig. ~~25B~~20B). Process-based classifications of modern shoreline systems are principally based on 2D areal morphology, ideally supported by data on hydrodynamics and sediment type (~~e.g. Coleman and Wright, 1975; Galloway, 1975; Hayes, 1979; Boyd et al., 1992; Hori and Saito, 2007; Ainsworth et al., 2011; Nyberg and Howell, 2016~~)(e.g. Coleman and Wright, 1975; Galloway, 1975; Hayes, 1979; Boyd et al., 1992; Hori and Saito, 2007; Ainsworth et al., 2011; Nyberg and Howell, 2016)) and sedimentary facies characteristics (~~e.g. Ta et al., 2002a; Lambiase et al., 2003; Salahuddin and Lambiase, 2013; Fanget et al., 2014; Gugliotta et al., 2018~~)(e.g. Ta et al., 2002a; Lambiase et al., 2003; Salahuddin and Lambiase, 2013; Fanget et al., 2014; Gugliotta et al., 2018)). Hence, the 2D morphologies of end-member tide-, wave- and fluvial-dominated shorelines are embedded in ternary-process models of shoreline depositional systems (~~Ainsworth et al., 2011; Ainsworth et al., 2011; Vakarelov and Ainsworth, 2013; Vakarelov and Ainsworth, 2013; Nyberg and Howell, 2016~~)(Ainsworth et al., 2011; Vakarelov and Ainsworth, 2013; Nyberg and Howell, 2016).

~~The morphological characteristics of tide~~Tide-dominated shorelines typically display ~~the following morphological characteristics~~: (1) complex and intricately branching networks of funnel-shaped (seaward-flaring) tidal channels, (2) elongate tidal bars (mainly subtidal but often with subaerial tops), which partly infill tidal channels and often extend seaward from channel mouths, and (3) more extensive ('land-fringing') intertidal and supratidal areas with, depending principally on latitude, salt marsh or mangrove colonization (~~e.g. Ainsworth et al., 2011; Nyberg~~

and Howell, 2016)(e.g. Ainsworth et al., 2011; Nyberg and Howell, 2016)). Tide-dominated shorelines are more likely to be rugose to funnel shaped, and *vice versa*, whereas straighter shorelines are more likely to be wave-dominated, and *vice versa* (e.g. Fig. 2) (e.g. Ainsworth et al., 2011; Nyberg and Howell, 2016)(e.g. Ainsworth et al., 2011; Nyberg and Howell, 2016)). These generalized relationships are useful but oversimplified, especially when they are an intrinsic component of algorithms for classifying modern shoreline process regime (Nyberg and Howell, 2016)(Nyberg and Howell, 2016)). For example, this relationship does not include quantifiable variations in tidal range, tidal prism and/or tidal bed shear with shoreline rugosity, or complex related feedbacks (e.g. D'Alpaos et al., 2010)(e.g. D'Alpaos et al., 2010)). A more rigorous, albeit ambitious, approach for determining the process regime along shorelines would be to compare measured values of tidal strength (bed shear stress), tidal range, wave strength, wave height and fluvial discharge (Harris et al., 2002)(Harris et al., 2002)) with those from numerical models, preferably including data assimilation.

The temporal resolution of rock-record data is highly dependent on the methodology of absolute dating and the degree of interpolation between control ages (Fig. 24C19C). For example, in the Cretaceous of the Western Interior Basin of North America, an estimated temporal resolution of c. 200 ka has been achieved because high-resolution ammonite biozones have been calibrated to radiometric age dates (Obradovich, 1993)(Obradovich, 1993)) (Krystinik and DeJarnett, 1995)(Krystinik and DeJarnett, 1995)). In contrast, a paucity of absolute age dates in the Miocene–Pliocene Baram Delta Province, and the vast majority of similar Tertiary delta provinces around the world, means biostratigraphic zones have a temporal resolution of >1 Ma, based partly on correlation to adjacent basins with absolute ages (Sandal, 1996).

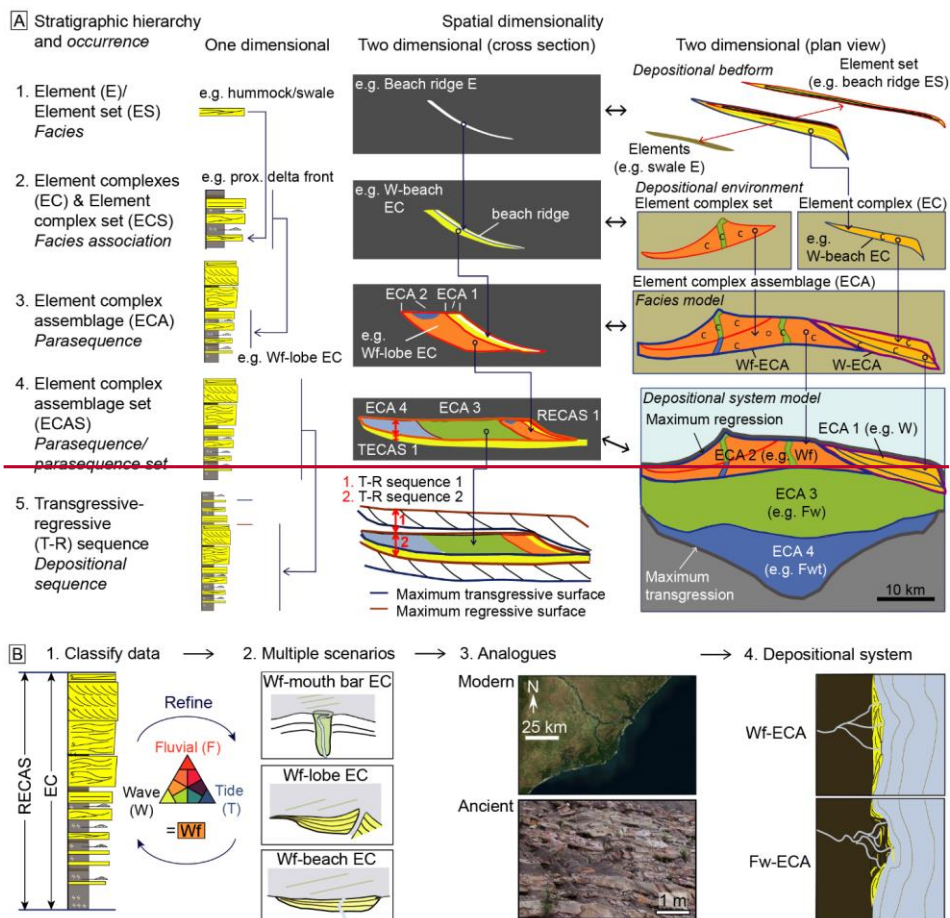




**Fig. 2419.** Variable resolution of palaeogeographic, tidal modelling and rock record data. (A) Illustration of the minimum temporal resolution of geologic data underpinning a palaeogeographic 'timeslice' (after [Markwick and Valdes, 2004](#)). Each data point is assumed to represent a single observation of equivalent area, but the temporal resolution of each point is generally variable (red cylinders), due in part to imprecise or uncertain dating and correlation. Defining a timeslice instead of a time-plane maximizes data density. (B) Thickness and spatial resolution of rock and model data. Rock data

are differentiated by general versus exceptional dataset quality: in this context, exceptional ~~being, for example, means~~ extensive and continuous outcrops or several tens of correlated cores and well logs. Numbers 1-5 represent ~~the~~ five hierarchical levels of rock data ~~(e.g. the “levels” of (or levels; e.g. Vakarelov and Ainsworth, 2013)(or levels; e.g. Vakarelov and Ainsworth, 2013)),~~ showing varying areal and thickness scales (see full text and legend in the bottom panel). Tidal model data is area based. (C) Temporal resolution of rock and model data-~~The inset (bottom panel) shows (i) the, showing (i)~~ five hierarchical levels of rock data ~~(Vakarelov and Ainsworth, 2013)(Vakarelov and Ainsworth, 2013));~~ (ii) the most common methods of absolute rock dating include geomagnetic, isotopic, biostratigraphy (calibrated to absolute dates), and interpolation between dates; and (iii) data quality types.





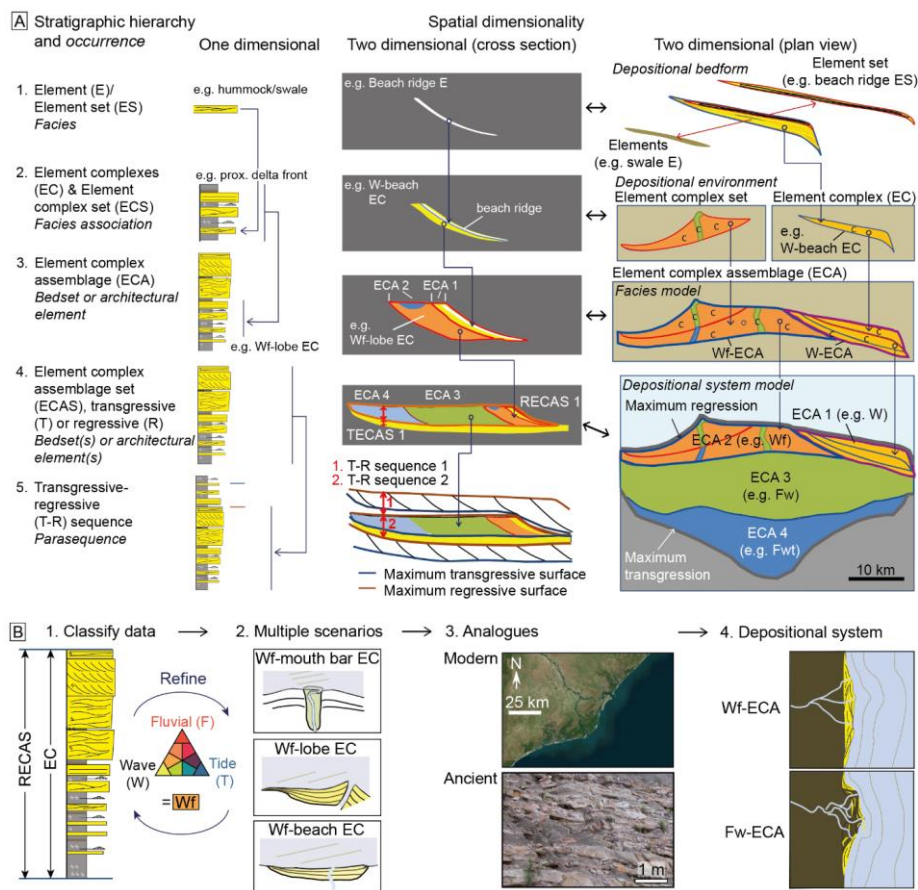


**Fig. 2520.** Scale and methodology of process classification and depositional model reconstruction (after Vakarelov and Ainsworth, 2013)(after Vakarelov and Ainsworth, 2013)).

(A) Five hierarchical levels of process-based architectural classification based on one-dimensional thickness and two-dimensional cross-section and plan-view data. For stratigraphic hierarchy levels 3 and 4, the stratigraphic occurrence–bedset(s) or architectural element(s) varies case-by-case.

(B) Simplified workflow for determining process depositional model from one-dimensional rock-record data. Refer to Figure 7 and Tables 2 and 3 in Vakarelov and Ainsworth (2013) Vakarelov and Ainsworth (2013) for further information.

### ~~5.1.1 Palaeotidal range and bed shear stress as proxies for depositional process regime~~

~~It is common for sedimentological and stratigraphic analysis of tidal range in the rock record to be limited to differentiating microtidal, mesotidal and macrotidal regimes (Wells et al., 2005a). Methods proposed for more detailed interpretation of palaeotidal range suffer from several assumptions and limitations (Section 3.2). In the present day, long-term tidal shoreline morphologies are related to the net exchange of water and sediment across the fluvial to marine transition zone, which is controlled by tidal range through its effect on the tidal prism (D'Alpaos et al., 2010). Furthermore, changes in tidal range and tidal prism impact the degree and physiography of tidal channelization, and vice versa (D'Alpaos et al., 2010). In mixed tide-wave systems, tidal range versus wave height is an approximate proxy for coastal energy regime and coastal morphology, especially for barrier islands (Hayes, 1979; FitzGerald, 1982; Davis and Hayes, 1984; Davis, 1994; FitzGerald et al., 1994; Anthony and Orford, 2002; McBride et al., 2013; Mulhern et al., 2017). However, coastal barrier morphologies in mixed tide-wave regimes are statistically indistinct from one another (Mulhern et al., 2017). Consequently, in ancient domains without quantitative information on both wave and tide processes, modelled palaeotidal range only indicates 'tidal potential'. Hence, coastlines with relatively high tidal ranges (i.e. high mesotidal to macrotidal) tend towards a 'higher potential' for tide dominance compared to coastlines with relatively low tidal ranges (microtidal to low mesotidal) and a 'lower tidal potential' (Wells et al., 2010a; Collins et al., 2018a). The precision of 'tidal potential' estimation is limited by the difficulties of quantifying tidal range from the rock record, and the complex relationships between tidal range, tidal dominance and shoreline morphology in the present day.~~

**Commented [CDSS22]:** This section has been deleted based on reviewer #1 recommendation

Tidal bed shear stress controls subaqueous sediment transport pathways and bedform distribution (e.g. [Stride, 1972](#); [Pingree and Griffiths, 1979](#); [Howarth, 1982](#); [Hulscher et al., 1993](#); [Ward et al., 2015](#)), but very few studies have compared tidal bed shear stress patterns to shoreline morphology (e.g. [Friedrichs, 1995](#); [Coco et al., 2013](#)). In models relating the tidal prism to equilibrium tidal channel physiography, the maximum bottom tidal shear stress equates to the critical threshold for incipient motion of sediment ([D'Alpaos et al., 2010](#)). At higher bed shear stresses, resultant bedform stability depends on the full range of flow conditions during transport and deposition (e.g. [Baas et al., 2016](#)). Consequently, modelled maximum palaeotidal bed shear stress, plotted as the equivalent transportable grain size based on critical bed shear stress thresholds, can be used as a proxy for tidal influence on sediment transport, bedform formation and shoreline morphology. This approximation is supported by favourable comparisons between model results and preserved sedimentary strata in earlier palaeotidal modelling case studies ([Mitchell et al., 2010](#); [Collins et al., 2017a](#); [Collins et al., 2018a](#)).

Bedform phase diagrams are predominantly based on laboratory experiments that use depth-averaged flow velocity or bed shear stress; narrow depth and grain size ranges; and the assumption that bedforms are in equilibrium with flow conditions (Figs. 10, 26A–B) ([Allen, 1968](#); [Rubin and McCulloch, 1980](#); [Allen, 1982b](#); [Harms et al., 1982](#); [Southard and Boguchwal, 1990](#); [Baas et al., 2016](#)). Bedform stability varies significantly with grain size and water depth, which has fundamental implications for comparison of modelled tidal bed shear stress and rock record data, and prediction of rock record characteristics based on modelled tidal bed shear stress. For a given water depth, if the minimum available grain size during deposition ('rock grain size') is finer than the potential grain size transportable by maximum strength modelled

tides ('model grain size'), the resultant bedform will be different from the equilibrium bedform (e.g. points V, X and Z; Fig. 26). For example, the resultant bedform may be in a different field (e.g. point V) or larger (e.g. point Z) (Fig. 26). If the minimum grain size available during deposition cannot be entrained by the modelled tides (Fig. 26C), tides will not influence bedform formation and sedimentary preservation (e.g. point Y; Fig. 26). The 'rock grain size' depends on the grain size available at the time of deposition, which is controlled by the geological and hydrological characteristics of the ancient source to sink system. The grain size range of available sediment is difficult to predict.

Bedform formation or type also varies significantly with water depth (Fig. 26A, B). For example, an increase in water depth from c. 20 cm to c. 20 m at point Z results increases the size of dune-scale cross bedding from decimetre to meter scale, but a similar increase in water depth at points U and W causes cessation of bedform formation (Fig. 26A, B). Comparing the preserved rock grain size and sedimentary structure to the model grain size can potentially be used to estimate water depth. For example, preservation of metre scale tidal cross stratification in coarse to very coarse sandstone in an area with sufficiently strong modelled tides would suggest a palaeowater depth of c. 20 m (e.g. point Z; Fig. 26). Alternative independent estimates of ancient water depth are extremely uncertain (e.g. Immenhauser, 2009).

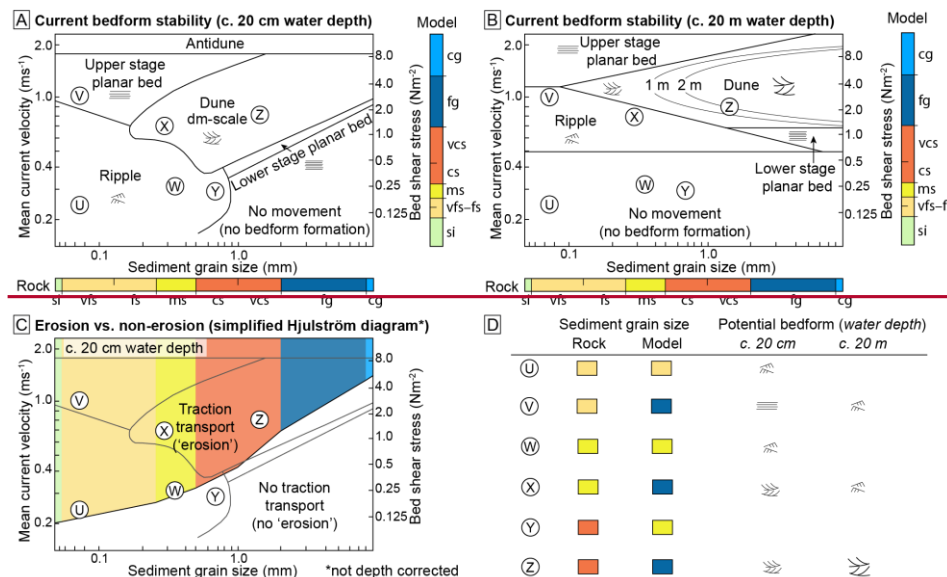


**Fig. 26.** The influence of current velocity, bed shear stress and sediment grain size on sediment traction, bedform stability and comparison of tidal model and rock record data. (A) Bedform stability diagram, including bed-shear stress, for unidirectional flow at c. 20 cm water depth (i.e. flume tank) (Harms et al., 1982; Mitchell et al., 2010). (B) Bedform stability diagram, including bed-shear stress, for unidirectional flow at c. 20 m water depth (Rubin and McCulloch, 1980). (C) Simplified Hjulström diagram constructed by plotting sediment grain size to threshold bed shear stress for sediment entrainment (Berenbrock and Tranmer, 2008) (Hjulström, 1939). (D) Simplified table of various plotted positions (U–Z) on the bedform stability and simplified Hjulström diagrams (A–C) comparing the rock record grain size to modeled grain size and the depth-dependence of potential bedform formation (or non-formation).

## 5.2 Controls on Tidal Processes tidal processes and Sedimentation sedimentation

### 5.2.1 Basin Physiography physiography

Formatted: Line spacing: Double

Formatted: Line spacing: Double

The influence of regional scale (100–1000s km) basin physiography on shoreline tides depends on the overall physiographic setting and regional scale physiography of the basin, and the influence of shelf width on tidal resonance.

Shoreline systems can be broadly subdivided into two physiographic categories. First, open-ocean systems directly face a typically large-scale (1000s km) open-ocean (e.g. modern Niger delta shelf facing the southern Atlantic Ocean). Second, partly enclosed systems face seas or oceans that are partly landlocked, have variable connectivity to an open ocean (s), and display a large variation in size (100s to 1000s km) (e.g. present-day North Sea). The case studies presented earlier (Section 4) are all partly enclosed systems.

For present-day open-ocean systems, there is no obvious systematic, qualitative relationship between tidal amplitude and latitude (e.g. Fig. 2). This is due to strong modification of tidal circulation by rotational, funnelling, shoaling and resonance effects, especially in shallower bathymetric areas and shoreline constrictions (Allen, 1997; Wells, 2008; Dalrymple and Padman, 2015). These effects are complicated and difficult to predict. However, numerical tidal modelling, such as shown here with Fluidity, integrates these effects and provides more rigorous and quantitative predictions of tidal potential in modern and ancient, open-ocean systems.

The overall physiography – size, shape and bathymetry – of the Earth’s global ocean, and constituent ocean basins (at present, the Pacific, Atlantic, Southern and Arctic oceans) is the first-order, largest-scale (1000s km) control on astronomical tides. A key consideration for understanding tidal processes and sedimentation along shorelines directly facing ocean basins (i.e. open-ocean shoreline systems) is therefore to estimate the influence of ocean-basin width and depth in controlling tidal resonance (Section 2.2.1). On geological timescales, of the order of



10s–100s Myr plate movements, ocean basins can move in and out of tidal resonant states in response to changing physiography (Green et al., 2017). For present-day open-ocean systems, there is no obvious systematic, qualitative relationship between tidal amplitude and latitude (e.g. Fig. 4) (Dalrymple and Padman, 2019). This is due to strong modification of tidal circulation by rotational, funnelling, shoaling and resonance effects, especially in shallower bathymetric areas and shoreline constrictions (Allen, 1997; Wells, 2008; Dalrymple and Padman, 2015; Dalrymple and Padman, 2019). These effects are complicated and difficult to predict. However, numerical tidal modelling provides a proven, robust method to understand the cumulative influence of these effects. This results in more rigorous and quantitative predictions of tidal potential in modern and ancient, open-ocean systems.

Shoreline systems facing water bodies that are partly enclosed by land, referred to herein as ‘partly enclosed’ systems, have variable degrees of connectivity to adjacent open ocean basin(s), and display a large variation in size (100s to 1000s km) (e.g. present-day North Sea). The case studies presented earlier (Section 3) are all partly enclosed systems. For partly enclosed systems, the foremost control on shoreline tides is the balance between the amount of tidal energy entering and exiting the basin – the tidal inflow and outflow (Fig. 27.21). Tidal potential is highest when tidal inflow exceeds outflow. Tidal inflow is mainly controlled by the physiography of the basin entrance(s) and the angle between the basin entrance(s) and tidal flow in the adjacent open ocean (Fig. 21A), which principally depends on latitude and Coriolis rotation (Leeder, 2011)(Leeder, 2011), and the physiography of the basin entrance (Fig. 27A). Tidal inflow will be relatively high where open-ocean tides flow directly towards the basin entrance, minimizing loss of tidal energy to frictional damping, and/or the entrance is relatively wide, deep and unobstructed (Fig. 27A.21A). Tidal outflow depends on the number, size, configuration and physiography of outflow connections (Fig. 27B.21B). Tidal outflow is highest if there are several multiple, wide, deep and unobstructed outflow connections (Fig. 27B). The



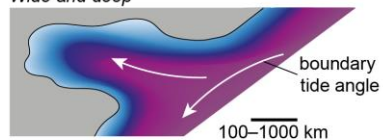
tidal energy distribution within partly enclosed systems depends on the relative ~~positioning~~ locations of inflow positions versus outflow positions and embayments, and the tidal flow dynamics within the basin. This point is clearly illustrated in palaeotidal modelling sensitivity tests of the Lower Greensand Seaway (section 4.2), in which the number and location of tidal inflow and outflow positions is varied (Fig. 4712).

Partly enclosed systems may also include relatively shallow (up to a few hundreds of metres) but wide (up to several 100s km) basins, for example, the present-day Baltic Sea and ancient epicontinental seaways. The physiography of these systems may also result in tidal resonance of the incoming boundary tide due to the tidal periodicity matching a natural oscillation frequency of water within the basin. Tidal resonance potential has been approximated for simple, rectangular-shaped, open-ended water bodies (Section 2.3; Fig. 4) but for (Wells, 2008). However, more complex ancient basin physiographies, palaeotidal modelling can be modelled to4) but for more complex ancient basin physiographies, palaeotidal modelling can provide quantitative information on integrated resonance potential for all tidal constituents.

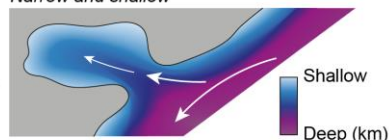
Regional-scale (100–1000s km) controls on tides (partly-enclosed basins)

**A** Inflow physiography

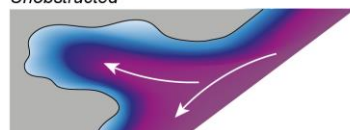
*Wide and deep*



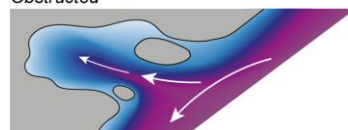
*Narrow and shallow*



*Unobstructed*

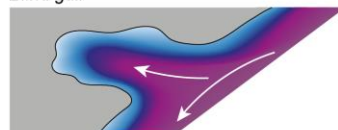


*Obstructed*

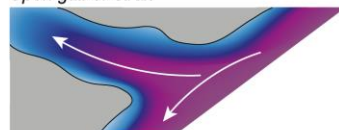


**B** Outflow configuration

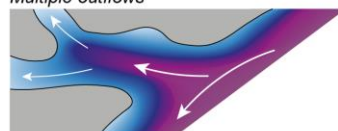
*Blind gulf*



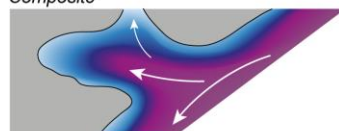
*Open gulf or strait*



*Multiple outflows*



*Composite*



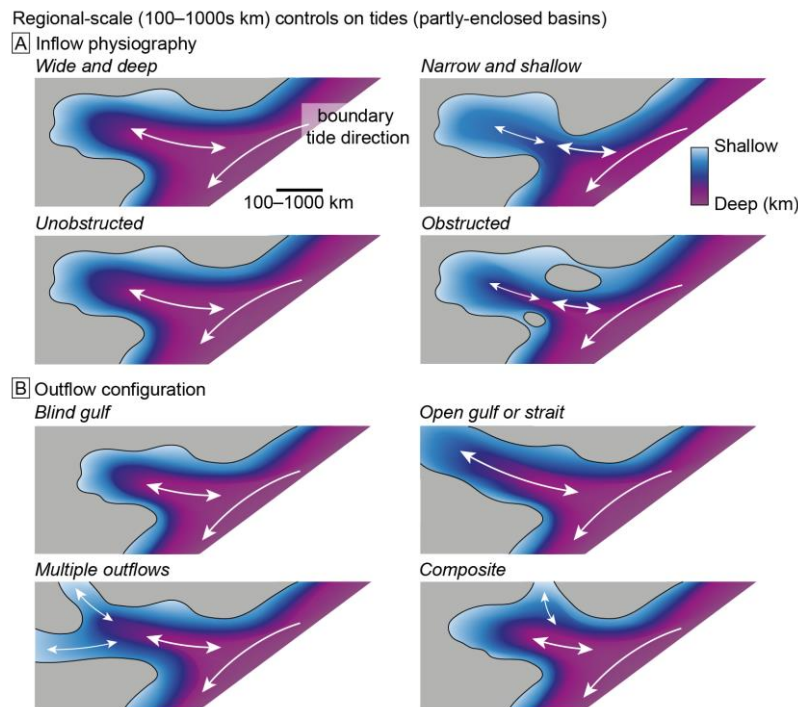


**Fig. 27.21.** Regional-scale (100–1000s km) basin physiographic controls on tidal energy potential in partly-enclosed basins, related to the balance ~~of~~in tidal energy flux into (inflow ~~versus~~) and out (outflow ~~-~~) of the partly enclosed basin. (A) The control of inflow physiography on tidal inflow includes the width, depth and degree of obstruction of the main tidal inflow position to the basin. Larger, thicker arrows indicate higher inflow-tidal energy flux into the partly enclosed basin. (B) The control of outflow physiography on tidal outflow includes the number, width, depth and degree of obstruction of main tidal outflow positions and their configuration with respect to the main tidal inflow positions and boundary tide pathway.

### 5.2.2 Tidal resonance on continental shelves

Funnelling, shoaling and resonance effects across continental shelves are ~~important~~ secondary widely recognised 10s–100s km-scale controls on tides- (sections 2.1.4 and 2.2.1).

Analysis of modern tides suggests that the relative importance of tides compared to wave and fluvial processes increases with shelf width perpendicular to the coastline (e.g. Redfield, 1958; Cram, 1979; Howarth, 1982; Ainsworth et al., 2011)(e.g. Redfield, 1958; Cram, 1979; Howarth, 1982; Ainsworth et al., 2011)). For example, analysis of 110 shoreline profiles surrounding Australia and 9 other global systems indicates that most wave dominated systems have shelf widths perpendicular to the coastline of <75 km, whereas most tide dominated systems have shelf widths >75 km (Heap et al., 2004; Ainsworth et al., 2011). This is principally due to an increase in tidal resonance (Howarth, 1982; Ainsworth et al., 2011) and shoaling effects, assuming sea-bed friction is ignored (Allen, 1997). Consequently, a 75 km shelf width is an approximate cut-off for high tidal resonance potential (>75 km) in predictive shoreline process models (Fig. 7).

However, it is important to consider potential variability in this relationship for ancient domains related to resonance theory, shelf width and regional controls. Simple resonance theory for straight, laterally extensive shelves with a boundary tide perpendicular to the shelf (Section 2.3) indicates that maximum tidal resonance occurs when shelf width is one quarter the tidal wavelength (and for widths 3/4, 5/4, etc.) (Fig. 3A and 28A–B). This is equivalent to several hundred kilometres for the dominant  $M_2$  and diurnal  $K_1$  tides (Fig. 3B) (e.g. Proudman, 1953; Howarth, 1982). In general, an increase in resonance potential with shelf width below one quarter tidal wavelength is partly offset by an increase in frictional drag (Fig. 28A–B). However, This is principally due to an increase in tidal resonance with shelf width (Section 2.2.1) (Howarth, 1982; Ainsworth et al., 2011), but some tidal energy will be lost to frictional drag on wider shelves (Allen, 1997). Furthermore, the relationship between shelf width, tidal range and

tidal dominance ([Nyberg and Howell, 2016](#)) varies globally due to changes in the following controls (Fig. [28C22](#)): (1) the relative amplitude of semi-diurnal to diurnal tidal constituents, which have significantly different wavelengths ([e.g. Kowalik and Luick, 2013](#))([e.g. Kowalik and Luick, 2013](#)); (2) the geometry of continental shelves; (3) the incidence angle of tides and tidal flow patterns, which partly relates to latitude and Coriolis rotation; and (4) frictional effects, which may exceed tidal amplification across wide shelves and seaways. Continental shelf width may change significantly on short geological timescales due to relative sea level changes related to global eustasy, isostatic adjustment, and tectonic subsidence and uplift ([e.g. Miller et al., 2005; Haq, 2014; Sames et al., 2016](#))([e.g. Miller et al., 2005; Haq, 2014; Sames et al., 2016](#)). Furthermore, within short-term eustatic sea level changes (10–100s ka), shelf width may change due to shoreline progradation, which is likely to be pronounced adjacent to major delta systems ([e.g. Burgess and Hovius, 1998; Hori et al., 2001; Ta et al., 2002a; Chamberlain et al., 2018](#))([e.g. Burgess and Hovius, 1998; Hori et al., 2001; Ta et al., 2002a; Chamberlain et al., 2018](#)). In addition, changes to regional-scale tidal flow can supersede the effect of shelf width changes on shelf tidal resonance. For example, despite a decrease in shelf width during 50 m sea-level lowstands, tidal range along northern SCS coastlines was higher during the Late Oligocene–Late Miocene because the boundary tide had a higher tidal range (section [4.1; Figs. 12, 133.1; Figs. 7, 8](#)). Likewise, resonance of the M2 tide in the modern Atlantic Ocean provides a higher boundary tide to the higher latitude Arctic Ocean (Fig. [4A12, 13](#)).

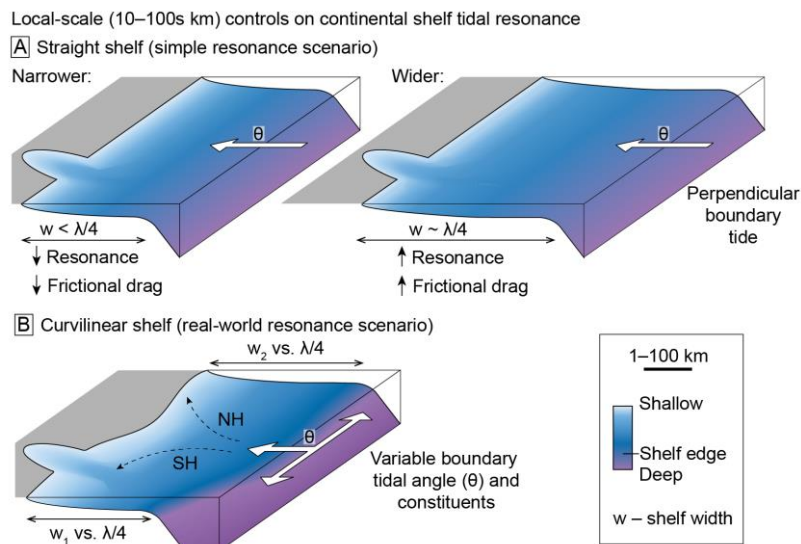


**Fig. 2822.** Local-scale (10–100s km) controls on continental shelf tidal resonance. (A–B) Simple resonance scenario for a straight shelf, perpendicular boundary tide and uniform shelf width ( $w$ ), where maximum tidal resonance occurs when shelf width is one-quarter the tidal wavelength ( $\lambda$ ) (cf. Fig. 3) (after Howarth, 1982) (after Howarth, 1982)). (C) A more realistic resonance scenario for a curvilinear shelf, variable angle ( $\theta$ ) and dominant tidal constituent of the boundary tide, Coriolis rotation and variable shelf width ( $w_1$  versus  $w_2$ ) compared to one-quarter the tidal wavelength. NH = Northern Hemisphere. SH = Southern Hemisphere.

### 5.2.3 Shoreline Geometry

~~Funnelling~~ Tidal amplification due to funnelling, shoaling and resonance effects in shoreline embayments are ~~tertiary~~ potentially very important smaller-scale (1–10s km) controls on tides (e.g. Slingerland, 1986; Dalrymple, 1992; Wells et al., 2007a; Ainsworth et al., 2011) (e.g. Slingerland, 1986; Dalrymple, 1992; Wells et al., 2007; Ainsworth et al., 2011)). ~~Protection from wave processes along embayed shorelines also increases the relative strength of tide and fluvial~~

processes (e.g. [Ainsworth et al., 2008](#); [Ainsworth et al., 2011](#); [Plink-Björklund, 2012](#)).

Consequently, increased shoreline rugosity is used as a proxy for increased tidal influence and decreased wave influence in predictive shoreline process models (Fig. 2) ([Ainsworth et al., 2008](#); [Ainsworth et al., 2011](#)). However, as outlined below, modern tides and palaeotidal modelling suggest that tidal amplification in coastal embayments is variable and depends on the balance between tidal amplification, ~~due to funnelling, shoaling and/or resonance effects,~~ and frictional damping.

Modern river-linked embayments (e.g. estuaries and interdistributary bays) are typically classified as either hyposynchronous, where tidal range decreases landward because frictional damping exceeds tidal amplification, or hypersynchronous, where tidal range initially increases landward due tidal amplification exceeding frictional damping, before decreasing to the tidal limit (~~e.g. [Godin, 1999](#); [Dalrymple and Choi, 2007](#)~~)(e.g. [Godin, 1999](#); [Dalrymple and Choi, 2007](#)). The degree of tidal amplification versus frictional damping can vary between adjacent embayments and show complex patterns within embayments, as seen along eastern North America and western India (Fig. ~~2923~~). Differentiating between ancient hypersynchronous and hyposynchronous embayments is difficult and requires interpretation of the process balance and extent of turbidity maximum zone in the fluvial-to-marine transition zone (~~e.g. [Gugliotta et al., 2016a](#)~~)(e.g. [Gugliotta et al., 2016a](#)). However, palaeotidal modelling can reveal spatial and temporal variations in tidal processes within ancient embayments. For example, as the entrance to the palaeo-Gulf of Thailand became wider and deeper during the Miocene, greater tidal inflow and reduced frictional damping shifted the tidal ~~maxima~~maximum landward (Fig. ~~127~~).

The relative strength of tidal amplification versus frictional damping depends on several factors:

- (1) The geometry and bathymetry of the embayment, especially its sinuosity (~~e.g.~~  
~~Slingerland, 1986; Allen, 1997~~)(e.g. Slingerland, 1986; Allen, 1997)). Frictional effects will be higher in more sinuous and rapidly shallowing embayments compared to straighter, gently shallowing embayments (Fig. 29, 30A23, 24A).
- (2) The geometry and bathymetry of the embayment entrance impacts inflow and outflow of tidal energy. A narrower, shallower and obstructed entrance increases dissipation and reflection of tidal energy (e.g. Mediterranean Ocean; Chesapeake Bay), whereas a wider, deeper and unobstructed entrance permits greater tidal inflow (e.g. Bay of Fundy) (Figs. 29, 30C23, 24C).
- (3) The angle between the embayment axis and incoming tide influences tidal inflow. Tidal inflow increases and frictional effects decrease when the incoming tide is more parallel to the embayment axis (Fig. 30B23, 24B).
- (4) Embayment physiography and the dominant tidal constituent control the resonance potential of embayment tides (Section 2.3).

Hyposynchronous embayments are more likely if the tidal inflow and resonance potential are low and frictional drag potential is high (Fig. 29A23A). Hypersynchronous embayments are more likely if tidal inflow and resonance potential are high and frictional drag potential is low (Fig. 29B23B). However, even if tidal amplification exceeds frictional effects, embayments may be dominated by fluvial or wave processes (Dalrymple, 1992).

Field Code Changed



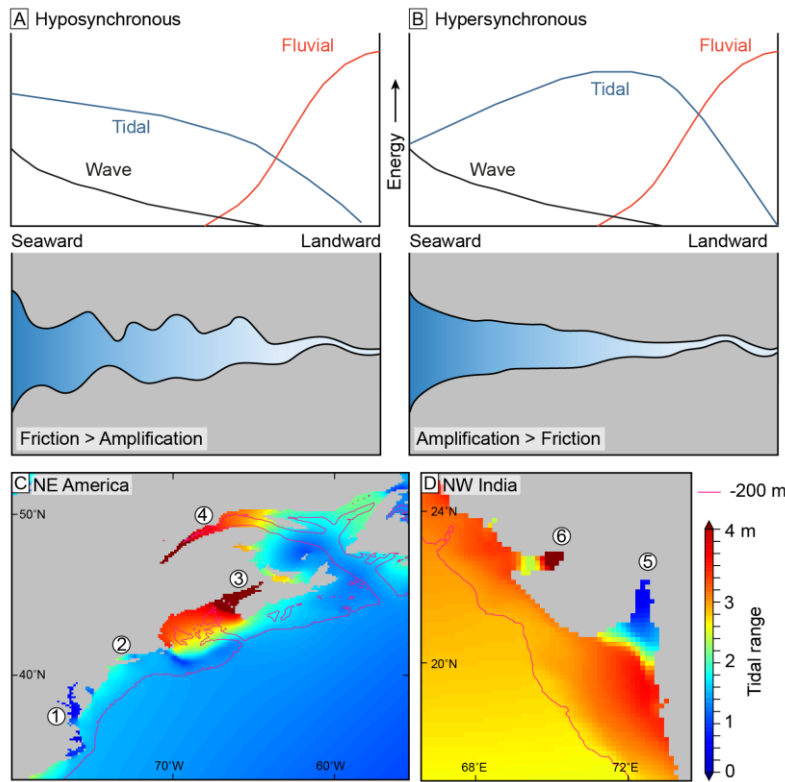


**Fig. 29.23.** Tides in shoreline embayments. (A) A hyposynchronous system in which frictional damping exceeds amplification of tides due to funneling, shoaling and resonance effect, resulting in a seaward to landward decrease in tidal range and tidal current speed. (B) A hypersynchronous system in which tidal amplification exceeds friction, causing a seaward-to-landward increase in tidal range and current speed, before friction causes tidal range and current speed to decrease to zero at the tidal limit (after Dalrymple and Choi, 2007). (C, D) Modeled tidal range from FES 2012 for north-east America (C) and north-west India (D) illustrating the varying relationship between tidal range and position within adjacent embayments: (1) hyposynchronous Chesapeake Bay; (2) moderately hypersynchronous Long Island Sound; (3) strongly hypersynchronous Bay of Fundy; (4) strongly hypersynchronous St.

Lawrence River mouth; (5) strongly hyposynchronous Gulf of Khambhat; and (6) complex hyposynchronous and hypersynchronous Gulf of Kutch.

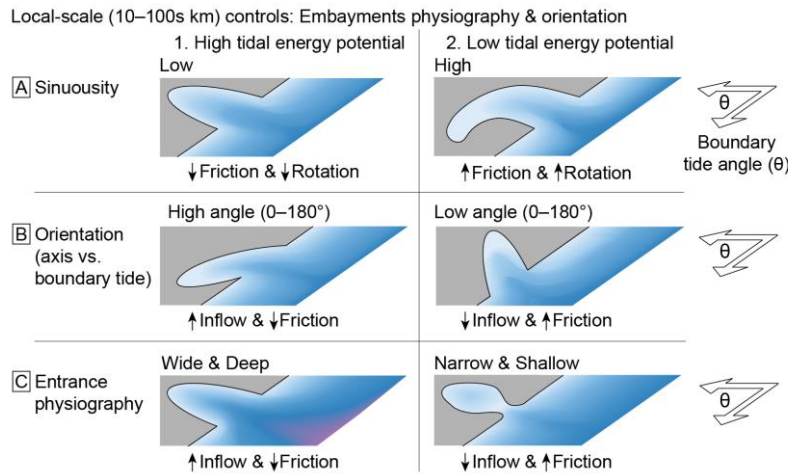


**Fig. 3024.** Physiographic controls on tides in shoreline embayments. A schematic matrix includes the influence of (A) shoreline geometry, for example, sinuosity and rugosity, (B) the relative orientation of the embayment axis and incoming tide, and (C) the physiography of the embayment entrance, on (1) high versus (2) low tidal energy potential within the embayment. Note this matrix excludes the influence of wave or fluvial processes.

### 5.3 Modified decision tree for prediction of shoreline processes—shelf depositional process regime

The original process-based, decision tree hierarchy for predicting shoreline-shelf systems uses the following sequential assessment procedure (Ainsworth et al., 2011) (Fig. 7A) of assessing 3A: (1) tidal resonance potential, wave versus (2) fluvial versus wave effectiveness, (3) low versus high A/S, (4) shoreline morphology geometry (relative degree of rugosity), and (5)

**Commented [CDSS23]:** Minor changes to this section include:  
-Including reference to the ocean-scale controls on tidal resonance  
-Discussing each hierarchical query in the revised decision tree sequentially, paragraph by paragraph, and explaining the omission of the A/S ratio query towards the end of the section

**Formatted:** Line spacing: Double

**Formatted:** Font: Bold

coastal process dominance. ~~Our evaluation proposes~~ (relative degree of fluvial, wave and tidal processes). ~~We propose~~ replacing this procedure with one that uses two decision trees, reflecting low and high wave energy potential, respectively. The procedure for using each decision tree comprises the following hierarchy (compare Figs. ~~7A3A~~ and ~~3426~~): (1) wave energy potential, (2) tidal energy potential, (3) shelf tidal resonance potential, (4) fluvial potential, and (5) shoreline geometry. The justification for this revision is outlined below, based on the preceding review of tidal theory, the physiographic influence on modern tides and present-day shoreline process regimes ~~(e.g. Nyberg and Howell, 2016)~~ (e.g. Nyberg and Howell, 2016), and the physiographic controls on tides highlighted by palaeotidal modelling studies and the ~~corresponding time-equivalent~~ stratigraphic record with preserved tidal ~~influence indicators~~.

The dominance of wave-dominated process regimes along present-day depositional shorelines (Fig. ~~62~~) ~~(Nyberg and Howell, 2016)~~ (Nyberg and Howell, 2016) supports this being the first-~~order control on decision for predicting~~-shoreline process regime (hierarchical query #1 in Fig. ~~3425~~). In modern systems, the height and strength of wind-generated surface waves are primarily controlled by the speed, duration and fetch of the wind ~~(e.g. Allen, 1997)~~ (e.g. Allen, 1997). Wave dominance also depends on the frequency of larger-magnitude storms-, overall meteorological conditions and the orientation of the shoreline relative to the wave-generating standing body of water. In ancient domains, determining the speed and duration of wind, and the effect on wave processes, would ideally require sophisticated analyses integrating palaeogeographic reconstructions and numerical climate and wave modelling. More generally, predicting wave energy potential along ancient shorelines relies on larger scale palaeogeographic reconstructions. If a system is open to a large water body or ocean, wave fetch and consequently

1  
2  
3  
4  
5  
6  
7  
8  
9  
10  
11 wave potential would be relatively high. Any protection that restricts access to oceanic waves  
12 will lower wave potential (~~e.g. Ainsworth et al., 2011~~)(e.g. Ainsworth et al., 2011)). Protection  
13 from ocean waves may be tectonic (e.g. emergent fault blocks, tectonically controlled seaways)  
14 or depositional (e.g. rugose coastal morphology, depositional headland, barrier islands,  
15  
16  
17  
18 ~~asymmetric~~asymmetrical deltas).

19  
20  
21  
22 The tidal energy potential of a basin (hierarchical query #2 in Fig. 3+25) is first dependent on  
23 whether the ~~basin is adjacent to an~~connected open ocean is at resonance with a particular tidal  
24 constituent (thus impacting the boundary tide amplitude), and second, whether the study area  
25 directly faces the open ocean or instead faces a partly enclosed water body. For systems facing  
26 an open- ocean-basins, tidal energy potential is assumed to be relatively high, given because of  
27 the relative lack of dissipation effects compared to partly enclosed systems. However, the  
28 absolute amount and distribution of tidal energy in an open-~~ocean basin is related~~relates to its  
29 ~~size, geometry and latitudinal distribution. For~~shape, bathymetry, which together determine  
30 ~~resonance, and only partly enclosed systems, relates to latitude (Dalrymple and Padman, 2019).~~  
31 As discussed (Section 4.2.1), the tidal energy potential in partly enclosed systems depends on the  
32 ~~balance of tidal energy~~ocean basin is related to its size, geometry and latitudinal distribution. For  
33 partly-enclosed systems, the tidal energy potential depends on the balance of tidal inflow versus  
34 outflow, ~~which is controlled by: (1) the relative orientation of the partly enclosed basin and~~  
35 ~~incoming tide; (2) the physiography of the basin entrance; and (3) the number, position and~~  
36 ~~physiography of outflow positions (Fig. 27). Tidal resonance may also be important in partly~~  
37 ~~enclosed systems of certain depth and geometry (Fig. 4)-21), as well as resonance (Section~~  
38 2.2.14).

Shelf resonance potential (hierarchical query #3 in Fig. 3+25) is related to shelf width and the dominant tidal constituent of the incoming tide (Figs. 3, 284, 23). Analysis of modern shoreline processes suggest a cut-off of c. 75 km between mainly tide-dominated (>75 km) and wave-dominated (<75 km) systems (Ainsworth et al., 2011)(Ainsworth et al., 2011)). However, tides only dominate on c. 50% of depositional shorelines associated with shelf widths of >75 km, with 47% being wave dominated (Fig. 62) (Nyberg and Howell, 2016)(Nyberg and Howell, 2016)). This suggests that a more representative shelf width threshold may be even higher, which would be closer to the theoretical shelf width for resonance of the typically dominant semi-diurnal M<sub>2</sub> or diurnal K<sub>1</sub> tidal components (Figs. 3, 28 Fig 23). However, without a more accurate and globally applicable cut-off value, the 75 km cut-off is retained in the proposed process prediction decision tree (Fig. 3+25). Nevertheless, this should be critically assessed on a case-by-case basis, considering other local geological factors.

Assessing fluvial potential (hierarchical query #4 in Fig. 3+25) relies on (1) measured or inferred drainage area, hinterland relief and rock types (e.g. Milliman and Syvitski, 1992; Syvitski and Milliman, 2007(Somme, 2009 #1471); (2) paleoclimate and its effects on water and sediment discharge (Hovius, 1998; Syvitski et al., 2003; Milliman and Farnsworth, 2011); (2) paleoclimatepaleoclimate and its effects on water and sediment discharge, and/or (3) observational evidence of fluvial influence in the rock record (Bhattacharya and Walker, 1992; MacEachern and Bann, 2008; Ainsworth et al., 2016); and/or (3) observational evidence of fluvial influence in the rock record (Bhattacharya and Walker, 1992; MacEachern and Bann, 2008; Ainsworth et al., 2016)(Bhattacharya and Walker, 1992; MacEachern and Bann, 2008;

Ainsworth et al., 2016). In general, large drainage basins would have higher fluvial potential than  
smaller drainage basins. However, anConversely, large rivers may have a disproportionate  
likelihood of being strongly tide influenced, or even tide dominated, at their mouth because of  
the larger tidal prism that is generated by the width of the river channel and its flat gradient,  
promoting long-distance penetration of the tide (Dalrymple, 2010b). An exception may be river  
systems with short, steep drainage basins subject to high rainfall storms, which often preserve  
river-influenced shoreline deposits (e.g. Bhattacharya and MacEachern, 2009; Collins et al.,  
2017b)(e.g. Bhattacharya and MacEachern, 2009; Collins et al., 2017b). The overwhelming  
dominance of wave- and tide-dominated shoreline morphologies along present-day coastlines  
indicates effective reworking of riverine sediment by marine processes (Fig. 6). However,  
sedimentary dynamics and deposition may still be dominated by river floods, even in deltas with  
lobate to cusped geometries typical of wave dominance (Rodriguez et al., 2000; Fielding et al.,  
2005; Gani and Bhattacharya, 2007)(Rodriguez et al., 2000; Fielding et al., 2005; Gani and  
Bhattacharya, 2007). Consequently, for ancient shoreline systems, any information suggesting a  
close proximity to a river system may suggest relatively high potential  
for river-influenced sedimentary dynamics and deposition influence (Fig. 3425. In general, large  
drainage basins would have higher fluvial potential than smaller drainage basins. However, an  
exception may be river systems with short, steep drainage basins subject to high rainfall storms,  
which often preserve river-influenced shoreline deposits (e.g. Bhattacharya and MacEachern,  
2009; Collins et al., 2017b). The overwhelming dominance of wave- and tide-dominated  
shoreline morphologies along present-day coastlines indicates effective reworking of riverine  
sediment by marine processes (Fig. 6). However, sedimentary dynamics and deposition may still  
be dominated by river floods, even in deltas with lobate-to-cusped geometries typical of wave

dominance (Rodriguez et al., 2000; Fielding et al., 2005; Gani and Bhattacharya, 2007).

Consequently, for ancient shoreline systems, any information suggesting a closely adjacent river system may suggest relatively high potential for river-influenced sedimentary dynamics and deposition (Fig. 31).

Shoreline geometry (hierarchical query #5 in Fig. 3425) mainly relates to the degree of rugosity, recognizing that tides are commonly amplified in many ~~present-day~~modern embayments and along embayed shorelines. However, ~~modern~~ embayments ~~along present-day shorelines~~ and those in palaeotidal simulations are not exclusively tide dominated (e.g. Figs. 6, 9, 342, 4, 26; cf. Fig. 2). ~~The 2) due to variations in the balance of between frictional damping and~~ tidal amplification ~~and frictional damping depends on the physiography and orientation of the~~ embayment (Fig. 30). ~~Tides may also undergo excess frictional damping compared to~~ amplification, due to funnelling, shoaling and/or resonance (as discussed in Section 4.2.3).

Embayed shorelines are also inevitably more protected from direct wave processes. However, wave processes may still be dominant along the back of moderately embayed shorelines, especially ~~adjacent to where~~ embayment mouths ~~with~~allow direct access to open ocean waves (Fig. 3425). In fluvially linked embayments, river processes may dominate over tides and waves (e.g. Dalrymple and Choi, 2007)(e.g. Dalrymple and Choi, 2007e.g. Dalrymple and Choi, 2007).

Therefore, shoreline geometry can have a variable potential influence on depositional processes.

The A/S ratio of a shoreline ~~selfshelf~~ system is a widely-used theoretical concept that links tectonics, eustatic sea-level change and sediment supply (Muto and Steel, 1997)(Muto and Steel, 1997)), and features prominently in the original process-based decision tree of Ainsworth et al.

(2011) (hierarchical query #3 in Fig. 7A-3A). However, A/S ratio has been removed from our revised predictive decision tree (Fig. 3025) due to limitations with the concept. For example, identifying relatively 'high' and 'low' A/S ratio relies on generalized relationships between A/S ratio and sequence stratigraphic systems tracts, which in turn relies on extensive datasets for sequence stratigraphic and/or shoreline trajectory analysis (Ainsworth et al., 2008)(Ainsworth et al., 2008)). Quantification of 'high' versus 'low' A/S ratios also relies upon sufficient well log, core and/or outcrop data to calculate the thickness of a sedimentary unit to approximate accommodation and the sand-to-shale ratio and approximate coarse sediment supply rate (Ainsworth, 2003; Ainsworth, 2005; Ainsworth et al., 2008)(Ainsworth, 2003; Ainsworth, 2005; Ainsworth et al., 2008; Ainsworth et al., 2018)). However, even if sufficient data are available, the exact ratios for 'high' and 'low' A/S regimes are yet to be determined. The reliance on available data and interpretations seriously limits reduces the applicability of the A/S ratio for predicting shoreline processes in ancient systems with, especially where data are limited data. Furthermore, the A/S ratio is a subordinate control on tides compared to the tidal energy potential of a basin, shelf tidal resonance potential and shoreline geometry. Process changes relating to A/S ratio only apply for moderately- to highly-embayed shorelines and relate to inferred are captured in changes to shoreline geometry (Section 1.2) (Ainsworth et al., 2011). In contrast We propose to replace the original three-tier process prediction scheme used in the original process-based decision tree of (Ainsworth, 2011 #345 @author-year) (Figs. 5A, 7A); we propose a 3A) (Ainsworth et al., 2011) with a two-tier process prediction scheme that is limited to reflects the primary and secondary processes (Figs. 5B, 31, 26). Analysis of modern shorelines suggests the thresholds for process classification in a three-tier scheme are can be

Field Code Changed



ambiguous (e.g. Fig. 62) (Nyberg and Howell, 2016)(Nyberg and Howell, 2016)). While a three-tier scheme has the superficial appearance of greater precision (Figs. 5A, 71A, 3) (Ainsworth et al., 2011)(Ainsworth et al., 2011)), it requires definitive process classification and quantitative analysis of potential quantification of formative processes for sedimentary structures that is rarely, if ever, availablepossible. At present, the range of mixed-process sedimentary structures and variability between different modern and ancient depositional systems are not yet fully documented or understood, leading to is incomplete, including ambiguities in the process interpretations of several sedimentary structures (Section 2.2) (e.g. Ainsworth et al., 2011; Dashtgard et al., 2012; Legler et al., 2014; Gugliotta et al., 2016a; Gugliotta et al., 2016b; Jablonski and Dalrymple, 2016; Rossi and Steel, 2016)-). A more holistic framework for interpreting mixed-process deposition and preservation would also include the effect of grain size availability on sedimentary facies characteristics and preservation, plus integration with a range of observational and interpretational techniques from both modern and ancient systems: (including numerical modelling).-However, the application of this understanding to such holistic analysis of the ancient record is still limited by several factors, includingnotably preservation bias in the rock record, dataset quality, and time available for data collection and process analysisstudy. The process prediction scheme proposed herein provides a quick, easily applied and robust interpretation of shoreline-shelf process regime to use, test and refine in subsequent studies. The scheme directly incorporates learnings from several numerical tidal modelling studies and can therefore be applied with a fair degree of confidence in the absence of potentially time-consuming and expensive numerical modelling.

# Decision trees for prediction of shoreline–shelf depositional process regime

## A Low wave energy potential:

### 1. Wave energy potential

### 2. Tidal energy potential

### 3. Shelf tidal resonance potential

### 4. Fluvial potential

### 5. Shoreline geometry

### Shoreline–shelf process regime

## B High wave energy potential:

### 1. Wave energy potential

### 2. Tidal energy potential

### 3. Shelf tidal resonance potential

### 4. Fluvial potential

### 5. Shoreline geometry

### Shoreline–shelf process regime

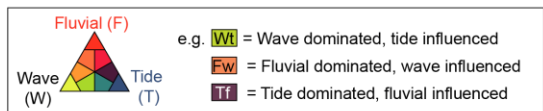


**Fig. 31. Proposed revision to decision trees for predicting shoreline process dominance (cf. Fig. 7A) (after Ainsworth et al., 2011)**

Decision trees for prediction of shoreline-shelf depositional process regime

**A Low wave energy potential:**

1. Wave energy potential

Low

2. Tidal energy potential

Low

High

3. Shelf tidal resonance potential

Low

High

Low

High

4. Fluvial potential

Low

High

Low

High

Low

High

Low

High

5. Shoreline geometry

SL ME HE

SL ME HE

SL ME HE

SL ME HE

SL ME HE

SL ME HE

SL ME HE

SL ME HE

SL ME HE

SL ME HE

SL ME HE

SL ME HE

Shoreline-shelf process regime

Wl Wt T

F F F

Tw Tw T

F F Tf

Tw T T

F F Tf

T T T

F F Tf

T T T

T T T

F F Tf

T T T

**B High wave energy potential:**

1. Wave energy potential

High

2. Tidal energy potential

Low

High

3. Shelf tidal resonance potential

Low

High

Low

High

4. Fluvial potential

Low

High

Low

High

Low

High

Low

High

5. Shoreline geometry

SL ME HE

SL ME HE

SL ME HE

SL ME HE

SL ME HE

SL ME HE

SL ME HE

SL ME HE

SL ME HE

SL ME HE

SL ME HE

SL ME HE

Shoreline-shelf process regime

Wl Wt Tw

Wl Fw Tf

Wl Tw Tw

Fw F F Tf

Wl Tw T

Fw F F Tf

Wl Tw T

Fw F F Tf

Tw T T

Tw T T

Fw Tw T

Fw Tw T

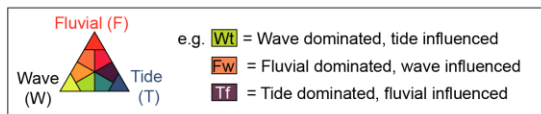


**Fig. 25. Proposed revision to decision trees for predicting shoreline process dominance (cf. Fig. 3A) (after Ainsworth et al., 2011) for systems with (A) low wave energy potential, and (B) high wave energy. The two decision trees each include five hierarchical queries: (1) wave energy**

1  
2  
3  
4  
5  
6  
7  
8  
9  
10  
11  
12  
13  
14  
15  
16  
17  
18  
19  
20  
21  
22  
23  
24  
25  
26  
27  
28  
29  
30  
31  
32  
33  
34  
35  
36  
37  
38  
39  
40  
41  
42  
43  
44  
45  
46  
47  
48  
49  
50  
51  
52  
53  
54  
55  
56  
57  
58  
59  
60  
61  
62  
63  
64  
65

potential of the basin; (2) tidal energy potential of the basin; (3) shelf tidal resonance potential;  
(4) fluvial potential; and (5) shoreline geometry. Key to ~~color~~colour coding is shown in the inset.  
Shoreline geometry abbreviations: SL-straight/lobate; ME-moderately embayed; HE-highly  
embayed.

Formatted: No Spacing, Line spacing: single  
Formatted: Font: 12 pt

## 6 CONCLUSIONS

Palaeotidal modelling investigations, integrating comparisons to the equivalent stratigraphic record, indicate that numerical tidal modelling can demonstrate the potential sensitivity of tides to physiographic uncertainty and potential influence of tidal processes along ancient shorelines. Present day global tidal measurements, and the spatio-temporal sensitivity of modelled ancient tides, indicate the following physiographic controls on tidal processes: (1) regional physiography (100–1000 km scale) controls tidal inflow versus outflow in partly enclosed oceans and seas; (2) shelf physiography (10–100 km scale), latitude, For shoreline–shelf systems, river, wave (including storm) and tide interactions are the primary determinants of sediment transport, morphodynamics and sedimentary preservation and are the cornerstones of process classification schemes. The preserved sedimentary record of these process interactions is widely interpreted, though the range of characteristics and corresponding process interpretation are debated and often ambiguous. Understanding the controls on river, wave and tidal processes benefits from an integrated approach combining numerical modelling and traditional facies analysis, which in turn improves prediction of shoreline–shelf processes classifications. We illustrate this approach in three case studies that combine palaeotidal modelling with process-based facies analysis of time-equivalent stratigraphy. The inferred controls on tides are discussed in the context of modern tidal processes and shoreline–shelf process regimes, resulting in a modification of predictive classification schemes for shoreline–shelf systems.

Tides are controlled by the following physiographic controls: (1) the impact of physiography – size, shape and bathymetry – on tidal resonance in the Earth's global ocean and constituent ocean basins (1000s km-scale), (2) in partly-enclosed water bodies, the physiography of ocean connections controls the balance between the amount of tidal energy entering and exiting the basin – the tidal inflow and outflow; (3) shelf physiography (10–100 km-scale) and the boundary tide orientation and dominant tidal constituent control shelf tidal resonance; and (34) embayment physiography (1–10 km-scale), especially at the entrance, and the relative orientation of the

**Commented [CDSS24]:** The conclusions have been completely rewritten to better reflect the rewritten abstract, introduction and restructuring of the paper, and summarise the intent: to review how predictions of modern and ancient shoreline-shelf process regime can be guided by insights from numerical modelling (with palaeotidal modelling as an example)

**Formatted:** Line spacing: Double

**Formatted:** Line spacing: single, Font Alignment: Auto

incoming tide, control tidal amplification (funnelling and shoaling) versus frictional effects in shoreline embayments. ~~However, validation~~ Validation of palaeotidal simulations using the rock record requires observations and process interpretations across a range of scales, from facies to depositional sequences, ideally integrating diverse data types. However, the validation is limited by ~~the difficulty in determining~~ three main uncertainties: (1) ancient tidal range prediction from stratigraphic data ~~and variability in;~~ (2) determining the relationship between bed shear stress, grain size and bedforms (and processes of primary sedimentary structures)-, and (3) preservational bias in the stratigraphic record. In contrast, numerical modelling of tides and other hydrodynamic processes are uniquely powerful tools in providing quantitative insights into the nature and intensity of ancient hydrodynamic processes. We show how this can significantly reduce ambiguities in palaeoenvironmental interpretations in a range of contrasting geological settings.

The overwhelming dominance of waves along modern shorelines indicates existing ~~predictive models for shoreline-shelf process regime-models~~ overstate the role of tides relative to waves. ~~This supports the proposed revised model for classifying and predicting modern and ancient shoreline process regimes, capturing the relative influence of fluvial, tide and wave processes.~~ ~~Our revised model includes the first-order control of~~ We propose a modified classification scheme for shoreline-shelf process regime that places wave fetch and associated meteorological conditions, ~~and improved understanding of physiographic controls on tides from as the first-order control,~~ with two initial strands for low and high wave energy potential, respectively. These two decision trees each include five hierarchical queries: (1) wave energy potential of the basin; (2) tidal energy potential of the basin; (3) shelf tidal resonance potential; (4) fluvial potential; and (5) shoreline geometry. The tidal prediction elements of both decision trees can be significantly enhanced by calibration with numerical tidal palaeotidal modelling. ~~However, determining,~~ as demonstrated by the case studies.

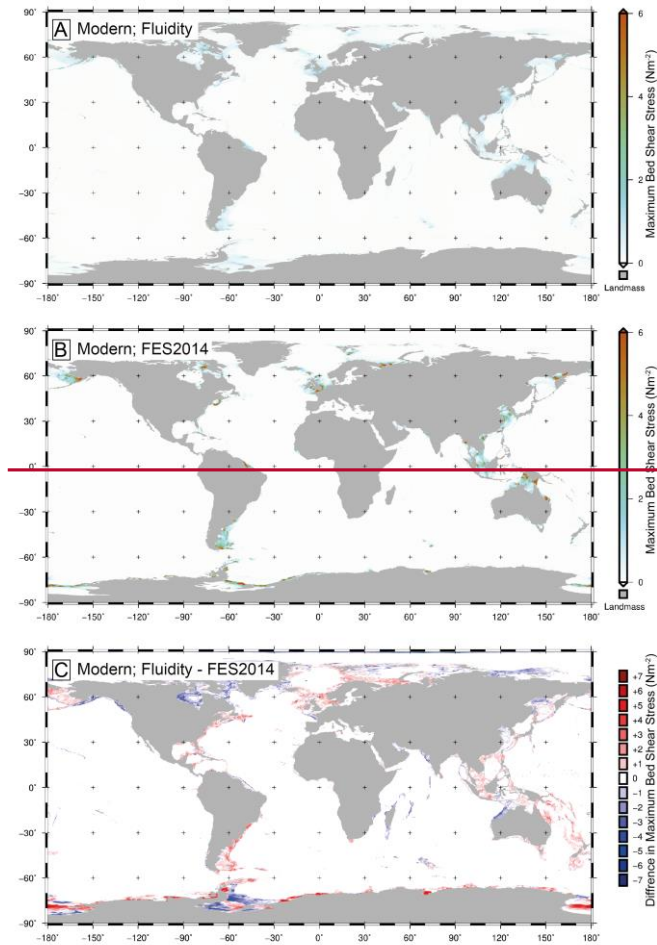
Determining process regime from ancient shoreline successions ~~is~~continues to be limited by ~~several factors that are undergoing renewed investigation, including: (1) the quality and availability of rock record data; (2) two critical aspects: (1) uncertainty and biases in the process classification of common sedimentary structures; (3) grain size controls on formation and preservation of sedimentary structures; and (4) and (2) skewed preservation of certain depositional processes in different environments and on different timescales. These uncertainties and limitations aspects, combined with these the challenges in classifying unravelling modern mixed-process modern shorelines, lead us regimes, lends support to advocate a two-tier approach to, rather than a three-tier, process classification of shoreline-shelf systems (identifying, in which emphasis is placed on only primary and secondary processes), but wider and consistent. Wider utilisation of these concepts is required to demonstrate their applicability this simpler yet robust predictive classification should enable more consistent and structured comparisons between ancient shoreline-shelf systems.~~

## ACKNOWLEDGEMENTS

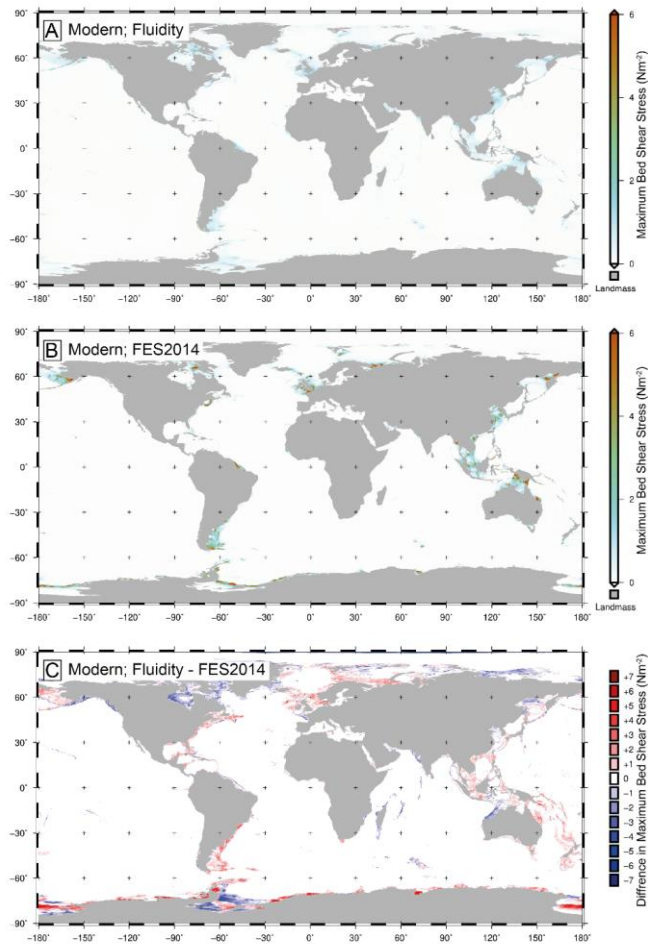
The authors acknowledge financial support from Natural Environment Research Council (NERC), Leverhulme Trust, Shell International Exploration and Production, and the Academy of Sciences of the Czech Republic. The authors thank Bob Dalrymple and Zheng Zhou for thorough, constructive reviewers and Jingping Xu for editorial comments. We also acknowledge support of Getech and Imperial College's Grantham Institute and High-Performance Computing Service. D.M. Hodgson, B.K. Levell, R.B. Ainsworth and B.K. Vakarelov are thanked for valuable comments and discussion.

Formatted: Line spacing: Double

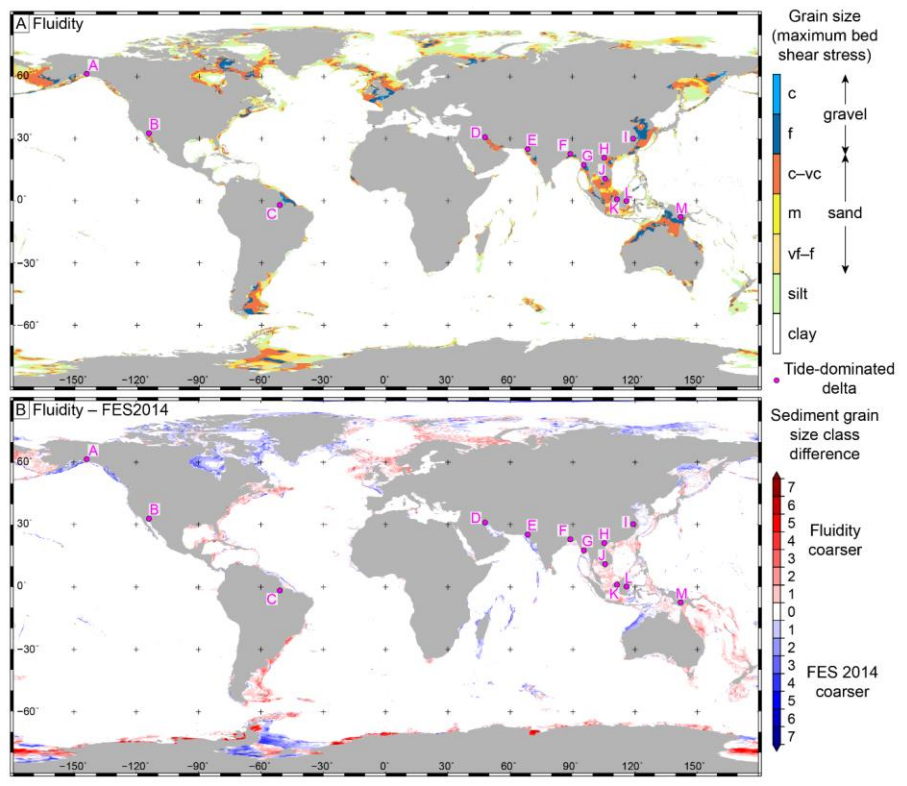
SUPPLEMENTARY MATERIAL



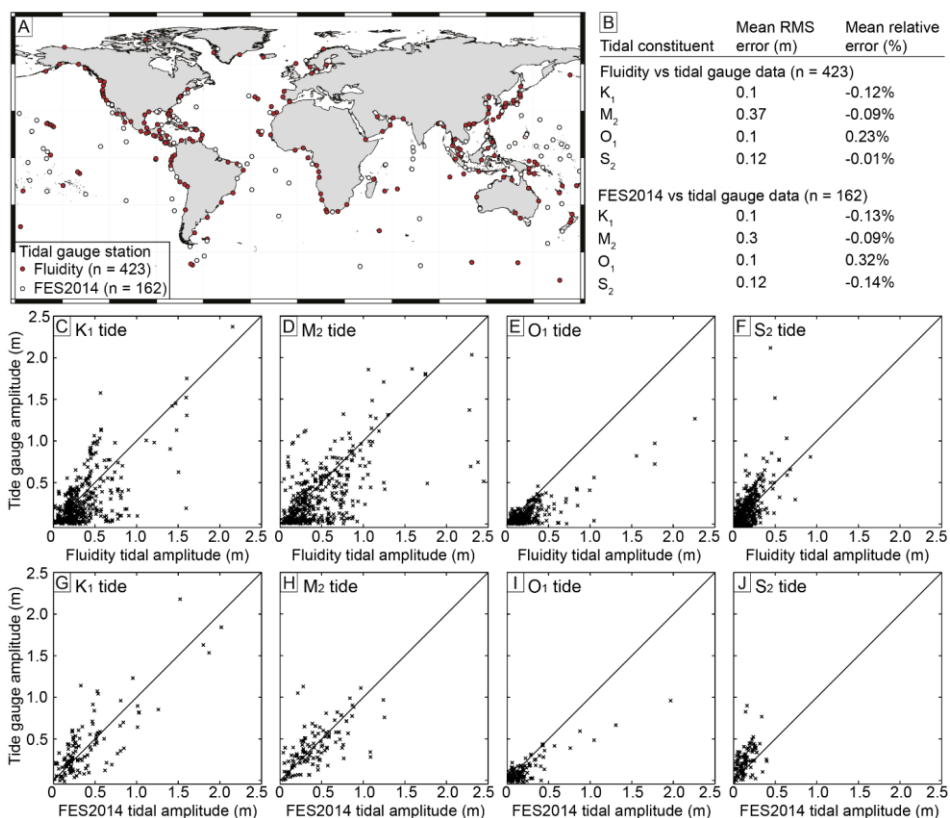




**Supplementary Fig. 1.** Global map of modern tidal bed shear stress calculated from (A) tidal modelling using Fluidity and (B) tidal velocity magnitude from FES2014. C) Difference in maximum tidal bed shear stress between (A) Fluidity and (B) FES2014; Blue indicates FES2014 has a higher maximum tidal bed shear stress.



**Supplementary Fig. 2.** (A) Maximum tidal bed shear stress modeled using Fluidity, plotted as the equivalent grain size that could be entrained if available. (B) Difference in sediment grain size class between maximum tidal bed shear stress for Fluidity (A) and FES2014 (Fig. 2D) (Carrère et al., 2015). Grain size abbreviations: vf = very fine; f = fine; m = medium; c = coarse; vc = very coarse. Pink dots show location of tide-dominated deltas (Goodbred and Saito, 2012): A) Copper; B) Colorado; C) Amazon; D) Shatt-al-Arab; E) Indus; F) Ganges-Brahmaputra; G) Irrawaddy; H) Red River; I) Yangtze; J) Mekong; K) Rajang; L) Mahakam; and M) Fly.



**Supplementary Fig. 3.** Validation of modeled tidal amplitude using Fluidity and FES2014 (Carrère et al., 2015). (A) Number (n) and position of a global set of tidal stations used for the comparisons to FES2014 (white circles, n = 162) and Fluidity (red circles, n = 423) model data. (B) Summary of root-mean-squared (RMS) and relative percentage errors between the model and tidal gauge data of tidal constituent amplitude. Tidal gauge amplitude data was derived by tidal harmonic analysis of sea surface elevation data. (C–J) Plots of tidal gauge versus modeled tidal amplitude for the  $K_1$  (C, G),  $M_2$  (D, H),  $O_1$  (E, I) and  $S_2$  (F, J) tidal constituents using Fluidity (C–F) and FES2014 (G–J).

## REFERENCES

- Abieda, H.S., Harith, Z.Z.T. and Rahman, A.H.A., 2005. Depositional controls on petrophysical properties and reservoir characteristics of Middle Miocene Miri Formation sandstones, Sarawak. *Bulletin of the Geological Society of Malaysia*, 5: 63-75.
- Ainsworth, R.B., 2003. Sequence stratigraphic-based analysis of depositional connectivity using 3-D reservoir modelling techniques, University of Liverpool, UK, 310 pp.
- Ainsworth, R.B., 2005. Sequence stratigraphic-based analysis of reservoir connectivity: influence of depositional architecture – a case study from a marginal marine depositional setting. *Petroleum Geoscience*, 11: 257–276.
- Ainsworth, R.B., Flint, S.S. and Howell, J.A., 2008. Predicting coastal depositional style: influence of basin morphology and accommodation to sediment supply ratio within a sequence stratigraphic framework. In: G.J. Hampson, R.J. Steel, P.M. Burgess and R.W. Dalrymple (Editors), *Recent Advances in Models of Siliclastic Shallow-Marine Stratigraphy*. SEPM Special Publication, pp. 237–263.
- Ainsworth, R.B., Hasiotis, S.T., Amos, K.J., Krapf, C.B., Payenberg, T.H., Sandstrom, M.L., Vakarelov, B.K. and Lang, S.C., 2012. Tidal signatures in an intracratonic playa lake. *Geology*, 40: 607-610.
- Ainsworth, R.B., Vakarelov, B.K., Lee, C., MacEachern, J.A., Montgomery, A.E., Ricci, L.P. and Dashtgard, S.E., 2015. Architecture and evolution of a regressive, tide-influenced marginal marine succession, Drumheller, Alberta, Canada. *Journal of Sedimentary Research*, 85: 596–625.
- Ainsworth, R.B., Vakarelov, B.K., MacEachern, J.A., Nanson, R.A., Lane, T.I., Rarity, F. and Dashtgard, S.E., 2016. Process-Driven Architectural Variability In Mouth-Bar Deposits: A Case Study From A Mixed-Process Mouth-Bar Complex, Drumheller, Alberta, Canada. *Journal of Sedimentary Research*, 86: 512-541.
- Ainsworth, R.B., Vakarelov, B.K. and Nanson, R.A., 2011. Dynamic spatial and temporal prediction of changes in depositional processes on clastic shorelines: Toward improved subsurface uncertainty reduction and management. *AAPG Bulletin*, 95: 267–297.
- Allen, G.P. and Chambers, J.L.C., 1998. Sedimentation in the modern and Miocene Mahakam Delta. *Indonesian Petroleum Association*, Jakarta, 236 pp.
- Allen, G.P. and Posamentier, H.W., 1993. Sequence stratigraphy and facies model of an incised valley fill; the Gironde Estuary, France. *Journal of Sedimentary Research*, 63: 378-391.
- Allen, J., 1981a. Lower Cretaceous tides revealed by cross-bedding with mud drapes. *Nature*, 289: 579.
- Allen, J.R.L., 1968. *Current Ripples: their relation to patterns of water and sediment motion*. North Holland, Amsterdam, 433 pp.
- Allen, J.R.L., 1981b. Palaeotidal speeds and ranges estimated from cross-bedding sets with mud drapes. *Nature*, 293: 394-396.
- Allen, J.R.L., 1982a. Mud drapes in sand-wave deposits: a physical model with application to the Folkestone Beds (early Cretaceous, southeast England). *Philosophical Transactions of the Royal Society of London A: Mathematical, Physical and Engineering Sciences*, 306: 291-345.

Formatted: Reference Head, Line spacing: Double

1  
2  
3  
4  
5  
6  
7  
8  
9  
10  
11  
12  
13  
14  
15  
16  
17  
18  
19  
20  
21  
22  
23  
24  
25  
26  
27  
28  
29  
30  
31  
32  
33  
34  
35  
36  
37  
38  
39  
40  
41  
42  
43  
44  
45  
46  
47  
48  
49  
50  
51  
52  
53  
54  
55  
56  
57  
58  
59  
60  
61  
62  
63  
64  
65

Allen, J.R.L., 1982b. Sedimentary structures, their character and physical basis, 1. Elsevier, Amsterdam, 592 pp.

Allen, P. and Homewood, P., 1984. Evolution and mechanics of a Miocene tidal sandwave. *Sedimentology*, 31: 63-81.

Allen, P.A., 1997. *Earth Surface Processes*. Blackwell Scientific Publications, Oxford, U.K., 404 pp.

Amir Hassan, M.H., Johnson, H.D., Allison, P.A. and Abdullah, W.H., 2013. Sedimentology and stratigraphic development of the upper Nyalau Formation (Early Miocene), Sarawak, Malaysia: A mixed wave- and tide-influenced coastal system. *Journal of Asian Earth Sciences*, 76: 301–311.

Amir Hassan, M.H., Johnson, H.D., Allison, P.A. and Abdullah, W.H., 2016. Sedimentology and stratigraphic architecture of a Miocene retrogradational, tide-dominated delta system: Balingian Province, offshore Sarawak, Malaysia. In: G.J. Hampson, A.D. Reynolds, B. Kostic and M.R. Wells (Editors), *Sedimentology of Paralic Reservoirs: Recent Advances*. Special Publications. Geological Society of London, London, UK, pp. SP444.12, 36 p.

Anderton, R., 1976. Tidal-shelf sedimentation: an example from the Scottish Dalradian. *Sedimentology*, 23: 429-458.

Anderton, R., 1985. Clastic facies models and facies analysis. In: P.J. Brenchley and B.P.J. Williams (Editors), *Sedimentology Recent Developments and Applied Aspects*. Special Publication 18. Geological Society, London, pp. 31-47.

Androsov, A., Kagan, B., Romanenkov, D. and Voltzinger, N., 2002. Numerical modelling of barotropic tidal dynamics in the strait of Messina. *Advances in Water Resources*, 25: 401-415.

Anthony, E.J. and Orford, J.D., 2002. Between wave-and tide-dominated coasts: the middle ground revisited. *Journal of Coastal Research*, 36: 8-15.

Anthony, E.J., Oyédé, L.M. and Lang, J., 2002. Sedimentation in a fluvially infilling, barrier-bound estuary on a wave- dominated, microtidal coast: the Ouémé River estuary, Benin, west Africa. *Sedimentology*, 49: 1095-1112.

Archer, A.W., 1995. Modeling of cyclic tidal rhythmities based on a range of diurnal to semidiurnal tidal-station data. *Marine Geology*, 123: 1-10.

Archer, A.W., Kvale, E.P. and Johnson, H.R., 1991. Analysis of modern equatorial tidal periodicities as a test of information encoded in ancient tidal rhythmities. In: S. DG, R. GE, Z. BA and R. RA (Editors), *Clastic Tidal Sedimentology*. Memoir of the Canadian Society of Petroleum Geologists, pp. 189–196.

Arnott, R.W.C. and Southard, J.B., 1990. Exploratory flow-duct experiments on combined-flow bed configurations, and some implications for interpreting storm-event stratification. *Journal of Sedimentary Research*, 60: 211-219.

Avdis, A., Candy, A.S., Hill, J., Kramer, S.C. and Piggott, M.D., 2018. Efficient unstructured mesh generation for marine renewable energy applications. *Renewable Energy*, 116: 842-856.

Baas, J.H., Best, J.L. and Peakall, J., 2016. Predicting bedforms and primary current stratification in cohesive mixtures of mud and sand. *Geological Society of London Journal*, 173: 12–45.

Banks, N., 1973. Tide- dominated offshore sedimentation, Lower Cambrian, north Norway. *Sedimentology*, 20: 213-228.

1  
2  
3  
4  
5  
6  
7  
8  
9  
10  
11  
12  
13  
14  
15  
16  
17  
18  
19  
20  
21  
22  
23  
24  
25  
26  
27  
28  
29  
30  
31  
32  
33  
34  
35  
36  
37  
38  
39  
40  
41  
42  
43  
44  
45  
46  
47  
48  
49  
50  
51  
52  
53  
54  
55  
56  
57  
58  
59  
60  
61  
62  
63  
64  
65

Barckhausen, U., Engels, M., Franke, D., Ladage, S. and Pubellier, M., 2014. Evolution of the South China Sea: Revised ages for breakup and seafloor spreading. *Marine and Petroleum Geology*, 58: 599-611.

Barckhausen, U. and Roeser, H.A., 2004. Seafloor spreading anomalies in the South China Sea revisited. In: P. Clift, W. Kuhnt, P. Wang and D. Hayes (Editors), *Continent-Ocean Interactions Within East Asian Marginal Seas*. Geophysical Monograph Series. AGU, Washington, DC, pp. 121-125.

Basilici, G., de Luca, P.H.V. and Poiré, D.G., 2012. Hummocky cross-stratification-like structures and combined-flow ripples in the Punta Negra Formation (Lower-Middle Devonian, Argentine Precordillera): A turbiditic deep-water or storm-dominated prodelta inner-shelf system? *Sedimentary Geology*, 267-268: 73-92.

Belderson, R., Johnson, M., Kenyon, N. and Stride, A., 1982. Bedforms. In: A.H. Stride (Editor), *Offshore tidal sands: processes and deposit*. Chapman and Hall, pp. 27-57.

Berenbrock, C. and Tranmer, A.W., 2008. Simulation of flow, sediment transport, and sediment mobility of the lower Coeur d'Alene River, Idaho. 2328-0328, U.S. Geological Survey, Reston, Virginia.

Bhattacharya, J.P. and Giosan, L., 2003. Wave-influenced deltas: Geomorphological implications for facies reconstruction. *Sedimentology*, 50: 187-210.

Bhattacharya, J.P. and MacEachern, J.A., 2009. Hyperpycnal Rivers and Prodeltaic Shelves in the Cretaceous Seaway of North America. *Journal of Sedimentary Research*, 79: 184-209.

Bhattacharya, J.P. and Walker, R.G., 1992. Deltas. In: R.G. Walker and N.P. James (Editors), *Facies Models: Response to Sea-Level Change*. Geological Association of Canada, St. John's, NL, pp. 157-177.

Boersma, J. and Terwindt, J., 1981. Neap-spring tide sequences of intertidal shoal deposits in a mesotidal estuary. *Sedimentology*, 28: 151-170.

Boersma, J.R., 1969. Internal structure of some tidal mega-ripples on a shoal in the Westerschelde estuary, the Netherlands: report of a preliminary investigation. *Geologie en Mijnbouw (Netherlands Journal of Geosciences)*, 48: 409-414.

Boyd, R., Dalrymple, R.W. and Zaitlin, B.A., 1992. Classification of clastic coastal depositional environments. *Sedimentary Geology*, 80: 139-150.

Boyd, R., Dalrymple, R.W. and Zaitlin, B.A., 2006. Estuarine and incised-valley facies models. In: H.W. Posamentier, Walker, R.G. (Editor), *Facies Models Revisited*. SEPM Special Publication, pp. 171-234.

Briais, A., Patriat, P. and Tapponnier, P., 1993. Updated interpretation of magnetic anomalies and seafloor spreading stages in the south China Sea: Implications for the Tertiary tectonics of Southeast Asia. *Journal of Geophysical Research*, 98: 6299-6328.

Bridges, P.H., 1982. Ancient offshore tidal deposits. In: A.H. Stride (Editor), *Offshore Tidal Sands, Processes and Deposits*. Chapman & Hall, London, UK, pp. 172-192.

Buatois, L.A., Santiago, N., Herrera, M., Plink-Björklund, P., Steel, R.J., Espin, M. and Parra, K., 2012. Sedimentological and ichnological signatures of changes in wave, river and tidal influence along a Neogene tropical deltaic shoreline. *Sedimentology*, 59: 1568-1612.

Burgess, P.M. and Hovius, N., 1998. Rates of delta progradation during highstands: consequences for timing of deposition in deep-marine systems. *Journal of the Geological Society*, 155: 217-222.

- Caldwell, P., Merrfield, M. and Thompson, P., 2015. Sea level measured by tide gauges from global oceans—the Joint Archive for Sea Level holdings (NCEI Accession 0019568), Version 5.5. National Oceanographic Data Center, NOAA. Dataset. 2015.
- Carrère, L., Lyard, F., Cancet, M. and Guillot, A., 2015. FES 2014, a new tidal model on the global ocean with enhanced accuracy in shallow seas and in the Arctic regio, EGU General Assembly 2015, Vienna, Austria.
- Casey, R., 1961. The stratigraphical palaeontology of the Lower Greensand. *Palaeontology*, 3: 487–621.
- Čech, S. and Uličný, D., 1996. Bohemian-Saxonian Cretaceous Basin—Overview. In: T. Voigt (Editor), *Stratigraphy and Facies of the Bohemian-Saxonian Cretaceous Basin. Field Trip Guide, Fifth International Cretaceous Symposium. Freiberg University of Mining and Technology, Freiberg*, pp. 1–8.
- Chamberlain, E.L., Törnqvist, T.E., Shen, Z., Mauz, B. and Wallinga, J., 2018. Anatomy of Mississippi Delta growth and its implications for coastal restoration. *Science advances*, 4: eaar4740.
- Charusiri, P. and Pum-Im, S., 2009. Cenozoic Tectonic Evolution of Major Sedimentary Basins in Central, Northern, and the Gulf of Thailand. *Bulletin of Earth Science Technology*, 2: 40–61.
- Chen, S., Steel, R.J., Dixon, J.F. and Osman, A., 2014. Facies and architecture of a tide-dominated segment of the Late Pliocene Orinoco Delta (Morne L'Enfer Formation) SW Trinidad. *Marine and Petroleum Geology*, 57: 208–232.
- Choi, K.S., Dalrymple, R.W., Chun, S.S. and Kim, S.-P., 2004. Sedimentology of modern, inclined heterolithic stratification (IHS) in the macrotidal Han River delta, Korea. *Journal of Sedimentary Research*, 74: 677–689.
- Chung, N.H., Quang, C.D. and Tham, N.T., 2015. A Review of Tertiary Palynomorph Assemblage in Cuu Long Basin: Case Study of Palynomorphs in Miocene–Oligocene Sediments. *International Journal of Sciences: Basic and Applied Research*, 24: 103–111.
- Clifton, H.E., 1983. Discrimination between subtidal and intertidal facies in Pleistocene deposits, Willapa Bay, Washington. *Journal of Sedimentary Research*, 53: 353–369.
- Coates, L. and MacEachern, J.A., 2007. The ichnological signatures of river- and wave-dominated delta complexes: differentiating deltaic and non-deltaic shallow marine successions, Lower Cretaceous Viking Formation and Upper Cretaceous Dunvegan Formation, west-central Alberta. In: J.A. MacEachern, K.L. Bann, M.K. Gingras and S.G. Pemberton (Editors), *Applied Ichnology. Short Course Notes 52. SEPM, Tulsa, Oklahoma*, pp. 227–254.
- Coco, G., Zhou, Z., van Maanen, B., Olabarrieta, M., Tinoco, R. and Townend, I., 2013. Morphodynamics of tidal networks: Advances and challenges. *Marine Geology*, 346: 1–16.
- Coleman, J.M. and Wright, L.D., 1975. Modern river deltas: variability of processes and sand bodies. In: M.L. Broussard (Editor), *Deltas: Models for Exploration. Houston Geological Society, Houston, Texas*, pp. 99–149.
- Collins, D.S., Avdis, A., Allison, P.A., Johnson, H.D., Hill, J., Piggott, M.D., Amir Hassan, M.H. and Damit, A.R., 2018a. Controls on Tidal Sedimentation and Preservation: Insights from Numerical Tidal Modelling in the Late Oligocene–Miocene South China Sea, Southeast Asia. *Sedimentology*, Accepted; In Press.

- Collins, D.S., Avdis, A., Allison, P.A., Johnson, H.D., Hill, J., Piggott, M.D., Hassan, M.H.A. and Damit, A.R., 2017a. Tidal dynamics and mangrove carbon sequestration during the Oligo–Miocene in the South China Sea. *Nature Communications*, 8: 15698.
- Collins, D.S., Johnson, H.D., Allison, P.A. and Damit, A.R., 2018b. Mixed Process, Humid-Tropical, Shoreline–Shelf Deposition: Middle Miocene–Modern Baram Delta Province, North-West Borneo. *Journal of Sedimentary Research*, 88: 399–430.
- Collins, D.S., Johnson, H.D., Allison, P.A., Guilpain, P. and Damit, A.R., 2017b. Coupled ‘storm-flood’ depositional model: Application to the Miocene–Modern Baram Delta Province, north-west Borneo. *Sedimentology*, 64: 1203–1235.
- Collins, D.S., Johnson, H.D. and Baldwin, C.T., 2020. Architecture and preservation in the fluvial to marine transition zone of a mixed- process humid- tropical delta: Middle Miocene Lambir Formation, Baram Delta Province, north- west Borneo. *Sedimentology*, 67: 1–46.
- Collinson, J. and Mountney, N.P., 2019. *Sedimentary Structures*. Dunedin Academic Press Ltd, 320 pp.
- Colombero, L. and Mountney, N.P., 2020a. Accommodation and sediment- supply controls on clastic parasequences: A meta- analysis. *Sedimentology*, 67: 1667–1709.
- Colombero, L. and Mountney, N.P., 2020b. On the geological significance of clastic parasequences. *Earth-Science Reviews*, 201: 103062.
- Colombero, L., Mountney, N.P. and McCaffrey, W.D., 2012. A relational database for the digitization of fluvial architecture concepts and example applications. *Petroleum Geoscience*, 18: 129–140.
- Comblen, R., Legrand, S., Deleersnijder, E. and Legat, V., 2009. A finite element method for solving the shallow water equations on the sphere. *Ocean Modelling*, 28: 12–23.
- Cooper, J., 2001. Geomorphological variability among microtidal estuaries from the wave-dominated South African coast. *Geomorphology*, 40: 99–122.
- Cooper, J.A.G., 1993. Sedimentation in a river dominated estuary. *Sedimentology*, 40: 979–1017.
- Cram, J.M., 1979. The influence of continental shelf width on tidal range: paleoceanographic implications. *The Journal of Geology*, 87: 441–447.
- Cummins, P.F. and Thupaki, P., 2018. A note on evaluating model tidal currents against observations. *Continental Shelf Research*, 152: 35–37.
- Cushman-Roisin, B., 1994. *Introduction to Geophysical Fluid Dynamics*. Prentice Hall, New Jersey, 320 pp.
- Cushman-Roisin, B. and Beckers, J.-M., 2011. *Introduction to Geophysical Fluid Dynamics: Physical and Numerical Aspects*. International Geophysics Series. Academic Press, Cambridge, MA, 875 pp.
- D’Alpaos, A., Lanzoni, S., Marani, M. and Rinaldo, A., 2010. On the tidal prism–channel area relations. *Journal of Geophysical Research: Earth Surface*, 115: F01003.
- d’Anglejan, B. and Brisebois, M., 1978. Recent sediments of the St. Lawrence middle estuary. *Journal of Sedimentary Research*, 48: 951–964.
- Dalrymple, R.W., 1992. Tidal depositional systems. In: R.G. Walker and N.P. James (Editors), *Facies Models: Response to Sea Level Change*. Geological Association of Canada, St. John’s, Newfoundland, pp. 195–218.
- Dalrymple, R.W., 2006. Incised valleys in time and space: an introduction to the volume and an examination of the controls on valley formation and filling. In: R.W. Dalrymple, D.A.



- Leckie and R.W. Tillman (Editors), *Incised Valleys in Time and Space*. SEPM Special Publication, pp. 5–12.
- Dalrymple, R.W., 2010. Interpreting sedimentary successions: facies, facies analysis and facies models. In: N.P. James and R.W. Dalrymple (Editors), *Facies Models 4*. Geological Association of Canada, pp. 3–18.
- Dalrymple, R.W., Baker, E.K., Harris, P.T. and Hughes, M.G., 2003. Sedimentology and stratigraphy of a tide-dominated, foreland-basin delta (Fly River, Papua New Guinea). In: F.H. Sidi, D. Nummedal, P. Imbert, H. Darman and H.W. Posamentier (Editors), *Tropical Deltas of Southeast Asia—Sedimentology, Stratigraphy, and Petroleum Geology*. SEPM Spec. Publ., pp. 147–173.
- Dalrymple, R.W. and Choi, K., 2007. Morphologic and facies trends through the fluvial–marine transition in tide-dominated depositional systems: A schematic framework for environmental and sequence-stratigraphic interpretation. *Earth-Science Reviews*, 81: 135–174.
- Dalrymple, R.W., Knight, R., Zaitlin, B.A. and Middleton, G.V., 1990. Dynamics and facies model of a macrotidal sand- bar complex, Cobequid Bay—Salmon River Estuary (Bay of Fundy). *Sedimentology*, 37: 577–612.
- Dalrymple, R.W., Kurcinka, C.E., Jablonski, B.V.J., Ichaso, A.A. and Mackay, D.A., 2015. Deciphering the relative importance of fluvial and tidal processes in the fluvial–marine transition. In: P.J. Ashworth, J.L. Best and D.R. Parsons (Editors), *Fluvial–Tidal Sedimentology*. Developments in Sedimentology. Elsevier, pp. 3–45.
- Dalrymple, R.W., Mackay, D.A., Ichaso, A.A. and Choi, K.S., 2012. Processes, morphodynamics, and facies of tide-dominated estuaries. In: R.A.J. Davis and R.W. Dalrymple (Editors), *Principles of Tidal Sedimentology*. Springer, New York, pp. 79–108.
- Dalrymple, R.W. and Padman, L., 2015. Tides at high latitudes, AAPG Hedberg Research Conference, Latitudinal Controls on Stratigraphic Models and Sedimentary Concept. AAPG Search and Discovery Article #120178, Banff.
- Dalrymple, R.W. and Rhodes, R.N., 1995. Estuarine dunes and bars. In: P. G.M.E. (Editor), *Geomorphology and Sedimentology of Estuaries*. Developments in Sedimentology. Elsevier, Amsterdam, pp. 359–422.
- Dalrymple, R.W., Zaitlin, B.A. and Boyd, R., 1992. Estuarine facies models: conceptual basis and stratigraphic implications: perspective. *Journal of Sedimentary Petrology*, 62: 1130–1146.
- Dashtgard, S.E., MacEachern, J.A., Frey, S.E. and Gingras, M.K., 2012. Tidal effects on the shoreface: towards a conceptual framework. *Sedimentary Geology*, 279: 42–61.
- Davis, R.A., 1994. Barrier island systems—a geologic overview. In: R.A. Davis Jr (Editor), *Geology of Holocene barrier island systems*. Springer, Heidelberg, pp. 1–46.
- Davis, R.A., 2012. Tidal signatures and their preservation potential in stratigraphic sequences. In: R.A. Davis and R.W. Dalrymple (Editors), *Principles of Tidal Sedimentology*. Springer, New York, pp. 35–55.
- Davis, R.A. and Hayes, M.O., 1984. What is a wave-dominated coast? *Marine Geology*, 60: 313–329.
- De Boer, P.L., Oost, A. and Visser, M., 1989. The diurnal inequality of the tide as a parameter for recognizing tidal influences. *Journal of Sedimentary Research*, 59: 912–921.

1  
2  
3  
4  
5  
6  
7  
8  
9  
10  
11  
12  
13  
14  
15  
16  
17  
18  
19  
20  
21  
22  
23  
24  
25  
26  
27  
28  
29  
30  
31  
32  
33  
34  
35  
36  
37  
38  
39  
40  
41  
42  
43  
44  
45  
46  
47  
48  
49  
50  
51  
52  
53  
54  
55  
56  
57  
58  
59  
60  
61  
62  
63  
64  
65

De Boer, P.L., Van Gelder, A. and Nio, S.D., 1988. Tide-influenced Sedimentary Environments and Facies. Reidel, Dordrecht, 530 pp.

De Raaf, J. and Boersma, J., 1971. Tidal deposits and their sedimentary structures (seven examples from Western Europe). *Geologie en Mijnbouw*, 50.

De Raaf, J., Reading, H. and Walker, R., 1965. Cyclic sedimentation in the Lower Westphalian of no Devon, England. *Sedimentology*, 4: 1-52.

De Raaf, J.F.M. and Boersma, J.R., 1977. Tidal deposits and their sedimentary structures (seven examples from Western Europe). *Geologie en Mijnbouw*, 50: 479-504.

de Vries Klein, G., 1977. Tidal circulation model for deposition of clastic sediment in epeiric and mioclinal shelf seas. *Sedimentary Geology*, 18: 1-12.

Dean, C.D., Collins, D.S., van Cappelle, M., Avdis, A. and Hampson, G.J., 2019. Regional-scale paleobathymetry controlled location, but not magnitude, of tidal dynamics in the Late Cretaceous Western Interior Seaway, USA. *Geology*, 47: 1083-1087.

Defant, A., 1961. *Physical Oceanography*, 11. Pergamon, New York, 598 pp.

Dercourt, J., Gaetani, M., Vrielynck, B., Barrier, E., Biju-Duval, B., Brunet, M.-F., Cadet, J.P., Crasquin, S. and Sandulescu, M., 2000. *Atlas Peri-Tethys Palaeogeographical Maps, I-XX. CCGM/CGMW*, 269 pp.

Dott, R.H., 1983. Episodic Sedimentation—How Normal Is Average? How Rare Is Rare? Does It Matter? *Journal of Sedimentary Petrology*, 53: 5-23.

Dott, R.H., 1996. Episodic event deposits versus stratigraphic sequences—shall the twain never meet? *Sedimentary Geology*, 104: 243-247.

Dott, R.H. and Bourgeois, J., 1982. Hummocky stratification: significance of its variable bedding sequences. *Geological Society of America Bulletin*, 93: 663–680.

Doust, H. and Sumner, H.S., 2007. Petroleum systems in rift basins—a collective approach in Southeast Asian basins. *Petroleum Geoscience*, 13: 127-144.

Dumas, S. and Arnott, R.W.C., 2006. Origin of hummocky and swaley cross-stratification— The controlling influence of unidirectional current strength and aggradation rate. *Geology*, 34: 1073–1076.

Egbert, G.D., Ray, R.D. and Bills, B.G., 2004. Numerical modeling of the global semidiurnal tide in the present day and in the last glacial maximum. *Journal of Geophysical Research: Oceans*, 109.

Ericksen, M.C. and Slingerland, R., 1990. Numerical simulations of tidal and wind-driven circulation in the Cretaceous Interior Seaway of North America. *Geological Society of America Bulletin*, 102: 1499-1516.

Fanget, A.-S., Berné, S., Jouet, G., Bassetti, M.-A., Dennielou, B., Maillet, G.M. and Tondut, M., 2014. Impact of relative sea level and rapid climate changes on the architecture and lithofacies of the Holocene Rhone subaqueous delta (Western Mediterranean Sea). *Sedimentary Geology*, 305: 35-53.

Fielding, C.R., Trueman, J. and Alexander, J., 2005. Sedimentology of the modern and Holocene Burdekin River Delta of north Queensland, Australia—controlled by river output, not by waves and tides. In: L. Giosan and J.P. Bhattacharya (Editors), *River Deltas—Concepts, Models, and Examples* Special Publication 18, pp. 467–496.

FitzGerald, D.M., 1982. Sediment bypassing at mixed energy tidal inlets, 18th International Conference on Coastal Engineering, pp. 1094-1118.

1  
2  
3  
4  
5  
6  
7  
8  
9  
10  
11  
12  
13  
14  
15  
16  
17  
18  
19  
20  
21  
22  
23  
24  
25  
26  
27  
28  
29  
30  
31  
32  
33  
34  
35  
36  
37  
38  
39  
40  
41  
42  
43  
44  
45  
46  
47  
48  
49  
50  
51  
52  
53  
54  
55  
56  
57  
58  
59  
60  
61  
62  
63  
64  
65

- FitzGerald, D.M., Rosen, P.S. and van Heteren, S., 1994. New England barriers. In: R.A. Davies Jr. (Editor), *Geology of Holocene Barrier Island Systems*. Springer, Heidelberg, pp. 305-394.
- Flemming, B.W. and Bartholoma, A., 1995. Tidal Signatures in Modern and Ancient Sediments. IAS Special Publication, 24, 358 pp.
- Foreman, M. and Henry, R., 1979. Tidal analysis based on high and low water observations, Institute of Ocean Sciences, Patricia Bay, Sidney, B.C.
- Foreman, M.G.G., 1979. Manual for Tidal Heights Analysis and Prediction. Pacific Marine Science Report 77-10. Institute of Ocean Sciences, Patricia Bay, Sidney, B.C., 58 pp.
- Franke, D., Barckhausen, U., Heyde, I., Tingay, M. and Ramli, N., 2008. Seismic images of a collision zone offshore NW Sabah/Borneo. *Marine and Petroleum Geology*, 25: 606-624.
- Frey, R.W. and Howard, J.D., 1986. Mesotidal estuarine sequences; a perspective from the Georgia Bight. *Journal of Sedimentary Research*, 56: 911-924.
- Friedrichs, C.T., 1995. Stability Shear Stress and Equilibrium Cross-Sectional Geometry of Sheltered Tidal Channels. *Journal of Coastal Research*, 11: 1062-1074.
- Gaina, C. and Müller, D., 2007. Cenozoic tectonic and depth/age evolution of the Indonesian gateway and associated back-arc basins. *Earth-Science Reviews*, 83: 177-203.
- Galloway, W.E., 1975. Process framework for describing the morphologic and stratigraphic evolution of deltaic depositional systems. In: M.L. Broussard (Editor), *Deltas: Models for Exploration*. Houston Geological Society, Houston, USA, pp. 87-98.
- Gani, M.R. and Bhattacharya, J.P., 2007. Basic building blocks and process variability of a Cretaceous delta: Internal facies architecture reveals a more dynamic interaction of river, wave, and tidal processes than is indicated by external shape. *Journal of Sedimentary Research*, 77: 284-302.
- Gardner, M.H., Cross, T.A., Levorsen, M., Chidsey, T., Adams, R. and Morris, T., 2004. Stacking patterns, sediment volume partitioning, and facies differentiation in shallow-marine and coastal-plain strata of the Cretaceous Ferron Sandstone, Utah. In: T.C. Chidsey, R.D. Adams and T.H. Morris (Editors), *Regional to Wellbore Analog for Fluvial-Deltaic Reservoir Modeling: The Ferron Sandstone of Utah*. American Association of Petroleum Geologists, Studies in Geology pp. 95-124.
- Geleynse, N., Storms, J.E.A., Walstra, D.-J.R., Jagers, H.R.A., Wang, Z.B. and Stive, M.J.F., 2011. Controls on river delta formation: insights from numerical modelling. *Earth and Planetary Science Letters*, 302: 217-226.
- Geuzaine, C. and Remacle, J.F., 2009. Gmsh: A 3-D finite element mesh generator with built-in pre-and post-processing facilities. *International Journal for Numerical Methods in Engineering*, 79: 1309-1331.
- Gil, J., García-Hidalgo, J., Segura, M., García, A. and Carenas, B., 2006. Stratigraphic architecture, palaeogeography and sea-level changes of a third order depositional sequence: the late Turonian-early Coniacian in the northern Iberian Ranges and Central System (Spain). *Sedimentary Geology*, 191: 191-225.
- Gingras, M.K. and MacEachern, J.A., 2012. Tidal ichnology of shallow-water clastic settings. In: R.A. Davis and R.W. Dalrymple (Editors), *Principles of Tidal Sedimentology*. Springer, New York, pp. 57-77.
- Gingras, M.K., MacEachern, J.A. and Dashtgard, S.E., 2012. The potential of trace fossils as tidal indicators in bays and estuaries. *Sedimentary Geology*, 279: 97-106.

- Ginsburg, R.N., 1975. Tidal Deposits – A Casebook of Recent Examples and Fossil Counterparts. Springer, New York, 428 pp.
- Giosan, L. and Bhattacharya, J.P. (Editors), 2005. River deltas: concepts, models, and examples. SEPM Special Publication 83, Tulsa, Oklahoma, 502 pp.
- Godin, G., 1993. On tidal resonance. *Continental Shelf Research*, 13: 89-107.
- Godin, G., 1999. The propagation of tides up rivers with special considerations on the upper Saint Lawrence River. *Estuarine, Coastal and Shelf Science*, 48: 307-324.
- Golonka, J., 2004. Plate tectonic evolution of the southern margin of Eurasia in the Mesozoic and Cenozoic. *Tectonophysics*, 381: 235-273.
- Golonka, J., 2007. Late Triassic and Early Jurassic palaeogeography of the world. *Palaeogeography, Palaeoclimatology, Palaeoecology*, 244: 297-307.
- Golonka, J., Gahagan, L., Krobicki, M., Marko, F. and Oszczytko, N., 2006. Plate-tectonic evolution and paleogeography of the circum-Carpathian region. In: J. Golonka and F.J. Picha (Editors), *The Carpathians and their Foreland: Geology and Hydrocarbon Resources*. AAPG Memoir, pp. 11–46.
- Gomis-Cartasio, L.E., Poyatos-Moré, M., Flint, S.S., Hodgson, D.M., Brunt, R.L. and Wickens, H.D., 2016. Anatomy of a mixed-influence shelf edge delta, Karoo Basin, South Africa. In: G.J. Hampson, A.D. Reynolds, B. Kostic and M.R. Wells (Editors), *Sedimentology of Paralic Reservoirs: Recent Advances*. Special Publication 444. Geological Society of London, pp. SP444.5.
- Goodbred, S.L. and Saito, Y., 2012. Tide-dominated deltas. In: R.A. Davis and R.W. Dalrymple (Editors), *Principles of Tidal Sedimentology*. Springer, New York, pp. 129-149.
- Gordon, A.L., Huber, B.A., Metzger, E.J., Susanto, R.D., Hurlburt, H.E. and Adi, T.R., 2012. South China Sea throughflow impact on the Indonesian throughflow. *Geophysical Research Letters*, 39: 1-7.
- Gorman, G.J., Piggott, M. and Pain, C.C., 2007. Shoreline approximation for unstructured mesh generation. *Computers & geosciences*, 33: 666-677.
- Gorman, G.J., Piggott, M., Wells, M., Pain, C.C. and Allison, P., 2008. A systematic approach to unstructured mesh generation for ocean modelling using GMT and Terreno. *Computers & Geosciences*, 34: 1721-1731.
- Greb, S.F. and Archer, A.W., 1995. Rhythmic sedimentation in a mixed tide and wave deposit, Hazel Patch sandstone (Pennsylvanian), eastern Kentucky coal field. *Journal of Sedimentary Research*, 65: 96-106.
- Grindrod, J., 1988. The palynology of Holocene mangrove and saltmarsh sediments, particularly in northern Australia. *Review of Palaeobotany and Palynology*, 55: 229-245.
- Gugliotta, M., Flint, S.S., Hodgson, D.M. and Veiga, G.D., 2015. Stratigraphic record of river-dominated crevasse subdeltas with tidal influence (Lajas Formation, Argentina). *Journal of Sedimentary Research*, 85: 265–284.
- Gugliotta, M., Flint, S.S., Hodgson, D.M. and Veiga, G.D., 2016a. Recognition criteria, characteristics and implications of the fluvial to marine transition zone in ancient deltaic deposits (Lajas Formation, Argentina). *Sedimentology*, 63: 1971–2001.
- Gugliotta, M., Kurcinka, C.E., Dalrymple, R.W., Flint, S.S. and Hodgson, D.M., 2016b. Decoupling seasonal fluctuations in fluvial discharge from the tidal signature in ancient deltaic deposits: an example from the Neuquén Basin, Argentina. *Journal of the Geological Society of London*, 173: 94–107.

- Gugliotta, M., Saito, Y., Nguyen, V.L., Oanh Ta, T.K. and Tamura, T., 2018. Sediment distribution and depositional processes along the fluvial to marine transition zone of the Mekong River delta, Vietnam. *Sedimentology*, Accepted; In Press.
- Guillocheau, F., Robin, C., Allemand, P., Bourquin, S., Brault, N., Dromart, G., Friedenberg, R., Garcia, J.-P., Gaulier, J.-M. and Gaumet, F., 2000. Meso-Cenozoic geodynamic evolution of the Paris Basin: 3D stratigraphic constraints. *Geodinamica Acta*, 13: 189-245.
- Gupta, R. and Johnson, H.D., 2002. High-resolution facies architecture of heterolithic tidal deposits: An integrated outcrop and electrofacies analysis of a complex reservoir. In: M. Lovell and N. Parkinson (Editors), *Geological application of well logs. AAPG Methods in Exploration No. 13*, pp. 161-184.
- Hadley, D.F., Arochukwu, E.C., Nishi, K., Sarginson, M.J., Salleh, H. and Omar, M., 2006. Depositional Modelling of Champion Field, Brunei, Society of Petroleum Engineers Asia Pacific Oil and Gas Conference and Exhibition. Society of Petroleum Engineers, Adelaide, Australia.
- Hall, R., 1996. Reconstructing Cenozoic SE Asia. In: R. Hall and D. Blundell (Editors), *Tectonic Evolution of Southeast Asia*. Geological Society, London, Special Publications, London, UK, pp. 153-184.
- Hall, R., 2002. Cenozoic geological and plate tectonic evolution of SE Asia and the SW Pacific: computer-based reconstructions, model and animations. *Journal of Asian Earth Sciences*, 20: 353-431.
- Hall, R., 2009. Southeast Asia's changing palaeogeography. *Blumea - Biodiversity, Evolution and Biogeography of Plants*, 54: 148-161.
- Hall, R., 2011. Australia–SE Asia collision: plate tectonics and crustal flow. Geological Society, London, Special Publications, 355: 75-109.
- Hall, R., 2013. The palaeogeography of Sundaland and Wallacea since the Late Jurassic. *Journal of Limnology*, 72: 1-17.
- Hall, R., Ali, J.R., Anderson, C.D. and Baker, S.J., 1995. Origin and motion history of the Philippine Sea Plate. *Tectonophysics*, 251: 229-250.
- Hallam, A., 1981. *Facies Interpretation and the Stratigraphic Record*. W.H. Freeman, Oxford, 291 pp.
- Hampson, G.J., Rodriguez, A.B., Storms, J.E.A., Johnson, H.D. and Meyer, C.T., 2008. Geomorphology and High-Resolution Stratigraphy of Progradational Wave-Dominated Shoreline Deposits: Impact on Reservoir-Scale Facies Architecture. 117-142.
- Hancock, J. and Rawson, P., 1992. Cretaceous. In: J. Cope, J. Ingham and P.F. Rawson (Editors), *Atlas of Palaeogeography and Lithofacies*. Geological Society London Memoir pp. 131-140.
- Hancock, J.M. and Kauffman, E., 1979. The great transgressions of the Late Cretaceous. *Journal of the Geological Society*, 136: 175-186.
- Hansen, C.D., MacEachern, J.A., Bann, K., Gingras, M. and Pemberton, S., 2007. Application of the asymmetric delta model to along-strike facies variations in a mixed wave-and river-influenced delta lobe, Upper Cretaceous Basal Belly River Formation, central Alberta. In: J.A. MacEachern, K.L. Bann, M.K. Gingras and S.G. Pemberton (Editors), *Applied Ichnology. SEPM Short Course Notes 52*. SEPM, Tulsa, Oklahoma, pp. 255–271.
- Haq, B.U., 2014. Cretaceous eustasy revisited. *Global and Planetary Change*, 113: 44-58.

1  
2  
3  
4  
5  
6  
7  
8  
9  
10  
11  
12  
13  
14  
15  
16  
17  
18  
19  
20  
21  
22  
23  
24  
25  
26  
27  
28  
29  
30  
31  
32  
33  
34  
35  
36  
37  
38  
39  
40  
41  
42  
43  
44  
45  
46  
47  
48  
49  
50  
51  
52  
53  
54  
55  
56  
57  
58  
59  
60  
61  
62  
63  
64  
65

Harms, J.C., Southard, J.B. and Walker, R.G., 1982. Structures and Sequences in Clastic Rocks. Short Course 9. SEPM, Tulsa, Oklahoma, 249 pp.

Harris, P.T., Heap, A.D., Bryce, S.M., Porter-Smith, R., Ryan, D.A. and Heggie, D.T., 2002. Classification of Australian Clastic Coastal Depositional Environments Based Upon a Quantitative Analysis of Wave, Tidal, and River Power. *Journal of Sedimentary Research*, 72: 858-870.

Hawkes, P., Fraser, A. and Einchcomb, C., 1998. The tectono-stratigraphic development and exploration history of the Weald and Wessex basins, Southern England, UK, Development, Evolution and Petroleum Geology of the Wessex Basin. Special Publications 133. Geological Society, London, pp. 39-65.

Hayes, M.O., 1975. Morphology of sand accumulations in estuaries: an introduction to the symposium. In: L.E. Cronin (Editor), *Estuarine Research*. Academic Press, New York, N.Y., pp. 3-22.

Hayes, M.O., 1979. Barrier island morphology as a function of tidal and wave regime. In: S.P. Leatherman (Editor), *Barrier Islands*. Academic Press, New York, pp. 1-27.

Hayes, M.O., 1980. General morphology and sediment patterns in tidal inlets. *Sedimentary geology*, 26: 139-156.

Hazebroek, H.P. and Tan, D.N.K., 1993. Tectonic evolution of the NW Sabah continental margin since the Late Eocene. In: G.H. Teh (Editor), *Proceedings symposium on the Tectonic framework and energy resources of the western margin of the Pacific Basin*. Special Publication. Geological Society of Malaysia, Kuala Lumpur, pp. 195-210.

Heap, A.D., Bryce, S. and Ryan, D.A., 2004. Facies evolution of Holocene estuaries and deltas: a large-sample statistical study from Australia. *Sedimentary Geology*, 168: 1-17.

Hinz, K., Fritsch, J., Kempter, E., Mohammad, M.A.M., Meyer, J., Mohamed, M.D., Vosberg, D.G.H., Weber, D.I.J. and Benavidez, M.J., 1989. Thrust tectonics along the north-western continental margin of Sabah/Borneo. *Geologische Rundschau*, 78: 705-730.

Hinz, K. and Schlüter, H., 1985. Geology of the Dangerous Grounds, South China Sea, and the continental margin off southwest Palawan: Results of SONNE cruises SO-23 and SO-27. *Energy*, 10: 297-315.

Hjulström, F., 1939. Transportation of Debris by Moving Water. In: P.D. Trask (Editor), *Recent Marine Sediments*. AAPG, Tulsa, OK, pp. 5-31.

Holgate, N.E., Jackson, C.A.L., Hampson, G.J. and Dreyer, T., 2013. Sedimentology and sequence stratigraphy of the Middle-Upper Jurassic Krossfjord and Fensfjord formations, Troll Field, northern North Sea. *Petroleum Geoscience*, 19: 237-258.

Holloway, N.H., 1982. North Palawan block, Philippines--Its relation to Asian mainland and role in evolution of South China Sea. *AAPG Bulletin*, 66: 1355-1383.

Honig, C. and Boyd, R., 1992. Estuarine sedimentation on the eastern shore of Nova Scotia. *Journal of Sedimentary Research*, 62: 569-583.

Hori, K. and Saito, Y., 2007. Classification, architecture, and evolution of large-river deltas. In: A. Gupta (Editor), *Large rivers: geomorphology and management*. John Wiley & Sons, Chichester, UK, pp. 75-96.

Hori, K., Saito, Y., Zhao, Q., Cheng, X., Wang, P., Sato, Y. and Li, C., 2001. Sedimentary facies of the tide-dominated paleo-Changjiang (Yangtze) estuary during the last transgression. *Marine Geology*, 177: 331-351.

1  
2  
3  
4  
5  
6  
7  
8  
9  
10  
11  
12  
13  
14  
15  
16  
17  
18  
19  
20  
21  
22  
23  
24  
25  
26  
27  
28  
29  
30  
31  
32  
33  
34  
35  
36  
37  
38  
39  
40  
41  
42  
43  
44  
45  
46  
47  
48  
49  
50  
51  
52  
53  
54  
55  
56  
57  
58  
59  
60  
61  
62  
63  
64  
65

Hori, K., Saito, Y., Zhao, Q. and Wang, P., 2002. Architecture and evolution of the tide-dominated Changjiang (Yangtze) River delta, China. *Sedimentary Geology*, 146: 249-264.

Hovikoski, J., Räsänen, M., Gingras, M., Ranzi, A. and Melo, J., 2008. Tidal and seasonal controls in the formation of Late Miocene inclined heterolithic stratification deposits, western Amazonian foreland basin. *Sedimentology*, 55: 499–530.

Hovius, N., 1998. Controls on sediment supply by large rivers. In: K.W. Shanley and P.J. McCabe (Editors), *Relative Role of Eustasy, Climate and Tectonics in Continental Rocks* SEPM Special Publication 59, pp. 3-16.

Howarth, M.J., 1982. Tidal currents of the continental shelf. In: A.H. Stride (Editor), *Offshore Tidal Sands: Processes and Deposits*. Chapman & Hall, London, pp. 10-26.

Hu, D., Wu, L., Cai, W., Gupta, A.S., Ganachaud, A., Qiu, B., Gordon, A.L., Lin, X., Chen, Z. and Hu, S., 2015. Pacific western boundary currents and their roles in climate. *Nature*, 522: 299–308.

Hubbard, S.M., Smith, D.G., Nielsen, H., Leckie, D.A., Fustic, M., Spencer, R.J. and Bloom, L., 2011. Seismic geomorphology and sedimentology of a tidally influenced river deposit, Lower Cretaceous Athabasca oil sands, Alberta, Canada. *AAPG bulletin*, 95: 1123-1145.

Huchon, P., Pichon, X.L. and Rangin, C., 1994. Indochina Peninsula and the collision of India and Eurasia. *Geology*, 22: 27-30.

Hulscher, S.J.M.H., de Swart, H.E. and de Vriend, H.J., 1993. The generation of offshore tidal sand banks and sand waves. *Continental Shelf Research*, 13: 1183-1204.

Hutchison, C.S., 1996. *South-East Asian oil, gas, coal, and mineral deposits*. Oxford University Press, Oxford, UK, 368 pp.

Hutchison, C.S., 2010. The North-West Borneo Trough. *Marine Geology*, 271: 32-43.

Hutchison, C.S., Bergman, S.C., Swauger, D.A. and Graves, J.E., 2000. A Miocene collisional belt in north Borneo: uplift mechanism and isostatic adjustment quantified by thermochronology. *Journal of the Geological Society*, 157: 783-793.

Ichaso, A.A. and Dalrymple, R.W., 2009. Tide- and wave-generated fluid mud deposits in the Tilje Formation (Jurassic), offshore Norway. *Geology*, 37: 539–542.

Immenhauser, A., 2009. Estimating palaeo-water depth from the physical rock record. *Earth-Science Reviews*, 96: 107-139.

Ingram, G.M., Chisholm, T.J., Grant, C.J., Hedlund, C.A., Stuart-Smith, P. and Teasdale, J., 2004. Deepwater North West Borneo: hydrocarbon accumulation in an active fold and thrust belt. *Marine and Petroleum Geology*, 21: 879-887.

Insole, A., Daley, B. and Gale, A., 1998. *The Isle of Wight: Geologists' Association Guide No. 60*. The Geologists' Association, London, UK, 132 pp.

Jablonski, B.V.J. and Dalrymple, R.W., 2016. Recognition of strong seasonality and climatic cyclicity in an ancient, fluvially dominated, tidally influenced point bar: Middle McMurray Formation, Lower Steepbank River, north-eastern Alberta, Canada. *Sedimentology*, 63: 552–585.

Jardine, E., 1997. Dual petroleum systems governing the prolific Pattani Basin, offshore Thailand. In: J.V.C. Howes and R.A. Noble (Editors), *International Conference on Petroleum Systems of SE Asia and Australasia*, Indonesian Petroleum Association, Jakarta, Indonesia, pp. 351-363.

1  
2  
3  
4  
5  
6  
7  
8  
9  
10  
11  
12  
13  
14  
15  
16  
17  
18  
19  
20  
21  
22  
23  
24  
25  
26  
27  
28  
29  
30  
31  
32  
33  
34  
35  
36  
37  
38  
39  
40  
41  
42  
43  
44  
45  
46  
47  
48  
49  
50  
51  
52  
53  
54  
55  
56  
57  
58  
59  
60  
61  
62  
63  
64  
65

Jerzykiewicz, T. and Wojewoda, J., 1986. The Radków and Szczeliniec sandstones: an example of giant foresets on a tectonically controlled shelf of the Bohemian Cretaceous Basin (Central Europe). In: J.R. Knight and J.R. McLean (Editors), *Shelf Sands and Sandstones*. Canadian Society of Petroleum Geologists, Memoir 11, pp. 1-15.

Johnson, H.D., 1975. Tide- and wave- dominated inshore and shoreline sequences from the late Precambrian, Finnmark, North Norway. *Sedimentology*, 22: 45-74.

Johnson, H.D. and Levell, B.K., 1995. Sedimentology of a transgressive, estuarine sand complex: the Lower Cretaceous Woburn Sands (Lower Greensand), southern England. In: A.G. Plint (Editor), *Sedimentary Facies Analysis: a Tribute to the Research and Teaching of Harold G. Reading*. IAS Special Publication 22. Blackwell Publishing Ltd., Oxford, UK, pp. 17-46.

Johnson, S.M. and Dashtgard, S.E., 2014. Inclined heterolithic stratification in a mixed tidal-fluvial channel: differentiating tidal versus fluvial controls on sedimentation. *Sedimentary Geology*, 301: 41-53.

Jopling, A.V. and Walker, R.G., 1968. Morphology and origin of ripple-drift cross-lamination, with examples from the Pleistocene of Massachusetts. *Journal of Sedimentary Research*, 38: 971-984.

Jouanneau, J.-M. and Latouche, C., 1981. *The Gironde Estuary*. Contributions to Sedimentology, 10. E. Schweizerbart'sche Verlagsbuchhandlung, Stuttgart.

Julien, P.Y. and Raslan, Y., 1998. Upper-regime plane bed. *Journal of Hydraulic Engineering*, 124: 1086-1096.

Kantha, L.H. and Clayson, C.A., 2000. *Numerical models of oceans and oceanic processes*, 66. Elsevier, 750 pp.

Klein, G.D., 1970a. Depositional and dispersal dynamics of intertidal sand bars. *Journal of Sedimentary Research*, 40: 1095-1127.

Klein, G.D., 1970b. Tidal origin of a Precambrian quartzite; the Lower Fine-grained quartzite (middle Dalradian) of Islay, Scotland. *Journal of Sedimentary Research*, 40: 973-985.

Klein, G.D., 1971. A sedimentary model for determining paleotidal range. *Geological Society of America Bulletin*, 82: 2585-2592.

Kowalik, Z. and Luick, J., 2013. *The Oceanography of Tides*. University of Alaska Fairbanks, Fairbanks, Alaska, 157 pp.

Kreisa, R. and Moila, R., 1986. Sigmoidal tidal bundles and other tide-generated sedimentary structures of the Curtis Formation, Utah. *Geological Society of America Bulletin*, 97: 381-387.

Krystinik, L.F. and DeJarnett, B.B., 1995. Lateral variability of sequence stratigraphic framework in the Campanian and Lower Maastrichtian of the Western Interior Seaway. In: J.C. Van Wagoner and G.T. Bertram (Editors), *Sequence Stratigraphy of Foreland Basin Deposits: Outcrop and Subsurface Examples from the Cretaceous of North America*. Memoir 64. AAPG, Tulsa, Oklahoma, pp. 11-26.

Kuhnt, W., Holbourn, A., Hall, R., Zuvela, M. and Käse, R., 2004. Neogene history of the Indonesian throughflow. In: P.C.W.K.P.W.D. Hayes (Editor), *Continent-Ocean Interactions within East Asian Marginal Seas*. Geophysical Monograph. American Geophysical Union, pp. 299-320.



- Kurcinka, C., Dalrymple, R.W. and Gugliotta, M., 2018. Facies and architecture of river-dominated to tide-influenced mouth bars in the lower Lajas Formation (Jurassic), Argentina. *AAPG Bulletin*, 102: 885-912.
- Kvale, E.P., 2006. The origin of neap-spring tidal cycles. *Marine Geology*, 235: 5-18.
- Kvale, E.P., 2012. Tidal constituents of modern and ancient tidal rhythmites: criteria for recognition and analyses. In: R.A. Davis and R.W. Dalrymple (Editors), *Principles of Tidal Sedimentology*. Springer, New York, pp. 1-17.
- Kvale, E.P., Archer, A.W. and Johnson, H.R., 1989. Daily, monthly, and yearly tidal cycles within laminated siltstones of the Mansfield Formation (Pennsylvanian) of Indiana. *Geology*, 17: 365-368.
- Lamb, M.P., Myrow, P.M., Lukens, C., Houck, K. and Strauss, J., 2008. Deposits from Wave-Influenced Turbidity Currents: Pennsylvanian Minturn Formation, Colorado, U.S.A. *Journal of Sedimentary Research*, 78: 480-498.
- Lambiase, J.J., Damit, A.R., Simmons, M.D., Abdoerrias, R. and Hussin, A., 2003. A depositional model and the stratigraphic development of modern and ancient tide-dominated deltas in NW Borneo. In: F.H. Sidi, D. Nummedal, P. Imbert, H. Darman and H.W. Posamentier (Editors), *Tropical Deltas of Southeast Asia—Sedimentology, Stratigraphy, and Petroleum Geology* SEPM Spec. Publ., pp. 109-123.
- Leckie, D.A. and Rumpel, T., 2003. Tide-influenced sedimentation in a rift basin—Cretaceous Qishn Formation, Masila Block, Yemen: A billion barrel oil field. *AAPG Bulletin*, 87: 987-1013.
- Lee, T.-Y. and Lawver, L.A., 1995. Cenozoic plate reconstruction of Southeast Asia. *Tectonophysics*, 251: 85-138.
- Leeder, M.R., 2011. *Sedimentology and sedimentary basins: from turbulence to tectonics*. Wiley-Blackwell, Oxford, UK, 784 pp.
- Legler, B., Hampson, G.J., Jackson, C.A.L., Johnson, H.D., Massart, B.Y.G., Sarginson, M. and Ravnås, R., 2014. Facies relationships and stratigraphic architecture of distal, mixed tide- and wave-influenced deltaic deposits: Lower Sego Sandstone, Western Colorado, U.S.A. *Journal of Sedimentary Research*, 84: 605-625.
- Legler, B., Johnson, H.D., Hampson, G.J., Massart, B.Y.G., Jackson, C.A.L., Jackson, M.D., El-Barkooky, A. and Ravnås, R., 2013. Facies model of a fine-grained, tide-dominated delta: Lower Dir Abu Lifa Member (Eocene), Western Desert, Egypt. *Sedimentology*, 60: 1313-1356.
- Levell, B.K., 1980. A late Precambrian tidal shelf deposit, the Lower Sandfjord Formation, Finnmark, north Norway. *Sedimentology*, 27: 539-557.
- Levell, B.K., 1987. The nature and significance of regional unconformities in the hydrocarbon-bearing Neogene sequences offshore West Sabah. *Bulletin of The Geological Society of Malaysia*, 21: 55-90.
- Levell, B.K., Johnson, H.D., Collins, D.S. and Van Cappelle, M., 2020. Deposition and preservation of fluvio- tidal shallow- marine sandstones: A re- evaluation of the Neoproterozoic Jura Quartzite (western Scotland). *Sedimentology*, 67: 173-206.
- Li, W., Bhattacharya, J.P., Zhu, Y., Garza, D. and Blankenship, E., 2011. Evaluating delta asymmetry using three- dimensional facies architecture and ichnological analysis, Ferron 'Notom Delta', Capital Reef, Utah, USA. *Sedimentology*, 58: 478-507.

- Li, Z., Bhattacharya, J.P. and Schieber, J., 2015. Evaluating along-strike variation using thin-bedded facies analysis, Upper Cretaceous Ferron Notom Delta, Utah. *Sedimentology*, 62: 2060–2089.
- Lockhart, B.E., Chinoroje, O., Enomoto, C.B. and Hollomon, G.A., 1997. Early Tertiary deposition in the southern Pattani Trough, Gulf of Thailand. In: P. Dheeradilok, C. Hinthong, P. Chaodumrong, P. Putthaphiban, W. Tansathien, C. Utha-aroon, N. Sattayarak, T. Nuchanong and S. Techawan (Editors), *The International Conference on Stratigraphy and Tectonic Evolution of Southeast Asia and the South Pacific*, Bangkok, Thailand, pp. 476-489.
- Longhitano, S.G., Mellere, D., Steel, R.J. and Ainsworth, R.B., 2012. Tidal depositional systems in the rock record: A review and new insights. *Sedimentary Geology*, 279: 2-22.
- Longhitano, S.G., Sabato, L., Tropeano, M. and Gallicchio, S., 2010. A mixed bioclastic–siliciclastic flood-tidal delta in a micro tidal setting: depositional architectures and hierarchical internal organization (Pliocene, Southern Apennine, Italy). *Journal of Sedimentary Research*, 80: 36-53.
- MacEachern, J.A. and Bann, K.L., 2008. The role of ichnology in refining shallow marine facies models. In: G.J. Hampson, R.J. Steel, P.M. Burgess and R.W. Dalrymple (Editors), *Recent Advances in Models of Siliciclastic Shallow-Marine Stratigraphy*. *SEPM Spec. Publ.*, pp. 73–116.
- MacEachern, J.A., Bann, K.L., Bhattacharya, J.P. and Howell, C.D., 2005. Ichnology of deltas: organism responses to the dynamic interplay of rivers, waves, storms, and tides. In: L. Giosan and J.P. Bhattacharya (Editors), *River Deltas—Concepts, Models, and Examples*. *SEPM Special Publication*. *SEPM*, pp. 45-85.
- MacMillan, D.H., 1966. *Tides*. American Elsevier Publishing Company, New York, 240 pp.
- Madec, G. and Imbard, M., 1996. A global ocean mesh to overcome the North Pole singularity. *Climate Dynamics*, 12: 381-388.
- Markwick, P.J. and Valdes, P.J., 2004. Palaeo-digital elevation models for use as boundary conditions in coupled ocean–atmosphere GCM experiments: a Maastrichtian (late Cretaceous) example. *Palaeogeography Palaeoclimatology Palaeoecology*, 213: 37-63.
- Martel, A.T., Allen, P.A. and Slingerland, R., 1994. Use of tidal-circulation modeling in paleogeographical studies: an example from the Tertiary of the Alpine perimeter. *Geology*, 22: 925-928.
- Martinius, A.W. and Gowland, S., 2011. Tide-influenced fluvial bedforms and tidal bore deposits (late Jurassic Lourinhã Formation, Lusitanian Basin, Western Portugal). *Sedimentology*, 58: 285–324.
- Martinius, A.W., Jablonski, B.V.J., Fustic, M., Strobl, R. and van den Berg, J.H., 2015. Fluvial to tidal transition zone facies in the McMurray Formation (Christina River, Alberta, Canada), with emphasis on the reflection of flow intensity in bottomset architecture. In: P.J. Ashworth, J.L. Best and D.R. Parsons (Editors), *Fluvial–Tidal Sedimentology. Developments in Sedimentology*. Elsevier, pp. 445–480.
- Martinius, A.W. and van den Berg, J.H., 2011. *Atlas of sedimentary structures in estuarine and tidally-influenced river deposits of the Rhine-Meuse-Scheldt system*. EAGE Publications BV, Houten, 298 pp.

- Maselli, V., Normandeau, A., Nones, M., Tesi, T., Langone, L., Trincardi, F. and Bohacs, K.M., 2020. Tidal modulation of river-flood deposits: How low can you go? *Geology*, 48: 663–667.
- Mazur, S., Green, C., Stewart, M.G., Whittaker, J.M., Williams, S. and Bouatmani, R., 2012. Displacement along the Red River Fault constrained by extension estimates and plate reconstructions. *Tectonics*, 31: TC5008.
- McBride, R.A., Anderson, J.B., Buynevich, I.V., Cleary, W., Fenster, M.S., Fitzgerald, D.M., Harris, M.S., Hein, C.J., Klein, A.H.F., Liu, B., de Menezes, J.T., Pejrup, M., Riggs, S.R., Short, A.D., Stone, G.W., Wallace, D.J. and Wang, P., 2013. Morphodynamics of barrier systems: a synthesis. In: J.F. Shroder (Editor), *Treatise on Geomorphology*. Academic Press, San Diego, CA, pp. 166–244.
- McCabe, P.J. and Jones, C.M., 1977. Formation of reactivation surfaces within superimposed deltas and bedforms. *Journal of Sedimentary Research*, 47: 707–715.
- McIlroy, D., 2006. Ichnology of a macrotidal tide-dominated deltaic depositional system: Lajas Formation, Neuquén Province, Argentina. In: R. Bromley, L.A. Buatois, J. Genise, M.G. Mángano and R. Melchor (Editors), *Sediment–Organism Interactions: A Multifaceted Ichnology*. Special Publication 88. SEPM, Tulsa, Oklahoma, pp. 195–211.
- McIlroy, D., 2007. Lateral variability in shallow marine ichnofabrics: implications for the ichnofabric analysis method. *Journal of the Geological Society*, 164: 359–369.
- Mellor, G.L., 1996. *Introduction to Physical Oceanography*. Springer-Verlag, New York, 248 pp.
- Miall, A.D., 2015. Updating uniformitarianism: stratigraphy as just a set of ‘frozen accidents’. In: D.G. Smith, R.J. Bailey, P.M. Burgess and A.J. Fraser (Editors), *Strata and Time: Probing the Gaps in Our Understanding*. Special Publication 404. Geological Society of London, pp. 11–36.
- Middleton, G.V., 1965. Primary sedimentary structures and their hydrodynamic interpretation, 12. SEPM Special Publication 265 pp.
- Miller, K.G., Kominz, M.A., Browning, J.V., Wright, J.D., Mountain, G.S., Katz, M.E., Sugarman, P.J., Cramer, B.S., Christie-Blick, N. and Pekar, S.F., 2005. The Phanerozoic record of global sea-level change. *Science*, 310: 1293–1298.
- Miller, K.G., Mountain, G.S., Wright, J.D. and Browning, J.V., 2011. A 180-Million-Year Record of Sea Level and Ice Volume Variations from Continental Margin and Deep-Sea Isotopic Records. *Oceanography*, 24: 40–53.
- Miller, K.G., Sugarman, P.J., Browning, J.V., Kominz, M.A., Hernández, J.C., Olsson, R.K., Wright, J.D., Feigenson, M.D. and Van Sickle, W., 2003. Late Cretaceous chronology of large, rapid sea-level changes: Glacioeustasy during the greenhouse world. *Geology*, 31: 585–588.
- Miller, M.C., McCave, I.N. and Komar, P.D., 1977. Threshold of sediment motion under unidirectional currents. *Sedimentology*, 24: 507–527.
- Milliman, J.D. and Farnsworth, K.L., 2011. *River discharge to the coastal ocean: a global synthesis*. Cambridge University Press, Cambridge, UK, 381 pp.
- Milliman, J.D. and Syvitski, J.P., 1992. Geomorphic/tectonic control of sediment discharge to the ocean: the importance of small mountainous rivers. *The Journal of Geology*, 100: 525–544.

- Mitchell, A.J., Allison, P.A., Gorman, G.J., Piggott, M.D. and Pain, C.C., 2011. Tidal circulation in an ancient epicontinental sea: The Early Jurassic Laurusian Seaway. *Geology*, 39: 207-210.
- Mitchell, A.J., Uličný, D., Hampson, G.J., Allison, P.A., Gorman, G.J., Piggott, M.D., Wells, M.R. and Pain, C.C., 2010. Modelling tidal current-induced bed shear stress and palaeocirculation in an epicontinental seaway: the Bohemian Cretaceous Basin, Central Europe. *Sedimentology*, 57: 359-388.
- Morley, C.K., 2016. Major unconformities/termination of extension events and associated surfaces in the South China Seas: Review and implications for tectonic development. *Journal of Asian Earth Sciences*, 120: 62-86.
- Morley, R.J., Swiecicki, T. and Pham, D.T.T., 2011. A sequence stratigraphic framework for the Sunda region, based on integration of biostratigraphic, lithological and seismic data from Nam Con Son basin, Vietnam, Indonesian Petroleum Association 35th Annual Convention, Jakarta, Indonesia, pp. IPA11-G-002.
- Mulhern, J.S., Johnson, C.L. and Martin, J.M., 2017. Is barrier island morphology a function of tidal and wave regime? *Marine Geology*, 387: 74-84.
- Müller, R.D., Roest, W.R., Royer, J.Y., Gahagan, L.M. and Sclater, J.G., 1997. Digital isochrons of the world's ocean floor. *Journal of Geophysical Research*, 102: 3211-3214.
- Murtaza, M., Rahman, A.H.A., Sum, C.W. and Konjing, Z., 2018. Facies associations, depositional environments and stratigraphic framework of the Early Miocene–Pleistocene successions of the Mukah–Balingian Area, Sarawak, Malaysia. *Journal of Asian Earth Sciences*, 152: 23-38.
- Muto, T. and Steel, R.J., 1997. Principles of regression and transgression: the nature of the interplay between accommodation and sediment supply. *Journal of Sedimentary Research*, 67: 994-1000.
- Mutti, E., Allen, G. and Rosell, J., 1984. Sigmoidal cross stratification and sigmoidal bars: depositional features diagnostic of tidal sandstones, 5th IAS European Regional Meeting, Marsiglia, pp. 312-313.
- Mutti, E., Rosell, J., Allen, G., Fonnesu, F. and Sgavetti, M., 1985. The Eocene Baronia tide dominated delta-shelf system in the Ager Basin. In: M.D. Mila and J. Rosell (Editors), *Excursion guidebook: 6th International Association of Sedimentologists European Regional Meeting*. International Association of Sedimentologists, Lleida, Spain, pp. 579-600.
- Myrow, P.M., Fischer, W. and Goodge, J.W., 2002. Wave-modified turbidites: combined-flow shoreline and shelf deposits, Cambrian, Antarctica. *Journal of Sedimentary Research*, 72: 641-656.
- Myrow, P.M. and Southard, J.B., 1996. Tempestite deposition. *Journal of Sedimentary Research*, 66: 992-1007.
- Nanson, R.A., Vakarelov, B.K., Ainsworth, R.B., Williams, F.M. and Price, D.M., 2013. Evolution of a Holocene, mixed-process, forced regressive shoreline: the Mitchell River delta, Queensland, Australia. *Marine Geology*, 339: 22-43.
- Narayan, J., 1971. Sedimentary structures in the lower Greensand of the Weald, England, and Bas-Boulonnais, France. *Sedimentary Geology*, 6: 73-109.

- Nguyen, V.L., Ta, T.K.O. and Tateishi, M., 2000. Late Holocene depositional environments and coastal evolution of the Mekong River Delta, Southern Vietnam. *Journal of Asian Earth Sciences*, 18: 427-439.
- Nio, S.-D. and Yang, C.-S., 1991. Diagnostic attributes of clastic tidal deposits: a review. In: D. Smith, G.G.E. Reinson, B.A. Zaitlin and R.A. Rahmani (Editors), *Clastic Tidal Sedimentology*. Canadian Society of Petroleum Geologists, Memoir 16, pp. 3-27.
- Nio, S., Siegenthaler, C. and Yang, C., 1983. Megaripple cross-bedding as a tool for the reconstruction of the paleo-hydraulics in a Holocene subtidal environment, SW Netherlands. *Geologie en Mijnbouw*, 62: 499-510.
- Nyberg, B. and Howell, J.A., 2015. Is the present the key to the past? A global characterization of modern sedimentary basins. *Geology*, 43: 643-646.
- Nyberg, B. and Howell, J.A., 2016. Global distribution of modern shallow marine shorelines. Implications for exploration and reservoir analogue studies. *Marine and Petroleum Geology*, 71: 83-104.
- Obradovich, J.D., 1993. A Cretaceous time scale. In: W.G.E. Caldwell and E.G. Kauffman (Editors), *Evolution of the Western Interior Basin*. Geological Association of Canada, Special Paper 39, St. John's, Newfoundland, pp. 379-396.
- Off, T., 1963. Rhythmic linear sand bodies caused by tidal currents. *AAPG Bulletin*, 47: 324-341.
- Ogg, J.G., Agterberg, F.P. and Gradstein, F.M., 2004. The Cretaceous period. In: G. F.M., O. J.G. and S. A.G (Editors), *A Geologic Time Scale 2004*. Cambridge University Press, Cambridge, pp. 344-383.
- Olson, W.S., 1972. Sedimentary Model for Determining Paleotidal Range: Discussion. *Geological Society of America Bulletin*, 83: 537-538.
- Open University Course Team, 1999. *Waves, Tides and Shallow-water Processes: Second Edition*. Butterworth-Heinemann, Oxford, UK, 227 pp.
- Orton, G.J. and Reading, H.G., 1993. Variability of deltaic processes in terms of sediment supply, with particular emphasis on grain size. *Sedimentology*, 40: 475-512.
- Pain, C.C., Piggott, M.D., Goddard, A.J.H., Fang, F., Gorman, G.J., Marshall, D.P., Eaton, M.D., Power, P.W. and De Oliveira, C.R.E., 2005. Three-dimensional unstructured mesh ocean modelling. *Ocean Modelling*, 10: 5-33.
- Peltzer, G. and Tapponnier, P., 1988. Formation and evolution of strike-slip faults, rifts, and basins during the India-Asia collision: An experimental approach. *Journal of Geophysical Research: Solid Earth*, 93: 15085-15117.
- Peng, Y., Steel, R.J., Rossi, V.M. and Olariu, C., 2018. Mixed-energy process interactions read from a compound-clinoform delta (paleo-Orinoco Delta, Trinidad): preservation of river and tide signals by mud-induced wave damping. *Journal of Sedimentary Research*, 88: 75-90.
- Perillo, M.M., Best, J.L. and Garcia, M.H., 2014. A new phase diagram for combined-flow bedforms. *Journal of Sedimentary Research*, 84: 301-313.
- Pietrzak, J., Jakobson, J.B., Burchard, H., Vested, H.J. and Petersen, O., 2002. A three-dimensional hydrostatic model for coastal and ocean modelling using a generalised topography following co-ordinate system. *Ocean Modelling*, 4: 173-205.
- Piggott, M.D., Gorman, G.J., Pain, C.C., Allison, P.A., Candy, A.S., Martin, B.T. and Wells, M.R., 2008. A new computational framework for multi-scale ocean modelling based on

1  
2  
3  
4  
5  
6  
7  
8  
9  
10  
11  
12  
13  
14  
15  
16  
17  
18  
19  
20  
21  
22  
23  
24  
25  
26  
27  
28  
29  
30  
31  
32  
33  
34  
35  
36  
37  
38  
39  
40  
41  
42  
43  
44  
45  
46  
47  
48  
49  
50  
51  
52  
53  
54  
55  
56  
57  
58  
59  
60  
61  
62  
63  
64  
65

adapting unstructured meshes. *International Journal for Numerical Methods in Fluids*, 56: 1003-1015.

Pingree, R.D. and Griffiths, D.K., 1979. Sand transport paths around the British Isles resulting from M2 and M4 tidal interactions. *Journal of the Marine Biological Association of the United Kingdom*, 59: 497-513.

Piper, D.J., Kontopoulos, N., Anagnostou, C., Chronis, G. and Panagos, A., 1990. Modern fan deltas in the western Gulf of Corinth, Greece. *Geo-Marine Letters*, 10: 5-12.

Plink-Björklund, P., 2012. Effects of tides on deltaic deposition: Causes and responses. *Sedimentary Geology*, 279: 107-133.

Posamentier, H.W. and Walker, R.G. (Editors), 2006. *Facies models revisited*. SEPM Special Publication 84.

Proudman, J., 1953. *Dynamical Oceanography*. Methuen-John Wiley, London, 409 pp.

Pugh, D.T., 1987. *Tides, surges and mean sea-level: a handbook for engineers and scientists*. John Wiley & Sons, Chichester, UK, 472 pp.

Ramli, N., 1986. Depositional model of a Miocene barred wave-and storm-dominated shoreface and shelf, southeastern Malay Basin, offshore West Malaysia. *AAPG Bulletin*, 70: 34-47.

Rawson, P.F., 2006. Cretaceous: sea levels peak as the North Atlantic opens, *The Geology of England and Wales*, 2nd Edition. Geological Society, London, London, UK, pp. 365-393.

Reading, H.G., 1978. *Sedimentary Environments and Facies*, 60. Blackwell Scientific Publications, Oxford, 557 pp.

Reading, H.G., 1996. *Sedimentary environments: processes, facies and stratigraphy*. Blackwell Publishing Ltd, Oxford, U.K., 615 pp.

Redfield, A.C., 1958. The influence of the continental shelf on the tides of the Atlantic coast of the United States. *Journal of Marine Research*, 17: 432-448.

Reineck, H.-E., 1963. Sedimentgefüge im Bereich der südlichen Nordsee. *Senckenbergische Naturforschende Gesellschaft, Abhandlungen*, 505: 1-138.

Reineck, H.-E. and Singh, I.B., 1980. *Depositional Sedimentary Environments: With Reference to Terrigenous Clastics*. Springer, Berlin, 549 pp.

Reineck, H.-E. and Wunderlich, F., 1968. Classification and Origin of Flaser and Lenticular Bedding. *Sedimentology*, 11: 99-104.

Replumaz, A. and Tapponnier, P., 2003. Reconstruction of the deformed collision zone between India and Asia by backward motion of lithospheric blocks. *Journal of Geophysical Research*, 108: B62285.

Ridd, M.F., Barber, A.J. and Crow, M.J., 2011. *The Geology of Thailand*. Geological Society of London, London, UK, 626 pp.

Robinson, A., 1966. Residual currents in relation to shoreline evolution of the East Anglian coast. *Marine Geology*, 4: 57-84.

Rodriguez, A.B., Hamilton, M.D. and Anderson, J.B., 2000. Facies and evolution of the modern Brazos Delta, Texas: wave versus flood influence. *Journal of Sedimentary Research*, 70: 283-295.

Rossi, V.M., Kim, W., Leva López, J., Edmonds, D., Geleynse, N., Olariu, C., Steel, R.J., Hiatt, M. and Passalacqua, P., 2016. Impact of tidal currents on delta-channel deepening, stratigraphic architecture, and sediment bypass beyond the shoreline. *Geology*, 44: 927-930.

- Rossi, V.M., Perillo, M.M., Steel, R.J. and Olariu, C., 2017. Quantifying mixed-process variability in shallow-marine depositional systems: What are sedimentary structures really telling us? *Journal of Sedimentary Research*, 87: 1060-1074.
- Rossi, V.M. and Steel, R.J., 2016. The role of tidal, wave and river currents in the evolution of mixed-energy deltas: Example from the Lajas Formation (Argentina). *Sedimentology*, 63: 824–864.
- Roy, P., Thom, B. and Wright, L., 1980. Holocene sequences on an embayed high-energy coast: an evolutionary model. *Sedimentary Geology*, 26: 1-19.
- Roy, P., Williams, R., Jones, A., Yassini, I., Gibbs, P., Coates, B., West, R., Scanes, P., Hudson, J. and Nichol, S., 2001. Structure and function of south-east Australian estuaries. *Estuarine, Coastal and Shelf Science*, 53: 351-384.
- Ru, K. and Pigott, J.D., 1986. Episodic rifting and subsidence in the South China Sea. *AAPG Bulletin*, 70: 1136-1155.
- Rubin, D.M. and McCulloch, D.S., 1980. Single and superimposed bedforms: a synthesis of San Francisco Bay and flume observations. *Sedimentary Geology*, 26: 207-231.
- Ruffell, A.H., 1992. Correlation of the Hythe Beds Formation (Lower Greensand Group: early-mid-Aptian), southern England. *Proceedings of the Geologists' Association*, 103: 273-291.
- Ruffell, A.H. and Wach, G.D., 1991. Sequence stratigraphic analysis of the Aptian-Albian Lower Greensand in southern England. *Marine and Petroleum Geology*, 8: 341-353.
- Safak, I., 2016. Variability of Bed Drag on Cohesive Beds under Wave Action. *Water*, 8: 131.
- Salahuddin and Lambiase, J.J., 2013. Sediment Dynamics and Depositional Systems of the Mahakam Delta, Indonesia: Ongoing Delta Abandonment On A Tide-Dominated Coast. *Journal of Sedimentary Research*, 83: 503–521.
- Sames, B., Wagerich, M., Wendler, J., Haq, B., Conrad, C., Melinte-Dobrinescu, M., Hu, X., Wendler, I., Wolfgring, E. and Yilmaz, I., 2016. Short-term sea-level changes in a greenhouse world—A view from the Cretaceous. *Palaeogeography, Palaeoclimatology, Palaeoecology*, 441: 393-411.
- Sandal, S.T., 1996. *The Geology and Hydrocarbon Resources of Negara Brunei Darussalam*. Brunei Shell Petroleum Company, Brunei Museum, Bandar Seri Begawan, Brunei Darussalam, 243 pp.
- Schwiderski, E.W., 1980. On charting global ocean tides. *Reviews of Geophysics*, 18: 243-268.
- Shanley, K.W., McCabe, P.J. and Hettinger, R.D., 1992. Tidal influence in Cretaceous fluvial strata from Utah, USA: a key to sequence stratigraphic interpretation. *Sedimentology*, 39: 905-930.
- Shanmugam, G., 2013. Modern internal waves and internal tides along oceanic pycnoclines: Challenges and implications for ancient deep-marine baroclinic sands. *AAPG Bulletin*, 97: 799-843.
- Shaw, D.P., 1964. *Time in Stratigraphy*. McGraw Hill, New York, 365 pp.
- Shoup, R.C., Morley, R.J., Swiecicki, T. and Clark, S., 2013. Tectono-stratigraphic Framework and Tertiary Paleogeogeography of Southeast Asia; Gulf of Thailand to South Vietnam Shelf. *Houston Geological Society Bulletin*, 55: 27-39.
- Siddiqui, N.A., Rahman, A.H.A., Sum, C.W., Mathew, M.J. and Menier, D., 2016. Onshore sandstone facies characteristics and reservoir quality of Nyalau Formation, Sarawak, East

1  
2  
3  
4  
5  
6  
7  
8  
9  
10  
11  
12  
13  
14  
15  
16  
17  
18  
19  
20  
21  
22  
23  
24  
25  
26  
27  
28  
29  
30  
31  
32  
33  
34  
35  
36  
37  
38  
39  
40  
41  
42  
43  
44  
45  
46  
47  
48  
49  
50  
51  
52  
53  
54  
55  
56  
57  
58  
59  
60  
61  
62  
63  
64  
65

Malaysia: an analogue to subsurface reservoir quality evaluation. *Arabian Journal for Science and Engineering*, 41: 267-280.

Sisulak, C.F. and Dashtgard, S.E., 2012. Seasonal Controls On the Development And Character of Inclined Heterolithic Stratification In A Tide-Influenced, Fluvially Dominated Channel: Fraser River, Canada. *Journal of Sedimentary Research*, 82: 244–257.

Sixsmith, P.J., Hampson, G.J., Gupta, S., Johnson, H.D. and Fofana, J.F., 2008. Facies architecture of a net transgressive sandstone reservoir analog: The Cretaceous Hosta Tongue, New Mexico. *AAPG Bulletin*, 92: 513-547.

Slater, R.D., 1985. A numerical model of tides in the Cretaceous Seaway of North America. *The Journal of Geology*, 93: 333-345.

Slingerland, R., 1986. Numerical computation of co-oscillating palaeotides in the Catskill epeiric Sea of eastern North America. *Sedimentology*, 33: 487-497.

Smith, D.G., 1988. Tidal bundles and mud couplets in the McMurray Formation, northeastern Alberta, Canada. *Bulletin of Canadian Petroleum Geology*, 36: 216-219.

Smith, D.G., Reinson, G.E., Zaitlin, B.A. and Rahmani, R.A., 1991. Clastic Tidal Sedimentology, 16. *Memoir of the Canadian Society of Petroleum Geologists*, 387 pp.

Sondi, I., Juračić, M. and Pravdić, V., 1995. Sedimentation in a disequilibrium river- dominated estuary: the Raša River Estuary (Adriatic Sea, Croatia). *Sedimentology*, 42: 769-782.

Soulsby, R., Hamm, L., Klopman, G., Myrhaug, D., Simons, R. and Thomas, G., 1993. Wave-current interaction within and outside the bottom boundary layer. *Coastal engineering*, 21: 41-69.

Southard, J.B. and Boguchwal, L.A., 1990. Bed configurations in steady unidirectional water flows. Part 2. Synthesis of flume data. *Journal of Sedimentary Research*, 60.

Staub, J.R. and Esterle, J.S., 1994. Peat-accumulating depositional systems of Sarawak, East Malaysia. *Sedimentary Geology*, 89: 91-106.

Staub, J.R. and Gastaldo, R., 2000. Seasonal sediment transport and deposition in the Rajang River delta, Sarawak, East Malaysia. *Sedimentary Geology*, 133: 249-264.

Stride, A.H., 1973. Sediment transport by the North Sea. In: E.D. Goldberg (Editor), *North Sea Science*. MIT Press, Cambridge, MA, pp. 101-130.

Stride, A.H., 1982. *Offshore tidal sands: processes and deposits*. Chapman & Hall, London, 222 pp.

Syvitski, J.P. and Milliman, J.D., 2007. Geology, geography, and humans battle for dominance over the delivery of fluvial sediment to the coastal ocean. *The Journal of Geology*, 115: 1-19.

Syvitski, J.P., Peckham, S.D., Hilberman, R. and Mulder, T., 2003. Predicting the terrestrial flux of sediment to the global ocean: a planetary perspective. *Sedimentary Geology*, 162: 5-24.

Syvitski, J.P. and Saito, Y., 2007. Morphodynamics of deltas under the influence of humans. *Global and Planetary Change*, 57: 261-282.

Ta, T.K.O., Nguyen, V.L., Tateishi, M., Kobayashi, I., Saito, Y. and Nakamura, T., 2002a. Sediment facies and Late Holocene progradation of the Mekong River Delta in Bentre Province, southern Vietnam: an example of evolution from a tide-dominated to a tide- and wave-dominated delta. *Sedimentary Geology*, 152: 313-325.



- 1
- 2
- 3
- 4
- 5
- 6
- 7
- 8
- 9
- 10
- 11 Ta, T.K.O., Nguyen, V.L., Tateishi, M., Kobayashi, I., Tanabe, S. and Saito, Y., 2002b.
- 12 Holocene delta evolution and sediment discharge of the Mekong River, southern
- 13 Vietnam. *Quaternary Science Reviews*, 21: 1807-1819.
- 14
- 15 Tapponnier, P., Peltzer, G. and Armijo, R., 1986. On the mechanics of the collision between
- 16 India and Asia. In: M.P. Coward and A.C. Ries (Editors), *Collision Tectonics*. Special
- 17 Publications. Geological Society, London, London, UK, pp. 113-157.
- 18
- 19 Tapponnier, P., Peltzer, G., Le Dain, A., Armijo, R. and Cobbold, P., 1982. Propagating
- 20 extrusion tectonics in Asia: New insights from simple experiments with plasticine.
- 21 *Geology*, 10: 611-616.
- 22
- 23 Taylor, B., 1992. Rifting and the volcanic-tectonic evolution of the Izu-Bonin-Mariana arc. In:
- 24 B. Taylor, K. Fujioaka and e. al. (Editors), *Proceedings of Ocean Drilling Program*
- 25 *Scientific Results*, College Station, TX, pp. 625-651.
- 26
- 27 Taylor, B. and Hayes, D.E., 1983. Origin and History of the South China Sea Basin. In: D.E.
- 28 Hayes (Editor), *The Tectonic and Geologic Evolution of Southeast Asian Seas and*
- 29 *Islands: Part 2. Geophysical Monograph*. American Geophysical Union, Washington,
- 30 D.C., pp. 23-56.
- 31
- 32 Terwindt, J., 1981. Origin and Sequences of Sedimentary Structures in Inshore Mesotidal
- 33 Deposits of the North Sea. In: S.D. Nio, R.T.E. Shüttenhelm and T.C.E.V. Weering
- 34 (Editors), *Holocene Marine Sedimentation in the North Sea Basin*. Special Publication.
- 35 *International Association of Sedimentologists*, pp. 4-26.
- 36
- 37 Terwindt, J. and Breusers, H., 1972. Experiments on the origin of flaser, lenticular and sand-
- 38 clay alternating bedding. *Sedimentology*, 19: 85-98.
- 39
- 40 Terwindt, J.H., 1971. Litho-facies of inshore estuarine and tidal-inlet deposits. *Geologie en*
- 41 *Mijnbouw*, 50: 515-526.
- 42
- 43 Thomas, R.G., Smith, D.G., Wood, J.M., Visser, J., Calverley-Range, E.A. and Koster, E.H.,
- 44 1987. Inclined heterolithic stratification—terminology, description, interpretation and
- 45 significance. *Sedimentary Geology*, 53: 123-179.
- 46
- 47 Tin, N.T. and Ty, N.D., 1995. Petroleum geology of the Nam Con Son Basin. *Bulletin of the*
- 48 *Geological Society of Malaysia*, 37: 1-11.
- 49
- 50 Tinterri, R., 2011. Combined flow sedimentary structures and the genetic link between
- 51 sigmoidal-and hummocky-cross stratification. *GeoActa*, 10: 1-43.
- 52
- 53 Todd, S.P., Dunn, M.E. and Barwise, A.J.G., 1997. Characterizing petroleum charge systems in
- 54 the Tertiary of SE Asia. In: A.J. Fraser, S.J. Matthews and R.W. Murphy (Editors),
- 55 *Petroleum Geology of Southeast Asia*. Special Publications 126. Geological Society
- 56 London, London, UK, pp. 25-47.
- 57
- 58 Togunwa, O.S., Abdullah, W.H., Hakimi, M.H. and Barbeito, P.J., 2015. Organic geochemical
- 59 and petrographic characteristics of Neogene organic-rich sediments from the onshore
- 60 West Baram Delta Province, Sarawak Basin: Implications for source rocks and
- 61 hydrocarbon generation potential. *Marine and Petroleum Geology*, 63: 115-126.
- 62
- 63 Tsimplis, M., Proctor, R. and Flather, R., 1995. A two- dimensional tidal model for the
- 64 Mediterranean Sea. *Journal of Geophysical Research: Oceans*, 100: 16223-16239.
- 65
- 66 Twilley, R.R., Rovai, A.S. and Riul, P., 2018. Coastal morphology explains global blue carbon
- 67 distributions. *Frontiers in Ecology and the Environment*, 16: 503-508.
- 68
- 69 Tyson, R. and Funnell, B., 1987. European Cretaceous shorelines, stage by stage.
- 70 *Palaeogeography, Palaeoclimatology, Palaeoecology*, 59: 69-91.

- Uličný, D., 2001. Depositional systems and sequence stratigraphy of coarse- grained deltas in a shallow- marine, strike- slip setting: the Bohemian Cretaceous Basin, Czech Republic. *Sedimentology*, 48: 599-628.
- Uličný, D., Laurin, J. and Čech, S., 2009. Controls on clastic sequence geometries in a shallow-marine, transtensional basin: the Bohemian Cretaceous Basin, Czech Republic. *Sedimentology*, 56: 1077-1114.
- Uličný, D. and Špičáková, L., 1996. Response to high frequency sea-level change in a fluvial to estuarine succession: Cenomanian palaeovalley fill, Bohemian Cretaceous Basin. *Geological Society, London, Special Publications*, 104: 247-268.
- Vakarelov, B.K. and Ainsworth, R.B., 2013. A hierarchical approach to architectural classification in marginal-marine systems: Bridging the gap between sedimentology and sequence stratigraphy. *AAPG Bulletin*, 97: 1121-1161.
- Vakarelov, B.K., Ainsworth, R.B. and MacEachern, J.A., 2012. Recognition of wave-dominated, tide-influenced shoreline systems in the rock record: Variations from a microtidal shoreline model. *Sedimentary Geology*, 279: 23-41.
- van Cappelle, M., Hampson, G.J. and Johnson, H.D., 2018. Spatial and Temporal Evolution of Coastal Depositional Systems and Regional Depositional Process Regimes: Campanian Western Interior Seaway, USA. *Journal of Sedimentary Research*, 88: 873-897.
- van Cappelle, M., Stukins, S., Hampson, G.J. and Johnson, H.D., 2016. Fluvial to tidal transition in proximal, mixed tide-influenced and wave-influenced deltaic deposits: Cretaceous lower Sego Sandstone, Utah, USA. *Sedimentology*, 63: 1333-1361.
- van den Berg, J.H., Boersma, J.R. and Gelder, A.v., 2007. Diagnostic sedimentary structures of the fluvial-tidal transition zone—Evidence from deposits of the Rhine and Meuse. *Netherlands Journal of Geosciences/Geologie en Mijnbouw*, 86: 287-306.
- van Hattum, M.W.A., Hall, R., Pickard, A.L. and Nichols, G.J., 2006. Southeast Asian sediments not from Asia: Provenance and geochronology of north Borneo sandstones. *Geology*, 34: 589.
- Van Straaten, L., 1953. Megaripples in the Dutch Wadden Sea and in the basin of Arcachon (France). *Geol. Mijnbouw*, 15: 1-11.
- Van Wagoner, J.C., Mitchum, R.M., Campion, K.M. and Rahmanian, V.D., 1990. Siliciclastic Sequence Stratigraphy in Well Logs, Cores, and Outcrops: Concepts for High-Resolution Correlation of Time and Facies. *Methods in Exploration*, 7. AAPG, 55 pp.
- Van Yperen, A.E., Poyatos- Moré, M., Holbrook, J.M. and Midtkandal, I., 2020. Internal mouth- bar variability and preservation of subordinate coastal processes in low-accommodation proximal deltaic settings (Cretaceous Dakota Group, New Mexico, USA). *The Depositional Record*.
- Vaucher, R., Pittet, B., Hormière, H., Martin, E.L. and Lefebvre, B., 2016. A wave-dominated, tide-modulated model for the Lower Ordovician of the Anti-Atlas, Morocco. *Sedimentology*, 64: 777-807.
- Visser, M.J., 1980. Neap-spring cycles reflected in Holocene subtidal large-scale bedform deposits: a preliminary note. *Geology*, 8: 543-546.
- Voigt, T. and Tröger, K., 1996. Sea-level changes during Late Cenomanian and early Turonian in the Saxonian Cretaceous Basin. *Mitteilungen aus dem Geologisch-Paläontologischen Institut der Universität Hamburg*, 77: 275-290.

- Walker, R.G., 1979. Facies Models. Geoscience Canada Reprint Series, 3. Geological Association of Canada, 211 pp.
- Walker, R.G. and James, N.P., 1992. Facies Models: Response to Sea Level Change. Geotext, 1. Geological Association of Canada, 409 pp.
- Walker, R.G. and Plint, A.G., 1992. Wave- and storm-dominated shallow marine systems. In: R.G. Walker and N.P. James (Editors), Facies Models: Response to Sea-Level Change. Geological Association of Canada, St. John's, Newfoundland, pp. 219-238.
- Wan Hsiah, A., 2003. Coaly source rocks of NW Borneo: role of suberinite and bituminite in oil generation and expulsion. Geological Society of Malaysia Bulletin, 47: 153-163.
- Ward, S.L., Neill, S.P., Van Landeghem, K.J.J. and Scourse, J.D., 2015. Classifying seabed sediment type using simulated tidal-induced bed shear stress. Marine Geology, 367: 94-104.
- Wei, X., Steel, R.J., Ravnås, R., Jiang, Z., Olariu, C. and Li, Z., 2016. Variability of tidal signals in the Brent Delta Front: New observations on the Rannoch Formation, northern North Sea. Sedimentary Geology, 335: 166-179.
- Wells, M.R., 2008. Tidal modelling of modern and ancient seas and oceans, Imperial College London, 527 pp.
- Wells, M.R., Allison, P.A., Hampson, G.J., Piggott, M.D. and Pain, C.C., 2005a. Modelling ancient tides: the Upper Carboniferous epi-continental seaway of Northwest Europe. Sedimentology, 52: 715-735.
- Wells, M.R., Allison, P.A., Piggott, M.D., Gorman, G.J., Hampson, G.J., Pain, C.C. and Fang, F., 2007a. Numerical Modeling of Tides in the Late Pennsylvanian Midcontinent Seaway of North America with Implications for Hydrography and Sedimentation. Journal of Sedimentary Research, 77: 843-865.
- Wells, M.R., Allison, P.A., Piggott, M.D., Hampson, G.J., Pain, C.C. and Gorman, G.J., 2010a. Tidal Modeling of an Ancient Tide-Dominated Seaway, Part 1: Model Validation and Application to Global Early Cretaceous (Aptian) Tides. Journal of Sedimentary Research, 80: 393-410.
- Wells, M.R., Allison, P.A., Piggott, M.D., Hampson, G.J., Pain, C.C. and Gorman, G.J., 2010b. Tidal Modeling of an Ancient Tide-Dominated Seaway, Part 2: The Aptian Lower Greensand Seaway of Northwest Europe. Journal of Sedimentary Research, 80: 411-439.
- Wells, M.R., Allison, P.A., Piggott, M.D., Pain, C.C., Hampson, G.J. and De Oliveira, C.R., 2005b. Large sea, small tides: the Late Carboniferous seaway of NW Europe. Journal of the Geological Society, 162: 417-420.
- Wells, M.R., Allison, P.A., Piggott, M.D., Pain, C.C., Hampson, G.J. and Dodman, A., 2007b. Investigating tides in the Early Pennsylvanian Seaway of NW Eurasia using the Imperial College Ocean Model. In: C. Holmden and B.R. Pratt (Editors), Dynamics of Epeiric Seas: Sedimentological, Paleontological and Geochemical Perspectives. Special Paper 48. Geological Association of Canada, pp. 363-387.
- Willis, B.J., 2005. Deposits of tide-influenced river deltas. In: L. Giosan and J.P. Bhattacharya (Editors), River Deltas—Concepts, Models, and Examples. SEPM Special Publication, pp. 87-129.
- Willis, B.J. and Fitris, F., 2012. Sequence Stratigraphy of Miocene Tide-Influenced Sandstones in the Minas Field, Sumatra, Indonesia. Journal of Sedimentary Research, 82: 400-421.

- Willis, B.J. and Gabel, S., 2001. Sharp-based, tide-dominated deltas of the Sego Sandstone, Book Cliffs, Utah, USA. *Sedimentology*, 48: 479–506.
- Wolanski, E.E.J., Mazda, Y.Y. and Ridd, P.P.V., 1992. Mangrove hydrodynamics. In: A.I. Robertson and D.M. Alongi (Editors), *Tropical Mangrove Ecosystems. Coastal and Estuarine Studies*. American Geophysical Union, Washington, DC, pp. 43–62.
- Wonham, J.P. and Elliott, T., 1996. High-resolution sequence stratigraphy of a mid-Cretaceous estuarine complex: the Woburn Sands of the Leighton Buzzard area, southern England. In: S.P. Hesselbo and D.N. Parkinson (Editors), *Sequence Stratigraphy in the British Isles. Special Publications 103*. Geological Society, London, pp. 41–62.
- Woodroffe, C.D., Rogers, K., McKee, K.L., Lovelock, C.E., Mendelssohn, I.A. and Saintilan, N., 2016. Mangrove sedimentation and response to relative sea-level rise. *Annual Review of Marine Science*, 8: 243–66.
- Yang, C.S. and Nio, S.D., 1985. The estimation of palaeohydrodynamic processes from subtidal deposits using time series analysis methods. *Sedimentology*, 32: 41–57.
- Yoshida, S., Johnson, H.D., Pye, K. and Dixon, R.J., 2004. Transgressive changes from tidal estuarine to marine embayment depositional systems: The Lower Cretaceous Woburn Sands of southern England and comparison with Holocene analogs. *AAPG Bulletin*, 88: 1433–1460.
- Yoshida, S., Steel, R.J. and Dalrymple, R.W., 2007. Changes in depositional processes—an ingredient in a new generation of sequence-stratigraphic models. *Journal of Sedimentary Research*, 77: 447–460.
- Zheng, W. and Deng, H., 2012. The Tidal Sandstone Characteristic of the Zhuhai Formation, Huizhou Oil Field, Pearl River Mouth Basin, South China Sea. *Petroleum Science and Technology*, 30: 567–574.
- Ziegler, P.A., 1990. *Geological Atlas of Western and Central Europe*. Maatschappij B.V., Shell Internationale Petroleum, The Hague, 239 pp.
- Zuchuat, V., Sleveland, A.R., Pettigrew, R.P., Dodd, T.J., Clarke, S.M., Rabbel, O., Braathen, A. and Midtkandal, I., 2019. Overprinted allocyclic processes by tidal resonance in an epicontinental basin: The Upper Jurassic Curtis Formation, east-central Utah, USA. *The Depositional Record*, 5: 272–305.